

University of Warwick institutional repository: <http://go.warwick.ac.uk/wrap>

**A Thesis Submitted for the Degree of PhD at the University of Warwick**

<http://go.warwick.ac.uk/wrap/46013>

This thesis is made available online and is protected by original copyright.

Please scroll down to view the document itself.

Please refer to the repository record for this item for information to help you to cite it. Our policy information is available from the repository home page.

## Library Declaration and Deposit Agreement

### 1. STUDENT DETAILS

Please complete the following:

Full name: .....

University ID number: .....

### 2. THESIS DEPOSIT

2.1 I understand that under my registration at the University, I am required to deposit my thesis with the University in BOTH hard copy and in digital format. The digital version should normally be saved as a single pdf file.

2.2 The hard copy will be housed in the University Library. The digital version will be deposited in the University's Institutional Repository (WRAP). Unless otherwise indicated (see 2.3 below) this will be made openly accessible on the Internet and will be supplied to the British Library to be made available online via its Electronic Theses Online Service (EThOS) service.

[At present, theses submitted for a Master's degree by Research (MA, MSc, LL.M, MS or MMedSci) are not being deposited in WRAP and not being made available via EThOS. This may change in future.]

2.3 In exceptional circumstances, the Chair of the Board of Graduate Studies may grant permission for an embargo to be placed on public access to the hard copy thesis for a limited period. It is also possible to apply separately for an embargo on the digital version. (Further information is available in the *Guide to Examinations for Higher Degrees by Research*.)

2.4 If you are depositing a thesis for a Master's degree by Research, please complete section (a) below. For all other research degrees, please complete both sections (a) and (b) below:

#### (a) Hard Copy

I hereby deposit a hard copy of my thesis in the University Library to be made publicly available to readers (please delete as appropriate) EITHER immediately OR after an embargo period of ..... months/years as agreed by the Chair of the Board of Graduate Studies.

I agree that my thesis may be photocopied. YES / NO (Please delete as appropriate)

#### (b) Digital Copy

I hereby deposit a digital copy of my thesis to be held in WRAP and made available via EThOS.

Please choose one of the following options:

EITHER My thesis can be made publicly available online. YES / NO (Please delete as appropriate)

OR My thesis can be made publicly available only after.....[date] (Please give date)  
YES / NO (Please delete as appropriate)

OR My full thesis cannot be made publicly available online but I am submitting a separately identified additional, abridged version that can be made available online.  
YES / NO (Please delete as appropriate)

OR My thesis cannot be made publicly available online. YES / NO (Please delete as appropriate)

**3. GRANTING OF NON-EXCLUSIVE RIGHTS**

Whether I deposit my Work personally or through an assistant or other agent, I agree to the following:

Rights granted to the University of Warwick and the British Library and the user of the thesis through this agreement are non-exclusive. I retain all rights in the thesis in its present version or future versions. I agree that the institutional repository administrators and the British Library or their agents may, without changing content, digitise and migrate the thesis to any medium or format for the purpose of future preservation and accessibility.

**4. DECLARATIONS**

(a) I DECLARE THAT:

- I am the author and owner of the copyright in the thesis and/or I have the authority of the authors and owners of the copyright in the thesis to make this agreement. Reproduction of any part of this thesis for teaching or in academic or other forms of publication is subject to the normal limitations on the use of copyrighted materials and to the proper and full acknowledgement of its source.
- The digital version of the thesis I am supplying is the same version as the final, hard-bound copy submitted in completion of my degree, once any minor corrections have been completed.
- I have exercised reasonable care to ensure that the thesis is original, and does not to the best of my knowledge break any UK law or other Intellectual Property Right, or contain any confidential material.
- I understand that, through the medium of the Internet, files will be available to automated agents, and may be searched and copied by, for example, text mining and plagiarism detection software.

(b) IF I HAVE AGREED (in Section 2 above) TO MAKE MY THESIS PUBLICLY AVAILABLE DIGITALLY, I ALSO DECLARE THAT:

- I grant the University of Warwick and the British Library a licence to make available on the Internet the thesis in digitised format through the Institutional Repository and through the British Library via the EThOS service.
- If my thesis does include any substantial subsidiary material owned by third-party copyright holders, I have sought and obtained permission to include it in any version of my thesis available in digital format and that this permission encompasses the rights that I have granted to the University of Warwick and to the British Library.

**5. LEGAL INFRINGEMENTS**

I understand that neither the University of Warwick nor the British Library have any obligation to take legal action on behalf of myself, or other rights holders, in the event of infringement of intellectual property rights, breach of contract or of any other right, in the thesis.

---

*Please sign this agreement and return it to the Graduate School Office when you submit your thesis.*

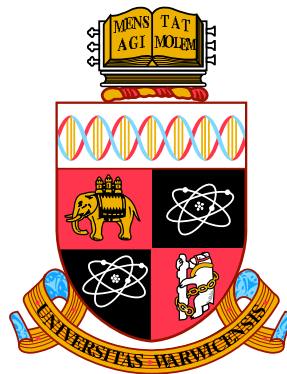
Student's signature: ..... Date: .....

Ras signalling in the fission yeast *Schizosaccharomyces pombe*

By

Michael Edward Bond

A THESIS SUBMITTED TO THE UNIVERSITY OF WARWICK FOR THE  
DEGREE OF  
DOCTOR OF PHILOSOPHY



Warwick Medical School,  
The University of Warwick.

February 2012

## Contents

Declaration of Authorship	xi
Acknowledgments	xii
Abstract	xiii
List of Tables	xiv
List of Figures	xv
Abbreviations	xxv
Chapter 1. General introduction	1
1.1. Cellular signalling	1
1.2. G proteins	2
1.2.1. Heterotrimeric G proteins	4
1.2.1.1. Heterotrimeric G protein activation	4
1.2.1.2. Signalling downstream of heterotrimeric G proteins	6
1.2.1.3. Termination of signalling through heterotrimeric G proteins	7
1.2.1.4. The localisation of heterotrimeric G proteins	7
1.2.2. Monomeric G proteins	8
1.2.2.1. The activation of monomeric GTPases	8
1.2.2.2. Termination of signalling through monomeric GTPases	9
1.2.2.3. The localisation of monomeric GTPases	10
1.3. Ras proteins	10
1.3.1. The discovery and clinical importance of ras	10
1.3.2. Activators of ras	11
1.3.3. The deactivation of ras	13
1.3.4. Signalling downstream of ras	15

1.3.5. Post-translational modification and localisation of ras	16
1.3.5.1. Farnesylation	16
1.3.5.2. Palmitoylation	18
1.3.5.3. Poly-basic domains	19
1.3.5.4. The two-signal hypothesis of plasma membrane association	19
1.3.5.5. Ras protein trafficking	19
1.3.6. Compartmentalised ras signalling	21
1.3.6.1. Signalling from endosomes	21
1.3.6.2. Signalling from the endomembranes	22
1.3.6.3. Signalling from plasma membrane microdomains	23
1.3.7. Ras localisation as a therapeutic target	25
1.4. The <i>Schizosaccharomyces pombe</i> model system	26
1.4.1. Nutrient-sensing in <i>Sz. pombe</i>	27
1.4.2. The <i>Sz. pombe</i> mating response	27
1.4.3. Pheromone-responsive signalling in <i>Sz. pombe</i>	29
1.4.3.1. Cell cycle arrest	29
1.4.3.2. Pheromone-induced morphology changes	30
1.4.3.3. The fusion of mating partners	30
1.4.3.4. Regulation of the cells response to pheromone	31
1.4.4. Regulation of polar cell morphology	32
1.4.4.1. Vegetative cell growth	32
1.4.4.2. Shmoo formation	34
1.4.5. The pathway-specific activation of Ras1	35
1.4.5.1. The differential regulation of Ras1	36
1.4.5.2. Compartmentalised ras signalling in <i>Sz. pombe</i>	36
1.4.6. Heterologous expression of signalling components in <i>Sz. pombe</i>	37
1.5. Aims	39
Chapter 2. Materials and methods	40
2.1. Materials	40

2.1.1.	General laboratory reagents.	40
2.1.2.	Molecular biology reagents.	40
2.1.3.	Gel documentation.	40
2.1.4.	Cell number analysis.	41
2.1.5.	P-factor synthesis.	41
2.1.6.	Growth media.	41
2.1.7.	Bacterial Strains.	44
2.1.8.	<i>Sz. pombe</i> strains.	44
2.1.9.	<i>Sz. pombe</i> genomic integration.	48
2.2.	Methods	49
2.2.1.	Cloning techniques.	49
2.2.2.	Transformation of <i>E. coli</i> .	49
2.2.3.	Transformation of <i>Sz. pombe</i> .	49
2.2.4.	Polymerase chain reaction (PCR)	49
2.2.4.1.	PCR amplification of DNA for cloning.	50
2.2.4.2.	Screening plasmid DNA from bacterial cells using PCR	50
2.2.4.3.	Screening yeast genomic DNA using PCR	50
2.2.5.	DNA sequencing.	50
2.2.6.	Preparation of yeast genomic DNA	50
2.2.7.	$\beta$ -galactosidase assays.	51
2.2.8.	Yeast mating assays.	52
2.2.9.	Fluorescence microscopy.	52
2.2.10.	Image analysis	53
2.2.11.	Western blot analysis.	53
2.2.11.1.	Preparation of yeast whole cell extracts.	53
2.2.11.2.	SDS-PAGE	53
2.2.11.3.	Western blot analysis.	53
2.2.11.4.	Staining with Coomassie Brilliant Blue.	54
2.2.12.	Flow cytometric analysis of cell cycle position.	55
2.2.13.	LIVE/DEAD assay for cell viability.	55

2.2.14. Chromosome instability assay.	56
2.2.15. Analysis of data.	56
Chapter 3. Creation of DNA constructs	57
3.1. Creation pREP3x expression constructs	57
3.1.1. Creation of pREP3x-ras constructs	57
3.1.2. Cloning of pREP3x-GFP-ras	59
3.1.3. Generating <i>1-40gpa1-gfp-ras1</i> fusions in pREP3x	59
3.2. Mutagenesis of <i>ras1</i>	62
3.2.1. Mutating <i>ras1</i> by inverse PCR	62
3.2.2. Mutating <i>ras1</i> using mutagenic cloning oligonucleotides	63
3.3. Creation of constructs for genomic integration	66
3.3.1. Generating constructs for integration of <i>ras</i> ORFs	66
3.3.2. Generating constructs for integration of <i>gfp-ras</i> fusions	67
3.3.3. Generating constructs for integration of <i>1-40gpa1-gfp-ras1</i> fusions	69
3.3.4. Creation of constructs for the integration of <i>tea1-mCherry</i>	71
Chapter 4. Characterisation of Ras1 signalling in <i>Sz. pombe</i>	77
4.1. Introduction	77
4.2. Analysis of Ras1 signalling in <i>Sz. pombe</i>	78
4.2.1. Development of a quantitative assay for mating.	78
4.2.2. Assessing mating efficiency in cells lacking endogenous Sxa2.	80
4.2.3. Constructing a Tea1-mCherry strain to visualise the cell tip.	82
4.2.4. Disruption of <i>ras1</i> .	85
4.2.5. Analysis of vegetative cell morphology using quantitative image analysis.	87
4.2.6. Analysis of pheromone-dependent G <sub>1</sub> arrest	89
4.3. The role of Ras1 signalling in <i>Sz. pombe</i>	91
4.3.1. Ras1 is required to maintain polar cell morphology	91
4.3.2. Ras1 is required for pheromone-responsive signalling	93

4.3.3.	Ras1 is required for pheromone-responsive cell cycle arrest.	96
4.3.4.	Ras1 is required for mating	98
4.4.	Constitutive expression of Ras1	99
4.4.1.	Plasmid-borne Ras1 can rescue pheromone-responsive signalling in $\Delta ras1$ strains.	101
4.4.2.	Constitutive Ras1 expression alters cell morphology and the localisation of the cell tip marker Tea1.	103
4.4.3.	Constitutive Ras1 expression causes the formation of multiple shmoo tips.	104
4.5.	The localisation of Ras1	107
4.5.1.	Constructing a GFP-Ras1 fusion	107
4.5.2.	Ras1 is localised to the plasma membrane	107
4.5.3.	GFP-Ras1 is functional but displays reduced signalling activity	109
4.5.4.	GFP-Ras1 is able to rescue mating when expressed from the <i>ras1</i> locus	114
4.6.	Investigation of Ras1 mutants displaying altered activity	116
4.6.1.	Integration of <i>ras1</i> mutants displaying altered activity	116
4.6.2.	Characterisation of Ras1 <sup>S22N</sup>	118
4.6.2.1.	Integrated Ras1 <sup>S22N</sup> does not rescue cell morphology.	118
4.6.2.2.	Pheromone responsive signalling in cells expressing Ras1 <sup>S22N</sup>	120
4.6.2.3.	pREP3x-Ras1 <sup>S22N</sup> did not support pheromone-dependent signalling.	124
4.6.3.	Characterisation of Ras1 <sup>G17V</sup> and Ras1 <sup>Q66L</sup>	126
4.6.3.1.	Integrated Ras1 <sup>G17V</sup> and Ras1 <sup>Q66L</sup> rescue elongated cell morphology.	126
4.6.3.2.	Ras1 <sup>G17V</sup> and Ras1 <sup>Q66L</sup> cause reduced signalling at high pheromone concentrations in $\beta$ -galactosidase assays	128
4.6.4.	JY1386 ( <i>ras1</i> <sup>Q66L</sup> ) and JY1272 ( <i>ras1</i> <sup>G17V</sup> ) display pheromone- dependent cell death.	132

4.6.5.	Analysis of Ras1 <sup>G17V</sup> and Ras1 <sup>Q66L</sup> activity when expressed from pREP3x	137
4.6.6.	Expression of Ras1 from pREP3x negatively effects cell viability.	139
4.6.7.	Increasing Ras1 activity affects chromosome segregation.	141
4.7.	The localisation of Ras1 mutants with differing activities	143
4.7.1.	Expression of GFP-Ras1 mutant fusions	143
4.7.2.	GFP-Ras1 <sup>Q66L</sup> (JY1495), GFP-Ras1 <sup>G17V</sup> (JY1496) and GFP-Ras1 <sup>S22N</sup> (JY1519) display the same localisation pattern as GFP-Ras1	143
4.7.3.	GFP-Ras1 <sup>Q66L</sup> (JY1495), GFP-Ras1 <sup>G17V</sup> (JY1496) and GFP-Ras1 <sup>S22N</sup> (JY1519) display reduced signalling activity through Scd1-Cdc42	144
4.7.4.	The GFP tag restores signalling at high concentrations of P-factor through Ras1 <sup>Q66L</sup> and Ras1 <sup>G17V</sup>	147
4.7.5.	Cells expressing GFP-Ras1 <sup>S22N</sup> displays little pheromone-responsive signalling	150
4.8.	Summary	153
Chapter 5.	The impact of Ras1 C-terminal modification and localisation on signalling in fission yeast	155
5.1.	Introduction	155
5.2.	Quantifying Ras1 localisation	156
5.2.1.	Comparing the localisation of GFP-Ras1 when expressed from the <i>ras1</i> locus and pREP3x	156
5.2.2.	Wild-type Ras1 displays predominantly plasma membrane localisation	156
5.2.3.	Expression of GFP-Ras1 from pREP3x restores pheromone dependent signalling in $\Delta ras1$ (JY1279) cells	160
5.2.4.	The localisation of Ras1 is altered in mutations which affect nucleotide binding and hydrolysis	162

5.3. Analysing the role of Ras1 C-terminal modification	162
5.3.1. Preventing lipid modification of Ras1 reduces plasma membrane localisation	163
5.3.2. Quantification of GFP-Ras1 <sup>C215S</sup> and GFP-Ras1 <sup>C216S</sup> localisation	164
5.3.3. Integration of Ras1 <sup>C215S</sup> and Ras1 <sup>C216S</sup>	167
5.3.4. Lipid modification of Ras1 is required to maintain elongated cell morphology	168
5.3.5. Cell polarity is not restored by the addition of cAMP in cells expressing Ras1 <sup>C215S</sup> and Ras1 <sup>C216S</sup>	170
5.3.6. The lipid modification of Ras1 is required for pheromone-responsive signalling	172
5.3.6.1. Analysis of pheromone-responsive changes in $\beta$ -galactosidase activity and average cell volume in cells expressing Ras1 <sup>C215S</sup> and Ras1 <sup>C216S</sup>	172
5.3.6.2. Analysis of pheromone-responsive cell elongation in cells expressing Ras1 <sup>C215S</sup> and Ras1 <sup>C216S</sup>	173
5.3.6.3. Analysis of pheromone-dependent cell cycle arrest in cells expressing Ras1 <sup>C215S</sup> and Ras1 <sup>C216S</sup>	176
5.3.7. GFP-Ras1 <sup>C215S</sup> and GFP-Ras1 <sup>C216S</sup> display a similar signaling profile to their non-tagged counterparts	177
5.3.8. Ras1 <sup>C215S</sup> and Ras1 <sup>C216S</sup> display strong pheromone dependent signalling when expressed from pREP3x	180
5.4. Prolonging the activity of Ras1 <sup>C215S</sup> rescues signalling	183
5.4.1. Expression of Ras1 <sup>Q66L, C215S</sup> .	183
5.4.2. The localisation of GFP-Ras1 <sup>C215S</sup> is unaltered by the addition of a Gln66Leu mutation	185
5.4.3. Prolonging the activity of Ras1 <sup>C215S</sup> partially restores elongated cell morphology	189

5.4.4.	Prolonging the activity of Ras1 <sup>C215S</sup> restores pheromone-responsive signalling	190
5.4.5.	GFP-Ras1 <sup>Q66L, C215S</sup> displays reduced signalling compared to Ras1 <sup>Q66L, C215S</sup>	194
5.4.6.	Ras1 <sup>Q66L, C215S</sup> displays a high level of pheromone-dependent signalling when expressed from pREP3x	196
5.5.	Summary	199
Chapter 6.	Targetting Ras1 to the plasma membrane	203
6.1.	Introduction	203
6.2.	Characterisation of Ras1-RitC	204
6.2.1.	Expression of Ras1-RitC	204
6.2.2.	Ras1-RitC is unable to rescue significant mating	204
6.2.3.	Ras1-RitC displays some signalling through Scd1	206
6.2.4.	Ras1-RitC displays reduced pheromone-responsive signaling compared to Ras1	208
6.2.5.	The localisation of Ras1-RitC	212
6.3.	Characterising 1-40Gpa1-GFP-Ras1	214
6.3.1.	Expression of 1-40Gpa1-GFP-Ras1 fusions	217
6.3.2.	1-40Gpa1-GFP-Ras1 fusion proteins display a high degree of plasma membrane localisation	217
6.3.3.	Vector-borne 1-40Gpa1-GFP-Ras1 displays signalling in response to pheromone	220
6.3.4.	Addition of the first 40 amino acids of Gpa1 to GFP-Ras1 <sup>C215S</sup> and GFP-Ras1 <sup>C216S</sup> increases signalling through Scd1	223
6.3.5.	Addition of the first 40 amino acids of Gpa1 to GFP-Ras1 increases pheromone-dependent signalling	228
6.3.5.1.	The analysis of $\beta$ -galactosidase activity and cell volume in cells expressing 1-40Gpa1-GFP-Ras1 fusions	228

6.3.5.2.	The analysis of cell elongation in cells expressing 1-40Gpa1-GFP-Ras1 fusions	231
6.3.5.3.	The analysis of cell cycle arrest in cells expressing 1-40Gpa1-GFP-Ras1 fusions	236
6.3.6.	Expression of 1-40Gpa1-GFP-Ras1, 1-40Gpa1-GFP-Ras1 <sup>C215S</sup> and 1-40Gpa1-GFP-Ras1 <sup>C216S</sup> rescues mating	238
6.4.	Summary	238
Chapter 7.	Functional expression of human ras proteins in fission yeast	242
7.1.	Introduction	242
7.2.	The localisation of human ras proteins in <i>Sz. pombe</i>	244
7.3.	Expression of human ras proteins in <i>Sz. pombe</i>	246
7.4.	The function of human ras proteins in <i>Sz. pombe</i>	248
7.4.1.	H-Ras, N-Ras and K-Ras4B all signal through Scd1	248
7.4.2.	H-Ras, N-Ras and K-Ras4B all propagate signalling in response to pheromone	249
7.4.3.	Addition of GFP to the N-terminus reduces pheromone-responsive signalling through H-Ras, N-Ras and K-Ras4B	255
7.4.4.	H-Ras, N-Ras and K-Ras4B display high levels of pheromone-responsive signalling upon expression from pREP3x	258
7.4.5.	H-Ras, N-Ras and K-Ras4B are only able to support limited mating	258
7.5.	Summary	259
Chapter 8.	Discussion	261
8.1.	Overview	261
8.2.	Quantifying Ras1 function and localisation in <i>Sz. pombe</i>	262
8.2.1.	Developing a quantitative assay for mating	262
8.2.2.	The use of quantitative imaging techniques in <i>Sz. pombe</i>	262
8.3.	Altering the activation and deactivation of Ras1	263
8.4.	The effects of increasing Ras1 signalling	264

8.4.1. Morphological defects and impaired mating upon constitutive expression of Ras1	264
8.4.2. Pheromone-dependent cell death in cells containing oncogenic Ras1 mutants	265
8.4.3. The effect of constitutive Ras1 expression on chromosome segregation	267
8.5. The role of C-terminal Ras1 modification	267
8.5.1. The effects of altering C-terminal modification on Ras1 localisation	268
8.5.2. The functional implications of preventing C-terminal Ras1 modification	269
8.5.3. Prolonging the activity of mislocalised Ras1	270
8.6. Increasing the level of Ras1 at the plasma membrane	271
8.6.1. The limitations of the Ras1-RitC fusion protein	271
8.6.2. The effect of 1-40Gpa1 on Ras1 localisation	272
8.6.3. The effect of 1-40Gpa1 on Ras1 function	272
8.6.4. The limitations of the 1-40Gpa1-GFP-Ras1 fusion	273
8.7. A revised model of Ras1 signalling in <i>Sz. pombe</i>	274
8.8. Human ras function in <i>Sz. pombe</i>	276
8.9. Perspectives and future directions	277
8.10. Conclusions	277
Bibliography	279

## Declaration of Authorship

I hereby declare that the work described in this thesis was conducted by myself under the supervision of Prof. John Davey and Dr. Graham Ladds, with the exception of those instances where the contributions of others have been specifically acknowledged.

None of the information herein has been used in any previous application for a degree.

All sources of information have been specifically acknowledged by means of reference.

Signed: \_\_\_\_\_

Date: \_\_\_\_\_

## Acknowledgments

I would like to first and foremost thank my supervisors Graham Ladds and John Davey for their instruction and help throughout my studies. I am very grateful for all the opportunities they have given me. A special thanks also to Graham for his hard work and support during the writing of this thesis, and throughout the whole of my PhD. I would like to also thank all the people who have been through the lab during my time there for making it such an enjoyable place to work.

Special thanks also goes to Michelle Bradley and Steven Charlton for their supportive and nurturing supervision during my time in industry, their help allowed me to start my scientific career in the best possible way.

Thanks go to all my family and friends, and especially Luci, for their support throughout my PhD and for generally being wicked.

## Abstract

Ras signalling is vital to many cellular processes. Ras proteins mediate a vast array of cellular signalling networks, and are conserved from humans to unicellular eukaryotes. The study of ras signalling in higher eukaryotes presents a number of technical challenges, due to the presence of multiple ras isoforms, regulatory proteins and activators. The fission yeast *Sz. pombe* represents an ideal system for the investigation of ras signalling, as it contains a single, non-essential ras protein (Ras1). In addition, Ras1 is involved in the regulation of a number of downstream pathways.

A number of studies in recent years have highlighted the role of subcellular localisation in ras signalling output. The localisation of Ras1 in *Sz. pombe* has also been described as key in effector selection, with Ras1 at the plasma membrane regulating mating and Ras1 at the endomembranes regulating cell morphology. This thesis describes a series of studies utilising Ras1 mutants and chimeric Ras1 proteins which display differing localisation patterns to determine the role of Ras1 localisation in signalling. The data presented herein support the notion of a revised model for the role of Ras1 localisation in signalling, suggesting that the localisation of Ras1 to the plasma membrane is key to all signalling events downstream of Ras1.

This thesis also describes the characterisation of oncogenic mutants of Ras1, demonstrating the importance of signalling magnitude in functional output. In addition, the importance of Ras1 regulation in cell viability and chromosome stability is also demonstrated. Finally, the functional expression of three human ras isoforms is described, validating the use of *Sz. pombe* as a model system for the heterologous expression of human ras signalling components.

## List of Tables

2.1 $\beta$ -galactosidase reporter and mating assay yeast strains	45
2.2 $\beta$ -galactosidase reporter yeast strains containing integrated GFP tagged ras proteins	46
2.3 Yeast strains used to determine Tea1 localisation	47
3.1 Oligonucleotides for amplification of <i>ras</i> ORFs	58
3.2 Oligonucleotides for mutating <i>ras1</i> by inverse PCR	64
3.3 Oligonucleotides to amplify <i>ras</i> ORFs for integration	66
5.1 Summary of the activity and localisation of Ras1 C-terminal modification mutants	202
6.1 Summary of the activity and localisation of 1-40Gpa1-GFP-Ras1 fusions	241

## List of Figures

1.1	The structural similarities between ras and G $\alpha$ proteins	3
1.2	The activation and deactivation of G proteins	4
1.3	Signalling from G protein-coupled receptors	6
1.4	Homology between members of the ras superfamily	9
1.5	Mitogen signalling through ras	12
1.6	The activation and regulation of human ras	14
1.7	C-terminal modification of ras proteins	17
1.8	The trafficking of human ras proteins	20
1.9	Mating in <i>Sz. pombe</i>	28
1.10	Pheromone-responsive signalling in <i>Sz. pombe</i>	29
1.11	The regulation of cell polarity in <i>Sz. pombe</i>	35
1.12	Compartmentalised Ras1 signalling in <i>Sz. pombe</i> .	37
3.1	Cloning of <i>ras</i> ORFs into pREP3x	58
3.2	Cloning of pREP3x-GFP-ras	60
3.3	Cloning of pREP3x-1-40Gpa1-GFP	61
3.4	Cloning of pREP3x-1-40Gpa1-GFP-Ras1	62
3.5	Mutating <i>ras1</i> using inverse PCR	64
3.6	Mutating the 215 <sup>th</sup> and 216 <sup>th</sup> codons of <i>ras1</i> using mutagenic cloning oligonucleotides	65
3.7	Generating constructs to integrate <i>ras</i> ORFs	67
3.8	Creating JD1847-GFP	68
3.9	Cloning of <i>gfp-ras</i> integration constructs	69

3.10 Cloning JD1847-1-40Gpa1-GFP	70
3.11 Cloning of <i>1-40gpa1-gfp-ras</i> integration constructs	71
3.12 Cloning of pKS-Tea1-3' Tea1 UTR	72
3.13 Inverse PCR of pKS-Tea1-3' Tea1 UTR	74
3.14 Cloning of JD3542-Ura4	75
3.15 Generating a <i>tea1-mCherry</i> integration construct	76
4.1 Isolation of spores using heat treatment	79
4.2 Restoration of mating in strains lacking Sxa2	81
4.3 Creation of a direct, in-frame Tea1-mCherry fusion at the <i>tea1</i> locus	83
4.4 Detection of Tea1-mCherry using fluorescence microscopy and immunoblotting	84
4.5 Disruption of Ras1	85
4.6 Confirming the disruption of <i>ras1</i> by immunoblotting	86
4.7 The morphology in cells transformed with vector alone and pREP3x-GFP	87
4.8 Analysis of cell morphology using Quimp image analysis software	88
4.9 Comparison of cell morphology parameters obtained using Quimp image analysis software	90
4.10 Analysis of pheromone-dependent G <sub>1</sub> arrest over time	91
4.11 The localisation of Tea1-mCherry in cells lacking Ras1	92
4.12 Pheromone-responsive transcription and cell volume changes in wild-type cells and cells lacking Ras1	94
4.13 Analysis of shmoo formation in JY544 ( <i>ras1</i> <sup>+</sup> ) and JY1279 ( $\Delta$ <i>ras1</i> ) using quantitative imaging	95

4.14 Pheromone-responsive cell cycle arrest in JY544 ( <i>ras1</i> <sup>+</sup> ) and JY1279 ( $\Delta$ <i>ras1</i> )	97
4.15 Loss of Ras1 prevents mating in <i>Sz. pombe</i>	99
4.16 Determining the expression of Ras1 from pREP3x using immunoblotting	100
4.17 Pheromone-responsive signalling in cells expressing Ras1 from pREP3x	102
4.18 Expression of Ras1 from pREP3x does not restore mating in $\Delta$ <i>ras1</i> cells	103
4.19 Expression of Ras1 from pREP3x disrupts polar cell morphology	105
4.20 Expression of Ras1 from pREP3x in $\Delta$ <i>ras1</i> cells causes the formation of multiple shmoo tips	106
4.21 Integration of GFP-Ras1	108
4.22 The localisation of GFP-Ras1	109
4.23 The morphology of cells expressing GFP-Ras1 from the endogenous <i>ras1</i> locus.	110
4.24 Pheromone-dependent changes in transcription and cell volume in cells expressing GFP-Ras1	111
4.25 Analysis of shmoo formation in cells expressing GFP-Ras1 using quantitative imaging	112
4.26 Pheromone-responsive changes in cell cycle position in cells expressing GFP-Ras1	113
4.27 Mating efficiency in cells expressing GFP-Ras1	115
4.28 Integration of <i>ras1</i> <sup>Q66L</sup> , <i>ras1</i> <sup>G17V</sup> and <i>ras1</i> <sup>S22N</sup> in the <i>sxa2</i> > <i>lacZ</i> reporter strain	117
4.29 Integration of <i>ras1</i> <sup>Q66L</sup> , <i>ras1</i> <sup>G17V</sup> and <i>ras1</i> <sup>S22N</sup> in the <i>Tea1-mCherry</i> , <i>sxa2</i> > <i>lacZ</i> strain	118

4.30	The morphology of cells expressing <i>ras1</i> <sup>S22N</sup>	119
4.31	Pheromone-responsive transcription and changes in cell volume in cells expressing Ras1 <sup>S22N</sup>	121
4.32	Analysis of shmoo formation in cells expressing Ras1 <sup>S22N</sup> using quantitative imaging	122
4.33	Pheromone-responsive changes in cell cycle position in cells expressing Ras1 <sup>S22N</sup>	123
4.34	Pheromone-responsive changes in transcription and cell size in cells expressing Ras1 <sup>S22N</sup> from pREP3x	125
4.35	Cell morphology in in cells expressing Ras1 <sup>G17V</sup> and Ras1 <sup>Q66L</sup>	127
4.36	Pheromone-responsive transcription and cell volume change in cells expressing Ras1 <sup>G17V</sup> and Ras1 <sup>Q66L</sup>	130
4.37	Pheromone-responsive changes in cell length in cells expressing Ras1 <sup>G17V</sup> and Ras1 <sup>Q66L</sup>	131
4.38	Pheromone-responsive changes in cell cycle position in cells expressing Ras1 <sup>G17V</sup> and Ras1 <sup>Q66L</sup>	133
4.39	JY1386 ( <i>ras1</i> <sup>Q66L</sup> ) and JY1272 ( <i>ras1</i> <sup>G17V</sup> ) display pheromone-dependent cell death	135
4.40	Analysis of pheromone-dependent cell death in JY1389 ( <i>ras1</i> <sup>Q66L</sup> ) over time	136
4.41	Pheromone-responsive changes in transcription and cell morphology in cells expressing GTPase deficient Ras1 mutants from pREP3x	138
4.42	Constitutive expression of Ras1 and GTPase deficient Ras1 mutants negatively impacts upon cell viability	140
4.43	Increased Ras1 activity causes an increase in chromosome instability	142

4.44	Expression of GFP-Ras1 <sup>Q66L</sup> (JY1495), GFP-Ras1 <sup>G17V</sup> (JY1496) and GFP-Ras1 <sup>S22N</sup> (JY1519)	144
4.45	The localisation of GFP-Ras1 <sup>Q66L</sup> , GFP-Ras1 <sup>G17V</sup> and GFP-Ras1 <sup>S22N</sup>	145
4.46	Analysis of the morphology of cells expressing GFP-Ras1 <sup>Q66L</sup> , GFP-Ras1 <sup>G17V</sup> and GFP-Ras1 <sup>S22N</sup>	146
4.47	Pheromone-dependent changes in transcription and cell volume in cells expressing GFP-Ras1 <sup>Q66L</sup> and GFP-Ras1 <sup>G17V</sup>	148
4.48	Analysing shmoo formation in cells expressing GFP-Ras1 <sup>Q66L</sup> (JY1495) and GFP-Ras1 <sup>G17V</sup> (JY1496) using quantitative image analysis	149
4.49	Pheromone-dependent changes in transcription and cell volume in cells expressing GFP-Ras1 <sup>S22N</sup> (JY1519)	151
4.50	Pheromone-dependent elongation in cells expressing GFP-Ras1 <sup>S22N</sup> (JY1519)	152
5.1	Comparing the localisation of GFP-Ras1 when expressed from the <i>ras1</i> locus and pREP3x	157
5.2	Quantifying the localisation of GFP-Ras1 using Quimp software	158
5.3	Pheromone-dependent changes in transcription and cell volume in cells expressing GFP-Ras1 from pREP3x	159
5.4	Analysing the localisation of GFP-Ras1 <sup>Q66L</sup> , GFP-Ras1 <sup>G17V</sup> and GFP-Ras1 <sup>S22N</sup> using Quimp software	161
5.5	Expression of GFP-Ras1 <sup>C215S</sup> (JY1522) and GFP-Ras1 <sup>C216S</sup> (JY1494)	164
5.6	The localisation of GFP-Ras1 <sup>C215S</sup> and GFP-Ras1 <sup>C216S</sup>	165
5.7	Analysing the localisation of GFP-Ras1 <sup>C215S</sup> and GFP-Ras1 <sup>C216S</sup> using Quimp software	166

5.8	Expression of Ras1 <sup>C215S</sup> (JY1378) and Ras1 <sup>C216S</sup> (JY1380) in the $\beta$ -galactosidase reporter strain	167
5.9	Expression of Ras1 <sup>C215S</sup> (JY1505) and Ras1 <sup>C216S</sup> (JY1506) in the Tea1-mCherry strain	168
5.10	Analysis of the morphology of cells expressing Ras1 <sup>C215S</sup> and Ras1 <sup>C216S</sup>	169
5.11	Polar cell morphology in <i>ras1</i> <sup>C215S</sup> (JY1378) and <i>ras1</i> <sup>C216S</sup> (JY1380) cells is not rescued by exogenous cAMP	171
5.12	Pheromone-dependent changes in transcription and cell volume in cells expressing Ras1 <sup>C215S</sup> and Ras1 <sup>C216S</sup>	174
5.13	Pheromone-dependent cell elongation in cells expressing Ras1 <sup>C215S</sup> and Ras1 <sup>C216S</sup>	175
5.14	Pheromone-responsive changes in cell cycle position in cells expressing Ras1 <sup>C215S</sup> and Ras1 <sup>C216S</sup>	176
5.15	Analysis of the morphology of cells expressing GFP-Ras1 <sup>C215S</sup> and GFP-Ras1 <sup>C216S</sup>	179
5.16	Pheromone-dependent changes in transcription on cell volume in cells expressing GFP-Ras1 <sup>C215S</sup> and GFP-Ras1 <sup>C216S</sup>	180
5.17	Pheromone-dependent changes in transcription on cell volume in cells expressing Ras1 <sup>C215S</sup> and Ras1 <sup>C216S</sup> from pREP3x	182
5.18	Expression of Ras1 <sup>Q66L, C215S</sup> in the $\beta$ -galactosidase reporter strain	183
5.19	Expression of Ras1 <sup>Q66L, C215S</sup> in the Tea1-mCherry strain	184
5.20	Expression of GFP-Ras1 <sup>Q66L, C215S</sup>	185
5.21	The localisation of GFP-Ras1 <sup>Q66L, C215S</sup>	186
5.22	Analysing the localisation of GFP-Ras1 <sup>Q66L, C215S</sup> using Quimp software	187

5.23	Analysis of the morphology of cells expressing Ras1 <sup>Q66L, C215S</sup>	188
5.24	Pheromone-dependent changes in transcription on cell volume in cells expressing Ras1 <sup>Q66L, C215S</sup>	191
5.25	Pheromone-dependent cell elongation in cells expressing Ras1 <sup>Q66L, C215S</sup>	192
5.26	Pheromone-responsive changes in cell cycle position in cells expressing Ras1 <sup>Q66L, C215S</sup>	193
5.27	Analysis of the morphology of cells expressing GFP-Ras1 <sup>Q66L, C215S</sup>	195
5.28	Pheromone-dependent changes in transcription on cell volume in cells expressing GFP-Ras1 <sup>Q66L, C215S</sup>	197
5.29	Pheromone-dependent changes in transcription on cell volume in cells expressing Ras1 <sup>Q66L, C215S</sup> from pREP3x	198
6.1	The homology between <i>Sz. pombe</i> Ras1 and human Rit	204
6.2	Integration of Ras1-RitC	205
6.3	Mating efficiency in cells expressing Ras1-RitC	206
6.4	The morphology of cells expressing Ras1-RitC from the endogenous <i>ras1</i> locus	207
6.5	Pheromone-dependent changes in transcription and cell volume in cells expressing Ras1-RitC	209
6.6	Analysis of shmoo formation in cells expressing Ras1-RitC using quantitative imaging	210
6.7	Pheromone-responsive changes in cell cycle position in cells expressing Ras1-RitC	211
6.8	Quantifying the localisation of GFP-Ras1-RitC using Quimp software	213

6.9	Integration of 1-40Gpa1-GFP-Ras1 in the $\beta$ -galactosidase reporter stain	215
6.10	Integration of 1-40Gpa1-GFP-Ras1 in the Tea1-mCherry strain	216
6.11	The localisation of 1-40Gpa1-GFP-Ras1 fusions	218
6.12	Quantifying the localisation of 1-40Gpa1-GFP-Ras1 fusions using Quimp software	219
6.13	Pheromone-dependent changes in transcription and cell volume in cells expressing 1-40Gpa1-GFP-Ras1 and 1-40Gpa1-GFP-Ras1 fusions with C-terminal modification defects from pREP3x	221
6.14	Pheromone-dependent changes in transcription and cell volume in cells expressing 1-40Gpa1-GFP-Ras1 and 1-40Gpa1-GFP-Ras1 fusions with altered nucleotide binding and hydrolysis from pREP3x	222
6.15	The morphology of cells expressing 1-40Gpa1-GFP-Ras1 fusions from the endogenous <i>ras1</i> locus	224
6.16	Quantification of the morphology of cells expressing 1-40Gpa1-GFP-Ras1 fusions from the endogenous <i>ras1</i> locus	225
6.17	Analysis of Tea1-mCherry localisation in cells expressing 1-40Gpa1-GFP-Ras1 fusions	227
6.18	Pheromone-dependent changes in transcription and cell volume in cells expressing 1-40Gpa1-GFP-Ras1 and 1-40Gpa1-GFP-Ras1 fusions with C-terminal modification defects	229
6.19	Pheromone-dependent changes in transcription and cell volume in cells expressing 1-40Gpa1-GFP-Ras1 and 1-	

40Gpa1-GFP-Ras1 fusions with altered nucleotide binding and hydrolysis	230
6.20 The morphology of cells expressing 1-40Gpa1-GFP-Ras1 fusions in the absence and presence of pheromone	232
6.21 Analysis of shmoo formation in cells expressing 1-40Gpa1-GFP-Ras1 fusions using quantitative imaging	233
6.22 Flow cytometric analysis of cell cycle position in cells expressing 1-40Gpa1-GFP-Ras1 fusions	234
6.23 Pheromone-responsive changes in cell cycle position in cells expressing 1-40Gpa1-GFP-Ras1 fusions	235
6.24 Quantitative analysis of mating efficiency in cells expressing 1-40Gpa1-GFP-Ras1, 1-40Gpa1-GFP-Ras1 <sup>C215S</sup> and 1-40Gpa1-GFP-Ras1 <sup>C216S</sup>	237
7.1 The homology between human ras proteins and <i>Sz. pombe</i> Ras1	243
7.2 Quantifying the localisation of GFP-human ras fusions using Quimp software	245
7.3 Integration of human H-Ras, N-Ras and K-Ras4B at the <i>ras1</i> locus of the $\beta$ -galactosidase reporter strain	246
7.4 Integration of human H-Ras, N-Ras and K-Ras4B at the <i>ras1</i> locus of the Tea1-mCherry strain	247
7.5 Integration of GFP-H-Ras, GFP-N-Ras and GFP-K-Ras4B at the <i>ras1</i> locus	248
7.6 Analysis of the morphology of cells expressing human H-Ras, N-Ras and K-Ras4B	250
7.7 Pheromone-dependent changes in transcription and cell volume in cells expressing human ras isoforms	252

7.8	Pheromone-dependent cell elongation in cells expressing human ras isoforms from the <i>ras1</i> locus	253
7.9	Pheromone-responsive changes in cell cycle position in cells expressing human ras isoforms from the <i>ras1</i> locus	254
7.10	Pheromone-dependent changes in transcription and cell volume in cells expressing GFP tagged human ras isoforms	256
7.11	Pheromone-dependent changes in transcription and cell volume in cells expressing human ras isoforms from pREP3x	257
7.12	Mating in cells expressing human H-Ras, N-Ras and K-Ras4B	259
8.1	The interaction between Ras1 signalling and cell division	268
8.2	The directed transport of palmitoylated ras	275

## Abbreviations

A	Adenine
a.a.	Amino Acid
APC	anaphase promoting complex
APT	acyl protein thioesterase
bp	base pair
cAMP	cyclic adenosine 3,5-monophosphate
CDC	cell-division cycle
CDK	cyclin-dependent kinase
cDNA	complementary deoxyribonucleic acid
cfu	colony forming unit
CRD	cysteine-rich domain
CRF	corticotrophin releasing factor
DAG	diacylglycerol
DIC	Differential interference contrast
dATP	deoxyadenosine triphosphate
dCTP	deoxycytidine triphosphate
dGTP	deoxyguanosine triphosphate
DHHC	Asp-His-His-Cys
DMM	defined minimal media
DNA	deoxyribonucleic acid
dNTP	deoxynucleotide triphosphate
DYRK	dual-specificity Yak-related kinase
dTTP	deoxythymidine triphosphate
<i>E.coli</i>	<i>Escherichia coli</i>

ECL	enhanced chemiluminescence
EDTA	ethylenediaminetetraacetic acid
EGF	epidermal growth factor
EM-CCD	electron-multiplying charge-coupled device
ER	endoplasmic reticulum
FOA	5' fluoro-orotic acid
FRET	fluorescence resonance energy transfer
FT	farnesyltransferase
FTI	farnesyltransferase inhibitor
GAP	GTPase activating protein
GDP	guanosine diphosphate
GEF	guanine nucleotide exchange factor
GFP	green fluorescent protein
GPCR	G protein-coupled receptor
G protein	guanine nucleotide-binding protein
GRK	G protein-coupled receptor kinase
GTP	guanosine triphosphate
h	hours
HMG	high mobility group
HPLC	high-performance liquid chromatography
HRP	horse-radish peroxidase
HVR	hypervariable region
IP <sub>3</sub>	inositol triphosphate
kb	kilo base
kDa	kilo Dalton
L	leucine
M	minus
MAP	mitogen activated protein
MAPK	mitogen activated protein kinase

MAPKK	mitogen activated protein kinase kinase
MAPKKK	mitogen activated protein kinase kinase kinase
mCherry	monomeric cherry
MCS	multi-cloning site
MEK	MAP kinase or ERK kinase
min	minutes
MSV	murine sarcoma virus
NETO	new end take off
NGF	nerve growth factor
OD	optical density
ONPG	<i>o</i> -nitrophenyl- $\beta$ -D-galactopyranoside
ORF	open reading frame
P	plus
PAGE	polyacrylamide gel electrophoresis
PAK	p21-activated kinase
PAT	protein acyl thioesterase
PBS	phosphate-buffered saline
PCR	polymerase chain reaction
PKA	protein kinase A
PKC	protein kinase C
PLC	phospholipase C
PM	plasma membrane
PVDF	polyvinylidene difluoride
RA	ras association
RBD	ras-binding domain
RGS	regulator of G protein signalling
RNA	ribonucleic acid
rpm	revolutions per minute

RTK	receptor tyrosine kinase
s	seconds
<i>S. cerevisiae</i>	<i>Saccharomyces cerevisiae</i>
SDS	sodium dodecyl sulphate
SEM	standard error of the mean
<i>Sz. pombe</i>	<i>Schizosaccharomyces pombe</i>
TAE	Tris acetic acid EDTA
TBS	Tris-buffered saline
TCR	T-cell receptor
TR	T rich
Tris	tris (hydroxymethy) aminomethane
TE	Tris EDTA
TEN	Tris EDTA NaCl
U	uracil
UTR	untranslated region
v/v	volume for volume
w/o	without
w/v	weight for volume
YE	yeast extract

## CHAPTER 1

### General introduction

#### 1.1. Cellular signalling

The ability of organisms to detect and respond to environmental changes is universally conserved. In addition, multicellular organisms require communication between cells to allow them to behave as a coordinated whole. To perform this function, an array of mechanisms have evolved to allow the detection of external cues and the control of cellular behavior in response to these cues.

All signalling pathways require the interpretation of an exogenous signal into an appropriate intracellular response. In most instances, the signal is unable to cross the cell membrane, requiring a means of transducing the signal from the exterior to the interior of the cell. Consequently, the majority of receptors for external signalling molecules, or ligands, are proteins which span the plasma membrane (trans-membrane proteins).

Upon transmission of a signal into the cell by a specific receptor, a cascade of interactions and reactions are employed to generate the required cellular response. Such signalling cascades do not function in isolation. Communication between pathways, or cross-talk, is commonplace, allowing the integration of multiple signals into complex cellular behaviors. In addition, multiple pathways often share common components despite regulating distinct cellular outcomes. Therefore, the study of individual signalling events in complex systems, such as higher eukaryotes, presents a number of technical challenges.

Many of the mechanisms employed by higher eukaryotes to transduce signals are conserved in simpler unicellular eukaryotes. Yeast have long been used as a model eukaryotic system due to their simplicity and genetic tractability.

Furthermore, they share many signalling components with higher eukaryotic cells. This thesis focusses on the use of the fission yeast *Schizosaccharomyces pombe* to study a highly conserved component of signalling, the monomeric G protein ras.

## 1.2. G proteins

Guanine nucleotide-binding proteins, or G proteins, are a highly conserved signalling component. They are part of a larger family of proteins which bind nucleotide triphosphates, such as the ATP-binding proteins, that utilise a conserved phosphate-binding loop (P-loop) (Saraste *et al.* 1990). P-loop proteins are divided into two families, the translation factor (TRAFAC) and the signal recognition particle, MinD, and BioD (SIMIBI) families, of which the TRAFAC group contains the majority of G proteins responsible for signal transduction (Leipe *et al.* 2002).

G proteins themselves can be broadly categorised into two classes, the monomeric G proteins and the heterotrimeric G proteins. Monomeric G proteins are grouped into the Ras superfamily, which is divided into five sub-families, the Ras, Rab, Rho, Ran and Arf families, on the basis of similarities in sequence and function (Wennerberg *et al.* 2005). The second broad category of G proteins, the heterotrimeric G proteins, exist as a dissociable  $G\alpha$ ,  $G\beta$  and  $G\gamma$  complex, of which the  $G\alpha$  subunit is the nucleotide-binding component (Hepler and Gilman 1992). All G proteins, either monomeric or heterotrimeric, bind the guanine nucleotides GDP and GTP with similar affinities. When inactive, G proteins are bound to a single molecule of GDP. Activation occurs through the exchange of GDP for GTP, and inactivation through the hydrolysis of GTP, returning the G protein to an inactive GDP bound state. Activation results in the stabilisation of the G protein effector binding site due to interactions between the  $\gamma$ -phosphate of the GTP and the conserved switch I and switch II regions of the protein (Sprang 1997). These functions are conferred

by a  $\sim 20$  kDa G domain, conserved across all G proteins (Figure 1.1) (Vetter and Wittinghofer 2001; Lambright *et al.* 1994). GTP binding results in a rearrangement of the conserved switch regions of the G protein. Hydrogen bonding between a DXXG motif of switch II, a conserved threonine residue of switch I and the  $\gamma$ -phosphate of GTP brings the switch region in closer proximity to the nucleotide binding pocket. The binding of GTP also requires the presence of a  $Mg^{2+}$  cofactor, which interacts with the same conserved threonine residue, and is involved in coordinating the  $\beta$ - and  $\gamma$ -phosphates. In ras, a conserved tyrosine residue in switch I is also involved in the binding of GTP (Lambright *et al.* 1994; Sprang 1997). In heterotrimeric G proteins these processes occur on the  $G\alpha$  subunit (Figure 1.1).

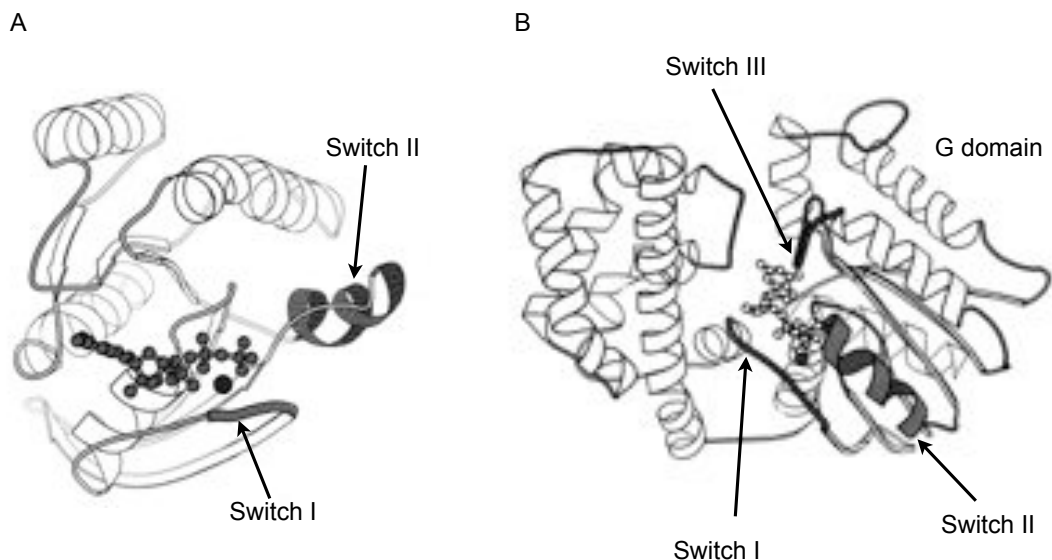


**Figure 1.1. The structural similarities between ras and  $G\alpha$  proteins**

The ribbon diagrams represent the structure of ras (A) and a  $G\alpha$  protein ( $G_{\alpha i}$ ) (B). Both proteins are depicted in complex with a non-hydrolysable GTP analog, indicated in the form of a ball and stick model. The solid sphere represents the  $Mg^{2+}$  cofactor of the two proteins. The switch regions are indicated in grey, and the G domain of the larger  $G_{\alpha i}$  protein is highlighted. Ras and the G domain of  $G_{\alpha i}$  display strong structural similarities, particularly with regard to the highly conserved switch regions. Figure modified from Sprang 1997.

G proteins have a certain level of spontaneous activation and intrinsic GTP hydrolysis activity. However, both nucleotide exchange and GTP hydrolysis are enhanced by two groups of regulatory proteins. Activation, through the exchange of GDP for GTP, is regulated and enhanced by the guanine nucleotide exchange factors (GEFs). GTP hydrolysis is regulated by a second class of proteins, the GTPase activating proteins (GAPs) (Boguski and McCormick 1993) (Figure 1.2).

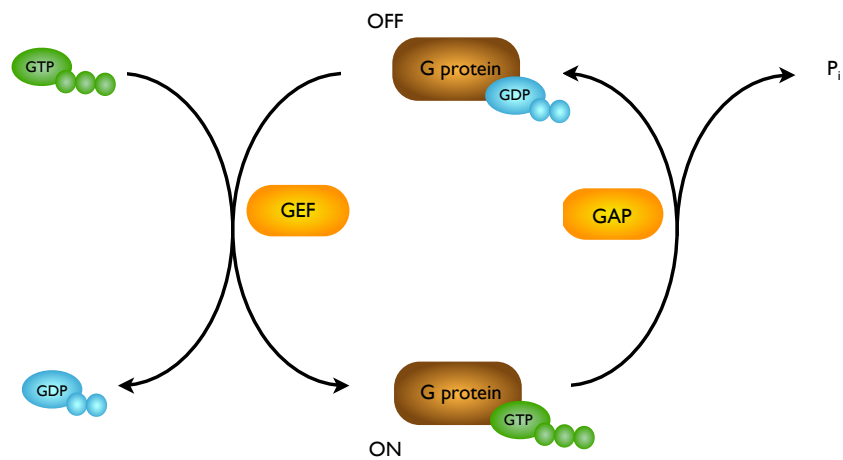


**Figure 1.2. The activation and deactivation of G proteins**

The activation and deactivation of G proteins follows the same canonical cycle. G proteins are switched from inactive to active through the exchange of GDP for GTP and are rendered inactive again by subsequent hydrolysis of GTP to GDP. The activities of regulatory guanine nucleotide exchange factors (GEFs), which include GPCRs in the case of heterotrimeric G proteins, and GTPase-activating proteins (GAPs), including RGS proteins, are also indicated.

### 1.2.1. Heterotrimeric G proteins.

1.2.1.1. *Heterotrimeric G protein activation.* Heterotrimeric G proteins act directly downstream of a specific class of receptors, the G protein-coupled receptors or GPCRs (Gilman 1987). GPCRs are one of the largest protein super-families, with greater than 800 coding regions in the human genome (Venter *et al.* 2001; Fredriksson *et al.* 2003). GPCRs are activated by a vast array of extracellular stimuli, including peptides, lipids, nucleotides, ions, odorants and photons. All GPCRs share a distinctive structure, consisting of seven  $\alpha$ -helical

trans-membrane domains linked by intracellular and extracellular loop regions, in addition to an N-terminal extracellular domain and C-terminal intracellular tail (Baldwin 1993).

GPCRs are grouped into six families based upon structural similarities, function and ligand-binding. The three largest families are 1/A, which are the rhodopsin related receptors, 2/B, which are the Glutamate related receptors and 3/C, known as the 'venus fly trap' receptors due to their large N-terminal region which forms two lobes that close around the ligand. The final three classes are the Adhesion (4/E), Frizzled/TAS2 (5/F), and fungal mating pheromone receptor (4/D) families (Josefsson 1999; Fredriksson *et al.* 2003).

Upon ligand-binding, the GPCR undergoes conformational changes, involving in particular the 3<sup>rd</sup> and 6<sup>th</sup> transmembrane domains (Ballesteros *et al.* 2001; Pierce *et al.* 2002), allowing the receptor to promote nucleotide exchange on the G $\alpha$  subunit of the G protein heterotrimer. The GPCR therefore assumes the role of a GEF protein in the activation of G $\alpha$  proteins. Following nucleotide exchange, the G $\alpha$  subunit and the G $\beta\gamma$  dimer dissociate to allow the initiation of downstream signalling events (Figure 1.3) (Lee *et al.* 1992).

GPCRs are not the only GEFs and upstream activators which act upon heterotrimeric G proteins. A number of non-receptor GEFs and activators have now been identified, including GAP-43, NG-GPA,  $\beta$ -APP, presenilin I, AGS1-8, Rhes, PBP/RKIP, and Ric-8. Like GPCRs, each have differing functional specificities. However, most non-receptor GEFs favor the activation of the G $\alpha_{i/o}$  family (reviewed in Sato *et al.* 2006). The AGS (activators of G protein signalling) family are of particular interest, as AGS1 is itself a monomeric G protein of the Ras superfamily. AGS1 is the only true GEF of the AGS family. Rhes (Ras homolog enriched in the striatum of the forebrain) is also a Ras superfamily member, with a similar function and 60% sequence identity to AGS1. AGS2-8 are quite different, and act independently of nucleotide exchange to promote G $\beta\gamma$  dissociation and signalling (Blumer *et al.* 2005).

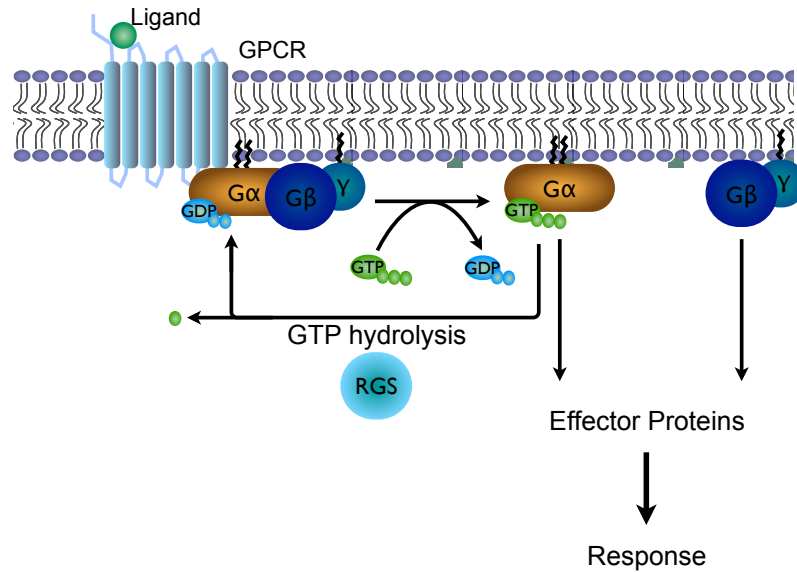


**Figure 1.3. Signalling from G protein-coupled receptors**

Signalling is initiated by the binding of a ligand to the GPCR. Conformational changes in the receptor then promote the exchange of GDP for GTP on the  $G\alpha$  subunit. The  $G\alpha$  and the  $G\beta\gamma$  then dissociate, allowing both to interact with effector proteins and initiate downstream signalling events. Signalling is terminated by GTP hydrolysis on the  $G\alpha$  subunit, catalysed by RGS proteins, resulting in reassociation of the G protein heterotrimer.

1.2.1.2. *Signalling downstream of heterotrimeric G proteins.* G protein heterotrimers are generally classified on the basis of their  $G\alpha$  subunit (Neves *et al.* 2002), however both the  $G\alpha$  subunit and the  $G\beta\gamma$  dimer are now known to initiate downstream signalling (Clapham and Neer 1997). The classification of  $G\alpha$  subunits is largely based upon the interacting partners of the protein, although  $G\alpha$  families do have overlapping functions. There are four main families of  $G\alpha$  protein, designated  $G\alpha_{i/o}$ ,  $G\alpha_{q/11}$ ,  $G\alpha_s$  and  $G\alpha_{12/13}$ . The  $G\alpha_{i/o}$  family contains the most widely expressed group of  $G\alpha$  proteins ( $G\alpha_i$ -type), which are responsible for the inhibition of adenylate cyclase. The  $G\alpha_{q/11}$  family are largely responsible for the mobilisation of intracellular calcium and regulation of protein kinase C (PKC). The  $G\alpha_s$  family act to stimulate the activity of adenylate cyclase. Finally,  $G\alpha_{12/13}$  family members are responsible for activating a number of effectors including phospholipase D (reviewed in Wettschureck and Offermanns 2005).

G $\beta\gamma$  subunits also activate a host of downstream effectors. These include K<sup>+</sup> channels, Ca<sup>2+</sup> channels, adenylate cyclase, mitogen activated protein kinases (MAPKs), phospholipases, phosphoinositide-3-kinases and G protein-coupled receptor kinases (GRKs) (reviewed in Clapham and Neer 1997).

1.2.1.3. *Termination of signalling through heterotrimeric G proteins.* The G $\alpha$  subunit of heterotrimeric G proteins contains two catalytic residues required for GTP hydrolysis. A glutamate on the switch II region is required for the orientation of the water molecule, allowing the transfer of the  $\gamma$ -phosphate from the GTP to the water. The second key residue is an arginine on the switch I region, which acts to stabilise the transition state of GTP hydrolysis (Sprang 1997).

G $\alpha$  subunits contain all the required catalytic residues to perform the GTPase function required for the termination of signalling. The intrinsic GTPase rate can be enhanced by a class of GAP proteins known as the regulators of G protein signalling (RGS) proteins (Figure 1.3). RGS proteins act allosterically to stabilise the transition state, increasing the rate of GTP hydrolysis by at least two orders of magnitude (Ross and Wilkie 2000).

1.2.1.4. *The localisation of heterotrimeric G proteins.* Heterotrimeric G proteins must target to the plasma membrane to allow signal transduction. All G $\beta\gamma$  dimers are modified with a hydrophobic prenyl group at the C-terminus of the G $\gamma$  subunit to promote membrane association. Prenylation occurs at a consensus CAAX (where A is any aliphatic residue and X is any amino acid) motif (Evanko *et al.* 2000). In addition, the N-terminus of most G $\alpha$  subunits is modified with a myristoyl and palmitoyl group. Myristoylation occurs at a consensus MG<sup>2</sup>XXXS<sup>6</sup> motif (Resh 1999). The heterotrimer is then assembled on the cytosolic face of the endoplasmic reticulum prior to transport to the plasma membrane (Marrari *et al.* 2007).

### 1.2.2. Monomeric G proteins.

The Ras superfamily contains five specific groups of structurally related but functionally distinct signalling proteins. The Ras (Rat sarcoma) family were the first proteins of the Ras superfamily to be described, due in no small part to their central role in oncogenesis. Ras proteins are now known to be involved in a vast array of signalling pathways, controlling processes including cell proliferation, cell death, differentiation and motility (Malumbres and Barbacid 2003). The Rho (Ras homologous) family are also involved in the transduction of signals in response to extracellular stimuli, regulating cytoskeletal elements, cell cycle progression and transcription. The Rab (Ras-like proteins in brain) and Arf (ADP-ribosylation factor) families are both involved in vesicular transport, whereas the Ran (Ras-like nuclear) family regulate the transport of proteins and RNA between the cytoplasm and nucleus (reviewed in Wennerberg *et al.* 2005). There is a high degree of conservation between Ras superfamily members. This is most apparent at the phosphate binding region (P region), which contains the conserved GXXXXGK(S/T) motif, and G region, which links the binding of the  $\gamma$ -phosphate and  $Mg^{2+}$  and contains the conserved DXXG motif (Figure 1.4) (Sprang 1997).

1.2.2.1. *The activation of monomeric GTPases.* All monomeric GTPases are activated by GEF proteins. All GEFs function to reduce the affinity of the G protein for guanine nucleotides by altering the phosphate binding site. As a consequence GDP is released and replaced by the more cellularly abundant GTP. GEFs are largely regulated by protein-protein interactions, protein-lipid interactions, the binding of second messengers and post-translational modification. These processes result in the activation of GEFs by three separate mechanisms, either through the translocation of GEFs to their site of action, the release of a regulatory domain from the G protein binding site or the induction of conformational changes in the active site of the protein (Bos *et al.* 2007).

```

1                P region                50
Ras  M-----TEYKLVVVGAGGVGKSALTIQLIQNHFVDEYDPTI
Rho  MTAAQAAGEEAPPGVRSVKVIVLVDGCGGKTSLLMVFADGAFPESEYIPTV
Cdc42 M-----QTIKCVVVGDAVGGKTCLLISYFTNKFPESEYIPTV
Rab  MLEE.DME-----VAIKMIVVVGNCIVGKSSMLQRYCKGIFTKDYKRTI
Ran  MAAQGEPEQ-----VQFKLVVVGDCGIGKTTFVKRHLTGFEFKKYVATL
Arf  MG-----NIFEKLF--KSLLGKMKMRLLLS--LDTAGKTI

51                G region                100
Ras  -EDSYRKQVVIDGFTCLLDLIDTAGOEYYSAMRDQVMRTGEGFLQVFAIN
Rho  -FERVMVNLQVKGKIPVHLLHWDTAGODDYDRLRPLFPDASVLLCCFDVT
Cdc42 -FDNYAVTVMIGGEPYTLGLFDTAGOEDYDRLRPLSPQTDVFLVCFQSVV
Rab  GVDFLERQIQVNDGDDVRLMLWDTAGOEFDALTKAYYRGAQACVLVFSIT
Ran  GVEVHPLVPHNTRGFIKFNVDWDTAGOEKFGGLRDGYVIQAQCALIMFDVT
Arf  ---LVKIKL---GETVP-AV-PIVG---F-CVETVEYKNNT--FAVVDVG

101                150
Ras  NTKSFDI-HQYREQIKRVKSDDDVPMVLVGNKCDL-AARTVESROAQDL
Rho  SPNSFDNIFNRWYPEVNH--CKKVPIIVGCKIDLKDKSLVNL-----L
Cdc42 SPSFENVKQKWPETIHH--CPKTPFLVGTQIDLRDDPSTIEK-----L
Rab  DRESFBAV-SSWREKVAE--VGDIPVVLVGNKIDLDDSCIKNEEAEL
Ran  SRVYKQNV-PNWHRDLVRV--CENIPVLCGNKVDIKDRK-VKAKST-VF
Arf  SH-FK-IGPLWQH-----FFONTK-ELSAQFAQ-----F

151                200
Ras  ARSYGLPIYIETSAK-----TRQGVEDAF--YTLVRELRQHKLR
Rho  RRN-GL-E--PVTYHRG--QE---MARS-VCAVA--YLECSARLHDNVH
Cdc42 AKN-KQK--PITPETA--EK---LARD-LKAVK--YVFCALTORGLK
Rab  AKRLKLRFYRTSVKEDLNVNEVFKYLAEKYLQKQQAEDPELTHSSSN
Ran  HRKKNLQYDISAKSNYNFEKPLWLRKLLGDPNLEFVAMPALAPPEV-
Arf  IKK--L--CGVTGTN-----DEASPGKLN--FLSTPSLQG----

201                248
Ras  ---KLNPPDE-----SGPGCMSCK-----CVLS
Rho  --AVFQEAEEVA-----LSSRGRNFWRRITQ-----GF--CVVT
Cdc42 --NVFDEAIIAA-----LEPPETQPKRK-----CCIF
Rab  KIGVFNTPGGSHSGQNSGTNGGDVINLRPNKQRTKKNRNPFFSSCSIP
Ran  ---VMDPALAAQYEH--LEVAQTAL-PDED-----DDL-----
Arf  ----MMPVN-----YFE

```

**Figure 1.4. Homology between members of the ras superfamily**

The protein sequences of representative members of the Ras, Rho, Rab, Ran and Arf families, in addition to the Rho GTPase Cdc42, were aligned using MultAlin version 5.4.1 (Corpet 1988). Gaps included to optimise the alignment are indicated with a -. Identical residues are shaded in black, conservative changes in grey and those without shading indicate non-conservative changes. Conserved regions between the closely related Ran and Rab families are shown in dark grey. The CAAX motifs of prenylated proteins are underlined. The two residues most commonly mutated in GTPase deficient mutants (Gly12 and Gln61 in ras) are highlighted in red.

1.2.2.2. *Termination of signalling through monomeric GTPases.* Like  $G\alpha$  subunits, monomeric G proteins contain the same conserved glutamate on the switch II region which is required for the coordination of the water molecule during GTP hydrolysis. Mutation of this residue, Gln61, is one of the most common activating mutations involved in ras mediated oncogenesis (Bos 1989). Monomeric G proteins do not contain the catalytic arginine which is also required for GTPase activity. In the case of monomeric G proteins it is

the GAP protein which contributes the catalytic arginine residue (Resat *et al.* 2001). The regulation of GAPs for monomeric GTPases employs the same basic strategies as those used for their GEF proteins (section 1.2.2.1) (Bos *et al.* 2007).

1.2.2.3. *The localisation of monomeric GTPases.* Like the  $G\beta\gamma$  dimer of heterotrimeric G proteins, the majority of small monomeric G proteins are modified at their C-terminus with a prenyl moiety to promote membrane attachment and transport to the plasma membrane. This modification occurs at a consensus CAAX motif. In a number of cases, monomeric G proteins are also modified with a palmitoyl moiety just upstream of the prenyl group (Wennerberg *et al.* 2005) (Figure 1.4). The Ran and Arf families are notable exceptions. Arf proteins, like most monomeric G proteins, are membrane associated, but are myristoylated at their N-terminus in a similar way to the  $G\alpha$  subunit of heterotrimeric G proteins (Donaldson 2008). Ran is required to shuttle between the cytoplasm and nucleoplasm to regulate nuclear transport. Ran proteins are not prenylated, but contain an acidic DEDDDL motif at their C terminus which promotes nuclear localisation, mediating interactions with a number of nuclear proteins (Lui and Huang 2009) (Figure 1.4).

### 1.3. Ras proteins

#### 1.3.1. The discovery and clinical importance of ras.

The first steps towards the discovery of ras proteins were taken with the identification of two acute transforming retroviruses in rodents, the Harvey-murine sarcoma virus (Ha-MSV) (Harvey 1964) and Kirsten-murine sarcoma virus (Ki-MSV) (Kirsten and Mayer 1967). As understanding of the nature of these viruses developed, it became clear that the viral genome contained regions of host sequence (Scolnick *et al.* 1973), and that the transforming genes in the viral genome originate from normal vertebrate genes that regulate cell growth

(Ellis *et al.* 1981). These genes were later classified as *ras* oncogenes (Coffin *et al.* 1981). The importance of *ras* oncogenes in human cancers was first demonstrated when homologues of the Harvey and Kirsten virus *ras* genes (*h-ras* and *k-ras*) were isolated from human bladder carcinomas (Der *et al.* 1982; Parada *et al.* 1982; Santos *et al.* 1982). It is now known that mutations in *ras* are responsible for a significant majority of human cancers (Bos 1989).

The first clues as to the biochemical activity of *ras* proteins came when it was demonstrated that *ras* from cells transformed with Ha-MSV and Ki-MSV bound GTP (Scolnick *et al.* 1979). Later *ras* was shown to hydrolyse GTP, and that the hydrolysis of GTP appeared impaired in oncogenic forms of the protein (Gibbs *et al.* 1984; Hurley *et al.* 1984; Sweet *et al.* 1984). Based upon these observations, it was suggested that the activity of *ras* in regulating cell proliferation was analogous to that of signal transducing G proteins. Hurley *et al.* (1984) were the first to demonstrate homology between *ras* and G $\alpha$  subunits of heterotrimeric G proteins.

### 1.3.2. Activators of *ras*.

The role of *ras* genes in cell proliferation suggested a link between *ras* and mitogen signalling. This link was later confirmed when epidermal growth factor (EGF) was shown to promote nucleotide exchange in *ras* proteins (Kamata and Feramisco 1984). The first upstream activator of a *ras* protein described was the *Saccharomyces cerevisiae* protein CDC25 (Broek *et al.* 1987), which was subsequently shown to display GEF activity (Jones *et al.* 1991). Following this, a number of mammalian GEFs were identified based upon homology to CDC25 (Wei *et al.* 1992), in addition to GEFs in model systems, such as the *Drosophila melanogaster* protein Sos (Simon *et al.* 1991).

The activation of *ras* by mitogens is now very well characterised. The recognition of ligand by mitogen receptors of the receptor tyrosine kinase (RTK) family results in receptor dimerisation. Upon dimerisation, one of the receptor

dimers phosphorylates multiple tyrosines on the intracellular C-terminus of the second binding partner. These phosphorylated tyrosines then act as sites of assembly for downstream signalling components (Ullrich and Schlessinger 1990). In the instance of ras activation, the adapter protein Grb2 binds phosphorylated tyrosines on the active receptor through a Src homology 2 (SH2) domain. Grb2 then acts as a bridge between the receptor and the ras GEF Sos through the binding of a proline-rich motif on Sos by a second domain of Grb2 (Src homology 3 or SH3 domain). The recruitment of Sos to the plasma membrane then allows the activation of ras (Figure 1.5) (reviewed in McCormick 1993). Studies have also highlighted a role for heterotrimeric G proteins in RTK signalling. The transactivation of RTKs such as the epidermal growth factor receptor (EGFR) has been demonstrated in response to G protein signalling, allowing subsequent ras activation (Daub *et al.* 1997).

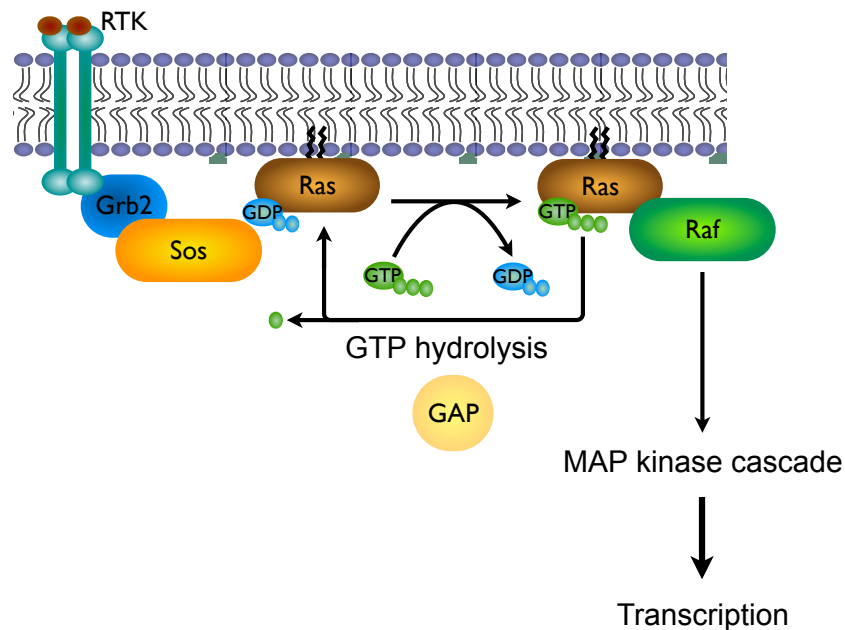


**Figure 1.5. Mitogen signalling through ras**

The binding of growth factors to their cognate receptor tyrosine kinases (RTKs) results in receptor homodimerisation and the phosphorylation of tyrosine residues in their cytoplasmic domains. The phosphorylated tyrosines then provide sites of binding for the SH2 domain of the adaptor protein Grb2. The ras GEF Sos is recruited to the cell surface through interaction with the SH3 domain of Grb2, where it is able to promote nucleotide exchange in ras. Ras then initiates a cascade of MAP kinase phosphorylation, resulting in transcription factor activation.

The linking of upstream signals to ras activity by the activation of GEF proteins is a common motif in ras signalling. Other known examples include, the activation of the GEFs RasGRF1 and RasGRF2 in response to increases in intracellular calcium and  $G\beta\gamma$  subunit signalling (Fernández-Medarde and Santos 2011) and the activation of the GEF RasGRP in response to phospholipase C (PLC) signalling and diacylglycerol (DAG) (Roose and Weiss 2000).

Finally, ras proteins have also been shown to act downstream of signalling from focal adhesions. Focal adhesions consist of membrane spanning proteins known as integrins, which bind extracellular matrix proteins forming heterodimers of  $\alpha$  and  $\beta$  integrin. Integrins themselves do not have catalytic activity, but couple to a family of tyrosine kinases known as the focal adhesion kinases (FAKs), such as p125FAK. p125FAK becomes autophosphorylated on tyrosine residues allowing the recruitment of Grb2-Sos. Cross-talk also occurs with GPCR signalling cascades through PKC-regulated FAK family kinases such as Pyk2 (reviewed in Luttrell *et al.* 1999) (Figure 1.6).

### 1.3.3. The deactivation of ras.

p120GAP was the first protein with RasGAP activity to be identified (Vogel *et al.* 1988). The discovery of p120GAP followed previous work which had demonstrated that a soluble cytoplasmic protein could stimulate the GTPase activity of normal N-Ras but not oncogenic forms of the protein (Trahey and McCormick 1987). A second GAP was later identified in the form of the NF1 protein (Ballester *et al.* 1990), mutation of which is responsible for type 1 neurofibromatosis. A number of ras GAP proteins have now been identified, each with differing functional profiles. Some of these functions include wound healing (NF1), cell adhesion (R-RasGAP), axonal development (SynGAP), anti-apoptotic signalling (p120GAP) and pro-apoptotic signalling (DIP1/2) (Iwashita and Song 2008).

The differing functional activities of ras GAPs are often conferred by differential expression patterns, and the presence of distinct protein-protein interaction domains. These include 14-3-3 domains (DIP1/2) and SH domains (p120GAP), and allow the recruitment of downstream signalling components. Different modes of membrane association also contribute to differing signalling characteristics. Specific examples include phosphoinositide binding through constitutive plekstrin homology (PH) domains ( $GAP1^{IP4BP}$ ) and calcium-responsive membrane association through calcium-binding C2 domains (CAPRI, RASL) (Iwashita and Song 2008) (Figure 1.6).

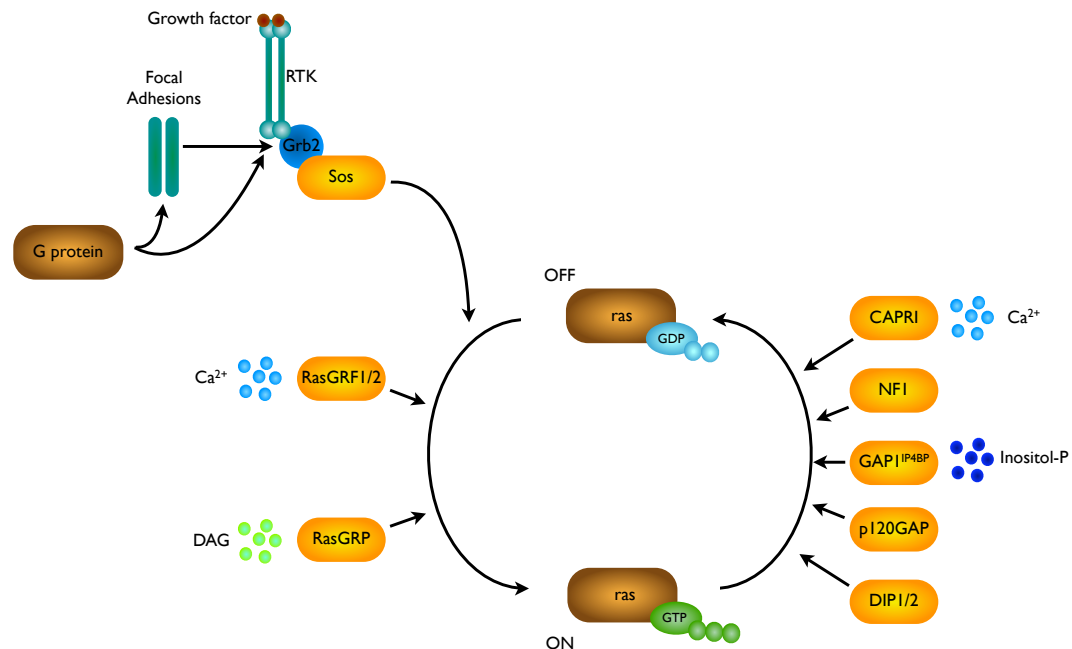


**Figure 1.6. The activation and regulation of human ras**

Human ras proteins are regulated by multiple processes and pathways. The best characterised pathway is initiated in response to growth factor stimulation, resulting receptor tyrosine kinase (RTK) activation, recruitment of the adaptor Grb2 and nucleotide exchange on ras promoted by the GEF Sos. Focal adhesions are also able to recruit Grb2 and initiate Sos GEF activity. The cross-talk between both of these processes and heterotrimeric G protein signalling is also indicated. The activation and deactivation of ras can also be influenced by second messengers, through second messenger regulated GEFs and GAPs. These include GEFs such as RasGRF1/2 ( $Ca^{2+}$ ) and RasGRP (Diacylglycerol or DAG), and the GAPs CAPRI ( $Ca^{2+}$ ) and  $GAP1^{IP4BP}$  (inositol-phosphates).

#### 1.3.4. Signalling downstream of ras.

Mitogen activated protein kinases (MAPKs) were the first identified effector of ras. An activated mutant of the MAP kinase kinase (MAPKK) MAPKK1 was shown to be sufficient for the transformation of cultured cells. In addition, it was shown that a dominant negative mutant of MAPKK1 could block transformation by oncogenic ras mutants (Cowley *et al.* 1994). The signalling events which occur downstream of ras in response to mitogens are now well established. Active ras at the plasma membrane recruits the serine/threonine kinase Raf1, causing Raf1 to become active. Raf1 then phosphorylates a MAP Kinase Kinase which, in turn, phosphorylates a MAP Kinase. The active MAP Kinase then translocates to the nucleus where it phosphorylates a number of substrates, resulting in changes in transcription (reviewed in Campbell *et al.* 1998).

Phosphatidylinositol-3-kinase (PI3K) also interacts with ras in a GTP-dependent manner. Early analysis demonstrated that dominant negative mutants of ras blocked the accumulation of 3' phosphorylated phosphoinositides in response to growth factors (Rodriguez-Viciana *et al.* 1994). It is now known that many proteins act downstream of PI3K, predominantly through the recognition of 3' phosphorylated phosphoinositides by plekstrin homology (PH) domains on these proteins. These include the serine/threonine kinase Akt and a number of monomeric G proteins (Vanhaesebroeck *et al.* 2010).

The modification of phospholipids as a consequence of ras activity is not limited to PI3K signalling. Phospholipase C $\epsilon$  (PLC $\epsilon$ ) is directly activated by GTP-bound ras (Kelley *et al.* 2001). PLC $\epsilon$  contains two ras association (RA) domains and a CDC25-like GEF domain. It is likely that the role of ras is to recruit PLC $\epsilon$  to the plasma membrane, as artificially targetting PLC $\epsilon$  to the plasma membrane overcomes a loss of ras binding (Bunney *et al.* 2006).

Ras also activates a number of GEFs for other monomeric GTPases. These include Ral GEFs (RalGDS, RGL, RGL2 and RGL3), Rab GEFs (RIN1, RIN2 and RIN3) and the Rac GEF Tiam1 (reviewed in Mitin *et al.* 2005).

### 1.3.5. Post-translational modification and localisation of ras.

The importance of localisation in ras signalling has been known for some time. An early study suggested that ras proteins displayed localisation to the inner surface of the plasma membrane (Willingham *et al.* 1980). It was also indicated that the localisation of ras to the plasma membrane was conferred by the C-terminus of the protein, and that plasma membrane localisation was required for the transforming activity of ras. A later study then demonstrated that a specific residue, the cysteine nearest the C-terminus of ras, was required for lipid binding and the transformation of cells in culture (Willumsen *et al.* 1984).

The localisation of ras proteins is conferred by a C-terminal domain known as the hypervariable region (HVR), which is highly divergent between ras isoforms. The HVR consists of two distinct domains. The C-terminal section of the HVR is the site of ras post-translational modification and the primary region responsible for ras trafficking and localisation. The region preceding this is known as the HVR linker, and acts as a bridge between the conserved G domain and the more divergent localisation domain of the ras protein (reviewed in Eisenberg and Henis 2008). In the following section the processes responsible for ras protein localisation are discussed.

1.3.5.1. *Farnesylation.* An early study indicated that the processing of ras into the mature membrane associated form of the protein occurred in two distinct stages (Gutierrez *et al.* 1989). During the first stage it was demonstrated that the protein undergoes C-terminal proteolysis, resulting in the removal of the final three amino acids, in addition to C-terminal carboxyl-methylation. It was also demonstrated that during this process ras gained hydrophobicity. This study suggested a requirement for the most C-terminal cysteine residue of ras in the first processing stage. The hydrophobicity gained during these

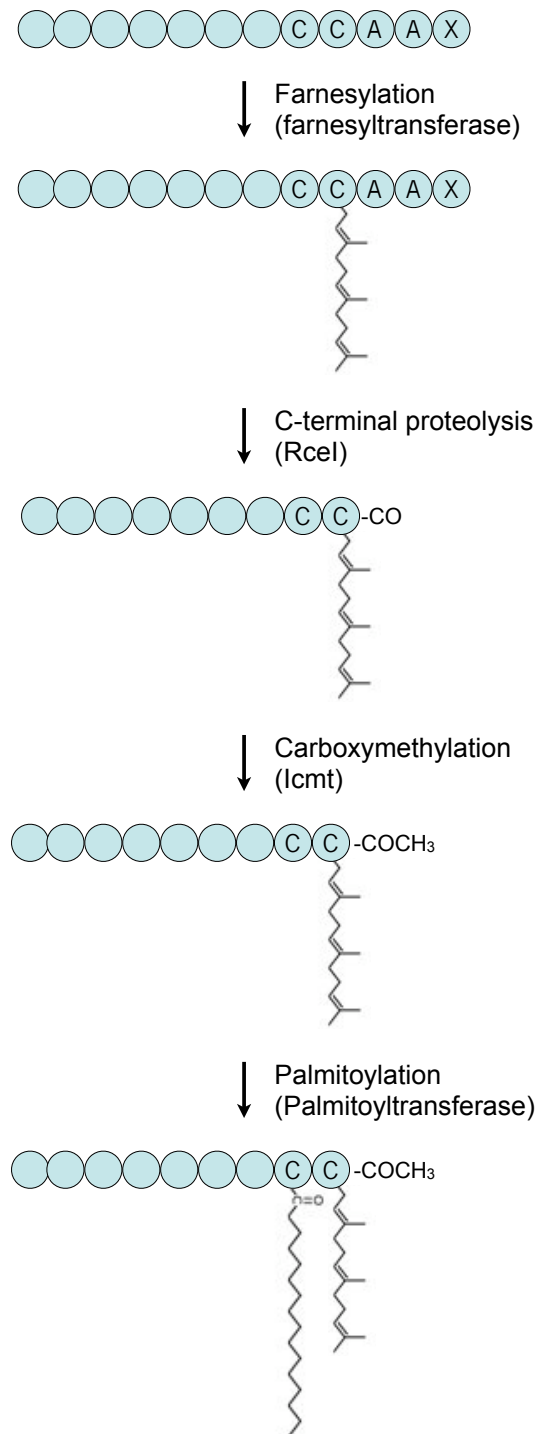


**Figure 1.7. C-terminal modification of ras proteins**

The modification of ras begins with farnesylation of the cysteine present in the C-terminal CAAX motif (where A is any aliphatic amino acid and X is any amino acid). Removal of the AAX is then catalysed by the protease Rce1 and carboxyl-methylation is performed by the protein Icmt. Palmitoylated ras isoforms are then modified with a palmitoyl group at an upstream cysteine residue.

initial processing steps is now known to be due to prenylation of the C-terminal cysteine (Hancock *et al.* 1989).

Subsequent studies have shown that the moiety added at this stage is a 15 carbon isoprenoid farnesyl group. The farnesylation of ras is catalysed by protein farnesyltransferases, which recognise the C-terminal CAAX motif (where A is any aliphatic amino acid and X is any amino acid) present in all ras proteins. Removal of the AAX of the protein farnesyltransferase recognition motif is then performed by the protease Rce1 (ras-converting enzyme), which is an integral membrane protein present at the endoplasmic reticulum. Carboxyl-methylation is then performed by the protein Icmt (Protein-S-isoprenylcysteine O-methyltransferase) (Figure 1.7) (Clarke 1992; Silvius 2002).

1.3.5.2. *Palmitoylation.* Despite farnesylation being the only modification conserved across all ras protein, palmitoylation was the first post-translational modification of ras to be described (Chen *et al.* 1985). Palmitoylation, the addition of a 16 carbon fatty acid chain, occurs at cysteine residues upstream of the farnesylated cysteine. H-Ras is palmitoylated at two cysteine residues and N-Ras contains a single palmitoyl moiety. However, not all ras proteins are palmitoylated. The K-Ras protein can exist as two splice variants, differing in their fourth exon. K-Ras4A contains a single palmitoylated cysteine, whereas K-Ras4B does not undergo palmitoylation (Figure 1.7) (Hancock *et al.* 1989).

Palmitoylation of ras comprises the second step of ras processing described in Gutierrez *et al.* (1989). Palmitoylation is catalysed by protein acyl transferases (PATs), which recognise the farnesylated C-terminus of ras and promote the addition of palmitoyl moieties to cysteines upstream of the farnesyl group. PATs largely fall into a single family of proteins, characterised by a cysteine rich domain (CRD) with a conserved DHHC (Asp-His-His-Cys) motif (CRD-DHHC proteins). Palmitoylated proteins are also actively de-palmitoylated by the cytoplasmic protein acylprotein thioesterase 1 (APT1) (reviewed in Eisenberg and Henis 2008).

1.3.5.3. *Poly-basic domains.* The efficient membrane binding of K-Ras4B is not dependent upon palmitoylation of the protein. Instead, it has been demonstrated that the association of K-Ras4B with the plasma membrane is enhanced by a stretch of lysine residues upstream of the C-terminal farnesylated cysteine, which promotes membrane association through ionic interactions with negatively charged lipid head groups at the plasma membrane. The presence of a polybasic region in K-Ras4B is required for the oncogenic transformation of cells in culture (Jackson *et al.* 1994).

1.3.5.4. *The two-signal hypothesis of plasma membrane association.* Many signalling proteins undergo modifications analogous to those seen in ras to allow association with the plasma membrane. No single membrane targeting signal, including palmitoylation, farnesylation or polybasic domains, is sufficient to promote efficient plasma membrane association. Soluble proteins therefore require the cooperative action of two or more plasma membrane targeting motifs to allow stable association with the plasma membrane (reviewed in Resh 1996). As a consequence, ras proteins employ a combination of farnesylation and a second signal such as palmitoylation or polybasic domains to promote membrane association (reviewed in Eisenberg and Henis 2008).

1.3.5.5. *Ras protein trafficking.* Based upon the processes that ras proteins undergo to become stably associated with the plasma membrane, a picture has been formed for ras trafficking. Ras is translated in the cytosol. Immediately following translation ras becomes farnesylated by cytosolic protein farnesyltransferases. The presence of the C-terminal farnesyl increases the hydrophobicity of ras, promoting the association of ras with the endoplasmic reticulum (ER). Ras is then further processed at the ER by Rce1 and Icmt, and palmitoylation of H-Ras and N-Ras is performed by ER associated PATs (Choy *et al.* 1999). H-Ras and N-Ras are then trafficked to the plasma membrane via

vesicular transport. The trafficking of K-Ras4B to the plasma membrane is less well characterised, but is independent of vesicular transport (Apolloni *et al.* 2000) (Figure 1.8).

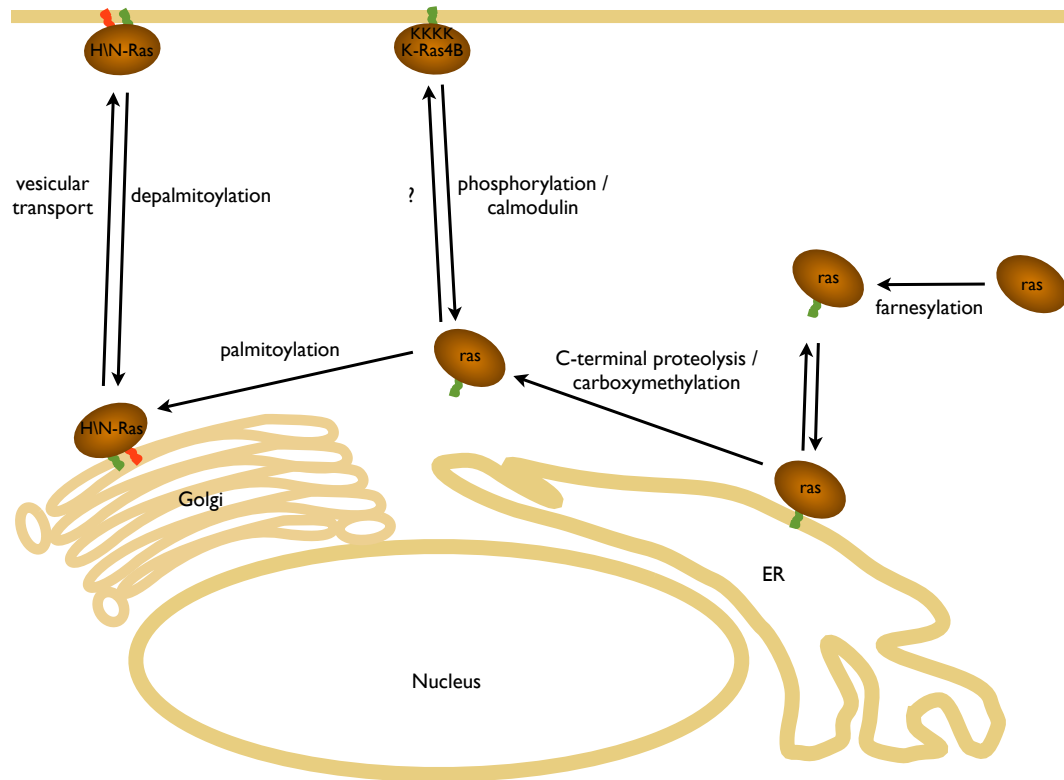


**Figure 1.8. The trafficking of human ras proteins**

All ras isoforms are farnesylated (green) in the cytosol by protein farnesyltransferases. Upon association with the ER, the protein undergoes C-terminal proteolysis and carboxymethylation, catalysed by Rce1 and Icmt respectively. At this point the processing of K-Ras4B is complete, and it is transported to the membrane via an unknown mechanism (right). H-Ras and N-Ras are further modified at the ER with two and one palmitoyl groups (red) respectively, in a process catalysed by protein acyl transferases (PATs). H-Ras and N-Ras are then trafficked to the plasma membrane through vesicular transport mechanisms (left). All ras isoforms can undergo retrograde transport from the plasma membrane. For K-Ras4B this process involves either calmodulin binding or phosphorylation. In the case of palmitoylated isoforms this process required depalmitoylation.

### 1.3.6. Compartmentalised ras signalling.

A number of factors have fostered the belief that ras signalling occurs solely from the plasma membrane. For example, the importance of ras plasma membrane localisation in the oncogenic transformation of cultured cells was a very early observation in the investigation of ras signalling (Willingham *et al.* 1980). Additionally, the role of ras in transducing signals from extracellular mitogens, and that these signals are detected by trans-membrane receptors (McCormick 1993), suggests that ras signalling is a plasma membrane-associated event. In the following section, however, the evidence for ras signalling from membrane compartments distinct from the plasma membrane will be discussed (reviewed in Mor and Philips 2006).

1.3.6.1. *Signalling from endosomes.* Receptor internalisation is a convenient means of down-regulating signalling from external stimuli. The internalisation of RTKs has been demonstrated to be involved in receptor down-regulation and degradation, reducing a cells stimulation in response to exogenous cues (Levkowitz *et al.* 1998). Studies, however, have demonstrated a role for internalisation in signalling. The accumulation of Grb2 and Sos has been shown on endosomes in response to EGF, indicating a possible role for endosomes as a platform for ras signalling (Di Guglielmo *et al.* 1994).

It now appears that endocytic trafficking of RTKs performs both a positive and negative role in signalling. Studies utilising endocytosis-defective cells reported reduced MAPK activation in response to EGF, supporting the notion of endosome-derived ras signalling in response to mitogens. Consistent with a dual positive and negative role in signalling, other signalling components became up-regulated when endocytosis was inhibited, such as PLC- $\gamma$  (Vieira *et al.* 1996). An endosome specific MAP kinase scaffold (MEK partner 1 or MP1) has also been identified, further indicating the importance of endosomal ras-MAPK activity (Teis *et al.* 2002).

One of the best characterised examples of endosomal signalling is that of neurotrophins. Nerve cells require signalling to occur over relatively long distances, and employ the retrograde transport of endosomes from nerve termini to the cell body to deliver information to the nucleus of the cell. The enrichment of active ras and MAPK signalling has been demonstrated on clathrin-coated vesicles in response to nerve growth factor (NGF) in cultured cells, again demonstrating a role for endosome-derived ras signalling (Howe *et al.* 2001).

1.3.6.2. *Signalling from the endomembranes.* A number of studies have demonstrated ras signalling from other endomembrane compartments. The depalmitoylation of isoforms such as H-Ras and N-Ras has been demonstrated to be key in the maintenance of their localisation to both the plasma membrane and internal structures such as the Golgi membranes. This endocytosis independent redistribution of ras from the plasma membrane to internal membranes has also been demonstrated for active GTP-bound H-Ras and N-Ras (Rocks *et al.* 2005). A second study also demonstrated ras activity on the Golgi and ER in response to mitogen signalling, and indicated that ras was able to activate downstream signals from these endomembrane compartments. This activity was shown to be independent of endocytosis, and potentially driven by ras depalmitoylation (Chiu *et al.* 2002).

In addition to the role of depalmitoylation in allowing ras activity for internal membranes, further studies have also explored a role for direct activation of ras at these sites. H-Ras can be activated at the Golgi in response to T-cell receptor (TCR) activation. TCR activation of H-Ras at the Golgi is dependent upon PLC- $\gamma$  and Ca<sup>2+</sup>, and results from the synergistic action of the Ca<sup>2+</sup>-dependent GEF RasGRP1 at the Golgi and the Ca<sup>2+</sup>-dependent translocation of the Ras GAP CAPRI to the plasma membrane. As a consequence ras becomes activated at the Golgi, but ras activity is inhibited at the plasma membrane (Bivona *et al.* 2003). Endoplasmic reticulum specific activation of

H-Ras has also been observed, regulated by the GEFs RasGRF1 and RasGRF2 (Arozarena *et al.* 2004).

The labile thioester bond between ras isoforms such as H-Ras and N-Ras and palmitoyl moieties at their C-terminus allows a reversible interaction with the plasma membrane through cycles of palmitoylation and depalmitoylation. The polybasic domain of K-Ras4B would appear a less dynamic localisation motif, as it is an intrinsic part of the protein's secondary structure. Despite this, a number of studies have demonstrated the dynamic redistribution of K-Ras4B in response to exogenous stimuli, in addition to endomembrane signalling. K-Ras4B displays rapid  $\text{Ca}^{2+}$ -dependent redistribution to endomembranes, including endosomes and the Golgi, upon the stimulation of hippocampal neurons with glutamate. The translocation required the binding of  $\text{Ca}^{2+}$ /calmodulin, leading to a redistribution of K-Ras4B and K-Ras4B activity (Fivaz and Meyer 2005). K-Ras4B translocation from the plasma membrane has also been demonstrated following phosphorylation of a specific serine residue (S181) within the C-terminal polybasic domain by protein kinase C (PKC). K-Ras4B redistributes to the endoplasmic reticulum, Golgi and mitochondria following phosphorylation. A PKC-dependent interaction with Bcl- $X_L$  (an anti-apoptotic Bcl-2 family protein) on the mitochondria was also observed, resulting in pro-apoptotic signalling (Bivona *et al.* 2006).

As with endosomal MAPK activity, a Golgi-specific MAPK scaffold also exists (Sef), further indicating a functional role for ras-MAPK signalling from the Golgi (Torii *et al.* 2004).

1.3.6.3. *Signalling from plasma membrane microdomains.* Compartmentalised signalling is not limited to different organelles, but also to different regions of an organelle. One example of this is the presence of distinct microdomains at the plasma membrane. The best studied membrane microdomain is the lipid raft. Lipid rafts are liquid-ordered membrane domains, rich in cholesterol and sphingolipids. It has been suggested that rafts play a role

in signal transduction, acting to both concentrate signalling components at the membrane and to segregate components to more tightly control signalling processes. A number of upstream components of ras signalling are associated with lipid rafts, including EGF receptors, T-cell receptors, NGF receptors and integrins, suggesting a role for lipid rafts in ras signalling (reviewed in Simons and Toomre 2000).

Another feature of some lipid rafts is the presence of caviolae. Caviolae are small invaginations present in some liquid ordered microdomains. The characteristic structure of caviolae is conferred by the polymerisation of caveolins, which are palmitoylated integral membrane proteins with a hairpin like structure (Simons and Toomre 2000). EGF receptors have been demonstrated to associate with caviolae, but also to exhibit ligand-dependent migration from caviolae-rich microdomains (Mineo *et al.* 1999). H-Ras has also been shown to associate with caveolin and lipid rafts. K-Ras4B, by contrast, displays specific localisation to liquid-disordered membranes. As seen in EGF receptor activation, H-Ras exhibits a stimulation-dependent redistribution from lipid rafts to liquid-disordered membranes upon GTP binding. Redistribution requires the presence of the H-Ras hypervariable region and is required for efficient Raf1 activation (Prior *et al.* 2001). Redistribution results from conformational changes in the catalytic domain, reducing the affinity of H-Ras for lipid raft structures (Rotblat *et al.* 2004). The second palmitoyl moiety of H-Ras appears key for this activity, as mono-palmitoylated H-Ras and wild-type N-Ras display the inverse effect, localising to liquid-disordered membranes when GDP-bound and redistributing to lipid rafts when active (Roy *et al.* 2005).

More recent studies have demonstrated the formation of clusters of 6-8 ras proteins which display reduced lateral mobility (ras nanoclusters). Ras nanoclusters display GTP-dependent stability and are required for efficient Raf activation ( Tian *et al.* 2007). The immobilisation of ras nanoclusters has been suggested to be dependent upon cytoskeletal elements, membrane proteins and liquid-disordered membrane microdomains (Abankwa *et al.* 2007).

### 1.3.7. Ras localisation as a therapeutic target.

Preventing the membrane association of ras is an attractive mechanism for the downregulation of oncogenic ras signalling. As a consequence, the development of farnesyltransferase inhibitors (FTIs) has been of significant interest as a cancer therapy. FTIs predominantly fall into two groups, compounds that act as farnesyl analogues or molecules that are competitive inhibitors of CAAX binding. Two compounds are currently being trialled which fall into the latter category, tipifarnib and lonafarnib (Appels *et al.* 2005). However, FTI therapy has not had the impact that was initially hoped, as ras proteins appear to become modified with a 20 carbon geranylgeranyl isoprenoid when farnesylation is inhibited (Downward 2003).

Another anti-cancer therapy that may modulate ras localisation is Bryostatins. Bryostatins activate PKC and is able to induce apoptosis in cultured cells. One study indicated that Bryostatins induced PKC-dependent phosphorylation of K-Ras4B, resulting in the localisation of K-Ras4B to the mitochondria and pro-apoptotic signalling through an interaction with Bcl-X<sub>L</sub> (Bivona *et al.* 2006).

More recently, a small molecule inhibitor of the de-palmitoylating enzyme APT1 has been identified (Palmostatin B). Inhibition of APT1 by Palmostatin B has been demonstrated to cause entropy driven indiscriminate membrane association of H-Ras and N-Ras, through disruption of the ras acylation cycle. Reversion in H-Ras transformed cultured cells was also observed upon Palmostatin B treatment (Dekker *et al.* 2010).

#### 1.4. The *Schizosaccharomyces pombe* model system

Yeast provide an ideal model system for the study of genetic and cellular processes. They employ a number of signalling cascades to sense environmental changes and control cellular behaviours, utilising components conserved in higher eukaryotic systems. In addition, their genetic tractability allows for the manipulation of components within signalling systems and the introduction of reporter constructs. Reporters can include auxotrophic markers, allowing growth-based signalling assays, and enzymes such as  $\beta$ -galactosidase, providing a colourimetric output for signalling activity. One such example in *Sz. pombe* is the *sxa2>lacZ*  $\beta$ -galactosidase reporter strain, in which the open reading frame of the pheromone-responsive gene *sxa2* has been replaced by the *lacZ* gene. This has allowed the quantitative analysis of pheromone-responsive signalling. The *sxa2* reporter system has been extended to include fluorescent reporters (Dr. Benjamin Smith, unpublished data) and luciferase (Antonia Nilsson, unpublished data). Both the budding yeast *S. cerevisiae* and the fission yeast *Sz. pombe* has been extensively utilised to study signalling events. Applications have included the study of GPCRs, heterotrimeric G proteins, MAP kinase cascades and ligand screens for novel therapeutic compounds (reviewed in Ladds *et al.* 2005).

*S. cerevisiae* and *Sz. pombe* both contain two G protein-mediated signalling cascades which detect external cues, mediating pheromone-responsive mating events and nutrient sensing. Both cascades are required to allow mating. *Sz. pombe* contains a single ras protein (Ras1), which is required for pheromone-responsive signalling. Ras signalling is involved in a further pathway in *Sz. pombe*, regulating cell morphology during mitotic growth (reviewed in Davey 1998 and Hoffman 2005a).

#### 1.4.1. Nutrient-sensing in *Sz. pombe*.

Monitoring the level of environmental nutrients is key to the survival of any organism. In addition, nutrient sensing in *Sz. pombe* is required for the regulation of mating events. Glucose-sensing is initiated by the binding of glucose to the GPCR Git3. Git3 propagates this signal through the activation of the G $\alpha$  subunit (Gpa2) of a heterotrimeric G protein complex (Welton and Hoffman 2000; Isshiki *et al.* 1992). GTP-bound Gpa2 then stimulates the activity of the adenylate cyclase Cyr1, resulting in an increase in the cellular concentration of cAMP (Ivey and Hoffman 2005). Increased cAMP levels stimulate cAMP-dependent protein kinase (PKA), resulting in the inhibition of sexual development (Maeda *et al.* 1990).

When nutrient levels become limiting, Cyr1 activity is no longer stimulated and cAMP levels fall as cAMP is converted to AMP by the phosphodiesterase Cgs2 (Maeda *et al.* 1990; Hoffman 2005b). The resultant reduction in PKA activity causes the expression of the transcription factor Ste11, resulting in the expression of genes required for mating (Reviewed in Yamamoto 1996).

#### 1.4.2. The *Sz. pombe* mating response.

*Sz. pombe* exists as two haploid mating types minus (M) and plus (P). During mitotic growth, *Sz. pombe* divides through a process of binary fission when the cell reaches a critical length. Under conditions of nutrient starvation, each mating type produces a diffusible pheromone. M cells express the P-factor receptor Mam2 and produce M-factor pheromone (Kitamura and Shimoda 1991), whereas P cells produce P-factor and express the M-factor receptor Map3 (Tanaka *et al.* 1993). Both mating pheromone receptors are GPCRs, and couple to the same G $\alpha$  subunit Gpa1 (Obara *et al.* 1991). The reciprocal exchange of pheromone, and pheromone receptor activation, brings about cellular changes, resulting in cell cycle arrest, polar growth of each cell towards the pheromone source and cell fusion (reviewed in Davey 1998) (Figure 1.9).

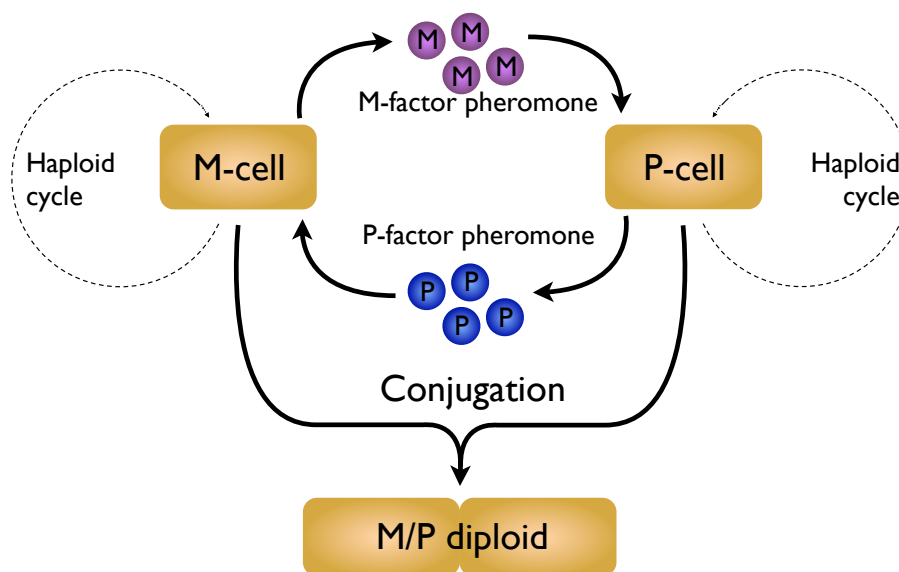


**Figure 1.9. Mating in *Sz. pombe***

Under normal conditions *Sz. pombe* exists as two haploid mating types and replicates by mitotic fission. Following nutrient limitation, cells of opposite mating types release mating-type specific mating pheromones. The detection of pheromone by cell surface receptors brings about cellular changes, resulting in chemotropic growth towards the mating partner, conjugation, cell fusion, meiosis and spore formation.

Ras1 is key to the signalling events underpinning mating. Pheromone binding to the mating type specific receptor induces exchange of GDP for GTP on Gpa1. Gpa1 then promotes nucleotide exchange on Ras1 through an as-yet undetermined mechanism, although it is known that the GEF Ste6 is required for Ras1 activation in response to pheromone (Hughes *et al.* 1990). Ras1 then initiates a MAP kinase cascade by promoting the translocation of the MAPKKK Byr2 to the plasma membrane (Bauman *et al.* 1998). Byr2 then phosphorylates Byr1 (Wang *et al.* 1991), which becomes active and phosphorylates Spk1 (Toda *et al.* 1991). The main target of Spk1 is the transcription factor Ste11 (Kjaerulff *et al.* 2005). Ste11 is a high mobility group (HMG) transcription factor which binds a 10bp T-rich (TR) consensus motif (TTCTTTGTTY) in the promoters of genes required for sexual differentiation, directing their expression (Sugimoto *et al.* 1991) (Figure 1.10).

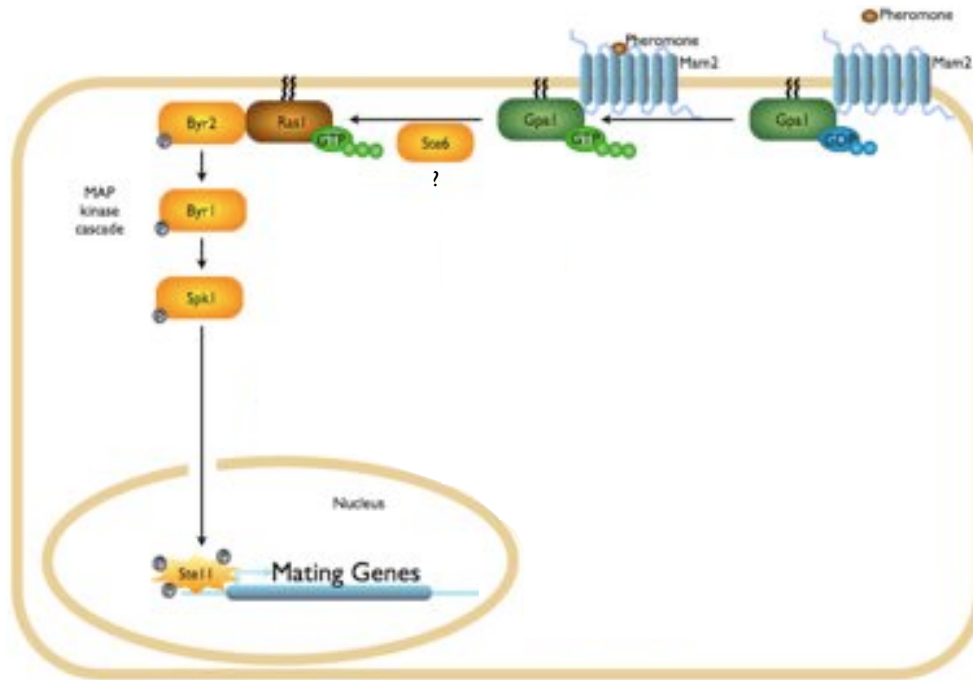


**Figure 1.10. Pheromone-responsive signalling in *Sz. pombe***

Pheromone-responsive signalling begins with pheromone binding to a mating-type specific GPCR, resulting in nucleotide exchange on Gpa1. Gpa1 signalling acts upstream of Ras1, regulating the ras GEF Ste6 through an as-yet undefined mechanism. GTP-bound Ras1 then promotes the translocation of the MAPKKK Byr2 to the plasma membrane. Pheromone-responsive transcription is brought about through sequential phosphorylation of kinases in the MAP kinase cascade (Byr2, Byr1 and Spk1) leading to phosphorylation of the transcription factor Ste11. Active Ste11 binds TR boxes in the promoter regions of specific genes, resulting in the expression of genes involved in cell cycle arrest, morphological changes and agglutination.

### 1.4.3. Pheromone-responsive signalling in *Sz. pombe*.

1.4.3.1. *Cell cycle arrest.* Upon mating, two haploid cells of opposite mating types fuse to form a diploid zygote. A key aspect of this process is maintaining cells in their haploid state prior to mating. As a consequence, an initial pheromone-dependent event is for cells to arrest in  $G_1$ . Investigation of this process is complex as nitrogen starvation, which is required for pheromone response in wild-type cells, also leads to a  $G_1$  arrest. A pheromone-dependent cell cycle arrest can, however, be observed when nutritional sensing is perturbed, such as in cells lacking Cyr1 (Davey and Niesen 1994; Imai and Yamamoto 1994).

Progress through the cell cycle is controlled by the cyclin-dependent kinase (CDK) Cdc2. The transition from  $G_1$  to S phase is primarily controlled by the B-cyclin Cig2, and to some degree Cdc13 (Mondesert *et al.* 1996). Pheromone acts to block cell cycle progression at  $G_1$  through inhibition of B-cyclin-Cdc2 kinase activity (Stern and Nurse 1997). Rum1 (replication uncoupled from mitosis) is the primary CDK inhibitor responsible for arrest in  $G_1$  (Moreno and Nurse 1994). Cells which lack Rum1 are defective in both starvation-induced arrest and pheromone-induced arrest. Rum1 inhibits the  $G_1$ -S transition by targetting Cdc13 for degradation by the anaphase-promoting complex (APC or cyclosome). Cig2 however is degraded by a mechanism independent of Rum1. Stern and Nurse (1998) described these processes, and suggested that pheromone brings about a transient  $G_1$  through Rum1-independent inhibition of Cig2-Cdc2. This then allows Rum1 transcription to become up-regulated, leading to Cdc13 degradation and a protracted  $G_1$  arrest. Both  $G_1$  arrest and Rum1 are also required for pheromone-dependent transcription (Stern and Nurse 1998).

1.4.3.2. *Pheromone-induced morphology changes.* One of the most marked changes a cell undergoes in response to pheromone is in the morphology of that cell. Following pheromone-dependent  $G_1$  arrest, cells continue to grow from one tip towards the source of the pheromone (shmoo) (Fukui *et al.* 1986a; Nielsen and Davey 1995). Shmooing cells display growth from a single projection tip, driven by the accumulation of filamentous actin, and requiring the orientation of microtubules along the long axis of the cell (Petersen *et al.* 1998). The concerted chemotropic growth exhibited by shmooing cells allows cells of opposite mating types to then meet and fuse.

1.4.3.3. *The fusion of mating partners.* Following the meeting of two cells of opposite mating types, cells undergo agglutination and cell fusion. Cell-cell contact is initially facilitated by transient hydrogen bonding, but later

becomes irreversible (Miyata *et al.* 1997). Agglutination is mediated by two mating-type specific agglutinin proteins, Map4 and Mam3 (Sharifmoghadam *et al.* 2006). The 1,3- $\beta$ -glucan of the cell wall at the point of conjugation is then degraded by a mating specific glucanase (Reichelt and Fleet 1981). The two cells then fuse, allowing nuclear fusion, meiosis and spore formation (Tanaka and Hirata 1982).

1.4.3.4. *Regulation of the cells response to pheromone.* Cells which do not mate are able to recover from stimulation and return to mitotic growth (Davey and Nielsen 1994; Imai and Yamamoto 1994). A key mechanism to allow recovery following stimulation in many signalling pathways is the degradation of extracellular ligands. Sxa2 is a serine carboxy-peptidase which inactivates exogenous P-factor through the removal of a single C-terminal leucine residue (Imai and Yamamoto 1994; Ladds *et al.* 1996; Ladds and Davey 2000). In contrast, there appears to be no equivalent mechanism for the inactivation of M-factor (Hughes and Davey 1997).

Another conserved mechanism of adaptation to extracellular stimuli is the removal of receptors from the cell surface. The internalisation of Map3 in response to pheromone has previously been suggested (Hirota *et al.* 2001). The internalisation of GPCRs is known to involve receptor phosphorylation (Ferguson 2001). Studies using GFP-tagged Mam2 have shown the rapid loss of Mam2 at the plasma membrane following pheromone stimulation (Wayne Croft, unpublished data). A number of potential phosphorylation sites have been identified on the C-terminus of Mam2, which is required for pheromone-dependent internalisation (Dr. Eilish McCann, unpublished data).

Dephosphorylation of MAP kinase cascade components is also a rapid means of attenuating signalling. The MAP kinase Spk1 is the primary site for inactivation of the cascade. It has been suggested that Spk1 is dephosphorylated by the phosphatase Pmp1 (Didmon *et al.* 2002). As a consequence, further phosphorylation of Ste11 is prevented, leading to a reduction

in pheromone-dependent transcription.

Two proteins with GAP activity also act upon the pheromone response pathway. Rgs1 is the only RGS protein present in *Sz. pombe*, and has GAP activity for the G $\alpha$  subunit Gpa1. Expression of *rgs1* is upregulated in response to pheromone through the action of Ste11, and cells which lack Rgs1 display a hypersensitivity to pheromone (Watson *et al.* 1999). Gap1 is the second protein with GAP activity which modulates pheromone-dependent signalling. Gap1 is the sole GAP protein for Ras1 in *Sz. pombe*. Loss of Gap1 results in a hypersensitivity to pheromone, indicating a role in the negative-regulation of pheromone-responsive Ras1 signalling (Imai *et al.* 1991).

The negative regulation of the pheromone response is key to functional signalling. Gap1, Rgs1, Pmp1 and Sxa2 are all required for efficient mating (Imai *et al.* 1991; Imai and Yamamoto 1992; Watson *et al.* 1999; Didmon *et al.* 2002). Furthermore, mathematical modeling of Gpa1 signalling has yielded a number of important insights into pathway regulation by the GAP activity of Rgs1, indicating the importance of GTP hydrolysis in both the negative and positive regulation of signal transduction (Smith *et al.* 2009). It has been suggested that GTP hydrolysis is required to release Gpa1 from an inactive GTP-bound state, possibly in an inactive Gpa1-effector complex, to allow further rounds of nucleotide exchange and effector activation. This study not only indicates that recovery from stimulation is important, but also suggests that negative regulators can positively influence signalling.

#### **1.4.4. Regulation of polar cell morphology.**

1.4.4.1. *Vegetative cell growth.* During mitotic growth, *Sz. pombe* cells grow through extension from the cell tip. Following division, growth is initially restricted to the end which existed prior to division (old end), but is initiated at the new end at a specific point in the cell cycle referred to as NETO (new end take off) (Davey 1998). Such controlled polar cell growth requires strict

regulation. Cytoskeletal elements are key to the establishment of cell polarity and polar cell growth in *Sz. pombe*. During cell growth, the distribution of actin closely matches the points of active cell elongation (Marks *et al.* 1986). Microtubules display polar orientation along the long axis of the cell, and are required for the establishment of cell polarity (Sawin and Nurse 1998). The main role of microtubules in cell polarity is the delivery of key proteins to the cell tip during the establishment of polar growth. The tip protein Tea1 is delivered to the tip of the cell by polar microtubules, and is retained at the tip through an interaction with the prenylated tip protein Mod5 (Snaith and Sawin 2003). Tea1 acts at the tip to regulate microtubule dynamics and recruit a host of downstream proteins required for polar cell growth (Behrens and Nurse 2002). Tea1 is required for the polar localisation of tip proteins such as Pom1, Tea2 and Tip1, forming a complex of proteins known as the polarisome, which are responsible for actin recruitment to the cell ends. Tea1 interacts with the tip protein Bud6 and the formin For3 to promote actin recruitment to the tip of the cell (Glynn *et al.* 2001; Feierbach and Chang 2001).

Another key factor in the maintenance of polar cell morphology is Pom1. Pom1 is a DYRK (dual-specificity Yak-related kinase) family protein, which is required for the positioning of the growth site at the cell pole. The localisation of Pom1 is dependent upon microtubules, Tea1 and the proteins intrinsic kinase activity (Bähler and Nurse 2001). Pom1 also links cell polarity with cell division, as it is required for correct positioning of the septum (Padte *et al.* 2006).

Ras1 signalling is required for polar cell morphology (Fukui *et al.* 1986b; Nadin-Davis *et al.* 1986). Ras1 acts to regulate polarity through activation of Scd1, a GEF for the Rho GTPase Cdc42 (Chang *et al.* 1994). The Ras1-Scd1-Cdc42 pathway exerts influence on cell polarity factors through the p21-activated kinase (PAK) Shk1 (Marcus *et al.* 1995). The interaction between Scd1, Cdc42 and Shk1 is facilitated by the scaffolding activity of Scd2 (Endo

*et al.* 2003). Tea1 is a direct target for the kinase activity of Shk1, which is likely one of the key links between Ras1 and cell polarity (Kim *et al.* 2003). Another target for Shk1 is Orb6, which is also required for polar cell morphology (Verde *et al.* 1995). Orb6 is required to limit Cdc42 activity to the cell tip and has been demonstrated to undergo Shk1-dependent phosphorylation (Das *et al.* 2009) (Figure 1.11). Ras1 and Cdc42 have an additional role in the regulation of chromosome segregation, which they perform through regulation of the proteins Yin6 and Moe1 (Yen and Chang 2000).

1.4.4.2. *Shmoo formation.* Upon stimulation with pheromone, the pattern of growth employed by *Sz. pombe* cells is dramatically altered. Cells undergo protracted extension from a single tip and are able to bend towards the source of pheromone. The mechanism by which cells alter their growth pattern is not precisely known, although components of the pathway controlling mitotic polar cell growth are also required for mating. These components include Scd1 and Scd2, which are required for mating and morphology but not pheromone-dependent transcription (Chang *et al.* 1994).

Despite this, key differences in polar cell organisation are observed between cells during the two modes of growth. The most significant observation is the delocalisation of Tea1, Tea2 and Tip1 from the growing tip upon pheromone stimulation. Cells lacking these three proteins also displayed accelerated shmoo formation and conjugation, suggesting that the loss of Tea1, Tea2 and Tip1 from the growing tip is required for shmoo formation to proceed. Pom1, by contrast, is required for the establishment of monopolar growth in response to pheromone (Niccoli and Nurse 2002). Such differences could represent a change in the cell from intrinsically controlled cell polarity to polar growth controlled by extrinsic signals from mating pheromones.

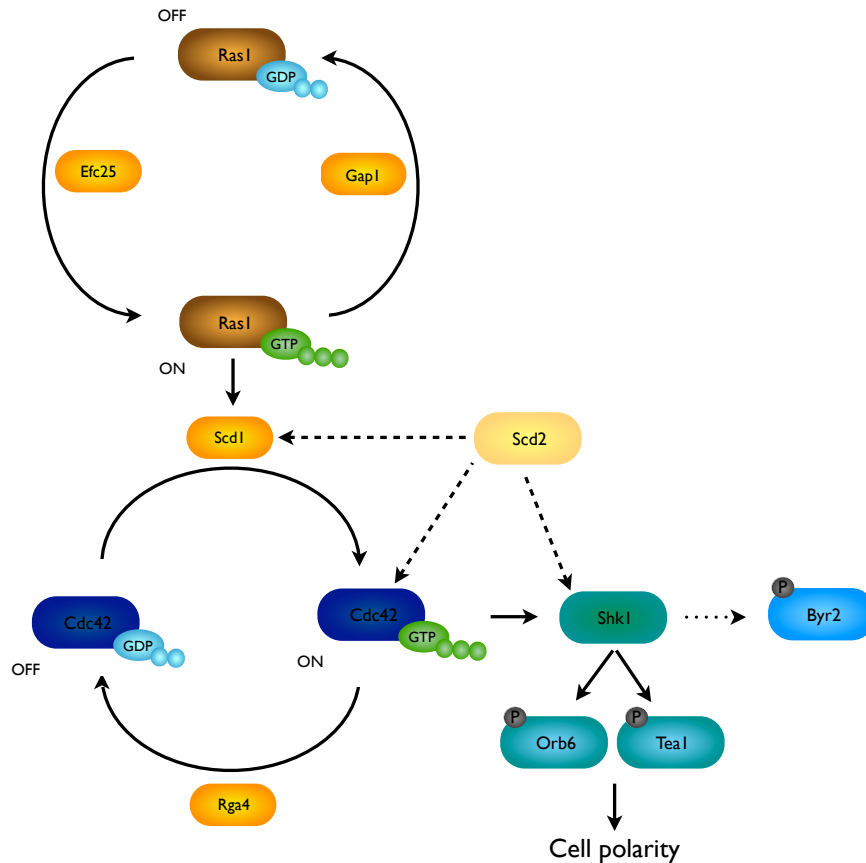


**Figure 1.11. The regulation of cell polarity in *Sz. pombe***

Ras1 exerts influence on cell polarity through activation of the Rho GEF Scd1. Scd1 then initiates nucleotide exchange on the Rho GTPase Cdc42. GTP-bound Cdc42 promotes the activity of the p21-activated kinase (PAK) Shk1, which directly phosphorylates the polarity factors Orb6 and Tea1. These processes are required for the maintenance of polar cell morphology. Rga4 is the GAP protein which returns Cdc42 to a GDP bound state. Shk1 also influences pheromone-responsive transcription through phosphorylation of Byr2. The scaffolding activity of Scd2 facilitates the interaction between Scd1, Cdc42 and Shk1, and is indicated by a dashed line.

#### 1.4.5. The pathway-specific activation of Ras1.

A striking aspect of Ras1 signalling in *Sz. pombe* is the ability of a single ras protein to regulate two distinct pathways in a single cell. Few studies have focussed on the differential activation of Ras1. Two mechanisms have, however, been proposed for the pathway-specific activity of Ras1. The first study to explore these processes highlighted the importance of differential GEF activity (Papadaki *et al.* 2002), which is a conserved motif in G protein signalling, and the second explored the emerging paradigm of compartmentalised ras sig-

nalling (Onken *et al.* 2006).

1.4.5.1. *The differential regulation of Ras1.* Ste6 was the first ras GEF described in *Sz. pombe*. The loss of Ste6 mirrored the mating defects observed in cells lacking Ras1, but Ste6 was not required for polar cell morphology (Hughes *et al.* 1990). A second GEF, Efc25, was later described which was not required for the mating response (Tratner *et al.* 1997). A later study demonstrated that Efc25, and more specifically the GEF domain of Efc25, was required for the maintenance of polar cell morphology. In addition, analysis of *ste6* and *efc25* expression indicated that *ste6* was upregulated in response to pheromone but *efc25* was not. Finally, the study demonstrated that Ste6 and Efc25 act in competition, with overexpression of each causing a reduction in signalling through the other (Papadaki *et al.* 2002). Taken together these results indicate that the pathway-specific activation of Ras1 is, in part, the result of differential regulation by Efc25 and Ste6, with Efc25 regulating polar morphology and Ste6 regulating mating.

1.4.5.2. *Compartmentalised ras signalling in Sz. pombe.* Only one study has explored the role of Ras1 localisation in signalling (Onken *et al.* 2006). The study indicated that the localisation of Ras1, like human N-Ras, was reliant on a single farnesyl group and a single palmitoyl group. It was suggested that preventing the palmitoylation of Ras1, through mutation of the palmitoylated cysteine to a serine (Ras1<sup>C215S</sup>), caused Ras1 to localise exclusively to the endomembranes. It was also suggested that Ras1<sup>C215S</sup> could support polar cell morphology but not mating. A second protein, in which the hypervariable region of Ras1 was replaced with the C-terminal targeting domain of the small GTPase Rit (RitC), was used to investigate plasma membrane signalling. The Ras1-RitC fusion was chosen, as it was trafficked to the plasma membrane without intermediate endomembrane localisation. Functional analysis indicated that Ras1-RitC could support mating but not morphology. These data

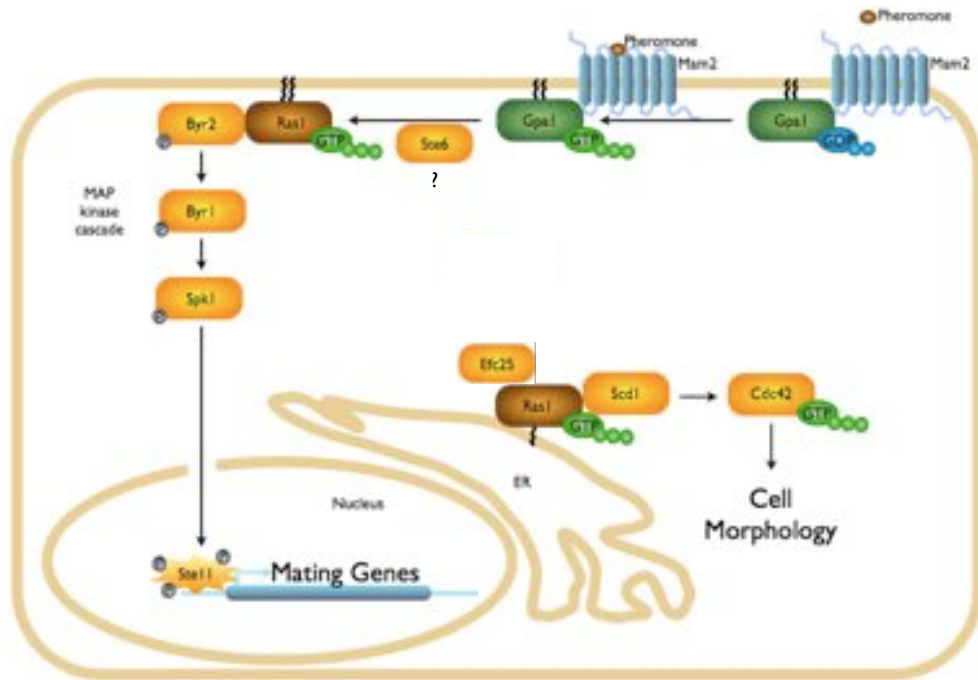


**Figure 1.12. Compartmentalised Ras1 signalling in *Sz. pombe*.**

Onken *et al.* (2006) suggested a model for the compartment specific regulation of Ras1 in *Sz. pombe*. In this model Ras1 at the plasma membrane is activated in response to pheromone by the GEF Ste6, resulting in the recruitment of Byr2, initiating a cascade of MAP kinase phosphorylation and culminating in the expression of genes required for mating. By contrast, nucleotide exchange on endomembrane localised Ras1 is initiated by the GEF Efc25, resulting in Scd1-Cdc42 activity and the regulation of polar cell morphology.

indicated that Ras1 on the plasma membrane regulated mating, and that Ras1 on the endomembranes regulated polar cell morphology (Figure 1.12).

#### 1.4.6. Heterologous expression of signalling components in *Sz. pombe*.

*Sz. pombe* has previously been used as a system for the heterologous expression of human signalling components. Studies have used *Sz. pombe* for the expression of human GPCRs, such as the D<sub>2S</sub> dopamine receptor (Sander *et al.* 1994), B<sub>2</sub> adrenergic receptor (Ficca *et al.* 1995) and NK<sub>2</sub> neurokinin receptor (Arkininstall *et al.* 1995). These studies highlighted the advantages of *Sz. pombe* as an expression system, but did not demonstrate signalling activity.

The functional expression of the corticotrophin releasing factor (CRF) receptor was later demonstrated. The study utilised a Gpa1 protein modified to contain the last five amino acids of human G $\alpha$  proteins, which confer coupling specificity (Ladds *et al.* 2003). The ability of human G $\alpha$  subunits to affect morphology in *Sz. pombe* has also been indicated upon the replacement of their last five amino acids with those from Gpa1. This finding has also allowed the investigation of human RGS protein specificity (Ladds *et al.* 2007). Human RGS4 has also been demonstrated to function in regulating Gpa1 (Hill *et al.* 2008), in addition to human G $\beta$  subunits (Goddard *et al.* 2006).

The functional expression of human H-Ras has also been highlighted in *Sz. pombe* (Nadin-Davis *et al.* 1986), however, little quantification of function has been performed.

**1.5. Aims**

- ◇ Develop quantitative measures of Ras1 function and localisation in *Sz. pombe*.
  
- ◇ Explore the role of Ras1 localisation in function using a quantitative approach.
  
- ◇ Determine the function and localisation of human ras isoforms in *Sz. pombe*.

## CHAPTER 2

### Materials and methods

#### 2.1. Materials

##### 2.1.1. General laboratory reagents.

General laboratory reagents were purchased from Sigma-Aldrich Co. Ltd. (Poole, Dorset, UK), and were of analytical grade unless stated otherwise.

##### 2.1.2. Molecular biology reagents.

Restriction enzymes, T4 deoxyribonucleic acid (DNA) ligase and *Taq* DNA polymerase (from *Thermus aquaticus*) were purchased from Invitrogen Ltd. (Paisley, Scotland, UK). Bacterial alkaline phosphatase was supplied by Fermentas (York, UK). FastStart high fidelity DNA polymerase blend was purchased from Roche Diagnostics Ltd. (Lewes, East Sussex, UK). All oligonucleotides were synthesised by Invitrogen Ltd. Ultrapure agarose was supplied by Helena Biosciences (Gateshead, Tyne & Wear, UK).

##### 2.1.3. Gel documentation.

All gels were visualised using a G:Box iChemi gel documentation system (Syngene, Cambridge, UK), with GeneTools analysis software (Syngene).

#### 2.1.4. Cell number analysis.

Cell densities and cell volumes were analysed using a Z2 Coulter<sup>®</sup> Particle counter and Isoton II azide-free electrolyte, supplied by Beckman Coulter (Luton, Bedfordshire, UK).

#### 2.1.5. P-factor synthesis.

P-factor was synthesised using a Biotech Instruments BT7300 Peptide Synthesiser by AltaBioscience (University of Birmingham, Birmingham, UK).

#### 2.1.6. Growth media.

Yeast extract, select agar and Luria broth were purchased from Invitrogen Ltd. Constituents of Amino Acid selective medium (AA) and Defined Minimal Medium (DMM) (Davey *et al.* 1995) were supplied by Sigma-Aldrich Co. Ltd.. AA plates were used for selective growth and DMM liquid media for all assays and selective growth. Yeast Extract (YE) liquid media and plates were used for routine cell growth. Nutritional supplements were included as required (YEALU = YE medium supplemented with adenine, leucine and uracil). Plates were made with the addition of 1.5% select agar.

#### DMM

Per litre:

NH <sub>4</sub> Cl	5 g
Na <sub>2</sub> HPO <sub>4</sub>	2.2 g
Phthalic Acid	3 g
Glucose	20 g
Salts (50x stock)	10 ml
Vitamins (1,000x stock)	1 ml
Minerals (10,000x stock)	0.1 ml

To make selective DMM (components as required):

L-adenine	0.5 g
L-leucine	0.5 g
L-uracil	0.5 g

Stock solution of salts (50x). Per litre:

MgCl <sub>2</sub> .6H <sub>2</sub> O	52.5 g
CaCl <sub>2</sub> .2H <sub>2</sub> O	0.735 g
KCl	50 g
Na <sub>2</sub> SO <sub>4</sub>	2 g

Stock solution of minerals (10000x). Per 100 ml:

Citric acid	1 g
Boric acid	0.5 g
MnSO <sub>4</sub> .H <sub>2</sub> O	0.5 g
ZnSO <sub>4</sub> .7H <sub>2</sub> O	0.4 g
Molybdic acid	0.305 g
FeCl <sub>3</sub> .6H <sub>2</sub> O	0.2 g
KI	0.1 g
CuSO <sub>4</sub> .5H <sub>2</sub> O	0.04 g

Stock solution of vitamins (1000x). Per 100 ml:

Nicotinic acid	1 g
Inositol	1 g
Pantothenic acid	0.1 g
Biotin	0.001 g

**YE**

Per litre:

Yeast extract	5 g
Glucose	30 g

To make YEALU supplement with:

L-adenine	0.5 g
L-leucine	0.5 g
L-uracil	0.5 g

**AA**

Per litre:

Yeast Nitrogen base w/o a.a.	
containing $(\text{NH}_4)_2\text{SO}_4$	6.7 g
Glucose	20 g
Amino acid mix	1.5 g
Select amino acid mix	0.5 g

Amino acid mix:

L-alanine	2 g
L-asparagine	2 g
L-cysteine	2 g
L-glutamine	2 g
L-glutamic acid	2 g
L-glycine	2 g
L-isoleucine	2 g
L-lysine	2 g
L-phenylalanine	2 g
L-proline	2 g

L-serine	2 g
L-theonine	2 g
L-tryptophan	2 g
L-tyrosine	2 g
L-valine	2 g
Myo-inositol	2 g
Para-amino benzoic acid	0.4 g

Select amino acid mix (components as required):

L-adenine	0.5 g
L-histidine	2 g
L-leucine	0.5 g
L-methionine	2 g
L-uracil	0.5 g

### 2.1.7. Bacterial Strains.

Cloning was performed using the *Escherichia coli* (*E. coli*) strain DH5 $\alpha$  (Stratagene, Cambridge, UK).

*E. coli* DH5 $\alpha$  genotype: *supE44 hsdR17 endA96 thi-1 relA1 recA1 gyrA96*.

### 2.1.8. *Sz. pombe* strains.

Standard nomenclature has been used to describe all *Sz. pombe* strains presented in this thesis. Deletions within genes are referred to as *yfg1-D10*, denoting the deletion of 1000 base pairs (bp) of the *yfg1* locus. Replacement of genes using a selectable *ura4*<sup>+</sup> cassette is presented as *yfg1::ura4*<sup>+</sup>, and gene replacement as *yfg1::yfg2*. Reporter strains, in which expression of a reporter gene is regulated by the promoter of an endogenous gene at the endogenous locus, are referred to as *pro1>rep1*.

**Table 2.1.  $\beta$ -galactosidase reporter and mating assay yeast strains**

Strain	Genotype
JY278	<i>mat1-M</i> , $\Delta$ <i>mat2/3::LEU2<sup>-</sup></i> , <i>leu1-32</i> , <i>ura4-D18</i> , <i>cyr1-D51</i>
JY444	<i>mat1-M</i> , $\Delta$ <i>mat2/3::LEU2<sup>-</sup></i> , <i>leu1-32</i> , <i>ura4-D18</i>
JY544	<i>mat1-M</i> , $\Delta$ <i>mat2/3::LEU2<sup>-</sup></i> , <i>leu1<sup>-</sup></i> , <i>ade6-M216</i> , <i>ura4-D18</i> , <i>cyr1-D51</i> , <i>sxa2&gt;lacZ</i>
JY1025	<i>mat1-P</i> , $\Delta$ <i>mat2/3::LEU2<sup>-</sup></i> , <i>leu1<sup>-</sup></i> , <i>ura4-D18</i>
JY1247	<i>mat1-M</i> , $\Delta$ <i>mat2/3::LEU2<sup>-</sup></i> , <i>leu1<sup>-</sup></i> , <i>ade6-M216</i> , <i>ura4-D18</i> , <i>cyr1-D51</i> , <i>sxa2&gt;lacZ</i> , $\Delta$ <i>ras1::ura4<sup>+</sup></i>
JY1272	<i>mat1-M</i> , $\Delta$ <i>mat2/3::LEU2<sup>-</sup></i> , <i>leu1<sup>-</sup></i> , <i>ade6-M216</i> , <i>ura4-D18</i> , <i>cyr1-D51</i> , <i>sxa2&gt;lacZ</i> , $\Delta$ <i>ras1::ras1<sup>G17V</sup></i>
JY1279	<i>mat1-M</i> , $\Delta$ <i>mat2/3::LEU2<sup>-</sup></i> , <i>leu1<sup>-</sup></i> , <i>ade6-M216</i> , <i>ura4-D18</i> , <i>cyr1-D51</i> , <i>sxa2&gt;lacZ</i> , <i>ras1-D6</i>
JY1351	<i>mat1-P</i> , $\Delta$ <i>mat2/3::LEU2<sup>-</sup></i> , <i>leu1<sup>-</sup></i> , <i>ura4-D18</i> , $\Delta$ <i>ras1::ura4<sup>+</sup></i>
JY1378	<i>mat1-M</i> , $\Delta$ <i>mat2/3::LEU2<sup>-</sup></i> , <i>leu1<sup>-</sup></i> , <i>ade6-M216</i> , <i>ura4-D18</i> , <i>cyr1-D51</i> , <i>sxa2&gt;lacZ</i> , $\Delta$ <i>ras1::ras1<sup>C215S</sup></i>
JY1380	<i>mat1-M</i> , $\Delta$ <i>mat2/3::LEU2<sup>-</sup></i> , <i>leu1<sup>-</sup></i> , <i>ade6-M216</i> , <i>ura4-D18</i> , <i>cyr1-D51</i> , <i>sxa2&gt;lacZ</i> , $\Delta$ <i>ras1::ras1<sup>C216S</sup></i>
JY1382	<i>mat1-M</i> , $\Delta$ <i>mat2/3::LEU2<sup>-</sup></i> , <i>leu1<sup>-</sup></i> , <i>ade6-M216</i> , <i>ura4-D18</i> , <i>cyr1-D51</i> , <i>sxa2&gt;lacZ</i> , $\Delta$ <i>ras1::ras1-ritc</i>
JY1384	<i>mat1-M</i> , $\Delta$ <i>mat2/3::LEU2<sup>-</sup></i> , <i>leu1<sup>-</sup></i> , <i>ade6-M216</i> , <i>ura4-D18</i> , <i>cyr1-D51</i> , <i>sxa2&gt;lacZ</i> , $\Delta$ <i>ras1::ras1<sup>S22N</sup></i>
JY1386	<i>mat1-M</i> , $\Delta$ <i>mat2/3::LEU2<sup>-</sup></i> , <i>leu1<sup>-</sup></i> , <i>ade6-M216</i> , <i>ura4-D18</i> , <i>cyr1-D51</i> , <i>sxa2&gt;lacZ</i> , $\Delta$ <i>ras1::ras1ras1<sup>Q66L</sup></i>
JY1388	<i>mat1-M</i> , $\Delta$ <i>mat2/3::LEU2<sup>-</sup></i> , <i>leu1<sup>-</sup></i> , <i>ade6-M216</i> , <i>ura4-D18</i> , <i>cyr1-D51</i> , <i>sxa2&gt;lacZ</i> , $\Delta$ <i>ras1::ras1ras1<sup>Q66L, C215S</sup></i>
JY1461	<i>mat1-M</i> , $\Delta$ <i>mat2/3::LEU2<sup>-</sup></i> , <i>leu1<sup>-</sup></i> , <i>ade6-M216</i> , <i>ura4-D18</i> , <i>cyr1-D51</i> , <i>sxa2&gt;lacZ</i> , $\Delta$ <i>ras1::h-ras</i>
JY1462	<i>mat1-M</i> , $\Delta$ <i>mat2/3::LEU2<sup>-</sup></i> , <i>leu1<sup>-</sup></i> , <i>ade6-M216</i> , <i>ura4-D18</i> , <i>cyr1-D51</i> , <i>sxa2&gt;lacZ</i> , $\Delta$ <i>ras1::n-ras</i>
JY1463	<i>mat1-M</i> , $\Delta$ <i>mat2/3::LEU2<sup>-</sup></i> , <i>leu1<sup>-</sup></i> , <i>ade6-M216</i> , <i>ura4-D18</i> , <i>cyr1-D51</i> , <i>sxa2&gt;lacZ</i> , $\Delta$ <i>ras1::k-ras4b</i>

**Table 2.2.  $\beta$ -galactosidase reporter yeast strains containing integrated GFP tagged ras proteins**

Strain	Genotype
JY1390	<i>mat1-M</i> , $\Delta$ <i>mat2/3::LEU2<sup>-</sup></i> , <i>leu1<sup>-</sup></i> , <i>ade6-M216</i> , <i>ura4-D18</i> , <i>cyr1-D51</i> , <i>sxa2&gt;lacZ</i> , $\Delta$ <i>ras1::gfp-ras1</i>
JY1494	<i>mat1-M</i> , $\Delta$ <i>mat2/3::LEU2<sup>-</sup></i> , <i>leu1<sup>-</sup></i> , <i>ade6-M216</i> , <i>ura4-D18</i> , <i>cyr1-D51</i> , <i>sxa2&gt;lacZ</i> , $\Delta$ <i>ras1::gfp-ras1<sup>C216S</sup></i>
JY1495	<i>mat1-M</i> , $\Delta$ <i>mat2/3::LEU2<sup>-</sup></i> , <i>leu1<sup>-</sup></i> , <i>ade6-M216</i> , <i>ura4-D18</i> , <i>cyr1-D51</i> , <i>sxa2&gt;lacZ</i> , $\Delta$ <i>ras1::gfp-ras1<sup>Q66L</sup></i>
JY1496	<i>mat1-M</i> , $\Delta$ <i>mat2/3::LEU2<sup>-</sup></i> , <i>leu1<sup>-</sup></i> , <i>ade6-M216</i> , <i>ura4-D18</i> , <i>cyr1-D51</i> , <i>sxa2&gt;lacZ</i> , $\Delta$ <i>ras1::gfp-ras1<sup>G17V</sup></i>
JY1497	<i>mat1-M</i> , $\Delta$ <i>mat2/3::LEU2<sup>-</sup></i> , <i>leu1<sup>-</sup></i> , <i>ade6-M216</i> , <i>ura4-D18</i> , <i>cyr1-D51</i> , <i>sxa2&gt;lacZ</i> , $\Delta$ <i>ras1::gfp-ras1<sup>Q66L, C215S</sup></i>
JY1498	<i>mat1-M</i> , $\Delta$ <i>mat2/3::LEU2<sup>-</sup></i> , <i>leu1<sup>-</sup></i> , <i>ade6-M216</i> , <i>ura4-D18</i> , <i>cyr1-D51</i> , <i>sxa2&gt;lacZ</i> , $\Delta$ <i>ras1::1-40gpa1-gfp-ras1<sup>C215S</sup></i>
JY1499	<i>mat1-M</i> , $\Delta$ <i>mat2/3::LEU2<sup>-</sup></i> , <i>leu1<sup>-</sup></i> , <i>ade6-M216</i> , <i>ura4-D18</i> , <i>cyr1-D51</i> , <i>sxa2&gt;lacZ</i> , $\Delta$ <i>ras1::1-40gpa1-gfp-ras1<sup>C216S</sup></i>
JY1500	<i>mat1-M</i> , $\Delta$ <i>mat2/3::LEU2<sup>-</sup></i> , <i>leu1<sup>-</sup></i> , <i>ade6-M216</i> , <i>ura4-D18</i> , <i>cyr1-D51</i> , <i>sxa2&gt;lacZ</i> , $\Delta$ <i>ras1::1-40gpa1-gfp-ras1<sup>Q66L</sup></i>
JY1501	<i>mat1-M</i> , $\Delta$ <i>mat2/3::LEU2<sup>-</sup></i> , <i>leu1<sup>-</sup></i> , <i>ade6-M216</i> , <i>ura4-D18</i> , <i>cyr1-D51</i> , <i>sxa2&gt;lacZ</i> , $\Delta$ <i>ras1::1-40gpa1-gfp-ras1<sup>Q66L C215S</sup></i>
JY1502	<i>mat1-M</i> , $\Delta$ <i>mat2/3::LEU2<sup>-</sup></i> , <i>leu1<sup>-</sup></i> , <i>ade6-M216</i> , <i>ura4-D18</i> , <i>cyr1-D51</i> , <i>sxa2&gt;lacZ</i> , $\Delta$ <i>ras1::gfp-n-ras</i>
JY1503	<i>mat1-M</i> , $\Delta$ <i>mat2/3::LEU2<sup>-</sup></i> , <i>leu1<sup>-</sup></i> , <i>ade6-M216</i> , <i>ura4-D18</i> , <i>cyr1-D51</i> , <i>sxa2&gt;lacZ</i> , $\Delta$ <i>ras1::gfp-k-ras4b</i>
JY1518	<i>mat1-M</i> , $\Delta$ <i>mat2/3::LEU2<sup>-</sup></i> , <i>leu1<sup>-</sup></i> , <i>ade6-M216</i> , <i>ura4-D18</i> , <i>cyr1-D51</i> , <i>sxa2&gt;lacZ</i> , $\Delta$ <i>ras1::1-40gpa1-gfp-ras1<sup>S22N</sup></i>
JY1519	<i>mat1-M</i> , $\Delta$ <i>mat2/3::LEU2<sup>-</sup></i> , <i>leu1<sup>-</sup></i> , <i>ade6-M216</i> , <i>ura4-D18</i> , <i>cyr1-D51</i> , <i>sxa2&gt;lacZ</i> , $\Delta$ <i>ras1::gfp-ras1<sup>S22N</sup></i>
JY1521	<i>mat1-M</i> , $\Delta$ <i>mat2/3::LEU2<sup>-</sup></i> , <i>leu1<sup>-</sup></i> , <i>ade6-M216</i> , <i>ura4-D18</i> , <i>cyr1-D51</i> , <i>sxa2&gt;lacZ</i> , $\Delta$ <i>ras1::1-40gpa1-gfp-ras1</i>
JY1523	<i>mat1-M</i> , $\Delta$ <i>mat2/3::LEU2<sup>-</sup></i> , <i>leu1<sup>-</sup></i> , <i>ade6-M216</i> , <i>ura4-D18</i> , <i>cyr1-D51</i> , <i>sxa2&gt;lacZ</i> , $\Delta$ <i>ras1::gfp-ras1<sup>C215S</sup></i>
JY1571	<i>mat1-M</i> , $\Delta$ <i>mat2/3::LEU2<sup>-</sup></i> , <i>leu1<sup>-</sup></i> , <i>ade6-M216</i> , <i>ura4-D18</i> , <i>cyr1-D51</i> , <i>sxa2&gt;lacZ</i> , $\Delta$ <i>ras1::gfp-h-ras</i>

**Table 2.3. Yeast strains used to determine Tea1 localisation**

Strain	Genotype
JY1466	<i>mat1-M</i> , $\Delta$ <i>mat2/3::LEU2<sup>-</sup></i> , <i>leu1<sup>-</sup></i> , <i>ade6-M216</i> , <i>ura4-D18</i> , <i>cyr1-D51</i> , <i>sxa2&gt;lacZ</i> , <i>tea1-ura4</i>
JY1469	<i>mat1-M</i> , $\Delta$ <i>mat2/3::LEU2<sup>-</sup></i> , <i>leu1<sup>-</sup></i> , <i>ade6-M216</i> , <i>ura4-D18</i> , <i>cyr1-D51</i> , <i>sxa2&gt;lacZ</i> , <i>tea1::tea1-mcherry</i>
JY1504	<i>mat1-M</i> , $\Delta$ <i>mat2/3::LEU2<sup>-</sup></i> , <i>leu1<sup>-</sup></i> , <i>ade6-M216</i> , <i>ura4-D18</i> , <i>cyr1-D51</i> , <i>sxa2&gt;lacZ</i> , <i>tea1::tea1-mcherry</i> , $\Delta$ <i>ras1::ura4<sup>+</sup></i>
JY1505	<i>mat1-M</i> , $\Delta$ <i>mat2/3::LEU2<sup>-</sup></i> , <i>leu1<sup>-</sup></i> , <i>ade6-M216</i> , <i>ura4-D18</i> , <i>cyr1-D51</i> , <i>sxa2&gt;lacZ</i> , <i>tea1::tea1-mcherry</i> , $\Delta$ <i>ras1::ras1<sup>C215S</sup></i>
JY1506	<i>mat1-M</i> , $\Delta$ <i>mat2/3::LEU2<sup>-</sup></i> , <i>leu1<sup>-</sup></i> , <i>ade6-M216</i> , <i>ura4-D18</i> , <i>cyr1-D51</i> , <i>sxa2&gt;lacZ</i> , <i>tea1::tea1-mcherry</i> , $\Delta$ <i>ras1::ras1<sup>C216S</sup></i>
JY1507	<i>mat1-M</i> , $\Delta$ <i>mat2/3::LEU2<sup>-</sup></i> , <i>leu1<sup>-</sup></i> , <i>ade6-M216</i> , <i>ura4-D18</i> , <i>cyr1-D51</i> , <i>sxa2&gt;lacZ</i> , <i>tea1::tea1-mcherry</i> , $\Delta$ <i>ras1::ras1<sup>Q66L</sup></i>
JY1508	<i>mat1-M</i> , $\Delta$ <i>mat2/3::LEU2<sup>-</sup></i> , <i>leu1<sup>-</sup></i> , <i>ade6-M216</i> , <i>ura4-D18</i> , <i>cyr1-D51</i> , <i>sxa2&gt;lacZ</i> , <i>tea1::tea1-mcherry</i> , $\Delta$ <i>ras1::ras1<sup>G17V</sup></i>
JY1509	<i>mat1-M</i> , $\Delta$ <i>mat2/3::LEU2<sup>-</sup></i> , <i>leu1<sup>-</sup></i> , <i>ade6-M216</i> , <i>ura4-D18</i> , <i>cyr1-D51</i> , <i>sxa2&gt;lacZ</i> , <i>tea1::tea1-mcherry</i> , $\Delta$ <i>ras1::ras1<sup>Q66L C215S</sup></i>
JY1510	<i>mat1-M</i> , $\Delta$ <i>mat2/3::LEU2<sup>-</sup></i> , <i>leu1<sup>-</sup></i> , <i>ade6-M216</i> , <i>ura4-D18</i> , <i>cyr1-D51</i> , <i>sxa2&gt;lacZ</i> , <i>tea1::tea1-mcherry</i> , $\Delta$ <i>ras1::h-ras</i>
JY1511	<i>mat1-M</i> , $\Delta$ <i>mat2/3::LEU2<sup>-</sup></i> , <i>leu1<sup>-</sup></i> , <i>ade6-M216</i> , <i>ura4-D18</i> , <i>cyr1-D51</i> , <i>sxa2&gt;lacZ</i> , <i>tea1::tea1-mcherry</i> , $\Delta$ <i>ras1::k-ras4b</i>
JY1512	<i>mat1-M</i> , $\Delta$ <i>mat2/3::LEU2<sup>-</sup></i> , <i>leu1<sup>-</sup></i> , <i>ade6-M216</i> , <i>ura4-D18</i> , <i>cyr1-D51</i> , <i>sxa2&gt;lacZ</i> , <i>tea1::tea1-mcherry</i> , $\Delta$ <i>ras1::1-40gpa1-gfp-ras1<sup>C215S</sup></i>
JY1513	<i>mat1-M</i> , $\Delta$ <i>mat2/3::LEU2<sup>-</sup></i> , <i>leu1<sup>-</sup></i> , <i>ade6-M216</i> , <i>ura4-D18</i> , <i>cyr1-D51</i> , <i>sxa2&gt;lacZ</i> , <i>tea1::tea1-mcherry</i> , $\Delta$ <i>ras1::1-40gpa1-gfp-ras1<sup>C216S</sup></i>
JY1514	<i>mat1-M</i> , $\Delta$ <i>mat2/3::LEU2<sup>-</sup></i> , <i>leu1<sup>-</sup></i> , <i>ade6-M216</i> , <i>ura4-D18</i> , <i>cyr1-D51</i> , <i>sxa2&gt;lacZ</i> , <i>tea1::tea1-mcherry</i> , $\Delta$ <i>ras1::1-40gpa1-gfp-ras1<sup>Q66L</sup></i>
JY1515	<i>mat1-M</i> , $\Delta$ <i>mat2/3::LEU2<sup>-</sup></i> , <i>leu1<sup>-</sup></i> , <i>ade6-M216</i> , <i>ura4-D18</i> , <i>cyr1-D51</i> , <i>sxa2&gt;lacZ</i> , <i>tea1::tea1-mcherry</i> , $\Delta$ <i>ras1::1-40gpa1-gfp-ras1<sup>Q66L C215S</sup></i>
JY1516	<i>mat1-M</i> , $\Delta$ <i>mat2/3::LEU2<sup>-</sup></i> , <i>leu1<sup>-</sup></i> , <i>ade6-M216</i> , <i>ura4-D18</i> , <i>cyr1-D51</i> , <i>sxa2&gt;lacZ</i> , <i>tea1::tea1-mcherry</i> , $\Delta$ <i>ras1::1-40gpa1-gfp-ras1<sup>S22N</sup></i>
JY1517	<i>mat1-M</i> , $\Delta$ <i>mat2/3::LEU2<sup>-</sup></i> , <i>leu1<sup>-</sup></i> , <i>ade6-M216</i> , <i>ura4-D18</i> , <i>cyr1-D51</i> , <i>sxa2&gt;lacZ</i> , <i>tea1::tea1-mcherry</i> , $\Delta$ <i>ras1::ras1<sup>S22N</sup></i>
JY1522	<i>mat1-M</i> , $\Delta$ <i>mat2/3::LEU2<sup>-</sup></i> , <i>leu1<sup>-</sup></i> , <i>ade6-M216</i> , <i>ura4-D18</i> , <i>cyr1-D51</i> , <i>sxa2&gt;lacZ</i> , <i>tea1::tea1-mcherry</i> , $\Delta$ <i>ras1::ras1</i>
JY1569	<i>mat1-M</i> , $\Delta$ <i>mat2/3::LEU2<sup>-</sup></i> , <i>leu1<sup>-</sup></i> , <i>ade6-M216</i> , <i>ura4-D18</i> , <i>cyr1-D51</i> , <i>sxa2&gt;lacZ</i> , <i>tea1::tea1-mcherry</i> , <i>ras1-D6</i>
JY1570	<i>mat1-M</i> , $\Delta$ <i>mat2/3::LEU2<sup>-</sup></i> , <i>leu1<sup>-</sup></i> , <i>ade6-M216</i> , <i>ura4-D18</i> , <i>cyr1-D51</i> , <i>sxa2&gt;lacZ</i> , <i>tea1::tea1-mcherry</i> , $\Delta$ <i>ras1::n-ras</i>

The *cyr1* gene encodes adenylate cyclase. Disruption of this open reading frame (ORF) allows *Sz. pombe* to undergo sexual differentiation during the mitotic growth cycle (Maeda *et al.* 1990).

The *sxa2* ORF encodes a secreted serine carboxypeptidase which degrades exogenous P-factor (Ladds *et al.* 1996; Ladds and Davey 2000). Loss of Sxa2 prolongs the response to P-factor stimulation, and increases signalling activity in reporter strains (Didmon *et al.* 2002).

*mat1-M Δmat2/3* strains are mating type stable M cells. Deletion of the *mat2* and *mat3* loci prevents mating type switching (Klar and Miglio 1986). *mat1-P Δmat2/3* strains are P cells incapable of switching mating type.

JY544 is an *sxa2>lacZ* reporter strain, in which activation of the pheromone-response pathway by P-factor results in the production of  $\beta$ -galactosidase.

#### **2.1.9. *Sz. pombe* genomic integration.**

Selection for the loss of *ura4*, upon replacement with sequence of interest, was performed using AA medium containing limited uracil (450  $\mu$ M) and 4.5 mM 5-fluoro-orotic acid (FOA, supplied by Toronto Research Chemicals Inc. Ontario, Canada). FOA is converted by Ura4 into the toxic uracil analogue 5-fluoro-uracil (Grimm *et al.* 1988).

## 2.2. Methods

### 2.2.1. Cloning techniques.

DNA preparation was performed using standard methods (Sambrook *et al.* 1989). All DNA modifying enzymes were used according to manufacturer's instructions. DNA fragments were analysed by electrophoresis on 1-3 % agarose gels containing 0.5 µg/ml ethidium bromide. DNA fragments were recovered from agarose gels using the QIAquick Gel Extraction Kit (Qiagen, West Sussex, UK).

### 2.2.2. Transformation of *E. coli*.

Competent *E. coli* DH5α (Stratagene) were produced and transformed as described in Sambrook *et al.* (1989).

### 2.2.3. Transformation of *Sz. pombe*.

*Sz. pombe* was transformed with plasmid DNA or linear DNA fragments using the lithium acetate method described by Okazaki *et al.* (1990).

### 2.2.4. Polymerase chain reaction (PCR).

*Taq* DNA polymerase (Invitrogen Ltd.) was used for screening bacterial colonies and yeast strains. FastStart high fidelity polymerase blend (Roche Diagnostics Ltd.) was used for amplifying DNA fragments for cloning. All polymerases were used according to manufacturer's instructions.

2.2.4.1. *PCR amplification of DNA for cloning.* A total reaction volume of 50  $\mu$ l was used, containing 1  $\mu$ g of sense and antisense oligonucleotide primer each, and 10-50 ng of template DNA. Deoxyribonucleoside triphosphates (dNTPs) (dATP, dCTP, dGTP and dTTP, Fermentas) were used at a final concentration of 0.2 mM. The PCR cycle consisted of a denaturation step of 94 °C held for 30 s, followed by an annealing step of between 40 and 60 °C held for 60 s. The extension step (72 °C) was held for 60 s per kilobase of product. 30 cycles of amplification were used per reaction. Reactions were concluded with 7 min incubation at 72 °C to allow complete product extension.

2.2.4.2. *Screening plasmid DNA from bacterial cells using PCR.* A single bacterial colony was suspended in 100  $\mu$ l of water and stored at 4 °C. 1  $\mu$ l of this suspension was used as the template in a 10  $\mu$ l PCR reaction.

2.2.4.3. *Screening yeast genomic DNA using PCR.* 1  $\mu$ l of yeast genomic DNA (200-400ng) was used as the template in a 10  $\mu$ l PCR reaction.

### **2.2.5. DNA sequencing.**

Plasmid DNA was sequenced by the Molecular Biology Service at the University of Warwick. Reactions utilised Big Dye Terminator 3.1 chemistry (Applied Biosystems, Foster City, CA, USA) and were run on a 3100 Genetic Analyser (Applied Biosystems).

### **2.2.6. Preparation of yeast genomic DNA.**

Genomic DNA was isolated from yeast using the protocol described in Hoffman and Winston (1987). Cells were grown to a density of  $\sim 1 \times 10^7$  cells/ml, harvested by centrifugation and washed once in sterile water. Cells were then resuspended in 200  $\mu$ l of Blue Buffer (2% Triton X-100, 1% sodium dodecyl

sulphate (SDS), 100 mM NaCl, 10 mM Tris-HCl (pH 8.0) and 1 mM ethylenediaminetetraacetic acid (EDTA)). 200  $\mu$ l of 1:1 phenol:chloroform and 400  $\mu$ l acid-washed glass beads (425-600  $\mu$ m diameter, Sigma-Aldrich Co. Ltd.) were added and the suspension was mixed for 3 min using a vortex mixer to promote cell lysis. 200  $\mu$ l Tris-EDTA (TE) (pH 7.5) was then added immediately, and the solid and aqueous phases were separated by centrifugation for 5 min at 13000 rpm, 4 °C. The aqueous phase was then transferred to 1 ml of ice-cold ethanol. The sample was mixed by inversion and genomic DNA was harvested by centrifugation for 10 min at 13000 rpm, 4 °C. The DNA pellet was washed with 70% ethanol, dried and resuspended in 50  $\mu$ l of TE (pH 7.5). The typical yield for this method is 10-20  $\mu$ g DNA.

#### 2.2.7. $\beta$ -galactosidase assays.

$\beta$ -galactosidase assays were performed using a method modified from Dohlman *et al.* (1995) (Didmon *et al.* 2002). *Sz. pombe* cells were cultured to a density of  $\sim 5 \times 10^5$  cells/ml in DMM. 500  $\mu$ l of cell culture was transferred to 2 ml Safe-Lock Eppendorf tubes (Eppendorf Ltd. Hamburg, Germany) containing varying concentrations of P-factor (diluted in high performance liquid chromatography (HPLC)-grade methanol and dried to remove the methanol). Tubes were then incubated at 29 °C for 16 h on a rotating wheel. 50  $\mu$ l was transferred to 750  $\mu$ l of Z-buffer containing 2.25 mM o-nitrophenyl- $\beta$ -D-galactopyranoside (ONPG, purchased from Sigma-Aldrich Co. Ltd.) and the reactions were incubated on a rotating wheel at 29 °C for 90 min. Reactions were stopped by the addition of 200  $\mu$ l of 2 M  $\text{Na}_2\text{CO}_3$ .  $\beta$ -galactosidase production was determined through measuring the accumulation of the coloured product ortho-nitrophenol (optical density (OD) at 420 nm), and expressed as  $\text{OD}_{420}$  per  $10^6$  cells (determined using a Z2 Coulter<sup>®</sup> Particle counter, Beckman Coulter).

***Z-buffer:***

60 mM Na<sub>2</sub>HPO<sub>4</sub>  
42 mM NaH<sub>2</sub>PO<sub>4</sub>  
10 mM KCl  
1 mM MgSO<sub>4</sub>  
50 mM β-mercaptoethanol  
0.5% (v/v) chloroform  
0.005% (w/v) SDS

**2.2.8. Yeast mating assays.**

Cells were cultured in liquid DMM to a density of  $\sim 5 \times 10^6$  cells/ml. 200  $\mu$ l of each mating type strain were mixed and harvested by centrifugation (2000 rpm for 3 min). Cells were resuspended in 10  $\mu$ l of sterile water and spotted onto DMM plates containing 100-fold lower NH<sub>4</sub>Cl than detailed in section 2.1.7. All assays also included separate non-mixed controls. Following 72 h incubation at 29 °C, plates were exposed to iodine crystals for 10 min, or until staining could be observed. Iodine staining of the starch contained within spore cell walls resulted in brown/black colony colouration, indicating mating (Egel *et al.* 1994).

**2.2.9. Fluorescence microscopy.**

Strains were cultured in the appropriate medium to a density of  $\sim 5 \times 10^6$  cells/ml. 5  $\mu$ l of cell culture was transferred directly to a CoverWell<sup>TM</sup> imaging chamber (Grace Bio-Labs, Oregon, USA) containing solid DMM (2% agarose), and residual liquid media was allowed to dry. Slides were covered and sealed and images were then obtained using a True Confocal Scanner Leica TCS SP5 microscope (Leica Microsystems Ltd. Milton Keynes, UK) or Nikon E800 epi-fluorescence microscope (Nikon UK Ltd. Kingston upon Thames, UK) fitted

with an Andor EM-CCD camera (Andor Technology Ltd. Belfast, Ireland).

#### **2.2.10. Image analysis.**

All image processing was performed using the open source software Image J (<http://rsb.info.nih.gov/ij/>). Cell segmentation was performed using the BOA plug-in of Image J, and image analysis using the Quantitative Imaging of Membrane Proteins (Quimp) package (Dormann *et al.* 2002; Bosgraaf *et al.* 2009).

#### **2.2.11. Western blot analysis.**

2.2.11.1. *Preparation of yeast whole cell extracts.* 10 ml of mid-log phase cell culture ( $\sim 1 \times 10^7$  cells/ml), cultured in the relevant media, was harvested by centrifugation (2000 rpm for 5 min) and washed once with TEN buffer (100 mM Tris (pH 6.8), 10 mM EDTA, 150 mM NaCl). Cells were then resuspended in 50  $\mu$ l TEN buffer containing protease inhibitors (1 Complete Mini protease inhibitor tablet, supplied by Roche Diagnostics Ltd. dissolved in 1.5ml of TEN buffer). Acid-washed glass beads (400  $\mu$ l) were added, cells were lysed by vortex mixing for 3 min, and 50  $\mu$ l of TEN buffer was added. 100  $\mu$ l of SDS-polyacrylamide gel electrophoresis (SDS-PAGE) sample buffer (125 mM Tris (pH 6.8), 8% glycerol, 5% SDS, 1%  $\beta$ -mercaptoethanol, 0.02% bromophenol blue) was added to each whole cell extract, and samples were heated at 100 °C for 5 min prior to SDS-PAGE (Ladds *et al.* 2003).

2.2.11.2. *SDS-PAGE.* SDS polyacrylamide gels were cast and run using a Geneflow OmniPAGE Mini vertical gel electrophoresis unit (Geneflow Ltd. Staffordshire, U.K.) according to the manufacturer's instructions.

2.2.11.3. *Western blot analysis.* Following separation by SDS-PAGE, protein was transferred to polyvinylidene difluoride (PVDF) membrane (Bio-Rad, Hemel Hempstead, UK) soaked in Half Towbin buffer (192 mM glycine, 25 mM Tris,

1.3 mM SDS and 10 % methanol) using an OmniBlot wet blotting unit (Gene-flow Ltd.) run at 60 mV for 1 h, with the membrane and gel placed between 3 layers of filter paper immersed in Half Towbin buffer. The membrane was blocked with 3 % Marvel (non-fat dried milk) in PBST (137 mM NaCl, 2.7 mM KCl, 8 mM Na<sub>2</sub>HPO<sub>4</sub>, 2 mM KH<sub>2</sub>PO<sub>4</sub>, 0.05 % (v/v) Tween 20 pH 7.4) for 2 h. The PVDF membrane was then incubated with primary antibody in PBST containing 3% Marvel overnight at 4°C with constant aggitation. The membrane was washed twice with water, and hybridised with the secondary antibody (in PBST containing 3 % Marvel) for 90 min at room temperature with constant aggitation. The membrane was then washed twice with water and once with PBST for 5 min. Signals were then detected using enhanced chemiluminescence (ECL) detection reagent (GE healthcare, Buckinghamshire, UK) and visualised using a G:Box iChemi gel documentation system (Syngene). A primary RAS10 anti-ras mouse monoclonal antibody (Millipore, Durham, UK) and secondary horseradish peroxidase-conjugated anti-mouse IgG antibody (Promega, Southampton, UK) were used for detection of ras proteins. A primary anti-fluorescent protein rabbit polyclonal antibody, raised against GFP, (Santa Cruz biotechnology, California, USA) and a secondary horseradish peroxidase-conjugated anti-rabbit IgG antibody (GE healthcare) were used for detection of fluorescent proteins.

2.2.11.4. *Staining with Coomassie Brilliant Blue.* Following SDS-PAGE, gels were placed in Coomassie Brilliant Blue stain (40% ethanol, 10% acetic acid, 0.2% Coomassie Brilliant Blue R250) and incubated for 30 min with constant agitation, to provide loading controls. The gel was then transferred to destain solution (40% ethanol, 10% acetic acid), and incubated until completely destained and bands were visible. Gels were visualised using a G:Box iChemi gel documentation system (Syngene).

### 2.2.12. Flow cytometric analysis of cell cycle position.

Cells were grown in the relevant culture medium to a density of  $\sim 1 \times 10^7$  cells/ml. 1 ml of culture was sonicated, harvested by centrifugation and fixed in 1 ml of ice cold 70% ethanol overnight. 300  $\mu$ l of fixed cells were then washed in 3 ml of 50 mM sodium citrate and resuspended in 500  $\mu$ l of 50 mM sodium citrate containing 0.1 mg/ml RNase A. Cells were incubated at 37 °C for 2 h before the addition of 500  $\mu$ l of 50 mM sodium citrate containing 8  $\mu$ g/ml propidium iodide. Flow cytometry was performed using a Becton, Dickinson and Company (BD) LSR II flow cytometer (BD Biosciences, Oxford, UK). Excitation was achieved using a 488 nm laser, and emission detected using a 575/26 band pass filter with a 550 long pass filter.

### 2.2.13. LIVE/DEAD<sup>®</sup> assay for cell viability.

Analysis of cell viability was performed using the LIVE/DEAD<sup>®</sup> *Funga* Light<sup>TM</sup> yeast viability kit (Invitrogen Ltd.). The protocol used the nucleic acid stains SYTO<sup>®</sup> 9 (green) and propidium iodide (red). SYTO<sup>®</sup> 9 labels all cells within a population and propidium iodide only labels those with damaged membranes. In cells with damaged membranes both dyes are present and SYTO<sup>®</sup> 9 fluorescence is reduced due to fluorescence resonance energy transfer (FRET) between the two dyes, causing cells with intact membranes to fluoresce green and cells with damaged membranes to fluoresce red (Zhang and Fang 2004).

Cells were cultured to a density of  $\sim 5 \times 10^5$  cells/ml in DMM. 500  $\mu$ l aliquots of cell culture were transferred to 2 ml Safe-Lock Eppendorf tubes (Eppendorf Ltd.) containing varying concentrations of P-factor pheromone (diluted in high performance liquid chromatography (HPLC)-grade methanol and dried to remove the methanol). Tubes were incubated at 29 °C for 16 h on a rotating wheel. The cells were washed twice with 1 ml of PBS and were then stained in 1 ml of PBS with 1  $\mu$ l of SYTO<sup>®</sup> 9 (3.34mM in dimethyl sulfoxide) and 1  $\mu$ l of propidium iodide (20mM in dimethyl sulfoxide). Flow cytometry

was performed using a BD LSR II flow cytometer. Excitation of both dyes was achieved using a 488 nm blue laser, and emission was detected using a 550 nm long pass filter with a 575/26 nm band pass filter for propidium iodide and a 505 nm long pass filter with a 530/30 nm band pass filter for SYTO<sup>®</sup> 9.

#### 2.2.14. Chromosome instability assay.

The fission yeast strain 2125 (Tinline-Purvis *et al.* 2009) contains the minichromosome Ch16, a non-essential 530kb derivative of chromosome III (Niwa *et al.* 1989). 2125 contains the mutation *ade6-210* on chromosome III and the complementary mutation *ade6-216* on Ch16 to rescue *ade6* activity. Loss of Ch16 results in an *ade<sup>-</sup>* phenotype and the formation of red colonies in the absence of exogenous adenine. To determine the rate of minichromosome loss, cells were cultured overnight in DMM lacking adenine and diluted to an OD<sub>600</sub> of 0.2 the following day. Cells were then grown to an OD<sub>600</sub> of 0.8, diluted 1 in 1000 in sterile water, and 100 µl of this dilution was then plated on YE plates lacking additional adenine. The presence of colonies displaying red and white sectors indicates the loss of the minichromosome in a subpopulation of cells within that colony. The presence of colonies displaying over half red colouration indicates the loss of Ch16 in the first division of that colony, allowing determination of minichromosome loss per division (Allshire *et al.* 1995).

2125 genotype: Ch3 *ade6-210, leu1-32, ura4-D18, his3-D1, arg3-D4 (h+)*.  
Ch16 *yps1::arg3, ert1::MATaG418, ade6-216, cid2::his3*.

#### 2.2.15. Analysis of data.

Non-linear regression of dose-response data and statistical analysis was completed using GraphPad Prism software version 4.03 for Windows (GraphPad Software Inc. San Diego, CA, USA). Statistical significance was determined using a one-way anova with a Tukey multiple comparison post test or an unpaired t test.

## CHAPTER 3

### Creation of DNA constructs

#### 3.1. Creation pREP3x expression constructs

This section details the construction of plasmids for the expression of proteins under the control of the *nmt1* promoter of pREP3x (Maundrell 1993).

##### 3.1.1. Creation of pREP3x-ras constructs.

The pREP vectors were constructed to allow the controlled expression of exogenous genes in *Sz. pombe* from a promoter that can be readily induced. To express ras proteins from the *nmt1* (no message in thiamine) promoter, the ORF in question was cloned into pREP3x. This allows control over the expression of each ras protein by the addition or removal of thiamine from the growth medium (Maundrell 1993). Each *ras* ORF was amplified using a sense oligonucleotide which started at the initiating ATG codon. The anti-sense oligonucleotide used in each case contained a full *Bam*HI site directly upstream of the endogenous stop anticodon. The PCR products were digested with *Bam*HI and ligated into *Eco*RV and *Bam*HI digested pREP3x, modified to contain an *Eco*RV site directly upstream of the *Bam*HI site (Figure 3.1). Human *ras* ORFs were amplified from cDNA clones obtained from the Guthrie cDNA Resource Centre ([www.cdna.org](http://www.cdna.org)). The *ras1-ritc* fusion was amplified from pRPGFP-Ras1-RitC, kindly supplied by Prof. Eric Chang (State University of New York at Buffalo). The pKS-Ras1 and pREP3x-Ras1 constructs used for the creation of all the *ras1* constructs used in this study, which lack the intron found in endogenous *ras1*, were created by Dr. Rachel Forfar. The oligonucleotides used for PCR amplification of *ras* ORFs are listed in table 3.1.

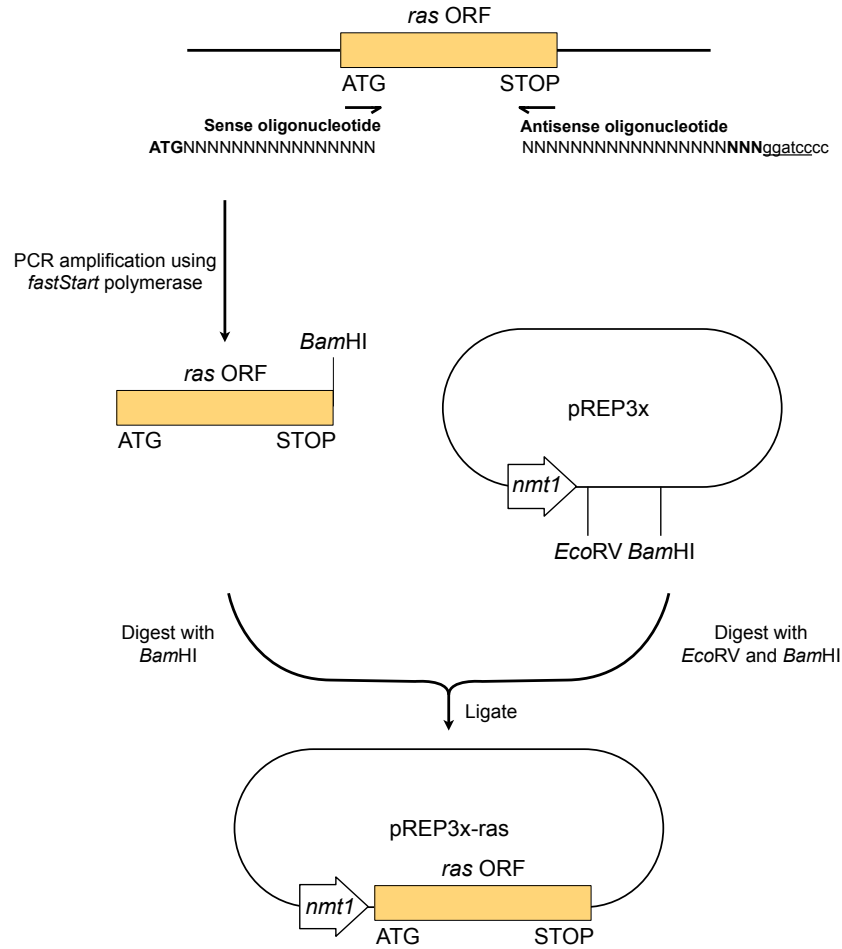


**Figure 3.1. Cloning of *ras* ORFs into pREP3x**

*ras* ORFs were amplified using the oligonucleotides listed in table 3.1. The amplified products were then digested with *Bam*HI and ligated into *Eco*RV and *Bam*HI digested pREP3x, modified to contain an *Eco*RV site directly upstream of the *Bam*HI site.

**Table 3.1. Oligonucleotides for amplification of *ras* ORFs**

<i>ras</i> ORF	Sense oligonucleotide	Antisense oligonucleotide
<i>ras1</i>	<b>ATG</b> AGG TCT ACC TAC TTA AGA GAG	ggggatcc <b>CTA</b> ACA TAT AAC ACA ACA
<i>ras1-ritc</i>	<b>ATG</b> AGG TCT ACC TAC TTA AGA GAG	ggggatcc <b>TCA</b> AGT TAC TGA ATC TTT CTT CT
<i>h-ras</i>	<b>ATG</b> ACG GAA TAT AAG C	ggggatcc <b>TCA</b> GGA GAG CAC ACA CTT GC
<i>n-ras</i>	<b>ATG</b> ACT GAG TAC AAA CTG	ggggatcc <b>TTA</b> CAT CAC CAC ACA TGG CAA TC
<i>k-ras4b</i>	<b>ATG</b> ACT GAA TAT AAA CTT G	ggggatcc <b>TTA</b> CAT AAT TAC ACA CTT TGT C

### 3.1.2. Cloning of pREP3x-GFP-ras.

Direct in-frame N-terminal *gfp-ras* fusions were made in pREP3x to allow the visualisation of ras localisation upon expression from the *nmt1* promoter. *ras* ORFs were amplified using the method detailed in section 3.1.1 and the oligonucleotides listed in table 3.1. The amplified *ras* ORFs were then digested with *Bam*HI and ligated into pREP3x-Nterm-GFP digested with *Eco*RV and *Bam*HI. The pREP3x-Nterm-GFP vector contains the *gfp* ORF lacking a stop codon, and contains an *Eco*RV immediately following the final codon of the *gfp* ORF followed by a *Bam*HI site (Dr. Claire Hill). As a consequence, ligation a *ras* ORF between the *Eco*RV and *Bam*HI sites generates a direct in-frame fusion separated by just one codon (GAT = Asn), resulting from the remaining half of the *Eco*RV site.

### 3.1.3. Generating 1-40gpa1-gfp-ras1 fusions in pREP3x.

*1-40gpa1-gfp-ras1* fusions were generated using a two step strategy. The first step was to generate a pREP3x vector containing the *1-40gpa1-gfp* fusion but lacking a stop codon. The second step was to generate the *1-40gpa1-gfp-ras1* fusion by subcloning the *ras1* ORF from existing *gfp-ras1* fusions utilising an endogenous *Nco*I site in the *gfp* ORF. A construct had previously been made containing the first 40 codons of the *gpa1* ORF followed by the *gfp* ORF (*1-40gpa1-gfp*) (Dr. Emma Godfrey). In order to allow expression of *1-40gpa1-gfp-ras1* fusion from pREP3x, *1-40gpa1-gfp* was amplified using a sense oligonucleotide beginning at the initiating ATG of *gpa1* (**ATG** GGA TGC ATG TCG AGT AAA TAC GC) and an antisense oligonucleotide containing a full *Bam*HI site immediately prior to the final coding anticodon of *gfp*, but lacking the endogenous stop anticodon (ggggatcc TTT GTA TAG TTC ATC CA). The PCR product was digested with *Bam*HI and ligated into *Eco*RV and *Bam*HI digested pREP3x (Figure 3.3).

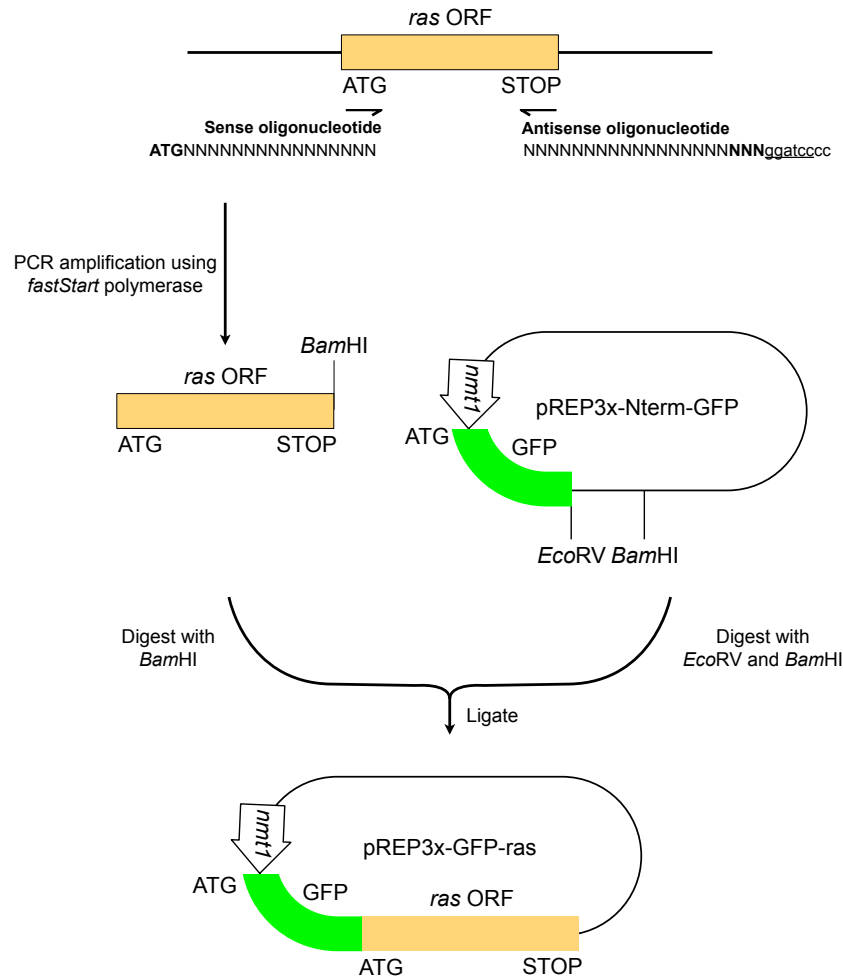


**Figure 3.2. Cloning of pREP3x-GFP-ras**

*ras* ORFs were amplified using the oligonucleotides listed in table 3.1. The amplified products were then digested with *Bam*HI and ligated into *Eco*RV and *Bam*HI digested pREP3x-Nterm-GFP, containing the *gfp* ORF lacking a stop codon directly upstream of an *Eco*RV site and *Bam*HI site.

pREP3x-1-40Gpa1-GFP-Ras1 was then generated by digesting pREP3x-GFP-Ras1 with *Nco*I and *Bam*HI, utilising an endogenous *Nco*I site in *gfp*, to yield a 3' portion of the *gfp* ORF fused to the whole *ras1* ORF. The pREP3x-1-40Gpa1-GFP construct detailed in Figure 3.3 was also digested with *Nco*I and *Bam*HI to yield linearised pREP3x containing 1-40*gpa1* fused to the 5' portion of the *gfp* ORF. Ligation of these two products reconstituted the *gfp* ORF, generating pREP3x-1-40Gpa1-GFP-Ras1 (Figure 3.4).

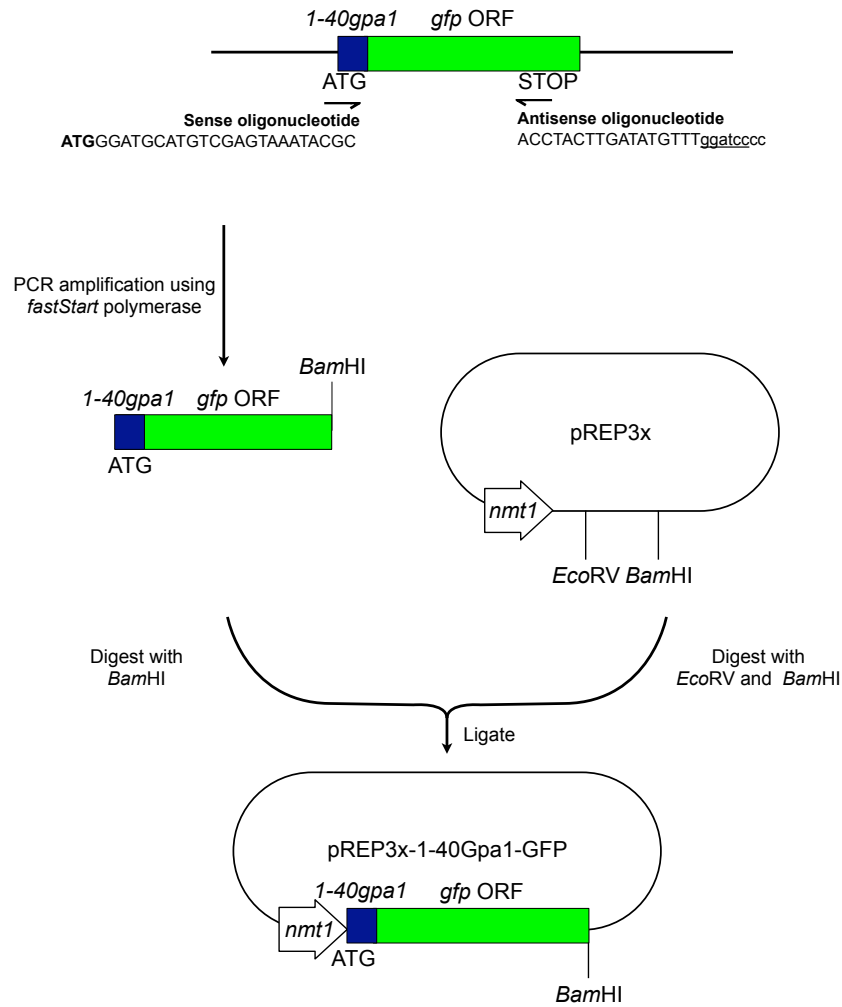


**Figure 3.3. Cloning of pREP3x-1-40Gpa1-GFP**

*1-40gpa1-gfp* was amplified from a pre-existing construct using a sense oligonucleotide beginning at the initiating ATG (ATG GGA TGC ATG TCG AGT AAA TAC GC) and an antisense oligonucleotide containing a full *Bam*HI site but lacking a stop anticodon (gggatcc TTT GTA TAG TTC ATC CA). The amplified product was then digested with *Bam*HI and ligated into *Eco*RV and *Bam*HI digested pREP3x, modified to contain an *Eco*RV site directly upstream of the *Bam*HI site.

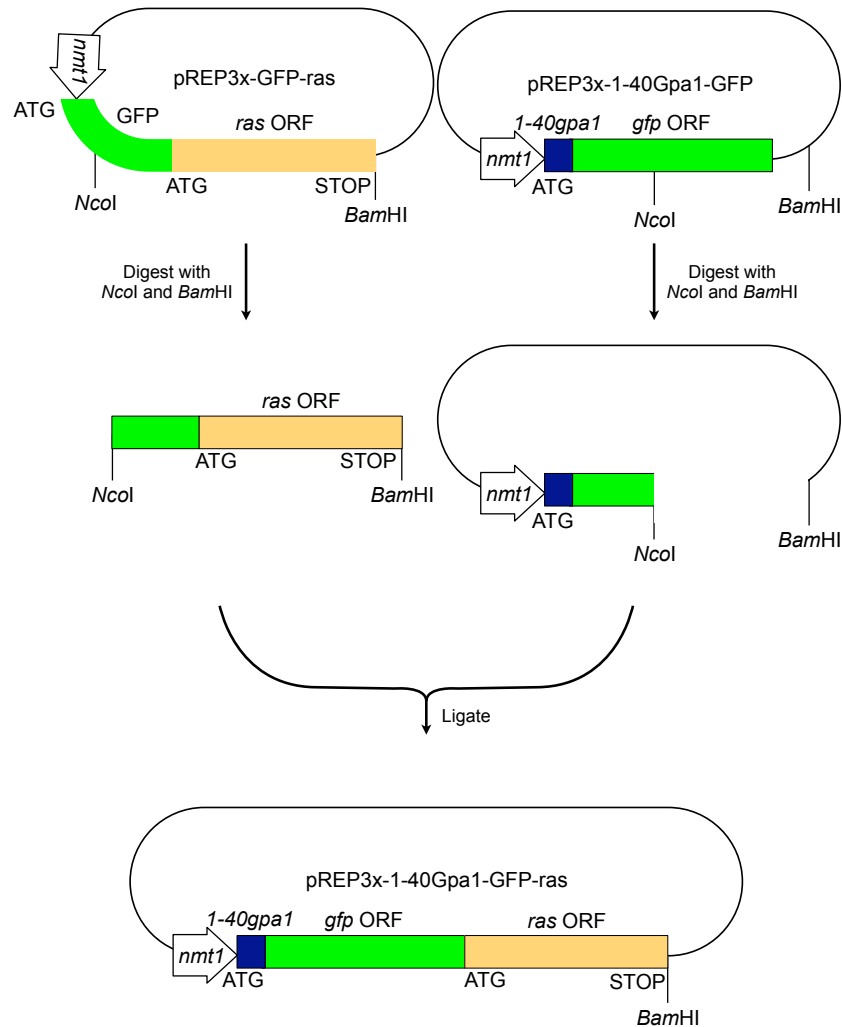


**Figure 3.4. Cloning of pREP3x-1-40Gpa1-GFP-Ras1**  
 pREP3x-GFP-Ras1 was digested with *NcoI* and *BamHI* to generate a 3' portion of the *gfp* ORF fused to the *ras1* ORF. pREP3x-1-40Gpa1-GFP was digested with *NcoI* and *BamHI* to generate linearised pREP3x containing 1-40gpa1 fused to the 5' portion of the *gfp* ORF. These two products were ligated together to generate pREP3x-1-40Gpa1-GFP-Ras1.

### 3.2. Mutagenesis of *ras1*

#### 3.2.1. Mutating *ras1* by inverse PCR.

To allow more detailed analysis of Ras1 function, a number of mutants were created with differing nucleotide binding and hydrolysis activities. Mutants were created by inverse PCR using a pKS-Ras1 template, in which the pKS vector has been modified to contain the pREP vector multi-cloning site (JD1766). Inverse PCR was performed using a sense oligonucleotide within the ORF and an antisense oligonucleotide beginning immediately 5' to the sense oligonucleotide,

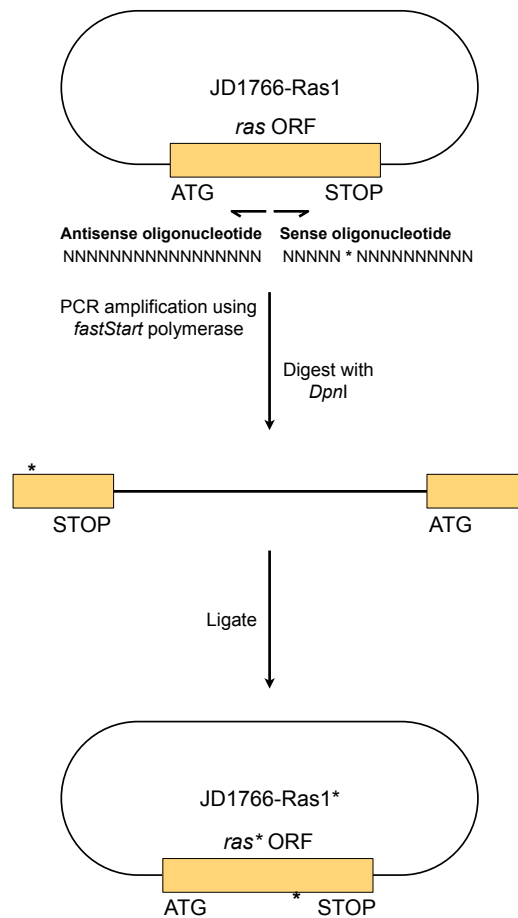
in which one of the two oligonucleotides contains the desired point mutation. The PCR product was then digested with *DpnI* to remove methylated template DNA (Sullivan and Folk 1988) and ligated to reconstitute the circular vector (Figure 3.5). Mutated *ras1* ORFs were then cloned into pREP3x using the method described in Figure 3.1 and fused with *gfp* using the method described in Figure 3.2. Creation of *1-40gpa1-gfp-ras1* fusions was performed as in Figure 3.4. The oligonucleotides used are given in table 3.2. Creation of *ras1*<sup>G17V</sup> was performed by Dr. Rachel Forfar.

### 3.2.2. Mutating *ras1* using mutagenic cloning oligonucleotides.

The residues involved in Ras1 post-translational modification are found at the far C-terminus of the protein. As a consequence, mutations which prevent these processes can be introduced using an antisense cloning oligonucleotide containing the desired mismatch. The *ras1* ORF was amplified using a sense oligonucleotide beginning at the initiating ATG codon (**ATG** AGG TCT ACC TAC TTA AGA GAG) and an antisense oligonucleotide containing the desired mismatch, and a *Bam*HI site immediately prior to the endogenous stop anticodon (*ras1*<sup>C215S</sup> = ggggatcc **CTA** CAT ATA ACA CAA CTT TTA GTT GA; *ras1*<sup>C216S</sup> = ggggatcc **CTA** CAT ATA ACA CTA CAT TTA G). The PCR products were digested with *Bam*HI and ligated into *Eco*RV and *Bam*HI digested pREP3x, modified to contain an *Eco*RV site directly upstream of the *Bam*HI site (Figure 3.6). *ras1*<sup>Q66L, C215S</sup> was created by amplification of *ras1*<sup>Q66L</sup> using the *ras1*<sup>C215S</sup> oligonucleotides. These mutant ORFs were fused to *gfp* using the method described in Figure 3.2, following amplification with the mutagenic antisense oligonucleotide described above. Creation of *1-40gpa1-gfp-ras1* fusions was performed as in Figure 3.4.

**Table 3.2. Oligonucleotides for mutating *ras1* by inverse PCR**

<i>ras</i> ORF	Sense oligonucleotide	Antisense oligonucleotide
<i>ras1</i> <sup>S22N</sup>	GGT GGT GTT GGT AAA AAT GCT TTG	ATC TCC TAC AAC TAC CAA TTT G
<i>ras1</i> <sup>Q66L</sup>	GAC ACG GCC GGT CTA GAG GAA TA	AAG GTG CGC TTT TAG ATG TAT TG
<i>ras1</i> <sup>G17V</sup>	T GGT GTT GGT AAA AGT GC	AC ATC TCC TAC AAC TAC CA

**Figure 3.5. Mutating *ras1* using inverse PCR**

The mutations *ras1*<sup>S22N</sup>, *ras1*<sup>Q66L</sup> and *ras1*<sup>G17V</sup> were created using inverse PCR. PCR amplification was performed on pKS-Ras1 using sense oligonucleotide within the ORF and an antisense oligonucleotide beginning immediately 5' to the sense oligonucleotide, in which one of the two oligonucleotides contains the desired point mutation, denoted by a \* (Table 3.2). The product was then digested with *DpnI* to remove template DNA and ligated to reconstitute the circularised vector.

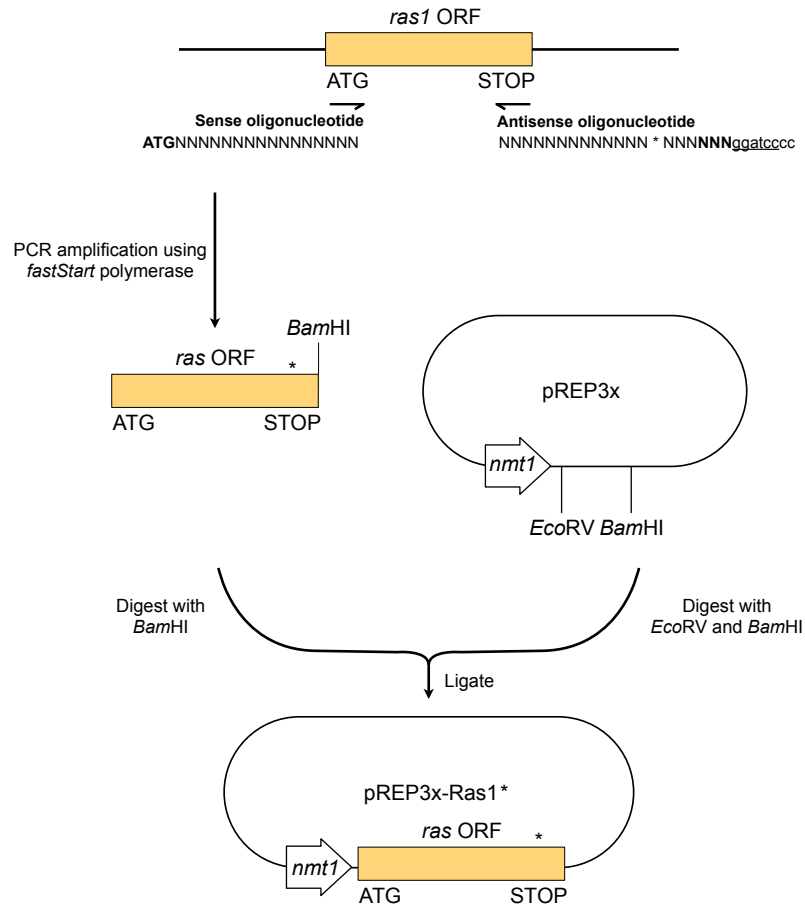


**Figure 3.6. Mutating the 215<sup>th</sup> and 216<sup>th</sup> codons of *ras1* using mutagenic cloning oligonucleotides**

Mutations in the 3' region of *ras1* were introduced using antisense oligonucleotides containing the desired point mutation. The *ras1* ORF was amplified using sense oligonucleotide beginning at the initiating ATG codon (ATG AGG TCT ACC TAC TTA AGA GAG) and a mutagenic antisense oligonucleotide (where the point mutation is denoted by a \*) containing a *Bam*HI site immediately prior to the endogenous stop anticodon (*ras1*<sup>C215S</sup> = ggggatcc CTA CAT ATA ACA CAA CTT TTA GTT GA; *ras1*<sup>C216S</sup> = ggggatcc CTA CAT ATA ACA CTA CAT TTA G). The product was digested with *Bam*HI and ligated into *Eco*RV and *Bam*HI digested pREP3x.

### 3.3. Creation of constructs for genomic integration

#### 3.3.1. Generating constructs for integration of *ras* ORFs.

A construct has previously been created containing the 5' and 3' flanking untranslated regions (UTRs) of the *ras1* locus separated by an *EcoRV* site (JD1847, Dr. Rachel Forfar). The construct was created to allow integration of exogenous sequence in place of the endogenous *ras1*, driven by homologous recombination with the flanking UTRs. All *ras* ORFs were amplified using a sense oligonucleotide beginning at the initiating ATG and an antisense oligonucleotide beginning at the endogenous stop anticodon (Table 3.3). *ras1*<sup>S22N</sup>, *ras1*<sup>Q66L</sup> and *ras1*<sup>G17V</sup> were amplified using the *ras1* oligonucleotides. *ras1*<sup>Q66L, C215S</sup> was amplified using the *ras1*<sup>C215S</sup> oligonucleotide set. Amplified products were then ligated into *EcoRV* digested JD1847 to create the final integration construct (Figure 3.7).

**Table 3.3. Oligonucleotides to amplify *ras* ORFs for integration**

<i>ras</i> ORF	Sense oligonucleotide	Antisense oligonucleotide
<i>ras1</i>	<b>ATG</b> AGG TCT ACC TAC TTA AGA GAG	<b>CTA</b> ACA TAT AAC ACA ACA TTA GTT GA
<i>ras1</i> <sup>C215S</sup>	<b>ATG</b> AGG TCT ACC TAC TTA AGA GAG	<b>CTA</b> CAT ATA ACA CAA CTT TTA GTT GA
<i>ras1</i> <sup>C216S</sup>	<b>ATG</b> AGG TCT ACC TAC TTA AGA GAG	<b>CTA</b> CAT ATA ACA CTA CAT TTA G
<i>ras1-ritc</i>	<b>ATG</b> AGG TCT ACC TAC TTA AGA GAG	<b>TCA</b> AGT TAC TGA ATC TTT CTT CT
<i>h-ras</i>	<b>ATG</b> ACG GAA TAT AAG C	<b>TCA</b> GGA GAG CAC ACA CTT GC
<i>n-ras</i>	<b>ATG</b> ACT GAG TAC AAA CTG	<b>TTA</b> CAT CAC CAC ACA TGG CAA TC
<i>k-ras4b</i>	<b>ATG</b> ACT GAA TAT AAA CTT G	<b>TTA</b> CAT AAT TAC ACA CTT TGT C

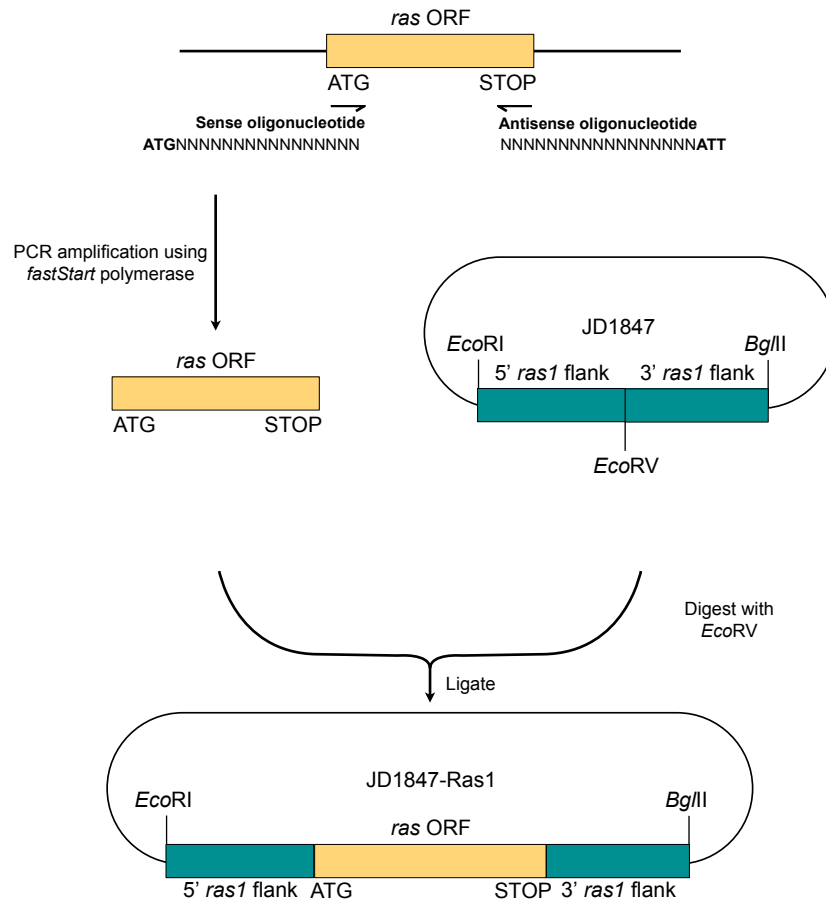


**Figure 3.7. Generating constructs to integrate *ras* ORFs**

The ORFs of different *ras* isoforms and mutants were amplified using sense oligonucleotides starting at the initiating ATG and antisense oligonucleotides beginning at the endogenous stop anticodon (Table 3.3). These products were then ligated between the flanking UTRs of the *ras1* locus in *EcoRV* digested JD1847.

### 3.3.2. Generating constructs for integration of *gfp-ras* fusions.

Constructs for the integration of *gfp-ras* fusions were generated using a two step cloning strategy, as described for *1-40gpa1-gfp-ras1* (section 3.1.3). The *gfp* ORF was first amplified using a sense oligonucleotide beginning at the initiating ATG (ATG AGT AAA GGA GAA GAA C) and an antisense oligonucleotide containing a full *Bam*HI site immediately prior to the final coding anticodon, but lacking the endogenous stop anticodon (ggggatcc TTT GTA TAG TTC ATC CA). This product was then ligated into *EcoRV* digested JD1847 (Figure 3.8).

*gfp-ras* fusions were generated by digesting pREP3x-GFP-*ras* constructs with *Nco*I and *Bam*HI, as detailed in Figure 3.4. JD1847-GFP (Figure 3.8) was also digested with *Nco*I and *Bam*HI and these two products were ligated to reconstitute the *gfp* ORF, generating JD1847-GFP-*ras* (Figure 3.9).

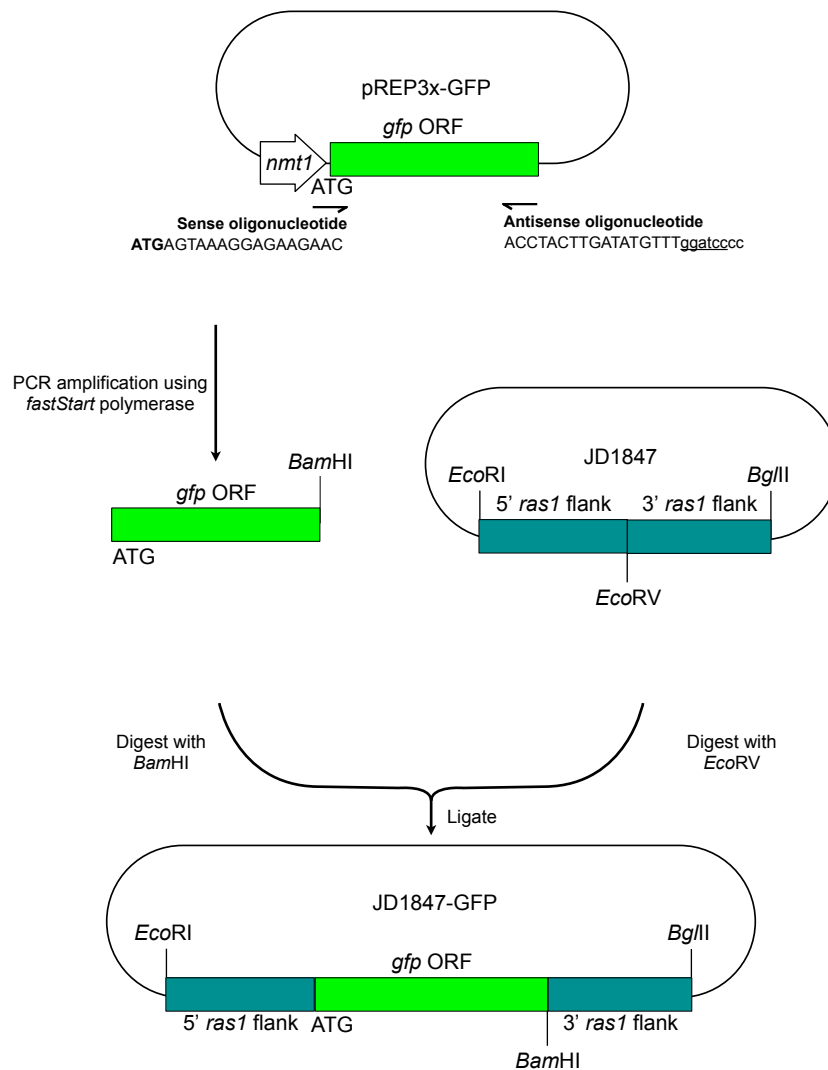


**Figure 3.8. Creating JD1847-GFP**

JD1847 was generated to allow creation of *gfp-ras* integration constructs (Figure 3.9). The *gfp* ORF was amplified using a sense oligonucleotide beginning at the initiating ATG (ATG AGT AAA GGA GAA GAA C) and an antisense oligonucleotide containing a full *Bam*HI site immediately prior to the final coding anticodon (ggggatcc TTT GTA TAG TTC ATC CA). This product was then ligated into *Eco*RV digested JD1847.

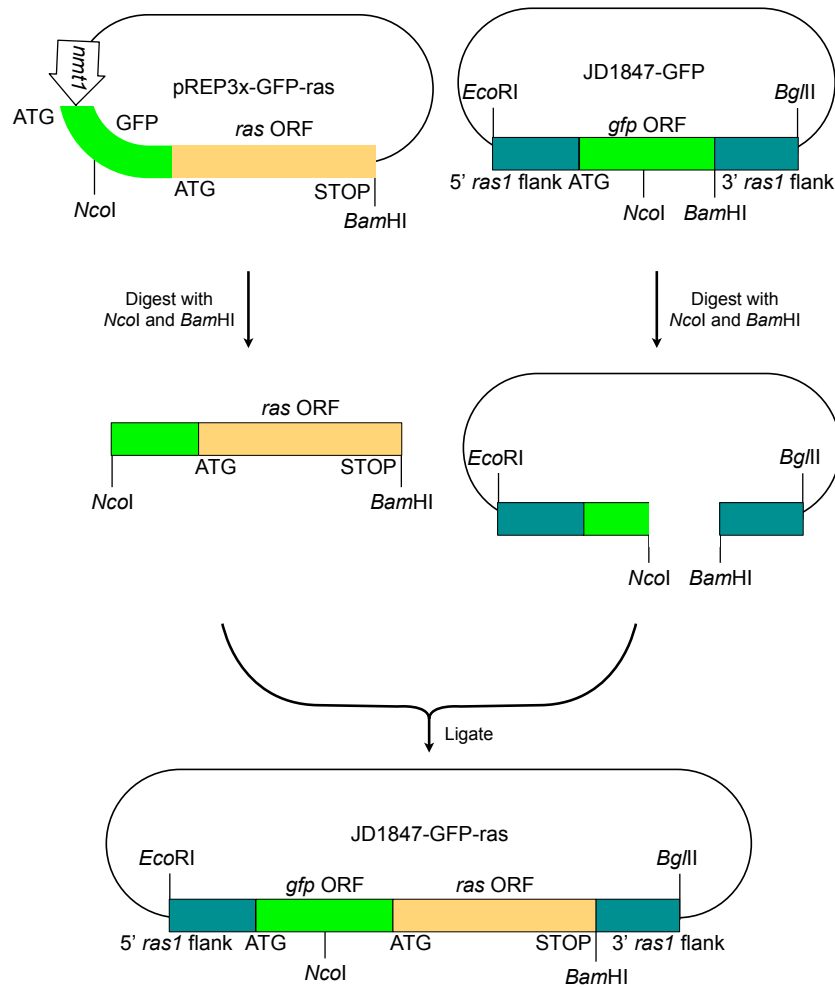


**Figure 3.9. Cloning of *gfp-ras* integration constructs**

pREP3x-GFP-*ras* constructs were digested with *Nco*I and *Bam*HI, utilising an endogenous *Nco*I site within the *gfp* ORF, to yield a 3' section of *gfp* fused to *ras*. This product was then ligated into *Nco*I and *Bam*HI digested JD1847-GFP, reconstituting the *gfp* ORF and generating *gfp-ras* fusions.

### 3.3.3. Generating constructs for integration of *1-40gpa1-gfp-ras1* fusions.

Constructs for the integration of *1-40gpa1-gfp-ras* fusions were generated using the same strategy as was used for *1-40gpa1-gfp-ras* fusions in pREP3x. *1-40gpa1-gfp* was first cloned between the *ras1* UTRs lacking a stop codon (Figure 3.10). *1-40gpa1-gfp-ras1* fusion were generated by subcloning the *ras1* ORF from existing *gfp-ras1* fusions utilising an endogenous *Nco*I site in the *gfp* ORF (Figure 3.11). *1-40gpa1-gfp* was amplified using a sense oligonucleotide beginning at the initiating ATG of *gpa1* (**ATG** GGA TGC ATG TCG AGT

AAA TAC GC) and an antisense oligonucleotide containing a full *Bam*HI site immediately prior to the final coding anticodon (ggggatcc TTT GTA TAG TTC ATC CA). This product was then ligated into *Eco*RV digested JD1847 (Figure 3.10).

*1-40gpa1-gfp-ras* fusions were then constructed by ligating *Nco*I and *Bam*HI digested *gfp-ras* fusions, from pREP3x-GFP-ras constructs, into *Nco*I and *Bam*HI digested JD1847-1-40Gpa1-GFP (Figure 3.11).

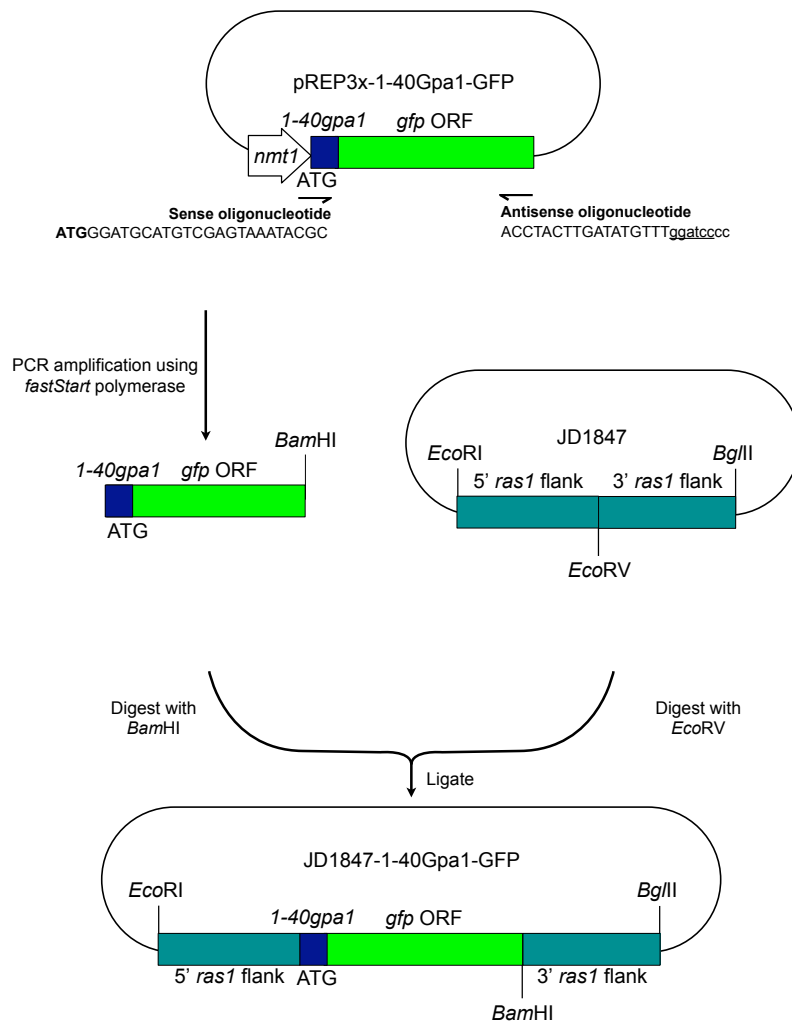


**Figure 3.10. Cloning JD1847-1-40Gpa1-GFP**

JD1847-1-40Gpa1-GFP was generated to allow creation of *1-40gpa1-gfp-ras* integration constructs (Figure 3.11). The *1-40gpa1-gfp* fusion was amplified using a sense oligonucleotide beginning at the initiating ATG of *gpa1* (ATG GGA TGC ATG TCG AGT AAA TAC GC) and an antisense oligonucleotide containing a full *Bam*HI site immediately prior to the final coding anticodon of *gfp* (ggggatcc TTT GTA TAG TTC ATC CA). This product was then ligated into *Eco*RV digested JD1847.

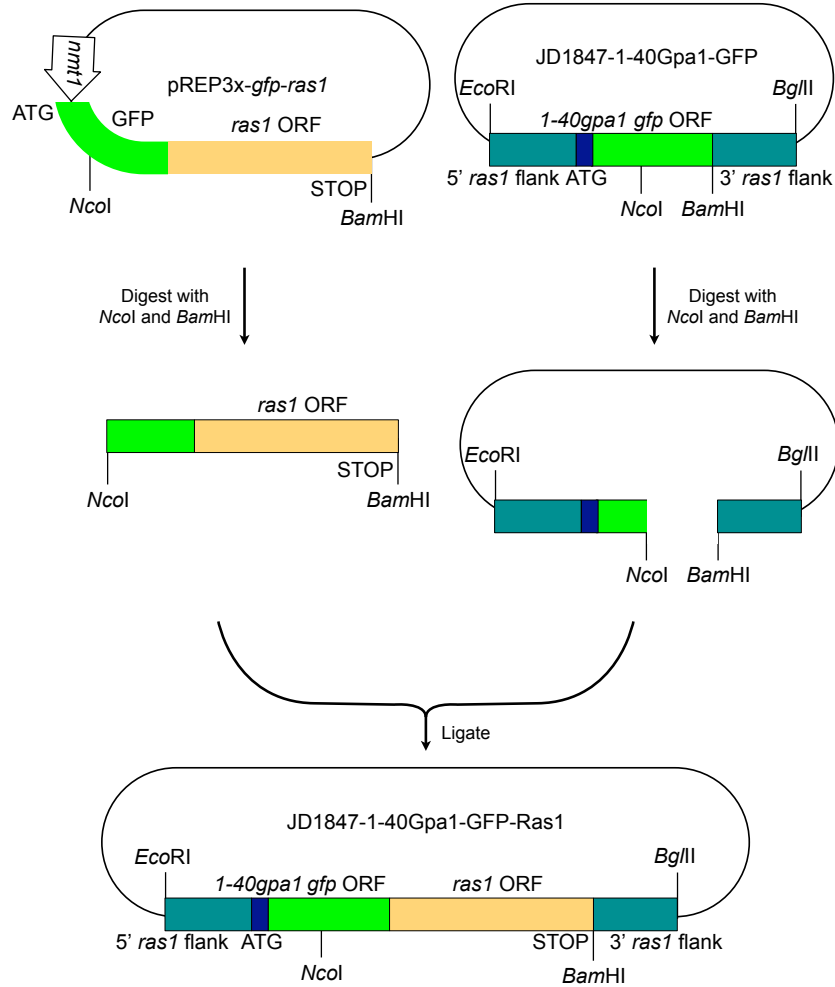


**Figure 3.11. Cloning of 1-40gpa1-gfp-ras integration constructs**  
pREP3x-GFP-ras constructs were digested with *NcoI* and *BamHI*, utilising an endogenous *NcoI* site within the *gfp* ORF, to yield a 3' section of *gfp* fused to *ras*. This product was then ligated into *NcoI* and *BamHI* digested JD1847-1-40Gpa1-GFP, reconstituting the *gfp* ORF and generating 1-40gpa1-gfp-ras fusions.

### 3.3.4. Creation of constructs for the integration of *tea1-mCherry*.

The cell tip protein Tea1 provides an ideal marker for cell polarity and polar cell growth. In order to visualise Tea1, a direct in-frame Tea1-mCherry fusion was made, expressed from the endogenous *tea1* locus.

To drive the integration of exogenous sequence downstream of the *tea1* ORF, the last 758 nucleotides of the *tea1* ORF and 658 nucleotides of the 3' UTR were amplified from *Sz. pombe* genomic DNA, using a sense oligonucleotide which included an endogenous *HindIII* site (G GGA AAG CTT GAG AAA CGG GAG) and an antisense oligonucleotide containing an endogenous

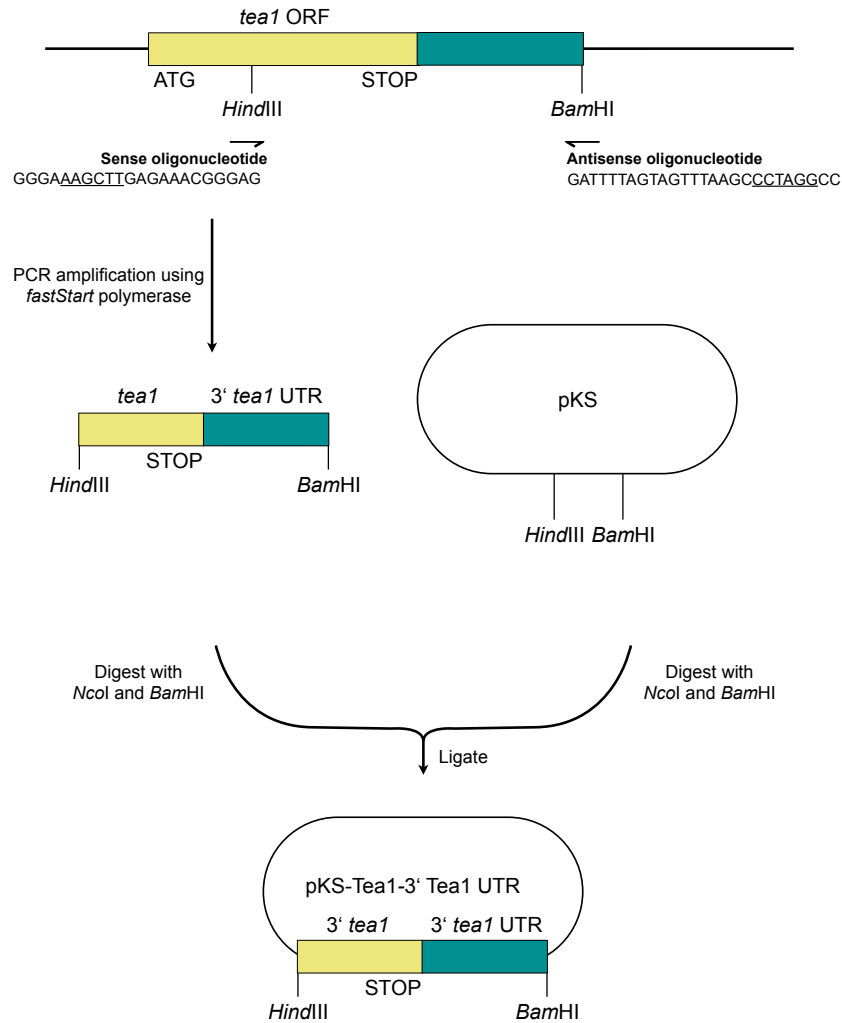


**Figure 3.12. Cloning of pKS-Tea1-3' Tea1 UTR**

The 3' region of the *tea1* ORF and 3' UTR of *tea1* were amplified from *Sz. pombe* genomic DNA using a sense oligonucleotide containing an endogenous *Hind*III site (G GGA AAG CTT GAG AAA CGG GAG) and an antisense oligonucleotide containing an endogenous *Bam*HI site (CCCGGATCCCGAATTTGATGATTTTAG). The PCR product was then digested with *Hind*III and *Bam*HI and ligated into pKS digested with *Hind*III and *Bam*HI.

*Bam*HI site (CCCGGATCCCGAA TTTGATGATTTTAG). This product was then digested with *Hind*III and *Bam*HI and ligated into pKS digested with *Hind*III and *Bam*HI (Figure 3.12).

To allow the generation of a *tea1-mcherry* fusion, the endogenous stop codon of the *tea1* ORF was removed from pKS-Tea1-3'Tea1 UTR and a *Bgl*II site was added directly after the last codon, to allow the cloning of sequence in-frame with *tea1*. This was achieved by inverse PCR amplification of pKS-

Tea1-3' Tea1 UTR using a sense oligonucleotide beginning immediately downstream of the *tea1* ORF and containing a full *Bgl*II site (gggagatctTAACTCTT TGGA ACTATTTTG), and an antisense oligonucleotide beginning at the last coding anticodon of *tea1*, and containing a full *Bgl*II site (cccagatct ATT TTC GTT GTC ATG GAC TGG). The product was digested with *Dpn*I to remove template DNA, digested with *Bgl*II and ligated to circularise the vector (JD3542) (Figure 3.13).

Integration of *mCherry* in frame with *tea1* was achieved using a two step strategy. A *ura4*<sup>+</sup> cassette was integrated first to allow subsequent integration of *mCherry* using FOA selection. To achieve this, the *ura4*<sup>+</sup> cassette was cloned into JD3542. The *ura4*<sup>+</sup> cassette was amplified using a sense oligonucleotide containing a full *Bam*HI site (ggggatccACCATGTAGCTACAAATCC) and an antisense oligonucleotide containing a full *Bam*HI site (ggggatccACCATGTAGTGATATTGAC). This product was then digested with *Bam*HI, an isocaudamer of *Bgl*II, producing the same overhanging nucleotide ends as a *Bgl*II digest (GATC). The product was then ligated into *Bgl*II digested JD3542 (Figure 3.14).

To create the final *tea1-mCherry* integration construct, the *mCherry* ORF was amplified using a sense oligonucleotide containing a full *Bgl*II site immediately prior to the initiating ATG (ggggagatct **ATG** GTG AGC AAG GGC GAG GA), and an antisense oligonucleotide containing a full *Bgl*II site immediately prior to the endogenous stop anticodon (ggggagatct **TTA** CTT GTA CAG CTC GTC CA). The PCR product was digested with *Bgl*II and ligated into *Bgl*II digested JD3542 creating an in-frame fusion of *tea1* and *mCherry* separated by two codons, generated by the linking *Bgl*II site (AGA and TCT to give an Arg and a Ser residue) (Figure 3.15).

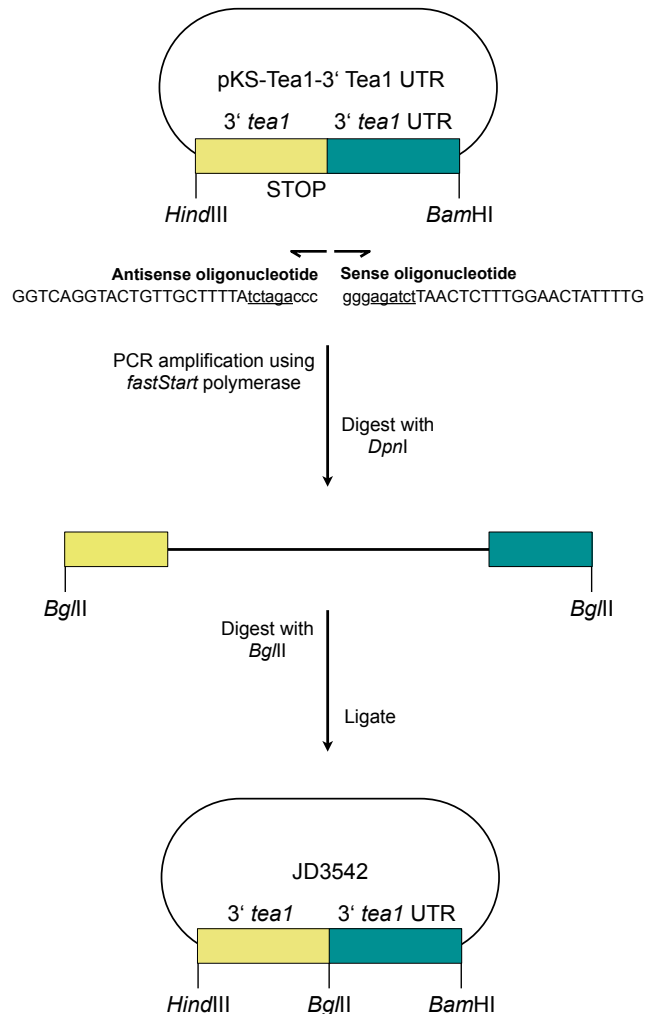


**Figure 3.13. Inverse PCR of pKS-Tea1-3' Tea1 UTR**

Inverse PCR amplification was performed on pKS-Tea1-3' Tea1 UTR to remove the stop codon of *tea1* and insert a *Bgl*II site directly downstream of the last codon of the *tea1* ORF. Amplification was performed using a sense oligonucleotide beginning immediately downstream of the *tea1* ORF and containing a full *Bgl*II site (gggagatctTAACTCTTTGGA ACTATTTTG), and an antisense oligonucleotide lacking the endogenous stop anticodon and containing a full *Bgl*II site (cccagatct ATT TTC GTT GTC ATG GAC TGG). The product was digested with *Dpn*I to remove template DNA, digested with *Bgl*II and ligated to circularise the vector (JD3542).

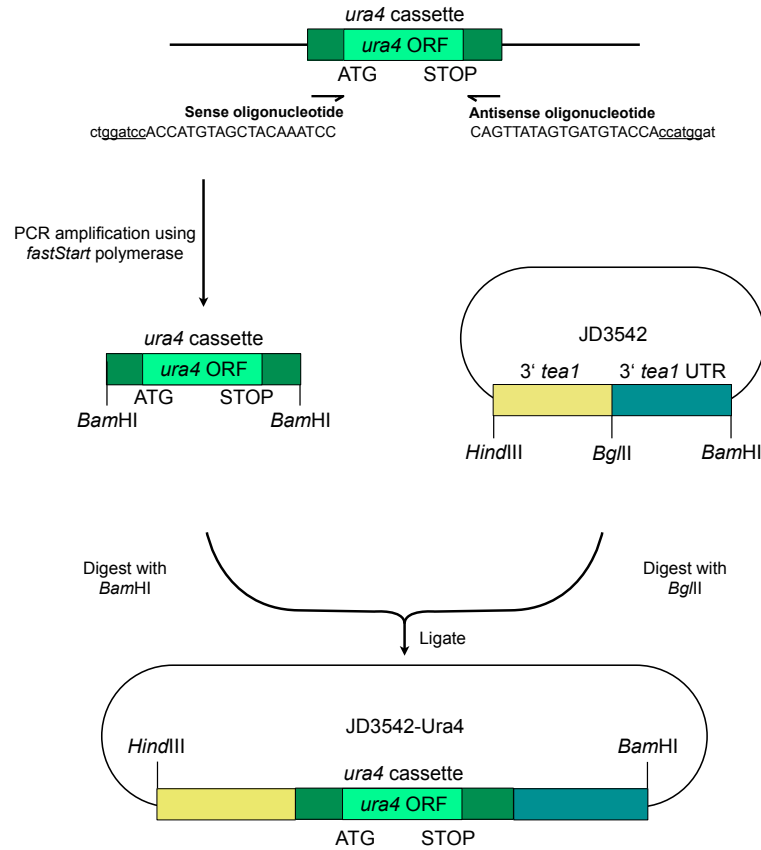


**Figure 3.14. Cloning of JD3542-Ura4**

The *ura4*<sup>+</sup> cassette was amplified using a sense oligonucleotide containing a full *Bam*HI site (ggggatccACCATGTAGCTACAAATCC) and an antisense oligonucleotide containing a full *Bam*HI site (ggggatccACCATGTAGTGATATTGAC). The PCR product was digested with *Bam*HI and ligated into *Bgl*II digested JD3542, abolishing the restriction endonuclease sites either side of the *ura4*<sup>+</sup> cassette.

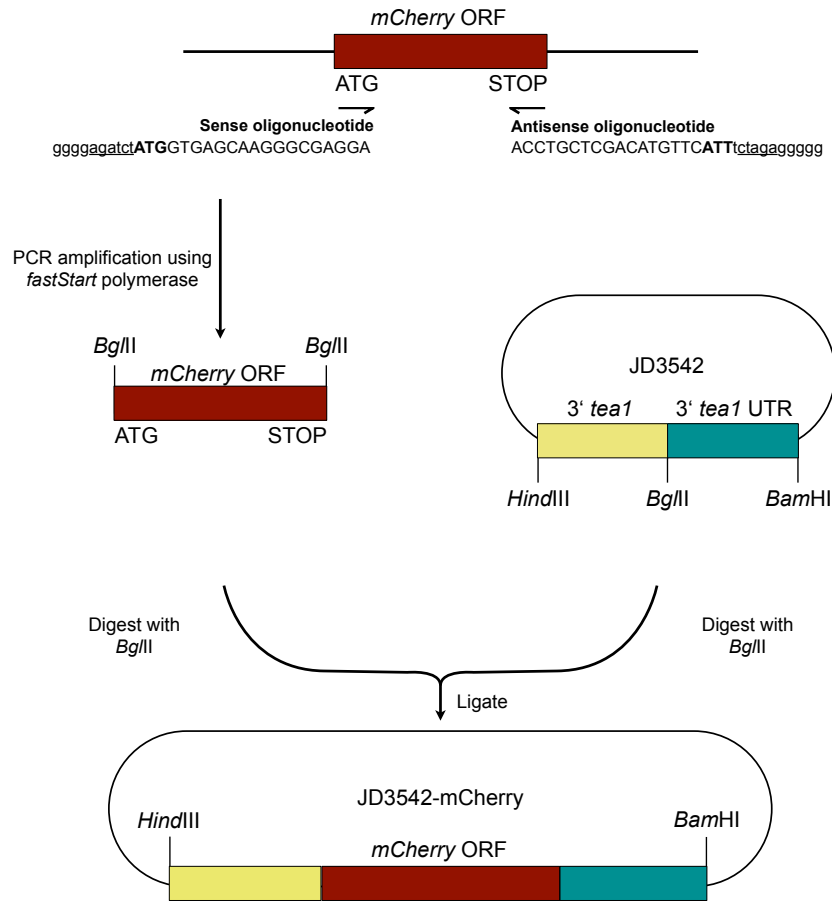


**Figure 3.15. Generating a *tea1-mCherry* integration construct**

The *mCherry* ORF was amplified using a sense oligonucleotide containing a full *Bgl*II site immediately prior to the initiating ATG (ggggagatct **ATG** GTG AGC AAG GGC GAG GA), and an antisense oligonucleotide containing a *Bgl*II site immediately prior to the endogenous stop anticodon (ggggagatct **TTA** CTT GTA CAG CTC GTC CA). The PCR product was digested with *Bgl*II and ligated into *Bgl*II digested JD3542.

## CHAPTER 4

### Characterisation of Ras1 signalling in *Sz. pombe*

#### 4.1. Introduction

The relative biochemical simplicity of ras activity belies a host of complexities. This is evident in higher eukaryotes, where multiple ras isoforms are expressed, each with differing but overlapping functional interactions (Malumbres and Barbacid 2003). As a consequence, the study of individual ras related signalling events in higher eukaryotes presents a number of technical challenges. Due to these compounding factors, previous studies have utilised simpler eukaryotic systems to investigate the activity of ras. The fission yeast *Sz. pombe* has proved an ideal system for the study of ras signalling, as it contains only a single ras protein (Ras1), which controls a number of downstream pathways. During mitotic growth, Ras1 regulates cell polarisation. During the switch from mitotic to meiotic development, Ras1 regulates pheromone-responsive changes in both gene expression and cell morphology, resulting in cellular changes which allow mating (Fukui *et al.* 1986b; Nielsen *et al.* 1992; Garcia *et al.* 2006).

Most previous studies documenting ras signalling in *Sz. pombe* have utilised qualitative measures of Ras1 function, including observation of cell morphology and the presence or absence of spores following the induction of mating (Fukui *et al.* 1986b; Papadaki *et al.* 2002; Onken *et al.* 2006). Simple experimental systems such as *Sz. pombe*, however, are ideally suited to quantitative population based assays for signalling behaviour. Such assays have been used to study many signalling components in *Sz. pombe*, including G protein-coupled receptors (GPCRs) (Ladds *et al.* 2003), heterotrimeric G proteins (Goddard *et al.* 2006; Ladds *et al.* 2007) and RGS proteins (Ladds *et al.* 2005; Hill *et*

*al.* 2008). Such a quantitative approach to Ras1 signalling could also prove highly informative, allowing a more detailed analysis of Ras1 function.

#### 4.2. Analysis of Ras1 signalling in *Sz. pombe*

The use of a pheromone-responsive *sxa2>lacZ*  $\beta$ -galactosidase reporter assay in *Sz. pombe* is already well established (Didmon *et al.* 2002). The assay provides a sensitive measure of pheromone-responsive signalling, allowing analysis of Ras1 activity following pheromone stimulation. Despite this, few quantitative assays exist for other aspects of Ras1 signalling. The development of such assays, investigating processes such as cell morphology, cell elongation in response to pheromone and mating, would be highly desirable, allowing a holistic analysis of Ras1 activity.

##### 4.2.1. Development of a quantitative assay for mating.

Most previous studies analysing mating in *Sz. pombe* have used qualitative measures of sporulation to indicate mating, either through microscopic examination of ascus formation or iodine staining of the starch rich spore cell wall (Egel *et al.* 1994). A quantitative assay from mating could prove a useful tool to allow the more meaningful comparison of strains with differing mating efficiencies.

Upon mating in *Sz. pombe*, four haploid spores are produced from two vegetative cells. Importantly, the spores produced are more resistant to external stresses than vegetative cells, a feature which can be exploited to isolate cells which have undergone mating from those which have not. Spore heat-resistance was used to isolate spores from vegetative cells, and spores were quantified by assessing the percentage of colony forming units (cfus) which recovered. Assays to develop this protocol were performed using the mating type stable M-cell strain JY444 and mating type stable P-cell strain JY1025.

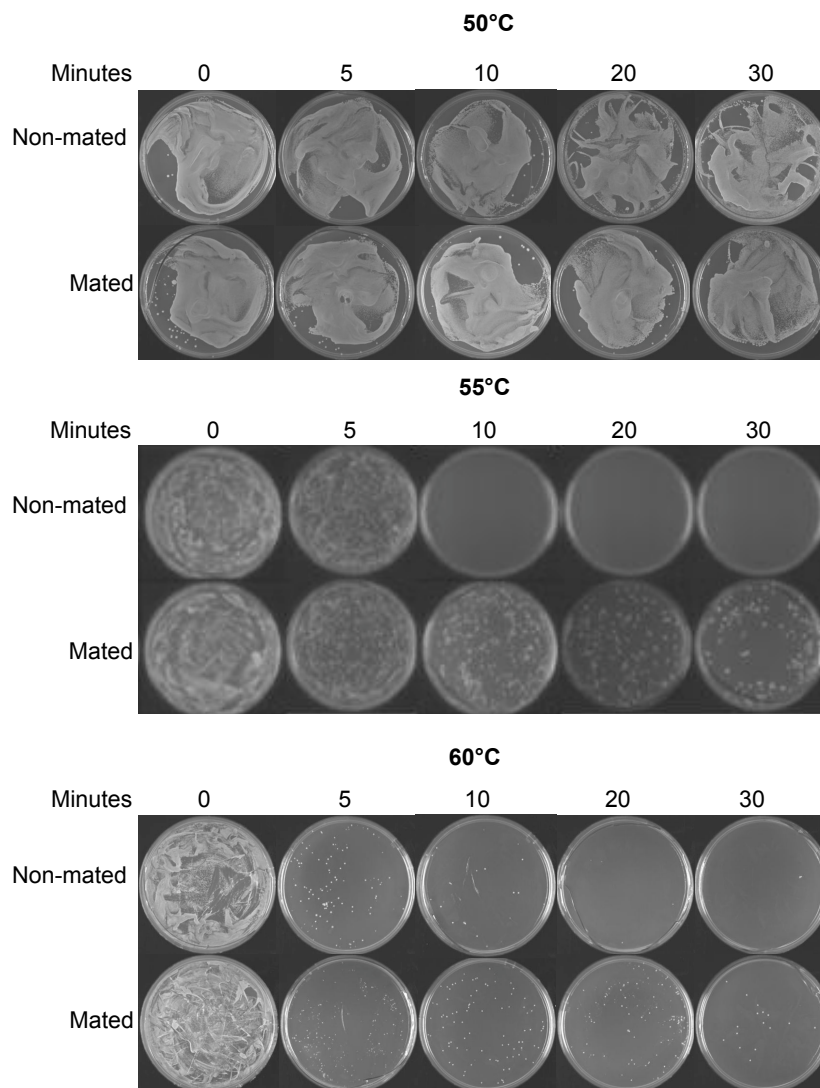


**Figure 4.1. Isolation of spores using heat treatment**

Mating in the *Sz. pombe* strains JY444 (M-cell) and JY1025 (P-cell) was investigated through the isolation of spores by heat treatment at 50°C to 60°C over a series of time points. Spore formation was assessed by quantification of colony forming units. Total vegetative cell death was seen after 10 minutes at 55°C, with no discernible reduction in spore viability.

Following the standard mating assay protocol (detailed in section 2.2.8), cells were suspended in 1 ml of sterile water and heated over a range of temperatures, from 50°C to 60°C, over periods of up to 30 minutes. Cells were then plated on rich media (YEALU) to allow recovery and colony formation (Figure 4.1). The number of colonies recovered following heat treatment was then used to determine the level of spore formation within that population and therefore the efficiency of mating in that strain.

Heating at 50°C did not achieve any discernible vegetative cell death after 30 mins. By contrast, heating at 60°C appeared to cause vegetative cell death but considerable reductions in cfu number were also observed in the mated population, possibly indicating a negative influence upon spore viability. Following these initial experiments, a temperature of 55°C and treatment period of 10 mins was chosen, as it represented a threshold at which high levels of cell death could be achieved in non-mated cell populations while maintaining significant cfu numbers in populations where mating had occurred. This allowed analysis of mating efficiency, by taking a percentage of cfus recovered after heat treatment compared to the number of cells in the non-heated population.

#### 4.2.2. Assessing mating efficiency in cells lacking endogenous Sxa2.

Wild-type M-cells (JY444) gave a cfu recovery of  $29 \pm 6\%$  upon mating with wild-type P-cells (JY1025), corresponding to strong spore staining when exposed to iodine (Figure 4.2A). However, the majority of strains used throughout this study were derived from the  $\beta$ -galactosidase reporter strain JY544, which lacks both *cyr1* and *sxa2*. The *cyr1* gene encodes adenylate cyclase, which is removed from these cells to allow sexual differentiation during mitotic growth. As such, the loss of *cyr1* does not negatively influence mating (Maeda *et al.* 1990) (JY444 (*cyr1*<sup>+</sup>) =  $29 \pm 6\%$  and JY278 (*cyr1*<sup>-</sup>) =  $24 \pm 3\%$ ). The loss of *sxa2*, a carboxypeptidase which degrades exogenous P-factor, causes cells to become sterile, preventing recovery following stimulation (Ladds *et al.* 1996). To rescue mating in these cells, Sxa2 was expressed from the vectors pREP3x, pREP41x and pREP81x (Ladds and Davey 2000), which contain thiamine repressible *nmt1* promoters of differing strengths, listed from highest to lowest (Maundrell 1993). Mating was restored upon expression of Sxa2 from all three vectors in the absence of thiamine (Figure 4.2B). The highest level of mating was observed in cells expressing Sxa2 from pREP41x, giving a cfu recovery of  $32 \pm 2\%$ , compared to  $21 \pm 2\%$  from pREP3x and  $21 \pm 1\%$  from

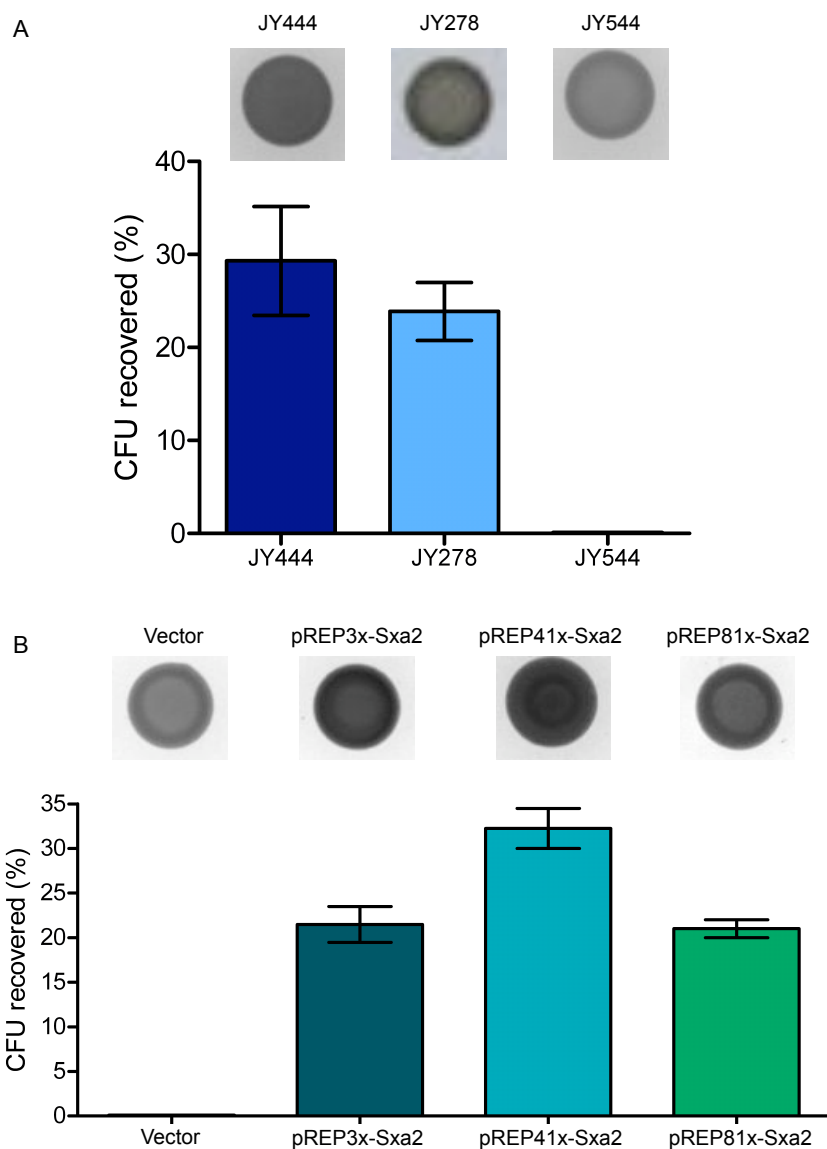


**Figure 4.2. Restoration of mating in strains lacking Sxa2**

Mating efficiency was assessed in the *sxa2*<sup>+</sup> and  $\Delta$ *sxa2* strains JY444 and JY544, in addition to the *sxa2*<sup>+</sup>, *cyr1*<sup>-</sup> strain JY278, upon mating with the mating type stable P-cell strain JY1025, using iodine staining and the mating efficiency assay described in 4.2.1 (A). No mating was observed in cells lacking *sxa2*. The assay was then performed using JY544 transformed with pREP alone (Vector), pREP3x-Sxa2, pREP41x-Sxa2 and pREP81x-Sxa2. Mating was restored in all strains expressing vector-borne *sxa2* (B). Data given is the mean of three independent experiments  $\pm$  SEM.

pREP81x. These figures are reflected in the levels of iodine staining observed in these populations, as the level of iodine staining appeared qualitatively darker in cells containing pREP41x-Sxa2, indicating a higher level of spore formation. Expression of Sxa2 from pREP41x was used in all subsequent mating assays

to restore mating in  $\Delta$ *sxa2* strains, as cells transformed with pREP41x-Sxa2 displayed the highest level of mating.

#### **4.2.3. Constructing a Tea1-mCherry strain to visualise the cell tip.**

A host of proteins act downstream of Ras1 at the tip of the cell to maintain cell polarity. The protein Tea1 displays Ras1-dependent localisation to the cell tips, acting downstream of the p21-activated kinase (PAK) Shk1 to regulate cytoskeletal elements (Kim *et al.* 2003). Consequently, Tea1 provides an ideal marker for Ras1 activity through the Scd1-Cdc42 pathway, as its tip localisation is reliant upon these signalling processes. The localisation of a fluorescent Tea1-mCherry fusion would therefore provide an additional means to determine Ras1 signalling, allowing the visualisation of polar cell organisation.

Tea1 was C-terminally tagged with the fluorescent protein mCherry at the *tea1* locus using a two-step integration strategy. The first step involved the removal of the endogenous stop codon of *tea1* and the insertion of a 1.8kb *ura4*<sup>+</sup> cassette directly downstream of the ORF, driven by homologous recombination (Figure 4.3A). The *ura4*<sup>+</sup> cassette was subsequently replaced with *mCherry* using FOA selection to select for the loss of the *ura4*<sup>+</sup> cassette, producing a direct, in-frame C-terminal fusion (Figure 4.3B). Fluorescence microscopy, using a Nikon E800 epifluorescence microscope fitted with an Andor EM-CCD camera, indicated defined tip localisation of the mCherry signal, consistent with the localisation of Tea1 observed in previous studies (Mata and Nurse 1997) (Figure 4.4A). Integration of the mCherry fluorescent protein in-frame with Tea1 was confirmed by immunoblotting. Immunoblotting was performed using a polyclonal primary antibody raised to GFP. Cross-reactivity with mCherry was confirmed in extracts from cells expressing mCherry from pREP3x, as a chemiluminescent signal was observed at a position consistent with the size of the mCherry protein (28.8 kDa). Cells lacking pREP3x-mCherry displayed

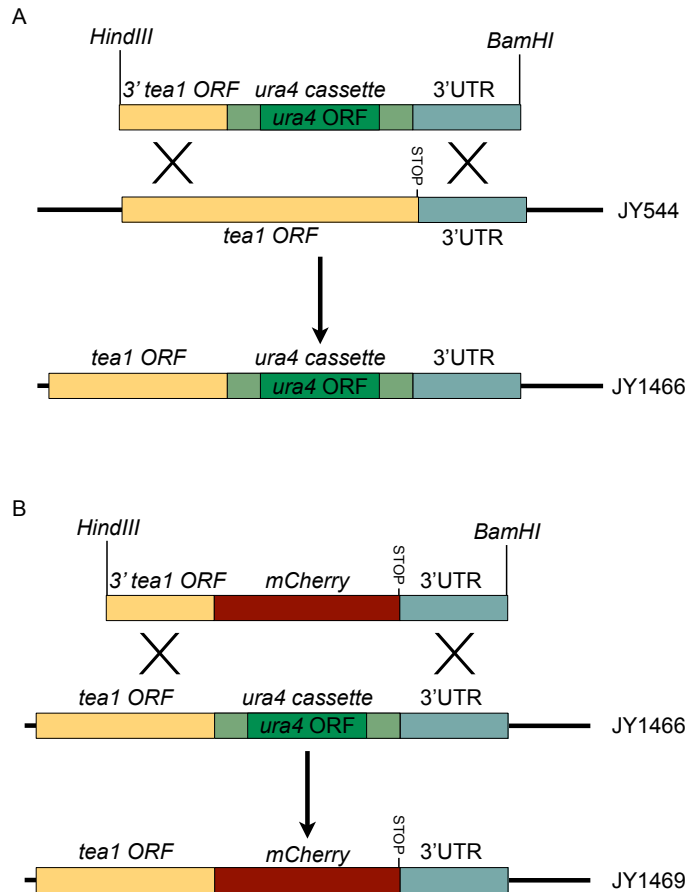


**Figure 4.3. Creation of a direct, in-frame Tea1-mCherry fusion at the *tea1* locus**

*tea1-mcherry* was generated at the *tea1* locus using a two step strategy. The endogenous stop codon was first replaced by a 1.8kb *ura4*<sup>+</sup> cassette using homologous recombination (A). The *ura4*<sup>+</sup> cassette was then replaced with *mcherry* to create an in frame C-terminal fusion (B).

no equivalent band, suggesting that the signal observed was a true mCherry signal. In cells containing the *tea1-mCherry* fusion, a chemiluminescent signal was observed at a position consistent with the predicted size of the fusion protein (~155 kDa). Only a single signal was detected, suggesting that the Tea1-mCherry fusion was not being cleaved (Figure 4.4B).

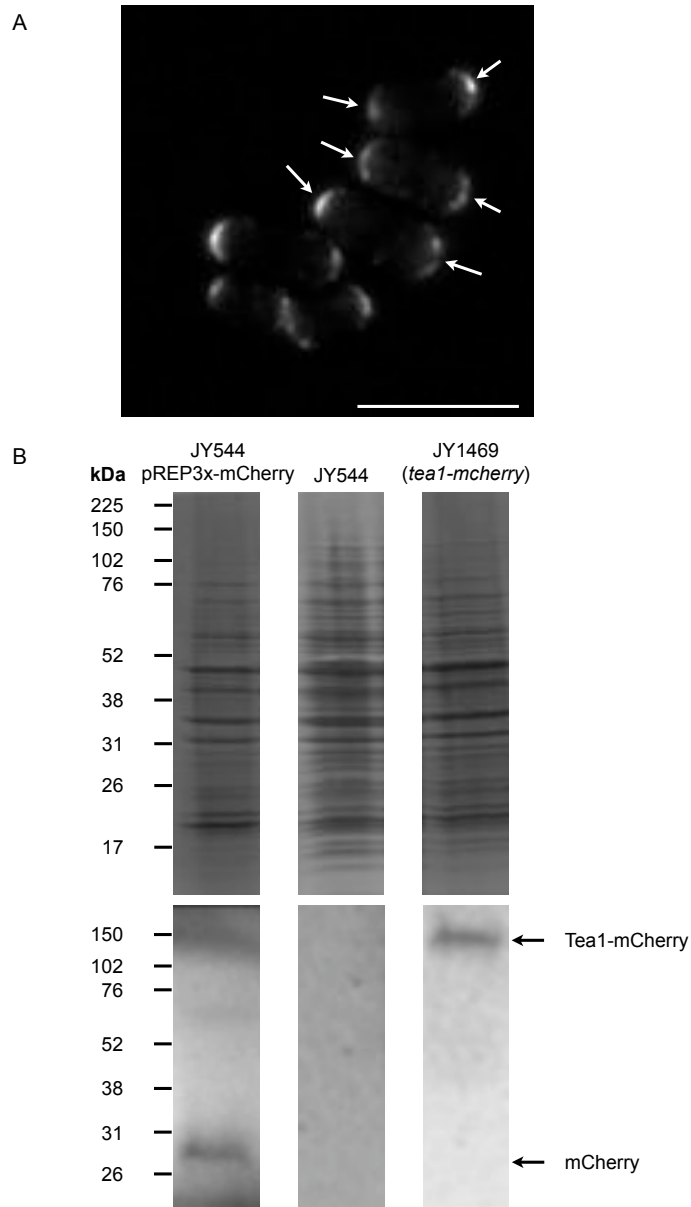


**Figure 4.4. Detection of Tea1-mCherry using fluorescence microscopy and immunoblotting**

Tea1-mCherry was visualised using a Nikon E800 epifluorescence microscope fitted with an Andor EM-CCD camera. The mCherry signal displayed a defined tip localisation, indicative of polar Tea1 distribution. Tip localisation of Tea1-mCherry is indicated with an arrow. The scale bar represents 10  $\mu\text{m}$  (A). Integration of mCherry in frame with Tea1 was confirmed via immunoblotting using a fluorescent protein polyclonal antibody raised to GFP. Extracts from cells expressing mCherry from pREP3x and extracts from the parent strain JY544 were included as controls. Coomassie stains of whole protein are included above the immunoblot as loading controls.

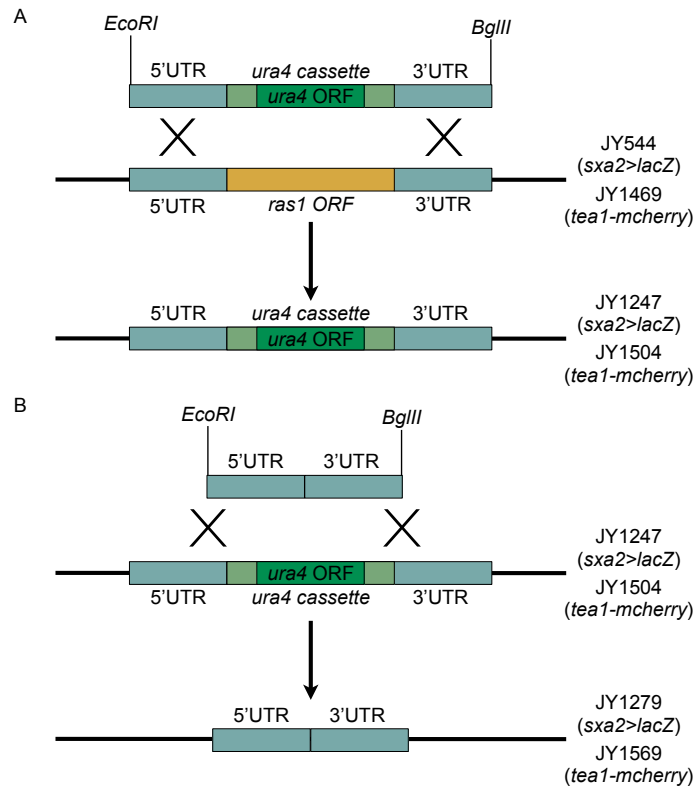


**Figure 4.5. Disruption of Ras1**

*ras1* was disrupted through replacement of the *ras1* ORF with the *ura4*<sup>+</sup> cassette, driven by homologous recombination with flanking regions of the ORF (A). The cassette was then removed by homologous recombination, using FOA selection to select for the loss of *ura4*<sup>+</sup> activity, to generate the final *ura4*<sup>-</sup>,  $\Delta ras1$  strain (B).

#### 4.2.4. Disruption of *ras1*.

The quantitative analysis of Ras1 signalling in *Sz. pombe* first required a detailed understanding of the phenotypes of cells containing and lacking Ras1. Ras1 was disrupted in the  $\beta$ -galactosidase reporter strain JY544 (*sxa2>lacZ*) and the strain JY1469 (*sxa2>lacZ, tea1-mCherry*) through direct replacement of the *ras1* ORF with the 1.8kb *ura4*<sup>+</sup> cassette, driven by homologous recombination (Figure 4.5A). The *ura4*<sup>+</sup> cassette was then removed through homologous recombination with the flanking regions of the *ras1* locus, using FOA selection to select for the loss of *ura4*<sup>+</sup> activity, generating JY1279 ( $\Delta ras1$ , *sxa2>lacZ*) and JY1569 ( $\Delta ras1$ , *tea1-mCherry*) (Figure 4.5B). JY1279 was generated by Dr. Rachel Forfar. Loss of Ras1 was confirmed through immunoblotting with a ras specific RAS10 antibody, which has previously been demonstrated to bind Ras1 (Onken *et al.* 2006) (Figure 4.6).

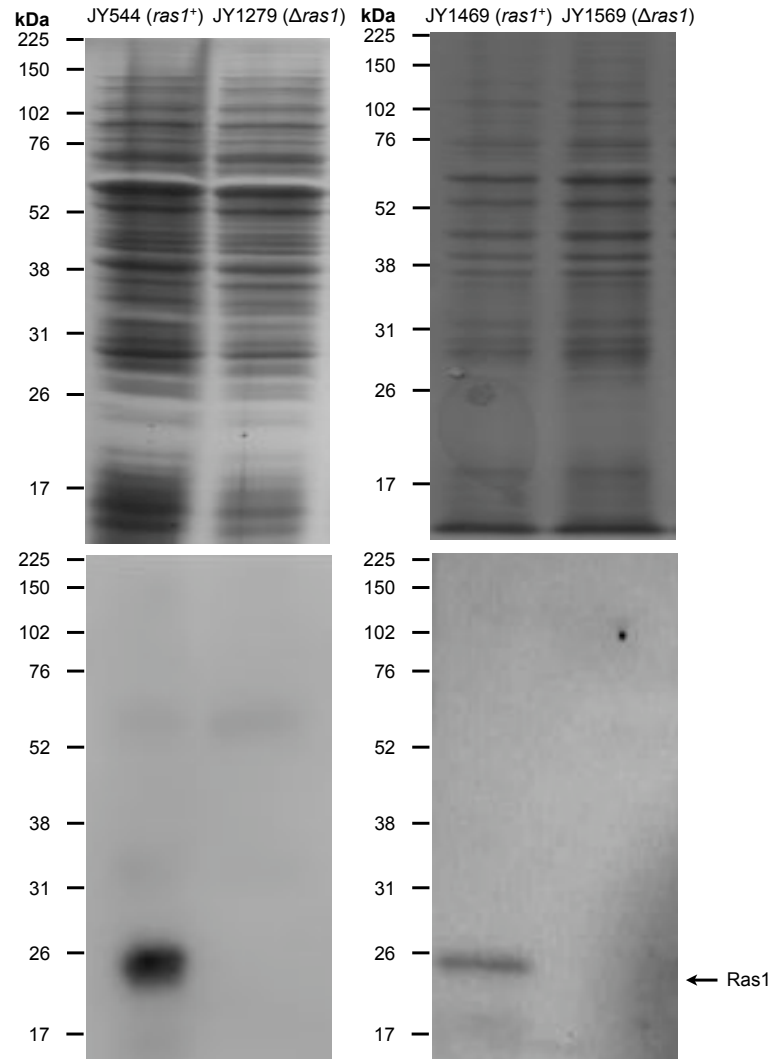


**Figure 4.6. Confirming the disruption of *ras1* by immunoblotting**

The loss of Ras1 from the strains JY544 (*sxa2>lacZ*) and JY1469 (*tea1-mcherry*) was confirmed through immunoblotting using the RAS10 anti-ras antibody. Whole cell extracts from both parent strains displayed a chemiluminescent signal at a position consistent with the presence of Ras1. Extracts from the  $\Delta ras1$  strains JY1279 (*sxa2>lacZ*) and JY1569 (*tea1-mCherry*) both displayed no Ras1 band. Coomassie stains of whole protein are included above the immunoblot as loading controls.

#### 4.2.5. Analysis of vegetative cell morphology using quantitative image analysis.

During vegetative cell growth Ras1 is responsible for maintaining polar cell morphology, with cells lacking Ras1 displaying a more rounded morphology than their wild-type counterparts (Fukui *et al.* 1986b). Importantly, the regulation of cell morphology by Ras1 utilises a distinct pathway from the mating response. Ras1, regulated by the GEF Efc25, activates the Rho GEF Scd1 which in turn initiates nucleotide exchange in Cdc42. Cdc42 then regulates cell morphology through the modulation of cytoskeletal elements (La Carbona *et al.* 2006).

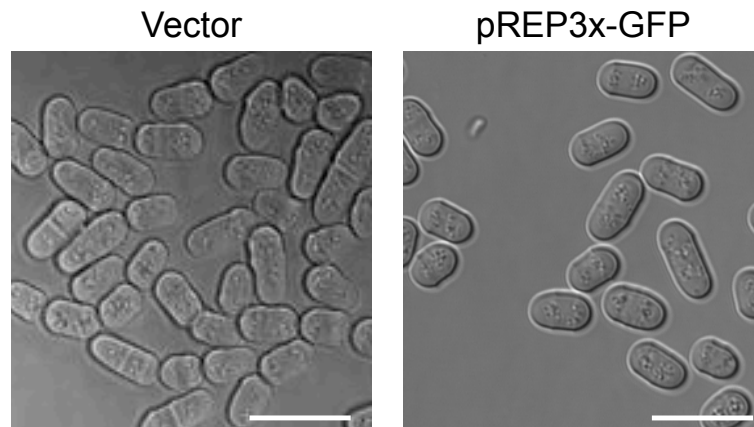


**Figure 4.7. The morphology in cells transformed with vector alone and pREP3x-GFP**

Populations of *ras1*<sup>+</sup> (JY544) cells transformed with pREP3x and pREP3x-GFP were visualised using a Leica SP5 scanning confocal microscope. No clear difference in cell morphology was observed upon the expression of GFP from pREP3x.

Quantitative image analysis provides a means to accurately determine the morphology of cells within a population. The Quimp plugin of ImageJ allows segmentation of cells within a fluorescent image (Dormann *et al.* 2002; Bosgraaf *et al.* 2009) (further development by Dr. Till Bretschneider and Richard Tyson). Quimp software has been developed to specifically analyse fluorescence images. As such, cellular fluorescence is required for Quimp analysis. For this series of studies expression of GFP from pREP3x was used, as

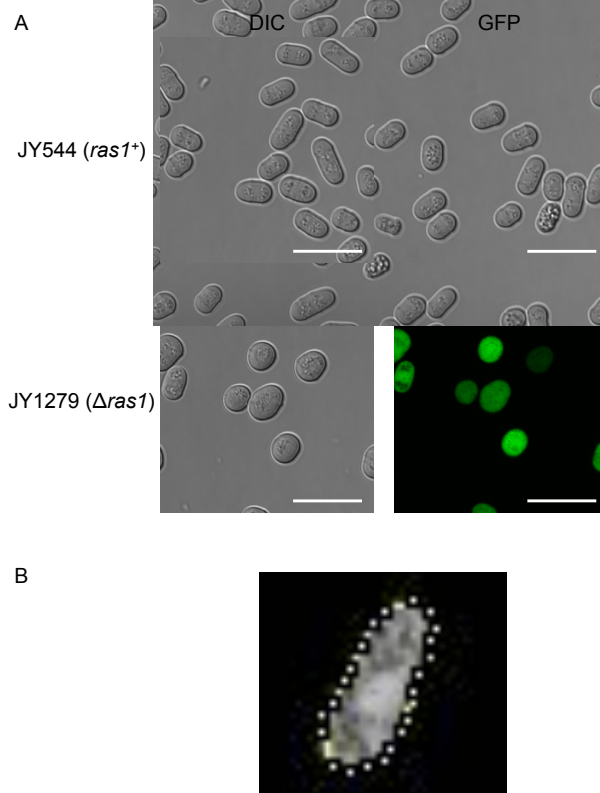


**Figure 4.8. Analysis of cell morphology using Quimp image analysis software**

Populations of *ras1*<sup>+</sup> (JY544) and  $\Delta$ *ras1* (JY1279) cells expressing GFP from pREP3x (A) were segmented using the Quimp image analysis plugin of ImageJ. Segmentation allowed the identification of the cell outline in fluorescence microscopy images (B). Images were obtained using a Leica SP5 scanning confocal microscope.

no discernible effect on cell morphology was observed (Figure 4.7). Following segmentation of a single cell, the Quimp software allows the analysis of a number of features of that cell. Two features which could prove informative in the analysis of cell morphology are the axial ratio, which takes the ratio of the longest and the shortest axis, and percentage circularity, which assigns a percentage based upon the cells identity to a circle (both equations given below).

$$Circularity = (4 \times \pi) \times \left( \frac{Area}{Perimeter^2} \right) \times 100$$

$$Axial\ ratio = \frac{long\ axis}{short\ axis}$$

Both parameters were used to analyse the same two populations of cells, a strain containing Ras1 (JY544) and a strain lacking Ras1 (JY1279). Images of these cells, expressing GFP from pREP3x and grown in DMM the absence of thiamine, were taken using a Leica SP5 scanning confocal microscope. These populations were selected as they represent examples of both polar cell morphology (JY544) and cells lacking polarity (JY1279) (Figure 4.8). Quimp software was then used to analyse the morphology of 30 individual cells from each strain using both parameters (cell circularity and axial ratio). Significant differences were observed between these populations using both analysis parameters. Cells exhibiting polar cell morphology (JY544) displayed a significantly higher mean axial ratio than cells lacking polarity (JY1279) ( $1.8 \pm 0.1$  compared to  $1.6 \pm 0.1$ ), and a significantly lower mean percent circularity ( $73.5 \pm 2.1$  % compared to  $85.9 \pm 1.6$  %). Of the two analysis parameters, percent circularity appeared the most sensitive, giving a P value of 0.0002 in an unpaired t test when comparing the two populations. Statistical analysis of the difference between these populations when comparing axial ratios gave a P value of 0.0255 (Figure 4.9). This observation would suggest that percent circularity could provide a robust assay for the analysis of cell morphology.

#### 4.2.6. Analysis of pheromone-dependent $G_1$ arrest.

All mating events in *Sz. pombe* require Rum1-dependent  $G_1$  arrest to proceed (Stern and Nurse 1998).  $G_1$  arrest can be measured using propidium iodide staining, allowing analysis of DNA complement using flow cytometry (Sazer and Sherwood 1990). This well established assay provides an additional quantitative measure of Ras1 signalling in response to pheromone. DNA complement was analysed in the strain JY544 (*sxa2>lacZ*) upon stimulation with 10  $\mu$ M pheromone in DMM, for periods of up to 8 h. A concentration of 10  $\mu$ M was chosen, as this has previously been demonstrated to produce a maximal pheromone-dependent signal (Smith *et al.* 2009). Cells were fixed with

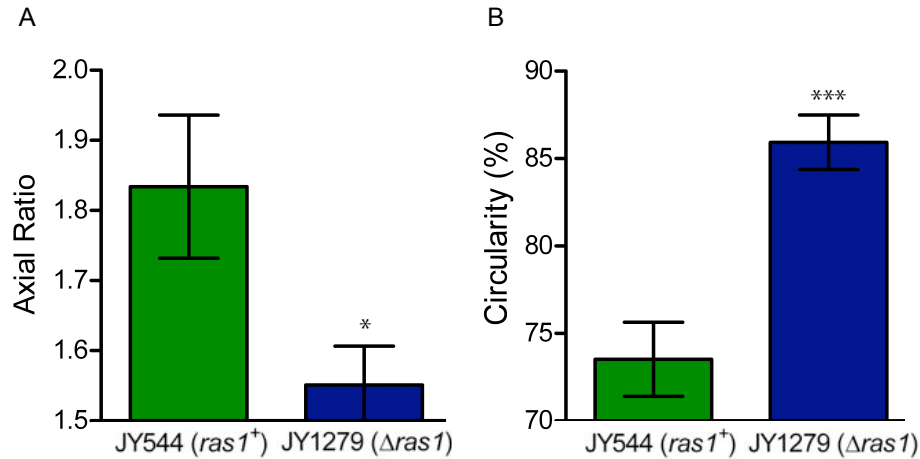


**Figure 4.9. Comparison of cell morphology parameters obtained using Quimp image analysis software**

Images of *ras1*<sup>+</sup> (JY544) and  $\Delta$ *ras1* (JY1279) cells were analysed using the axial ratio and percent circularity outputs of the Quimp image analysis plugin of ImageJ. Significant differences in morphology were observed between the two populations using both analysis parameters. Statistical significance was determined using an unpaired t test. One asterisk indicates a P-value of 0.0255 and three asterisks indicates a P-value of 0.0002. Data representative of 30 individual cells  $\pm$  SEM.

ethanol, stained with propidium iodide, and 30000 cells per sample were analysed using a Becton, Dickinson and Company (BD) LSRII flow cytometer. Excitation was achieved using a 488 nm laser, and emission detected using a 575/26 band pass filter with a 550 long pass filter. The time course was performed to determine the appropriate time of stimulation for subsequent G<sub>1</sub> arrest assays. Successive increases in the number of cells in G<sub>1</sub> were observed up to 6 h (Figure 4.10). Following 6 h of stimulation, increased numbers of cells in G<sub>2</sub> were observed as cells recovered from stimulation. These data indicate that 6 h stimulation gives maximal pheromone-dependent cell cycle arrest.

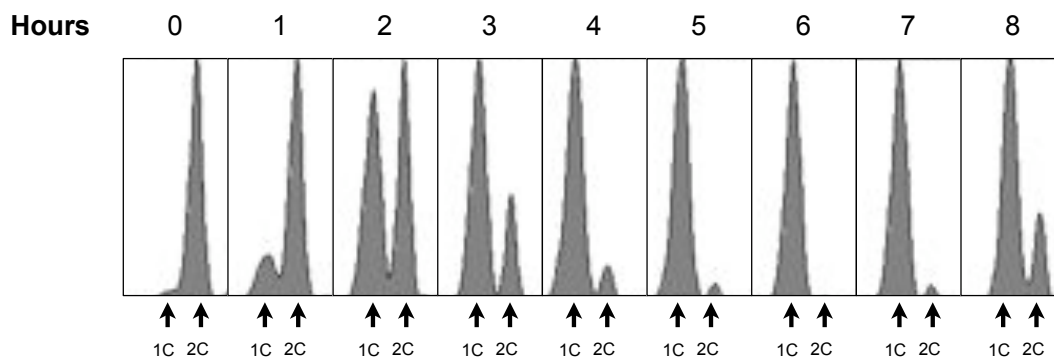


**Figure 4.10. Analysis of pheromone-dependent  $G_1$  arrest over time**  
 Cell cycle position was analysed in the strain JY544, upon stimulation with 10  $\mu$ M pheromone for periods up to 8 h. DNA complement was determined using propidium iodide staining and flow cytometry. Analysis was performed for 30000 cells. Maximal  $G_1$  arrest was observed following 6 h stimulation.

The methods detailed in the preceding section allow the detailed analysis of a number of features of Ras1 function. The assays developed in this section were then employed to characterise Ras1 function, in addition to the function of an array of Ras1 mutants and chimeras.

### 4.3. The role of Ras1 signalling in *Sz. pombe*

In the remaining sections of this chapter, the role of Ras1 in *Sz. pombe* is characterised using the assays described in section 4.2. In addition, a number of mutants with altered activities are used to further highlight the role of Ras1. Finally, the localisation of Ras1 is also analysed. These experiments were performed to provide a detailed account of Ras1 signalling in fission yeast.

#### 4.3.1. Ras1 is required to maintain polar cell morphology.

Previous studies have demonstrated that the loss of Ras1 causes a loss of polar cell morphology (Fukui *et al.* 1986b). Additionally, the data presented in Figures 4.8 and 4.9 demonstrate that significant differences in cell morphology can be observed between *ras1*<sup>+</sup> (JY544) and  $\Delta$ *ras1* (JY1279) cells, with  $\Delta$ *ras1* cells displaying a significantly more rounded morphology. To determine

whether this change results in the altered localisation of tip specific proteins, the distribution of Tea1-mCherry was observed in the  $\Delta ras1$  strain JY1569 using a Nikon E800 epifluorescence microscope fitted with an Andor EM-CCD camera, and compared to that observed in a strain containing Ras1 (JY1469) (Figure 4.11). The strain JY1569 displays little defined tip localisation of Tea1-mCherry. Tea1 appears in some of these cells to localise preferentially to opposite sides of the cell, although Tea1 could be observed over the whole of the cortex. This observation could suggest that the majority of microtubules, which are required for the transport of Tea1 to the cortex, still orient along one axis in the cell. The localisation of Tea1-mCherry in JY1569 is very different to that observed in *ras1*<sup>+</sup> cells (JY1469), in which Tea1 appears to exclusively localise to discrete patches at the tips of the cell. The tip localised Tea1-mCherry is indicated with an arrow.

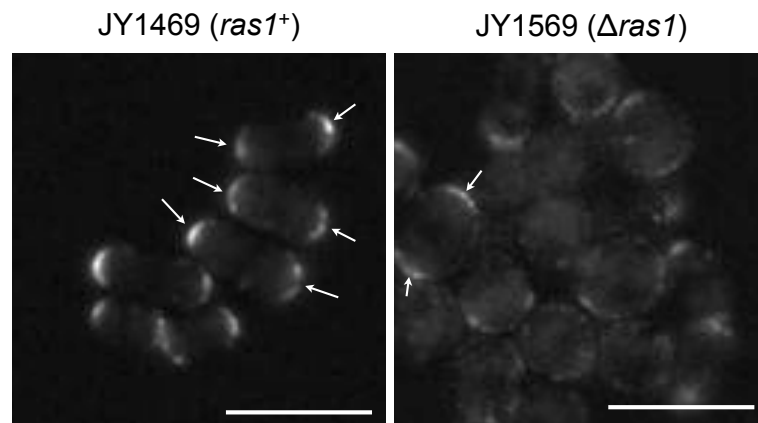


**Figure 4.11. The localisation of Tea1-mCherry in cells lacking Ras1**

The localisation of Tea1-mCherry was determined in a *ras1*<sup>+</sup> strain (JY1469) and  $\Delta ras1$  strain (JY1569) using a Nikon E800 epifluorescence microscope fitted with an Andor EM-CCD camera. The majority of polar Tea1 localisation is lost in the strain lacking Ras1, with Tea1 distributed around most of the cortex. Tip localisation of Tea1-mCherry is indicated with an arrow. The scale bar represents 10  $\mu\text{m}$ .

### 4.3.2. Ras1 is required for pheromone-responsive signalling.

Pheromone-responsive signalling in *Sz. pombe* results in a number of cellular changes. These changes include the expression of mating genes, cell cycle arrest, cell elongation (shmoo formation) and mating (Davey 1998). All these processes require signalling through Ras1, and can all be used to analyse Ras1 activity.

The *sxa2>lacZ*  $\beta$ -galactosidase reporter assay provides a quantitative read-out for pheromone-responsive transcription (Didmon *et al.* 2002). In addition, the assay utilises a Z2 Coulter<sup>®</sup> particle counter, allowing concurrent analysis of cell volume, and providing an indirect measure of cell elongation (shmoo formation). To quantify the effects of removing Ras1 upon the pheromone response cascade, the strains JY544 (*sxa2>lacZ*, *ras1*<sup>+</sup>) and JY1279 (*sxa2>lacZ*,  $\Delta$ *ras1*) were grown in DMM and exposed to varying concentrations of P-factor (1 nM - 100  $\mu$ M) for 16 h.  $\beta$ -galactosidase activity was then determined using ONPG as a substrate (Didmon *et al.* 2002). Cells expressing Ras1 displayed a dose-response profile to pheromone with a pEC<sub>50</sub> of  $7.0 \pm 0.1$  and maximal response of  $21.8 \pm 0.6$  (Figure 4.12A). A similar dose-response was also observed in cell volume, indicating shmoo formation in response to pheromone. Cells displayed an increase in volume from  $67.18 \pm 0.84$  fl to  $94.5 \pm 0.8$  fl with a pEC<sub>50</sub> to pheromone of  $6.7 \pm 0.1$ . In contrast, a pheromone-dependent increase in  $\beta$ -galactosidase activity or cell volume was not observed in cells lacking Ras1 (Figure 4.12B).  $\Delta$ *ras1* cells did however display a higher basal cell volume ( $89.1 \pm 1.7$  fl) than the *ras1*<sup>+</sup> strain. This observation could be due to the width of  $\Delta$ *ras1* cells, which have previously been demonstrated to be wider than wild-type cells (Kelly and Nurse 2011). This may result in a higher cell volume reading when analysed using the Z2 Coulter<sup>®</sup> particle counter. Images indicate that cells lacking Ras1 (JY1279) are visibly wider than cells containing Ras1 (JY544), which have one long axis and one markedly shorter axis (Figure 4.8).

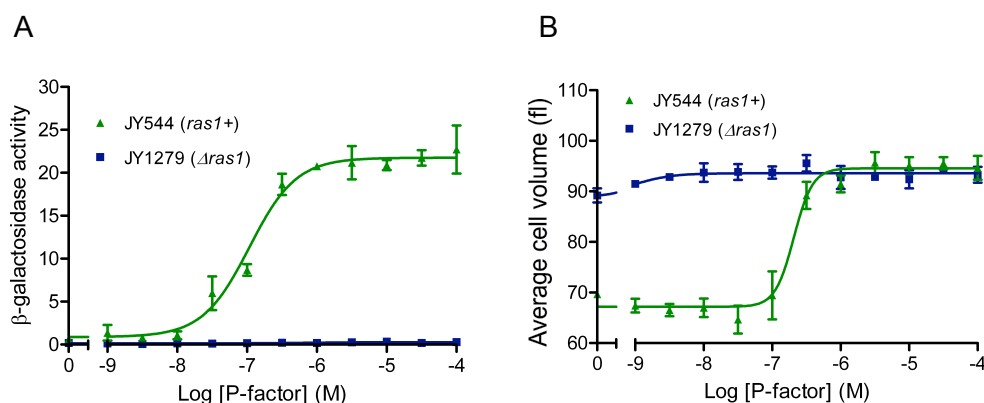


**Figure 4.12. Phormone-responsive transcription and cell volume changes in wild-type cells and cells lacking Ras1**

Phormone-responsive changes in transcription and cell volume were observed in *ras1*<sup>+</sup> (JY544) and  $\Delta ras1$  (JY1279) cells. Cells were grown in the presence of 1 nM to 100  $\mu$ M phormone in DMM for 16 h. Assays were then performed for  $\beta$ -galactosidase activity (A) and average cell volume (B). Cells lacking Ras1 displayed a loss of phormone-responsive signalling. Data shown is an average of three independent determinants ( $\pm$ SEM).

Cell volume measurements using the Z2 Coulter<sup>®</sup> particle counter appear to be affected by multiple aspects of cell morphology, including cell width. As a consequence, it becomes more challenging to dissect changes in cell size from altered cell morphology. Therefore, other methods of analysing shmoo formation may provide more accurate data.

In addition to the parameters mentioned in section 4.2.5, the Quimp software can also give a measurement of cell length along the longest axis. As shmoo formation in *Sz. pombe* is characterised by a unidirectional increase in cell length, this would appear a more accurate assay for phormone-responsive changes in morphology. Cell length was determined in images of *ras1*<sup>+</sup> (JY544) and  $\Delta ras1$  (JY1279) cell populations, expressing GFP from pREP3x, grown in the presence (10  $\mu$ M) and absence of P-factor in DMM lacking thiamine for 16 h (Figure 4.13B). Images were obtained using a Leica SP5 scanning confocal microscope. 10  $\mu$ M P factor was used as it elicited a maximal phormone response (Figure 4.12). The cells used in this assay were expressing GFP from pREP3x in the absence of thiamine to allow detection of the cell by the software. Analysis was performed on 30 individual cells of each strain under each

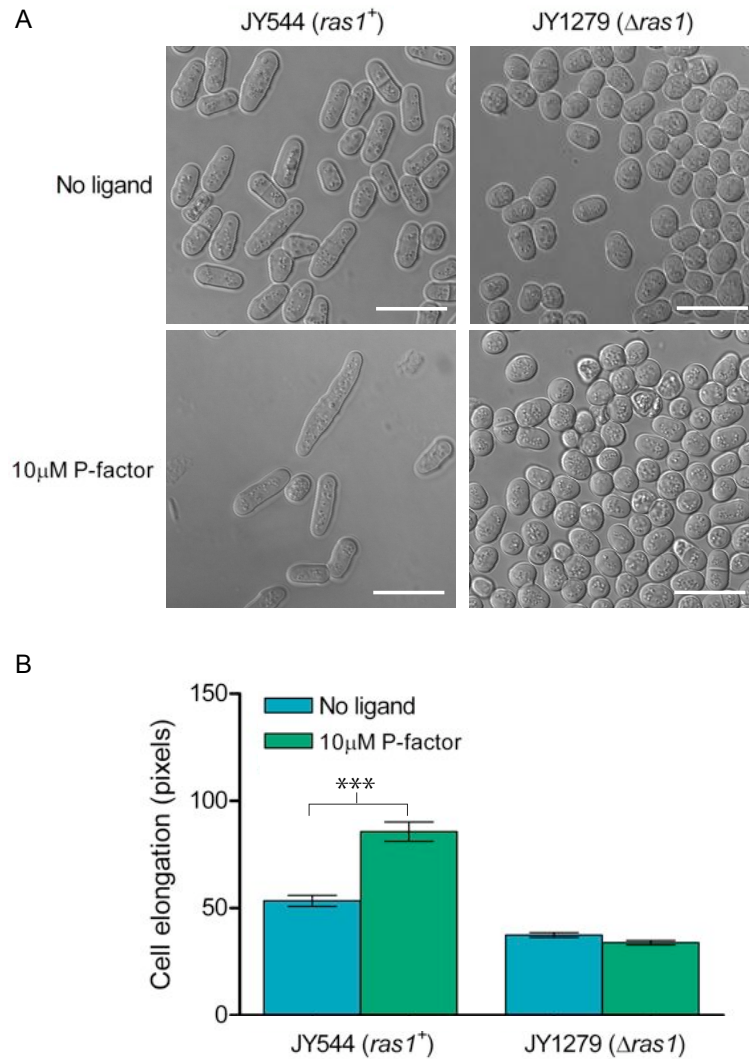


**Figure 4.13. Analysis of shmoo formation in JY544 (*ras1*<sup>+</sup>) and JY1279 ( $\Delta$ *ras1*) using quantitative imaging**

Images of cells containing wild-type Ras1 (JY544) and cells lacking Ras1 (JY1279) were obtained following growth in the absence and in the presence of 10  $\mu$ M pheromone after 16 h using a Leica SP5 scanning confocal microscope. Representative images are displayed in panel A. JY544 (*ras1*<sup>+</sup>) displayed a statistically significant ( $P = 0.001$ ), pheromone-dependent increase in cell length, whereas none was seen in JY1279 (B). Data shown is representative of 30 individual cells  $\pm$  SEM. Statistical significance was determined using a one-way anova with a Tukey multiple comparison post test. Three asterisks indicates a P-value of 0.001. Images from the populations analysed illustrate the pheromone responsive change in morphology observed in JY544. The scale bar represents 10  $\mu$ m.

assay condition. Cell length increased significantly in JY544 upon pheromone stimulation from  $53.4 \pm 2.6$  pixels to  $85.5 \pm 4.5$  pixels ( $P = 0.001$ ). Pheromone-responsive changes in cell length were not observed in cells lacking Ras1. The basal cell length of these cells was lower than that of JY544 ( $37.5 \pm 6.1$  pixels), indicating a shorter vegetative morphology. Cell elongation is also visible in images of JY544 upon pheromone stimulation. No change in morphology is seen in JY1279 (Figure 4.13A).

#### 4.3.3. Ras1 is required for pheromone-responsive cell cycle arrest.

To characterise the role of Ras1 in establishing a  $G_1$  cell cycle arrest, *ras1*<sup>+</sup> (JY544) and  $\Delta ras1$  (JY1279) cells were cultured in the presence (10  $\mu$ M P-factor) and absence of pheromone in DMM for 16 h (Figure 4.14). DNA complement was analysed using propidium iodide staining and flow cytometry for 30000 cells per strain and assay condition. In the absence of pheromone  $25.0 \pm 1.5$  % of cells containing Ras1 (JY544) were in  $G_1$ . This figure appears high for cells in the absence of pheromone, as *Sz. pombe* cells predominantly reside in  $G_2$  during mitotic growth. However, all cells used in this study were *cyr1*<sup>-</sup>, a genotype which mimics nutrient starvation. It is known that nutrient starvation also induces  $G_1$  arrest (Egel and Egel-Mitani 1974). As a consequence, the lack of Cyr1 in these cells could account for the high number of cells in  $G_1$ . JY1279 ( $\Delta ras1$ ) displayed lower levels of  $G_1$  cells, with  $8.4 \pm 1.8$  % of non-stimulated cells in  $G_1$ . Ras1 therefore appears to influence the number of cells in  $G_1$  in the absence of pheromone stimulation. These data could indicate a link between Ras1 and cell cycle progression in the absence of stimulation in a strain lacking Cyr1, and that Ras1 may influence cell cycle progression in response to nutrient starvation.

Upon pheromone stimulation for 6 h, JY544 cells displayed a significant shift from predominantly  $G_2$  to predominantly  $G_1$ , increasing from  $25.0 \pm 1.5$

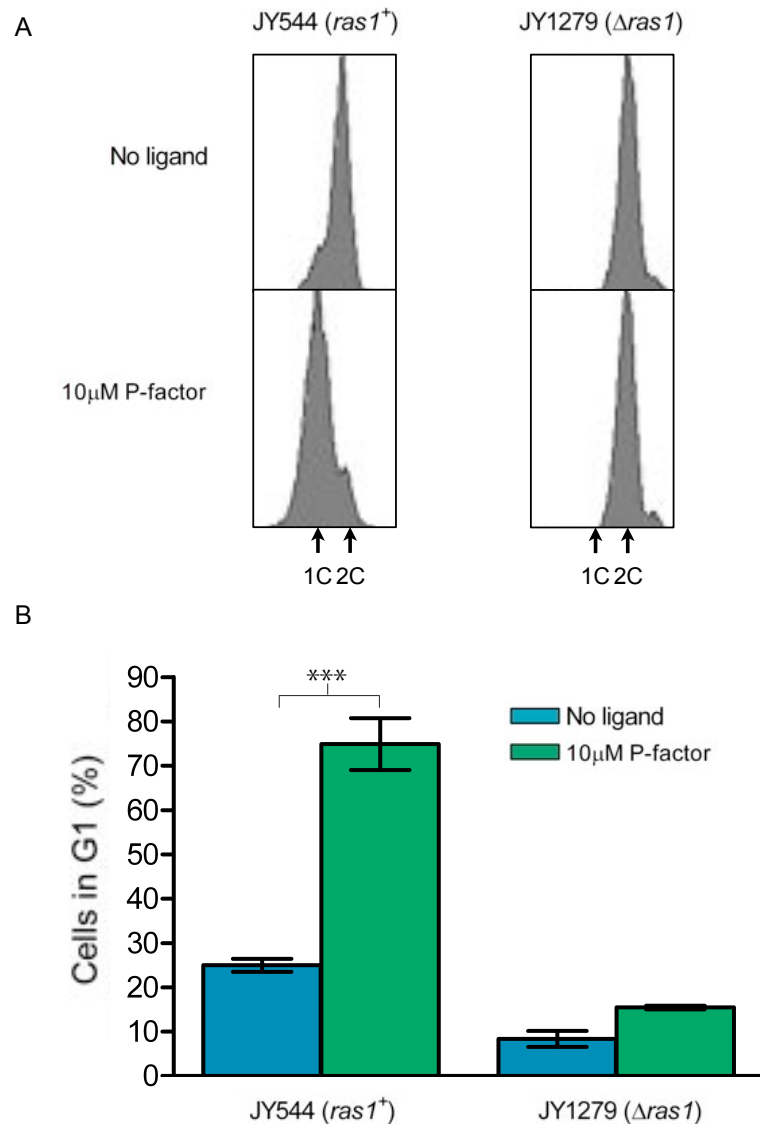


**Figure 4.14. Pheromone-responsive cell cycle arrest in JY544 (*ras1*<sup>+</sup>) and JY1279 ( $\Delta$ *ras1*)**

Cell cycle arrest was analysed in the strains JY544 and JY1279 using propidium iodide staining and flow cytometry after 6 h growth in the presence (10  $\mu$ M P-factor) and absence of pheromone. This analysis allowed the distinction between cells containing a single complement (1C) and double complement (2C) of DNA (A). JY544, but not JY1279, displayed a significant shift from cells largely residing in G<sub>2</sub> to cells largely residing in G<sub>1</sub> ( $P = 0.001$ ) (B). Data shown representative of three independent determinants  $\pm$  SEM. Statistical significance was determined using a one-way anova with a Tukey multiple comparison post test. Three asterisks indicates a P-value of 0.001.

% of cells in G<sub>1</sub> to  $74.9 \pm 5.8$  % of cells in G<sub>1</sub> ( $P = 0.001$ ). Cells lacking Ras1 displayed a small but not significant pheromone-dependent change in cell cycle position, increasing from  $8.4 \pm 1.8$  % to  $15.5 \pm 0.4$  % of cells in G<sub>1</sub>.

#### 4.3.4. Ras1 is required for mating.

To determine the requirement for Ras1 in mating, *ras1*<sup>+</sup> (JY544) and  $\Delta$ *ras1* (JY1279) cells expressing Sxa2 from pREP41x were assayed using the quantitative mating assay described in section 4.2.1. No iodine staining was observed following incubation of  $\Delta$ *ras1* (JY1279) cells with cells of the opposite mating type (JY1025). By contrast, iodine staining was observed in the population containing JY544, indicative of spore formation and mating. Quantitative analysis of mating indicated no cfu recovery in the population containing JY1279. JY544 exhibited a cfu recovery of  $32 \pm 2$  %. These data indicated that the loss of Ras1 caused cells to become sterile. (Figure 4.15). This observation is in concert with previous studies (Nadin-Davis *et al.* 1986).

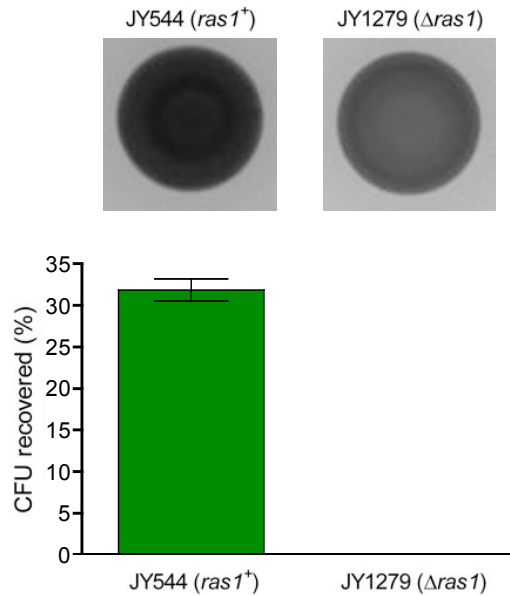


**Figure 4.15. Loss of Ras1 prevents mating in *Sz. pombe***

The mating of *ras1*<sup>+</sup> (JY544) and  $\Delta$ *ras1* (JY1279) strains expressing Sxa2 from pREP41x was assessed using the quantitative mating assay detailed in section 4.2.1. No mating was seen either through use of this assay or through iodine staining of spores in the strain JY1279. Data shown is representative of three independent determinants  $\pm$  SEM.

#### 4.4. Constitutive expression of Ras1

pREP vectors allow the controlled expression of specific genes within *Sz. pombe*. Expression from pREP vectors was used to determine the activity of Ras1 when expressed at a constant level, independent of control from the *ras1* promoter. Ras1 was expressed from the vector pREP3x, which contains a full strength *nmt1* promoter (Maundrell 1993), in the  $\Delta$ *ras1* strain JY1279 following growth in the absence of thiamine for 48h. The expression of Ras1 from pREP3x was then analysed by immunoblotting, using an anti-ras RAS10 antibody. A strong chemiluminescent signal was observed upon immunoblotting in whole cell extracts from cells expressing Ras1 from pREP3x. A second, smaller band was also seen. Due to the cross reactivity of the RAS10 antibody with multiple ras isoforms, it is likely that the antibody binds the more conserved N-terminus. The second band is therefore likely to contain an N-terminal region of the protein. This smaller band could be indicative of the

breakdown of Ras1 in these cells. In addition, it is possible that this represents a population of Ras1 which has not undergone C-terminal modification, or is a modification intermediate of Ras1 (Figure 4.16). The presence of a greater amount of Ras1 could allow the detection of such intermediates, which may be at very low concentrations in cells expressing Ras1 at wild-type levels.

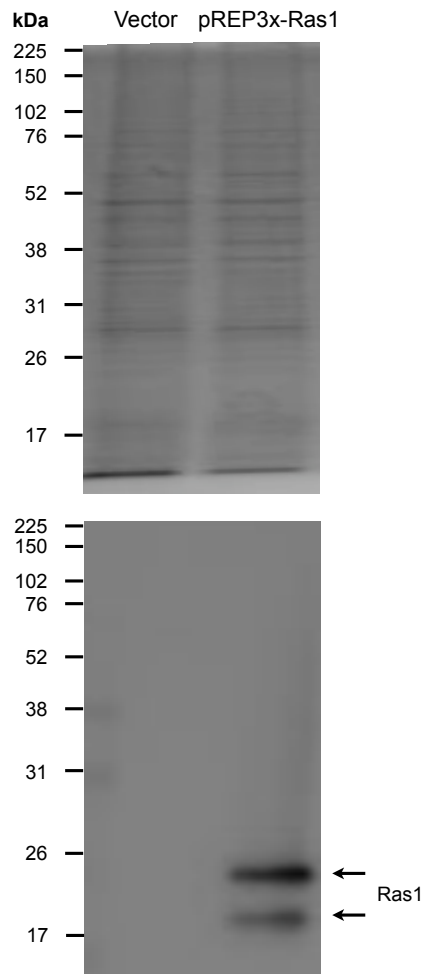


**Figure 4.16. Determining the expression of Ras1 from pREP3x using immunoblotting**

Expression of Ras1 from pREP3x in the  $\Delta ras1$  strain JY1279 was analysed through immunoblotting using a RAS10 anti-ras antibody. A strong chemiluminescent signal at a position consistent with the size of Ras1 was observed in whole cell extracts from these cells, but not from those containing vector alone. In addition, a second smaller band was seen, possibly indicating some breakdown of Ras1, or the presence of a modification intermediate. Coomassie stains of whole protein are included above the immunoblot as loading controls.

#### 4.4.1. Plasmid-borne Ras1 can rescue pheromone-responsive signalling in $\Delta ras1$ strains.

The signalling of cells expressing Ras1 from pREP3x was first determined through analysis of pheromone-responsive transcription and cell volume changes in response to pheromone. JY1279 ( $\Delta ras1$ ) transformed with pREP3x alone or pREP3x-Ras1 were grown with 1 nM to 100  $\mu$ M pheromone for 16 h in DMM lacking thiamine. Analysis of  $\beta$ -galactosidase activity revealed that cells containing pREP3x-Ras1 displayed a dose-response profile comparable to that observed in cells expressing Ras1 from the endogenous locus (pEC<sub>50</sub> of  $6.5 \pm 0.1$  compared to  $7.0 \pm 0.1$ ) (Figure 4.17A). However, the maximal signal was much lower than that observed in JY544, reaching only  $11.66 \pm 0.24$  compared to  $21.76 \pm 0.62$ . This observation appears counter-intuitive, as the constitutive expression of a positive regulator of signalling would not be expected to have a negative influence upon maximal signal. It would therefore suggest that the tight regulation of Ras1 expression is key to the magnitude of functional output.

Analysis of cell volume in cells containing pREP3x-Ras1 indicated an increase in cell size upon exposure to pheromone ( $75.9 \pm 1.1$  fl to  $85.0 \pm 0.7$  fl), however the cells displayed a high cell volume at basal signalling levels (Figure 4.17B). Images of these cells indicated that cells expressing Ras1 from pREP3x were markedly larger in the absence of pheromone (Figure 4.17C).

Expression of Ras1 from pREP3x elicited some pheromone-dependent signalling. To determine whether this signalling was sufficient to support mating, Ras1 was expressed from pREP3x in the  $\Delta ras1$  P-cell strain JY1351 (Prof. John Davey). JY1351 was used in this instance as pREP3x and pREP41x share the same selection marker, preventing the expression of Sxa2 from pREP41x. Mating was performed with the M-cell strain JY444. Quantitative analysis of spore formation indicated a degree of cfu recovery was observed ( $0.6 \pm 0.8$  %), however, it was not at a level significantly above that observed in the vector

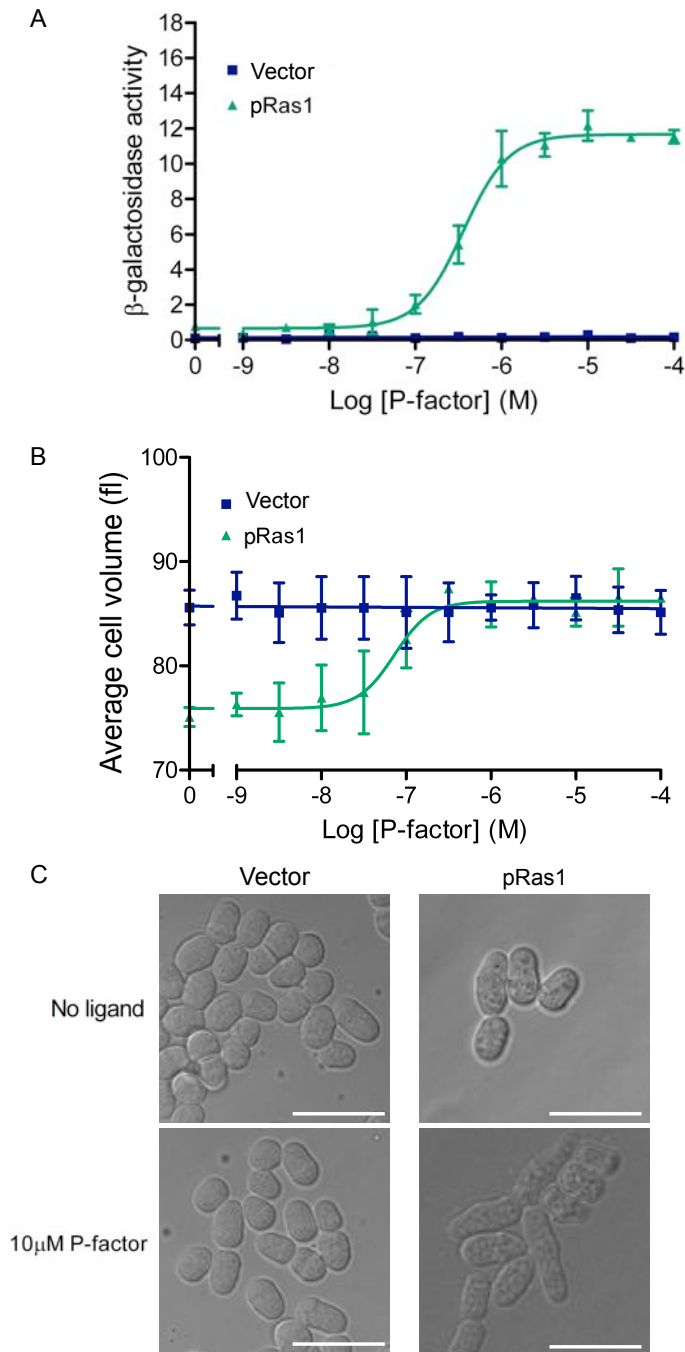


**Figure 4.17. Pheromone-responsive signalling in cells expressing Ras1 from pREP3x**

Pheromone-responsive changes in transcription and cell volume were observed in  $\Delta ras1$  (JY1279) cells transformed with vector alone and pREP3x-Ras1. Cells were grown in the presence of 1 nM to 100  $\mu$ M pheromone for 16 h in DMM lacking thiamine. Assays were then performed for  $\beta$ -galactosidase activity (A) and average cell volume (B). Images were also taken of each cell population (C). The scale bar represents 10  $\mu$ m. DIC images were taken using a Leica SP5 scanning confocal microscope. Pheromone-responsive signalling was observed in cells expressing Ras1 from pREP3x. Data shown is an average of three independent determinants ( $\pm$ SEM).

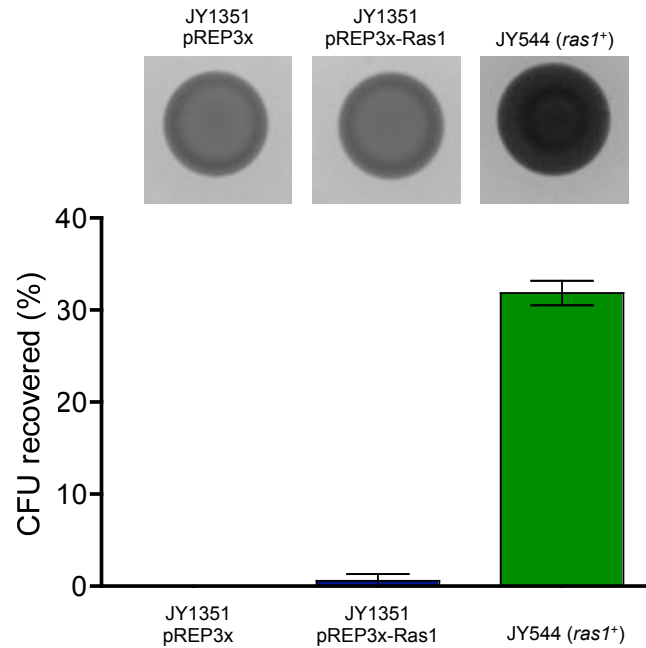


**Figure 4.18. Expression of Ras1 from pREP3x does not restore mating in  $\Delta ras1$  cells**

The mating of  $\Delta ras1$  (JY1351) cells transformed with vector alone and pREP3x-Ras1 was assessed using the quantitative mating assay detailed in section 4.2.1. The *ras1*<sup>+</sup> strain JY544 expressing Sxa2 from pREP41x is included as a control. No significant mating was seen in JY1351 transformed with either vector alone or pREP3x-Ras1. Data shown representative of three independent determinants  $\pm$  SEM.

alone control. This was reflected in the lack of iodine staining observed in this population, indicating a lack of mating and spore formation. By contrast, JY544 (*ras1*<sup>+</sup>) transformed with pREP41x-Sxa2 exhibited a cfu recovery of  $32 \pm 2$  % upon incubation with cells of the opposite mating type (Figure 4.18).

#### 4.4.2. Constitutive Ras1 expression alters cell morphology and the localisation of the cell tip marker Tea1.

Images of cells expressing Ras1 from pREP3x indicate an enlarged and more rounded morphology than that expected for wild-type cells (Figure 4.19A). This observation could indicate a change in the regulation of polar growth when Ras1 expression is not regulated by the *ras1* promoter. Thus, the localisation of the tip marker Tea1-mCherry was determined in  $\Delta ras1$  cells (JY1569)

transformed with pREP3x alone and pREP3x-Ras1, in order to establish the ability of Ras1 expressed from pREP3x to maintain polar cell organisation.

Images of these cells were obtained using a Nikon E800 epifluorescence microscope fitted with an Andor EM-CCD camera. In addition, images of  $\Delta ras1$  cells (JY1279) expressing Ras1 from pREP3x, and expressing GFP from pREP4x, were obtained using a Leica SP5 scanning confocal microscope. Cell circularity was then determined for 30 individual cells in these populations using Quimp software (Figure 4.19).

As is seen in  $\Delta ras1$  cells and the vector alone control, Tea1-mCherry in cells containing pREP3x-Ras1 showed some preferential localisation to opposite sides of the cortex, but Tea1-mCherry could be seen over the extent of the cell periphery (Figure 4.19C). Additionally, cells expressing Ras1 from pREP3x displayed a rounded morphology similar to the vector alone control ( $85.9 \pm 1.0$  % compared to  $87.2 \pm 1.8$  %) (Figure 4.19A and B). In contrast, cells expressing Ras1 from the *ras1* locus (JY544) exhibit the discrete localisation of Tea1-mCherry to opposite poles of the cell, and a significantly lower percentage cell circularity ( $73.5 \pm 1.2$ %,  $P = 0.001$ ). These data suggest that the regulation of Ras1 expression is also key to correct Ras1 function through Scd1-Cdc42.

#### **4.4.3. Constitutive Ras1 expression causes the formation of multiple shmoo tips.**

A key aspect of mating in fission yeast is the polar growth of a cell towards a cell of the opposite mating type. As a consequence, the loss of polarity observed in cells expressing Ras1 from pREP3x (Figure 4.19) could account for some of the loss of mating seen in these cells (Figure 4.18). Examination of JY1279 expressing Ras1 from pREP3x indicates that a number of cells form multiple projection tips (indicated by black arrows) upon stimulation with  $10 \mu\text{M}$  P-factor for 16 h (Figure 4.20). This observation could indicate that the

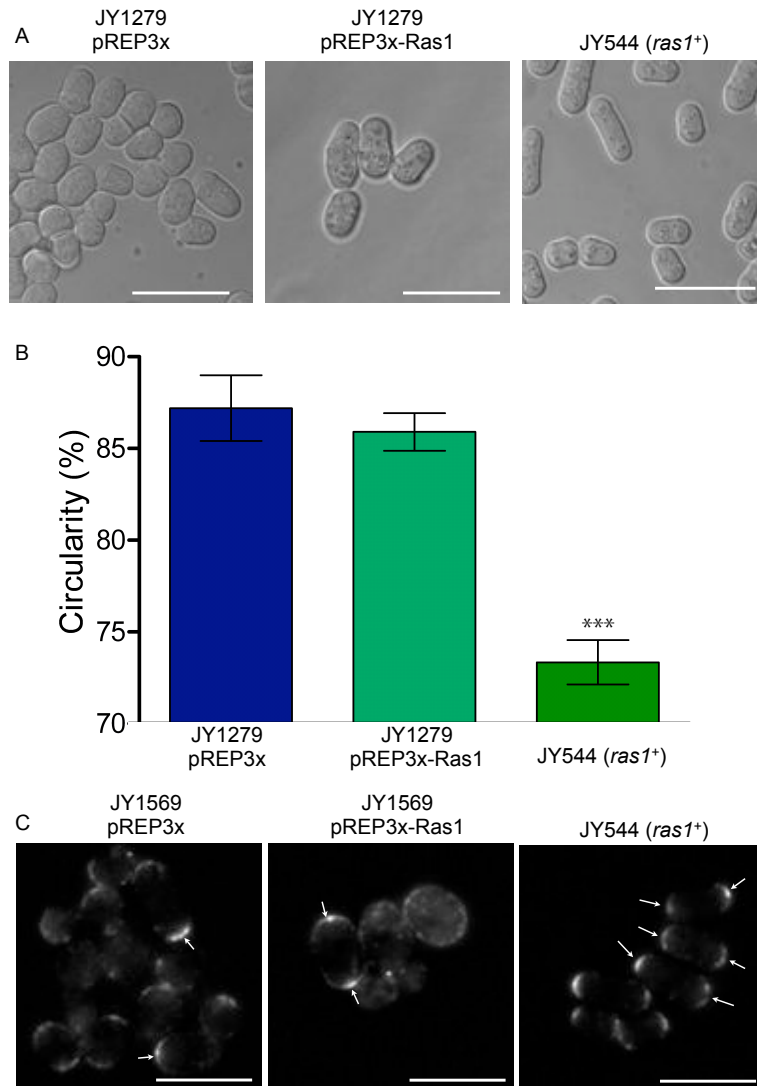


**Figure 4.19. Expression of Ras1 from pREP3x disrupts polar cell morphology**

Images of  $\Delta ras1$  cells (JY1279) transformed with vector alone and pREP3x-Ras1, expressing GFP from pREP4x, were obtained using a Leica SP5 scanning confocal microscope. Representative DIC images are displayed in panel A. Cell circularity was determined in these populations using Quimp software (B). Data representative of 30 individual cells  $\pm$  SEM. Cells containing pREP3x-Ras1 displayed a rounded morphology. Tea1-mCherry localisation was determined in a  $\Delta ras1$  strain (JY1569) transformed with vector alone and pREP3x-Ras1 using a Nikon E800 epifluorescence microscope fitted with an Andor EM-CCD camera (C). Tea1 was distributed around most of the cortex in cells containing pREP3x-Ras1. The scale bar represents 10  $\mu$ m. JY544 (*ras1*<sup>+</sup>) is also displayed to represent a wild-type phenotype.

regulation of Ras1 expression is important in directional sensing during mating and shmoo formation, and may explain the lack of mating observed in Figure 4.18.

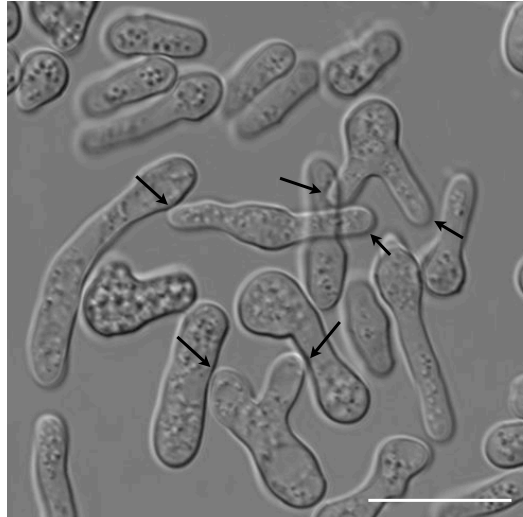


**Figure 4.20. Expression of Ras1 from pREP3x in  $\Delta ras1$  cells causes the formation of multiple shmoo tips**

The morphology of cells expressing Ras1 from pREP3x was examined following incubation in the presence of 10  $\mu\text{M}$  pheromone for 16 h. A number of cells within the population displayed multiple shmoo tips. DIC images were taken using a Leica SP5 scanning confocal microscope. The scale bar represents 10  $\mu\text{m}$ .

## 4.5. The localisation of Ras1

### 4.5.1. Constructing a GFP-Ras1 fusion.

Many previous studies have demonstrated the use of N-terminal GFP-ras fusions as a means of assessing ras localisation, while maintaining ras function (Choy *et al.* 1999; Chiu *et al.* 2002; Matallanas *et al.* 2006; Onken *et al.* 2006). A direct in-frame N-terminal *gfp-ras1* fusion was created at the *ras1* locus, to allow analysis of Ras1 localisation. Integration of *gfp-ras1* in the strain JY1247 (*ras1::ura4<sup>+</sup>*, *sxa2>lacZ*) was achieved using homologous recombination between flanking regions of the *ras1* locus and homologous regions flanking the *gfp-ras1* fusion in a linearised vector (Figure 4.21A). FOA selection was used to select for the loss of the *ura4<sup>+</sup>* cassette and integration of the fusion, generating the strain JY1390. Immunoblotting using an anti-ras RAS10 antibody gave a chemiluminescent signal consistent with the predicted size of the GFP-Ras1 fusion ( $\sim 52$ kDa) in whole cell extracts generated from JY1390. Little breakdown of the fusion was also observed (Figure 4.21B).

### 4.5.2. Ras1 is localised to the plasma membrane.

To determine the cellular localisation of Ras1, fluorescence images of cells from the strain JY1390 (*gfp-ras1*), grown in DMM, were obtained using a Nikon E800 epifluorescence microscope fitted with an Andor EM-CCD camera (Figure 4.22). The fluorescence level observed from these cells was very low, indicating that the GFP-Ras1 fusion was expressed at low levels. Despite this, the localisation of GFP-Ras1 could be observed at the plasma membrane, and was particularly apparent at the septa of dividing cells. Some localisation to peri-nuclear endomembrane structures may also have been present. The localisation of GFP-Ras1 has previously been described in one study, in which GFP-Ras1 was expressed from integrated plasmids containing the *ras1* promoter (Onken *et al.* 2006). As such, the localisation demonstrated in Figure

4.22 is the first localisation of GFP-Ras1 from the endogenous *ras1* locus described. The pattern of localisation seen in Figure 4.22 closely matches that previously observed.

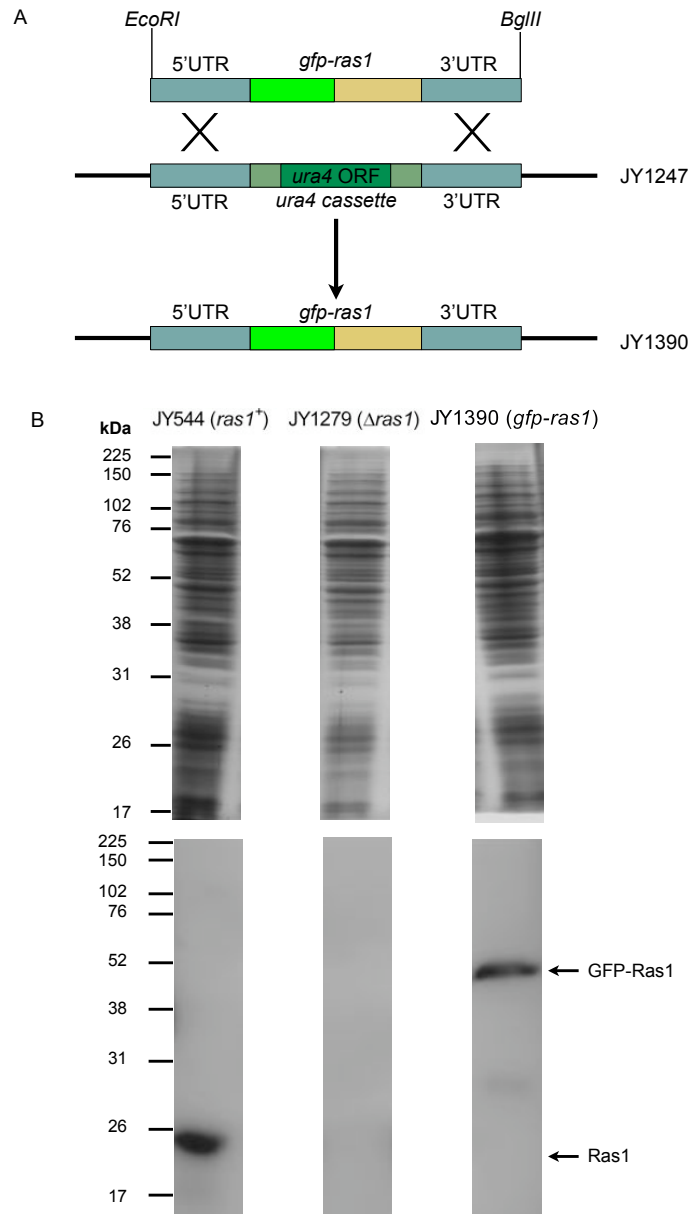


**Figure 4.21. Integration of GFP-Ras1**

Integration of GFP-Ras1 in the *ras1::ura4<sup>+</sup>, sxa2>lacZ* strain JY1247 was achieved by homologous recombination between flanking regions of the *ras1* ORF and homologous regions on a linearised vector (A). FOA selection was used to select for the loss of *ura4*. Expression was confirmed via immunoblotting using a RAS10 antibody (B). Expression of GFP-Ras1 (JY1390) was demonstrated, and a chemiluminescent signal was observed at a position consistent with the size of the fusion (~ 52kDa). Coomassie stains of whole protein are included above the immunoblot as loading controls.

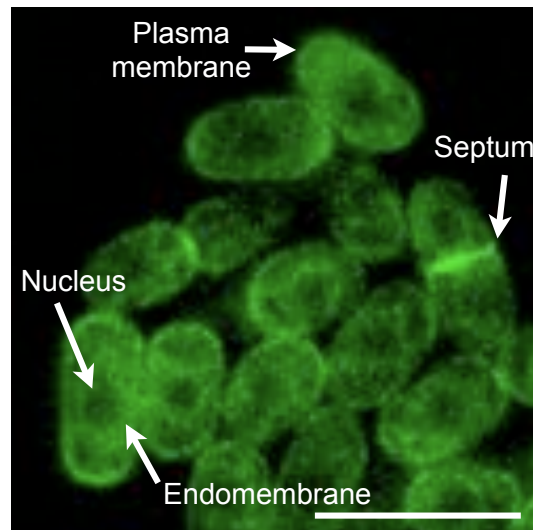


**Figure 4.22. The localisation of GFP-Ras1**

The localisation of GFP-Ras1 in the strain JY1390 (*gfp-ras1*) was determined using a Nikon E800 epifluorescence microscope fitted with an Andor EM-CCD camera. GFP-Ras1 was observed at the plasma membrane and peri-nuclear endomembrane structures. The scale bar represents 10  $\mu\text{m}$ .

#### 4.5.3. GFP-Ras1 is functional but displays reduced signalling activity.

To determine whether the activity of Ras1 was affected by the addition of GFP to the N-terminus, the activity of GFP-Ras1 was first analysed through the investigation of cell morphology (Figure 4.23). Images of *ras1*<sup>+</sup> (JY544),  $\Delta$ *ras1* (JY1279) and *gfp-ras1* (JY1390) cells, expressing GFP from pREP3x to allow detection of the cell, were obtained using a Leica SP5 scanning confocal microscope. Quimp software was used to determine the morphology 30 individual cells within these populations. pREP3x-GFP was used as the GFP-Ras1 signal was not sufficient to allow detection of the cell upon visualisation using the Leica SP5 scanning confocal microscope.

JY1390 cells displayed a significantly lower percent circularity than  $\Delta$ *ras1* cells ( $P = 0.001$ ). JY1390 cells displayed only a slightly more rounded morphology than *ras1*<sup>+</sup> cells (JY544) ( $78.3 \pm 1.1\%$  compared to  $73.4 \pm 1.2\%$ ), possibly indicating a slightly decreased signalling activity through GFP-Ras1.

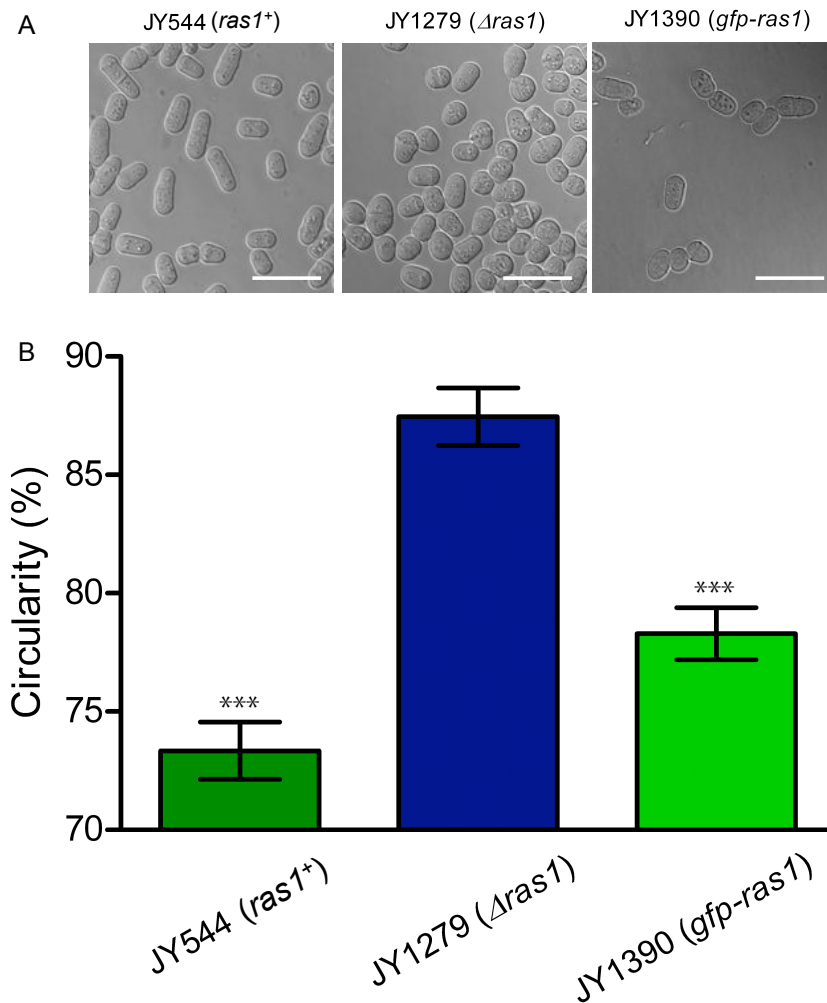


**Figure 4.23.** The morphology of cells expressing GFP-Ras1 from the endogenous *ras1* locus.

Images of *ras1*<sup>+</sup> (JY544),  $\Delta$ *ras1* (JY1279) and *gfp-ras1* (JY1390) cells, expressing GFP from pREP3x, were obtained using a Leica SP5 scanning confocal microscope. Representative DIC images are displayed in panel A. Cell circularity was determined using Quimp software (B). Cells expressing GFP-Ras1 displayed a significantly lower percentage circularity than cells lacking Ras1 ( $P = 0.001$ ). Data representative of 30 individual cells  $\pm$  SEM. Statistical significance was determined using a one-way anova with a Tukey multiple comparison post test. Three asterisks indicates a P-value of 0.001. The scale bar represents 10  $\mu$ m.

Cells expressing GFP-Ras1 exhibited a slightly reduced level of signalling through the cell polarity pathway. To determine whether the pheromone response was also impaired, the pheromone-dependent signalling of GFP-Ras1 was first investigated through analysis of transcription and cell volume.  $\beta$ -galactosidase activity and average cell volume were determined in cells grown in a range of pheromone concentrations (1 nM to 100  $\mu$ M) in DMM for 16

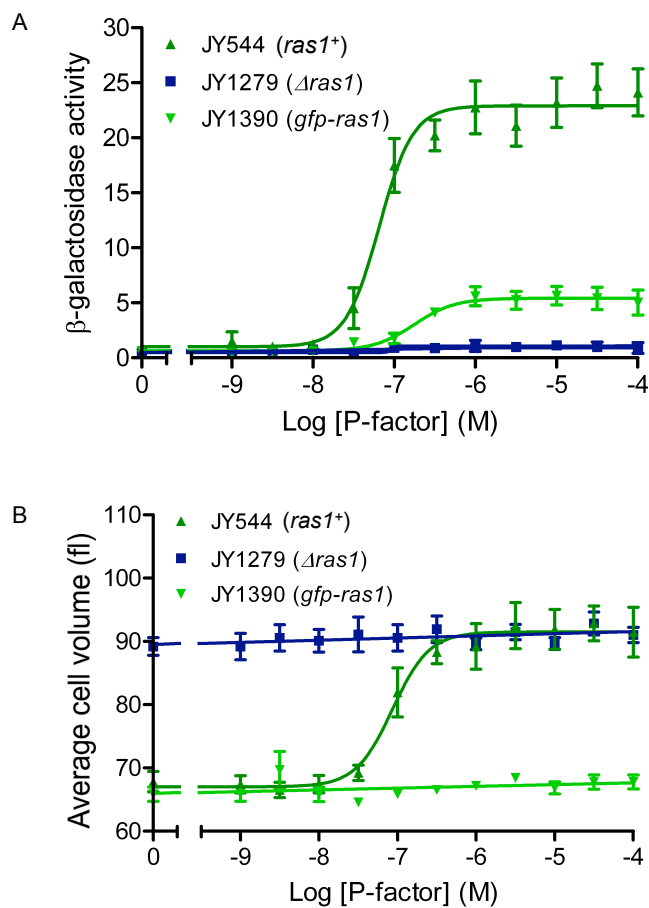


**Figure 4.24. Pheromone-dependent changes in transcription and cell volume in cells expressing GFP-Ras1**

Pheromone-responsive changes in transcription and cell volume were observed in *ras1*<sup>+</sup> (JY544),  $\Delta$ *ras1* (JY1279) and *gfp-ras1* (JY1390) cells. Cells were grown in 1 nM to 100  $\mu$ M pheromone in DMM for 16 h. Assays were then performed for  $\beta$ -galactosidase activity (A) and average cell volume (B). Reduced maximal  $\beta$ -galactosidase activity was seen in JY1390 compared to JY544, and no pheromone-dependent increase in cell volume was observed. Data shown is an average of three independent determinants ( $\pm$ SEM).

h. In  $\beta$ -galactosidase assays for pheromone-responsive transcription, JY1390 (*gfp-ras1*) displayed a markedly lower level of maximal signalling than JY544 (*ras1*<sup>+</sup>) ( $5.4 \pm 0.3$  compared to  $22.9 \pm 0.7$ ) but a similar  $pEC_{50}$  to pheromone ( $6.8 \pm 0.1$  compared to  $7.2 \pm 0.1$ ) (Figure 4.24A). No change in cell volume was observed upon pheromone stimulation in JY1390, however the strain displayed a low basal cell volume consistent with cells containing wild-type Ras1 (Figure 4.24B). This observation again indicates that GFP-Ras1 has a reduced signalling activity.

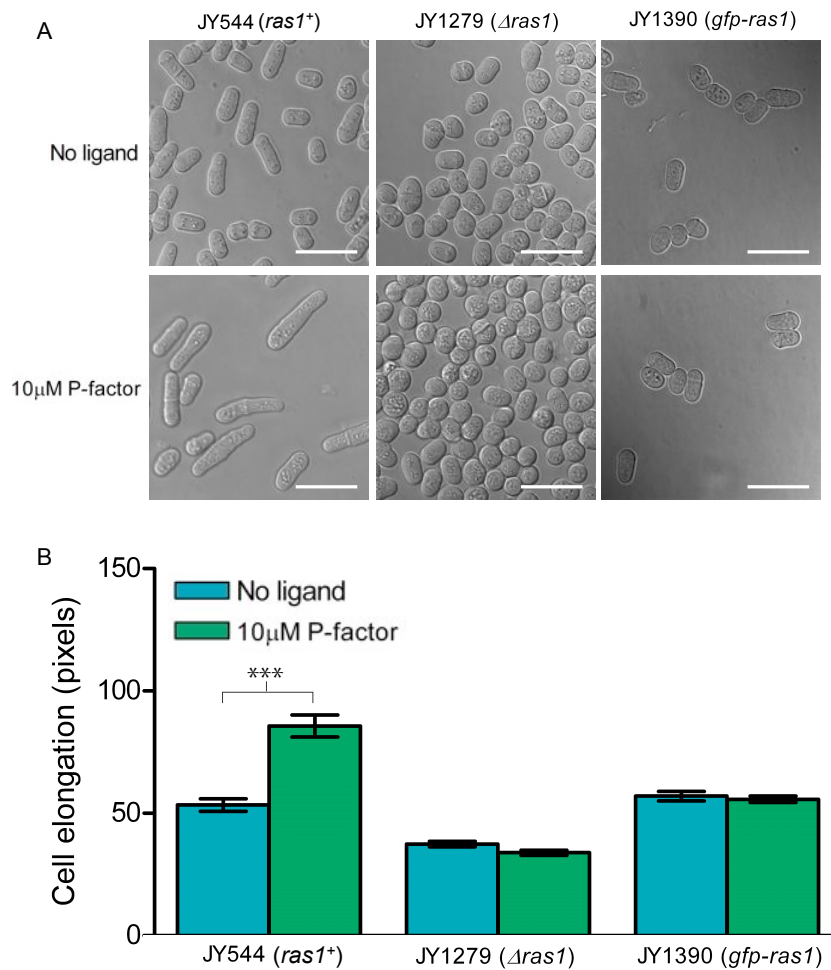


**Figure 4.25. Analysis of shmoo formation in cells expressing GFP-Ras1 using quantitative imaging**

Images of cells containing wild-type Ras1 (JY544), GFP-Ras1 (JY1390) and cells lacking Ras1 (JY1279), expressing GFP from pREP3x, were obtained following growth in the absence and in the presence of 10  $\mu$ M pheromone after 16 h, using a Leica SP5 scanning confocal microscope. Representative DIC images are displayed in panel A. JY1279 ( $\Delta$ *ras1*) and JY1390 (*gfp-ras1*) display no pheromone dependent change in cell length. Cells expressing GFP-Ras1 displayed a basal cell length consistent with that seen in JY544 (B). Data shown is representative of 30 individual cells  $\pm$  SEM. Statistical significance was determined using a one-way anova with a Tukey multiple comparison post test. Three asterisks indicates a P-value of 0.001. Images from the populations analysed indicate no pheromone dependent change in cell morphology in cells expressing GFP-Ras1. The scale bar represents 10  $\mu$ m.

No pheromone-dependent change in cell volume was seen in JY1390 (*gfp-ras1*). Quantitative analysis of cell length, however, provides a more direct measure of cell elongation in response to pheromone. To determine whether any shmoo formation could be observed in these cells, images of *ras1*<sup>+</sup> (JY544),

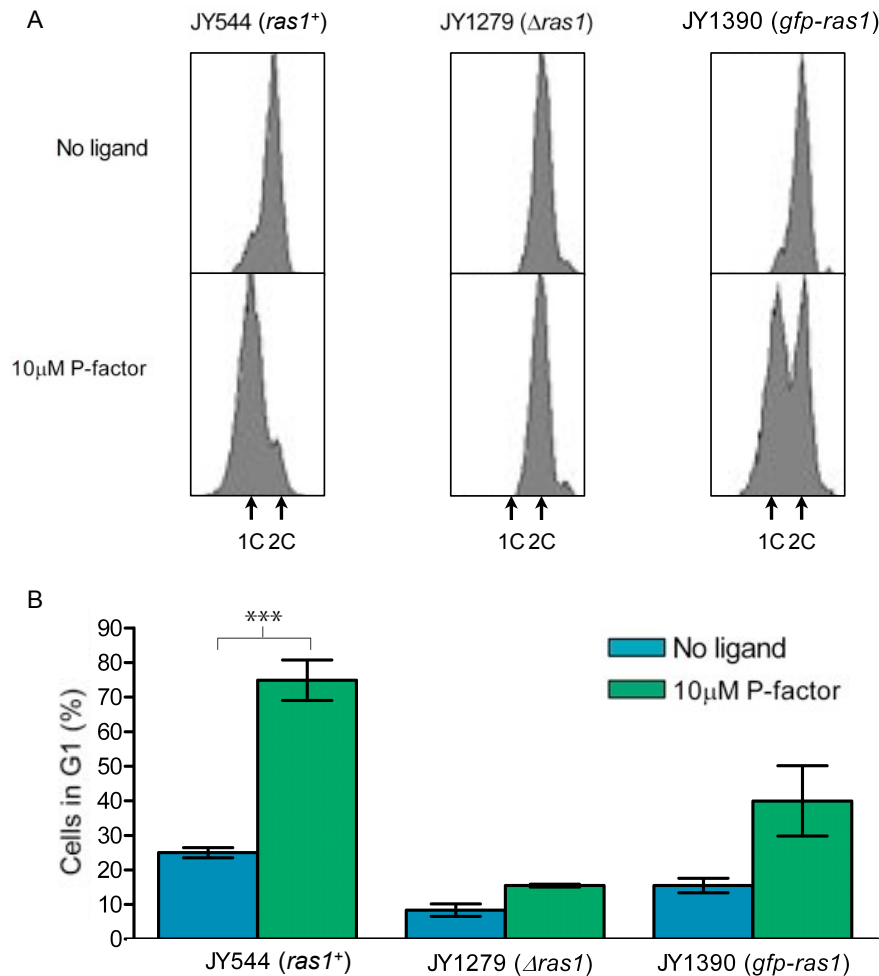


**Figure 4.26. Phormone-responsive changes in cell cycle position in cells expressing GFP-Ras1**

Cell cycle arrest was analysed in strains the JY544 (*ras1*<sup>+</sup>), JY1279 ( $\Delta$ *ras1*) and JY1390 (*gfp-ras1*) using propidium iodide staining and flow cytometry after growth in the presence (10 µM P-factor) and absence of pheromone in DMM for 6 h. This analysis allowed the distinction between cells containing a single complement (1C) and double complement (2C) of DNA (A). Cells expressing GFP-Ras1 (JY1390) displayed some phormone-dependent G<sub>1</sub> arrest (B). Data shown representative of three independent determinants  $\pm$  SEM. Analysis was performed for 30000 cells. Statistical significance was determined using a one-way anova with a Tukey multiple comparison post test. Three asterisks indicates a P-value of 0.001.

$\Delta$ *ras1* (JY1279) and *gfp-ras1* (JY1390) cells, expressing GFP from pREP3x, were obtained using a Leica SP5 scanning confocal microscope. Images were taken of cells grown in the presence (10 µM P-factor) and absence of pheromone in DMM lacking thiamine for 16 h. The length of 30 individual cells of each strain and each assay condition was analysed using Quimp quantitative imaging software (Figure 4.25B). JY1390 displayed a basal cell length consistent

with that observed in *ras1*<sup>+</sup> (JY544) cells ( $57.0 \pm 1.9$  pixels and  $53.4 \pm 2.6$  respectively), indicative of an elongated vegetative morphology. No pheromone-dependent increase in cell length was observed in JY1390. Images of these cells also indicate no change in morphology upon pheromone stimulation (Figure 4.25A). These data confirm the observations described in Figure 4.24.

In all measures of pheromone-dependent signalling utilised to this point, cells expressing GFP-Ras1 exhibit a reduced level of activity. To determine whether pheromone-dependent G<sub>1</sub> arrest was also reduced, analysis of cell cycle position in response to pheromone was also performed in the *gfp-ras1* strain JY1390. Cells were analysed using propidium iodide staining and flow cytometry following growth in the presence (10  $\mu$ M P-factor) and absence of pheromone in DMM for 6 h. JY1390 displayed an increase in the percentage of cells in G<sub>1</sub> upon stimulation with 10  $\mu$ M P-factor ( $17.9 \pm 3.2$  % to  $40.0 \pm 10.1$  %) (Figure 4.26B). Although this increase was not statistically significant, a clear increase in cells containing a single complement of chromosomal DNA (1C) could be seen upon stimulation with pheromone (Figure 4.26A). The increase in G<sub>1</sub> arrest observed in JY1390 is however markedly lower than that exhibited by JY544, again indicating a reduced level of signalling in cell containing GFP-Ras1.

#### **4.5.4. GFP-Ras1 is able to rescue mating when expressed from the *ras1* locus.**

GFP-Ras1 displayed signalling activity in most of the assays performed, albeit at reduced levels compared to wild-type Ras1. To determine whether GFP-Ras1 could support mating, JY1390 (*gfp-ras1*), expressing Sxa2 from pREP41x, was mixed with a wild-type P-cell (JY1025) strain, and a quantitative mating assay was performed (as detailed in section 4.2.1). JY1390 displayed a mating efficiency comparable to JY544, giving a cfu recovery of  $31 \pm 7$  % compared to  $32 \pm 2$  %. These data indicate that GFP-Ras1 is able

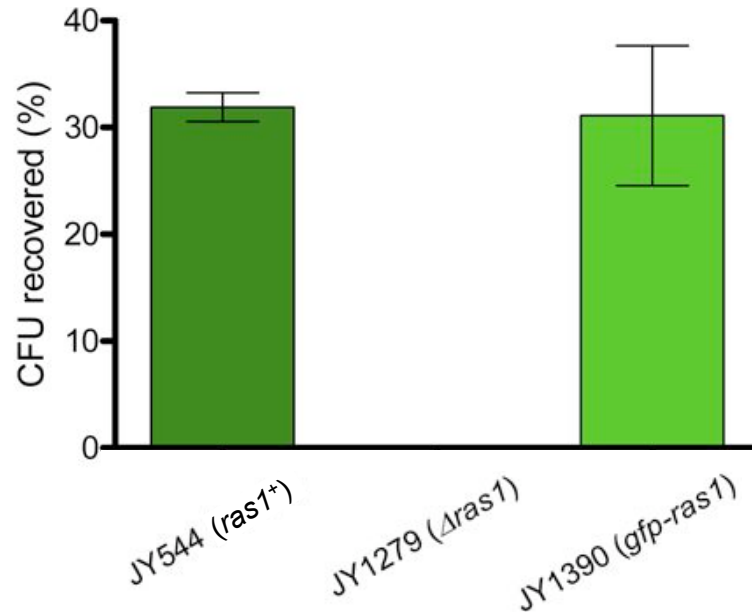


**Figure 4.27. Mating efficiency in cells expressing GFP-Ras1**

The mating of *ras1*<sup>+</sup> (JY544),  $\Delta$ *ras1* (JY1279) and *gfp-ras1* (JY1390) cells expressing Sxa2 from pREP41x was assessed using the quantitative mating assay detailed in section 4.2.1. JY544 and JY1390 displayed similar levels of mating. Data shown representative of three independent determinants  $\pm$  SEM. Statistical significance was determined using a one-way anova with a Tukey multiple comparison post test. No statistically significant difference in mating was observed between JY544 and JY1390.

to fully restore mating, despite supporting lower levels for transcriptional activity and no shmoo formation in response to pheromone. The observation could indicate that in denser cell populations cell proximity negates the need for extensive morphological changes in response to pheromone.

In the preceding section, the localisation and activity of GFP-Ras1, expressed from the *ras1* locus, was described. In this series of experiments GFP-Ras1 was demonstrated to localise predominantly to the plasma membrane, with some localisation to endomembranes. This localisation is in agreement with that previously described (Onken *et. al.* 2006). The level of expression of this fusion was however extremely low. GFP-Ras1 was also demonstrated to be functional in regulating cell morphology, pheromone-response and mating, but with a slightly reduced activity.

#### 4.6. Investigation of Ras1 mutants displaying altered activity

Mutation of ras is of high clinical significance, most notably in the progression of cancer. As a consequence, many mutations in ras have been studied extensively. The majority of these mutants fall into two broad categories, those which are deficient in their GTPase activity and those which are deficient in GDP-GTP exchange. The first category of mutant is the most clinically relevant, being involved in a significant majority of human cancers (McCormick 1989). Most of these mutations occur in regions responsible for interacting with the  $\gamma$ -phosphate of GTP, such as the Gly12Val mutant in human ras isoforms, or regions involved in the catalysis of GTP hydrolysis, such as the Gln61Leu mutant in human ras (Krengel *et al.* 1990; Tong *et al.* 1991). These mutants prevent the inactivation of ras following GTP binding. Of the inactive mutants, the majority are deficient in their interaction with GEFs, such as the Ser17Asn mutant in human ras (Feig and Cooper 1988; Jung *et al.* 1994), or in their interaction with downstream effectors, such as the Asp38Asn mutant (Akasaka *et al.* 1996). As a result, these mutations prevent ras signalling. Such mutants provide highly informative tools to analyse the characteristics of ras signalling, allowing the investigation of ras proteins with specific changes in their signalling activity.

##### 4.6.1. Integration of *ras1* mutants displaying altered activity.

Ras1 expression levels appear key to correct function (section 4.4). As such, three separate *ras1* mutants with altered activity were integrated at the *ras1* locus. The first two mutants, *ras1*<sup>Q66L</sup> and *ras1*<sup>G17V</sup>, are based on the best characterised oncogenic mutations (Gly12Val and Gln61Leu) in human ras isoforms. The third mutation, *ras1*<sup>S22N</sup>, is derived from the inactive ras mutant Ser17Asn. This mutant was used as the Asp38Asn inactive mutation has been shown to still interact with the downstream Ras1 binding protein Byr2 (Akasaka *et al.* 1996; Kae *et al.* 2004). Integration was performed in the

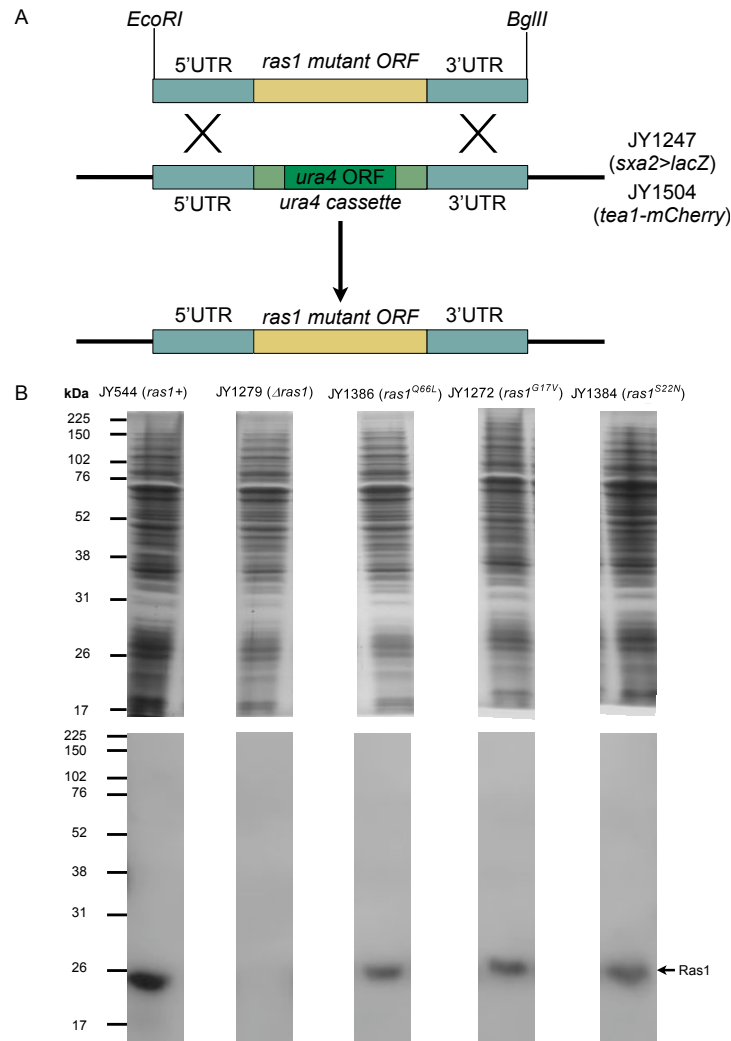


**Figure 4.28. Integration of  $ras1^{Q66L}$ ,  $ras1^{G17V}$  and  $ras1^{S22N}$  in the  $sxa2>lacZ$  reporter strain**

Integration of  $ras1^{Q66L}$ ,  $ras1^{G17V}$  and  $ras1^{S22N}$  was achieved through homologous recombination and FOA selection for the loss of  $ura4$  (A). Integration was confirmed by immunoblotting in JY1247 ( $sxa2>lacZ$ ) (B) using an anti-ras RAS10 antibody. Coomassie stains of whole protein are included above the immunoblot as loading controls.

$\Delta ras1::ura4^+$  strains JY1247 ( $sxa2>lacZ$ ), to enable analysis of pheromone-dependent transcription, and JY1504 ( $tea1-mCherry$ ), to allow visualisation of polar cell organisation. The mutant  $ras1$  ORFs were introduced using homologous recombination and selection for the loss of the  $ura4^+$  cassette by culturing on FOA. Integration was confirmed by immunoblotting, using the anti-ras antibody RAS10 (Figures 4.28 and 4.29). JY1272 was generated by Dr. Rachel Forfar.

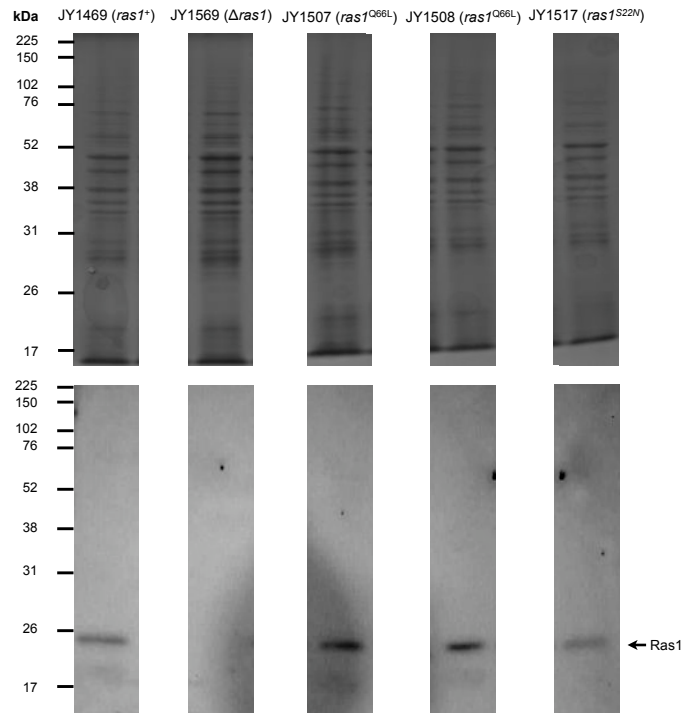


**Figure 4.29.** Integration of  $ras1^{Q66L}$ ,  $ras1^{G17V}$  and  $ras1^{S22N}$  in the *Tea1-mCherry*, *sxa2>lacZ* strain

Integration of  $ras1^{Q66L}$ ,  $ras1^{G17V}$  and  $ras1^{S22N}$  was achieved through homologous recombination and FOA selection (as detailed in Figure 4.28A). Integration was confirmed by immunoblotting in JY1569 (*tea1-mCherry*) using an anti-ras RAS10 antibody. Coomassie stains of whole protein are included above the immunoblot as loading controls.

#### 4.6.2. Characterisation of Ras1<sup>S22N</sup>.

4.6.2.1. *Integrated Ras1<sup>S22N</sup> does not rescue cell morphology.* The ser17Asn mutation in human ras isoforms prevents ras activity. To determine whether the equivalent mutation in Ras1 (Ser22Asn) also results in inactivity, the morphology of the strain JY1384 ( $ras1^{S22N}$ , *sxa2>lacZ*) was determined using quantitative imaging. The localisation of Tea1-mCherry was analysed in the strain JY1517 ( $ras1^{S22N}$ , *tea1-mCherry*) to investigate the activity of  $ras1^{S22N}$  in regulating cell morphology. Images of Tea1-mCherry localisation were obtained using a Nikon E800 epifluorescence microscope fitted with an Andor EM-CCD camera. Cells expressing ( $ras1^{S22N}$ ) displayed a lack of polar Tea1-mCherry localisation, comparable to that seen in  $\Delta ras1$  cells (Figure 4.30C).

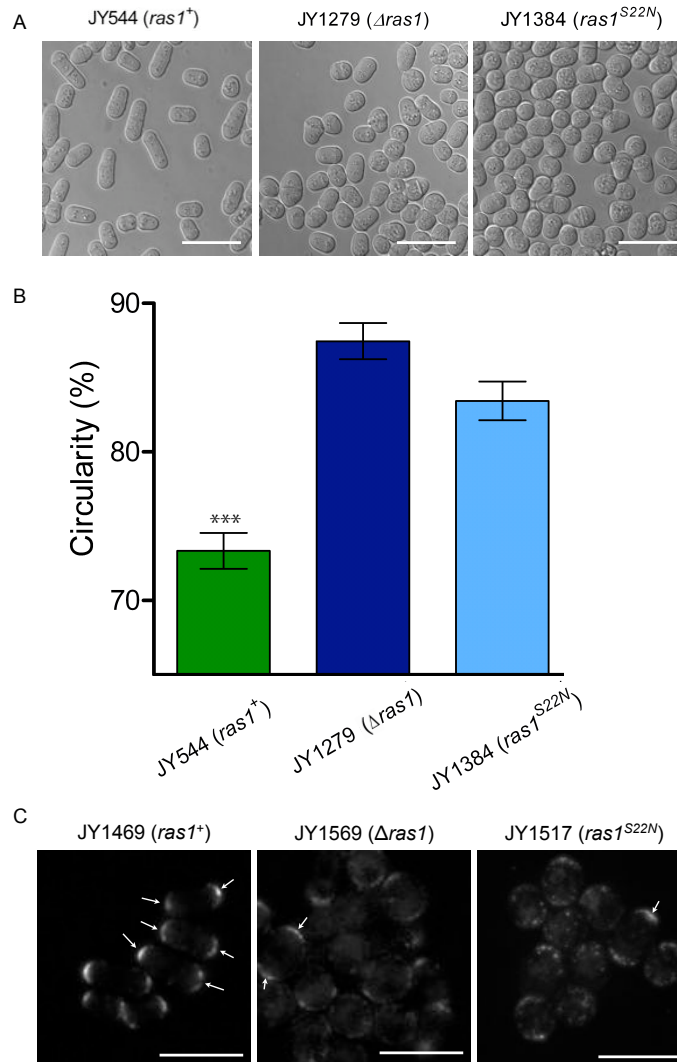


**Figure 4.30.** The morphology of cells expressing *ras1*<sup>S22N</sup>

Images of cells lacking *ras1* (JY1279), cells expressing *ras1*<sup>S22N</sup> (JY1386) and cells expressing *ras1* (JY544), expressing GFP from pREP3x, were obtained using a Leica SP5 scanning confocal microscope. Representative DIC images are displayed in panel A. Cell circularity was determined using Quimp software (B). Cells expressing Ras1<sup>S22N</sup> displayed a high percent circularity comparable to cells lacking Ras1. Data representative of 30 individual cells  $\pm$  SEM. Three asterisks indicates a P value of 0.001. The localisation of Tea1-mCherry was determined in *ras1*<sup>+</sup> cells (JY1469),  $\Delta$ *ras1* cells (JY1569) and cells expressing Ras1<sup>S22N</sup> (JY1517) using a Nikon E800 epifluorescence microscope fitted with an Andor EM-CCD camera (C). Cells lacking Ras1 and those expressing Ras1<sup>S22N</sup> displayed a loss of polar Tea1-mCherry localisation. The scale bar represents 10  $\mu$ m.

The majority of cells containing *ras1*<sup>S22N</sup> exhibited Tea1-mCherry localisation to the extent of the cell periphery. Some cells displayed a degree of polar Tea1-mCherry localisation, although this was less defined than in cells containing wild-type Ras1.

Images of *ras1*<sup>+</sup> (JY544),  $\Delta$ *ras1* (JY1279) and *ras1*<sup>S22N</sup> (JY1384) cells, expressing GFP from pREP3x, were obtained using a Leica SP5 scanning confocal microscope, to allow analysis of their morphology. Quimp software was then used to determine the morphology 30 individual cells within these populations. Cells expressing *ras1*<sup>S22N</sup> exhibited a predominantly rounded morphology, similar to cells lacking Ras1 (Figure 4.30A). This corresponded with a high percent circularity in these cells ( $83.4 \pm 1.3$  % compared to  $87.5 \pm 1.2$  % in cells lacking Ras1) (Figure 4.30B).

A previous study (Jung *et al.* 1994), had suggested that the *ras1*<sup>S22N</sup> mutant still supported polar cell morphology. This study presented single polar cells in highly heterogenous populations as evidence of signalling. The data presented in Figure 4.30 suggest that within a heterogenous population the overriding morphology is that of a rounded cell (based upon quantitative imaging) that lacks polarity (based upon Tea1-mCherry localisation). This observation highlights the importance of population based analysis of signalling activity, reducing the influence of outlying cells.

4.6.2.2. *Pheromone responsive signalling in cells expressing Ras1*<sup>S22N</sup>. Previous studies (Jung *et al.* 1994) have indicated that Ras1<sup>S22N</sup> is unable to support conjugation and mating. These data suggest that Ras1<sup>S22N</sup> is unable to signal through Byr2. To confirm this hypothesis,  $\beta$ -galactosidase activity and average cell volume were determined for cells grown in a range of pheromone concentrations (1 nM to 100  $\mu$ M) in DMM for 16, using the strain JY1384 (*ras1*<sup>S22N</sup>). Cells expressing Ras1<sup>S22N</sup> displayed a slight increase in  $\beta$ -galactosidase activity upon pheromone stimulation ( $1.0 \pm 0.1$  to  $2.4 \pm 1.2$ ) (Figure 4.31A), and no increase in average cell volume was observed (Figure

4.31B). The slight increase in  $\beta$ -galactosidase activity observed could indicate that Ras1<sup>S22N</sup> retains some function, although not enough to support mating or cell polarity.

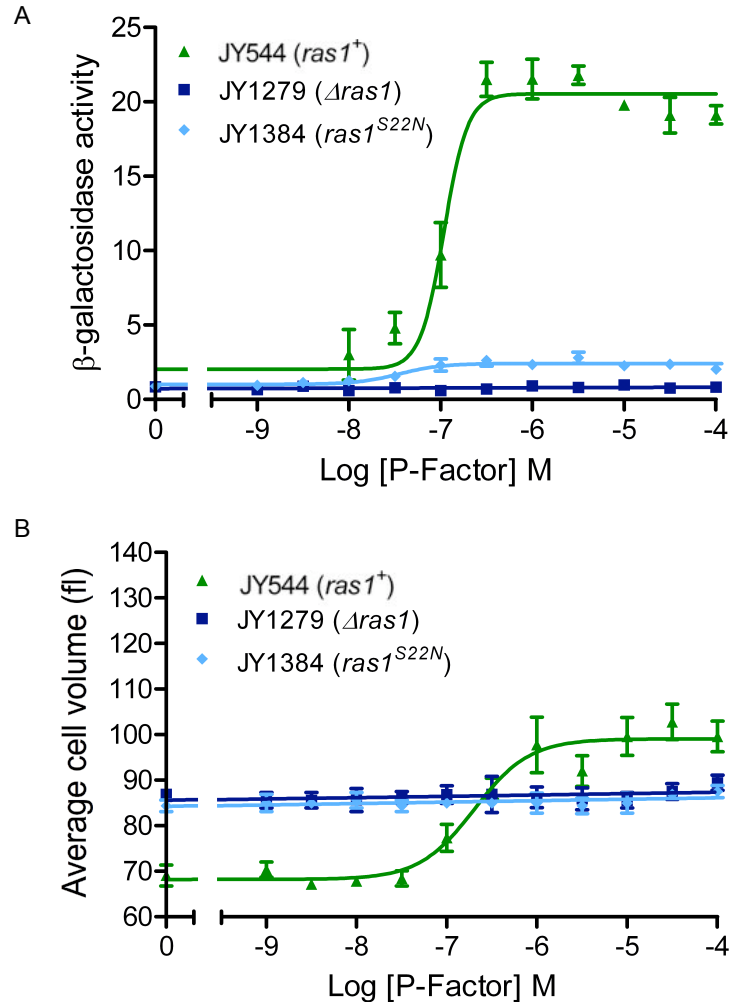


**Figure 4.31. Pheromone-responsive transcription and changes in cell volume in cells expressing Ras1<sup>S22N</sup>**

Pheromone-responsive changes in transcription and cell volume were observed in *ras1*<sup>+</sup> (JY544) cells,  $\Delta$ *ras1* (JY1279) cells, and cells expressing Ras1<sup>S22N</sup>. Analysis was performed following growth in 1 nM to 100  $\mu$ M pheromone in DMM for 16 h. Assays were then performed for  $\beta$ -galactosidase activity (A) and average cell volume (B). Cells expressing Ras1<sup>S22N</sup> displayed a small increase in  $\beta$ -galactosidase activity upon pheromone stimulation, but no increase in cell volume. Data shown is an average of three independent determinants ( $\pm$ SEM).

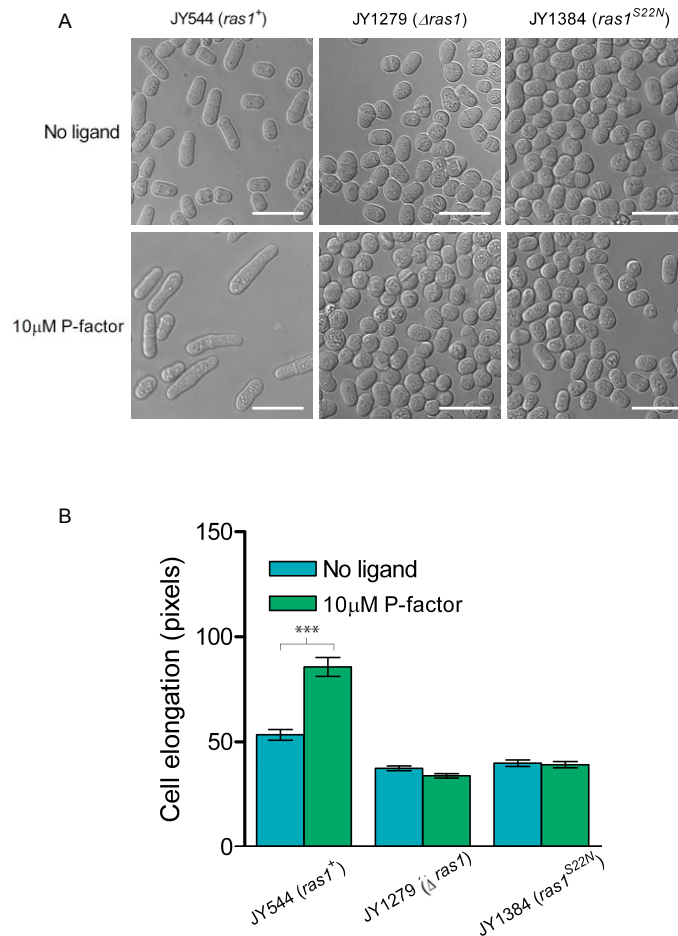


**Figure 4.32. Analysis of shmoo formation in cells expressing Ras1<sup>S22N</sup> using quantitative imaging**

Images of *ras1*<sup>+</sup> (JY544),  $\Delta$ *ras1* (JY1279) and *ras1*<sup>S22N</sup> (JY1384) cells were obtained following 16 h growth in the absence and in the presence of 10  $\mu$ M pheromone in DMM lacking thiamine, using a Leica SP5 scanning confocal microscope. Representative DIC images are displayed in panel A. Quimp software was then used to determine cell length. JY1279 ( $\Delta$ *ras1*) and JY1384 (*ras1*<sup>S22N</sup>) display no pheromone dependent change in cell length. Data shown is representative of 30 individual cells  $\pm$  SEM. Statistical significance was determined using a one-way anova with a Tukey multiple comparison post test. Three asterisks indicates a P-value of 0.001. Images from the populations analysed indicate no pheromone dependent change in cell morphology in cells expressing Ras1<sup>S22N</sup>. The scale bar represents 10  $\mu$ m.

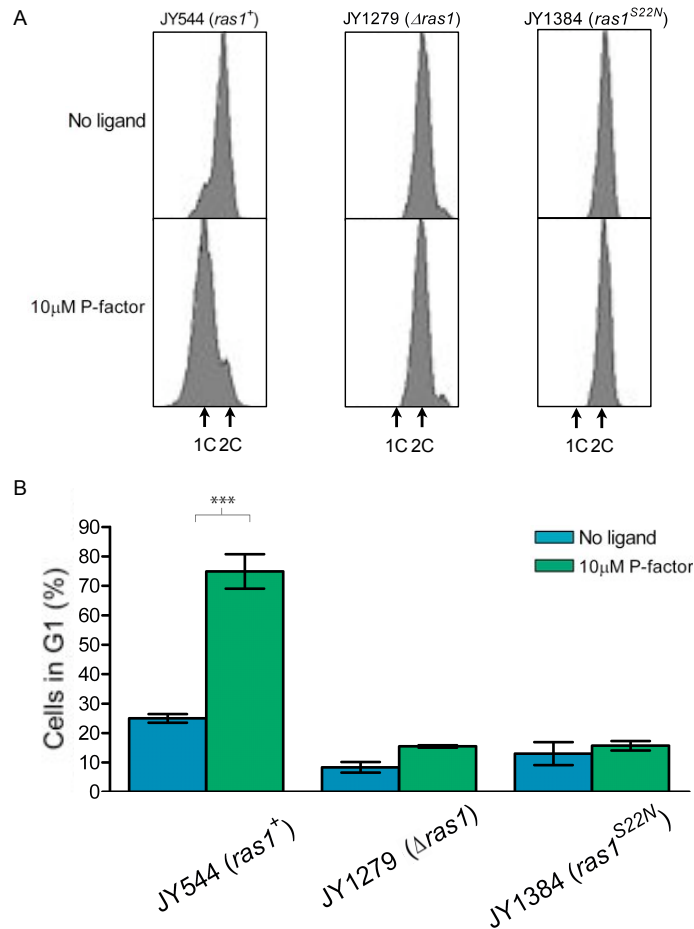


**Figure 4.33. Phormone-responsive changes in cell cycle position in cells expressing Ras1<sup>S22N</sup>**

Cell cycle arrest was analysed in *ras1*<sup>+</sup> (JY544),  $\Delta$ *ras1* (JY1279) and *ras1*<sup>S22N</sup> (JY1384) cells using propidium iodide staining and flow cytometry, after 6 h growth in the presence (10  $\mu$ M P-factor) and absence of pheromone in DMM. This analysis allowed the distinction between cells containing a single complement (1C) and double complement (2C) of DNA (A). Cells lacking Ras1 (JY1279) and those expressing Ras1<sup>S22N</sup> (JY1384) displayed no phormone-dependent G<sub>1</sub> arrest (B). Analysis was performed for 30000 cells. Data shown representative of three independent determinants  $\pm$  SEM. Statistical significance was determined using a one-way anova with a Tukey multiple comparison post test. Three asterisks indicates a P-value of 0.001.

Shmoo formation in these cells was also analysed using quantitative imaging (Figure 4.32B). Cells expressing GFP from pREP3x were imaged following 16 h growth in DMM lacking thiamine in the absence of pheromone and in the presence of 10  $\mu$ M P-factor, using a Leica SP5 scanning confocal microscope. Quimp software was then used to analyse 30 individual cells for each strain and under each assay condition. Image analysis of cell length using Quimp software

indicated no pheromone-dependent change in cell length in cells expressing Ras1<sup>S22N</sup>. Images of these populations also indicated no morphological change in cells expressing Ras1<sup>S22N</sup> in response to pheromone, as the cells maintain a rounded morphology (Figure 4.32A).

Analysis of G<sub>1</sub> arrest in response to pheromone in cells expressing Ras1<sup>S22N</sup> was performed following 6 h growth in the absence of pheromone and in the presence of 10  $\mu$ M P-factor in DMM, using propidium iodide staining and flow cytometry. The assay was performed for 30000 cells (Figure 4.33). A low percentage of cells expressing Ras1<sup>S22N</sup> were in G<sub>1</sub> in the absence of pheromone and no significant cell cycle arrest was observed following stimulation ( $13.0 \pm 3.9$  % in the absence of pheromone and  $15.7 \pm 1.6$  % following stimulation), similar to that observed in cells lacking Ras1. These data further demonstrate the inability of Ras1<sup>S22N</sup> to transduce the pheromone signal.

#### 4.6.2.3. *pREP3x-Ras1<sup>S22N</sup> did not support pheromone-dependent signalling.*

Increasing the cellular concentration of a defective signalling protein could potentially rescue signalling defects, as if the protein has a partial activity a greater concentration may support more activity. Expression from pREP3x, in the absence of thiamine, was used to determine whether any signalling could be observed through Ras1<sup>S22N</sup> upon constitutive expression. The ability of Ras1<sup>S22N</sup> to transduce signal through Byr2 was then determined by analysis of  $\beta$ -galactosidase activity and cell volume in response to pheromone (Figure 4.34).

$\beta$ -galactosidase activity and average cell volume were determined in cells grown in a range of pheromone concentrations (1 nM to 100  $\mu$ M) in DMM lacking thiamine for 16 h. Cells expressing Ras1<sup>S22N</sup> from pREP3x displayed a small pheromone-dependent increase in  $\beta$ -galactosidase activity ( $0.82 \pm 0.17$  to  $1.56 \pm 0.23$ ), similar to that observed upon expression from the *ras1* locus (Figure 4.34A). The magnitude of the increase in  $\beta$ -galactosidase activity observed did not, however, appear to be affected by the expression of Ras1<sup>S22N</sup>

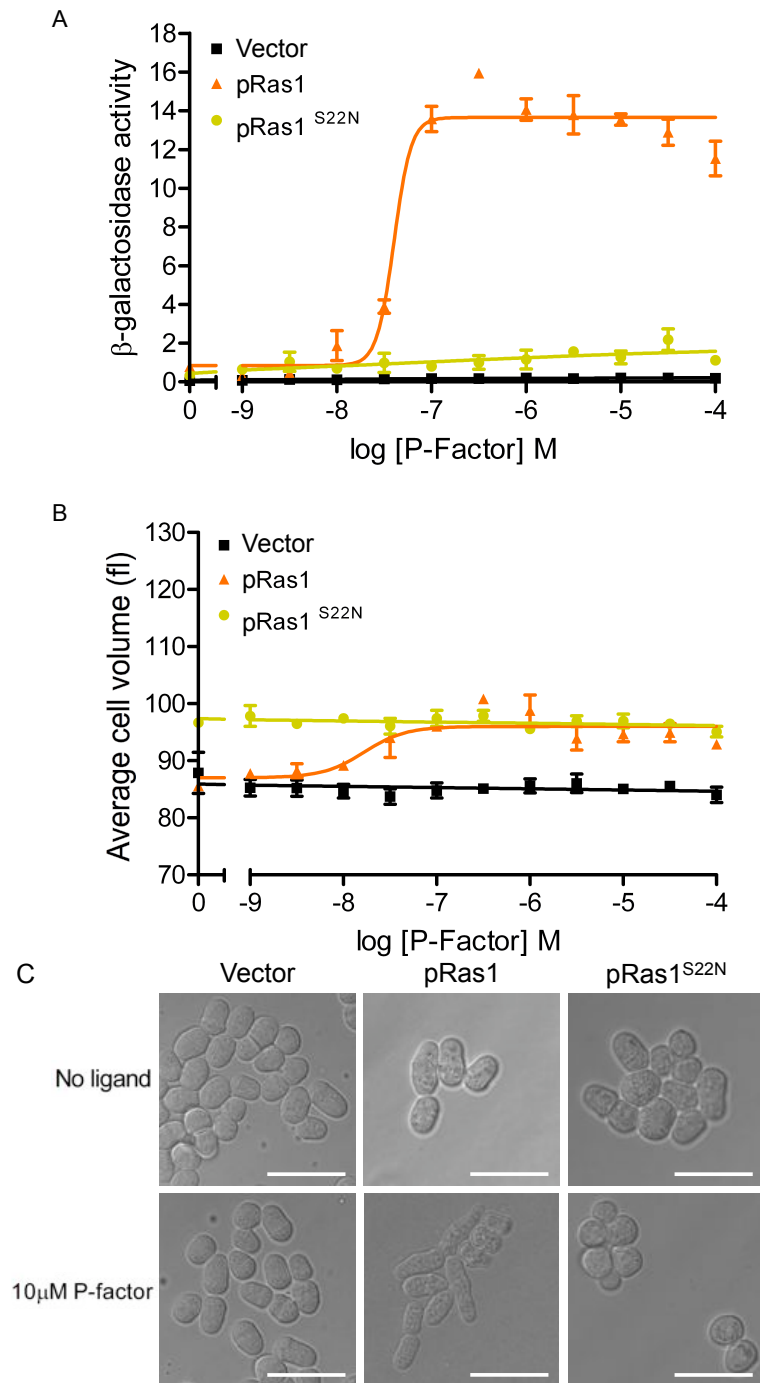


**Figure 4.34. Pheromone-responsive changes in transcription and cell size in cells expressing Ras1<sup>S22N</sup> from pREP3x**

Pheromone-responsive changes in transcription and cell volume were observed in  $\Delta ras1$  (JY1279) cells transformed with pREP3x-Ras1, pREP3x-Ras1<sup>S22N</sup> and vector alone. Assays were then performed for  $\beta$ -galactosidase activity (A) and average cell volume (B) following growth in a range of pheromone concentrations (1 nM to 100  $\mu$ M) in DMM lacking thiamine for 16 h. Cells expressing Ras1<sup>S22N</sup> from pREP3x displayed a slight increase in  $\beta$ -galactosidase activity upon pheromone stimulation but no increase in cell volume. Data shown is an average of three independent determinants ( $\pm$ SEM). Images indicate no pheromone dependent change in cell morphology in cells expressing Ras1<sup>S22N</sup> from pREP3x (C). DIC images were taken using a Leica SP5 scanning confocal microscope. The scale bar represents 10  $\mu$ m.

from the constitutive *nmt1* promoter.

No pheromone dependent change in cell volume or cell morphology was observed in cells expressing Ras1<sup>S22N</sup> from pREP3x (Figure 4.34B and C). These cells did, however, display a slightly elevated cell volume ( $96.73 \pm 0.25$  fl) compared to cells containing pREP3x alone ( $85.25 \pm 0.30$  fl), possibly indicating a slightly altered morphology. Despite this, images of cells expressing Ras1<sup>S22N</sup> from pREP3x indicate a rounded morphology. These data again indicate that Ras1<sup>S22N</sup> is unable to transduce a signal, despite constitutive expression from the *nmt1* promoter.

The data presented in this section all indicates that Ras1<sup>S22N</sup> is unable to activate signalling.

#### 4.6.3. Characterisation of Ras1<sup>G17V</sup> and Ras1<sup>Q66L</sup>.

The Ras1<sup>G17V</sup> mutant has been previously studied in *Sz. pombe*. These studies have indicated that the Gly17Val mutation causes a hypersensitivity to pheromone (Fukui *et al.* 1986b; Davey 1991). In addition, it was suggested that Ras1<sup>G17V</sup> rescues elongated cell morphology and pheromone-response in strains lacking upstream components such as Ral2 (Fukui *et al.* 1989). These studies have also suggested that Ras1<sup>G17V</sup> has a negative effect upon mating. However, no studies have investigated other types of GTPase deficient mutants, such as those based on Gln61Leu, or investigated multiple signalling outputs from these mutants using a quantitative approach. The analysis of such mutants, which should exhibit prolonged signalling activity, could prove highly informative. The integration of the GTPase deficient mutants Ras1<sup>G17V</sup> and Ras1<sup>Q66L</sup> is detailed in section 4.6.1.

4.6.3.1. *Integrated Ras1<sup>G17V</sup> and Ras1<sup>Q66L</sup> rescue elongated cell morphology.* Having investigated the characteristics of a Ras1 mutant which is unable to undergo activation (Ras1<sup>S22N</sup>, section 4.6.2), the activity of mutants which

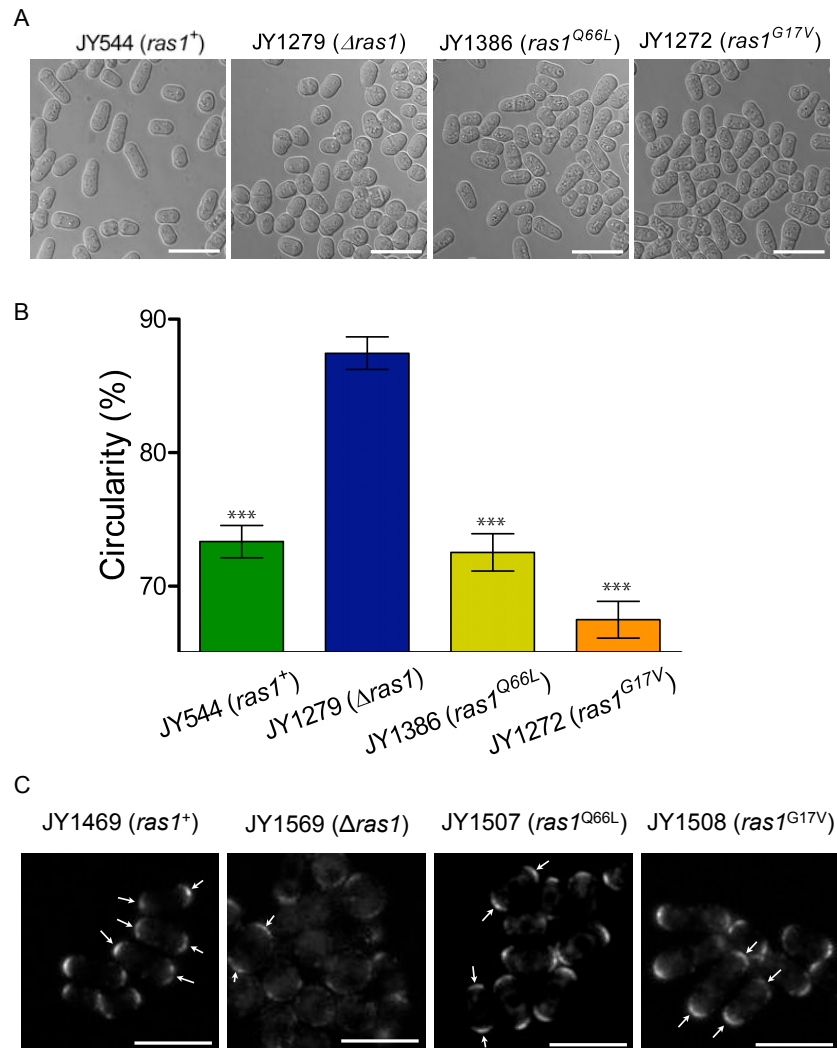


**Figure 4.35. Cell morphology in cells expressing Ras1<sup>G17V</sup> and Ras1<sup>Q66L</sup>**

Images of cells lacking Ras1 and those expressing Ras1, Ras1<sup>G17V</sup> and Ras1<sup>Q66L</sup> from the *ras1* locus were obtained using a Leica SP5 scanning confocal microscope. All strains were also expressing GFP from pREP3x. Representative DIC images are displayed in panel A. Cell circularity was determined using Quimp software (B). These data indicated that Ras1<sup>Q66L</sup> and Ras1<sup>G17V</sup> rescued elongated morphology. Three asterisks indicates a P-value of 0.001. Data representative of 30 individual cells  $\pm$  SEM. The localisation of Tea1-mCherry was determined in *ras1*<sup>+</sup> cells (JY1469),  $\Delta$ *ras1* cells (JY1569), cells expressing Ras1<sup>Q66L</sup> (JY1507) and cells expressing Ras1<sup>G17V</sup> (JY1508), using a Nikon E800 epifluorescence microscope fitted with an Andor EM-CCD camera (C). Cells expressing Ras1<sup>Q66L</sup> and Ras1<sup>G17V</sup> displayed polar Tea1 localisation consistent with that seen in JY1469. The scale bar represents 10  $\mu$ m.

should display protracted signalling was assessed. The morphology of cells expressing Ras1<sup>G17V</sup> and Ras1<sup>Q66L</sup> from the *ras1* locus was determined in images of each strain expressing GFP from pREP3x in the absence of thiamine, obtained using a Leica SP5 scanning confocal microscope. The circularity of 30 individual cells within each population was then analysed using Quimp software. The localisation of Tea1-mCherry was also investigated in cells expressing these two mutants from the *ras1* locus, using a Nikon E800 epifluorescence microscope fitted with an Andor EM-CCD camera.

Cells expressing both mutants displayed specific tip localisation of Tea1-mCherry, consistent with that seen in cells expressing wild-type Ras1 (Figure 4.35C). The discrete tip localisation of Tea1-mCherry indicates that both mutants are functional in the regulation of polar cell organisation. Both mutant strains also displayed low percent circularity, significantly different from  $\Delta ras1$  cells ( $P = 0.001$ ) (Figure 4.35A and B). JY1507 (*ras1*<sup>Q66L</sup>) displays a percent circularity consistent with JY544 (*ras1*<sup>+</sup>) ( $72.5 \pm 1.4$  % compared to  $73.4 \pm 1.2$  %). By contrast, JY1508 (*ras1*<sup>G17V</sup>) displays a markedly lower percent circularity ( $67.5 \pm 1.4$  %). The low percentage circularity observed for both strains is indicative of an elongated polar morphology, again suggesting that Ras1<sup>G17V</sup> and Ras1<sup>Q66L</sup> are functional in regulating polar cell morphology.

4.6.3.2. *Ras1*<sup>G17V</sup> and *Ras1*<sup>Q66L</sup> cause reduced signalling at high pheromone concentrations in  $\beta$ -galactosidase assays. Reducing the ability of Ras1 to hydrolyse GTP would be expected to positively influence signalling in response to pheromone, leading to prolonged signalling activity. To investigate this hypothesis,  $\beta$ -galactosidase activity and cell volume were used to analyse the effect of the Gly17Val and Gln66Leu mutations on Ras1 activity through the Byr2-Byr1-Spk1 MAP kinase cascade (Figure 4.36). Analysis was performed following growth in a range of pheromone concentrations (1 nM to 100  $\mu$ M) in DMM for 16 h.

Cells expressing either mutation did not display a typical dose-response profile to pheromone in assays for pheromone-responsive transcription or cell volume. Both strains reached a peak maximal signal at between 100 nM and 1  $\mu$ M, at a level comparable to the maximal signal observed in JY544 (*ras1*<sup>+</sup>), followed by a sharp reduction in both  $\beta$ -galactosidase activity and cell volume at higher pheromone concentrations. Cells expressing Ras1<sup>Q66L</sup> displayed a basal cell volume greater than that observed in wild type cells ( $79.8 \pm 0.1$  fl compared to  $66.6 \pm 1.5$  fl). As these cells have a polar morphology, this observation could indicate an increase in cell size, possibly due to unregulated Ras1 signalling through the cell morphology pathway.

Ras1<sup>G17V</sup> and Ras1<sup>Q66L</sup> also supported increased pheromone-dependent transcription at lower concentrations of pheromone, indicating a greater sensitivity to pheromone in these cells. However, no increase in basal signalling was observed, suggesting that both mutants still required activation, and were not constitutively active in the absence of pheromone. Interestingly, cells expressing Ras1<sup>G17V</sup> and Ras1<sup>Q66L</sup> appeared to reach a maximal signal at around the EC<sub>50</sub> concentration of P-factor for wild-type cells ( $\sim 100$ nM). This effect was also mirrored in assays for cell volume. A sharp reduction in pheromone-dependent signalling and cell size at higher pheromone concentrations had not previously been observed in cells expressing wild-type Ras1 or other Ras1 mutants.

Analysis of cell volume in these cells produced an unexpected reduction in volume at higher pheromone concentrations. Analysis of shmoo formation using quantitative imaging however reveals quite differing activities between the two mutations. The strains JY1386 (*ras1*<sup>Q66L</sup>) and JY1272 (*ras1*<sup>G17V</sup>), expressing GFP from pREP3x, were analysed following growth in the absence or presence of 10  $\mu$ M P-factor in DMM lacking thiamine for 16 h. Images were obtained using a Leica SP5 scanning confocal microscope. Quimp software was then used to analyse 30 individual cells of each strain and under each assay condition (Figure 4.37B). JY1386 (*ras1*<sup>Q66L</sup>) displayed a strong, significant

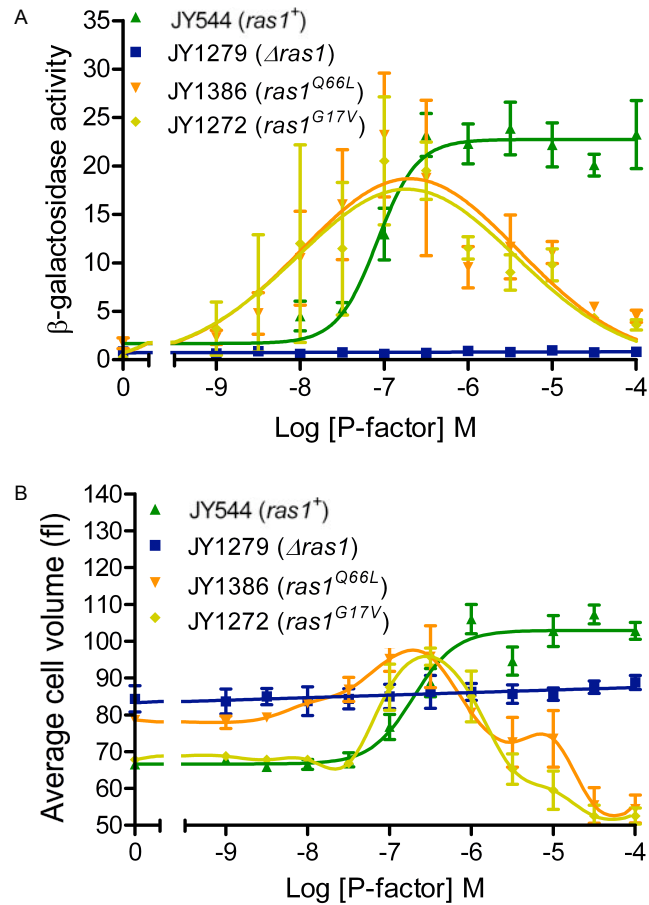


**Figure 4.36. Pheromone-responsive transcription and cell volume change in cells expressing Ras1<sup>G17V</sup> and Ras1<sup>Q66L</sup>**

Pheromone-responsive changes in transcription and cell volume were observed in *ras1*<sup>+</sup> (JY544) cells,  $\Delta$ *ras1* (JY1279) cells, cells expressing Ras1<sup>Q66L</sup> (JY1507) and cells expressing Ras1<sup>G17V</sup> (JY1508). Strains were grown in the presence of 1 nM to 100  $\mu$ M pheromone in DMM for 16 h. Assays were then performed for  $\beta$ -galactosidase activity (A) and average cell volume (B). Cells expressing Ras1<sup>Q66L</sup> and Ras1<sup>G17V</sup> displayed increased  $\beta$ -galactosidase activity and cell volume up to 1  $\mu$ M P-factor, followed by a sharp reduction in both parameters at higher pheromone concentrations. Data shown is an average of three independent determinants ( $\pm$ SEM).

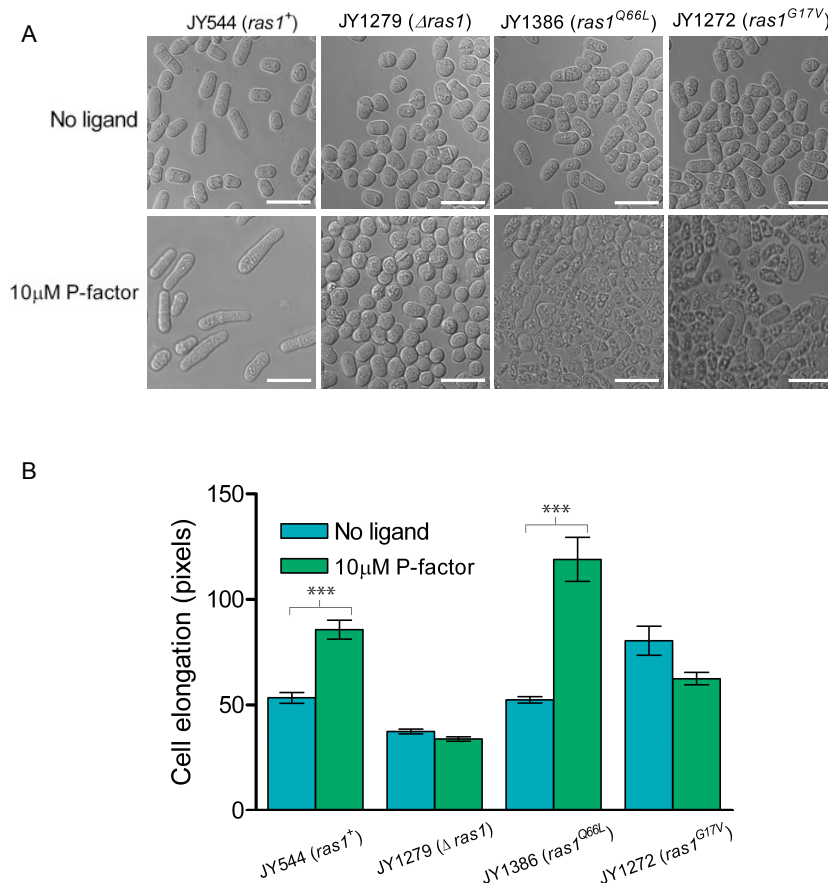


**Figure 4.37. Phormone-responsive changes in cell length in cells expressing *Ras1*<sup>G17V</sup> and *Ras1*<sup>Q66L</sup>**

Images of *ras1*<sup>+</sup> (JY544),  $\Delta$ *ras1* (JY1279), *ras1*<sup>Q66L</sup> (JY1386) and *ras1*<sup>G17V</sup> (JY1272) cells were obtained after 16 h growth in the absence and in the presence of 10 µM phormone in DMM lacking thiamine, using a Leica SP5 scanning confocal microscope. Representative DIC images are displayed in panel A. Cells expressing *Ras1*<sup>Q66L</sup> (JY1386) displayed a significant increase in cell length upon phormone stimulation ( $P = 0.001$ ) (B). Cells expressing *Ras1*<sup>G17V</sup> (JY1272) were longer in the absence of phormone than JY544, but displayed a decrease in cell length upon phormone stimulation. Data shown is representative of 30 individual cells  $\pm$  SEM. Statistical significance was determined using a one-way anova with a Tukey multiple comparison post test. Three asterisks indicates a P-value of 0.001. Images from indicate a large number of dead cells in the phormone treated populations of JY1386 and JY1272.

phormone-dependent increase in cell length ( $52.4 \pm 1.5$  pixels to  $119.0 \pm 10.4$  pixels,  $P = 0.001$ ). JY1272 (*ras1*<sup>G17V</sup>) displayed a high basal cell length ( $80.4 \pm 6.9$  pixels), consistent with the low circularity observed in this strain, but a relative reduction in cell length upon phormone stimulation ( $62.5 \pm 2.9$  pixels). Images of both strains indicate the presence of a large number of

dense pitted cells, possibly due to an increase in cell death upon stimulation with pheromone (Figure 4.37A). As the analysis of cell morphology requires the expression of GFP it will favor viable cells. This could explain why cell length appears to drop in response to pheromone in JY1272, as responding cells may have died. Cell death at higher pheromone concentrations could also explain why  $\beta$ -galactosidase activity and average cell volume appear lower in the presence of high levels of pheromone in both strains expressing GTPase deficient mutants (Figure 4.36).

Cell cycle progression in response to pheromone was analysed as a final measure of pheromone-dependent signalling. Pheromone-dependent G<sub>1</sub> arrest was analysed following 6 h growth in the absence of pheromone and in the presence of 10  $\mu$ M P-factor in DMM, using propidium iodide staining and flow cytometry. Analysis was performed for 30000 cells. Analysis of G<sub>1</sub> arrest also indicated a reduced level of pheromone-dependent G<sub>1</sub> arrest in cells expressing Ras1<sup>G17V</sup> and Ras1<sup>Q66L</sup> compared to those expressing wild-type Ras1 (Figure 4.38). JY1386 (*ras1*<sup>Q66L</sup>) displayed an increase in cells in G<sub>1</sub> from 22.07  $\pm$  5.99 % to 48.97  $\pm$  2.83 % and JY1272 (*ras1*<sup>G17V</sup>) displayed an increase from 26.3  $\pm$  5.14 % to 39.93  $\pm$  10.48 %. Cells expressing wild-type Ras1 display an increase from 25.0  $\pm$  1.5 % to 74.9  $\pm$  5.8 %, which is markedly higher than in the two strains containing GTPase deficient mutants. These results again could be confounded by the presence of a large number of dead cells, as these cells would still display propidium iodide staining.

#### 4.6.4. JY1386 (*ras1*<sup>Q66L</sup>) and JY1272 (*ras1*<sup>G17V</sup>) display pheromone-dependent cell death.

Images of cells expressing Ras1<sup>G17V</sup> and Ras1<sup>Q66L</sup> indicate that both strains die in a pheromone dependent manner (Figure 4.37). As a consequence, these data suggest that prolonged Ras1 activity may be detrimental to cell viability. A number of tools are available in *Sz. pombe* for the analysis of cell death.

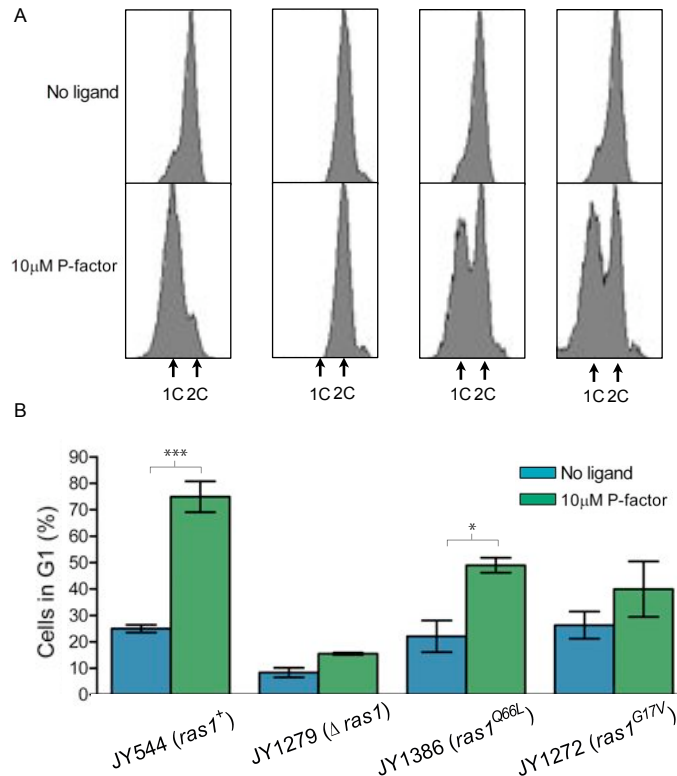


**Figure 4.38. Phormone-responsive changes in cell cycle position in cells expressing Ras1<sup>G17V</sup> and Ras1<sup>Q66L</sup>**

Cell cycle arrest was analysed in *ras1*<sup>+</sup> (JY544),  $\Delta$ *ras1* (JY1279), *ras1*<sup>Q66L</sup> (JY1386) and *ras1*<sup>G17V</sup> (JY1272) cells using propidium iodide staining and flow cytometry after 6 h growth in the presence (10  $\mu$ M P-factor) and absence of pheromone in DMM. This analysis allowed the distinction between cells containing a single complement (1C) and double complement (2C) of DNA (A). Both strains expressing the GTPase deficient mutants displayed some phormone-dependent cell cycle arrest (B). Data shown representative of three independent determinants  $\pm$  SEM. Analysis was performed for 30000 cells. Statistical significance was determined using a one-way anova with a Tukey multiple comparison post test. One asterisk indicates a P-value of 0.05 and three asterisks indicates a P-value of 0.001.

The LIVE/DEAD<sup>®</sup> *Funga* Light<sup>TM</sup> cell viability assay utilises two nucleic acid stains, SYTO<sup>®</sup> 9 and propidium iodide. SYTO<sup>®</sup> 9 is able to cross both intact and compromised membranes, whereas propidium iodide is only able to cross the compromised membranes of non-viable cells. As a consequence, living cells are only stained with SYTO<sup>®</sup> 9 (green), whereas dead cells are stained with SYTO<sup>®</sup> 9 (green) and propidium iodide (red). The presence of both dyes in non-viable cells causes a reduction in the green signal due to FRET between the two fluorophores. Flow cytometric analysis is then used to distinguish the

green live cells from the red non-viable cells (Zhang and Fang 2004).

To determine the extent of cellular mortality upon pheromone exposure, the strains JY544 (*ras1*<sup>+</sup>), JY1279 ( $\Delta$ *ras1*), JY1389 (*ras1*<sup>Q66L</sup>) and JY1272 (*ras1*<sup>G17V</sup>) were analysed using the LIVE/DEAD<sup>®</sup> *Funga* Light<sup>TM</sup> assay. Analysis was performed following 16 h incubation with 0, 100 nM and 10  $\mu$ M P-factor in DMM (Figure 4.39). Fluorescence was determined for 30000 cells by flow cytometry using an LSRII flow cytometer. Excitation of both dyes was achieved using a 488 nm laser, and emission detected using a 550 nm long pass filter with a 575/26 nm band pass filter for propidium iodide, and a 505 nm long pass filter with a 530/30 nm band pass filter for SYTO<sup>®</sup> 9.

JY544 (*ras1*<sup>+</sup>) displayed a small increase in cell death upon pheromone stimulation, increasing from  $1.83 \pm 0.6$  % to  $8.7 \pm 1.5$  %. These data indicate that pheromone signalling causes some cell death wild-type cells. JY1279 ( $\Delta$ *ras1*) exhibited a very slight increase in cell death at higher P-factor concentrations ( $2.0 \pm 0.4$  % to  $3.9 \pm 0.8$  %). The strains JY1389 (*ras1*<sup>Q66L</sup>) and JY1272 (*ras1*<sup>G17V</sup>) displayed a significant pheromone-dependent increase in cell death ( $P = 0.001$ ). The percentage of non-viable cells observed in JY1389 (*ras1*<sup>Q66L</sup>) increased from  $2.2 \pm 0.8$  % to  $52.4 \pm 8.8$  % and  $89.7 \pm 0.8$  % across the three pheromone concentrations used. A similar increase was also observed in JY1272 (*ras1*<sup>G17V</sup>) upon pheromone stimulation ( $2.8 \pm 1.1$  % to  $48.3 \pm 13.9$  % to  $89.1 \pm 1.1$  %). These data confirm the observation made in Figure 4.37A that pheromone appears to negatively effect cell viability in these strains, and also provides an explanation for the apparent reduction in pheromone-dependent signalling observed in these strains at higher pheromone concentrations.

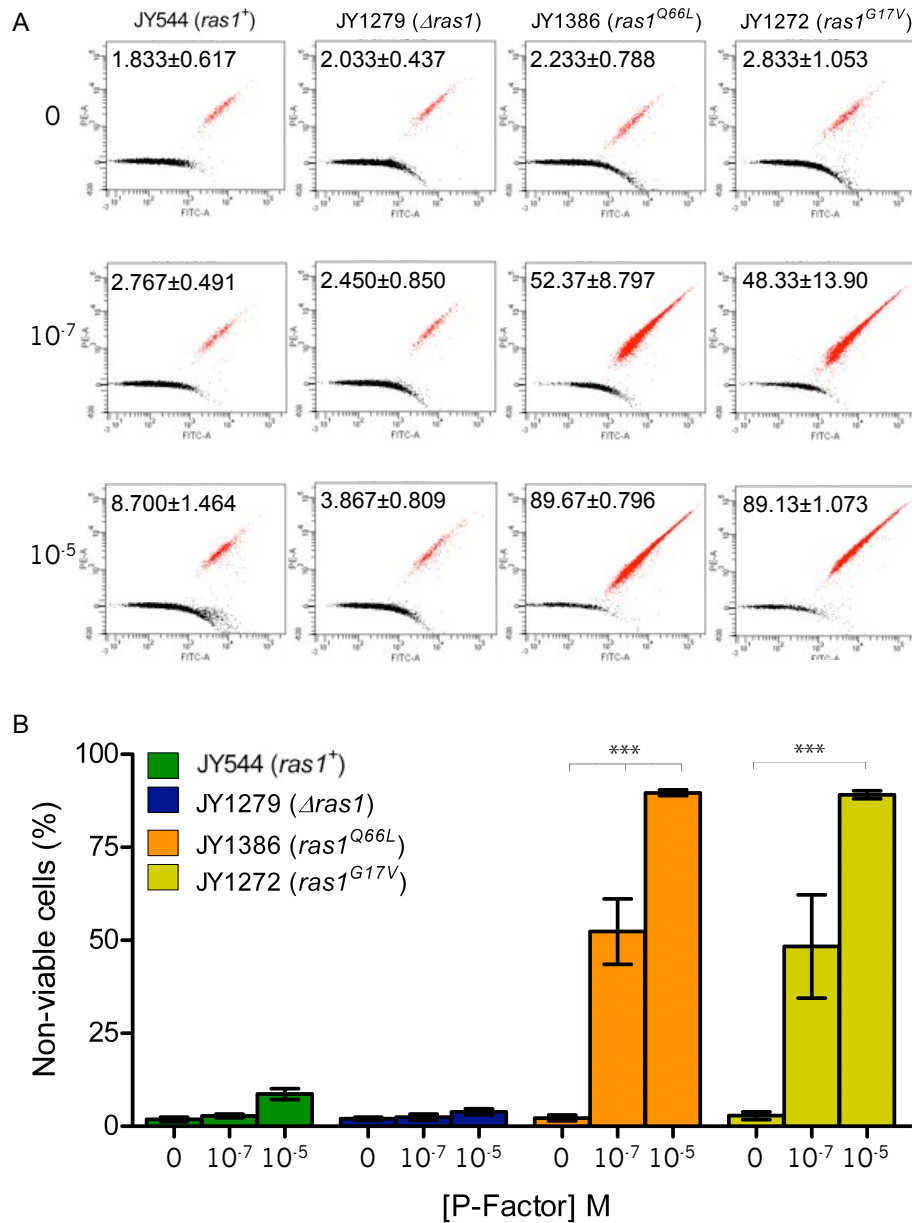


**Figure 4.39. JY1386 (*ras1*<sup>Q66L</sup>) and JY1272 (*ras1*<sup>G17V</sup>) display pheromone-dependent cell death**

Cell viability in *ras1*<sup>+</sup> (JY544) cells,  $\Delta$ *ras1* (JY1279) cells, cells expressing Ras1<sup>Q66L</sup> (JY1507) and cells expressing Ras1<sup>G17V</sup> (JY1508) was analysed using the LIVE/DEAD<sup>®</sup> *Funga* Light<sup>™</sup> assay. Flow cytometric analysis was performed following 16 h growth in the absence of pheromone and in the presence of 100 nM and 10  $\mu$ M P-factor in DMM (A). Cells expressing Ras1<sup>Q66L</sup> (JY1507) and cells expressing Ras1<sup>G17V</sup> (JY1508) both displayed pheromone-dependent cell death (B). Percentage non-viable cells is indicated on each dot plot  $\pm$ SEM. Non-viable cells are indicated in red. Data shown is an average of three independent determinants ( $\pm$ SEM). Analysis was performed for 30000 cells. Statistical significance was determined using a one-way anova with a Tukey multiple comparison post test. Three asterisks indicates a P-value of 0.001.

To determine the timing of cell death in response to pheromone, DIC images were taken of JY1389 (*ras1<sup>Q66L</sup>*) stimulated with 10  $\mu$ M P-factor over a period of 5 h. JY1389 (*ras1<sup>Q66L</sup>*) was used as a representative example of a strain containing a GTPase deficient Ras1 mutant. Analysis revealed cell death could be observed after 1 h, marked by the appearance of pitted dense cells. The number of dead cells increased with time up to 5 h, indicating that cell death was occurring in a time-dependent manner in response to pheromone (Figure 4.40).

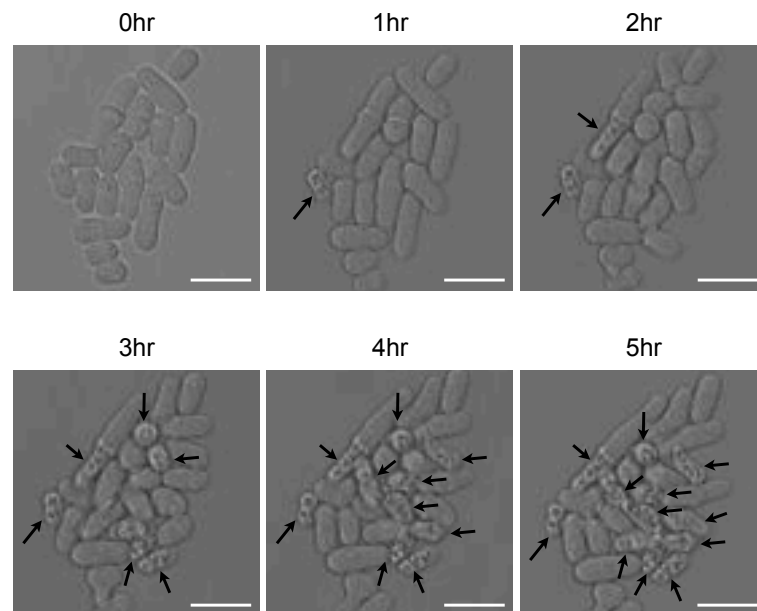


**Figure 4.40. Analysis of pheromone-dependent cell death in JY1389 (*ras1<sup>Q66L</sup>*) over time**

JY1389 (*ras1<sup>Q66L</sup>*) was stimulated with 10  $\mu$ M P factor and images were taken every hour. DIC images were taken using a Leica SP5 scanning confocal microscope. Cell death could be observed after 1 h of stimulation. Dead cells are highlighted with arrows. The scale bar represents 10  $\mu$ m.

#### 4.6.5. Analysis of Ras1<sup>G17V</sup> and Ras1<sup>Q66L</sup> activity when expressed from pREP3x.

The pheromone-dependent signalling of cells expressing Ras1<sup>G17V</sup> and Ras1<sup>Q66L</sup> was reduced at higher pheromone concentrations. To determine whether the constitutive expression of these mutants caused similar or more pronounced effects, the activity of Ras1<sup>G17V</sup> and Ras1<sup>Q66L</sup> was also investigated when expressed from pREP3x in the  $\Delta ras1$  strain JY1279. Assays for  $\beta$ -galactosidase activity and average cell volume were performed for cells grown in a range of pheromone concentrations (1 nM to 100  $\mu$ M) for 16 h in DMM lacking thiamine. Ras1<sup>G17V</sup> and Ras1<sup>Q66L</sup> supported a large dose-dependent increase in  $\beta$ -galactosidase activity when expressed from pREP3x, displaying maximal signals of  $23.1 \pm 0.7$  and  $36.2 \pm 1.8$  respectively (Figure 4.41A). Both strains displayed pEC<sub>50</sub> values comparable to those seen in cell expressing wild-type Ras1 ( $6.5 \pm 0.1$ ), with cells expressing Ras1<sup>G17V</sup> giving a pEC<sub>50</sub> of  $7.0 \pm 0.1$  and cells expressing Ras1<sup>Q66L</sup> giving a pEC<sub>50</sub> of  $7.5 \pm 0.1$ . This result may appear counter-intuitive, as the regulated expression of these mutants from the *ras1* locus was detrimental to cell viability at higher pheromone concentrations. Constitutive expression of Ras1<sup>G17V</sup> and Ras1<sup>Q66L</sup>, like expression of these mutants from the *ras1* locus, caused a pheromone-dependent reduction in cell volume (Figure 4.41B). In the absence of pheromone, however, these cells displayed a very large cell volume. Cells expressing Ras1<sup>G17V</sup> exhibited a volume of  $110.3 \pm 2.1$  fl and cells expressing Ras1<sup>Q66L</sup> a volume of  $182.4 \pm 1.8$  fl.

Examination of cell morphology revealed the expression of these mutants, most notably Ras1<sup>Q66L</sup>, caused a marked increase in cell size (Figure 4.41C). Upon pheromone stimulation these cells also undergo a concerted increase in cell size, but with no defined polarity. The reduction in cell volume observed in Figure 4.41B could therefore also be due to cell death in these populations.

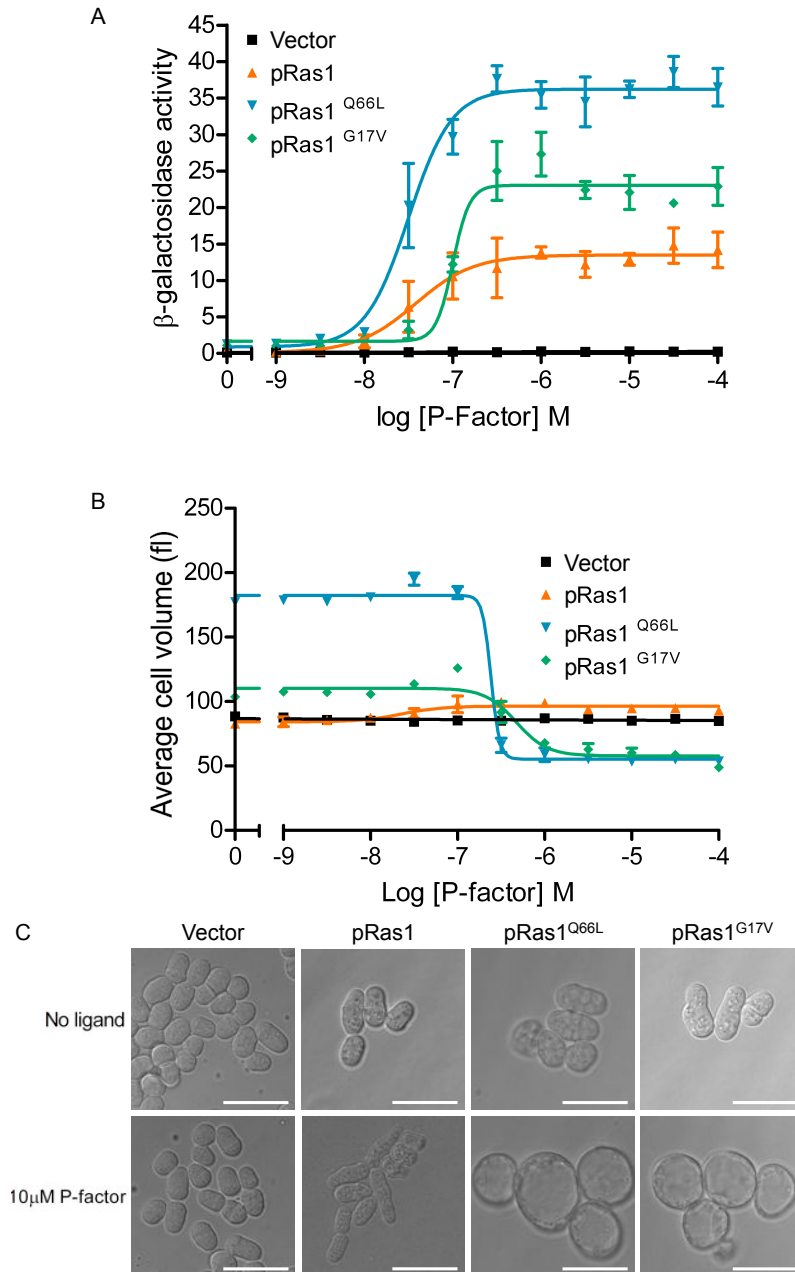


**Figure 4.41. Phormone-responsive changes in transcription and cell morphology in cells expressing GTPase deficient Ras1 mutants from pREP3x**

Phormone-responsive changes in transcription and cell volume were observed in  $\Delta ras1$  (JY1279) cells transformed with pREP3x-Ras1, pREP3x-Ras1<sup>Q66L</sup>, pREP3x-Ras1<sup>G17V</sup> and vector alone. Assays were performed for  $\beta$ -galactosidase activity (A) and average cell volume (B) following growth in 1 nM to 100  $\mu$ M phormone for 16 h in DMM lacking thiamine. Cells expressing Ras1<sup>Q66L</sup> and Ras1<sup>G17V</sup> from pREP3x displayed large dose-dependent increases in  $\beta$ -galactosidase activity upon phormone stimulation but reductions in cell volume. Data shown is an average of three independent determinants ( $\pm$ SEM). Images from the populations analysed indicate that the expression of Ras1<sup>Q66L</sup> and Ras1<sup>G17V</sup> caused an increased basal cell volume and a non-polar increase in cell size in response to phormone (C). DIC images were taken using a Leica SP5 scanning confocal microscope. The scale bar represents 10  $\mu$ m.

#### 4.6.6. Expression of Ras1 from pREP3x negatively effects cell viability.

Cells expressing Ras1<sup>G17V</sup> and Ras1<sup>Q66L</sup> from pREP3x did not display a drop in signalling at higher pheromone concentrations. This observation would appear counter-intuitive, as the constitutive expression of a GTPase deficient mutant would be expected to reinforce the effects seen upon regulated expression from the *ras1* locus. The LIVE/DEAD<sup>®</sup> *Funga* Light<sup>TM</sup> assay was used to determine the effect of pheromone on cell viability in  $\Delta ras1$  (JY1279) cells transformed with pREP3x-Ras1, pREP3x-Ras1<sup>Q66L</sup>, pREP3x-Ras1<sup>G17V</sup> and vector alone (Figure 4.42). Cells were stained with propidium iodide and SYTO<sup>®</sup> 9 following 16 h incubation with 0, 100 nM and 10  $\mu$ M P-factor in DMM lacking thiamine. Flow cytometric analysis was then performed using an LSRII flow cytometer for 30000 individual cells.

The results observed in all strains expressing Ras1 from pREP3x starkly contrast those seen when expression of Ras1 is driven by the endogenous *ras1* promoter, as high levels of cell death can be observed in all conditions. In the absence of pheromone  $10.7 \pm 6.2$  % of cells are non-viable in the vector alone control, compared to  $34.9 \pm 11.8$  %,  $42.1 \pm 7.0$  % and  $45.1 \pm 5.0$  % in those expressing Ras1, Ras1<sup>Q66L</sup> and Ras1<sup>G17V</sup> respectively. A dose-dependent increase in cell death was observed in all these populations upon pheromone stimulation. This effect was not as pronounced as in cell expressing Ras1<sup>Q66L</sup> and Ras1<sup>G17V</sup> from the *ras1* locus, due to the high levels of basal cell death. This could account for the seemingly counter-intuitive observation that expression of Ras1 from pREP3x reduces signalling, as a large number of cells within the population would be dead (Figure 4.17). In addition, it may explain why constitutive expression of the GTPase-deficient mutants does not cause a drop in signalling at higher pheromone concentrations (Figure 4.41), as viability is impacted even in the absence of pheromone. These results could indicate a level of basal Ras1 signalling, possibly due to increased Ras1 activity due to Efc25 mediated nucleotide exchange.

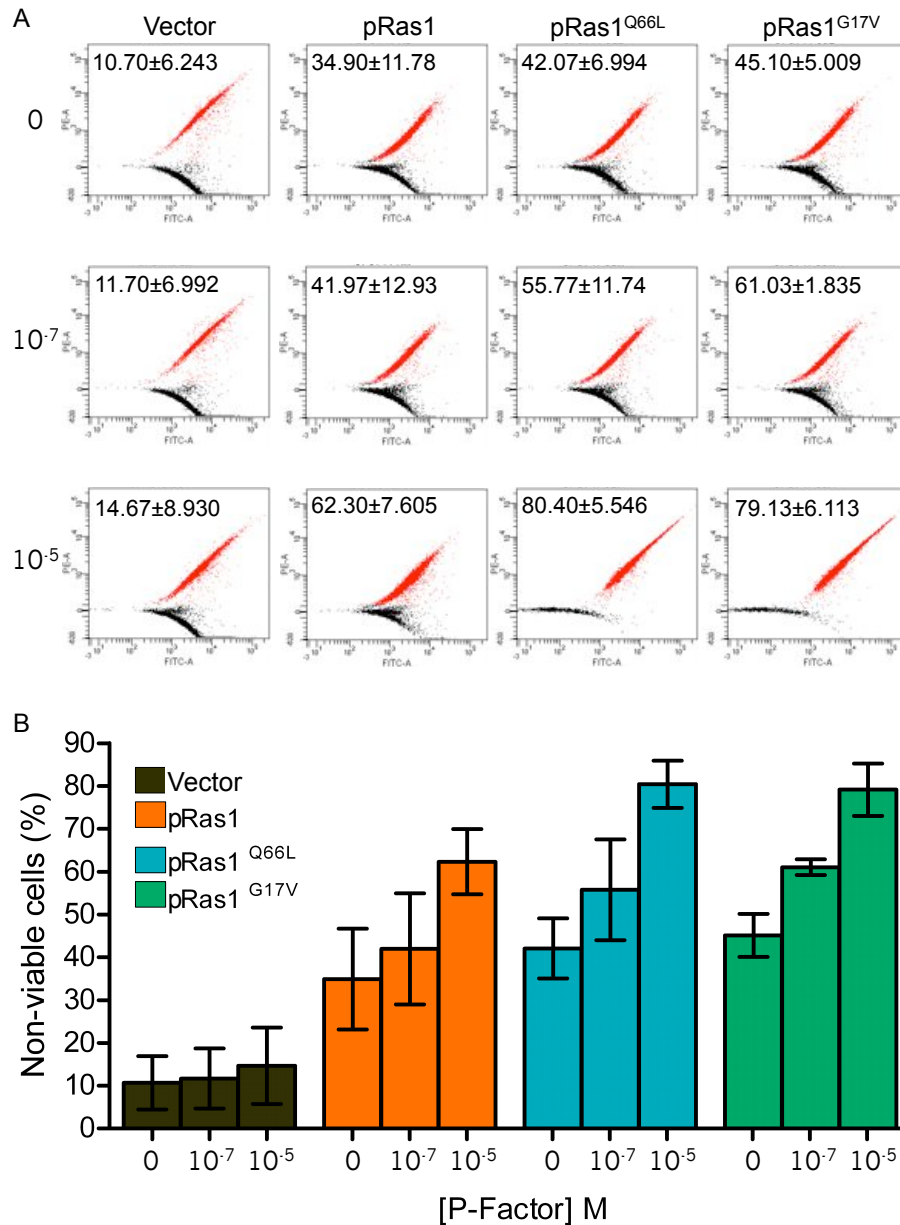


**Figure 4.42. Constitutive expression of Ras1 and GTPase deficient Ras1 mutants negatively impacts upon cell viability**

Cell viability in  $\Delta ras1$  (JY1279) cells transformed with pREP3x-Ras1, pREP3x-Ras1<sup>Q66L</sup>, pREP3x-Ras1<sup>G17V</sup> and vector alone, was analysed using the LIVE/DEAD<sup>®</sup> *Funga* Light<sup>™</sup> assay. Flow cytometric analysis was performed following 16 h growth in the absence of pheromone and in the presence of 100 nM and 10  $\mu$ M P-factor in DMM lacking thiamine (A). Cells expressing Ras1, Ras1<sup>Q66L</sup> and Ras1<sup>G17V</sup> displayed high levels of cell death in all conditions (B). Percentage non-viable cells is indicated on each dot plot  $\pm$ SEM. Non-viable cells are indicated in red. Analysis was performed for 30000 cells. Data shown is an average of three independent determinants ( $\pm$ SEM).

It should be noted that, cells containing vector alone displayed a higher level of cell death ( $10.7 \pm 6.2$  %) than the cells lacking pREP3x presented in Figure 4.39. This result could be due to the selective media used to prevent loss of the vector, as these cells are not provided with exogenous leucine. Growth in slightly less rich media could account for a slight increase in cell death

#### 4.6.7. Increasing Ras1 activity affects chromosome segregation.

Previous studies have suggested a link between Ras1 signalling and chromosome segregation (Li *et al.* 2000). It has been indicated that the loss of Ras1, or the Ras1 effector Scd1, from *Sz. pombe* causes an increase in chromosome missegregation. Due to this link between Ras1 and chromosome segregation, it is possible that chromosome instability could be contributing to the decrease in cell viability observed in cells expressing Ras1 or the GTPase-deficient mutants from pREP3x.

Chromosome stability was determined using the strain 2125 (Tinline-Purvis *et al.* 2009), which contains a non-essential minichromosome (Ch16). The strain contains the mutation *ade-210* on chromosome III and a complementary *ade-216* mutation on Ch16 to rescue *ade6* function. Loss of the minichromosome, a function of chromosome instability, results in a loss of *ade6* activity and the formation of red colonies (Niwa *et al.* 1989). The presence of sectored colonies indicates chromosome loss within that clonal cell population.

The strain 2125 was transformed with pREP3x-Ras1, pREP3x-Ras1<sup>Q66L</sup>, pREP3x-Ras1<sup>G17V</sup> and vector alone. Following growth in DMM lacking adenine, thiamine and leucine, cells were cultured on rich media (YE) lacking additional adenine. The presence of sectored colonies was then determined in a total of >20000 colonies.

An increase in sectored colonies was observed upon constitutive expression of Ras1, Ras1<sup>Q66L</sup> and Ras1<sup>G17V</sup> in 2125. In 2125 transformed with vector alone, the rate of chromosome loss in an individual colony was >0.005 %. In

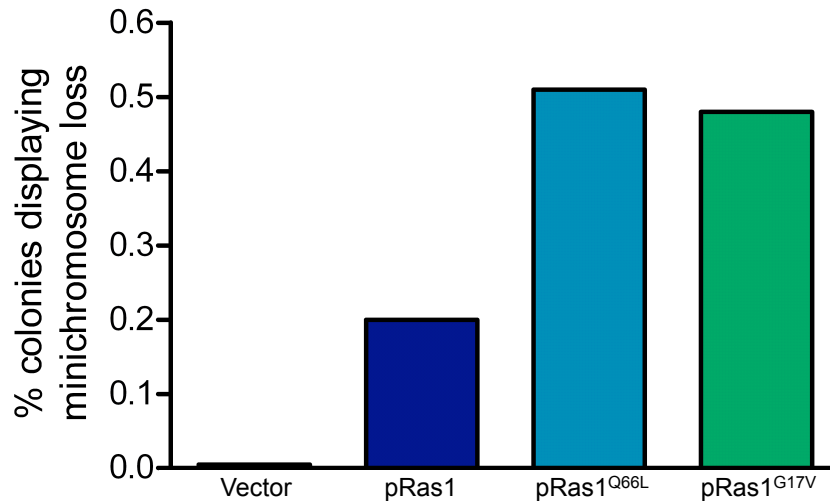


**Figure 4.43. Increased Ras1 activity causes an increase in chromosome instability**

Chromosome stability was determined in the minichromosome strain 2125 transformed with pREP3x-Ras1, pREP3x-Ras1<sup>Q66L</sup>, pREP3x-Ras1<sup>G17V</sup> and vector alone. Cells expressing Ras1 from pREP3x displayed an increase in minichromosome loss compare to the vector alone control. A further increase was observed upon expression of either GTPase deficient Ras1 mutant. Data representative of >20000 colonies.

cells expressing Ras1 from pREP3x this rate increased to 0.200 % and in cells expressing Ras1<sup>Q66L</sup> and Ras1<sup>G17V</sup> from pREP3x this increased to 0.510 % and 0.480 % respectively (Figure 4.43). No colonies displayed red colouration over more than 50 % of the colony, which would indicate chromosome loss at the first division of that colony and allow the analysis of chromosome loss per division. These data indicate that increasing Ras1 activity negatively impacts upon chromosome segregation, probably through altering the interaction of Ras1 with Scd1 (Li *et al.* 2000), which may contribute to Ras1-dependent cell death. Although the chromosome instability observed in this assay was not due to pheromone stimulation, these data could provide a rationale as to why increased Ras1 signalling could influence viability.

## 4.7. The localisation of Ras1 mutants with differing activities

### 4.7.1. Expression of GFP-Ras1 mutant fusions.

Ras1<sup>Q66L</sup>, Ras1<sup>G17V</sup> and Ras1<sup>S22N</sup> all displayed differing functional activities, which may also affect their localisation. To determine whether there was a link between altered activity and localisation in these mutants, integration of GFP-Ras1 fusions was performed in the *ras1::ura4<sup>+</sup>, sxa2>lacZ* strain JY1247 (as highlighted in Figure 4.28A). GFP-Ras1<sup>Q66L</sup> (JY1495), GFP-Ras1<sup>G17V</sup> (JY1496) and GFP-Ras1<sup>S22N</sup> (JY1519) were all integrated at the *ras1* locus. Expression was confirmed by immunoblotting using an anti-ras RAS10 antibody. The bands observed were at a position consistent with the predicted size of the GFP-Ras1 fusions ( $\sim 52$ kDa), and little evidence of protein cleavage was observed (Figure 4.44).

### 4.7.2. GFP-Ras1<sup>Q66L</sup> (JY1495), GFP-Ras1<sup>G17V</sup> (JY1496) and GFP-Ras1<sup>S22N</sup> (JY1519) display the same localisation pattern as GFP-Ras1.

The localisation of GFP-Ras1 (JY1390), GFP-Ras1<sup>Q66L</sup> (JY1495), GFP-Ras1<sup>G17V</sup> (JY1496) and GFP-Ras1<sup>S22N</sup> (JY1519), expressed from the endogenous *ras1* promoter, was established using a Nikon E800 epifluorescence microscope fitted with an Andor EM-CCD camera. All three mutant GFP-Ras1 proteins displayed a localisation pattern comparable to that observed for GFP-Ras1, being present predominantly at the plasma membrane but also displaying some localisation to endomembrane structures (Figure 4.45). The fluorescence signal from each fusion was very low, and similar to that observed for GFP-Ras1. These data indicate that altering the nucleotide exchange or GTPase activity of Ras1 has little effect upon Ras1 localisation.

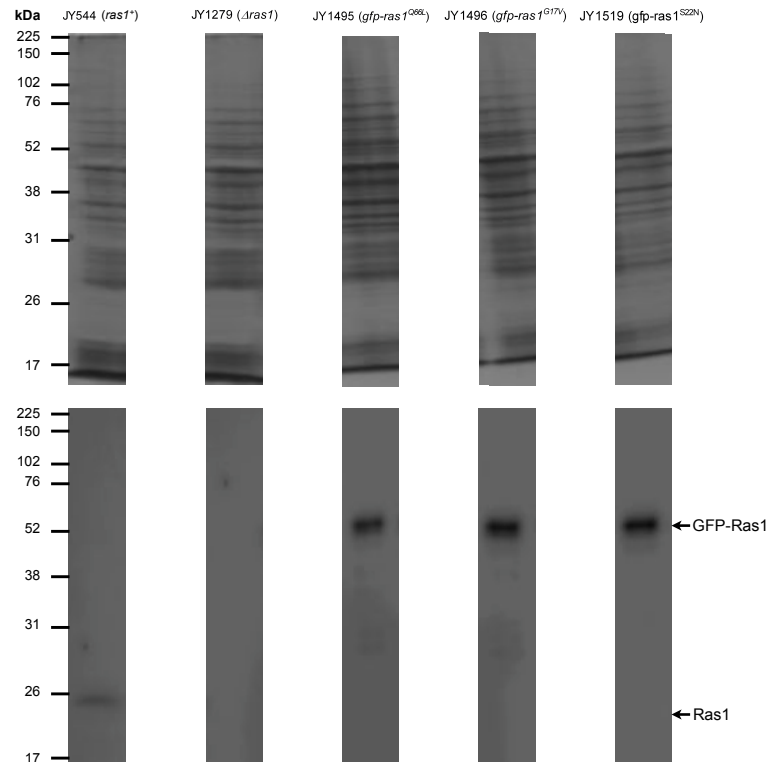


**Figure 4.44. Expression of GFP-Ras1<sup>Q66L</sup> (JY1495), GFP-Ras1<sup>G17V</sup> (JY1496) and GFP-Ras1<sup>S22N</sup> (JY1519)**

Integration of GFP-Ras1<sup>Q66L</sup> (JY1495), GFP-Ras1<sup>G17V</sup> (JY1496) and GFP-Ras1<sup>S22N</sup> (JY1519) at the *ras1* locus in the *sxa2>lacZ* reporter strain JY1247 was confirmed via immunoblotting using a RAS10 antibody. Coomassie stains of whole protein are included above the immunoblot as loading controls.

#### **4.7.3. GFP-Ras1<sup>Q66L</sup> (JY1495), GFP-Ras1<sup>G17V</sup> (JY1496) and GFP-Ras1<sup>S22N</sup> (JY1519) display reduced signalling activity through Scd1-Cdc42.**

GFP-Ras1 displayed reduced signalling activity compared to wild-type Ras1. As a consequence, the activity of Ras1<sup>Q66L</sup>, Ras1<sup>G17V</sup> and Ras1<sup>S22N</sup> may also be altered by the addition of an N-terminal GFP tag. To determine the activity of GFP-Ras1<sup>Q66L</sup>, GFP-Ras1<sup>G17V</sup> and GFP-Ras1<sup>S22N</sup>, signalling was first analysed through the Scd1-Cdc42 mediated cell morphology pathway. Images of cells in each population, expressing GFP from pREP3x, were obtained using a Leica SP5 scanning confocal microscope. Cell circularity was then determined using the Quimp image analysis software for 30 cells of each strain (Figure 4.46). Both GTPase deficient Ras1 mutants displayed reduced activity when

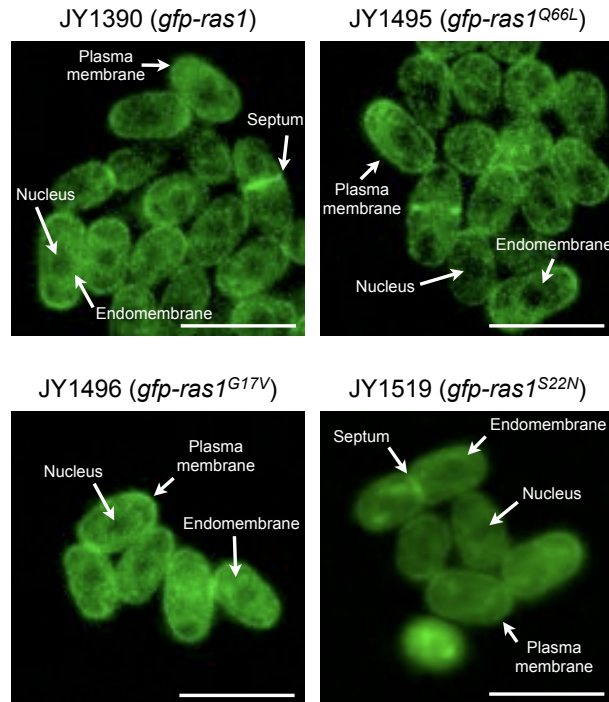


**Figure 4.45.** The localisation of GFP-Ras1<sup>Q66L</sup>, GFP-Ras1<sup>G17V</sup> and GFP-Ras1<sup>S22N</sup>

The localisation of GFP-Ras1 (JY1390), GFP-Ras1<sup>Q66L</sup> (JY1495), GFP-Ras1<sup>G17V</sup> (JY1496) and GFP-Ras1<sup>S22N</sup> (JY1519) was determined using a Nikon E800 epifluorescence microscope fitted with an Andor EM-CCD camera. All GFP-Ras1 fusions displayed localisation to the plasma membrane and peri-nuclear endomembrane structures. The scale bar represents 10  $\mu\text{m}$ .

tagged with GFP. Cells expressing GFP-Ras1<sup>Q66L</sup> (JY1495) still displayed a significantly less rounded morphology ( $78.2 \pm 1.2\%$ ,  $P = 0.001$ ) than  $\Delta ras1$  cells (JY1279) ( $85.9 \pm 1.5\%$ ), similar to that observed in cells expressing GFP-Ras1 ( $78.3 \pm 1.1\%$ ). The strain containing GFP-Ras1<sup>G17V</sup> however, displayed a rounded morphology ( $90.6 \pm 0.7\%$ ) consistent with that observed in  $\Delta ras1$  cells. These results indicate quite considerable differences in the effect of the GFP tag on these mutants, as the non-tagged version of Ras1<sup>G17V</sup> displayed the more elongated morphology of the two mutants. Despite this, the localisation of Ras1<sup>G17V</sup> appeared largely similar to GFP-Ras1, suggesting that this effect is likely due to impaired activity rather than altered localisation. GFP-Ras1<sup>S22N</sup>, like Ras1<sup>S22N</sup>, displayed no signalling through this pathway ( $94.9 \pm 0.4\%$  circularity).

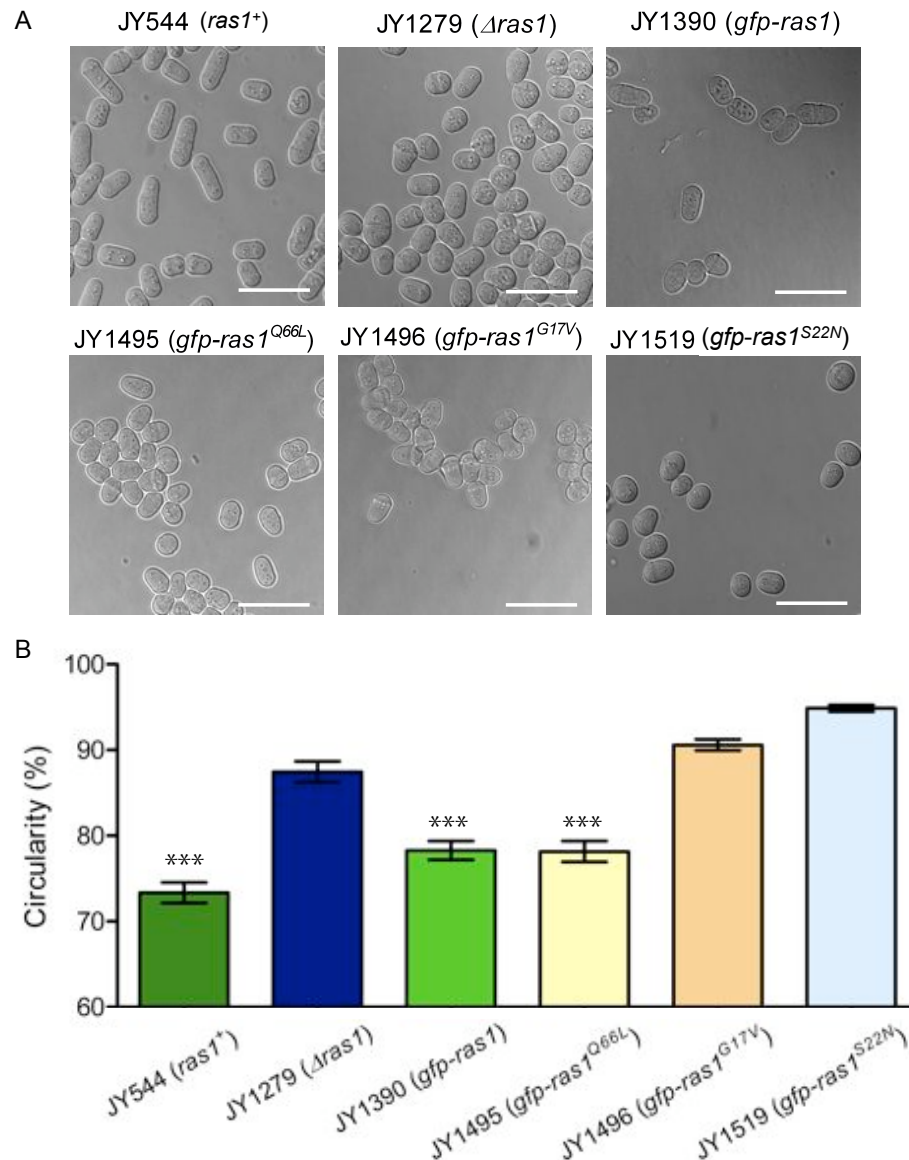


**Figure 4.46. Analysis of the morphology of cells expressing GFP-Ras1<sup>Q66L</sup>, GFP-Ras1<sup>G17V</sup> and GFP-Ras1<sup>S22N</sup>**

Images of populations of *ras1*<sup>+</sup> (JY544),  $\Delta$ *ras1* (JY1279), *gfp-ras1* (JY1390), *gfp-ras1*<sup>Q66L</sup> (JY1495), *gfp-ras1*<sup>G17V</sup> (JY1496) and *gfp-ras1*<sup>S22N</sup> (JY1519) cells, expressing GFP from pREP3x, were obtained using a leica SP5 scanning confocal microscope. Representative DIC images are displayed in panel A. Cell circularity was calculated using Quimp software (B). GFP-Ras1<sup>Q66L</sup> was the only mutant which supported significant signalling through Scd1-Cdc42 (P = 0.001). Data representative of 30 individual cells  $\pm$  SEM. Statistical significance was determined using a one-way anova with a Tukey multiple comparison post test. Three asterisks indicates a P-value of 0.001. The scale bar represents 10  $\mu$ m

#### 4.7.4. The GFP tag restores signalling at high concentrations of P-factor through Ras1<sup>Q66L</sup> and Ras1<sup>G17V</sup>.

Ras1<sup>Q66L</sup> and Ras1<sup>G17V</sup> both caused reduced signalling at higher P-factor concentrations, due to pheromone dependent cell death. These effects appear to be caused by prolonged Ras1 signalling, due to the inability of these mutants to hydrolyse GTP. As GFP-Ras1<sup>G17V</sup> and GFP-Ras1<sup>Q66L</sup> display a reduced level of signalling compared to their non-tagged counterparts (Figure 4.46), it is possible that the effect of these mutations on cell viability may be reduced.

To test this hypothesis, pheromone-dependent signalling was initially analysed using assays for  $\beta$ -galactosidase activity and average cell volume, following growth in a range of pheromone concentrations (1 nM to 100  $\mu$ M) in DMM for 16 h. Cells expressing GFP-Ras1<sup>Q66L</sup> (JY1495) and GFP-Ras1<sup>G17V</sup> (JY1496) displayed a classic sigmoidal dose-response profile to pheromone in  $\beta$ -galactosidase assays (Figure 4.47A). In addition, both displayed higher maximal signalling than JY1390 (*gfp-ras1*) ( $5.4 \pm 0.3$ ), with JY1495 (*gfp-ras1*<sup>Q66L</sup>) giving a maximal signal of  $13.3 \pm 0.5$  and JY1496 (*gfp-ras1*<sup>G17V</sup>) giving a maximal signal of  $18.3 \pm 0.6$ . Both displayed pEC<sub>50</sub>s comparable to wild-type cells (JY544) (JY1495 =  $7.4 \pm 0.1$ , JY1496 =  $7.1 \pm 0.1$  and JY544 =  $6.8 \pm 0.1$ ). JY1495 (*gfp-ras1*<sup>Q66L</sup>) and JY1496 (*gfp-ras1*<sup>G17V</sup>) also displayed a pheromone-dependent increase in cell volume, although both displayed higher basal cell volumes than wild type cells (JY1495 (*gfp-ras1*<sup>Q66L</sup>) =  $74.9 \pm 1.1$  fl, JY1496 (*gfp-ras1*<sup>G17V</sup>) =  $77.7 \pm 0.8$  fl and JY544 (*ras1*<sup>+</sup>) =  $67.0 \pm 1.3$  fl). JY1495 (*gfp-ras1*<sup>Q66L</sup>) displayed an increase in cell volume comparable with JY1390 (*gfp-ras1*), reaching a maximum of  $82.1 \pm 0.9$  fl. JY1496 (*gfp-ras1*<sup>G17V</sup>) gave a higher maximal cell volume, more consistent with wild-type cells (JY544), reaching  $93.2 \pm 0.9$  fl. These data suggest that GFP-Ras1<sup>G17V</sup> and GFP-Ras1<sup>Q66L</sup> do not cause pheromone dependent cell death, and may allow a more informative analysis of the signalling of these mutants.

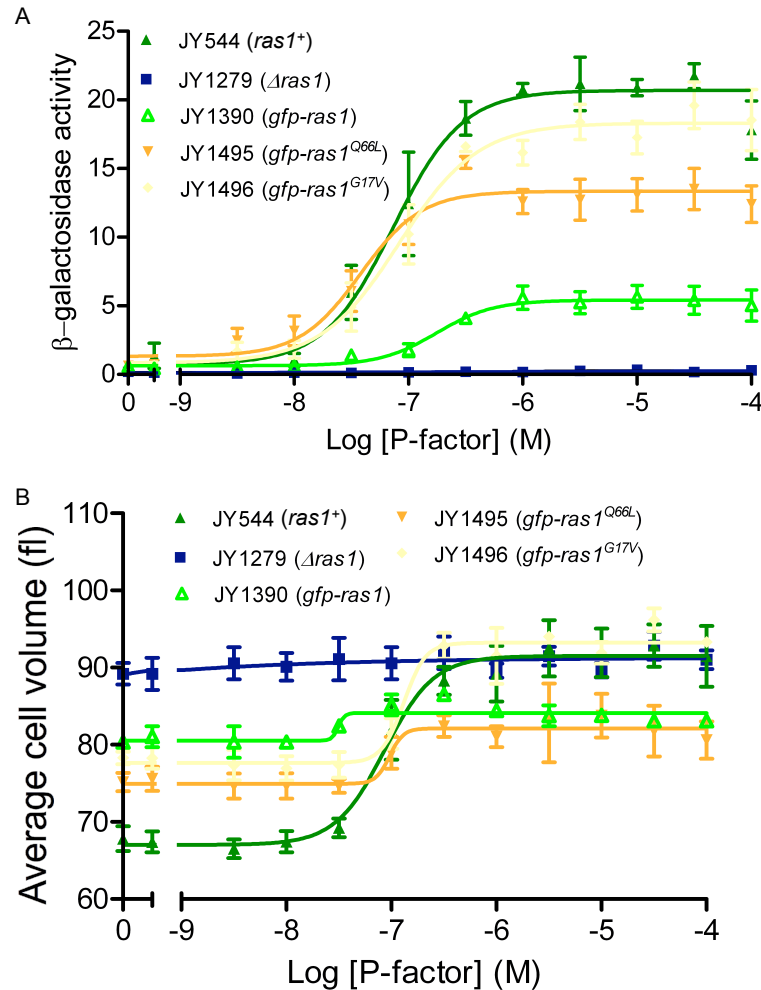


**Figure 4.47. Phormone-dependent changes in transcription and cell volume in cells expressing GFP-Ras1<sup>Q66L</sup> and GFP-Ras1<sup>G17V</sup>**

Phormone-responsive changes in transcription and cell volume were observed in *ras1*<sup>+</sup> (JY544),  $\Delta$ *ras1* (JY1279), *gfp-ras1* (JY1390), *gfp-ras1*<sup>Q66L</sup> (JY1495) and *gfp-ras1*<sup>G17V</sup> (JY1496) cells. Cells were grown in the presence of 1 nM to 100  $\mu$ M phormone in DMM for 16 h. Assays were then performed for  $\beta$ -galactosidase activity (A) and average cell volume (B). JY1495 and JY1496 both displayed maximal  $\beta$ -galactosidase activity higher than JY1390, and both displayed an increase in cell volume upon phormone stimulation. Data shown is an average of three independent determinants ( $\pm$ SEM).

Cells expressing GFP-Ras1<sup>G17V</sup> and GFP-Ras1<sup>Q66L</sup> exhibited a phormone-dependent increase in cell volume. To determine whether this increase in cell volume corresponded to an increase in cell length, images of the strains JY1495 (*gfp-ras1*<sup>Q66L</sup>) and JY1496 (*gfp-ras1*<sup>G17V</sup>), expressing GFP from pREP3x, were obtained following 16 h growth in the absence and in the presence of 10  $\mu$ M phormone in DMM lacking thiamine. Images were taken using a Leica SP5

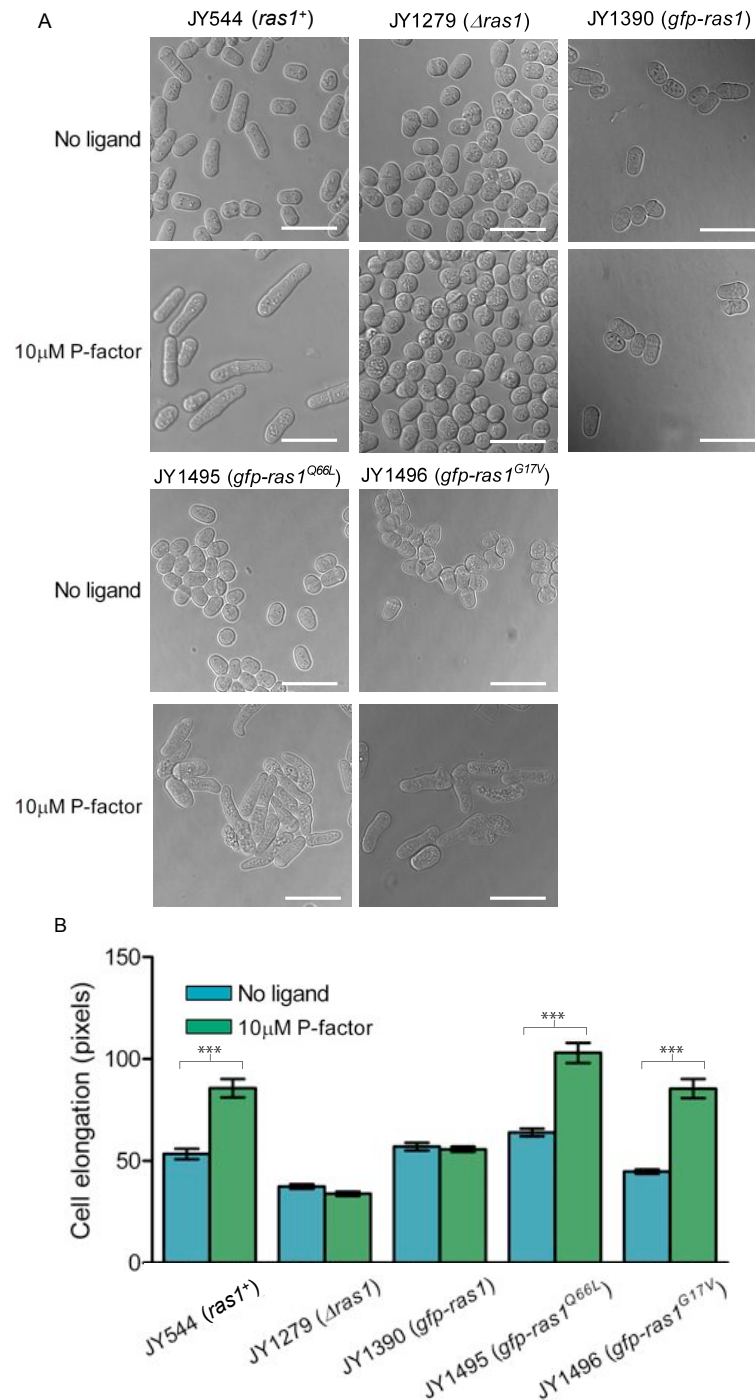


**Figure 4.48. Analysing shmoo formation in cells expressing GFP-Ras1<sup>Q66L</sup> (JY1495) and GFP-Ras1<sup>G17V</sup> (JY1496) using quantitative image analysis**

Images of *ras1*<sup>+</sup> (JY544),  $\Delta$ *ras1* (JY1279), *gfp-ras1* (JY1390), *gfp-ras1*<sup>Q66L</sup> (JY1495) and *gfp-ras1*<sup>G17V</sup> (JY1496) cells were obtained following 16 h growth in the absence and in the presence of 10  $\mu$ M pheromone in DMM lacking thiamine, using a Leica SP5 scanning confocal microscope. Representative DIC images are displayed in panel A. JY1495 (*gfp-ras1*<sup>Q66L</sup>) and JY1496 (*gfp-ras1*<sup>G17V</sup>) displayed a significant pheromone-dependent increase in cell length ( $P = 0.001$ ) (B). Data shown is representative of 30 individual cells  $\pm$  SEM. Statistical significance was determined using a one-way anova with a Tukey multiple comparison post test. Three asterisks indicates a P-value of 0.001. Images from the populations analysed demonstrate shmoo formation in response to pheromone in JY1495 (*gfp-ras1*<sup>Q66L</sup>) and JY1496 (*gfp-ras1*<sup>G17V</sup>) (B). The scale bar represents 10  $\mu$ m.

scanning confocal microscope. The Quimp image analysis software was then used to determine cell length for 30 cells of each strain and under each assay condition (Figure 4.48). Both strains displayed a pheromone-dependent increase in cell length comparable to that observed in wild-type cells. JY1495 (*gfp-ras1<sup>Q66L</sup>*) exhibited an increase from  $63.98 \pm 1.87$  pixels to  $103.0 \pm 5.0$  pixels and JY1496 (*gfp-ras1<sup>G17V</sup>*) exhibited an increase from  $44.8 \pm 1.1$  pixels to  $85.5 \pm 4.7$  pixels. Shmoo formation could also be observed in images of these cells, with cells exhibiting marked elongation following pheromone stimulation. These data again indicate that GFP-Ras1<sup>G17V</sup> and GFP-Ras1<sup>Q66L</sup> display signalling at higher pheromone concentrations, without any influence upon cell viability.

#### 4.7.5. Cells expressing GFP-Ras1<sup>S22N</sup> displays little pheromone-responsive signalling.

Ras1<sup>G17V</sup> and Ras1<sup>Q66L</sup> displayed quite differing signalling characteristics when tagged with GFP. To determine the signalling activity of GFP-Ras1<sup>S22N</sup> in response to pheromone,  $\beta$ -galactosidase activity and average cell volume were analysed following growth in a range of pheromone concentrations (1 nM to 100  $\mu$ M) in DMM for 16 h. GFP-Ras1<sup>S22N</sup> supported a slight pheromone-dependent increase in  $\beta$ -galactosidase activity, consistent with that observed in cells expressing Ras1<sup>S22N</sup> from both the endogenous *ras1* locus and pREP3x (Figure 4.49A). JY1519 (*gfp-ras1<sup>S22N</sup>*) did not display any increase in cell volume in response to pheromone, and exhibited a high basal cell volume ( $86.3 \pm 0.4$  fl) indicative of a rounded morphology (Figure 4.49B).

Images of JY1519 (*gfp-ras1<sup>S22N</sup>*), expressing GFP from pREP3x, were obtained following 16 h growth in the absence and in the presence of 10  $\mu$ M pheromone in DMM lacking thiamine, using a Leica SP5 scanning confocal microscope. The Quimp image analysis software was then used to determine cell length for 30 cells under each assay condition. JY1519 (*gfp-ras1<sup>S22N</sup>*) showed

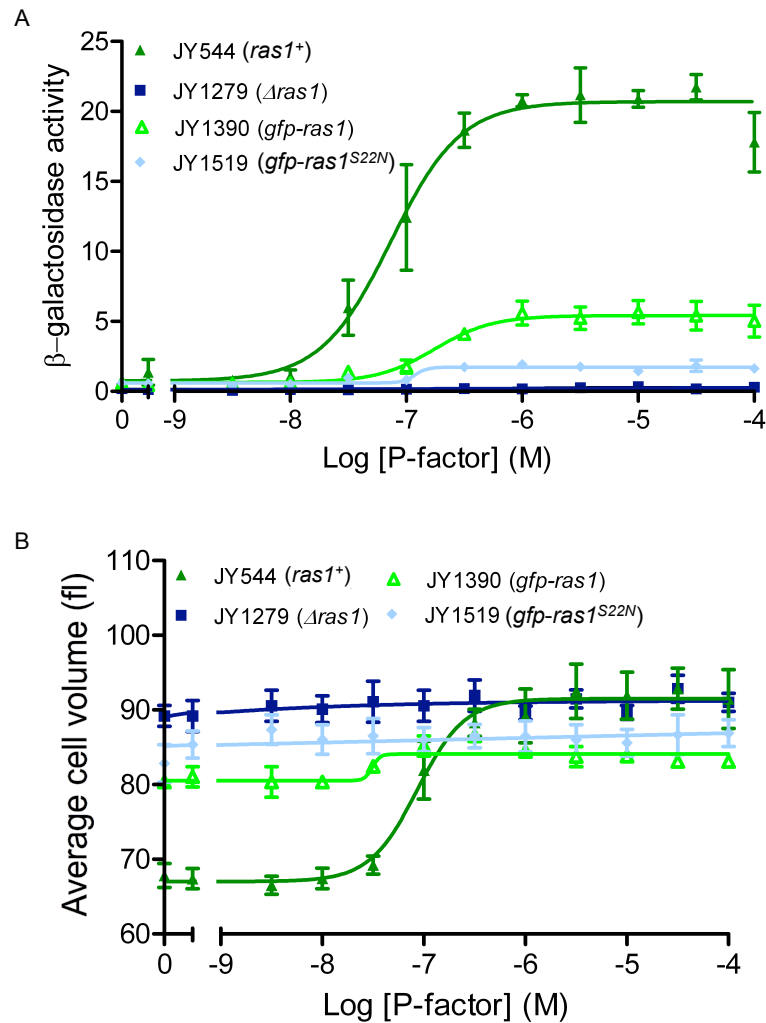


**Figure 4.49. Phormone-dependent changes in transcription and cell volume in cells expressing GFP-Ras1<sup>S22N</sup> (JY1519)**

Phormone-responsive changes in transcription and cell volume were observed in *ras1*<sup>+</sup> (JY544),  $\Delta$ *ras1* (JY1279), *gfp-ras1* (JY1390) and *gfp-ras1*<sup>S22N</sup> (JY1519) cells. Cells were grown in 1 nM to 100  $\mu$ M phormone in DMM for 16 h. Assays were then performed for  $\beta$ -galactosidase activity (A) and average cell volume (B). JY1519 displayed a small increase in  $\beta$ -galactosidase activity in response to phormone, and no increase in cell volume. Data shown is an average of three independent determinants ( $\pm$ SEM).

no increase in cell length in response to phormone (Figure 4.50B). These cells also exhibited a rounded morphology similar to that seen in cells lacking Ras1 (JY1279) (Figure 4.50A). These data indicate that GFP-Ras1<sup>S22N</sup>, like Ras1<sup>S22N</sup>, displays little signalling activity.

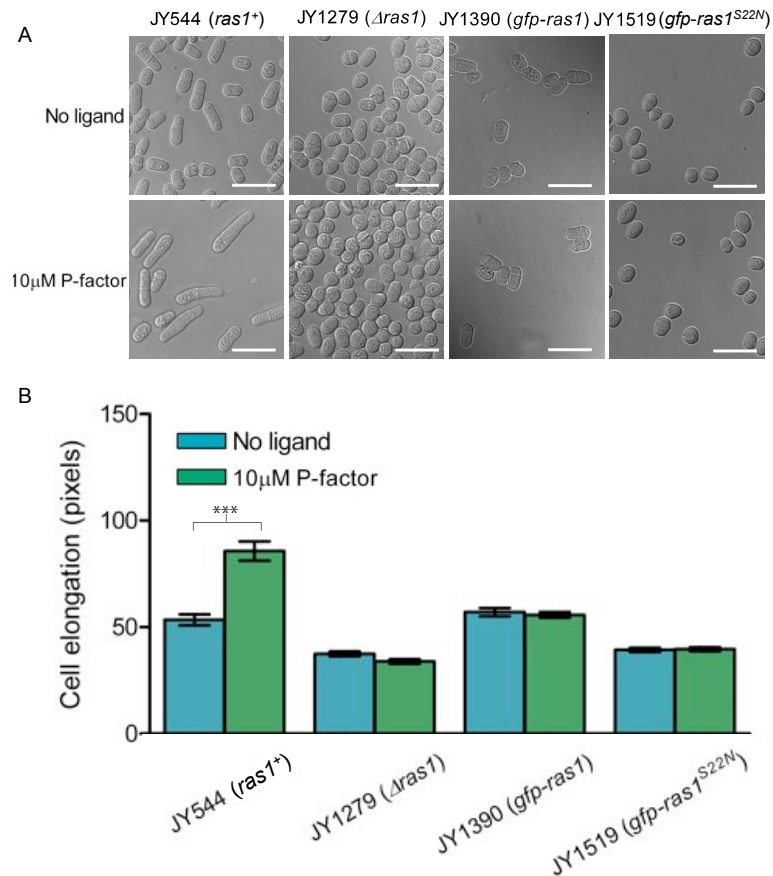


**Figure 4.50. Phormone-dependent elongation in cells expressing GFP-Ras1<sup>S22N</sup> (JY1519)**

Quimp software was used to determine the length of cells grown in the absence and in the presence of 10 µM phormone in DMM lacking thiamine for 16 h. Images were taken using a Leica SP5 scanning confocal microscope. Representative DIC images are shown in panel A. JY1519 (*gfp-ras1*<sup>S22N</sup>) displayed no phormone-dependent increase in cell length (B). Data shown is representative of 30 individual cells  $\pm$  SEM. Statistical significance was determined using a one-way anova with a Tukey multiple comparison post test. Three asterisks indicates a P-value of 0.001. Images from the populations analysed demonstrate no change in morphology in response to phormone in JY1519. The scale bar represents 10 µm.

## 4.8. Summary

The *Sz. pombe* pheromone response and cell polarity pathways provide ideal systems for the study of ras signalling. Despite this, few previous studies have sought to quantitatively characterise Ras1 signalling through these pathways. This chapter details the development of a quantitative assay for mating, in addition to the application of quantitative imaging techniques to the study of cell morphology in *Sz. pombe*. These assays were then used in conjunction with well established assays, such as the  $\beta$ -galactosidase assay for pheromone-responsive transcription and propidium iodide assay for cell cycle arrest, to characterise Ras1 signalling. In addition, a Tea1-mCherry strain was constructed for the analysis of cell polarity. Ras1 activity was analysed through the study of *ras1*<sup>+</sup> and  $\Delta$ *ras1* strains, indicating that Ras1 has an essential role in these processes.

The signalling activity of three Ras1 mutants were also discussed in this chapter. The first mutant, Ras1<sup>S22N</sup>, was based upon mutants in human ras isoforms which are unable to interact with GEF proteins effectively. Most signalling was lost through this mutant in all assays for Ras1 activity. The one exception to this was the small pheromone-dependent increase in  $\beta$ -galactosidase activity observed in cells expressing this mutant. The level of activity observed in cells containing Ras1<sup>S22N</sup> was very low and not increased upon constitutive expression from pREP3x. This could indicate the retention of some scaffolding activity, for example through low affinity binding of Byr2, which is not present in cells lacking Ras1 but is not dependent upon GEF mediated nucleotide exchange.

The other mutants assayed in this chapter were both based upon GTPase deficient mutants in human ras isoforms. This class of mutants are of high clinical relevance, as they are implicated in a significant majority of human cancers, causing aberrant mitogenic signalling. The two mutants, Ras1<sup>Q66L</sup> and Ras1<sup>G17V</sup>, differ in the mechanism of their GTPase deficiency. The Gly17Val

mutation alters the interaction between ras and the  $\gamma$ -phosphate of GTP, whereas the Gln66Leu mutant prevents the catalysis of GTP hydrolysis. Despite these differences both had a very similar effect upon signalling. Both gave strong pheromone-dependent signalling at low P-factor concentrations, but an apparent reduction in activity at higher ligand concentrations, due to cell death. This effect was less apparent upon constitutive expression of the mutants from pREP3x, as cell viability was affected even in the absence of pheromone. The greatest difference between the two mutants was in their effect upon morphology. Ras1<sup>G17V</sup>, but not Ras1<sup>Q66L</sup>, caused a hyperelongated phenotype, possibly indicating an increase in signalling through Scd1-Cdc42. As a consequence, in addition to the effects upon cell viability, little pheromone dependent elongation was seen in this strain at higher pheromone concentrations.

It was found that the constitutive expression of Ras1 resulted in an increase in chromosome missegregation. This effect was further compounded by the constitutive expression of GTPase deficient mutants. Based upon previous work (Li *et al.* 2000), it is likely that this effect is due to an aberrant interaction with Scd1. The effect of increased Ras1 expression and activity upon chromosome instability could in part explain the reduced cell viability observed in these strains.

The functional expression of a GFP-Ras1 fusion protein from the *ras1* locus was also described. In addition, it was demonstrated that GFP-Ras1 localised to the plasma membrane and endomembranes. It was also indicated that mutations which affected nucleotide binding and GTP hydrolysis did not significantly affect localisation. Finally, the analysis of GFP-Ras1<sup>G17V</sup> and GFP-Ras1<sup>Q66L</sup> function indicated signalling activity at high pheromone concentrations. These data suggest that cell viability was not impaired in these populations. Both strains exhibited higher pheromone-dependent signalling than in cells expressing GFP-Ras1. These effects could not be directly observed in strains expressing Ras1<sup>G17V</sup> and Ras1<sup>Q66L</sup> due to impaired cell viability.

## The impact of Ras1 C-terminal modification and localisation on signalling in fission yeast

### 5.1. Introduction

As with many components which translate extracellular signals into intracellular responses, ras requires membrane association for correct function. The localisation of ras proteins is a function of their C-terminus, which is the most highly divergent region between most ras proteins. All ras proteins undergo a process of cysteine farnesylation, catalysed by farnesyltransferases, at a C-terminal CAAX motif (where A is any aliphatic residue and X is any amino acid). However, this modification is not sufficient to promote stable membrane association, and a second plasma membrane targeting motif is required (Eisenberg and Henis 2008). In Ras1, the second motif is a palmitoylated cysteine residue directly upstream of the farnesylated cysteine (Figure 1.7).

One previous study has investigated the role of Ras1 C-terminal modification in signalling (Onken *et al.* 2006). The study suggested that preventing the palmitoylation of Ras1 blocked all transport of Ras1 to the plasma membrane. In addition, it was indicated that preventing the plasma membrane localisation of Ras1 disrupted mating but not polar cell morphology. It was concluded that the signalling of Ras1 from the plasma membrane promoted mating through activation of Byr2, and that endomembrane associated Ras1 was responsible for regulating cell polarity through activation of Scd1.

In the following chapter, the quantitative analysis of Ras1 localisation and activity is detailed in mutants exhibiting C-terminal modification defects. In addition, the localisation of the mutants displaying altered nucleotide binding and hydrolysis phenotypes discussed in chapter 4 is also analysed.

## 5.2. Quantifying Ras1 localisation

### 5.2.1. Comparing the localisation of GFP-Ras1 when expressed from the *ras1* locus and pREP3x.

Expression of GFP-Ras1 from the *ras1* locus allowed the visualisation of Ras1 localisation (Figure 4.22). Despite this, expression of the fusion was at very low levels, preventing the detailed analysis of localisation. In an attempt to increase expression, GFP-Ras1 was expressed from pREP3x in the  $\Delta ras1$  strain JY1279. The localisation of GFP-Ras1 when expressed from the *ras1* locus or from pREP3x was qualitatively similar. Both exhibited localisation predominantly to the plasma membrane, in addition to some localisation to endomembrane structures (Figure 5.1). Due to the low level of expression observed from the *ras1* locus, GFP-Ras1 could only be detected using an electron multiplying charge-coupled device (EM-CCD) camera, in which the signal at each pixel is increased prior to visualisation. GFP-Ras1 expressed from the *ras1* locus could not be detected using a scanning confocal microscope (Leica SP5), whereas GFP-Ras1 expressed from pREP3x gave a very strong signal. Due to the strength of this signal the image also contained markedly less noise. Given this improved image quality, and the apparent lack of effect upon localisation, expression from pREP3x could provide a means to analyse Ras1 localisation at greater resolution and detail.

### 5.2.2. Wild-type Ras1 displays predominantly plasma membrane localisation.

The higher level of expression observed from pREP3x allowed the generation of higher resolution images of GFP-Ras1 localisation (Figure 5.1). Such images should allow a more detailed analysis of GFP-Ras1 localisation. In addition to the analysis of morphology, one of the primary functions of the Quimp plugin

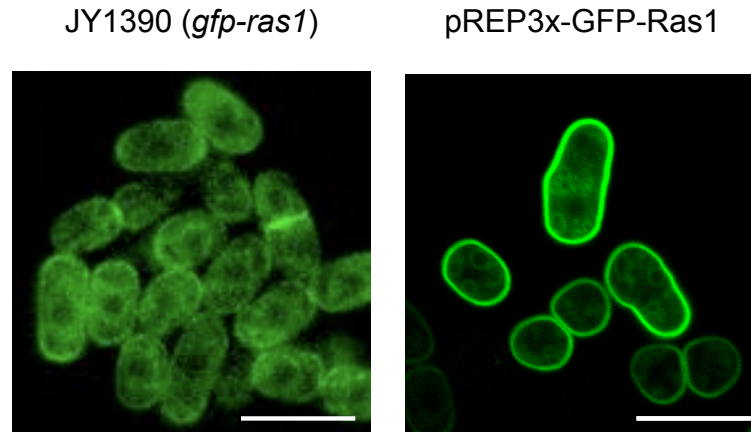


**Figure 5.1. Comparing the localisation of GFP-Ras1 when expressed from the *ras1* locus and pREP3x**

Images of GFP-Ras1 expressed from the *ras1* locus were taken using a Nikon E800 epifluorescence microscope fitted with an Andor EM-CCD camera, as GFP-Ras1 was not detected using a scanning confocal microscope (Leica SP5). Images of GFP-Ras1 expressed from pREP3x were collected using a Leica SP5 scanning confocal microscope. The scale bar represents 10  $\mu\text{m}$ .

of ImageJ is to analyse the distribution of fluorescence in a cell, with a specific focus on fluorescence at the cortex of the cell. This analysis therefore allows the quantification of plasma membrane localisation. Images of  $\Delta ras1$  cells (JY1279) expressing GFP and GFP-Ras1 from pREP3x were obtained using a Leica SP5 scanning confocal microscope (Figure 5.2A). Quimp software was then used to separate fluorescence at the periphery of the cell from the interior, and the intensity of fluorescence in each of these compartments was determined (Figure 5.2B). The level of plasma membrane fluorescence in cells expressing GFP alone was determined to be  $3.1 \pm 1.0 \%$ , representing a small proportion of soluble GFP in close proximity to the membrane. By contrast, GFP-Ras1 displayed predominantly plasma membrane localisation ( $78.0 \pm 3.5 \%$ ) (Figure 5.2C). Examination of GFP-Ras1 localisation indicates that the majority of GFP-Ras1 not at the plasma membrane was located on endomembrane structures. These observations are in agreement with those made in previous studies, in which it was reported that Ras1 localised mainly to the plasma membrane and displays some endomembrane localisation (Onken *et al.* 2006).

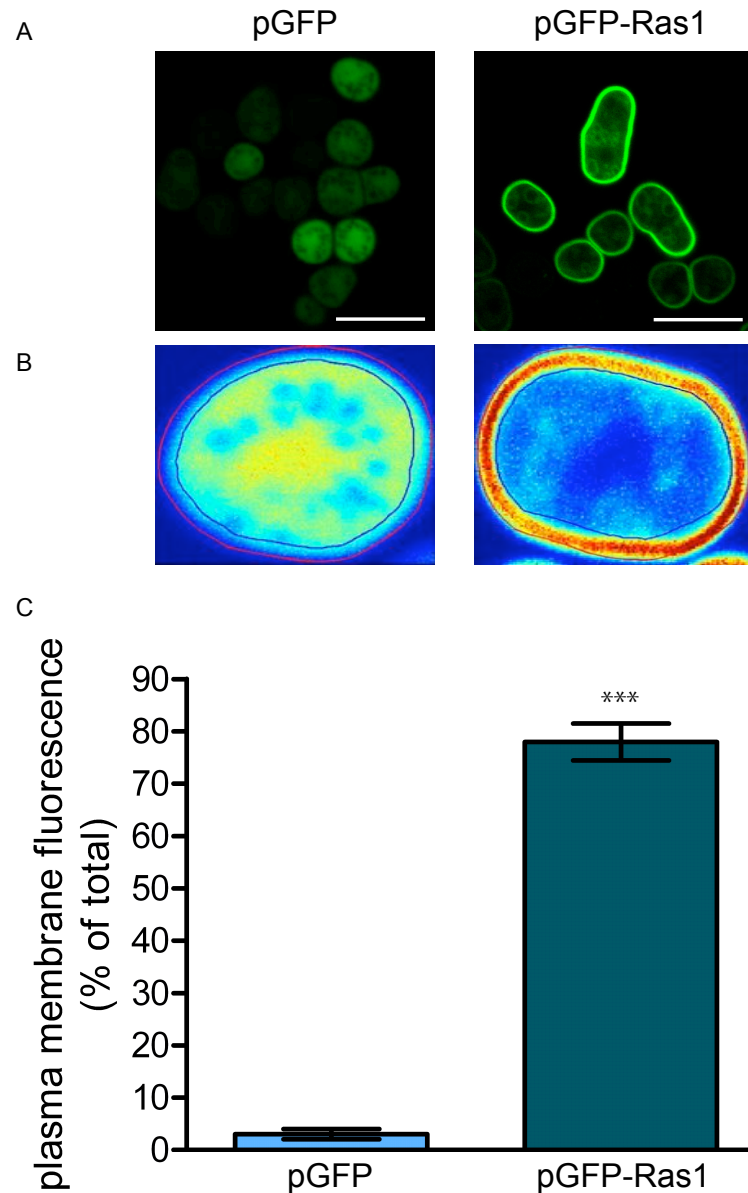


**Figure 5.2.** Quantifying the localisation of GFP-Ras1 using Quimp software

Images of  $\Delta ras1$  cells (JY1279) expressing GFP and GFP-Ras1 from pREP3x were obtained using a Leica SP5 scanning confocal microscope (A). The intensity of fluorescence at the periphery compared to the interior of the cell was determined using Quimp software (B), and percentage plasma membrane fluorescence was calculated (C). The analysis indicated that GFP-Ras1 displayed predominantly plasma membrane fluorescence. Statistical significance was determined using a one-way anova with a Tukey multiple comparison post test. Three asterisks indicates a P-value of 0.001. The scale bar represents 10  $\mu\text{m}$ .

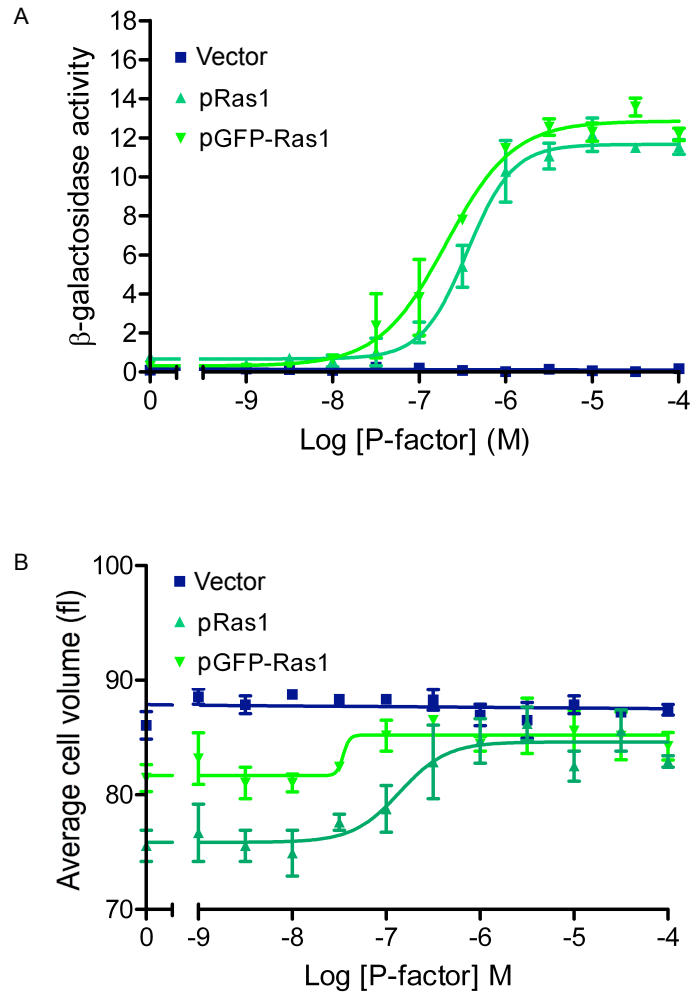


**Figure 5.3. Phormone-dependent changes in transcription and cell volume in cells expressing GFP-Ras1 from pREP3x**

Phormone-responsive changes in transcription and cell volume were observed  $\Delta ras1$  (JY1279) cells transformed with pREP3x-Ras1, pREP3x-GFP-Ras1 and vector alone. Cells were grown in the presence of 1 nM to 100  $\mu$ M phormone in DMM for 16 h. Assays were then performed for  $\beta$ -galactosidase activity (A) and average cell volume (B). Both Ras1 and GFP-Ras1 displayed comparable  $\beta$ -galactosidase activity, and both displayed an increase in cell volume upon phormone stimulation. Data shown is an average of three independent determinants ( $\pm$ SEM).

### 5.2.3. Expression of GFP-Ras1 from pREP3x restores pheromone dependent signalling in $\Delta ras1$ (JY1279) cells.

Expression of GFP-Ras1 from pREP3x was used to allow the quantification of Ras1 localisation. Signalling in response to pheromone was analysed to determine whether GFP-Ras1 could support signalling when expressed from pREP3x in the  $\Delta ras1$  strain JY1279. Assays for  $\beta$ -galactosidase activity and average cell volume were performed following growth in a range of pheromone concentrations (1 nM to 100  $\mu$ M) in DMM lacking thiamine for 16 h. Cells expressing GFP-Ras1 and Ras1 from pREP3x displayed very similar dose-response profiles. Cells containing pREP3x-GFP-Ras1 gave a maximal signal of  $12.9 \pm 0.5$  and a pEC<sub>50</sub> of  $6.7 \pm 0.1$ , compared to a maximal signal of  $11.7 \pm 0.3$  and a pEC<sub>50</sub> of  $6.5 \pm 0.1$  in cells expressing Ras1 (Figure 5.3A).

The expression of GFP-Ras1 and Ras1 from pREP3x also supported similar pheromone-dependent increases in cell volume. Cells expressing GFP-Ras1 exhibited a maximal volume of  $86.30 \pm 1.4$  fl and pEC<sub>50</sub> of  $7.6 \pm 0.3$ . Similarly, cells containing Ras1 exhibited a maximal volume of  $85.8 \pm 1.3$  fl and pEC<sub>50</sub> of  $6.8 \pm 0.3$ . Cells containing GFP-Ras1 displayed a higher basal cell volume than those expressing Ras1 ( $81.6 \pm 1.9$  fl compared to  $76.4 \pm 1.2$  fl), possibly indicating a slightly more rounded morphology than cells expressing Ras1 (Figure 5.3B). The expression of GFP-Ras1 from pREP3x causes an increase in maximal signalling compared to when expressed from the *ras1* locus (Figure 4.24). This is the inverse effect of that seen with wild-type Ras1, in which constitutive expression causes reduced signalling, due to cell death (Figure 4.42). These data could suggest that the constitutive expression of GFP-Ras1 is not as detrimental to cell viability as that of wild-type Ras1.

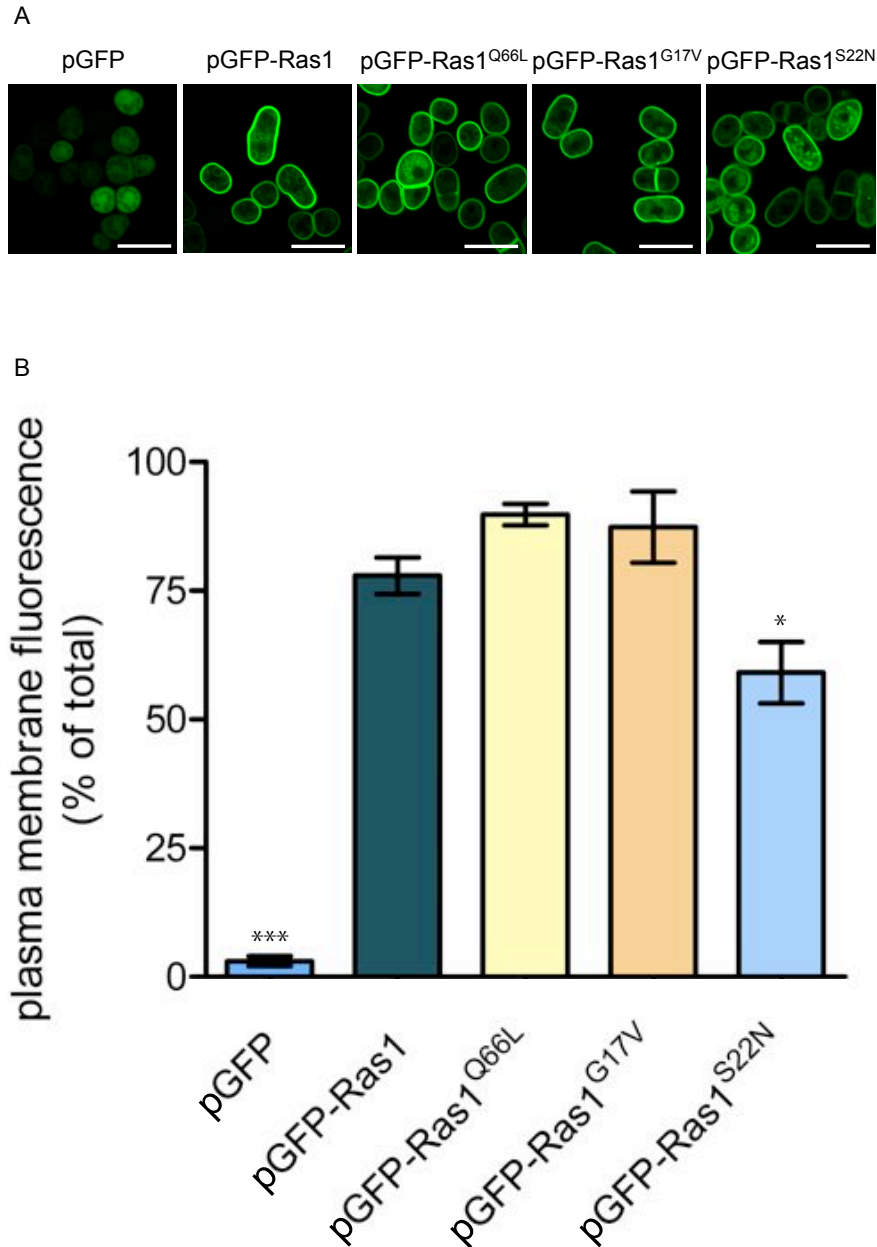


**Figure 5.4. Analysing the localisation of GFP-Ras1<sup>Q66L</sup>, GFP-Ras1<sup>G17V</sup> and GFP-Ras1<sup>S22N</sup> using Qimp software**

Images of  $\Delta ras1$  cells (JY1279) expressing GFP and GFP-Ras1 fusions from pREP3x were obtained using a Leica SP5 scanning confocal microscope (A). The intensity of fluorescence at the periphery compared to the interior of the cell was determined using Qimp software, and percentage plasma membrane fluorescence was calculated (B). GFP-Ras1<sup>Q66L</sup> and GFP-Ras1<sup>G17V</sup> both displayed plasma membrane localisation comparable to GFP-Ras1. GFP-Ras1<sup>S22N</sup> displayed a lower level of plasma membrane localisation. Statistical significance was determined using a one-way anova with a Tukey multiple comparison post test. Data representative of 10 individual cells  $\pm$  SEM. One asterisk indicates a P-value of 0.05 and three asterisks indicates a P-value of 0.001. The scale bar represents 10  $\mu$ m.

#### 5.2.4. The localisation of Ras1 is altered in mutations which affect nucleotide binding and hydrolysis.

Expression of GFP-Ras1<sup>Q66L</sup>, GFP-Ras1<sup>G17V</sup> and GFP-Ras1<sup>S22N</sup> from the *ras1* locus revealed no clear change in the localisation of all three mutants compared to wild-type Ras1 (Figure 4.45). However, as discussed in the preceding sections, the expression of GFP-Ras1 fusions from the *ras1* locus does not allow the detailed analysis of localisation. To increase their expression, GFP-Ras1<sup>Q66L</sup>, GFP-Ras1<sup>G17V</sup> and GFP-Ras1<sup>S22N</sup> were expressed in the  $\Delta ras1$  strain JY1279 from pREP3x. Fluorescence images were then obtained using a Leica SP scanning confocal microscope (Figure 5.4A), and Quimp software was used to determine the level of fluorescence at the plasma membrane (Figure 5.4B).

Both GFP-Ras1<sup>Q66L</sup> and GFP-Ras1<sup>G17V</sup> displayed high levels of plasma membrane localisation. Both exhibited higher mean percentage plasma membrane fluorescence ( $89.8 \pm 2.1$  % and  $87.4 \pm 6.9$  % respectively) than GFP-Ras1 ( $78.0 \pm 3.5$  %), although this difference was not statistically significant in either case. GFP-Ras1<sup>S22N</sup>, by contrast, displayed a significantly lower percentage membrane fluorescence ( $59.1 \pm 6.0$  %,  $P = 0.05$ ). These data could indicate that the functional interactions of Ras1, which require nucleotide exchange, influence the levels of Ras1 at the plasma membrane.

### 5.3. Analysing the role of Ras1 C-terminal modification

Ras1 is modified at two C-terminal residues to promote plasma membrane association (Onken *et al.* 2006). Cys216, which is contained within a canonical CAAX farnesylation motif, is the first residue to be modified by the addition of farnesyl group. This event is required for all downstream modifications to proceed. The AAX is then cleaved and the C-terminal cysteine is methyl esterified (Eisenberg and Henis 2008). Finally, the Cys215 residue is palmitoylated and the C-terminal modification of Ras1 is complete. The modification of

these residues can be prevented through the use of analogues which sequester the enzymes responsible for these modification, such as 2-bromo-palmitate (Resh 2006), or the more direct approach of site-directed mutagenesis. In the following section, the use of conservative cysteine to serine mutations to prevent farnesylation and palmitoylation is discussed. Both the function of these mutants, determined using the assays describe in chapter 4, and their localisation, determined using the techniques described in the preceding section, is described.

### 5.3.1. Preventing lipid modification of Ras1 reduces plasma membrane localisation.

N-terminal GFP fusions of the palmitoylation deficient Ras1<sup>C215S</sup> mutant and palmitoylation and farnesylation deficient Ras1<sup>C216S</sup> mutant were created at the *ras1* locus, to allow analysis of the effects of these mutants upon Ras1 localisation. Integration was performed using the method described previously (Figure 4.28A). Expression was confirmed by immunoblotting using an anti-ras RAS10 antibody, giving a signal at a position consistent with the predicted size of the fusion ( $\sim 53$  kDa) (Figure 5.5).

In order to determine the effect of altering the C-terminal modification of Ras1 upon Ras1 localisation, images of cells expressing GFP-Ras1, GFP-Ras1<sup>C215S</sup> and GFP-Ras1<sup>C216S</sup> from the endogenous *ras1* promoter were obtained. Images were taken using a Nikon E800 epifluorescence microscope fitted with an Andor EM-CCD camera (Figure 5.6). Little plasma membrane localisation of GFP-Ras1<sup>C215S</sup> or GFP-Ras1<sup>C216S</sup> was observable. However, the fluorescence signal was extremely low, preventing clear analysis of the localisation of either mutant. GFP-Ras1<sup>C215S</sup> displayed some localisation to internal structures, which could represent endomembranes. GFP-Ras1<sup>C216S</sup> appeared to be present throughout the cytosol.

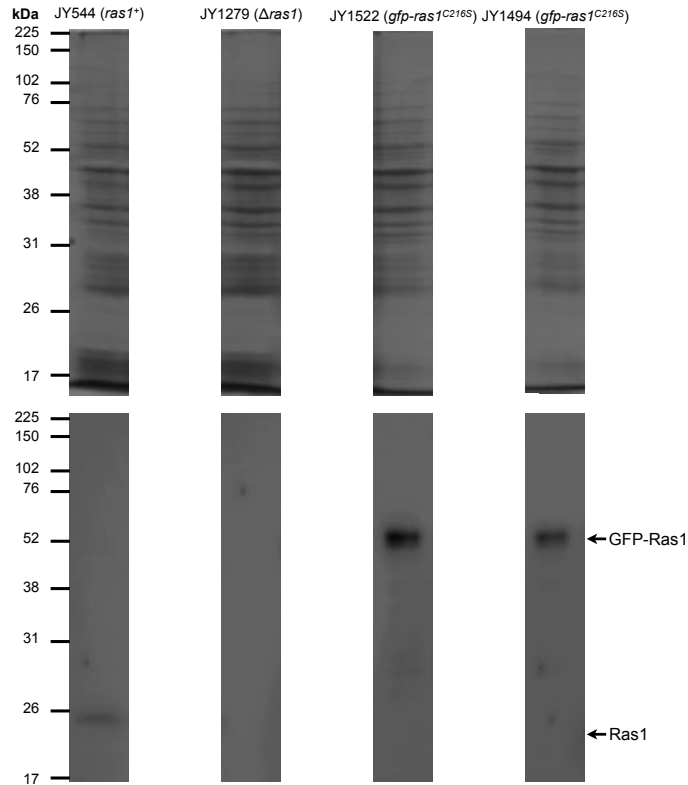


**Figure 5.5. Expression of GFP-Ras1<sup>C215S</sup> (JY1522) and GFP-Ras1<sup>C216S</sup> (JY1494)**

Integration of GFP-Ras1<sup>C215S</sup> (JY1522) and GFP-Ras1<sup>C216S</sup> (JY1494) in the *ras1::ura4<sup>+</sup>, sxa2>lacZ* reporter strain JY1247 was confirmed via immunoblotting using an anti-ras RAS10 antibody. Coomassie stains of whole protein are included above the immunoblot as loading controls.

### 5.3.2. Quantification of GFP-Ras1<sup>C215S</sup> and GFP-Ras1<sup>C216S</sup> localisation.

Neither GFP-Ras1<sup>C215S</sup> or GFP-Ras1<sup>C216S</sup> exhibited clear plasma membrane localisation when expressed from the *ras1* locus. However, the quality of these images was very poor. To allow the generation of higher resolution images of GFP-Ras1<sup>C215S</sup> and GFP-Ras1<sup>C216S</sup>, their localisation was determined through expression from pREP3x in the  $\Delta ras1$  strain JY1279. Fluorescence images were obtained using a Leica SP5 scanning confocal microscope (Figure 5.7A), and the images were analysed using Quimp software to determine the level of fluorescence at the periphery compared to the interior of the cell (Figure 5.7B). The loss of C-terminal modifications had profound effects upon Ras1 localisation. The loss of the palmitoyl group caused a reduction in plasma

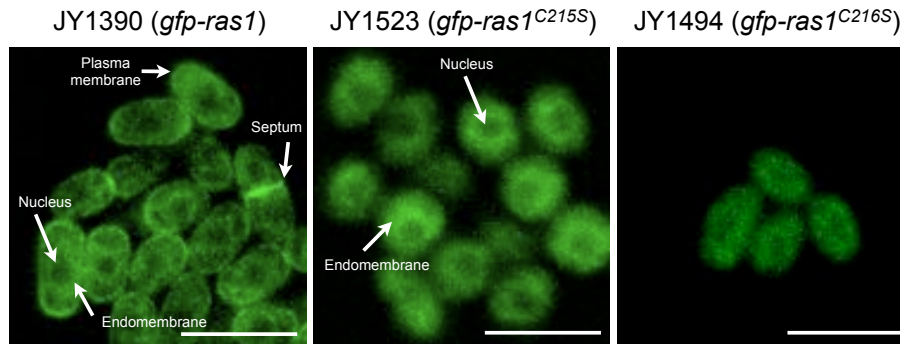


**Figure 5.6. The localisation of GFP-Ras1<sup>C215S</sup> and GFP-Ras1<sup>C216S</sup>**

The localisation of GFP-Ras1, GFP-Ras1<sup>C215S</sup> and GFP-Ras1<sup>C216S</sup>, upon expression from the *ras1* locus, was determined using a Nikon E800 epifluorescence microscope fitted with an Andor EM-CCD camera. GFP-Ras1 was observed at the plasma membrane and peri-nuclear endomembrane structures. GFP-Ras1<sup>C215S</sup> appeared to localise to endomembrane structures and GFP-Ras1<sup>C216S</sup> exhibited diffuse cytosolic localisation. The scale bar represents 10  $\mu\text{m}$ .

membrane localisation, with plasma membrane fluorescence falling from  $78.0 \pm 3.5 \%$  of wild-type GFP-Ras1 to  $16.6 \pm 1.8 \%$  of GFP-Ras1<sup>C215S</sup>. Despite this drop, Ras1 was still observed at the plasma membrane, an observation which contradicts a previous study where it was suggested the loss of the palmitoyl group prevents Ras1 from reaching the plasma membrane (Onken *et al.* 2006). However, more recent studies have suggested that monolipidated proteins, such as GFP-Ras1<sup>C215S</sup>, do not display preferential localisation to specific membrane compartments, with their localisation simply reflecting membrane density (Rocks *et al.* 2010). This observation is in concert with the localisation of GFP-Ras1<sup>C215S</sup> observed in Figure 5.7, in which GFP-Ras1<sup>C215S</sup> displays a uniform distribution across the plasma membrane and endomembranes. GFP-Ras1<sup>C216S</sup> displayed no specific membrane localisation and appeared largely cytosolic, exhibiting a plasma membrane fluorescence comparable to GFP alone ( $4.4 \pm 1.5 \%$  compared to  $3.1 \pm 1.0 \%$ ).

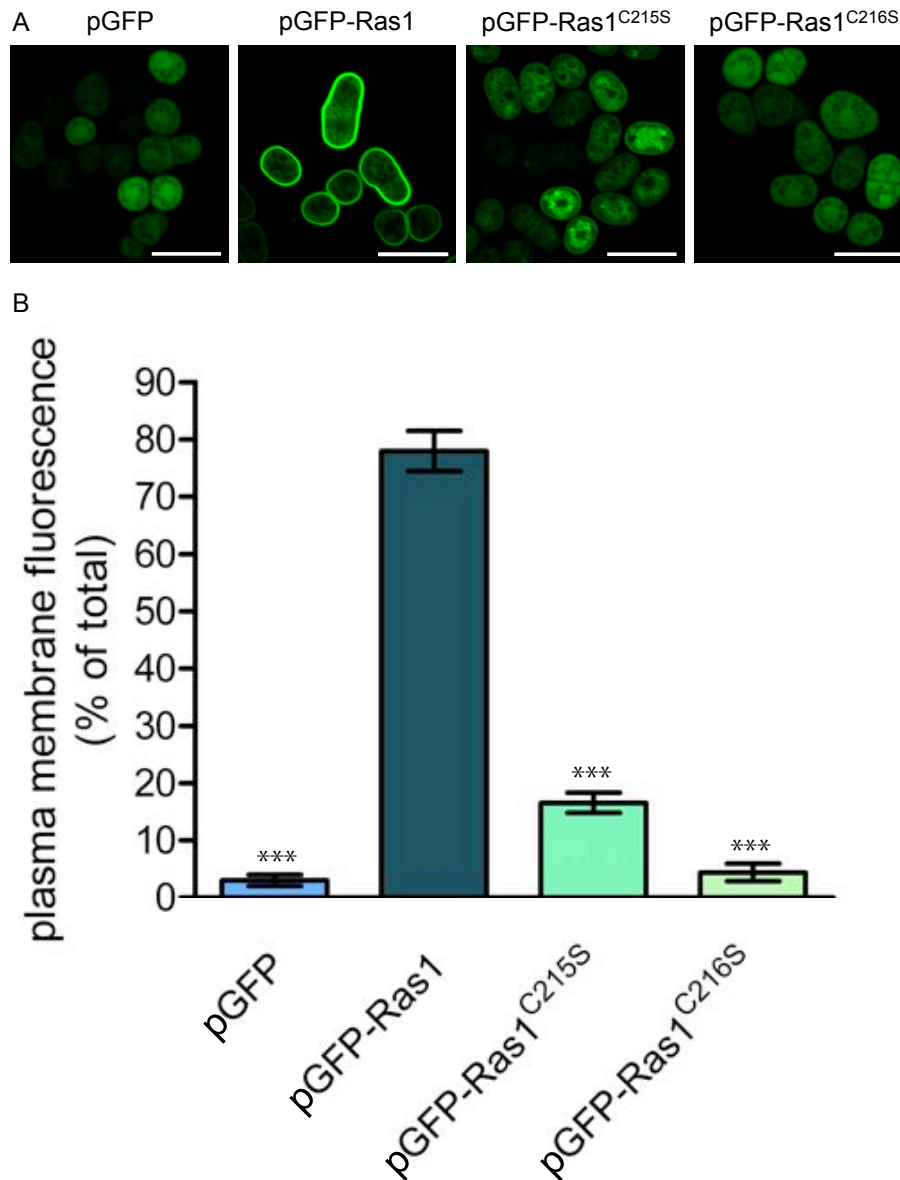


**Figure 5.7. Analysing the localisation of GFP-Ras1<sup>C215S</sup> and GFP-Ras1<sup>C216S</sup> using Quimp software**

Images of  $\Delta ras1$  cells (JY1279) expressing GFP and GFP-Ras1 fusions from pREP3x were obtained using a Leica SP5 scanning confocal microscope (A). The intensity of fluorescence at the periphery compared to the interior of the cell was determined using Quimp software, and percentage plasma membrane fluorescence was calculated (B). Preventing lipid modification caused a reduction in the plasma membrane localisation of Ras1. Statistical significance was determined using a one-way anova with a Tukey multiple comparison post test. Three asterisks indicates a P-value of 0.001. Data representative of 10 individual cells  $\pm$  SEM. The scale bar represents 10  $\mu$ m.

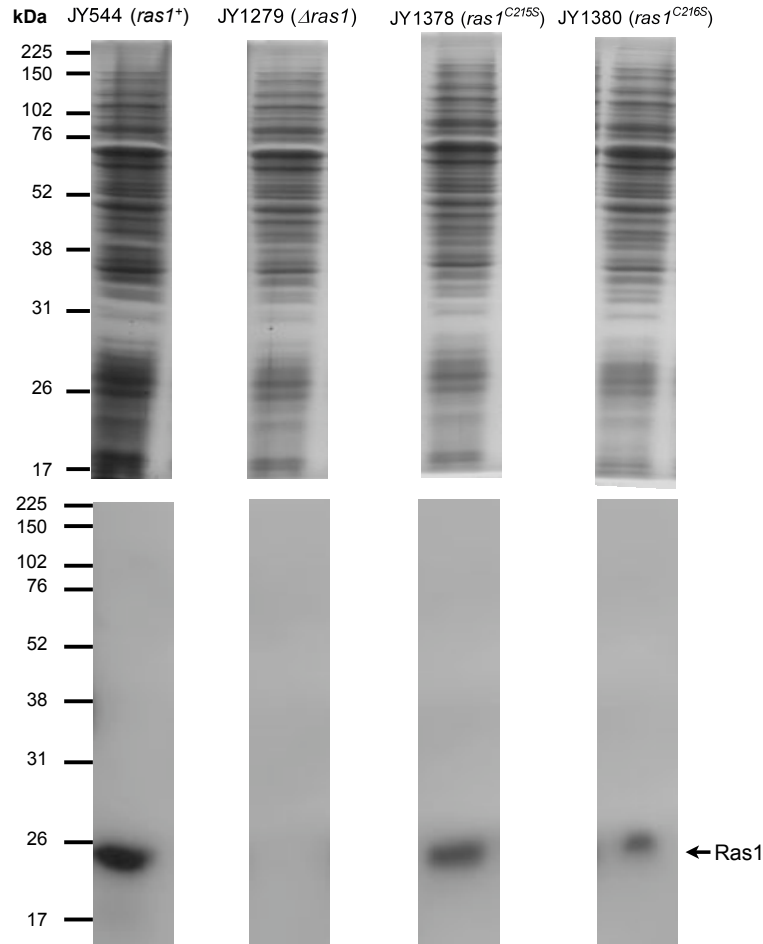


**Figure 5.8. Expression of Ras1<sup>C215S</sup> (JY1378) and Ras1<sup>C216S</sup> (JY1380) in the  $\beta$ -galactosidase reporter strain**

Integration of Ras1<sup>C215S</sup> (JY1378) and Ras1<sup>C216S</sup> (JY1380) in the *ras1::ura4<sup>+</sup>, sxa2>lacZ* reporter strain JY1247 was confirmed via immunoblotting using an anti-ras RAS10 antibody. Coomassie stains of whole protein are included above the immunoblot as loading controls.

### 5.3.3. Integration of Ras1<sup>C215S</sup> and Ras1<sup>C216S</sup>.

In order to analyse the function of Ras1<sup>C215S</sup> and Ras1<sup>C216S</sup> when expressed from the endogenous *ras1* promoter, both mutants were integrated at the *ras1* locus in the *ras1::ura4<sup>+</sup>, sxa2>lacZ* strain JY1247 (Figure 5.8) and the *ras1::ura4<sup>+</sup>, tea1-mCherry* strain JY1504 (Figure 5.9) using the method described previously (Figure 4.28A). Expression was confirmed by immunoblotting using an anti-ras RAS10 antibody.

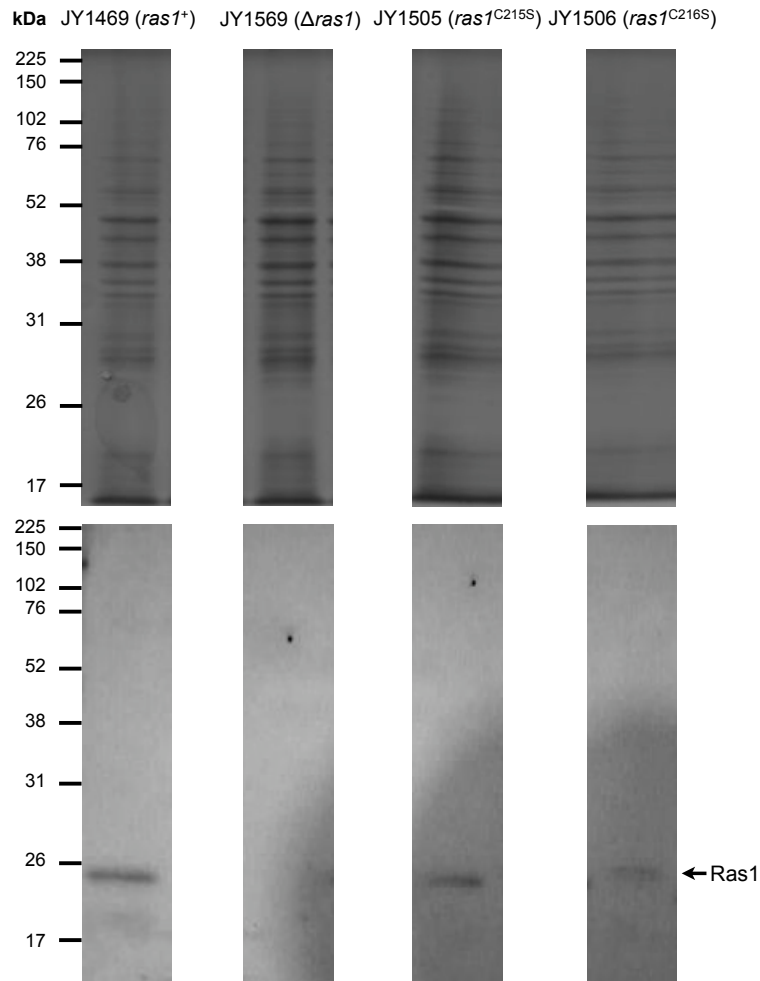


**Figure 5.9. Expression of Ras1<sup>C215S</sup> (JY1505) and Ras1<sup>C216S</sup> (JY1506) in the Tea1-mCherry strain**

Integration of Ras1<sup>C215S</sup> (JY1505) and Ras1<sup>C216S</sup> (JY1506) in the *ras1::ura4<sup>+</sup>, tea1-mCherry* strain JY1569 was confirmed via immunoblotting using an anti-ras RAS10 antibody. Coomassie stains of whole protein are included above the immunoblot as loading controls.

#### 5.3.4. Lipid modification of Ras1 is required to maintain elongated cell morphology.

GFP-Ras1<sup>C215S</sup> and GFP-Ras1<sup>C216S</sup> both exhibited altered localisation compared to GFP-Ras1. It has previously been suggested that the localisation of Ras1 to the plasma membrane is not required to maintain elongated morphology, and that this process is controlled at the endomembranes. As a consequence, it would be expected that morphology was unaffected in cells expressing Ras1<sup>C215S</sup> (Onken *et al.* 2006), which exhibited high levels of

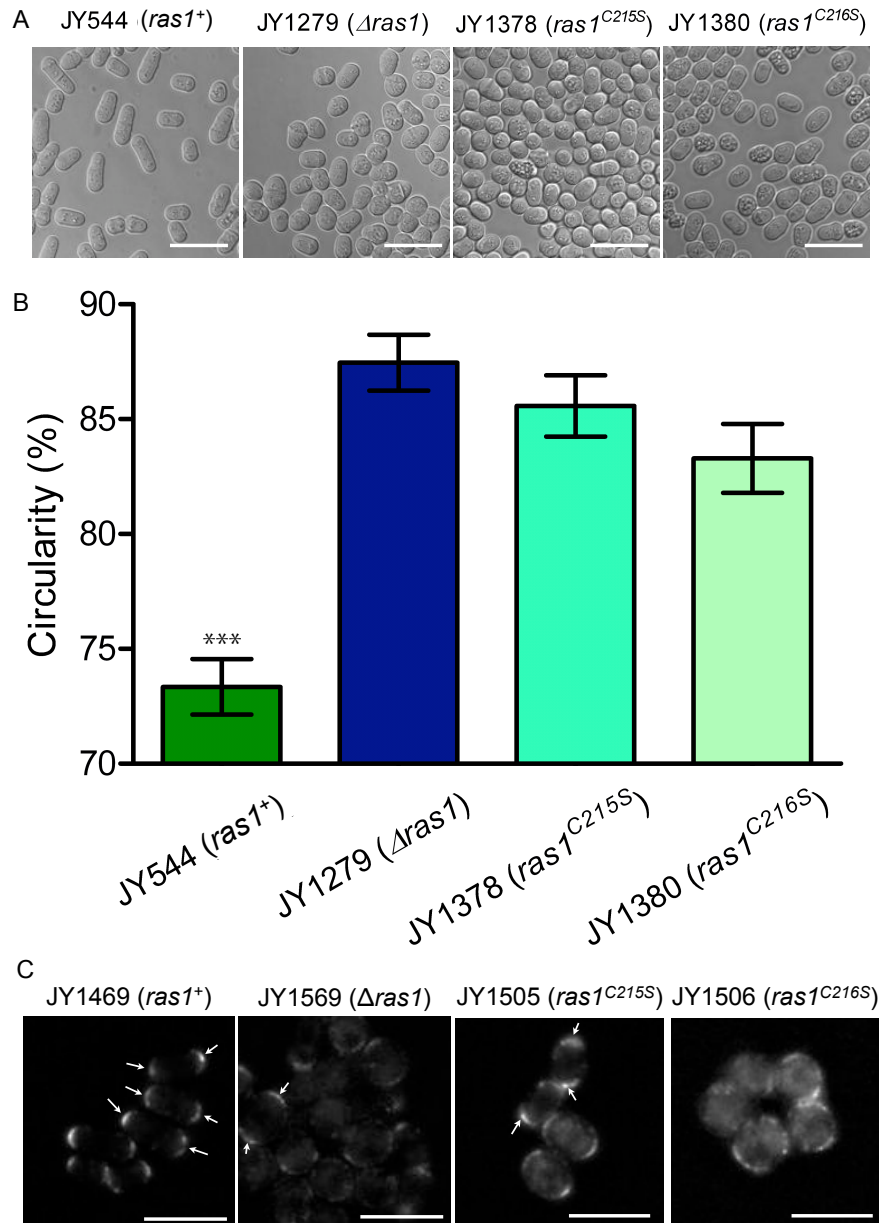


**Figure 5.10. Analysis of the morphology of cells expressing *Ras1*<sup>C215S</sup> and *Ras1*<sup>C216S</sup>**

Images of *ras1*<sup>+</sup> (JY544),  $\Delta$ *ras1* (JY1279), *ras1*<sup>C215S</sup> (JY1378) and *ras1*<sup>C216S</sup> (JY1380) cells, expressing GFP from pREP3x, were obtained using a Leica SP5 scanning confocal microscope. Representative DIC images are displayed in panel A. Cell circularity was determined using Quimp software (B). *ras1*<sup>C215S</sup> (JY1378) and *ras1*<sup>C216S</sup> (JY1380) cells both displayed rounded morphologies consistent with cells lacking Ras1. The localisation of Tea1-mCherry was determined in *ras1*<sup>+</sup> (JY1469),  $\Delta$ *ras1* (JY1569), *ras1*<sup>C215S</sup> (JY1505) and *ras1*<sup>C216S</sup> (JY1506) cells using a Nikon E800 epifluorescence microscope fitted with an Andor EM-CCD camera (C). *ras1*<sup>C215S</sup> (JY1505) and *ras1*<sup>C216S</sup> (JY1506) cells displayed little polar Tea1 localisation. The scale bar represents 10  $\mu$ m. Data representative of 30 individual cells  $\pm$  SEM. Three asterisks indicates a P value of 0.001.

endomembrane Ras1 localisation. To test this hypothesis, cell polarity was analysed in cells expressing Ras1<sup>C215S</sup> and Ras1<sup>C216S</sup> through analysis of Tea1 localisation and percentage circularity.

The localisation of Tea1-mCherry was determined in cells expressing the mutants Ras1<sup>C215S</sup> and Ras1<sup>C216S</sup> from the *ras1* locus using a Nikon E800 epifluorescence microscope fitted with an Andor EM-CCD camera. Some polar Tea1-mCherry localisation was observed in cells expressing Ras1<sup>C215S</sup>, however Tea1-mCherry was not as exclusively localised to the cell tips as in wild-type cells, displaying localisation to other regions of the plasma membrane (Figure 5.10C). Cells expressing Ras1<sup>C216S</sup> exhibited little polar Tea1-mCherry localisation, displaying localisation to the extent of the cell cortex in a pattern consistent with that observed in cells lacking Ras1.

Images of cells expressing Ras1<sup>C215S</sup> and Ras1<sup>C216S</sup> from the *ras1* locus, and expressing GFP from pREP3x, were obtained using a Leica SP5 scanning confocal microscope. Quimp software was then used to determine the circularity of 30 individual cells of each strain. The reduced tip-specific localisation of Tea1-mCherry in cells expressing Ras1<sup>C215S</sup> was reflected in a high percentage circularity in the strain JY1378 (*ras1*<sup>C215S</sup>) ( $85.6 \pm 1.3$  %) (Figure 5.10A and B). This observation contradicts previous reports, suggesting that palmitoylation of Ras1 is not required to maintain polar cell morphology. Ras1<sup>C216S</sup>, which displays little membrane association, did not support polar Tea1-mCherry localisation or elongated morphology, with these cells displaying a percentage circularity of  $83.3 \pm 1.5$  %.

### 5.3.5. Cell polarity is not restored by the addition of cAMP in cells expressing Ras1<sup>C215S</sup> and Ras1<sup>C216S</sup>.

The strains JY544 and JY1469, and all subsequent strains generated from either strain, contain a chromosomal deletion of *cyr1*<sup>-</sup>. Cyr1 is known to affect morphology, causing cells to become shorter and appear less polar (Jin

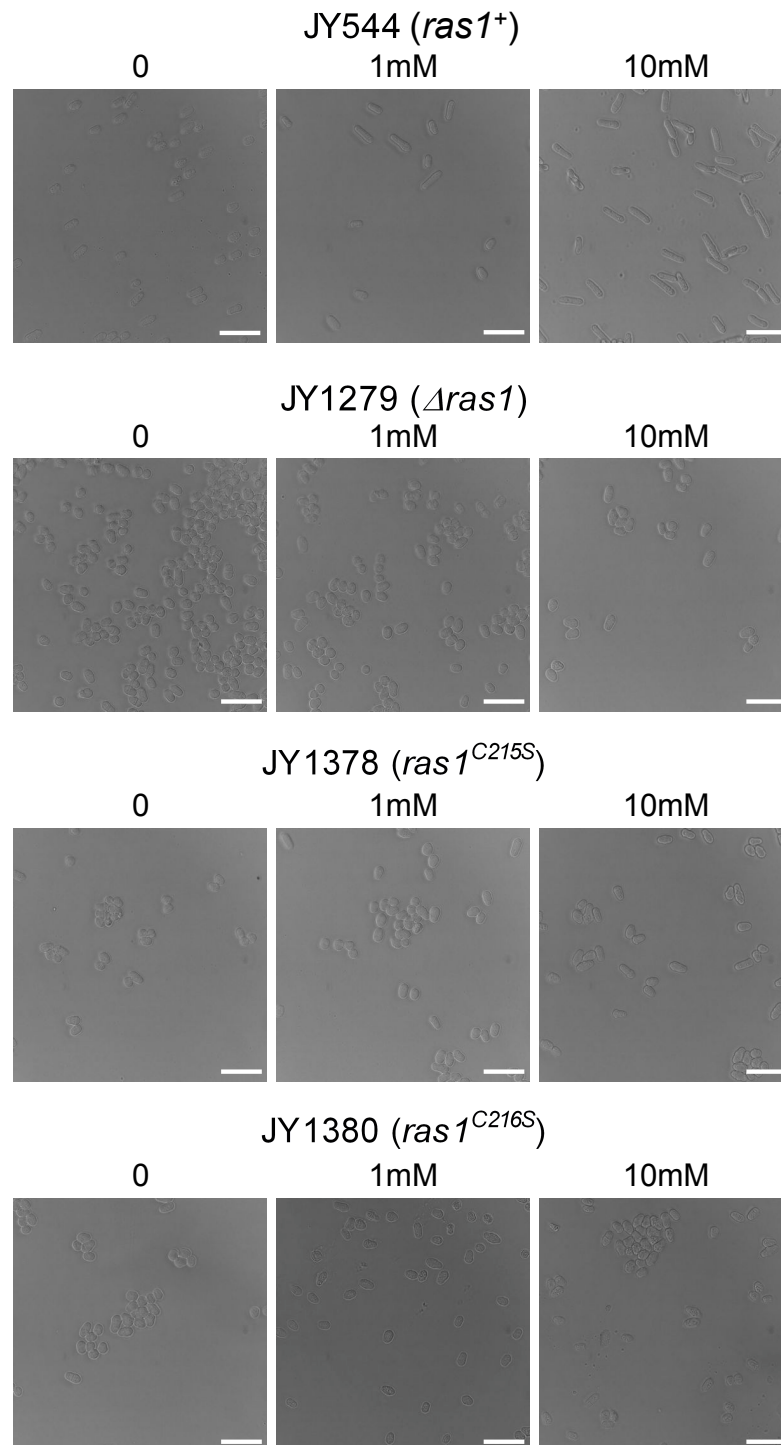


**Figure 5.11. Polar cell morphology in *ras1*<sup>C215S</sup> (JY1378) and *ras1*<sup>C216S</sup> (JY1380) cells is not rescued by exogenous cAMP**  
*ras1*<sup>+</sup> (JY544),  $\Delta$ *ras1* (JY1279), *ras1*<sup>C215S</sup> (JY1378) and *ras1*<sup>C216S</sup> (JY1380) cells were grown in the presence of up to 10 mM cAMP in DMM for 24 h. DIC images were then obtained using a Leica SP5 scanning confocal microscope. JY544 displayed a dose-dependent increase in cell length, whereas none was seen in JY1279, JY1378 or JY1380. The scale bar represents 10  $\mu$ m.

*et al.* 1995). Therefore, the strain background used in this study could be a criticism of the results described in Figure 5.10. Loss of *Cyr1*, however, can be recovered through the addition of exogenous cAMP (Demirbas *et al.* 2011). The strains JY544 (*ras1*<sup>+</sup>), JY1279 (*ras1*<sup>-</sup>), JY1378 (*ras1*<sup>C215S</sup>) and JY1380 (*ras1*<sup>C216S</sup>) were grown in DMM containing a range of cAMP concentration (0, 1mM and 10mM), and were imaged after 24 h growth using a Leica SP5 scanning confocal microscope (Figure 5.11). JY544 displayed a marked increase in cell length upon the addition of cAMP. JY1378 (*ras1*<sup>C215S</sup>) and JY1380 (*ras1*<sup>C216S</sup>) displayed a slight increase in cell length, with cells appearing slightly more elongated. However, a similar effect was also observed in cells lacking Ras1. This observation confirms the finding detailed in Figure 5.10 that neither Ras1<sup>C215S</sup> or Ras1<sup>C216S</sup> are able to rescue cell polarity.

### 5.3.6. The lipid modification of Ras1 is required for pheromone-responsive signalling.

5.3.6.1. *Analysis of pheromone-responsive changes in  $\beta$ -galactosidase activity and average cell volume in cells expressing Ras1<sup>C215S</sup> and Ras1<sup>C216S</sup>.* Ras1 is known to interact with Byr2 at the plasma membrane (Bauman *et al.* 1998). As a consequence, it would be expected that Ras1 C-terminal modification is key to pheromone-dependent signalling. To determine the requirement for Ras1 C-terminal modification in pheromone-responsive processes, the signalling activity of cells expressing Ras1<sup>C215S</sup> and Ras1<sup>C216S</sup> was analysed through the investigation of  $\beta$ -galactosidase activity and average cell volume. Analysis was performed following growth in a range of pheromone concentrations (1 nM to 100  $\mu$ M) in DMM for 16 h.

Cells expressing Ras1<sup>C215S</sup> exhibited reduced maximal signalling compared to wild-type cells (JY544) in  $\beta$ -galactosidase assays ( $3.7 \pm 0.2$  compared to  $20.0 \pm 0.6$ ) (Figure 5.12A), indicating that reducing the level of Ras1 at the plasma membrane reduces the magnitude of signalling. Cells expressing Ras1<sup>C215S</sup>

gave a lower pEC<sub>50</sub> to pheromone ( $6.4 \pm 0.1$ ) than cells expressing Ras1 ( $7.2 \pm 0.1$ ), potentially due to the lower level of maximal signalling observed in these cells. Ras1<sup>C216S</sup> gave little signalling. Neither mutant supported a pheromone-dependent increase in cell volume (Figure 5.12B). These observations suggest that Ras1 plasma membrane localisation is key to pheromone-dependent signalling. Both also exhibited higher basal cell volumes (*ras1*<sup>C215S</sup> cells =  $77.0 \pm 2.0$  fl, *ras1*<sup>C216S</sup> cells =  $78.3 \pm 2.3$  fl), similar to that observed for cells lacking Ras1 ( $81.8 \pm 2.2$  fl), and indicative of the rounded morphology of these cells.

5.3.6.2. *Analysis of pheromone-responsive cell elongation in cells expressing Ras1<sup>C215S</sup> and Ras1<sup>C216S</sup>.* Neither Ras1 mutant displayed a pheromone-dependent increase in cell volume. However, the measurement of cell volume is complicated by changes in cell width (section 4.3.2), which is also influenced by Ras1 signalling (Kelly and Nurse 2011). In order to more accurately measure shmoo formation, cell elongation in response to pheromone was also analysed using quantitative imaging. Images of cells expressing Ras1<sup>C215S</sup> and Ras1<sup>C216S</sup> from the *ras1* locus, with concurrent expression of GFP from pREP3x, were obtained using a Leica SP5 scanning confocal microscope. Analysis was performed following growth in the presence (10  $\mu$ M P-factor) and absence of pheromone in DMM lacking thiamine for 16 h. Quimp software was then used to determine the length of 30 individual cells of each strain under each assay condition.

Cells expressing Ras1<sup>C216S</sup> did not increase in cell length in response to pheromone, although a small increase in cell length was observed in cell expressing Ras1<sup>C215S</sup> of 5.18 pixels on average (Figure 5.13). Cell expressing Ras1<sup>C215S</sup> and Ras1<sup>C216S</sup> both exhibited a reduced basal cell length, similar to that observed in cells lacking Ras1 (*ras1*<sup>C215S</sup> =  $35.7 \pm 1.8$ , *ras1*<sup>C216S</sup> =  $40.8 \pm 1.7$  and  $\Delta$ *ras1* =  $37.5 \pm 1.1$ ). These values are indicative of a shorter, and potentially more rounded morphology. Images of the strains JY1378 (*ras1*<sup>C215S</sup>) and JY1380 (*ras1*<sup>C216S</sup>) indicate no clear shmoo formation.

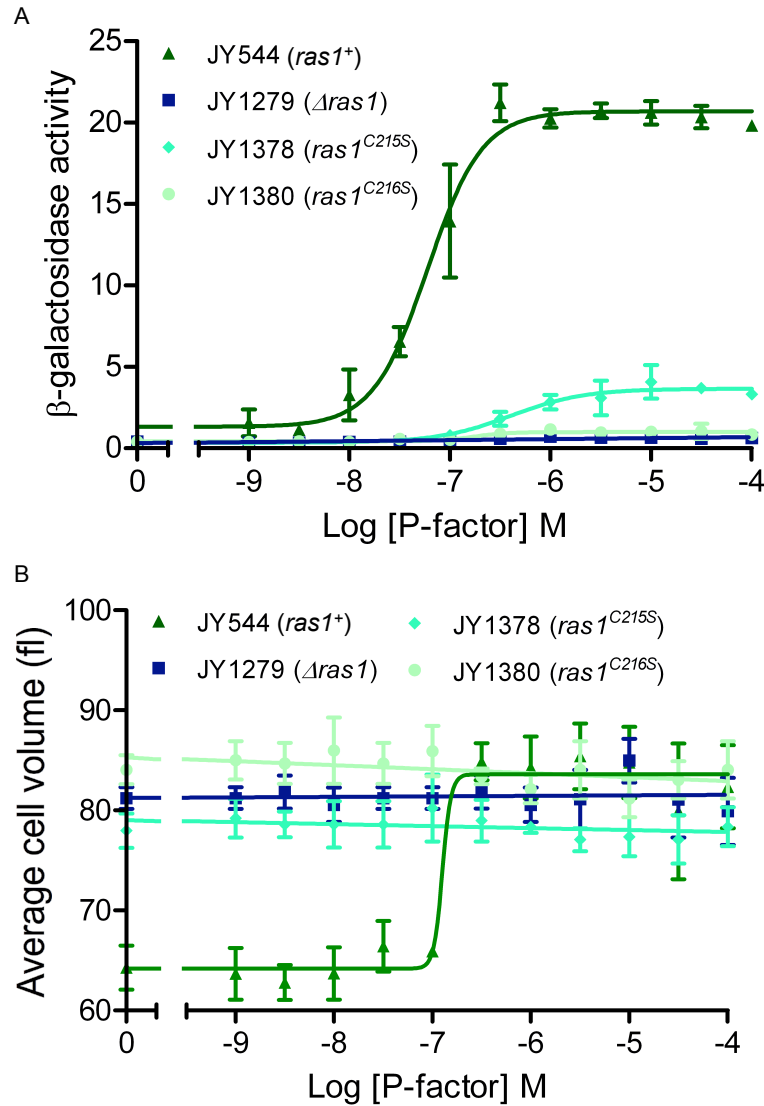


**Figure 5.12. Pheromone-dependent changes in transcription and cell volume in cells expressing Ras1<sup>C215S</sup> and Ras1<sup>C216S</sup>**

Pheromone-responsive changes in transcription and cell volume were observed in *ras1*<sup>+</sup> (JY544),  $\Delta$ *ras1* (JY1279), *ras1*<sup>C215S</sup> (JY1378) and *ras1*<sup>C216S</sup> (JY1380) cells. Cells were grown in 1 nM to 100  $\mu$ M pheromone in DMM for 16 hs. Assays were then performed for  $\beta$ -galactosidase activity (A) and average cell volume (B). JY1378 displayed pheromone-dependent  $\beta$ -galactosidase activity, but to a lesser extent than JY544. Ras1<sup>C215S</sup> and Ras1<sup>C216S</sup> did not support pheromone-responsive changes in cell volume. Data shown is an average of three independent determinants ( $\pm$ SEM).

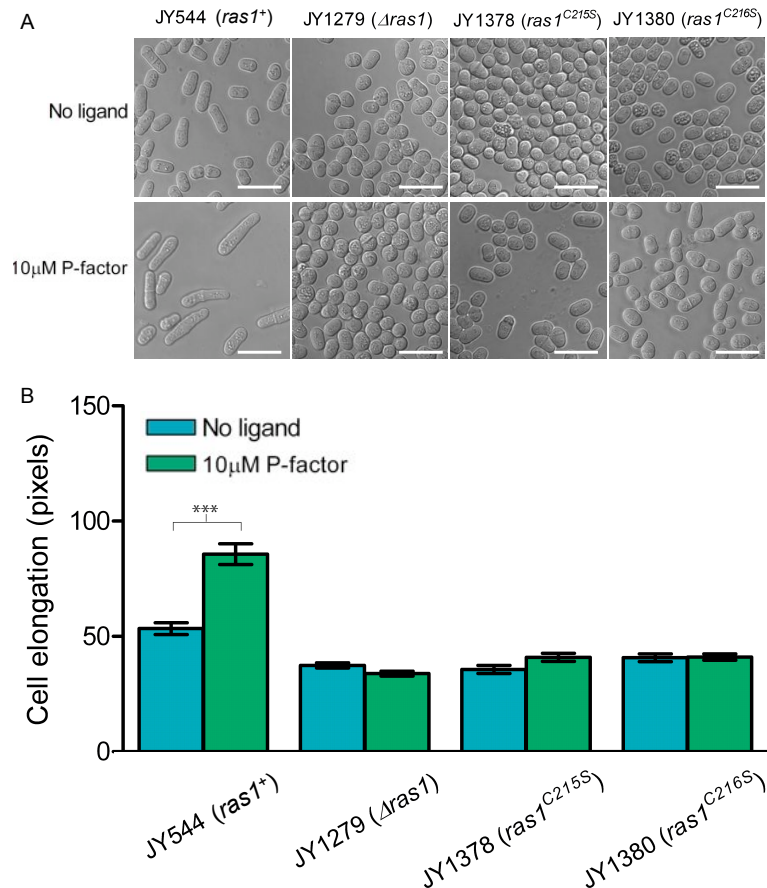


**Figure 5.13. Phormone-dependent cell elongation in cells expressing *Ras1*<sup>C215S</sup> and *Ras1*<sup>C216S</sup>**

Images of cells containing wild-type *Ras1* (JY544), *Ras1*<sup>C215S</sup> (JY1378), *Ras1*<sup>C216S</sup> (JY1380) and cells lacking *Ras1* (JY1279) were obtained following growth in the absence and in the presence of 10  $\mu$ M phormone in DMM lacking thiamine for 16 h, using a Leica SP5 scanning confocal microscope. Representative DIC images are displayed in panel A. Cell length was then determined for 30 cells using Quimp software. Cells expressing *Ras1*<sup>C215S</sup> and *Ras1*<sup>C216S</sup> displayed no significant increase in cell length in response to phormone (B). Data shown is representative of 30 individual cells  $\pm$  SEM. Statistical significance was determined using a one-way anova with a Tukey multiple comparison post test. Three asterisks indicates a P-value of 0.001. Images from the populations analysed demonstrate no change in morphology in response to phormone. The scale bar represents 10  $\mu$ m.

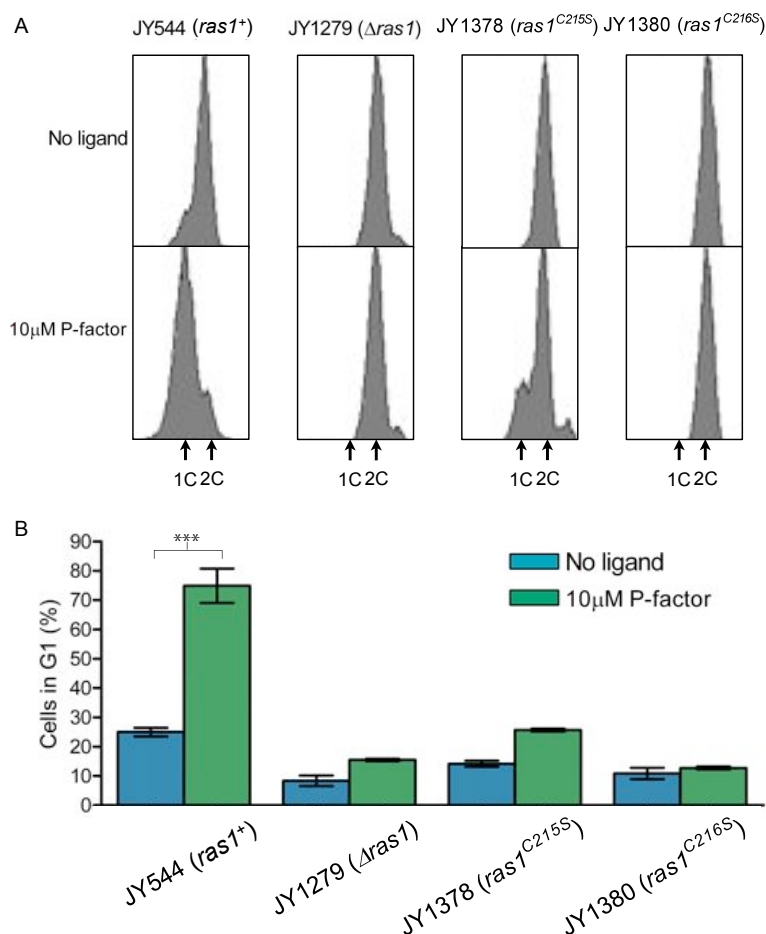


**Figure 5.14. Phormone-responsive changes in cell cycle position in cells expressing *Ras1*<sup>C215S</sup> and *Ras1*<sup>C216S</sup>**

Cell cycle arrest was analysed in *ras1*<sup>+</sup> (JY544),  $\Delta$ *ras1* (JY1279), *ras1*<sup>C215S</sup> (JY1378) and *ras1*<sup>C216S</sup> (JY1380) cells using propidium iodide staining and flow cytometry, after growth in the presence (10 µM P-factor) and absence of phormone in DMM for 6 h. This analysis allowed the distinction between cells containing a single complement (1C) and double complement (2C) of DNA (A). Cells expressing *Ras1*<sup>C215S</sup> (JY1380) displayed some phormone-dependent G<sub>1</sub> arrest (B). Data shown representative of three independent determinants  $\pm$  SEM. Analysis was performed for 30000 cells. Statistical significance was determined using a one-way anova with a Tukey multiple comparison post test. Three asterisks indicates a P-value of 0.001.

5.3.6.3. *Analysis of phormone-dependent cell cycle arrest in cells expressing *Ras1*<sup>C215S</sup> and *Ras1*<sup>C216S</sup>.* Cells expressing *Ras1*<sup>C215S</sup> and *Ras1*<sup>C216S</sup> both display limited phormone-dependent signalling. To investigate their ability to induce a phormone-dependent cell cycle arrest, cell cycle position was determined following growth in the presence (10 µM P-factor) and absence of

pheromone in DMM for 6 h. Cell cycle position was analysed using propidium iodide staining and flow cytometry. Analysis indicated little pheromone-responsive G<sub>1</sub> arrest in cells expressing Ras1<sup>C216S</sup>. Cells expressing Ras1<sup>C215S</sup> showed an increase in cells in G<sub>1</sub> following pheromone stimulation ( $14.2 \pm 1.0\%$  to  $25.7 \pm 0.5\%$ ), however the increase was not statistically significant (Figure 5.14). Despite this, an increase in cells containing a single complement of DNA (1C) was visible upon pheromone stimulation (Figure 5.14A).

Due to the low levels of pheromone responsive-signalling observed in cells containing Ras1<sup>C215S</sup> and the lack of signalling displayed by cells expressing Ras1<sup>C216S</sup>, it would be expected that neither mutant would support mating. The mating of strains expressing Ras1<sup>C215S</sup> or Ras1<sup>C216S</sup> from the *ras1* locus was determined using the quantitative assay for spore formation detailed in section 4.2.1. Neither mutant was able to support any mating when expressed from the *ras1* locus, in conjunction with expression of Sxa2 from pREP41x (0% in all assays).

### 5.3.7. GFP-Ras1<sup>C215S</sup> and GFP-Ras1<sup>C216S</sup> display a similar signalling profile to their non-tagged counterparts.

Analysis of the signalling of GFP-tagged mutants has previously proved informative of their function, allowing the characterisation of signalling through GTPase deficient mutants at high pheromone concentrations (Figure 4.47). However, Ras1<sup>C215S</sup> and Ras1<sup>C216S</sup> were unable to support polar cell morphology when expressed from the *ras1* locus. As the addition of GFP to Ras1 predominantly reduces signalling activity, it would be expected that cells containing GFP-Ras1<sup>C215S</sup> and GFP-Ras1<sup>C216S</sup> would also not display polar cell morphology. To determine whether GFP-Ras1<sup>C215S</sup> and GFP-Ras1<sup>C216S</sup> could support cell polarity, images of cells expressing Ras1<sup>C215S</sup> and Ras1<sup>C216S</sup> from the *ras1* locus, and expressing GFP from pREP3x, were obtained using a Leica SP5 scanning confocal microscope. Quimp software was then used to

determine the circularity of 30 cells within each population. Strains expressing both GFP-tagged mutants displayed a rounded morphology, consistent with a lack of signalling through Scd1-Cdc42 (Figure 5.15). Cells expressing GFP-Ras1<sup>C215S</sup> exhibited a percentage circularity of  $94.3 \pm 0.4$  % and cells expressing GFP-Ras1<sup>C216S</sup> exhibited a percentage circularity of  $90.3 \pm 0.7$  %. The  $\Delta ras1$  strain JY1279 displayed a similar percentage circularity of  $87.5 \pm 1.2$  %.

Despite the lack of polar cell morphology observed in cells expressing GFP-Ras1<sup>C215S</sup> and GFP-Ras1<sup>C216S</sup>, Ras1<sup>C215S</sup> have previously been shown to exhibit some pheromone-dependent signalling (Figure 5.12 and 5.14). As such, GFP-Ras1<sup>C215S</sup> may also retain some function, allowing cells to respond to pheromone stimulation. Analysis of pheromone-dependent signalling, through the investigation of  $\beta$ -galactosidase activity and average cell volume, indicated a similar pattern of signalling in cells expressing GFP-Ras1<sup>C215S</sup> and GFP-Ras1<sup>C216S</sup> as that observed in cells containing their non-tagged counterparts.  $\beta$ -galactosidase activity and average cell volume were analysed following growth in a range of pheromone concentrations (1 nM to 100  $\mu$ M) in DMM for 16 h.

Cells expressing GFP-Ras1<sup>C215S</sup> displayed reduced maximal signalling in  $\beta$ -galactosidase assays compared to both Ras1 and GFP-Ras1 ( $2.4 \pm 0.3$  compared to  $20.7 \pm 0.7$  and  $5.4 \pm 0.3$  respectively) (Figure 5.16A). Cells containing GFP-Ras1<sup>C216S</sup> displayed no pheromone-dependent  $\beta$ -galactosidase activity. Neither supported an increase in cell volume in response to pheromone (Figure 5.16B). Cells expressing GFP-Ras1<sup>C215S</sup> and GFP-Ras1<sup>C216S</sup> also exhibited a high basal cell volume ( $83.3 \pm 2.4$  fl and  $87.7 \pm 1.3$  fl respectively), similar to that observed in cells lacking Ras1 ( $88.74 \pm 1.6$  fl).

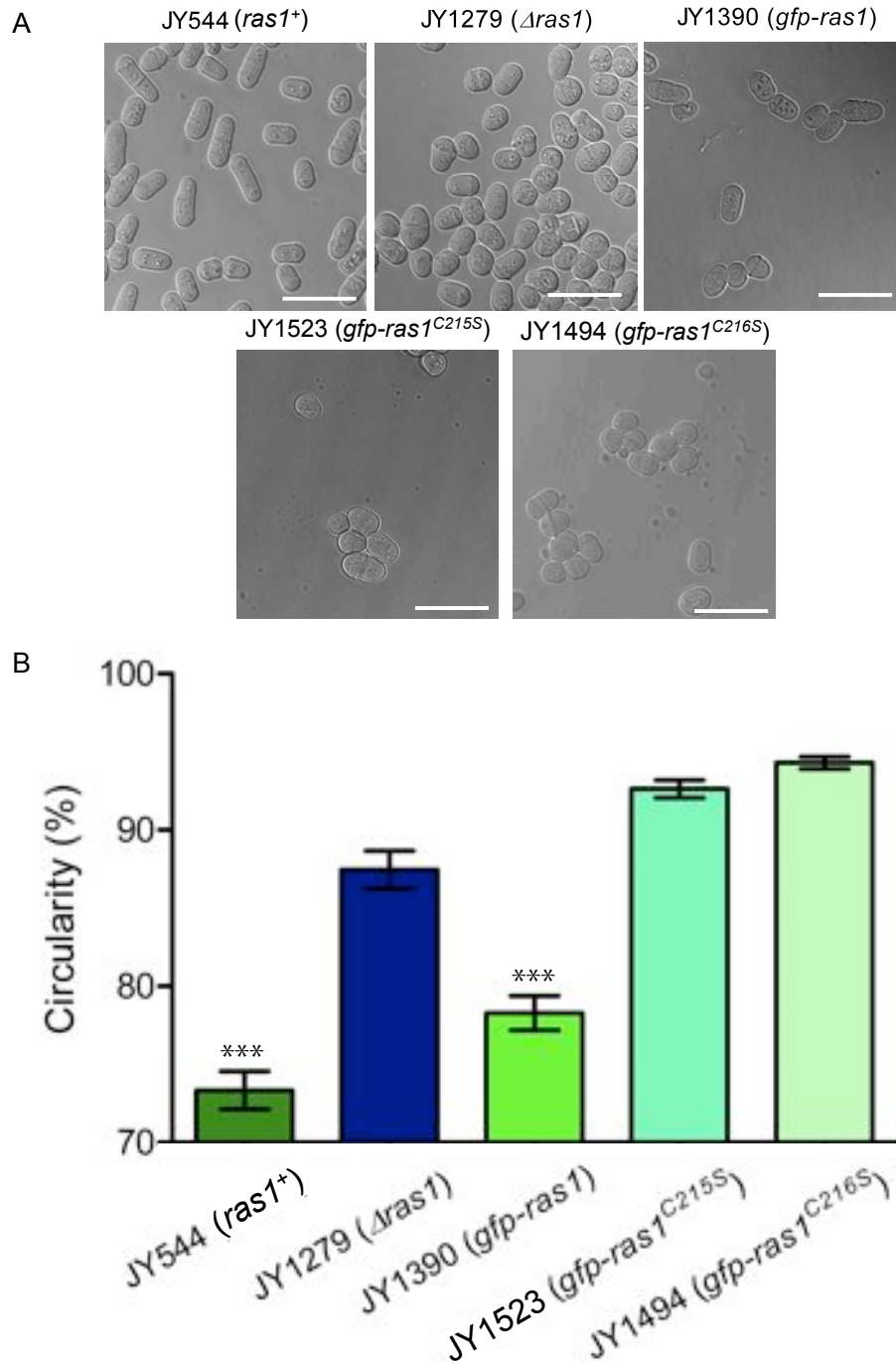


**Figure 5.15. Analysis of the morphology of cells expressing GFP-Ras1<sup>C215S</sup> and GFP-Ras1<sup>C216S</sup>**

Images of *ras1*<sup>+</sup> (JY544),  $\Delta$ *ras1* (JY1279), *gfp-ras1*<sup>C215S</sup> (JY1494) and *gfp-ras1*<sup>C216S</sup> (JY1522) cells, expressing GFP from pREP3x were obtained using a Leica SP5 scanning confocal microscope. Representative DIC images are displayed in panel A. Cell circularity was determined using Quimp software (B). *gfp-ras1*<sup>C215S</sup> (JY1494) and *gfp-ras1*<sup>C216S</sup> (JY1522) cells both displayed rounded morphologies consistent with cells lacking Ras1. Data representative of 30 individual cells  $\pm$  SEM. The scale bar represents 10  $\mu$ m. Statistical significance was determined using a one-way anova with a Tukey multiple comparison post test. Three asterisks indicates a P-value of 0.001.

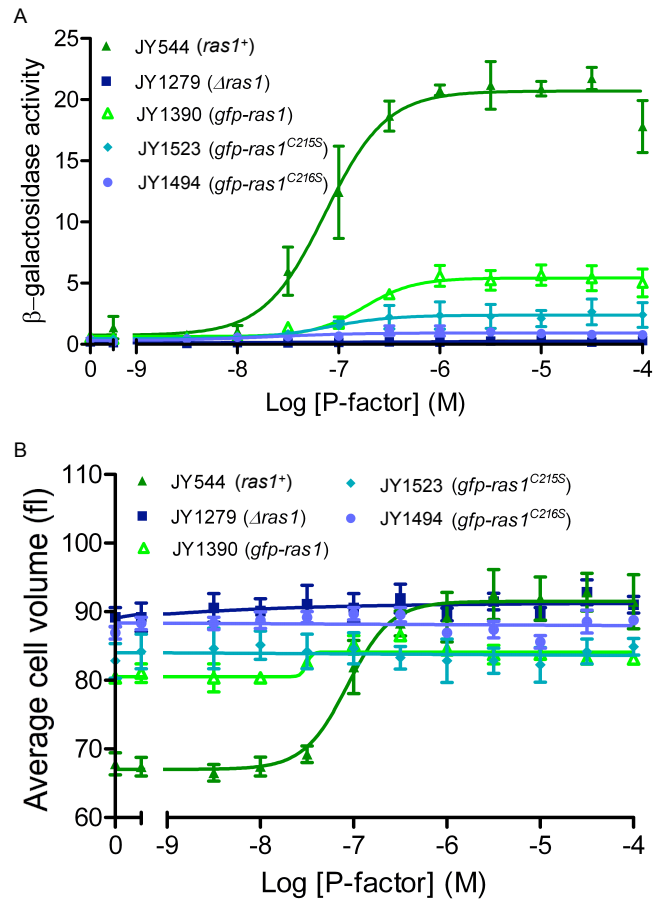


**Figure 5.16. Phormone-dependent changes in transcription on cell volume in cells expressing GFP-Ras1<sup>C215S</sup> and GFP-Ras1<sup>C216S</sup>**

Phormone-responsive changes in transcription and cell volume were observed in *ras1*<sup>+</sup> (JY544),  $\Delta$ *ras1* (JY1279), *gfp-ras1* (JY1390), *gfp-ras1*<sup>C215S</sup> (JY1494) and *gfp-ras1*<sup>C216S</sup> (JY1522) cells. Cells were grown in 1 nM to 100  $\mu$ M pheromone in DMM for 16 h. Assays were then performed for  $\beta$ -galactosidase activity (A) and average cell volume (B). JY1494 (*gfp-ras1*<sup>C215S</sup>) displayed reduced phormone-dependent  $\beta$ -galactosidase activity compared to JY544 (*ras1*<sup>+</sup>) and JY1390 (*gfp-ras1*). JY1522 (*gfp-ras1*<sup>C216S</sup>) displayed no  $\beta$ -galactosidase activity. Cells expressing both GFP fused Ras1 mutants did not display phormone-responsive changes in cell volume. Data shown is an average of three independent determinants ( $\pm$ SEM).

### 5.3.8. Ras1<sup>C215S</sup> and Ras1<sup>C216S</sup> display strong phormone dependent signalling when expressed from pREP3x.

The results observed for Ras1<sup>C215S</sup> and Ras1<sup>C216S</sup> to this point indicate that preventing the localisation of Ras1 to the plasma membrane causes it to become limiting in both the phormone response and the regulation of cell morphology. Based upon this observation, the constitutive expression of Ras1<sup>C215S</sup> and Ras1<sup>C216S</sup> mutants should increase their signalling output, as increasing their

concentration throughout the cell should increase their local concentration at the plasma membrane.

To test this hypothesis, Ras1<sup>C215S</sup> and Ras1<sup>C216S</sup> were expressed from the pREP3x vector in the  $\Delta ras1$  strain JY1279, and signalling in response to pheromone was determined through analysis of  $\beta$ -galactosidase activity and average cell volume.  $\beta$ -galactosidase activity and average cell volume were analysed following growth in a range of pheromone concentrations (1 nM to 100  $\mu$ M) in DMM lacking thiamine for 16 h.

Both Ras1<sup>C215S</sup> and Ras1<sup>C216S</sup> supported high levels of  $\beta$ -galactosidase activity in response to pheromone (Figure 5.17A). Cells expressing Ras1<sup>C215S</sup> from pREP3x gave a maximal response of  $24.9 \pm 1.0$  and Ras1<sup>C216S</sup> a maximal response of  $18.0 \pm 0.5$ , compared to  $12.2 \pm 0.4$  in those expressing wild-type Ras1. This increased activity relative to cells expressing Ras1 from pREP3x could be due to the reduced cell viability observed in cells containing pREP3x-Ras1 (Figure 4.42). As Ras1<sup>C215S</sup> and Ras1<sup>C216S</sup> are less active, their unregulated expression from pREP3x may be less harmful to the cell. Cells containing pREP3x-Ras1<sup>C216S</sup> displayed a reduced pEC<sub>50</sub> to pheromone ( $6.7 \pm 0.1$ ) than those containing pREP3x-Ras1<sup>C215S</sup> and pREP3x-Ras1 ( $7.1 \pm 0.1$  and  $7.4 \pm 0.2$ ) despite displaying a high maximal response to pheromone, possibly due to the lack of a membrane tether holding Ras1 in proximity to upstream activators.

The expression of Ras1<sup>C215S</sup> from pREP3x in cells lacking Ras1 elicited a large pheromone-dependent increase in cell volume, increasing from  $82.6 \pm 1.3$  fl to  $112.6 \pm 1.1$  fl (Figure 5.17B). Cells containing pREP3x-Ras1<sup>C216S</sup> displayed a less pronounced increase in cell volume, increasing from  $76.4 \pm 0.8$  fl to  $81.9 \pm 0.1$ . By contrast, cells expressing wild-type Ras1 from pREP3x exhibited only a slight increase in cell volume ( $83.0 \pm 1.9$  fl to  $85.8 \pm 0.7$ ). These data further highlight the significant pheromone-dependent signalling supported by Ras1<sup>C215S</sup> and Ras1<sup>C216S</sup> when expressed from pREP3x.

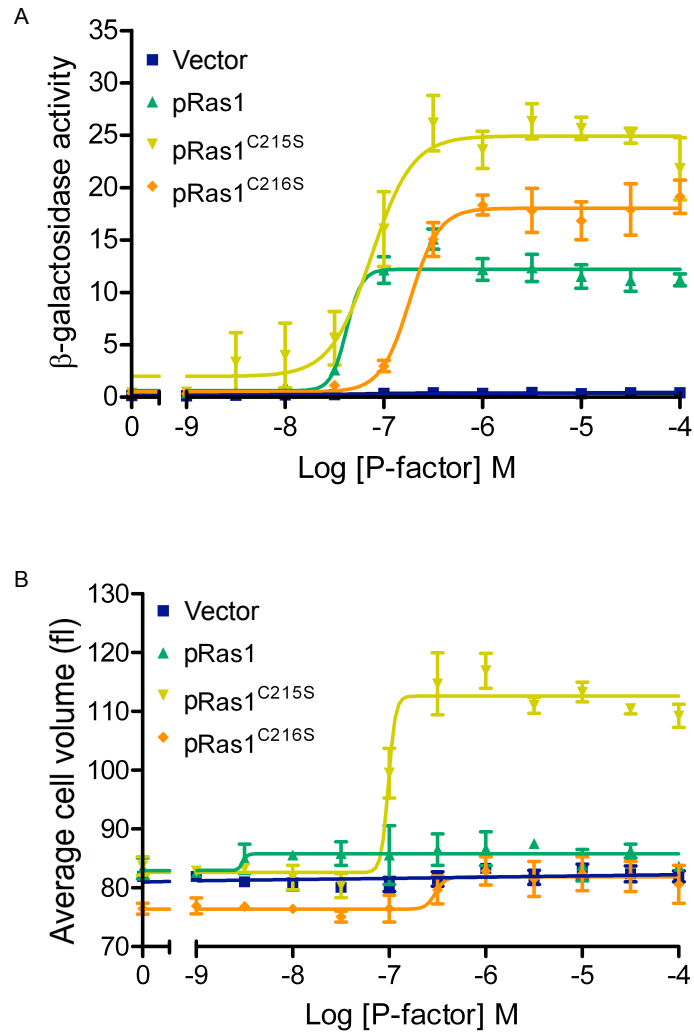


**Figure 5.17. Phormone-dependent changes in transcription on cell volume in cells expressing Ras1<sup>C215S</sup> and Ras1<sup>C216S</sup> from pREP3x**

Phormone-responsive changes in transcription and cell volume were observed in  $\Delta ras1$  (JY1279) cells transformed with pREP3x-Ras1<sup>C215S</sup>, pREP3x-Ras1<sup>C216S</sup>, pREP3x-Ras1 and vector alone. Cells were grown in 1 nM to 100  $\mu$ M phormone in DMM lacking thiamine for 16 h. Assays were then performed for  $\beta$ -galactosidase activity (A) and average cell volume (B). Cells expressing both Ras1 mutants from pREP3x exhibited phormone-dependent  $\beta$ -galactosidase activity and increases in average cell volume. Data shown is an average of three independent determinants ( $\pm$ SEM).

## 5.4. Prolonging the activity of Ras1<sup>C215S</sup> rescues signalling

### 5.4.1. Expression of Ras1<sup>Q66L, C215S</sup>.

The results discussed in section 5.3 suggest that reducing the concentration of Ras1 at the plasma membrane results in Ras1 becoming limiting in both pheromone-responsive signalling and the regulation of cell morphology. One way of corroborating this observation is to determine whether allowing Ras1<sup>C215S</sup> to activate more downstream effectors would increase functional output. This was investigated through increasing the period of activation of the Ras1<sup>C215S</sup> mutant, with the addition of the Gln66Leu GTPase deficiency mutation.

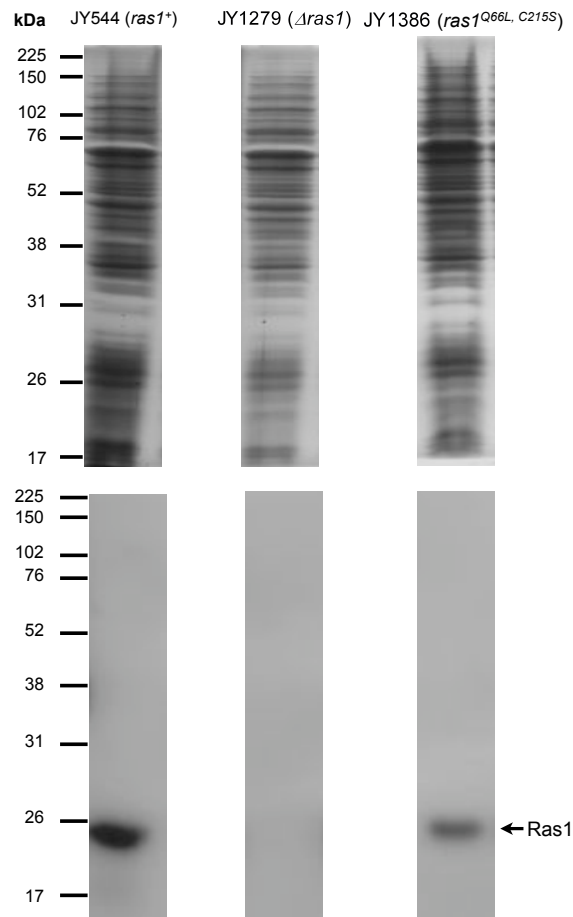


**Figure 5.18. Expression of Ras1<sup>Q66L, C215S</sup> in the  $\beta$ -galactosidase reporter strain**

Integration of Ras1<sup>Q66L, C215S</sup> into the *ras1::ura4<sup>+</sup>, sxa2>lacZ* reporter strain JY1247 was confirmed via immunoblotting using an anti-ras RAS10 antibody. Coomassie stains of whole protein are included above the immunoblot as loading controls.

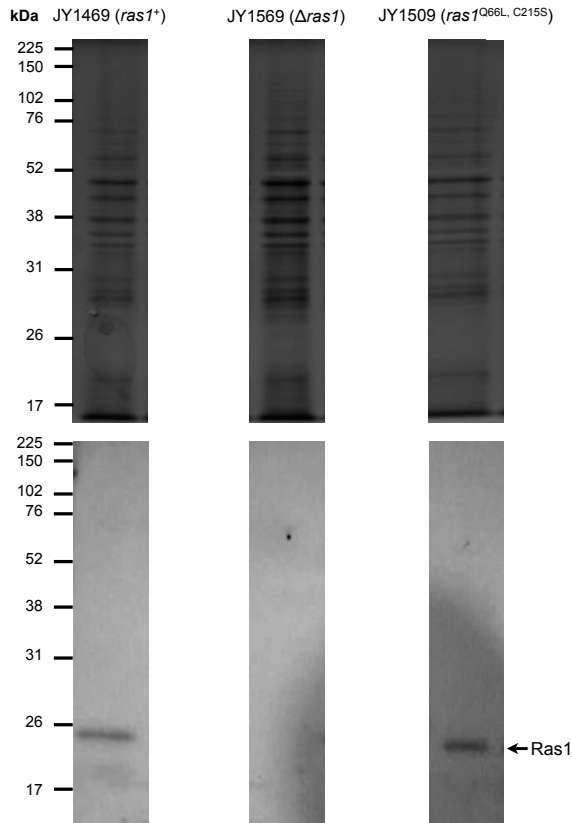


**Figure 5.19. Expression of Ras1<sup>Q66L, C215S</sup> in the Tea1-mCherry strain**

Integration of Ras1<sup>Q66L, C215S</sup> into the *ras1::ura4<sup>+</sup>, tea1-mCherry* strain JY1569 was confirmed via immunoblotting using an anti-ras RAS10 antibody. Coomassie stains of whole protein are included above the immunoblot as loading controls.

Ras1<sup>Q66L, C215S</sup> was integrated at the *ras1* locus in the strains JY1247 ( $\Delta ras1::ura4^+$ , *sxa2>lacZ*) (Figure 5.18) and JY1504 ( $\Delta ras1::ura4^+$ , *tea1-mCherry*) (Figure 5.19) as previously described (Figure 4.28A). Expression was confirmed by immunoblotting using the anti-ras RAS10 antibody. In addition, a direct in-frame N-terminal GFP-Ras1<sup>Q66L, C215S</sup> fusion was created at the *ras1* locus in the *sxa2>lacZ* reporter strain. Expression of GFP-Ras1<sup>Q66L, C215S</sup> from the *ras1* locus was also confirmed by immunoblotting, giving a chemiluminescent signal at a position consistent with the predicted size of the fusion ( $\sim 52$ kDa) and exhibiting no evidence of breakdown (Figure 5.20).

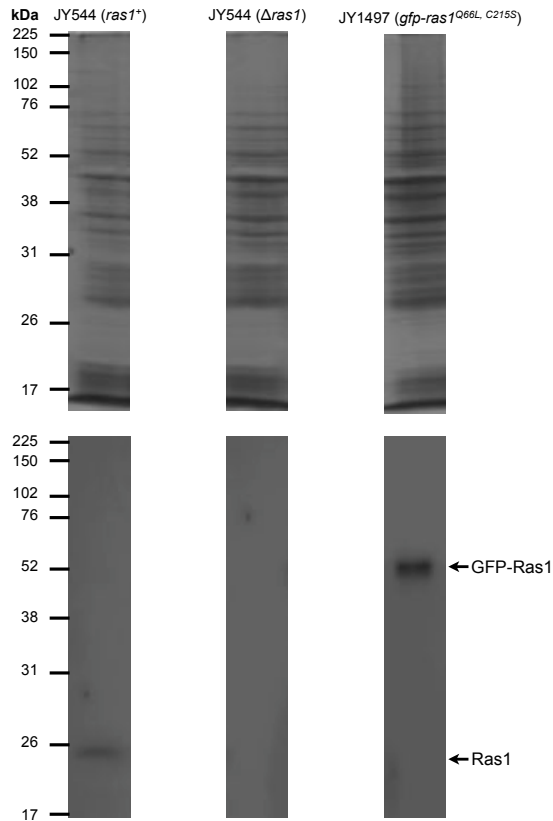


**Figure 5.20. Expression of GFP-Ras1<sup>Q66L, C215S</sup>**

Integration of GFP-Ras1<sup>Q66L, C215S</sup> into the *ras1::ura4<sup>+</sup>, sxa2>lacZ* reporter strain was confirmed via immunoblotting using an anti-ras RAS10 antibody. Coomassie stains of whole protein are included above the immunoblot as loading controls.

#### 5.4.2. The localisation of GFP-Ras1<sup>C215S</sup> is unaltered by the addition of a Gln66Leu mutation.

In order to determine whether increasing the duration of Ras1<sup>C215S</sup> activation rescues signalling, it is important to ensure that the localisation of GFP-Ras1<sup>C215S</sup> is not altered by the addition of a Gln66Leu mutation. If the localisation of GFP-Ras1<sup>C215S</sup> and GFP-Ras1<sup>Q66L, C215S</sup> differ, any change in activity cannot be solely attributed to the increased duration of Ras1<sup>Q66L, C215S</sup> activity. The localisation of GFP-Ras1<sup>Q66L, C215S</sup> was first analysed upon expression from the *ras1* locus using a Nikon E800 epifluorescence microscope fitted with an Andor EM-CCD camera. GFP-Ras1<sup>Q66L, C215S</sup> appeared to localise predominantly to endomembrane structures, largely surrounding the nucleus of the cell, and displayed a localisation pattern consistent with GFP-Ras1<sup>C215S</sup>

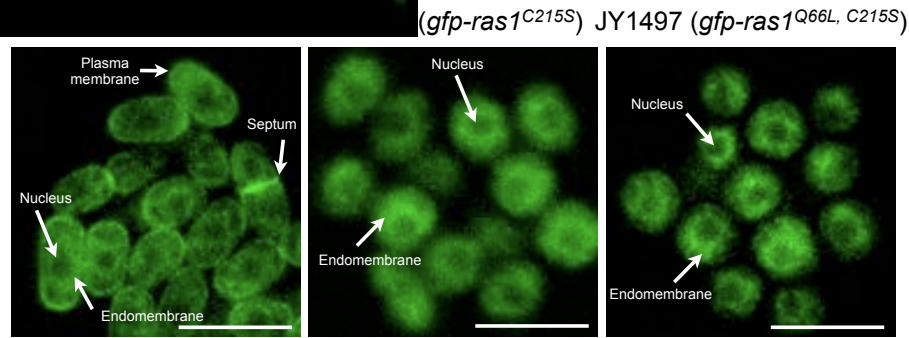


**Figure 5.21. The localisation of GFP-Ras1<sup>Q66L, C215S</sup>**

The localisation of GFP-Ras1, GFP-Ras1<sup>C215S</sup> and GFP-Ras1<sup>Q66L, C215S</sup>, upon expression from the *ras1* locus, was determined using a Nikon E800 epifluorescence microscope fitted with an Andor EM-CCD camera. GFP-Ras1 was observed at the plasma membrane and peri-nuclear endomembrane structures. GFP-Ras1<sup>C215S</sup> and GFP-Ras1<sup>Q66L, C215S</sup> displayed endomembrane localisation. The scale bar represents 10  $\mu\text{m}$ .

(Figure 5.21). These data suggest that the localisation of GFP-Ras1<sup>C215S</sup> is not perturbed by altering the ability of the protein to hydrolyse GTP.

In order to perform a more detailed analysis of GFP-Ras1<sup>Q66L, C215S</sup> localisation, the peripheral fluorescence of GFP-Ras1<sup>Q66L, C215S</sup> was quantified upon expression from pREP3x in the  $\Delta ras1$  strain JY1279. Fluorescence images were obtained using a Leica SP5 scanning confocal microscope (Figure 5.22A), and the percentage fluorescence at the periphery relative to the interior of the cell was calculated using Quimp software (Figure 5.22B). GFP-Ras1<sup>C215S</sup> was previously determined to have a percent plasma membrane localisation of  $16.6 \pm 1.8 \%$ . This appeared unchanged upon the addition of the Gln66Leu mutation in GFP-Ras1<sup>Q66L, C215S</sup> ( $15.3 \pm 1.3 \%$ ). Both displayed a significantly lower level of plasma membrane localisation than GFP-Ras1 ( $78.0 \pm 3.5 \%$ ,  $P = 0.001$ ), exhibiting high levels of endomembrane localisation. This observation suggests that any change in function observed in Ras1<sup>Q66L, C215S</sup> compared to Ras1<sup>C215S</sup> is a consequence of the GTPase deficiency conferred by the Gln66Leu mutation, as opposed to an alteration in localisation.

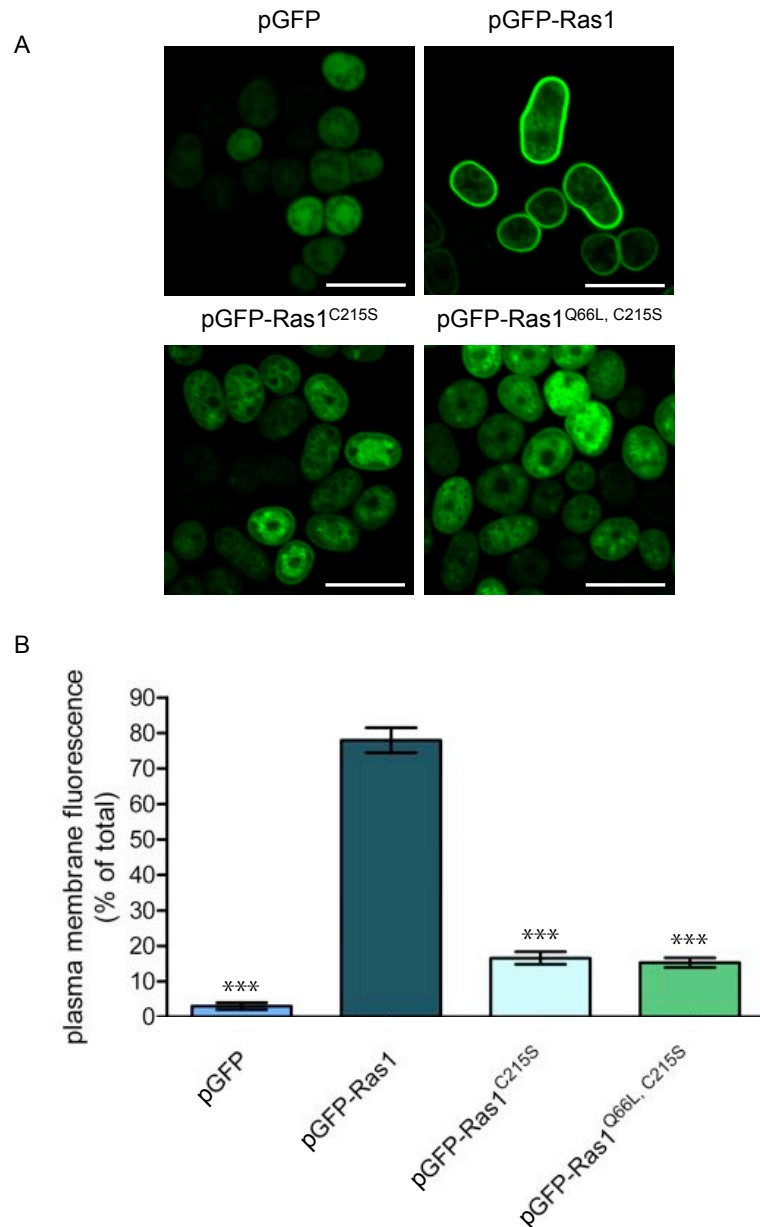


**Figure 5.22. Analysing the localisation of GFP-Ras1<sup>Q66L, C215S</sup> using Quimp software**

Images of  $\Delta ras1$  cells (JY1279) expressing GFP and GFP-Ras1 fusions from pREP3x were obtained using a Leica SP5 scanning confocal microscope (A). The intensity of fluorescence at the periphery compared to the interior of the cell was determined using Quimp software, and percentage plasma membrane fluorescence was calculated (B). GFP-Ras1<sup>Q66L, C215S</sup> displayed a reduced plasma membrane localisation compared to GFP-Ras1, similar to that of GFP-Ras1<sup>C215S</sup>. Statistical significance was determined using a one-way anova with a Tukey multiple comparison post test. Three asterisks indicates a P-value of 0.001. The scale bar represents 10  $\mu\text{m}$ .

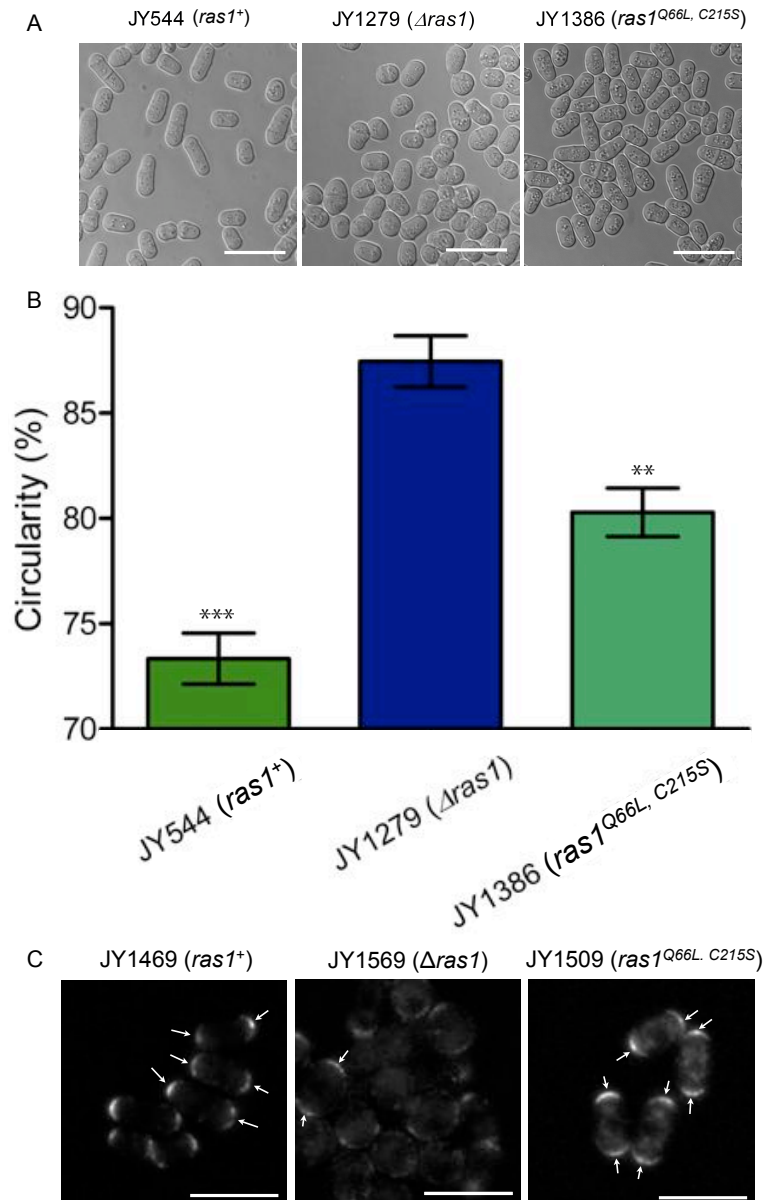


**Figure 5.23. Analysis of the morphology of cells expressing Ras1<sup>Q66L, C215S</sup>**

Images of populations of *ras1*<sup>+</sup> (JY544),  $\Delta$ *ras1* (JY1279) and *ras1*<sup>Q66L, C215S</sup> (JY1386) cells, expressing GFP from pREP3x, were obtained using a Leica SP5 scanning confocal microscope. Representative DIC images are displayed in panel A. Cell circularity was determined using Quimp software (B). *ras1*<sup>Q66L, C215S</sup> (JY1386) cells displayed a reduced percentage circularity compared to cells lacking Ras1. The localisation of Tea1-mCherry was determined in *ras1*<sup>+</sup> (JY1469),  $\Delta$ *ras1* (JY1569) and *ras1*<sup>Q66L, C215S</sup> (JY1509) cells using a Nikon E800 epifluorescence microscope fitted with an Andor EM-CCD camera (C). Cells expressing Ras1<sup>Q66L, C215S</sup> displayed polar Tea1-mCherry localisation. The scale bar represents 10  $\mu$ m. Data representative of 30 individual cells  $\pm$  SEM. Statistical significance was determined using a one-way anova with a Tukey multiple comparison post test. Two asterisks indicates a P value of 0.01 and three asterisks indicates a P-value of 0.001.

### 5.4.3. Prolonging the activity of Ras1<sup>C215S</sup> partially restores elongated cell morphology.

GFP-Ras1<sup>Q66L, C215S</sup> exhibited the same localisation pattern as GFP-Ras1<sup>C215S</sup>. In order to determine whether the increased duration of Ras1<sup>Q66L, C215S</sup> activity rescued the lack of polar morphology previously observed in cells expressing Ras1<sup>C215S</sup> (Figure 5.10), the signalling of Ras1<sup>Q66L, C215S</sup> through Scd1-Cdc42 was determined through the analysis of Tea1 localisation and cell circularity. The localisation of Tea1-mCherry was examined in cells expressing Ras1<sup>Q66L, C215S</sup> from the *ras1* locus, using a Nikon E800 epifluorescence microscope fitted with an Andor EM-CCD camera. Tea1-mCherry in JY1509 (*ras1*<sup>Q66L, C215S</sup>) displayed discrete localisation to the tips of the cells, with little localisation to the surrounding cell cortex. This observation is consistent with significant Ras1 signalling through Scd1-Cdc42 (Figure 5.23C). In addition, the localisation of Tea1-mCherry was not dissimilar to that observed in cells expressing wild-type Ras1. These data provide a clear indication that Ras1<sup>Q66L, C215S</sup> is able to promote polar cell growth.

In order to quantify the morphology of these cells, images of the strain JY1386 (*ras1*<sup>Q66L, C215S</sup>), expressing GFP from pREP3x, were obtained using a Leica SP5 scanning confocal microscope. Quimp software was then used to determine the circularity of 30 cells within the population (Figure 5.23A and B).

JY1386 (*ras1*<sup>Q66L, C215S</sup>) exhibited a significantly lower percentage circularity than cells lacking Ras1 ( $80.3 \pm 1.2\%$  compared to  $87.5 \pm 1.2\%$ ,  $P = 0.01$ ). This represents a significant but partial rescue of wild-type cell morphology, as cell circularity was not reduced to wild-type levels ( $73.4 \pm 1.2\%$ ). This reduced circularity is indicative of signalling through Scd1-Cdc42 and, further to the polar localisation of Tea1-mCherry observed in JY1509 (*ras1*<sup>Q66L, C215S</sup>), demonstrates that prolonging the activity of Ras1<sup>C215S</sup> can rescue polar cell morphology.

#### 5.4.4. Prolonging the activity of Ras1<sup>C215S</sup> restores pheromone-responsive signalling.

The addition of the Gln66Leu mutation to Ras1<sup>C215S</sup> partially restored signalling through Scd1-Cdc42, suggesting that moving Ras1 away from the plasma membrane results in Ras1 becoming limiting through the cell morphology pathway. As it is known that Ras1 activity causes the accumulation of Byr2 at the plasma membrane (Bauman *et al.* 1998), it would be expected that abolishing the GTPase activity of Ras1<sup>C215S</sup> would also increase pheromone-dependent signalling.

To test this hypothesis, the pheromone-responsive signalling of cells expressing Ras1<sup>Q66L, C215S</sup> was first analysed using assays for  $\beta$ -galactosidase activity and average cell volume.  $\beta$ -galactosidase activity and average cell volume were analysed following growth in a range of pheromone concentrations (1 nM to 100  $\mu$ M) in DMM for 16 h.

Cells expressing Ras1<sup>Q66L, C215S</sup> from the *ras1* locus displayed maximal signalling at near wild-type levels, with JY1386 (*ras1*<sup>Q66L, C215S</sup>) displaying a maximal signal of  $18.8 \pm 0.9$  and JY544 (*ras1*<sup>+</sup>) displaying a maximal signal of  $22.7 \pm 0.9$  (Figure 5.24A). JY1386 (*ras1*<sup>Q66L, C215S</sup>) and JY544 (*ras1*<sup>+</sup>) also displayed comparable pEC<sub>50</sub>s to pheromone (JY544 (*ras1*<sup>+</sup>) =  $7.0 \pm 0.1$  and JY1386 (*ras1*<sup>Q66L, C215S</sup>) =  $7.1 \pm 0.1$ ). Ras1<sup>Q66L, C215S</sup> supported a pheromone-dependent increase in cell volume ( $81.4 \pm 1.4$  fl to  $98.2 \pm 1.6$  fl) but exhibited a high basal cell volume compared to cells expressing wild-type Ras1 ( $66.6 \pm 1.5$ ) (Figure 5.24B).

Cells expressing Ras1<sup>Q66L, C215S</sup> exhibited a pheromone-dependent increase in cell volume. However, cell elongation provides a more direct measure of shmoo formation. Cell elongation in response to pheromone was determined using quantitative imaging. Images of JY1386 (*ras1*<sup>Q66L, C215S</sup>) cells, expressing GFP from pREP3x, were obtained following growth in the presence (10  $\mu$ M P-factor) and absence of pheromone in DMM lacking thiamine for 16 h. Quimp software was then used to determine the length of 30 cells per image.

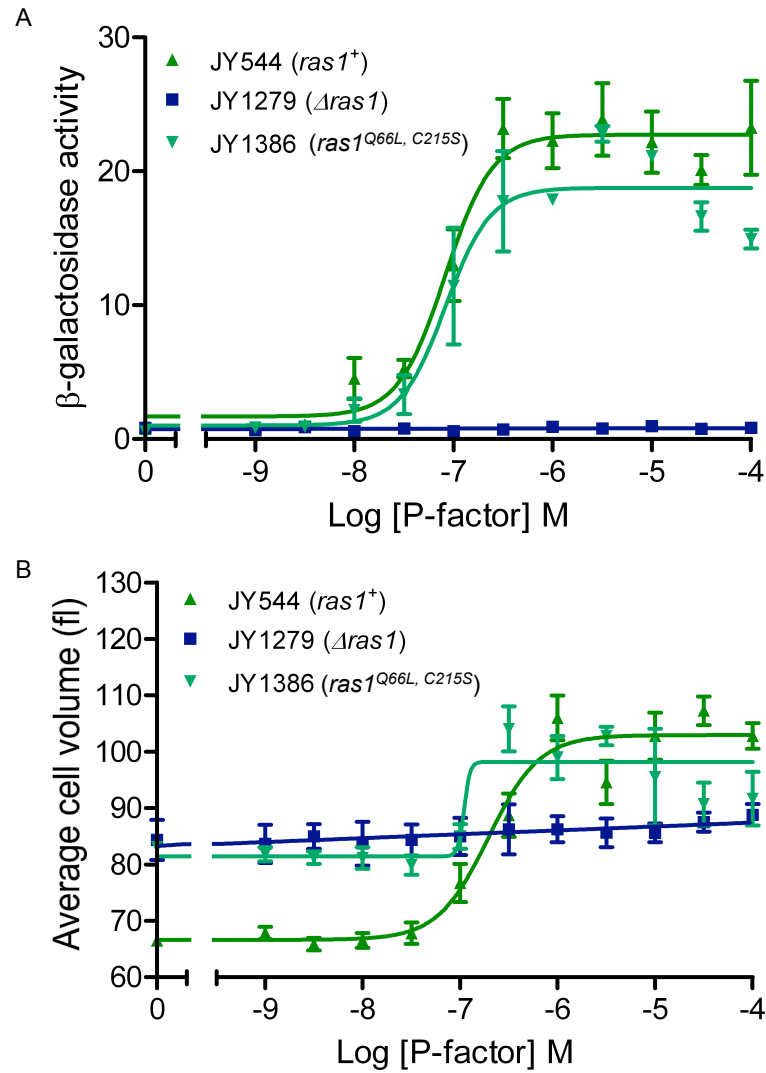


**Figure 5.24. Phormone-dependent changes in transcription on cell volume in cells expressing Ras1<sup>Q66L, C215S</sup>**

Phormone-responsive changes in transcription and cell volume were observed in *ras1*<sup>+</sup> (JY544),  $\Delta$ *ras1* (JY1279) and *ras1*<sup>Q66L, C215S</sup> (JY1386) cells. Cells were grown in 1 nM to 100  $\mu$ M phormone in DMM for 16 h. Assays were then performed for  $\beta$ -galactosidase activity (A) and average cell volume (B). Expression of Ras1<sup>Q66L, C215S</sup> supported phormone-responsive transcription and an increase in cell volume following stimulation. Data shown is an average of three independent determinants ( $\pm$ SEM).

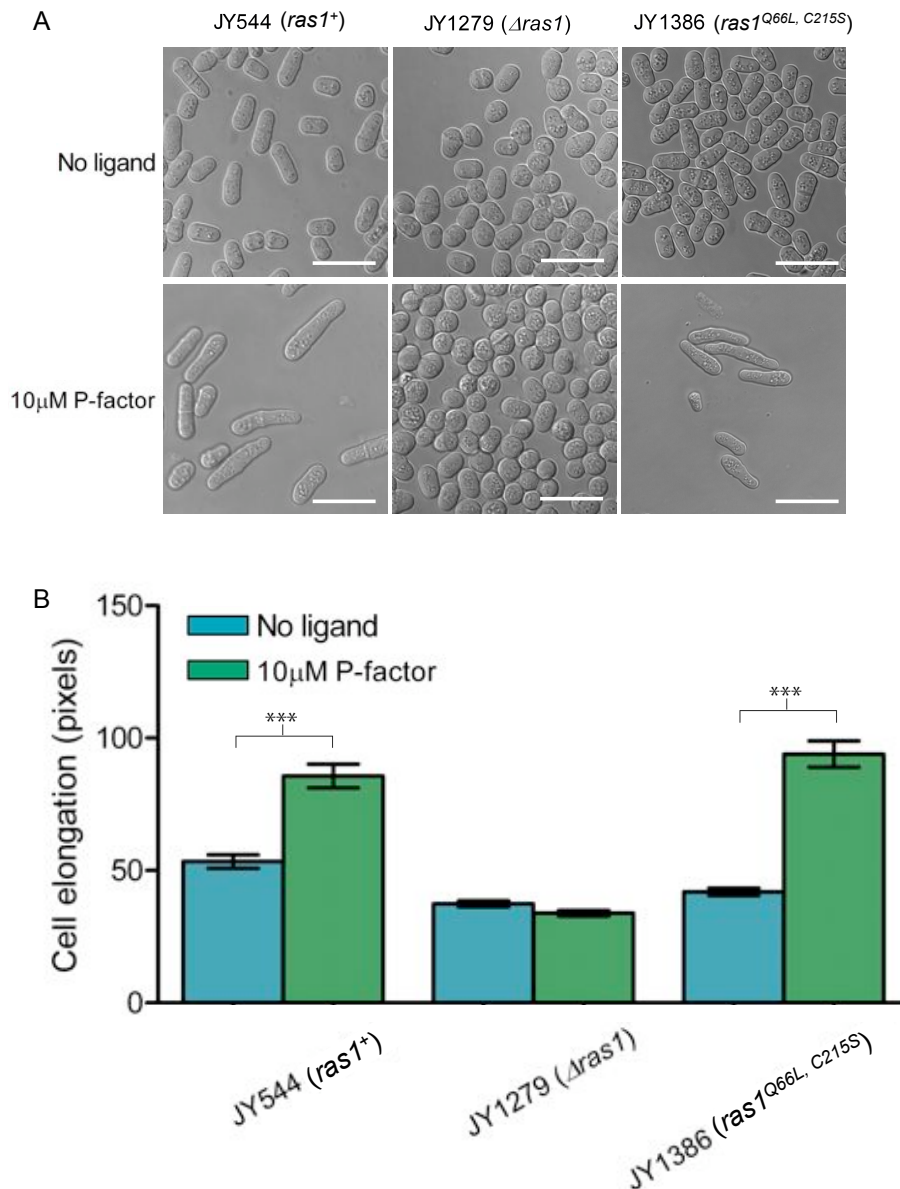


**Figure 5.25. Phormone-dependent cell elongation in cells expressing Ras1<sup>Q66L, C215S</sup>**

Quimp software was used to determine the length of cells in the absence and in the presence of 10  $\mu$ M pheromone after 16 h. Images were taken using a Leica SP5 scanning confocal microscope. Representative DIC images are displayed in panel A. Cells expressing Ras1<sup>Q66L, C215S</sup> displayed a significant increase in cell length in response to pheromone ( $P = 0.001$ ) (B). Data shown is representative of 30 individual cells  $\pm$  SEM. Statistical significance was determined using a one-way anova with a Tukey multiple comparison post test. Three asterisks indicates a P-value of 0.001. Images from the populations analysed demonstrate that Ras1<sup>Q66L, C215S</sup> supports clear shmoo formation (B). The scale bar represents 10  $\mu$ m.

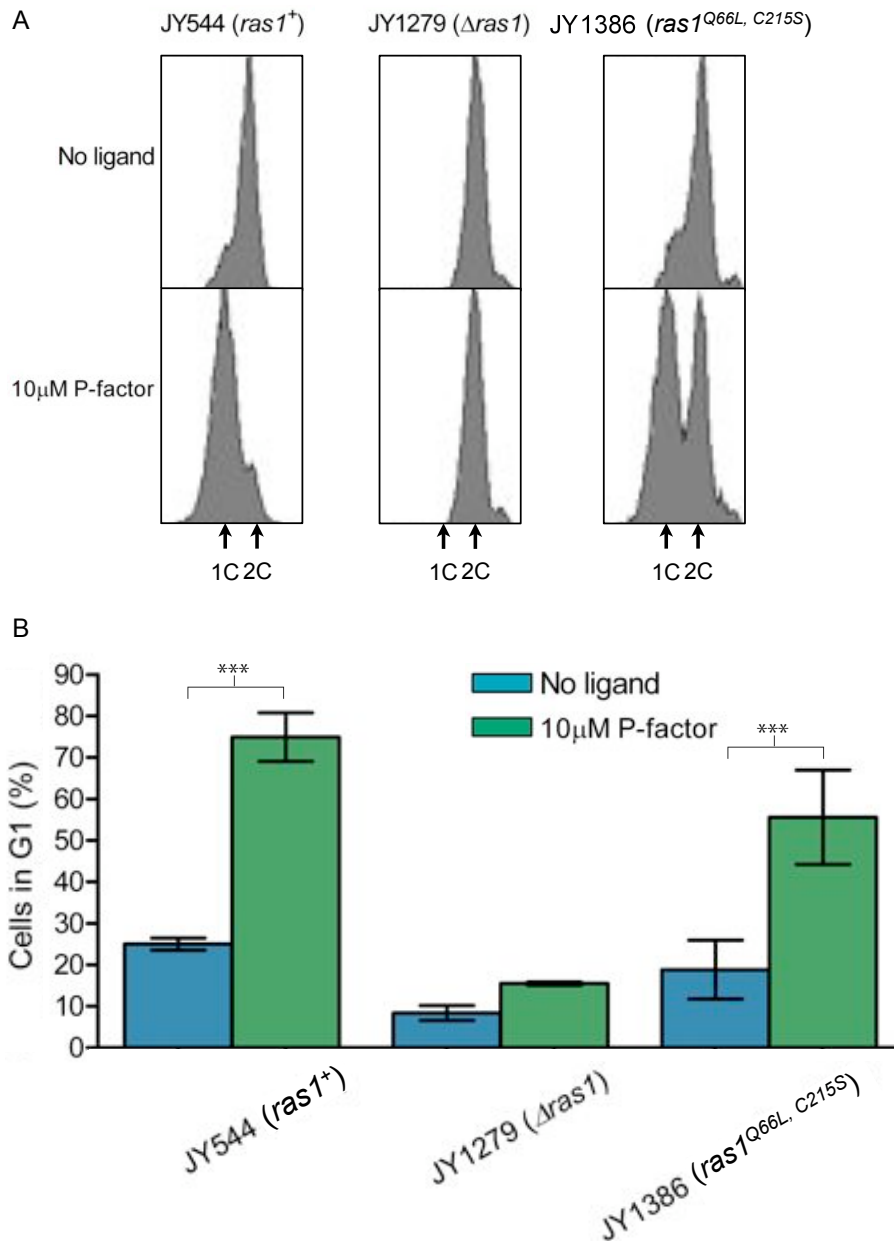


**Figure 5.26. Pheromone-responsive changes in cell cycle position in cells expressing Ras1<sup>Q66L, C215S</sup>**

Cell cycle arrest was analysed in *ras1*<sup>+</sup> (JY544),  $\Delta$ *ras1* (JY1279) and *ras1*<sup>Q66L, C215S</sup> (JY1386) cells using propidium iodide staining and flow cytometry, following growth in the presence (10  $\mu$ M P-factor) and absence of pheromone in DMM for 6 h. This analysis allowed the distinction between cells containing a single complement (1C) and double complement (2C) of DNA (A). Cells expressing Ras1<sup>Q66L, C215S</sup> displayed a significant pheromone-dependent G<sub>1</sub> arrest (B). Data shown representative of three independent determinants  $\pm$  SEM. Analysis was performed for 30000 cells. Statistical significance was determined using a one-way anova with a Tukey multiple comparison post test. Three asterisks indicates a P-value of 0.001.

Cells expressing Ras1<sup>Q66L, C215S</sup> displayed significant elongation in response to pheromone, increasing from  $41.97 \pm 1.3$  pixels to  $94.0 \pm 5.0$  pixels ( $P = 0.001$ ) (Figure 5.25B). No significant increase in cell length was observed previously in cells expressing Ras1<sup>C215S</sup> from the *ras1* locus. Images of JY1386 (*ras1*<sup>Q66L, C215S</sup>) also indicate the presence of shmooing cells (Figure 5.25A).

In order to further characterise the pheromone-dependent signalling of cells expressing Ras1<sup>Q66L, C215S</sup>, the cell cycle position of JY1386 (*ras1*<sup>Q66L, C215S</sup>) cells was also determined using propidium iodide staining and flow cytometry after growth in the presence (10  $\mu$ M P-factor) and absence of pheromone in DMM for 6 h. Analysis was performed for 30000 cells. Cells expressing Ras1<sup>Q66L, C215S</sup> displayed a significant level of G<sub>1</sub> arrest upon pheromone stimulation, increasing from  $23.1 \pm 2.0$  % to  $54.9 \pm 11.4$  % ( $P = 0.001$ ) (Figure 5.26). A clear increase in cells containing a single complement (1C) of chromosomal DNA can also be seen in these cells following pheromone stimulation (Figure 5.26A). By contrast, cells expressing Ras1<sup>C215S</sup> displayed only a small, non-significant increase in cells in G<sub>1</sub> upon stimulation with pheromone.

The ability of Ras1<sup>Q66L, C215S</sup> to support mating was also investigated using the quantitative assay for spore formation detailed in section 4.2.1. No mating was observed in JY1386 (*ras1*<sup>Q66L, C215S</sup>) cells upon incubation with cells of the opposite mating type (JY1025), possibly due to the inability of these cells to recover following stimulation as a consequence of the GTPase deficiency conferred by the Gln66Leu mutation.

#### 5.4.5. GFP-Ras1<sup>Q66L, C215S</sup> displays reduced signalling compared to Ras1<sup>Q66L, C215S</sup>.

Accurate analysis of GFP-Ras1<sup>Q66L, C215S</sup> localisation is key to the interpretation of the results presented in this section. As a consequence, the activity of GFP-Ras1<sup>Q66L, C215S</sup> is of significant interest. To investigate the signalling of GFP-Ras1<sup>Q66L, C215S</sup>, cell morphology was first determined in JY1497 (*gfp-*

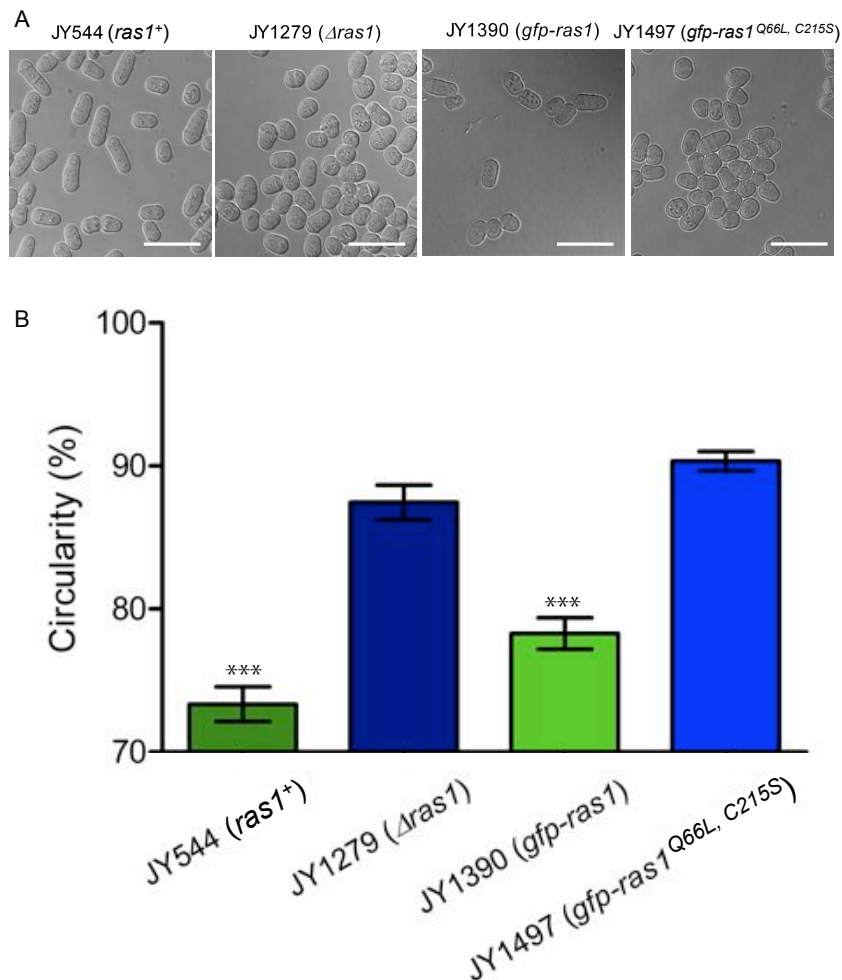


**Figure 5.27. Analysis of the morphology of cells expressing GFP-Ras1<sup>Q66L, C215S</sup>**

Images of *ras1*<sup>+</sup> (JY544),  $\Delta$ *ras1* (JY1279) and *gfp-ras1*<sup>Q66L, C215S</sup> (JY1497) cells, expressing GFP from pREP3x were obtained using a Leica SP5 scanning confocal microscope. Quimp software was then used to determine the circularity of cells within these populations. Representative DIC images are displayed in panel A. *gfp-ras1*<sup>Q66L, C215S</sup> (JY1497) cells displayed a rounded morphology consistent with cells lacking Ras1 (B). Data representative of 30 individual cells  $\pm$  SEM. Statistical significance was determined using a one-way anova with a Tukey multiple comparison post test. Three asterisks indicates a P-value of 0.001.

*ras1*<sup>Q66L, C215S</sup>) cells, expressing GFP from pREP3x. Images of these cells were obtained using a Leica SP5 scanning confocal microscope, and Quimp software was used to determine the circularity of 30 cells within the population (Figure 5.27). JY1497 displayed a rounded morphology consistent with a lack of Ras1 signalling through Scd1-Cdc42 ( $90.33 \pm 0.67$  %), indicating that the addition of GFP to Ras1<sup>Q66L, C215S</sup> had a significant detrimental effect upon signalling.

Although GFP-Ras1<sup>Q66L, C215S</sup> was unable to support polar cell morphology, the fusion may still retain function in regulating the pheromone response. The pheromone-dependent signalling of cells expressing GFP-Ras1<sup>Q66L, C215S</sup> was determined using assays for  $\beta$ -galactosidase activity and average cell volume, following growth in a range of pheromone concentrations (1 nM to 100  $\mu$ M) in DMM for 16 h. The addition of the GFP-tag to Ras1<sup>Q66L, C215S</sup> also had a marked effect upon pheromone dependent signalling. JY1497 (*gfp-ras1*<sup>Q66L, C215S</sup>) displayed a maximal signal of just  $7.91 \pm 0.63$  in  $\beta$ -galactosidase assays (Figure 5.28A), and displayed only a slight increase in cell volume in response to pheromone ( $80.8 \pm 0.3$  fl to  $83.8 \pm 1.4$  fl) (Figure 5.28B). By contrast, cells expressing Ras1<sup>Q66L, C215S</sup> exhibited a maximal signal of  $18.8 \pm 0.9$  in assays for  $\beta$ -galactosidase activity and a pheromone-dependent increase in cell volume from  $81.4 \pm 1.4$  fl to  $98.2 \pm 1.6$  fl (Figure 5.24). These data indicate that the addition of GFP to the N-terminus has a significant effect upon the signalling of Ras1<sup>Q66L, C215S</sup> through both the pheromone-response and cell morphology pathways.

#### 5.4.6. Ras1<sup>Q66L, C215S</sup> displays a high level of pheromone-dependent signalling when expressed from pREP3x.

Both increasing the expression of Ras1<sup>C215S</sup>, through expression from pREP3x (Figure 5.17), and increasing the activity of Ras1<sup>C215S</sup>, with the addition of the Gln66Leu mutation (Figure 5.24-5.26), increased pheromone-dependent signalling. As such increasing the expression of the Ras1<sup>Q66L, C215S</sup> double mutant may further increase signalling in response to pheromone. The pheromone-dependent signalling of  $\Delta ras1$  (JY1279) cells expressing Ras1<sup>Q66L, C215S</sup> from pREP3x was determined through analysis of  $\beta$ -galactosidase activity and cell volume changes in response to pheromone. Assays for  $\beta$ -galactosidase activity and average cell volume were performed following growth in a range of

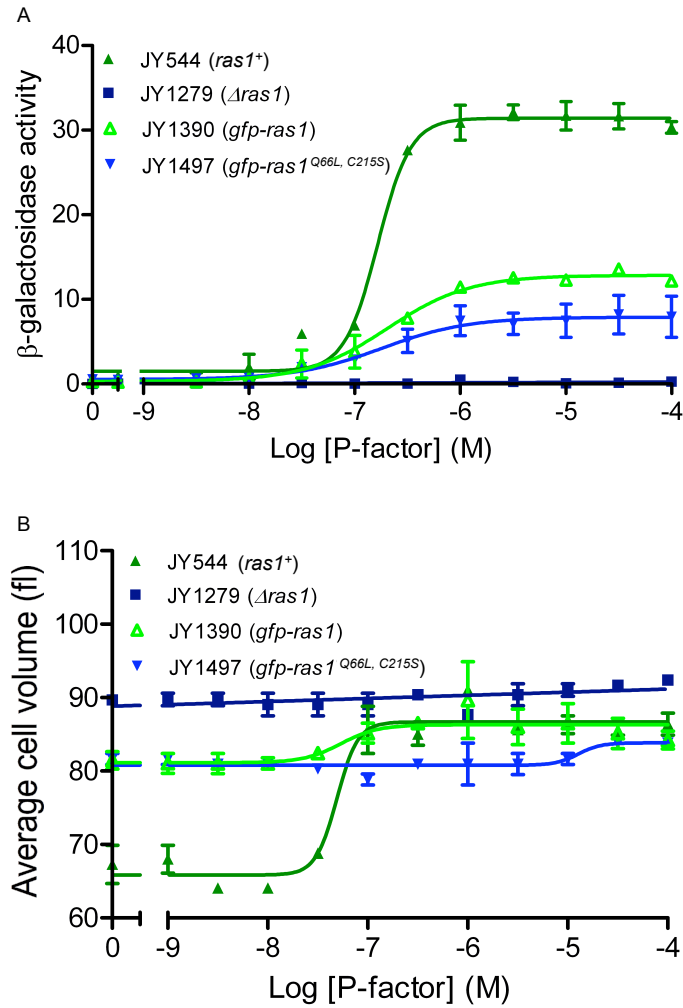


**Figure 5.28. Phormone-dependent changes in transcription on cell volume in cells expressing GFP-Ras1<sup>Q66L, C215S</sup>.**

Phormone-responsive changes in transcription and cell volume were observed in *ras1*<sup>+</sup> (JY544),  $\Delta$ *ras1* (JY1279) and *gfp-ras1*<sup>Q66L, C215S</sup> (JY1497) cells. Cells were grown in 1 nM to 100  $\mu$ M phormone in DMM for 16 h. Assays were then performed for  $\beta$ -galactosidase activity (A) and average cell volume (B). GFP-Ras1<sup>Q66L, C215S</sup> displayed reduced  $\beta$ -galactosidase activity compared to non-tagged Ras1<sup>Q66L, C215S</sup> and only a small increase in cell volume. Data shown is an average of three independent determinants ( $\pm$ SEM).

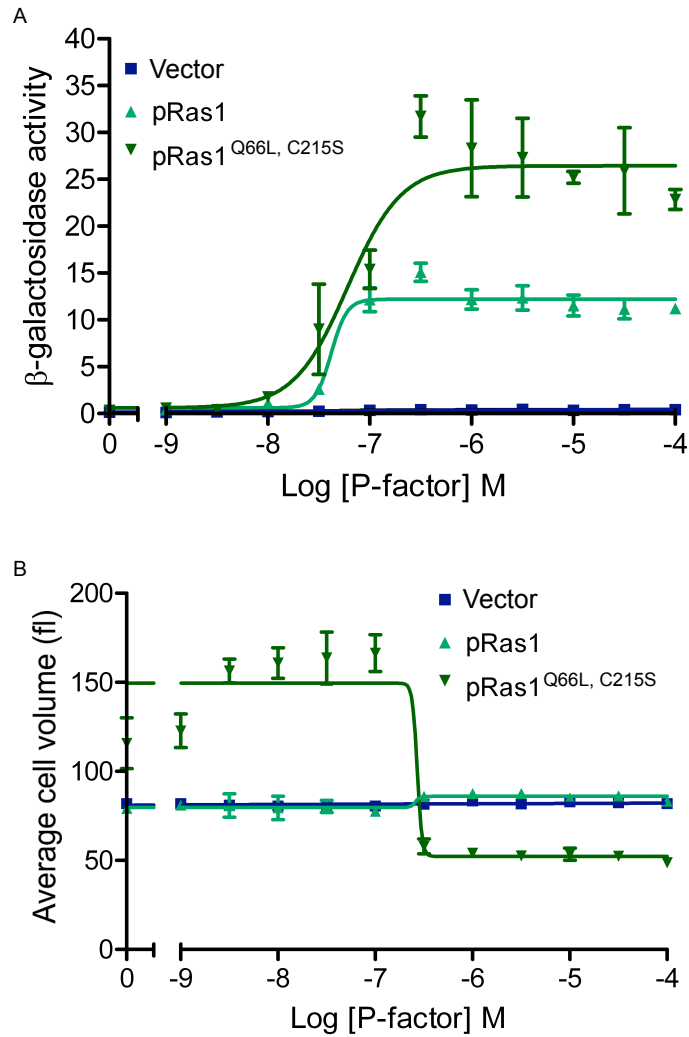


**Figure 5.29. Phormone-dependent changes in transcription on cell volume in cells expressing Ras1<sup>Q66L, C215S</sup> from pREP3x**

Phormone-responsive changes in transcription and cell volume were observed in  $\Delta ras1$  (JY1279) cells transformed with pREP3x-Ras1<sup>Q66L, C215S</sup>, pREP3x-Ras1 and vector alone. Cells were grown in 1 nM to 100  $\mu$ M phormone in DMM lacking thiamine for 16 h. Assays were then performed for  $\beta$ -galactosidase activity (A) and average cell volume (B). Ras1<sup>Q66L, C215S</sup> supported strong phormone dependent  $\beta$ -galactosidase activity. Cells expressing Ras1<sup>Q66L, C215S</sup> displayed a high basal cell volume and a reduction in cell volume upon phormone stimulation. Data shown is an average of three independent determinants ( $\pm$ SEM).

pheromone concentrations (1 nM to 100  $\mu$ M) in DMM lacking thiamine for 16 h.

JY1279 ( $\Delta ras1$ ) cells expressing Ras1<sup>Q66L, C215S</sup> from pREP3x displayed higher maximal signalling than those expressing wild-type Ras1 from pREP3x ( $18.0 \pm 0.5$  compared to  $12.2 \pm 0.4$  respectively), but did exhibit a drop in signalling at higher pheromone concentrations (Figure 5.29A). These cells also displayed a very high cell volume in the absence of pheromone ( $149.5 \pm 4.9$  fl), consistent with that observed in cells expressing Ras1<sup>Q66L</sup> from pREP3x. Ras1<sup>Q66L, C215S</sup>, when expressed from pREP3x, also caused a reduction in cell volume at higher pheromone concentrations ( $52.3 \pm 4.7$  fl), again consistent with cells expressing Ras1<sup>Q66L</sup> from pREP3x (Figure 5.29B). These data could indicate that constitutive expression of Ras1<sup>Q66L, C215S</sup> causes cell death in response to pheromone in a similar manner to the Ras1<sup>Q66L</sup> mutant.

### 5.5. Summary

The relationship between Ras1 C-terminal modification, localisation and function has previously been cited as a key example of compartment specific ras signalling (Chang and Philips 2006; Onken *et al.* 2006). The preceding chapter has dealt with the use of quantitative assays to analyse the effects of altering Ras1 C-terminal modification on localisation and function. It was found that preventing palmitoylation and farnesylation had dramatic effects upon the localisation of Ras1. Preventing farnesylation and palmitoylation caused Ras1 to become cytosolic. This mutation had the most severe effect upon signalling, preventing all Ras1 activity when expressed from the endogenous *ras1* locus. Preventing just palmitoylation caused a significant reduction in plasma membrane localisation, with Ras1 displaying indiscriminate membrane localisation. This observation is consistent with that described for other monolipidated substrates (Rocks *et al.* 2010), but is not in agreement with the

localisation of Ras1<sup>C215S</sup> described previously, where it was reported to associate exclusively with endomembranes (Onken *et al.* 2006). In addition, the activity of Ras1<sup>C215S</sup> is quite different from that described in Onken *et al.* 2006. It was suggested that Ras1<sup>C215S</sup> was unable to propagate pheromone dependent signalling, as it was not present on the plasma membrane. In this present study however, some pheromone-dependent signalling was observed, consistent with the presence of a small population of Ras1 at the plasma membrane. More significantly, it was found that Ras1<sup>C215S</sup> could not support elongated cell morphology. This is again in disagreement with the published activity of Ras1<sup>C215S</sup>, which is described as supporting signalling through Scd1-Cdc42 from the endomembranes. Population based quantitative analysis of morphology and analysis of Tea1 localisation, however, does not support this finding.

Based upon these observations it appears that reducing the level of Ras1 at the plasma membrane causes Ras1 to become limiting in both Ras1-dependent signalling pathways. This supposition is supported by the finding that increasing the duration of Ras1<sup>C215S</sup> activity, through the addition of the Gln66Leu GTPase deficiency mutation, rescues some signalling activity through both pathways. These results are summarised in table 5.1. In addition, it was found that increasing the concentration of Ras1<sup>C215S</sup>, through expression from pREP3x caused increased pheromone-dependent signalling, again suggesting that Ras1<sup>C215S</sup> becomes limiting when expressed from the *ras1* locus.

Ras1<sup>C216S</sup> could also support pheromone-dependent signalling when expressed from pREP3x, although these cells displayed a reduced pEC<sub>50</sub> to pheromone. A previous study (Kholodenko *et al.* 2000), using a systems biology approach to study membrane-associated signalling proteins, suggested that membrane tethering and membrane recruitment allowed the formation of more, longer lasting signalling complexes. As a result, more sensitive signalling could be achieved when signalling proteins form membrane complexes. This could explain the reduced potency of P-factor in cells containing cytosolic Ras1.

Finally, the localisation of the inactive Ras1 mutant Ras1<sup>S22N</sup> and the two GTPase deficient mutants Ras1<sup>G17V</sup> and Ras1<sup>Q66L</sup> was assessed. All three mutants displayed predominantly plasma membrane localisation. Ras1<sup>S22N</sup> however, displayed significantly lower plasma membrane localisation than Ras1. This observation could indicate that the localisation of Ras1 to the plasma membrane is, in part, a consequence of the functional interactions of Ras1. As a result, preventing Ras1 function leads to a significantly altered localisation pattern.

Table 5.1. Summary of the activity and localisation of Ras1 C-terminal modification mutants

Strain	Ras1 PM localisation	Cell polarity	Pheromone response	Mating
<i>ras1</i> <sup>+</sup>	++	++	++	++
$\Delta$ <i>ras1</i>	-	-	-	-
<i>ras1</i> <sup>C215S</sup>	+	-	+	-
<i>ras1</i> <sup>C216S</sup>	-	-	-	-
<i>ras1</i> <sup>Q66L, C215S</sup>	+	+	++	-

## CHAPTER 6

# Targetting Ras1 to the plasma membrane

### 6.1. Introduction

Mutants which prevent Ras1 C-terminal modification allow the analysis of Ras1 signalling at reduced plasma membrane concentrations. To analyse the role of compartmentalisation in Ras1 signalling, it would also be advantageous to investigate the effect of increasing plasma membrane targetting. One previous study (Onken *et al.* 2006) used a fusion of the N-terminus of Ras1 with the C-terminal localisation domain of the small monomeric GTPase Rit (RitC), which is not processed through the endomembranes before reaching the plasma membrane. Ras1 and Rit share significant sequence homology, but differ in their C-terminal localisation domain (Figure 6.1). It was suggested in this study that the Ras1-RitC fusion could support signalling in response to pheromone, as this occurs at the plasma membrane, but could not support polar cell morphology, as it was suggested that this was controlled at the endomembranes. The chimera, in which the last 48 amino acids of Ras1 were replaced with the last 62 amino acids of Rit, was kindly supplied by Prof. Eric Chang.

In the preceding chapter a series of evidence was presented which suggested that the plasma membrane localisation of Ras1 is important in both the pheromone response and polar cell morphology. This observation is not in agreement with the published activity of the Ras1-RitC fusion. In the following chapter a number of Ras1 fusion proteins, including the Ras1-RitC fusion, are characterised which display increased plasma membrane localisation.



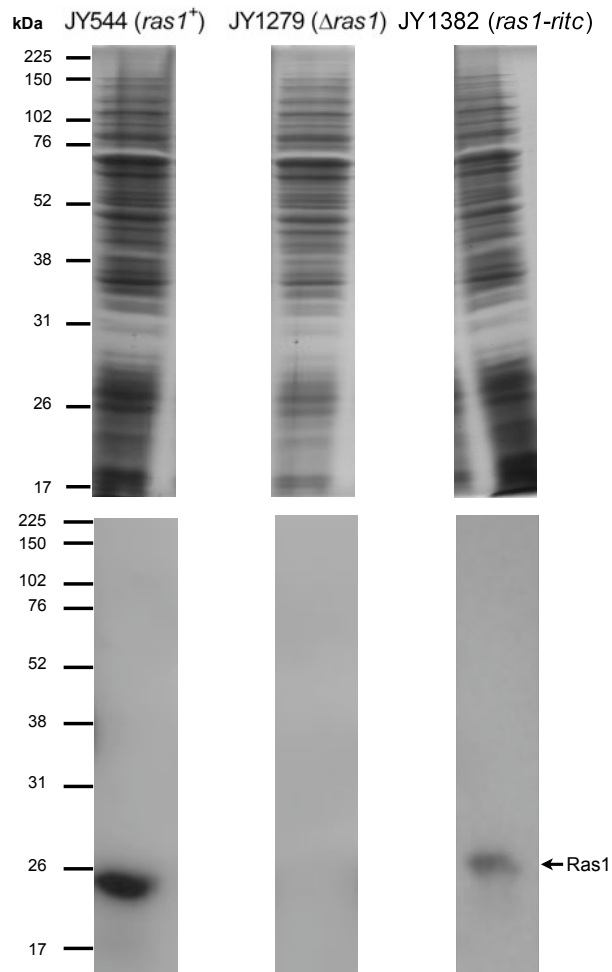


**Figure 6.2. Integration of Ras1-RitC**

Integration of Ras1-RitC in the *ras1::ura4*<sup>+</sup>, *sxa2*>*lacZ* strain JY1247 was confirmed via immunoblotting using an anti-ras RAS10 antibody. Coomassie stains of whole protein are included above the immunoblot as loading controls.

strain (JY1025), ascus spores could be detected by microscopy using a Leica SP5 scanning confocal microscope (Figure 6.3A). Mating in this strain however was occurring at a very low efficiency, and population wide analysis using quantitative assays for spore formation suggested little significant mating (0.27% in just one assay of three replicates) (Figure 6.3B).

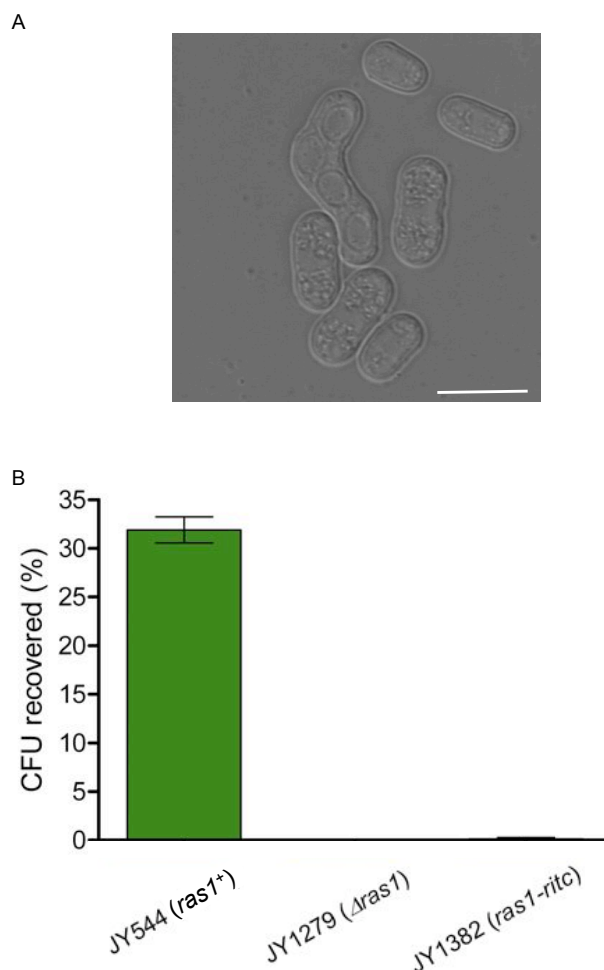


**Figure 6.3. Mating efficiency in cells expressing Ras1-RitC**

The mating of *ras1*<sup>+</sup> (JY544),  $\Delta$ *ras1* (JY1279) and *ras1-ritc* (JY1382) cells, expressing Sxa2 from pREP4x, was assessed by microscopic examination (A) and the quantitative mating assay detailed in section 4.2.1 (B). JY1382 displayed no significant mating, but some spore formation could be observed. Data shown representative of three independent determinants  $\pm$  SEM. Statistical significance was determined using a one-way anova with a Tukey multiple comparison post test. Images were obtained using a Leica SP5 scanning confocal microscope. The scale bar represents 10  $\mu$ m.

**6.2.3. Ras1-RitC displays some signalling through Scd1.**

Ras1-RitC displayed little mating. However, some function may be observable upon analysis of other measures of Ras1 signalling. The activity of Ras1-RitC through the cell polarity pathway was the first measure of Ras1 activity employed. The morphology of cells expressing Ras1-RitC from the endogenous *ras1* locus (JY1382) were determined using quantitative imaging. Images of these cells, expressing GFP from pREP3x, were obtained using a Leica SP5

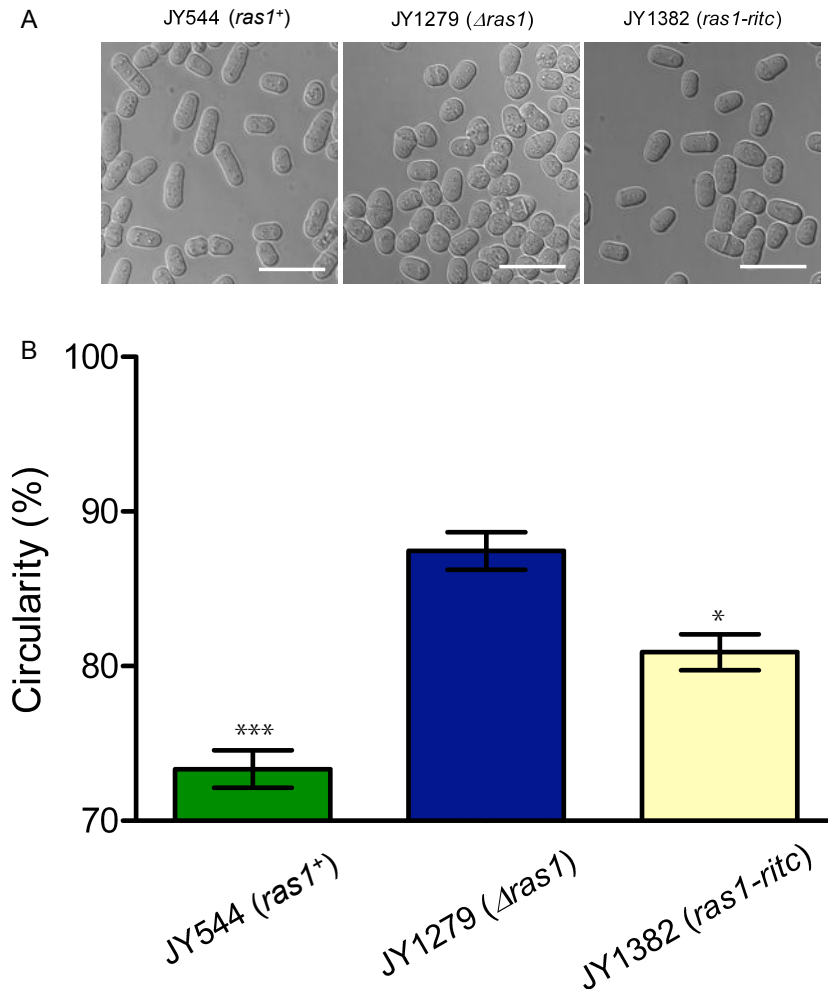


**Figure 6.4.** The morphology of cells expressing Ras1-RitC from the endogenous *ras1* locus

Images of *ras1*<sup>+</sup> (JY544),  $\Delta$ *ras1* (JY1279) and *ras1-ritc* (JY1382) cells, expressing GFP from pREP3x, were obtained using a Leica SP5 scanning confocal microscope. Representative DIC images are displayed in panel A. Cell circularity was determined using Quimp software (B). Cells expressing Ras1-RitC displayed a significantly lower percentage circularity than cells lacking Ras1 ( $P = 0.05$ ), but higher than that observed in *ras1*<sup>+</sup> (JY544) cells. Data representative of 30 individual cells  $\pm$  SEM. Statistical significance was determined using a one-way anova with a Tukey multiple comparison post test. One asterisks indicates a P-value of 0.05 and three asterisks indicates a P-value of 0.001. The scale bar represents 10  $\mu$ m.

confocal microscope. Quimp software was then used to determine the circularity of 30 individual cells within the population (Figure 6.4). JY1382 (*ras1-ritc*) displayed significantly reduced percentage circularity ( $80.9 \pm 1.6$  %,  $P = 0.05$ ) compared to  $\Delta$ *ras1* (JY1279) cells ( $87.5 \pm 1.2$  %). This did not represent a full restoration of signalling, as *ras1*<sup>+</sup> (JY544) cells display a lower percentage cir-

cularity ( $73.4 \pm 1.2$  %). Images of cells expressing Ras1-RitC also indicate the presence of polar, barrel shaped cells. These results indicate that Ras1-RitC is able to signal through the cell polarity pathway, a result which contradicts the activity described previously for this fusion protein (Onken *et al.* 2006).

#### **6.2.4. Ras1-RitC displays reduced pheromone-responsive signalling compared to Ras1.**

Ras1-RitC has previously been demonstrated to rescue mating (Onken *et al.* 2006), and in this study displayed some spore formation (Figure 6.3). As such, it would be expected that Ras1-RitC would demonstrate some pheromone-dependent signalling. The ability of Ras1-RitC to transduce signal in response to pheromone was first determined using assays for  $\beta$ -galactosidase activity and average cell volume, following growth in a range of pheromone concentrations (1 nM to 100  $\mu$ M) in DMM for 16 h. *ras1-ritc* (JY1382) cells displayed a lower maximal signal ( $8.7 \pm 0.3$ ) compared to *ras1*<sup>+</sup> (JY544) cells ( $20.7 \pm 0.6$ ), but a similar pEC<sub>50</sub> ( $6.6 \pm 0.1$  and  $7.2 \pm 0.1$  respectively) in assays for  $\beta$ -galactosidase activity (Figure 6.5A). Cells expressing Ras1-RitC also displayed a pheromone-dependent increase in cell volume ( $72.5 \pm 0.7$  fl to  $80.7 \pm 1.1$  fl), although these cells exhibited a higher cell volume in the absence of pheromone than *ras1*<sup>+</sup> cells ( $64.2 \pm 1.4$  fl), potentially indicative of a more rounded morphology (Figure 6.5B).

Cells expressing Ras1-RitC exhibited a pheromone-dependent increase in cell volume. To determine whether this was due to an increase in cell length, and hence shmoo formation, morphological changes in *ras1-ritc* (JY1382) cells in response to pheromone were also analysed using quantitative imaging. Images of cells, expressing GFP from pREP3x, following growth in the absence and in the presence of 10  $\mu$ M pheromone for 16 h, were obtained using a Leica SP5 scanning confocal microscope (Figure 6.6A). Quimp software was then used to determine the length of 30 cells under each assay condition. Cells ex-

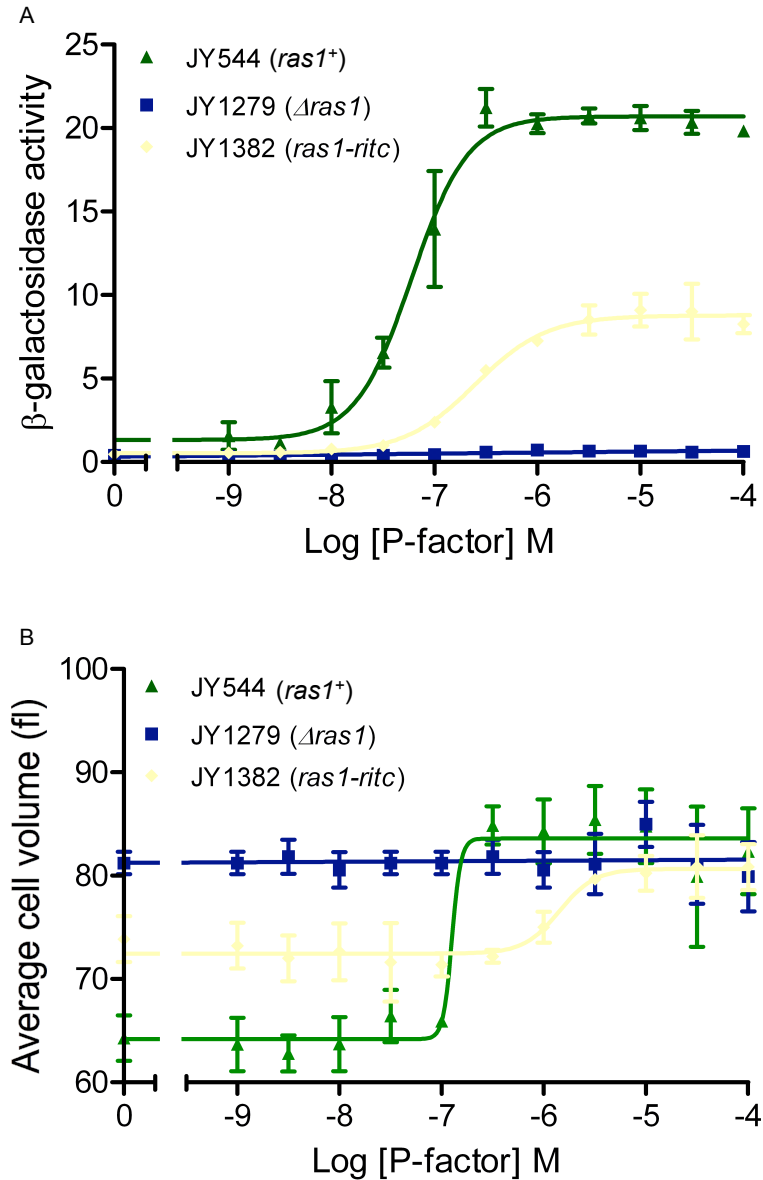


**Figure 6.5. Pheromone-dependent changes in transcription and cell volume in cells expressing Ras1-RitC**

Pheromone-responsive changes in transcription and cell volume were observed in *ras1*<sup>+</sup> (JY544),  $\Delta$ *ras1* (JY1279) and *ras1-ritc* (JY1382) cells. Cells were grown in 1 nM to 100  $\mu$ M pheromone in DMM for 16 h. Assays were then performed for  $\beta$ -galactosidase activity (A) and average cell volume (B). Reduced maximal  $\beta$ -galactosidase activity and cell volume were seen in JY1382 compared to JY544. JY1382 also displayed an increased basal cell volume. Data shown is an average of three independent determinants ( $\pm$ SEM).

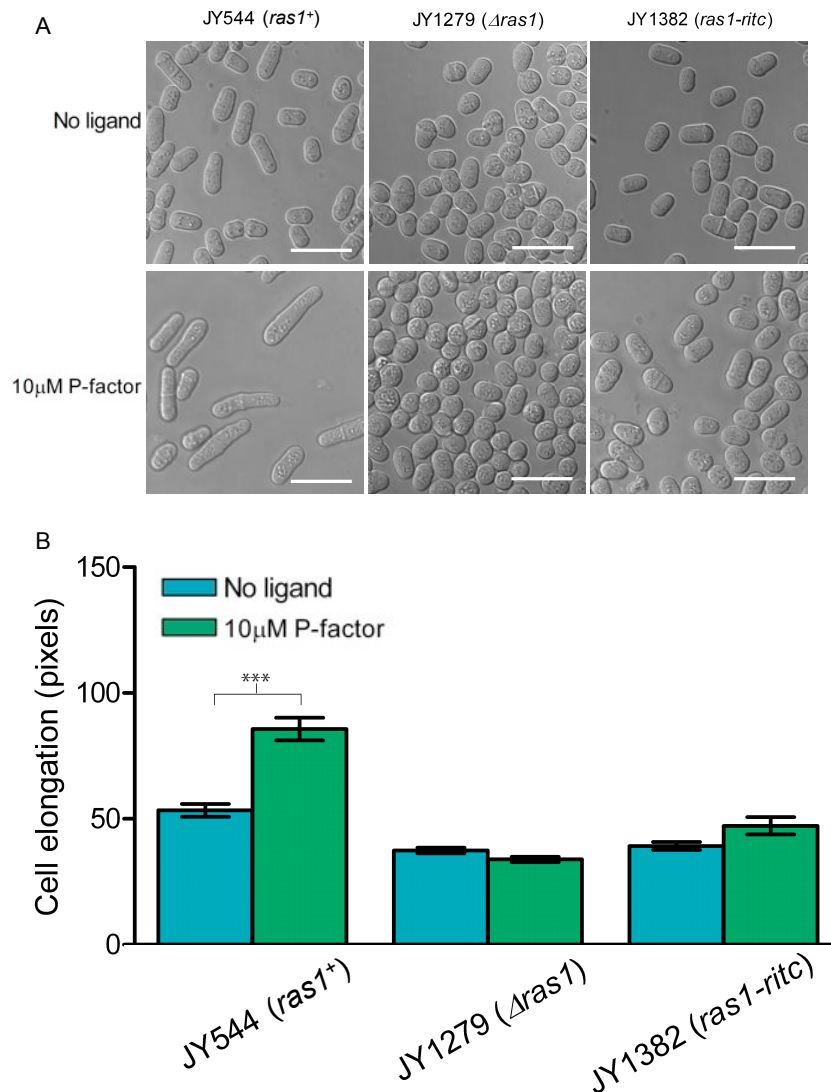


**Figure 6.6. Analysis of shmoo formation in cells expressing Ras1-RitC using quantitative imaging**

Quimp software was used to determine the length of cells in the absence and in the presence of 10  $\mu$ M pheromone after 16 h. Images were taken using a Leica SP5 scanning confocal microscope. Representative DIC images are displayed in panel A. JY1279 ( $\Delta$ *ras1*) and JY1382 (*ras1-ritc*) display no significant pheromone dependent change in cell length. JY1382 did however display a trend towards increased cell length in response to pheromone (B). Data shown is representative of 30 individual cells  $\pm$  SEM. Statistical significance was determined using a one-way anova with a Tukey multiple comparison post test. Three asterisks indicates a P-value of 0.001. Images from the populations analysed indicate no clear pheromone dependent change in cell morphology in cells expressing Ras1-RitC. The scale bar represents 10  $\mu$ m.

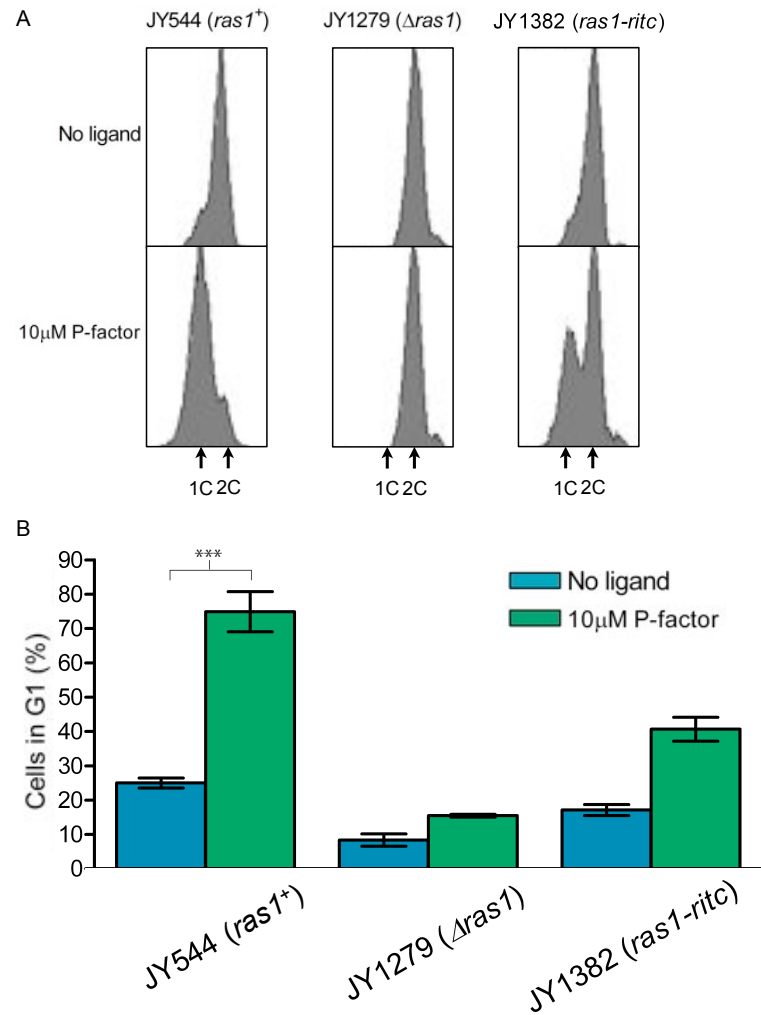


**Figure 6.7. Phormone-responsive changes in cell cycle position in cells expressing Ras1-RitC**

Cell cycle arrest was analysed in *ras1*<sup>+</sup> (JY544),  $\Delta$ *ras1* (JY1279) and *ras1-ritc* (JY1382) cells using propidium iodide staining and flow cytometry, following growth in the presence (10  $\mu$ M P-factor) and absence of pheromone in DMM for 6 h. This analysis allowed the distinction between cells containing a single complement (1C) and double complement (2C) of DNA (A). Cells expressing Ras1-RitC (JY1382) displayed some phormone-dependent G<sub>1</sub> arrest (B). Data shown representative of three independent determinants  $\pm$  SEM. Analysis was performed for 30000 cells. Statistical significance was determined using a one-way anova with a Tukey multiple comparison post test. Three asterisks indicates a P-value of 0.001.

pressing Ras1-RitC displayed a trend towards increased cell length in response to pheromone ( $39.2 \pm 1.6$  pixels to  $47.2 \pm 3.5$  pixels), however this change was not statistically significant (Figure 6.6B). No clear morphological change in response to pheromone could be observed in images of these cells (Figure 6.6A).

The final assay for pheromone-dependent signalling used to determine the activity of Ras1-RitC was the analysis of cell cycle arrest. DNA complement was determined in cells using propidium iodide staining and flow cytometry, following growth in the presence ( $10 \mu\text{M}$  P-factor) and absence of pheromone in DMM for 6 h. The number of *ras1-ritc* (JY1382) cells in  $G_1$  increased from  $17.1 \pm 1.6$  % to  $40.7 \pm 3.5$  % upon pheromone stimulation (Figure 6.7). This increase, although not statistically significant, is supported by a marked increase in cell containing a single complement (1C) of chromosomal DNA when *ras1-ritc* cells are treated with pheromone (Figure 6.7A). These data suggest a degree of pheromone-dependent cell cycle arrest.

### 6.2.5. The localisation of Ras1-RitC.

Ras1-RitC was previously described as solely localising to the plasma membrane (Onken *et al.* 2006). To confirm this, analysis of Ras1-RitC localisation was performed using an N-terminal GFP-Ras1-RitC fusion protein expressed from pREP3x in the  $\Delta ras1$  strain JY1279 (Figure 6.8A). Images were obtained using a Leica SP5 scanning confocal microscope, and analysed using Quimp software to determine the relative levels of fluorescence at the periphery compared to the interior of the cell (Figure 6.8B). The level of GFP-Ras1-RitC at the plasma membrane ( $79.9 \pm 8.7$  %) was determined to be similar to that of GFP-Ras1 ( $78.0 \pm 3.5$  %). This observation does not indicate that Ras1-RitC displays an increased level of plasma membrane localisation compared to Ras1, as was previously reported (Onken *et al.* 2006). Images of these cells indicate that, in addition to a high degree of plasma membrane localisation, GFP-Ras1-

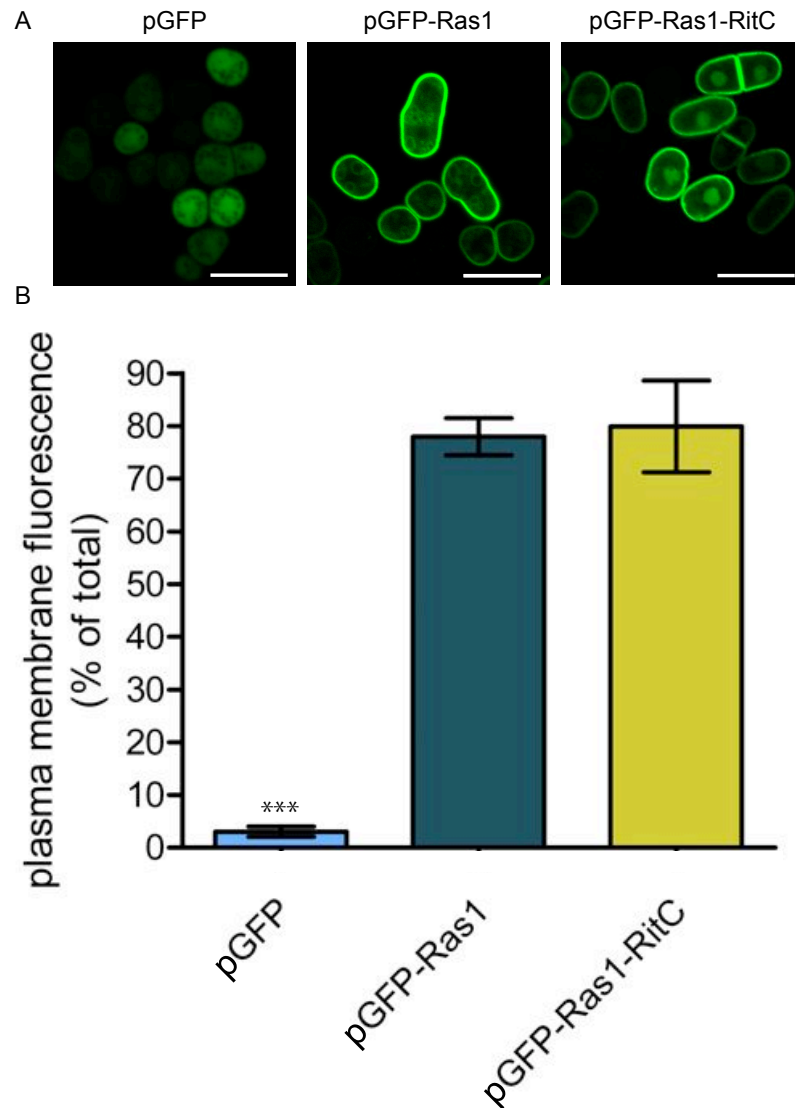


**Figure 6.8. Quantifying the localisation of GFP-Ras1-RitC using Quimp software**

Images of  $\Delta ras1$  cells (JY1279) expressing GFP, GFP-Ras1 and GFP-Ras1-RitC from pREP3x were obtained using a Leica SP5 scanning confocal microscope (A). The intensity of fluorescence at the periphery compared to the interior of the cell was determined using Quimp software, and percentage plasma membrane fluorescence was calculated (B). The analysis indicated that GFP-Ras1-RitC displayed predominantly plasma membrane fluorescence, comparable to that observed for GFP-Ras1. Data representative of 10 individual cells. Statistical significance was determined using a one-way anova with a Tukey multiple comparison post test. Three asterisks indicates a P-value of 0.001. The scale bar represents 10  $\mu\text{m}$ .

RitC is also extensively localised to the cytoplasm and nucleus, suggesting the presence of a pool of soluble GFP-Ras1-RitC.

The Ras1-RitC construct does not display a specific plasma membrane localisation. In addition, the chimeric protein displayed impaired function in all assays for Ras1 activity. As a consequence, a different means of promoting the plasma membrane localisation may provide more conclusive data.

### 6.3. Characterising 1-40Gpa1-GFP-Ras1

G $\alpha$  subunits of heterotrimeric G proteins employ a different means of promoting plasma membrane localisation to Ras1 and Rit. Most G $\alpha$  subunits are modified at their N-terminus with a myristoyl and palmitoyl moiety to promote membrane association (Resh 1999). Such modifications may prove useful in promoting a stronger association between Ras1 with the plasma membrane. The N-terminus of the G $\alpha$  subunit Gpa1 contains a consensus MG<sup>2</sup>XXXS<sup>6</sup> myristoylation sequence (Johnson *et al.* 1994) and a downstream cysteine, which is likely to be a target for palmitoylation.

Previous work has demonstrated that mutating these potential myristoylation (Gly2Ala) and palmitoylation (Cys3Ser) sites reduces the plasma membrane localisation of Gpa1, and that the first 40 amino acids of Gpa1 (1-40Gpa1) form an efficient plasma membrane targeting motif (Godfrey 2009). The following section explores the use of the N-terminal plasma membrane localisation domain of Gpa1 as a motif to increase the level of Ras1 at the plasma membrane, investigating the localisation and function of this novel protein.

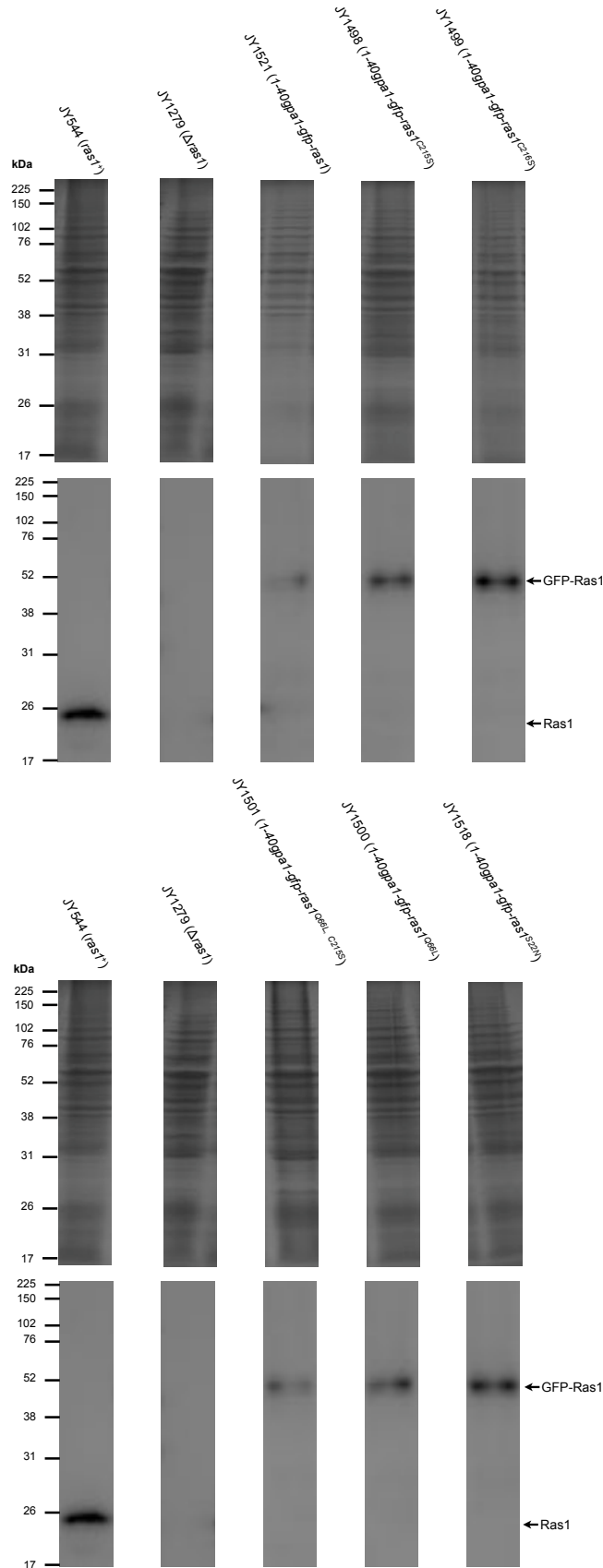


**Figure 6.9. Integration of 1-40Gpa1-GFP-Ras1 in the  $\beta$ -galactosidase reporter strain**

Integration of 1-40Gpa1-GFP-Ras1 fusions in the *ras1::ura4<sup>+</sup>, sxa2>lacZ* strain JY1247 was confirmed via immunoblotting using an anti-ras RAS10 antibody. Coomassie stains of whole protein are included above the immunoblot as loading controls.

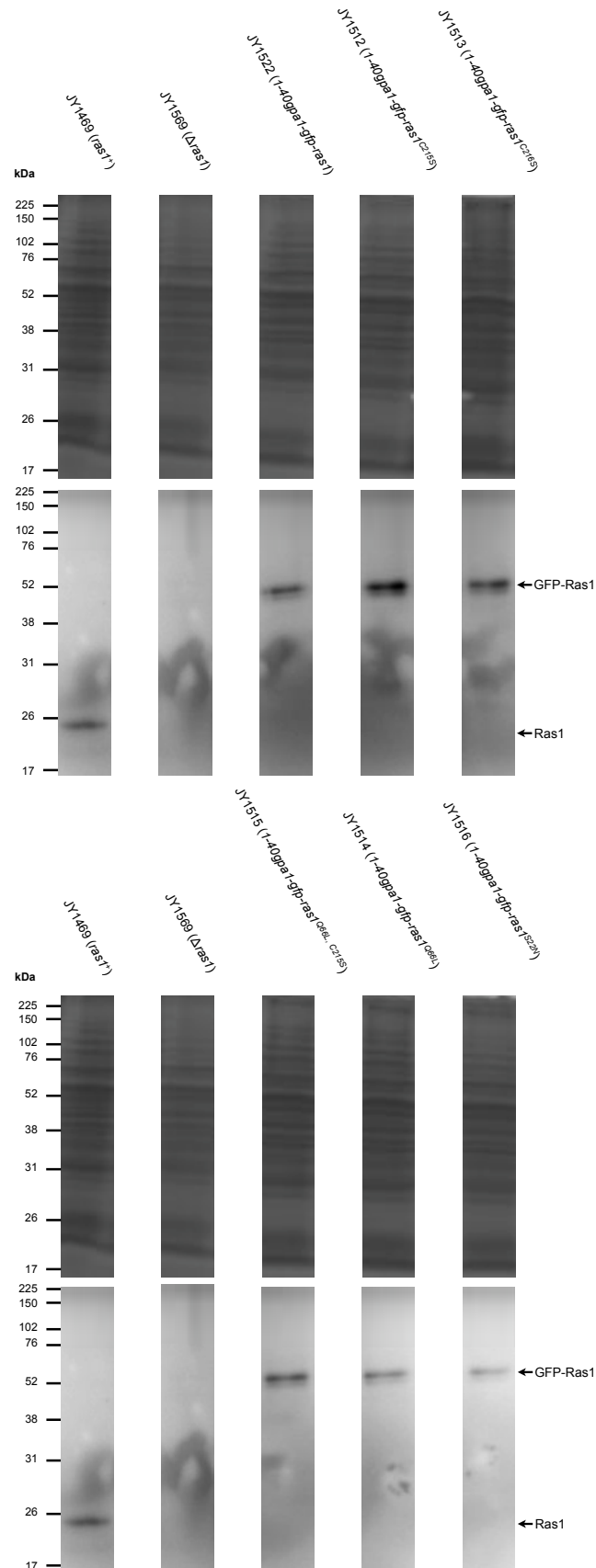


**Figure 6.10. Integration of 1-40Gpa1-GFP-Ras1 in the Tea1-mCherry strain**

Integration of 1-40Gpa1-GFP-Ras1 fusions in the *ras1::ura4<sup>+</sup>, tea1-mCherry* strain JY1569 was confirmed via immunoblotting using an anti-ras RAS10 antibody. Coomassie stains of whole protein are included above the immunoblot as loading controls.

### 6.3.1. Expression of 1-40Gpa1-GFP-Ras1 fusions.

Chimeric proteins containing the first 40 amino acids of Gpa1 (1-40Gpa1) fused to GFP-Ras1 were created containing wild-type Ras1, the palmitoylation and palmitoylation/farnesylation deficient mutants Ras1<sup>C215S</sup> and Ras1<sup>C216S</sup>, the palmitoylation and GTPase deficient mutant Ras1<sup>Q66L, C215S</sup>, the GTPase deficient mutant Ras1<sup>Q66L</sup> and the inactive mutant Ras1<sup>S22N</sup>. All six fusions were created at the *ras1* locus, using the method previously described in Figure 4.28A. Expression of these proteins from the *ras1* locus of the *sxa2>lacZ* (Figure 6.9) and *tea1-mCherry* (Figure 6.10) strains was confirmed by immunoblotting using an anti-ras RAS10 antibody, giving a signal at a position consistent with the predicted size of the fusion (~ 58 kDa).

### 6.3.2. 1-40Gpa1-GFP-Ras1 fusion proteins display a high degree of plasma membrane localisation.

The aim of creating the 1-40Gpa1-GFP-Ras1 fusions was to increase the level of Ras1 at the plasma membrane. The localisation of 1-40Gpa1-GFP-Ras1 fusion proteins was initially determined when expressed from the *ras1* locus, using a Nikon E800 epifluorescence microscope fitted with an Andor EM-CCD camera. All six fusions displayed plasma membrane localisation. Despite the low fluorescence signal, plasma membrane localisation could be observed in all strains and was particularly apparent at the septa of dividing cells, providing a good indication of plasma membrane localisation (Figure 6.11).

The 1-40Gpa1-GFP-Ras1 fusion proteins, when expressed from the *ras1* locus, appeared to predominantly localised to the plasma membrane. However, the low level of expression observed from the *ras1* locus prevents the detailed analysis of localisation. In order to increase the fluorescent signal, all six 1-40Gpa1-GFP-Ras1 fusion proteins were expressed from pREP3x in the  $\Delta ras1$  strain JY1279, allowing quantitative analysis of their localisation. Fluorescence images were obtained using a Leica SP5 scanning confocal micro-

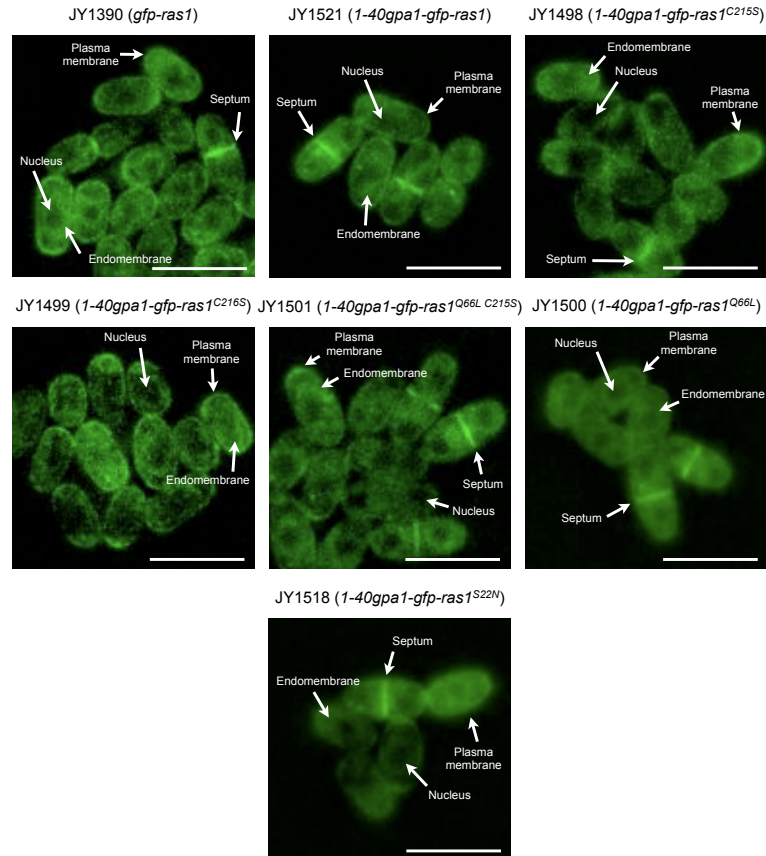


**Figure 6.11. The localisation of 1-40Gpa1-GFP-Ras1 fusions**

The localisation of 1-40Gpa1-GFP-Ras1 proteins, upon expression from the *ras1* locus, was determined using a Nikon E800 epifluorescence microscope fitted with an Andor EM-CCD camera. All displayed plasma membrane localisation. The scale bar represents 10  $\mu\text{m}$ .

scope (Figure 6.12A) and Quimp software was used to separate peripheral from cytosolic fluorescence (Figure 6.12B). All 1-40Gpa1-GFP-Ras1 fusions demonstrated predominantly plasma membrane localisation. 1-40Gpa1-GFP-Ras1 exhibited a slight, but not significant increase in plasma membrane localisation ( $86.9 \pm 4.4\%$ ) compared to GFP-Ras1 alone ( $78.0 \pm 3.5\%$ ). Both 1-40Gpa1-GFP-Ras1<sup>C215S</sup> and 1-40Gpa1-GFP-Ras1<sup>C216S</sup> displayed plasma membrane localisation ( $73.6 \pm 6.0\%$  and  $62.0 \pm 3.5\%$  respectively) to a greater extent compared to GFP-Ras1<sup>C215S</sup> and GFP-Ras1<sup>C216S</sup> alone ( $16.6 \pm 1.8\%$  and  $4.4 \pm 1.5\%$  respectively). 1-40Gpa1-GFP-Ras1<sup>C216S</sup> was the only 1-40Gpa1-GFP-Ras1 fusion protein to display a significantly lower percentage membrane fluorescence than GFP-Ras1 ( $P = 0.05$ ).

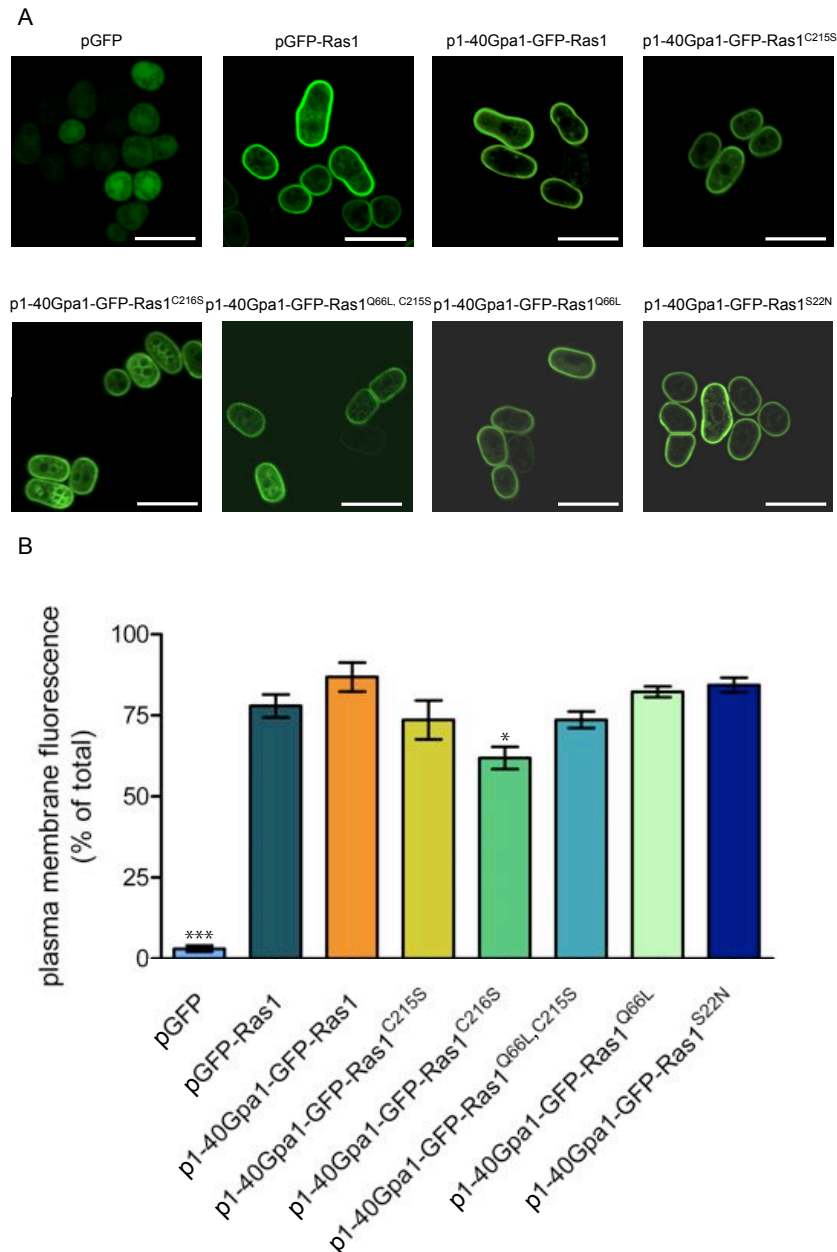


**Figure 6.12. Quantifying the localisation of 1-40Gpa1-GFP-Ras1 fusions using Quimp software**

Images of  $\Delta ras1$  cells (JY1279) expressing GFP, GFP-Ras1 and 1-40Gpa1-GFP-Ras1 fusions from pREP3x were obtained using a Leica SP5 scanning confocal microscope (A). The intensity of fluorescence at the periphery compared to the interior of the cell was determined using Quimp software (B). All 1-40Gpa1-GFP-Ras1 fusions displayed predominantly plasma membrane localisation. Data representative of 10 individual cells. Statistical significance was determined using a one-way anova with a Tukey multiple comparison post test. One asterisk indicates a P value of 0.05 and three asterisks indicates a P-value of 0.001. The scale bar represents 10  $\mu$ m.

The nucleotide binding and hydrolysis activity of Ras1 did not appear to affect the localisation of 1-40Gpa1-GFP-Ras1. 1-40Gpa1-GFP-Ras1<sup>Q66L</sup> and 1-40Gpa1-GFP-Ras1<sup>S22N</sup> both displayed levels of plasma membrane localisation comparable to GFP-Ras1 and 1-40Gpa1-GFP-Ras1. 1-40Gpa1-GFP-Ras1<sup>Q66L</sup> displayed a percentage plasma membrane fluorescence of  $82.3 \pm 1.7$  % and 1-40Gpa1-GFP-Ras1<sup>S22N</sup> gave a plasma membrane fluorescence of  $84.4 \pm 2.2$  %. 1-40Gpa1-GFP-Ras1<sup>Q66L, C215S</sup> exhibited a percentage plasma membrane fluorescence ( $73.7 \pm 2.6$  %) comparable to 1-40Gpa1-GFP-Ras1<sup>C215S</sup>.

### 6.3.3. Vector-borne 1-40Gpa1-GFP-Ras1 displays signalling in response to pheromone.

The localisation of 1-40Gpa1-GFP-Ras1 fusions was determined upon expression from pREP3x. The pheromone-responsive signalling of each fusion, expressed from the pREP3x vector in the  $\Delta ras1$  strain JY1279, was analysed to determine the functional activity of the fusions under these expression conditions.  $\beta$ -galactosidase activity and average cell volume were analysed following growth in a range of pheromone concentrations (1 nM to 100  $\mu$ M) in DMM lacking thiamine for 16 h. 1-40Gpa1-GFP-Ras1, 1-40Gpa1-GFP-Ras1<sup>C215S</sup> and 1-40Gpa1-GFP-Ras1<sup>C216S</sup> all supported signalling at a magnitude comparable to GFP-Ras1 in  $\beta$ -galactosidase assays (Figure 6.13A). 1-40Gpa1-GFP-Ras1 elicited a maximal signal of  $15.1 \pm 0.9$ , 1-40Gpa1-GFP-Ras1<sup>C215S</sup> a maximal signal of  $16.9 \pm 0.7$  and 1-40Gpa1-GFP-Ras1<sup>C216S</sup> a maximal signal of  $11.5 \pm 0.4$ , compared to  $12.9 \pm 0.5$  in cells expressing GFP-Ras1 from pREP3x. All strains also displayed an increase in cell volume in response to pheromone (1-40Gpa1-GFP-Ras1 =  $85.8 \pm 1.0$  fl to  $90.4 \pm 0.8$  fl, 1-40Gpa1-GFP-Ras1<sup>C215S</sup> =  $81.2 \pm 1.2$  fl to  $90.0 \pm 0.9$  fl and 1-40Gpa1-GFP-Ras1<sup>C216S</sup> =  $87.1 \pm 0.6$  fl to  $92.3 \pm 0.7$  fl ) (Figure 6.13B).

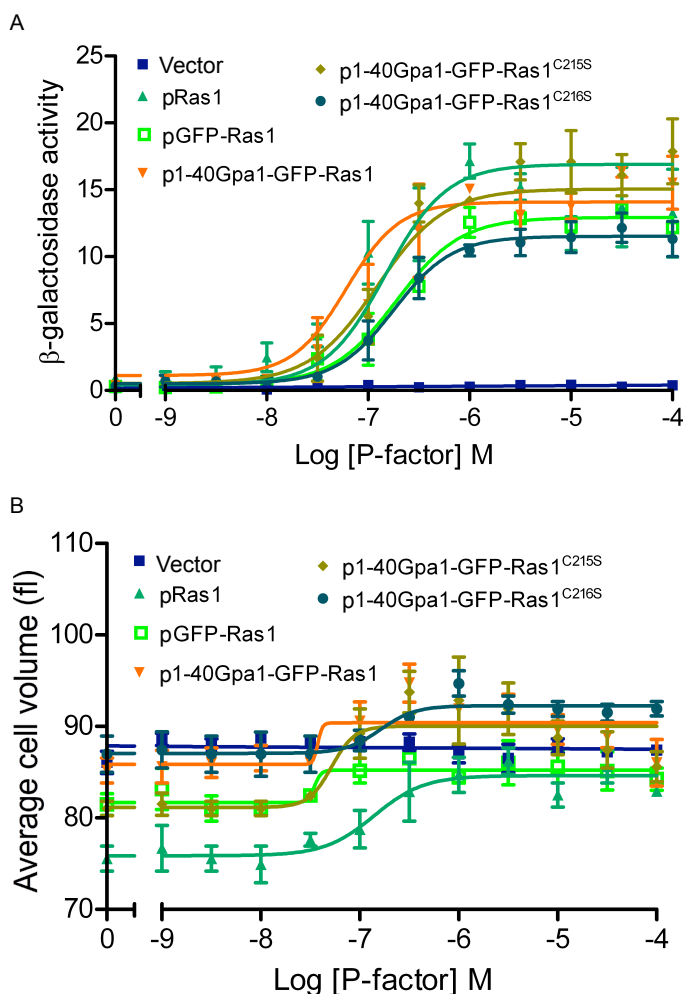


**Figure 6.13. Pheromone-dependent changes in transcription and cell volume in cells expressing 1-40Gpa1-GFP-Ras1 and 1-40Gpa1-GFP-Ras1 fusions with C-terminal modification defects from pREP3x**

Pheromone-responsive changes in transcription and cell volume were observed in  $\Delta ras1$  (JY1279) cells expressing 1-40Gpa1-GFP-Ras1 and 1-40Gpa1-GFP-Ras1 fusions containing C-terminal modification defects from pREP3x. Cells were grown in 1 nM to 100  $\mu$ M pheromone in DMM lacking thiamine for 16 h. Assays were then performed for  $\beta$ -galactosidase activity (A) and average cell volume (B). All 1-40Gpa1-GFP-Ras1 fusions supported  $\beta$ -galactosidase activity and cell volume changes in response to pheromone. Data shown is an average of three independent determinants ( $\pm$ SEM).

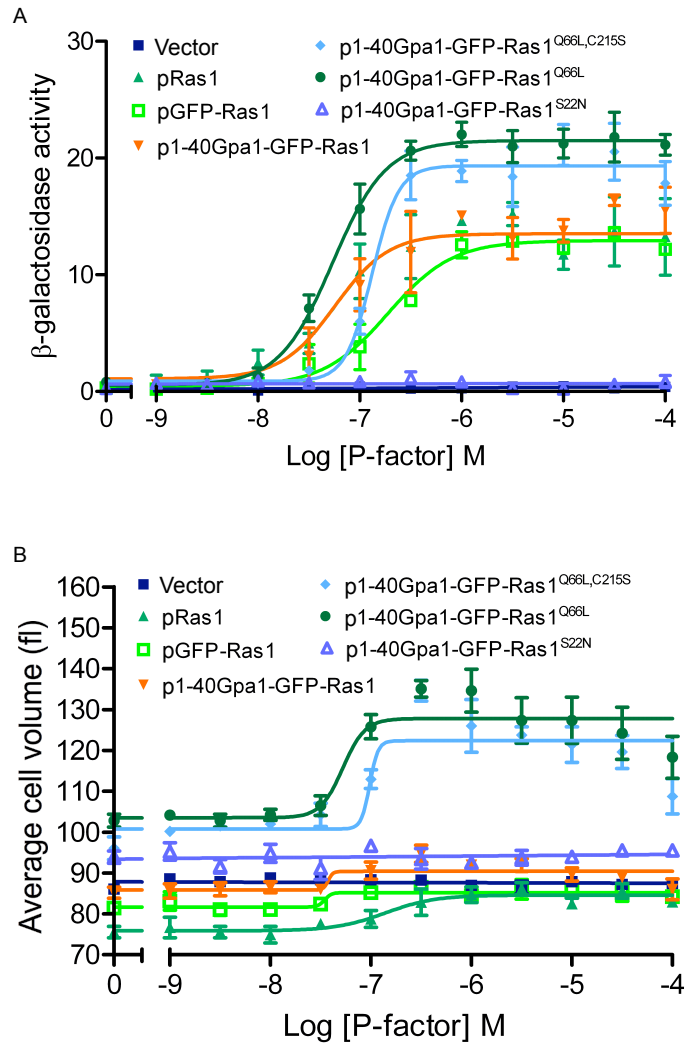


**Figure 6.14.** Pheromone-dependent changes in transcription and cell volume in cells expressing 1-40Gpa1-GFP-Ras1 and 1-40Gpa1-GFP-Ras1 fusions with altered nucleotide binding and hydrolysis from pREP3x

Pheromone-responsive changes in transcription and cell volume were observed in  $\Delta ras1$  (JY1279) cells expressing 1-40Gpa1-GFP-Ras1 and 1-40Gpa1-GFP-Ras1 fusions with altered nucleotide binding and hydrolysis from pREP3x. Cells were grown in 1 nM to 100  $\mu$ M pheromone in DMM lacking thiamine for 16 h. Assays were then performed for  $\beta$ -galactosidase activity (A) and average cell volume (B). 1-40Gpa1-GFP-Ras1<sup>Q66L, C215S</sup> and 1-40Gpa1-GFP-Ras1<sup>Q66L</sup> supported high levels of pheromone-dependent signalling. 1-40Gpa1-GFP-Ras1<sup>S22N</sup> displayed no pheromone-responsive signalling. Data shown is an average of three independent determinants ( $\pm$ SEM).

Cells expressing both 1-40Gpa1-GFP-Ras1<sup>Q66L, C215S</sup> and 1-40Gpa1-GFP-Ras1<sup>Q66L</sup> displayed a strong pheromone-dependent response in  $\beta$ -galactosidase assays (Figure 6.14A). The expression of 1-40Gpa1-GFP-Ras1<sup>Q66L, C215S</sup> from pREP3x gave a maximal response of  $19.3 \pm 0.6$  and expression of 1-40Gpa1-GFP-Ras1<sup>Q66L</sup> a maximal signal of  $21.5 \pm 0.5$ . Both populations also displayed a larger basal cell volume than cells expressing Ras1 or GFP-Ras1 from pREP3x, with cells expressing 1-40Gpa1-GFP-Ras1<sup>Q66L C215S</sup> displaying a basal cell volume of  $100.8 \pm 2.2$  fl and cells expressing 1-40Gpa1-GFP-Ras1<sup>Q66L</sup> displaying a basal cell volume of  $103.5 \pm 2.1$  fl. Both also displayed an increase in cell volume upon pheromone stimulation, with cells containing 1-40Gpa1-GFP-Ras1<sup>Q66L C215S</sup> reaching a volume of  $122.4 \pm 1.9$  fl and cells containing 1-40Gpa1-GFP-Ras1<sup>Q66L</sup> reaching a volume of  $127.8 \pm 1.7$  fl (Figure 6.14B). 1-40Gpa1-GFP-Ras1<sup>S22N</sup> displayed no pheromone-dependent signalling.

#### 6.3.4. Addition of the first 40 amino acids of Gpa1 to GFP-Ras1<sup>C215S</sup> and GFP-Ras1<sup>C216S</sup> increases signalling through Scd1.

The first 40 amino acids of Gpa1 did not cause a significant change in the levels of GFP-Ras1, GFP-Ras1<sup>Q66L</sup> and GFP-Ras1<sup>S22N</sup> at the plasma membrane. As such, it would be expected that these fusions would not display significantly altered function. In order to determine whether any change in activity could be observed, the morphology of cells expressing these fusions was analysed using quantitative imaging. Images of cells expressing 1-40Gpa1-GFP-Ras1<sup>Q66L</sup> and 1-40Gpa1-GFP-Ras1<sup>S22N</sup> from the *ras1* locus grown in DMM lacking thiamine, and expressing GFP from pREP3x, were obtained using a Leica SP5 scanning confocal microscope. The circularity of 30 cells of each strain was then determined using Quimp software. No significant difference in cell morphology (Figure 6.15) or percentage circularity (Figure 6.16) was observed in cells expressing these GFP-tagged Ras1 proteins upon addition of 1-40Gpa1 (GFP-

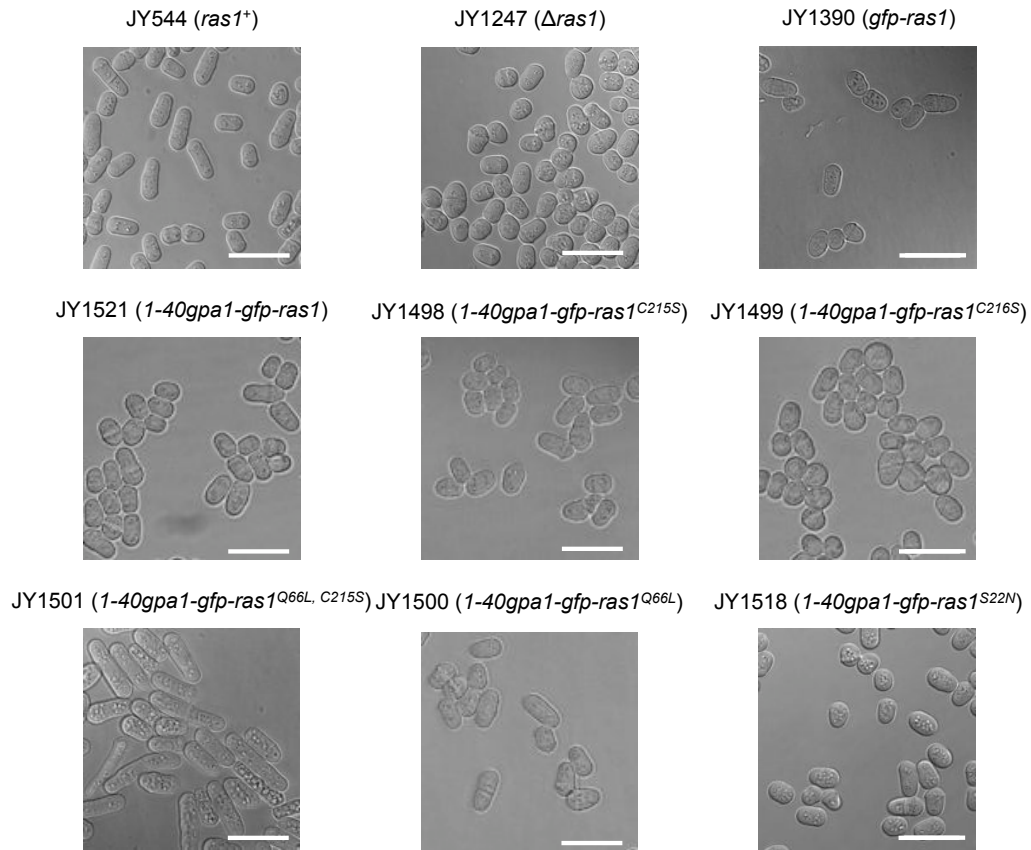


**Figure 6.15. The morphology of cells expressing 1-40Gpa1-GFP-Ras1 fusions from the endogenous *ras1* locus**

Images of populations of *ras1*<sup>+</sup> (JY544) cells,  $\Delta$ *ras1* (JY1279) cells, *gfp-ras1* (JY1390) cells, and cells expressing 1-40Gpa1-GFP-Ras1 fusions from the endogenous *ras1* locus were obtained using a Leica SP5 scanning confocal microscope. With the exception of cells expressing 1-40Gpa1-GFP-Ras1<sup>S22N</sup> and 1-40Gpa1-GFP-Ras1<sup>C216S</sup>, the majority of strains containing 1-40Gpa1-GFP-Ras1 fusions display polar cell morphology. The scale bar represents 10  $\mu$ m.

Ras1 =  $78.3 \pm 1.1$  %, 1-40Gpa1-GFP-Ras1 =  $79.4 \pm 1.0$  %, GFP-Ras1<sup>Q66L</sup> =  $78.2 \pm 1.2$  % 1-40Gpa1-GFP-Ras1<sup>Q66L</sup> =  $77.3 \pm 1.4$  %, GFP-Ras1<sup>S22N</sup> =  $94.9 \pm 0.4$  % and 1-40Gpa1-GFP-Ras1<sup>S22N</sup> =  $92.1 \pm 1.0$  %).

The same analysis of morphology was also performed for all other 1-40Gpa1-GFP-Ras1 fusions. The addition of 1-40Gpa1 had the greatest effect upon mutants which alone displayed low levels of plasma membrane localisation. GFP-Ras1<sup>C215S</sup> displayed a significantly rounded morphology, exhibiting a percentage circularity of  $92.6 \pm 0.6$  %. The addition of 1-40Gpa1 caused a reduction in percentage circularity to  $81.4 \pm 1.2$  %, a figure significantly lower

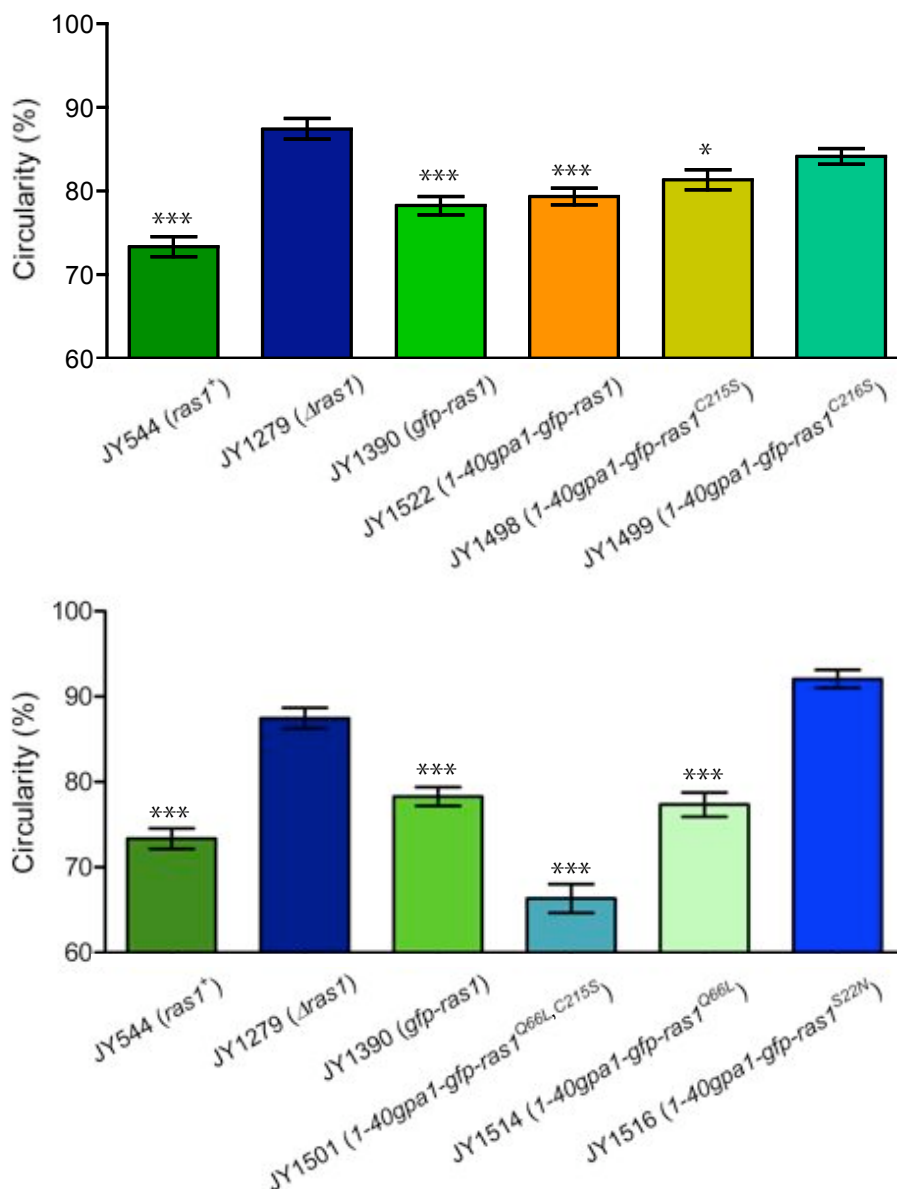


**Figure 6.16. Quantification of the morphology of cells expressing 1-40Gpa1-GFP-Ras1 fusions from the endogenous *ras1* locus**

Cell circularity was determined in populations of *ras1*<sup>+</sup> (JY544) cells,  $\Delta$ *ras1* (JY1279) cells, *gfp-ras1* (JY1390) cells, and cells expressing 1-40Gpa1-GFP-Ras1 fusions from the endogenous *ras1* locus. All strains were expressing GFP from pREP3x following growth in DMM lacking thiamine, and analysis of morphology was performed using Quimp software. Cells expressing 1-40Gpa1-GFP-Ras1 fusions containing C-terminal modification mutants (A) and mutants displaying altered nucleotide binding and hydrolysis phenotypes (B) were analysed. All fusions except 1-40Gpa1-GFP-Ras1<sup>C216S</sup> and 1-40Gpa1-GFP-Ras1<sup>S22N</sup> displayed a percentage circularity significantly lower than cells lacking Ras1. Data representative of 30 individual cells  $\pm$  SEM. Statistical significance was determined using a one-way anova with a Tukey multiple comparison post test. One asterisk indicates a P-value of 0.05 and three asterisks indicates a P-value of 0.001.

than that seen in cells lacking Ras1 ( $P = 0.05$ ). Cells expressing 1-40Gpa1-GFP-Ras1<sup>C215S</sup> also appeared more elongated (Figure 6.15). GFP-Ras1<sup>C216S</sup> also displayed a reduction in percentage circularity from  $94.3 \pm 0.4$  % to  $84.2 \pm 1.0$  % upon addition of the first 40 amino acids of Gpa1. The addition of 1-40Gpa1 to GFP-Ras1<sup>Q66L, C215S</sup> caused the largest reduction in percentage circularity, falling from  $90.3 \pm 0.7$  % to  $66.3 \pm 1.7$  % (Figure 6.16), with these cells exhibiting a marked hyper-elongated morphology (Figure 6.15).

As an additional measure of Ras1 activity through Scd1-Cdc42, the localisation of Tea1-mCherry in strains expressing 1-40Gpa1-GFP-Ras1 fusions from the *ras1* locus was determined using a Nikon E800 epifluorescence microscope fitted with an Andor EM-CCD camera. Images of each strain indicated that all, with the exception of the inactive mutant 1-40Gpa1-GFP-Ras1<sup>S22N</sup>, displayed a degree of polar Tea1-mCherry localisation in most cells (Figure 6.17). This observation is most notable in strains expressing 1-40Gpa1-GFP-Ras1<sup>C215S</sup>, as Ras1<sup>C215S</sup> supported little polar Tea1 localisation, and strains expressing 1-40Gpa1-GFP-Ras1<sup>C216S</sup>, as cells expressing Ras1<sup>C216S</sup> alone displayed no clear tip localisation of Tea1-mCherry (Figure 5.10). These data, in addition to those presented in Figures 6.15 and 6.16, indicate that promoting the association of Ras1<sup>C215S</sup> and Ras1<sup>C216S</sup> with the plasma membrane, through an additional plasma membrane targetting domain, restores some signalling through Scd1-Cdc42. This observation again indicates that plasma membrane localisation of Ras1 is important for the maintenance of polar cell morphology in addition to pheromone-dependent signalling.

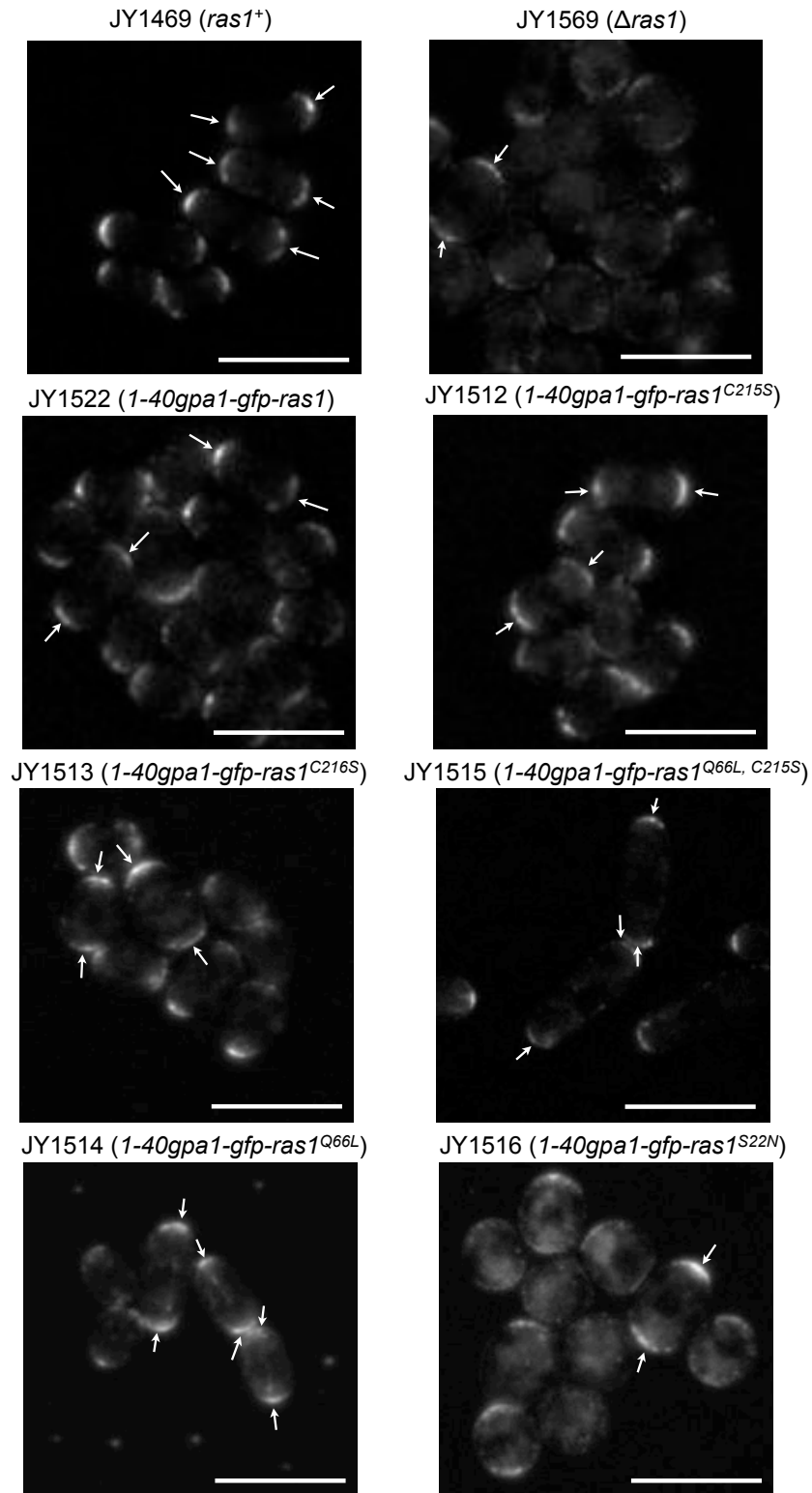


**Figure 6.17.** Analysis of Tea1-mCherry localisation in cells expressing 1-40Gpa1-GFP-Ras1 fusions

The localisation of Tea1-mCherry was determined in *ras1*<sup>+</sup> (JY1469) cells,  $\Delta$ *ras1* (JY1569) cells and cells expressing 1-40Gpa1-GFP-Ras1 fusions using a Nikon E800 epifluorescence microscope fitted with an Andor EM-CCD camera. Arrows indicate the tip localisation of Tea1-mCherry. All fusions except 1-40Gpa1-GFP-Ras1<sup>S22N</sup> displayed polar Tea1-mCherry localisation in the majority of cells imaged. The scale bar represents 10  $\mu$ m.

### 6.3.5. Addition of the first 40 amino acids of Gpa1 to GFP-Ras1 increases pheromone-dependent signalling.

6.3.5.1. *The analysis of  $\beta$ -galactosidase activity and cell volume in cells expressing 1-40Gpa1-GFP-Ras1 fusions.* Addition of 1-40Gpa1 to GFP-Ras1 fusion proteins would be expected to increase signalling in response to pheromone, as all indications suggest this process is regulated at the plasma membrane (Bauman *et al.* 1998; Onken *et al.* 2006). In order to test this assertion, pheromone-dependent signalling was determined using assays for  $\beta$ -galactosidase activity and average cell volume, following growth in a range of pheromone concentrations (1 nM to 100  $\mu$ M) in DMM for 16 h. Analysis of  $\beta$ -galactosidase activity in response to pheromone indicated that cells expressing 1-40Gpa1-GFP-Ras1 displayed a slightly higher maximal signal ( $6.2 \pm 0.3$ ) than cell expressing GFP-Ras1 alone ( $5.4 \pm 0.3$ ) (Figure 6.18A). GFP-Ras1 however displays reduced maximal signalling compared to wild-type Ras1 (Figure 4.24). 1-40Gpa1-GFP-Ras1<sup>C215S</sup> exhibited a maximal signal slightly below that of GFP-Ras1 ( $4.7 \pm 0.2$ ), but markedly higher than that of GFP-Ras1<sup>C215S</sup> alone ( $2.4 \pm 0.3$ ) (Figure 5.16). Cells expressing 1-40Gpa1-GFP-Ras1<sup>C216S</sup> also displayed  $\beta$ -galactosidase activity in response to pheromone, giving a maximal signal of  $2.6 \pm 0.2$  (Figure 6.18A), whereas no pheromone-dependent signalling was observed in strains expressing GFP-Ras1<sup>C216S</sup> (Figure 5.16). Cells expressing 1-40Gpa1-GFP-Ras1 displayed a slight pheromone-responsive increase in cell volume, with the 1-40Gpa1-GFP-Ras1 strain exhibiting an increase from  $70.0 \pm 0.7$  fl to  $74.1 \pm 1.2$  fl. 1-40Gpa1-GFP-Ras1<sup>C215S</sup> and 1-40Gpa1-GFP-Ras1<sup>C216S</sup> did not support an increase in cell volume (Figure 6.18B).

The activity of 1-40Gpa1-GFP-Ras1 mutants displaying altered nucleotide binding and hydrolysis properties was also determined through analysis of  $\beta$ -galactosidase activity and cell volume. As with all previous Ras1 proteins containing the Ser22Asn mutation, 1-40Gpa1-GFP-Ras1<sup>S22N</sup> displayed no significant pheromone dependent signalling. 1-40Gpa1-GFP-Ras1<sup>Q66L</sup>, <sup>C215S</sup> and 1-40Gpa1-GFP-Ras1<sup>Q66L</sup> however, displayed strong pheromone-dependent sig-

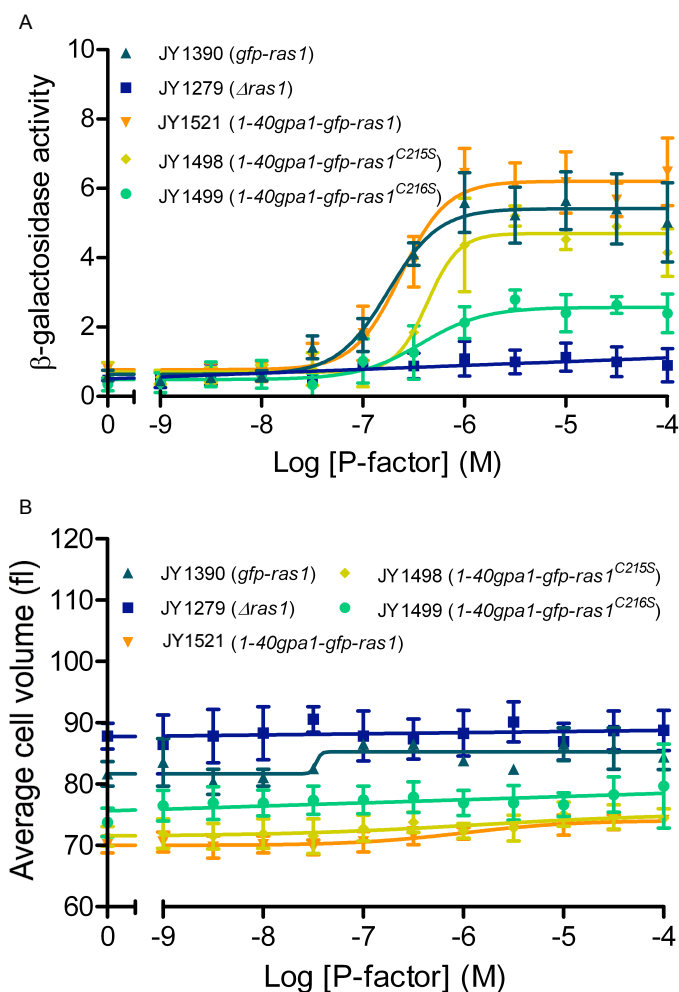


**Figure 6.18. Pheromone-dependent changes in transcription and cell volume in cells expressing 1-40Gpa1-GFP-Ras1 and 1-40Gpa1-GFP-Ras1 fusions with C-terminal modification defects**

Pheromone-responsive changes in transcription and cell volume were observed in *gfp-ras1* (JY1390) cells,  $\Delta$ *ras1* (JY1279) cells and cells expressing 1-40Gpa1-GFP-Ras1 fusions from the *ras1* locus. Cells were grown in 1 nM to 100  $\mu$ M pheromone in DMM for 16 h. Assays were then performed for  $\beta$ -galactosidase activity (A) and average cell volume (B). All 1-40Gpa1-GFP-Ras1 fusions displayed pheromone-responsive  $\beta$ -galactosidase activity. Data shown is an average of three independent determinants ( $\pm$ SEM).

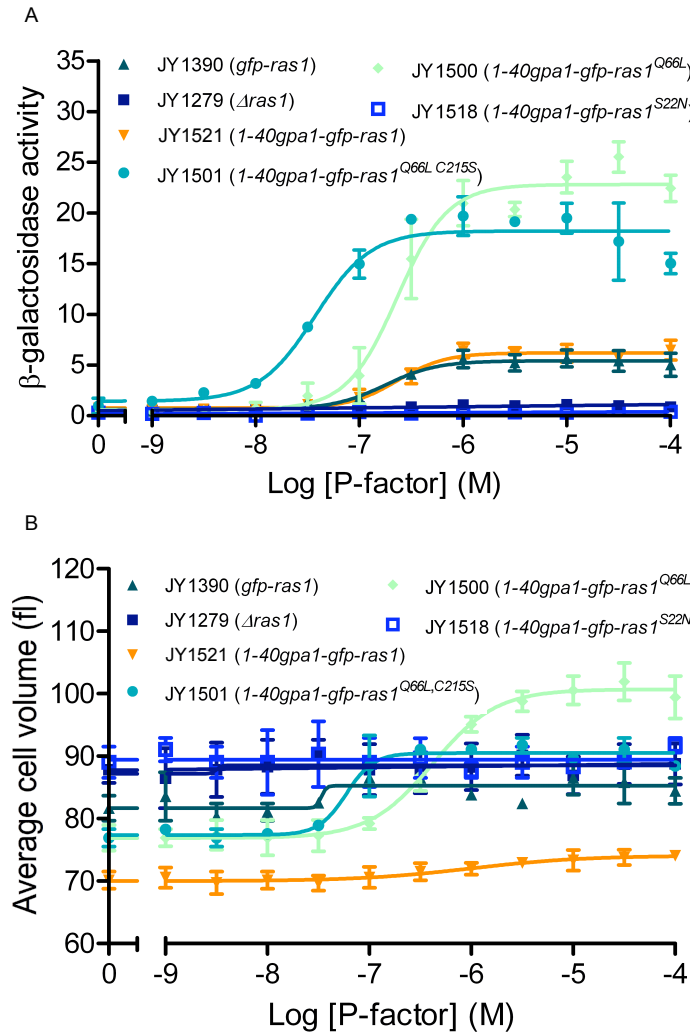


**Figure 6.19. Pheromone-dependent changes in transcription and cell volume in cells expressing 1-40Gpa1-GFP-Ras1 and 1-40Gpa1-GFP-Ras1 fusions with altered nucleotide binding and hydrolysis**

Pheromone-responsive changes in transcription and cell volume were observed in *gfp-ras1* (JY1390) cells,  $\Delta ras1$  (JY1279) cells and cells expressing 1-40Gpa1-GFP-Ras1 fusions from the *ras1* locus. Cells were grown in 1 nM to 100  $\mu$ M pheromone in DMM for 16 h. Assays were then performed for  $\beta$ -galactosidase activity (A) and average cell volume (B). 1-40Gpa1-GFP-Ras1<sup>Q66L C215S</sup> and 1-40Gpa1-GFP-Ras1<sup>Q66L</sup> displayed elevated pheromone-responsive  $\beta$ -galactosidase activity and cell volume changes. 1-40Gpa1-GFP-Ras1<sup>S22N</sup> exhibited little signalling. Data shown is an average of three independent determinants ( $\pm$ SEM).

nalling. Cells expressing 1-40Gpa1-GFP-Ras1<sup>Q66L, C215S</sup> exhibited a maximal signal of  $18.2 \pm 0.7$  in  $\beta$ -galactosidase assays, higher than GFP-Ras1<sup>Q66L, C215S</sup> alone (Figure 5.28). This strain also demonstrated a greater sensitivity to pheromone, giving a pEC<sub>50</sub> of  $7.4 \pm 0.1$  compared to  $6.7 \pm 0.1$  in cells expressing GFP-Ras1 (Figure 6.19A). Cells expressing 1-40Gpa1-GFP-Ras1<sup>Q66L</sup> gave a maximal signal of  $22.8 \pm 0.8$  in  $\beta$ -galactosidase assays. Both strains displayed an increase in cell volume in response to pheromone, with the 1-40Gpa1-GFP-Ras1<sup>Q66L C215S</sup> strain showing an increase from  $77.4 \pm 0.8$  fl to  $90.5 \pm 0.6$  fl, and the 1-40Gpa1-GFP-Ras1<sup>Q66L</sup> strain showing an increase from  $76.9 \pm 0.9$  fl to  $100.7 \pm 1.2$  fl (Figure 6.19B).

6.3.5.2. *The analysis of cell elongation in cells expressing 1-40Gpa1-GFP-Ras1 fusions.* The majority of 1-40Gpa1-GFP-Ras1 fusions displayed only a small increase in cell volume in response to pheromone. Cell length, however, provides a more direct measure of shmoo formation. Cell elongation in response to pheromone was determined in these strains using quantitative image analysis. Images of each strain, expressing GFP from pREP3x, were obtained using a Leica SP5 scanning confocal microscope, following 16 h incubation in the absence and in the presence of 10  $\mu$ M pheromone (Figure 6.20). Quimp software was then used to determine the length of 30 cells of each strain under each assay condition. 1-40Gpa1-GFP-Ras1 displayed a significant increase in cell length in response to pheromone ( $50.0 \pm 1.4$  pixels to  $59.9 \pm 2.2$  pixels,  $P = 0.05$ ) (Figure 6.21A). Of the other five 1-40Gpa1-GFP-Ras1 fusions 1-40Gpa1-GFP-Ras1<sup>Q66L</sup> was the only mutant which displayed a significant increase in cell length ( $64.0 \pm 1.9$  pixels to  $103.0 \pm 5.0$  pixels,  $P = 0.05$ ). 1-40Gpa1-GFP-Ras1<sup>Q66L, C215S</sup> displayed a hyper-elongated morphology in the absence of pheromone ( $82.5 \pm 3.7$  pixels) (Figure 6.21B).

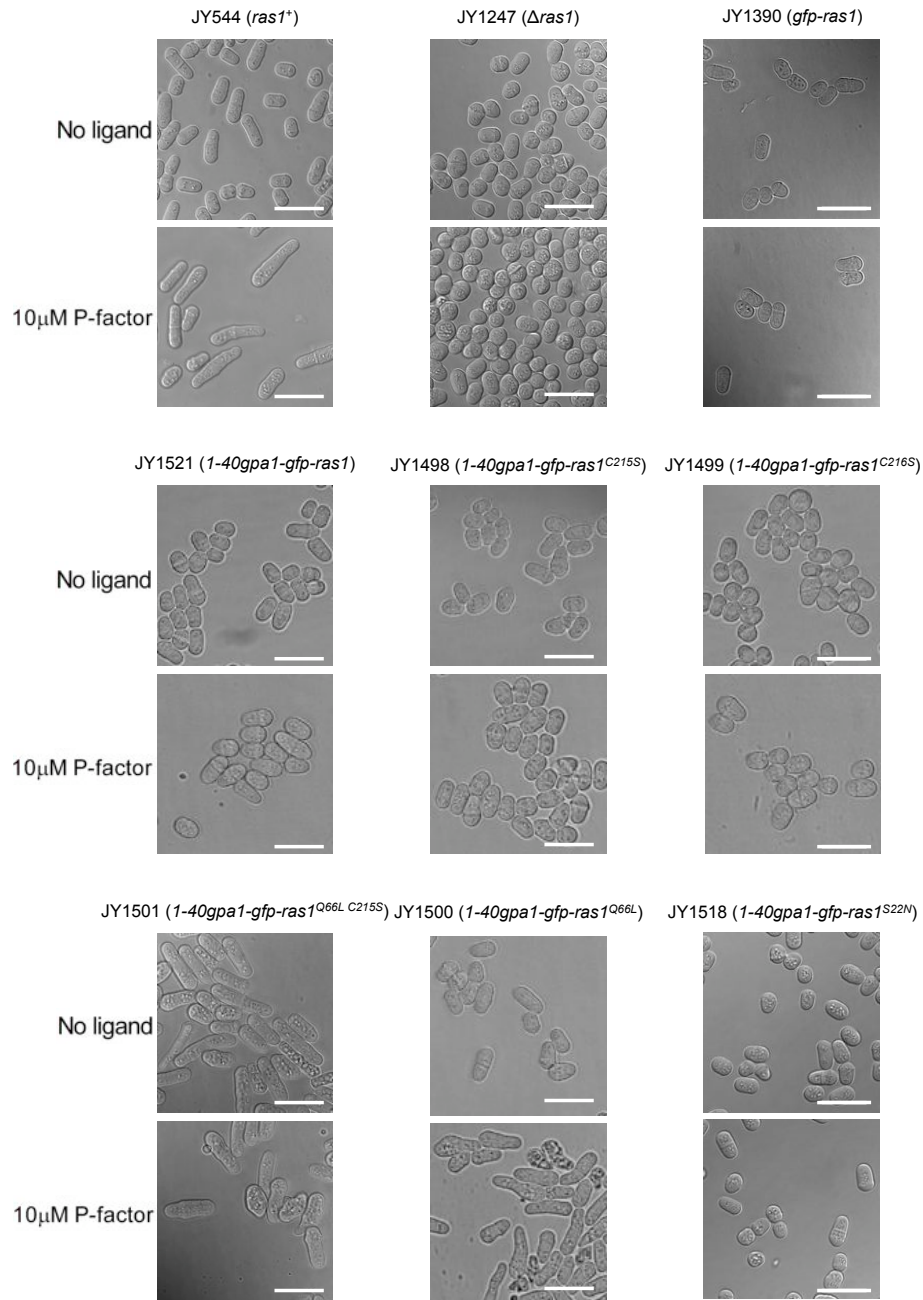


**Figure 6.20. The morphology of cells expressing 1-40Gpa1-GFP-Ras1 fusions in the absence and presence of pheromone**

DIC images of cells expressing 1-40Gpa1-GFP-Ras1 fusions from the *ras1* locus were obtained using a Leica SP5 scanning confocal microscope, following growth in the absence and in the presence of 10  $\mu$ M pheromone in DMM lacking thiamine for 16 h. Only the strain containing 1-40Gpa1-GFP-Ras1<sup>Q66L</sup> displayed marked morphological changes in response to pheromone. The scale bar represents 10  $\mu$ m.

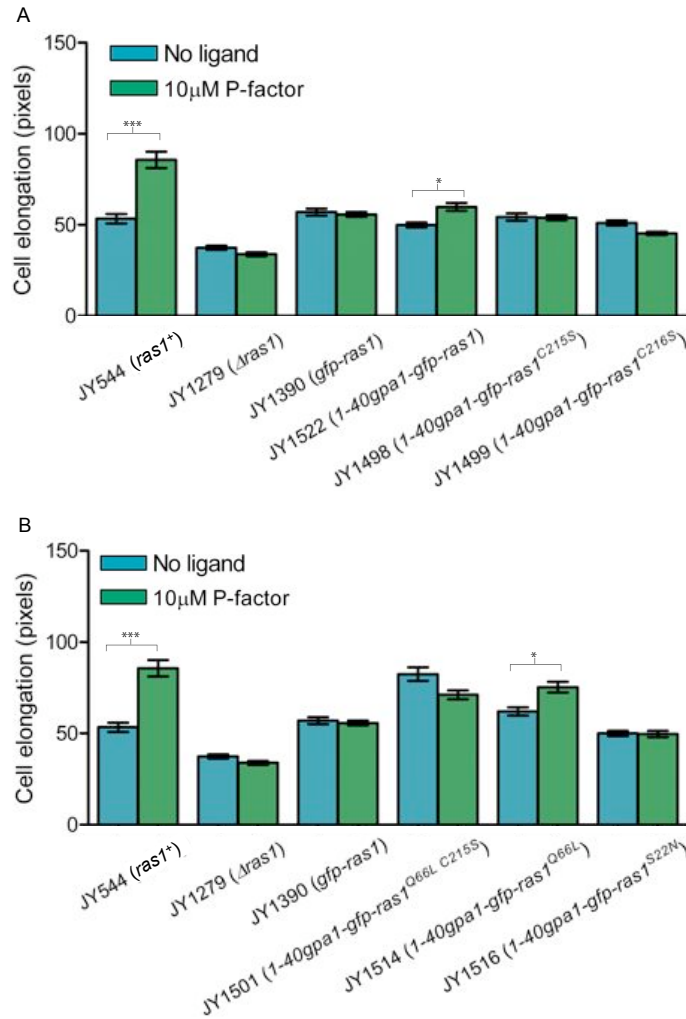


**Figure 6.21. Analysis of shmoo formation in cells expressing 1-40Gpa1-GFP-Ras1 fusions using quantitative imaging**

Quimp software was used to determine the length of cells expressing 1-40Gpa1-GFP-Ras1 fusions, following growth in the absence and in the presence of 10  $\mu$ M pheromone in DMM lacking thiamine for 16 h. 1-40Gpa1-GFP-Ras1 and 1-40Gpa1-GFP-Ras1<sup>Q66L</sup> supported a significant pheromone-dependent increase in cell length ( $P = 0.05$ ). Data shown is representative of 30 individual cells  $\pm$  SEM. Statistical significance was determined using a one-way anova with a Tukey multiple comparison post test. One asterisk indicates a P value of 0.05 and three asterisks indicates a P-value of 0.001.

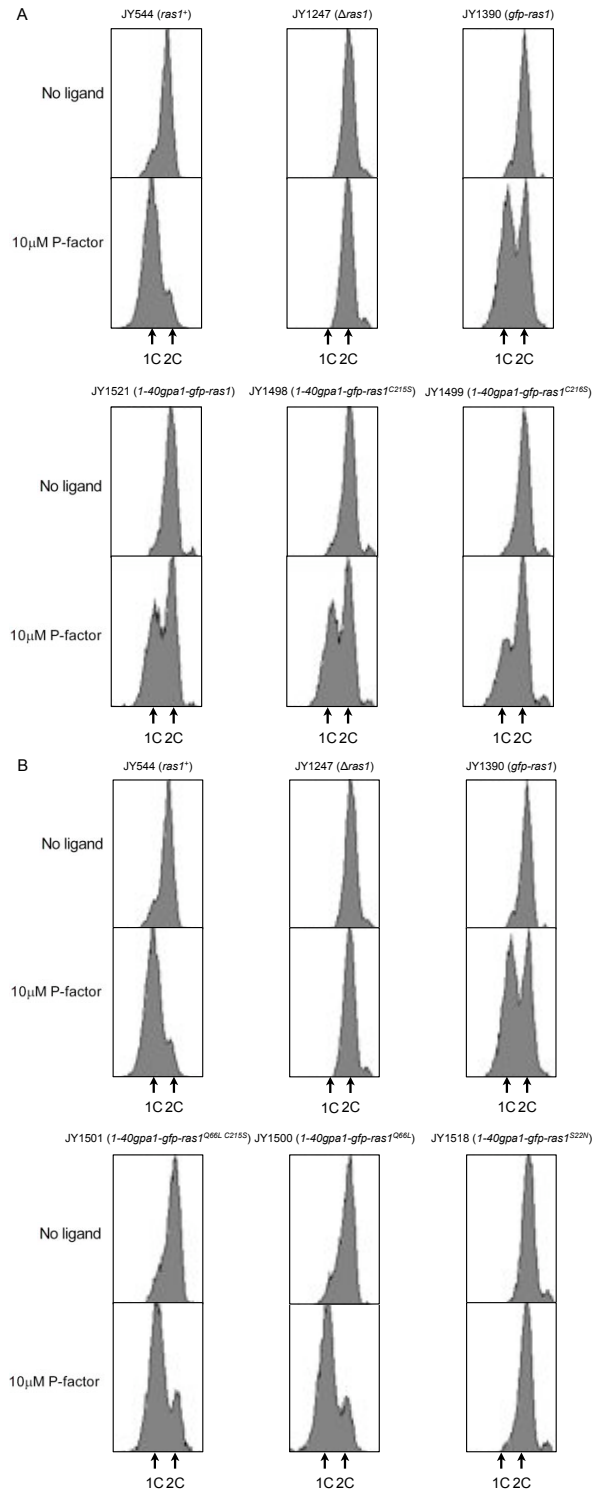


**Figure 6.22. Flow cytometric analysis of cell cycle position in cells expressing 1-40Gpa1-GFP-Ras1 fusions**

Cell cycle arrest was analysed in *ras1*<sup>+</sup> (JY544) cells,  $\Delta$ *ras1* (JY1279) cells, *gfp-ras1* (JY1390) cells and cells expressing 1-40Gpa1-GFP-Ras1, fusions containing C-terminal modification defects (A) and fusions with altered nucleotide binding and hydrolysis (B), using propidium iodide staining and flow cytometry. Analysis was performed following growth in the presence (10  $\mu$ M P-factor) and absence of pheromone in DMM for 6 h. Flow cytometric analysis allowed the distinction between cells containing a single complement (1C) and double complement (2C) of DNA. 1-40Gpa1-GFP-Ras1<sup>S22N</sup> was the only fusion not to support a marked increase in cells containing a single complement of genomic DNA. Analysis was performed for 30000 cells.

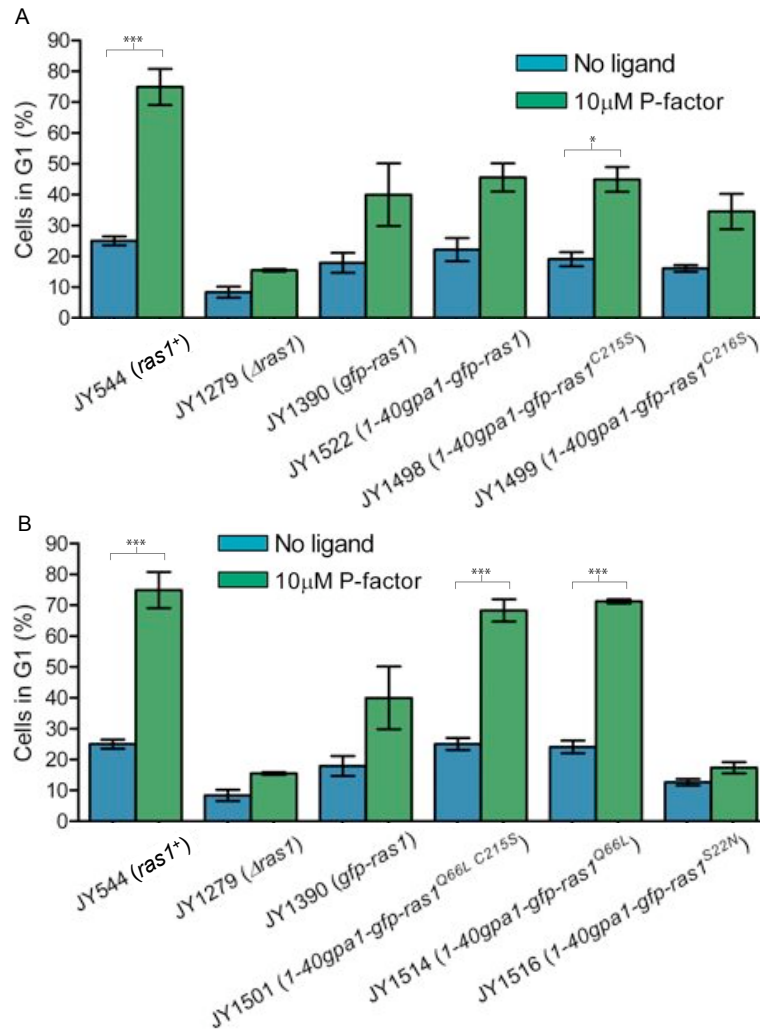


**Figure 6.23. Pheromone-responsive changes in cell cycle position in cells expressing 1-40Gpa1-GFP-Ras1 fusions**

Cell cycle arrest was analysed in *ras1<sup>+</sup>* (JY544) cells,  $\Delta$ *ras1* (JY1279) cells, *gfp-ras1* (JY1390) cells and cells expressing 1-40Gpa1-GFP-Ras1, fusions containing C-terminal modification defects (A) and fusions with altered nucleotide binding and hydrolysis (B) using propidium iodide staining and flow cytometry. Analysis was performed following growth in the presence (10  $\mu$ M P-factor) and absence of pheromone in DMM for 6 h. Most fusions exhibited some pheromone-dependent G<sub>1</sub> arrest. 1-40Gpa1-GFP-Ras1<sup>C215S</sup>, 1-40Gpa1-GFP-Ras1<sup>Q66L C215S</sup> and 1-40Gpa1-GFP-Ras1<sup>Q66L</sup> supported a significant increase in cells in G<sub>1</sub> in response to pheromone (P = 0.05, 0.001 and 0.001 respectively). Data shown representative of three independent determinants  $\pm$  SEM. Analysis was performed for 30000 cells. Statistical significance was determined using a one-way anova with a Tukey multiple comparison post test. One asterisk indicates a P value of 0.05 and three asterisks indicates a P-value of 0.001.

Images of these strains following stimulation only reveal marked shmoo formation in cells expressing 1-40Gpa1-GFP-Ras1<sup>Q66L</sup> (Figure 6.20). As suggested in Figure 6.16, cells expressing 1-40Gpa1-GFP-Ras1<sup>Q66L, C215S</sup> exhibit a marked hyper-elongated morphology.

6.3.5.3. *The analysis of cell cycle arrest in cells expressing 1-40Gpa1-GFP-Ras1 fusions.* Cell cycle arrest provides an additional, sensitive measure of Ras1 signalling following pheromone stimulation. Cell cycle position was analysed in strains expressing 1-40Gpa1-GFP-Ras1 fusions from the endogenous *ras1* locus following growth in the presence (10  $\mu$ M P-factor) and absence of pheromone in DMM for 6 h, using propidium iodide staining and flow cytometry (Figure 6.22). Analysis was performed for 30000 cells. Most fusion proteins supported an increase in the percentage of cells in G<sub>1</sub> upon stimulation with pheromone. 1-40Gpa1-GFP-Ras1 ( $22.2 \pm 3.8$  % to  $45.6 \pm 4.6$  %) and 1-40Gpa1-GFP-Ras1<sup>C216S</sup> ( $16.1 \pm 1.1$  % to  $34.5 \pm 5.8$  %) supported some pheromone dependent increase in G<sub>1</sub> arrest in response to pheromone. Cells expressing Ras1<sup>C216S</sup> alone displayed no discernible pheromone-dependent G<sub>1</sub> arrest (Figure 5.14). Strains containing 1-40Gpa1-GFP-Ras1<sup>C215S</sup> ( $19.1 \pm 2.3$  % to  $44.9 \pm 4.0$  %), 1-40Gpa1-GFP-Ras1<sup>Q66L, C215S</sup> ( $25.0 \pm 2.0$  % to  $68.3 \pm 3.6$  %) and 1-40Gpa1-GFP-Ras1<sup>Q66L</sup> ( $24.1 \pm 2.1$  % to  $71.2 \pm 0.7$  %) all displayed a significant increase in the number of cells in G<sub>1</sub> following incubation with pheromone (P = 0.05, 0.001 and 0.001 respectively) (Figure 6.23). Ras1<sup>C215S</sup> alone did not support a significant increase in G<sub>1</sub> arrest upon stimulation with pheromone (Figure 5.14). All these strains displayed a marked increase in cells containing a single complement (1C) of chromosomal DNA following pheromone stimulation (Figure 6.22). Cells expressing 1-40Gpa1-GFP-Ras1<sup>S22N</sup> exhibited a slight increase in G<sub>1</sub> arrest in response to pheromone ( $12.7 \pm 1.1$  % to  $17.3 \pm 1.8$  %), however this was not significant.

These data again indicate that increasing the levels of Ras1 at the plasma membrane promotes signalling in response to pheromone.

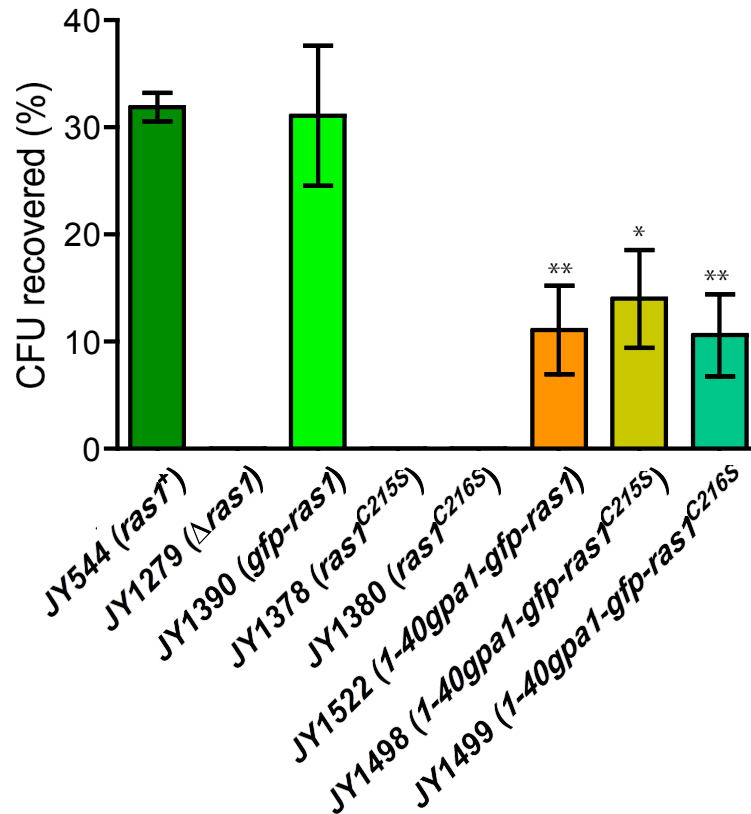


**Figure 6.24.** Quantitative analysis of mating efficiency in cells expressing 1-40Gpa1-GFP-Ras1, 1-40Gpa1-GFP-Ras1<sup>C215S</sup> and 1-40Gpa1-GFP-Ras1<sup>C216S</sup>

The mating of *ras1*<sup>+</sup> (JY544) cells,  $\Delta$ *ras1* (JY1279) cells, *gfp-ras1* (JY1390) cells and cells containing Ras1<sup>C215S</sup>, Ras1<sup>C216S</sup>, 1-40Gpa1-GFP-Ras1, 1-40Gpa1-GFP-Ras1<sup>C215S</sup> and 1-40Gpa1-GFP-Ras1<sup>C216S</sup>, expressing Sxa2 from pREP41x, was assessed using the quantitative mating assay detailed in section 4.2.1. All three 1-40Gpa1-GFP-Ras1 fusions supported mating. Data shown representative of three independent determinants  $\pm$  SEM. Statistical significance was determined using a one-way anova with a Tukey multiple comparison post test. Two asterisks indicates a P-value of 0.01. One asterisk indicates a P-value of 0.05.

### 6.3.6. Expression of 1-40Gpa1-GFP-Ras1, 1-40Gpa1-GFP-Ras1<sup>C215S</sup> and 1-40Gpa1-GFP-Ras1<sup>C216S</sup> rescues mating.

Cells containing 1-40Gpa1-GFP-Ras1, 1-40Gpa1-GFP-Ras1<sup>C215S</sup> and 1-40Gpa1-GFP-Ras1<sup>C216S</sup> all displayed significant pheromone-dependent signalling. To determine whether these strains could also mate, JY1522 (*1-40gpa1-gfp-ras1*), JY1498 (*1-40gpa1-gfp-ras1<sup>C215S</sup>*) and JY1499 (*1-40gpa1-gfp-ras1<sup>C216S</sup>*), expressing Sxa2 from pREP41x, were incubated with wild-type P-cells (JY1025), and a quantitative mating assay was performed, as detailed in section 4.2.1 (Figure 6.24). Mating was observed in all three strains, albeit at a lower level than was observed in cells expressing wild-type Ras1. JY1522 (*1-40gpa1-gfp-ras1*) displayed a cfu recovery of  $11.12 \pm 4.12$  %, JY1498 (*1-40gpa1-gfp-ras1<sup>C215S</sup>*) a recovery of  $17.10 \pm 4.48$  % and JY1499 (*1-40gpa1-gfp-ras1<sup>C216S</sup>*) of  $16.57 \pm 6.53$  %. These were the only 1-40Gpa1-GFP-Ras1 fusions to support mating. The Ras1<sup>C215S</sup> and Ras1<sup>C216S</sup> mutants alone did not support mating, again indicating that increasing the level of these Ras1 mutants at the plasma membrane promotes pheromone-responsive signalling.

## 6.4. Summary

The results detailed in chapter 5 discussed the role of Ras1 C-terminal modification in signalling activity and localisation. These results suggested that the localisation of Ras1 to the plasma membrane was key to both pheromone-dependent signalling and polar cell morphology. In order to further investigate this finding, in the preceding chapter a number of chimeric Ras1 proteins were characterised which displayed increased plasma membrane avidity. The first chimeric Ras1 protein utilised was the Ras1-RitC fusion, which has been used previously to investigate Ras1 signalling from the plasma membrane (Onken *et al.* 2006). In this study it was suggested that Ras1-RitC localised solely to the plasma membrane and was only able to propagate signalling in response to pheromone. In the data presented in section 6.2 it is indicated that Ras1-RitC

displays predominantly plasma membrane localisation, but also substantial cytosolic and nuclear localisation. In addition, functional assays indicated that Ras1-RitC displayed signalling through both Byr2 in response to pheromone and Scd1 in maintaining polar cell morphology, although this activity was reduced in both cases compared to wild-type Ras1. It was also suggested in Onken *et al.* 2006 that Ras1-RitC was able to rescue mating. In this present study however, it was found that mating occurred at a very low efficiency in cells expressing Ras1-RitC.

Ras1-RitC did not display specific plasma membrane localisation, and only exhibited partial activity in all assays for Ras1 function. Due to the limitations of the Ras1-RitC fusion, a different approach to increasing the plasma membrane localisation of Ras1 was adopted. Section 6.3 details the use of the N-terminal plasma membrane targeting domain of Gpa1 to increase Ras1 plasma membrane localisation, adding a myristoyl and palmitoyl group to N-terminus of the protein. The first 40 amino acids of Gpa1 were fused to GFP-Ras1, GFP-Ras1<sup>C215S</sup>, GFP-Ras1<sup>C216S</sup>, GFP-Ras1<sup>Q66L C215S</sup>, GFP-Ras1<sup>Q66L</sup> and GFP-Ras1<sup>S22N</sup>, and their activity and localisation was investigated. All displayed a high degree of plasma membrane localisation, however in most instances little difference was observed in function compared to the equivalent proteins lacking 1-40Gpa1. The most significant effect was observed upon fusions containing the palmitoylation deficient mutant Ras1<sup>C215S</sup> and the palmitoylation/farnesylation deficient mutant Ras1<sup>C216S</sup>. Both displayed a significant increase in plasma membrane localisation upon addition of the first 40 amino acids of Gpa1. 1-40Gpa1-GFP-Ras1<sup>C215S</sup> supported increased pheromone-responsive signalling, statistically significant polar cell morphology, polar Tea1 localisation and mating. In contrast, Ras1<sup>C215S</sup> alone was unable to rescue polar cell morphology or mating. 1-40Gpa1-GFP-Ras1<sup>C216S</sup> supported pheromone-responsive signalling, a reduced cell circularity compared to Ras1<sup>C216S</sup> alone, some polar Tea1 localisation and mating. Ras1<sup>C216S</sup> was previously unable to propagate any signalling when expressed from the *ras1*

locus. These data again highlight the importance of plasma membrane localisation in Ras1 signalling, as shifting the localisation of Ras1<sup>C215S</sup> and Ras1<sup>C216S</sup> back to the plasma membrane lead to an increase in all measures of Ras1 function. These data are summarised in table 6.1.

Table 6.1. Summary of the activity and localisation of 1-40Gpa1-GFP-Ras1 fusions

Strain	Ras1 PM localisation	Cell polarity	Pheromone response	Mating
<i>ras1</i> <sup>+</sup>	++	++	++	++
$\Delta$ <i>ras1</i>	-	-	-	-
<i>1-40gpa1-gfp-ras1</i>	++	++	+	+
<i>1-40gpa1-gfp-ras1</i> <sup>C215S</sup>	++	+	+	+
<i>1-40gpa1-gfp-ras1</i> <sup>C216S</sup>	++	-	+	+
<i>1-40gpa1-gfp-ras1</i> <sup>Q66L, C215S</sup>	++	++	++	-
<i>1-40gpa1-gfp-ras1</i> <sup>Q66L</sup>	++	++	++	-
<i>1-40gpa1-gfp-ras1</i> <sup>S22N</sup>	++	-	-	-

## CHAPTER 7

# Functional expression of human ras proteins in fission yeast

### 7.1. Introduction

The development of pheromone-responsive reporter strains (Didmon *et al.* 2002; Ladds *et al.* 2003) has facilitated the use of *Sz. pombe* as a model system for studying human signalling components. Previous applications have included expression of human G $\alpha$  subunits (Ladds *et al.* 2003), human G $\beta$  subunits (Goddard *et al.* 2006) and human RGS proteins (Ladds *et al.* 2007; Hill *et al.* 2008). Further studies have explored the heterologous expression of human ras proteins in fission yeast (Nadin-Davis *et al.* 1986), however none have sought to quantify signalling through multiple pathways or compare multiple human ras isoforms.

Human ras proteins and *Sz. pombe* Ras1 share significant sequence homology (Figure 7.1A). The N-terminal region, which is involved in nucleotide binding and effector interaction and contains the guanine nucleotide-binding (G region) and phosphate-binding (P region) domains (Vetter and Wittinghofer 2001), is highly conserved between human ras proteins and Ras1. Most sequence divergence is observed in the C-terminal region, or hypervariable domain, which is involved in ras localisation (Eisenberg and Henis 2008). All isoforms contain a C-terminal CAAX farnesylation motif to promote membrane association. Ras1 and N-Ras each contain a single palmitoyl group to further aid plasma membrane localisation. H-Ras, by contrast, contains two palmitoyl groups and K-Ras4B is not palmitoylated but contains a poly-basic domain to allow interaction with lipid head groups at the plasma membrane (Bijlmakers and Marsh 2003; Eisenberg and Henis 2008; Smotrys and Linder 2004). In



addition, the sequences immediately upstream of these modifications, which have previously been implicated in localisation (Hancock 2003), are highly divergent between the isoforms (Figure 7.1B). In Ras1 this upstream region is considerably larger than human ras isoforms, however the significance of this remains to be determined. As a result, the C-terminal localisation domain of Ras1 could display properties that differ from human ras proteins. Despite this divergence, the high level of homology in the nucleotide binding and effector interaction domains of these proteins suggests human ras and Ras1 might be functionally interchangeable.

### 7.2. The localisation of human ras proteins in *Sz. pombe*

The highly divergent C-termini of human H-Ras, N-Ras and K-Ras4B could confer quite differing localisation patterns in *Sz. pombe*. As a consequence, these isoforms could prove informative in determining the link between ras localisation and function in fission yeast. The localisation of the three human ras isoforms H-Ras, N-Ras and K-Ras4B was determined using GFP-ras fusions expressed from pREP3x in the  $\Delta ras1$  strain JY1279. Images were obtained using a Leica SP5 scanning confocal microscope (Figure 7.2A) and the relative level of fluorescence at the periphery compared to the interior of the cell was determined using Quimp software (Figure 7.2B). GFP-K-Ras4B displayed the highest plasma membrane localisation of the three human ras isoforms ( $67.5 \pm 4.7$  %). GFP-H-Ras exhibited an intermediate level of plasma membrane localisation ( $41.5 \pm 8.2$  %), and GFP-N-Ras displayed the lowest ( $11.3 \pm 3.1$  %). All however displayed a lower level of plasma membrane localisation than GFP-Ras1 ( $78.0 \pm 3.5$  %). These differences in localisation are likely due to the quite differing C-terminal localisation domains of these three proteins (Figure 7.1B).

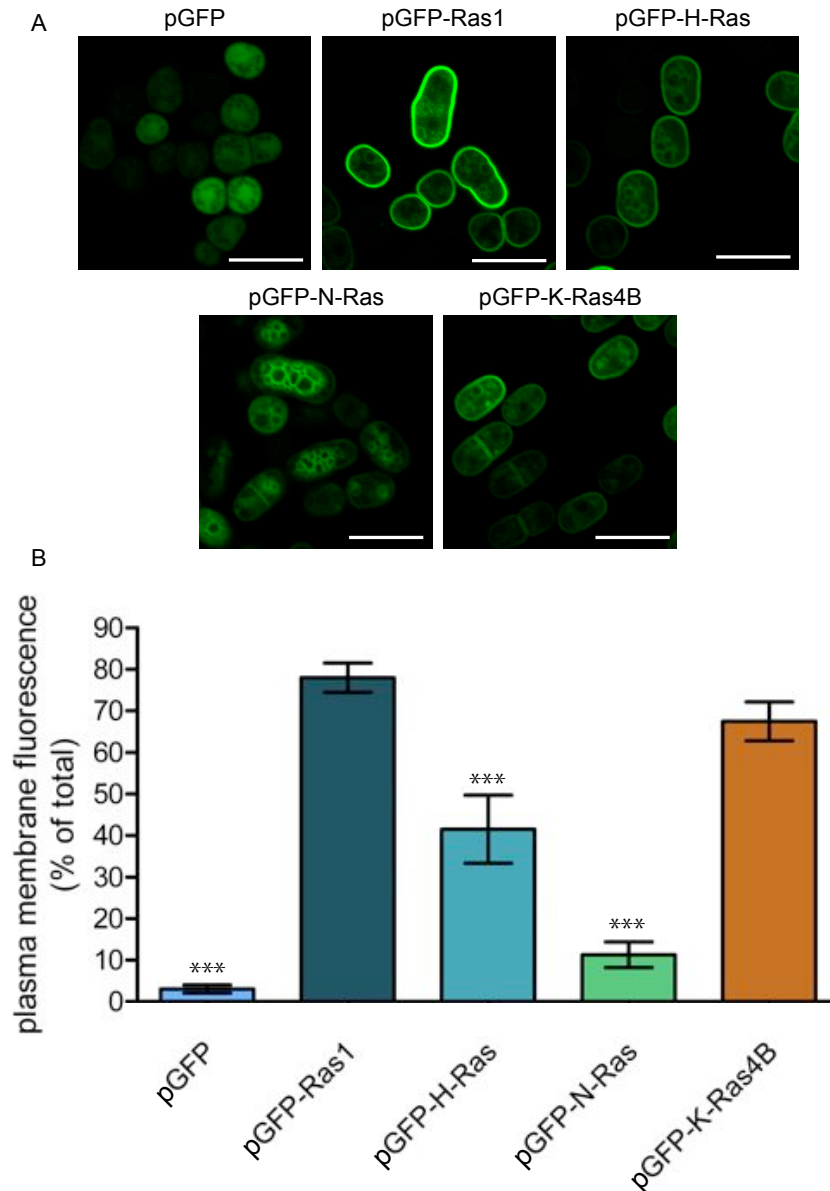


**Figure 7.2. Quantifying the localisation of GFP-human ras fusions using Quimp software**

Images of  $\Delta ras1$  cells (JY1279) expressing GFP, GFP-Ras1, GFP-H-Ras, GFP-N-Ras and GFP-K-Ras4B from pREP3x were obtained using a Leica SP5 scanning confocal microscope (A). The intensity of fluorescence at the periphery compared to the interior of the cell was determined using Quimp software (B). GFP-K-Ras4B displayed plasma membrane fluorescence comparable to GFP-Ras1. GFP-H-Ras and GFP-N-Ras exhibited significantly lower plasma membrane localisation. Data representative of 10 individual cells. Statistical significance was determined using a one-way anova with a Tukey multiple comparison post test. Three asterisks indicates a P-value of 0.001. The scale bar represents 10  $\mu$ m.

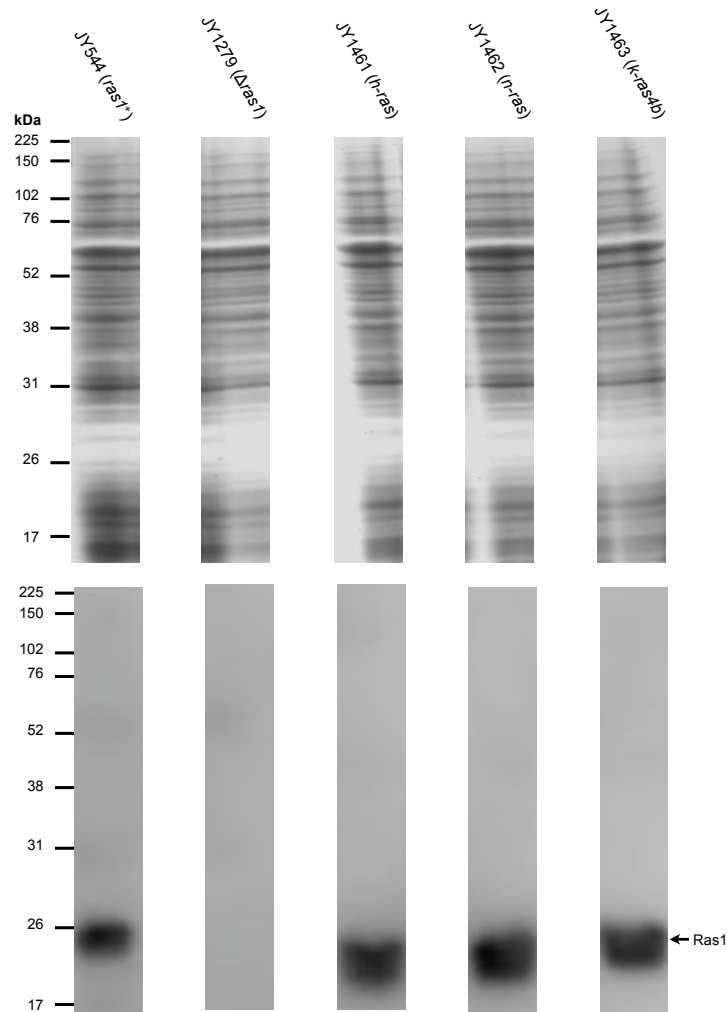


**Figure 7.3. Integration of human H-Ras, N-Ras and K-Ras4B at the *ras1* locus of the  $\beta$ -galactosidase reporter strain**

Integration of human H-Ras, N-Ras and K-Ras4B in the *ras1::ura4<sup>+</sup>, sxa2>lacZ* strain JY1247 was confirmed via immunoblotting using an anti-ras RAS10 antibody. Coomassie stains of whole protein are included above the immunoblot as loading controls.

### 7.3. Expression of human ras proteins in *Sz. pombe*

To allow the analysis of human ras activity in fission yeast at endogenous Ras1 levels, the human ras isoforms H-Ras, N-Ras and K-Ras4B were integrated at the *ras1* locus in the  $\beta$ -galactosidase reporter strain (*sxa2>lacZ*) (Figure 7.3) and the *tea1-mCherry* (Figure 7.4) strain using the method previously described (Figure 4.28A). Expression was confirmed by immunoblotting using an anti-ras RAS10 antibody. Direct, in-frame N-terminal GFP-H-Ras, GFP-N-Ras and GFP-K-Ras4B fusions were also created at the *ras1* locus in

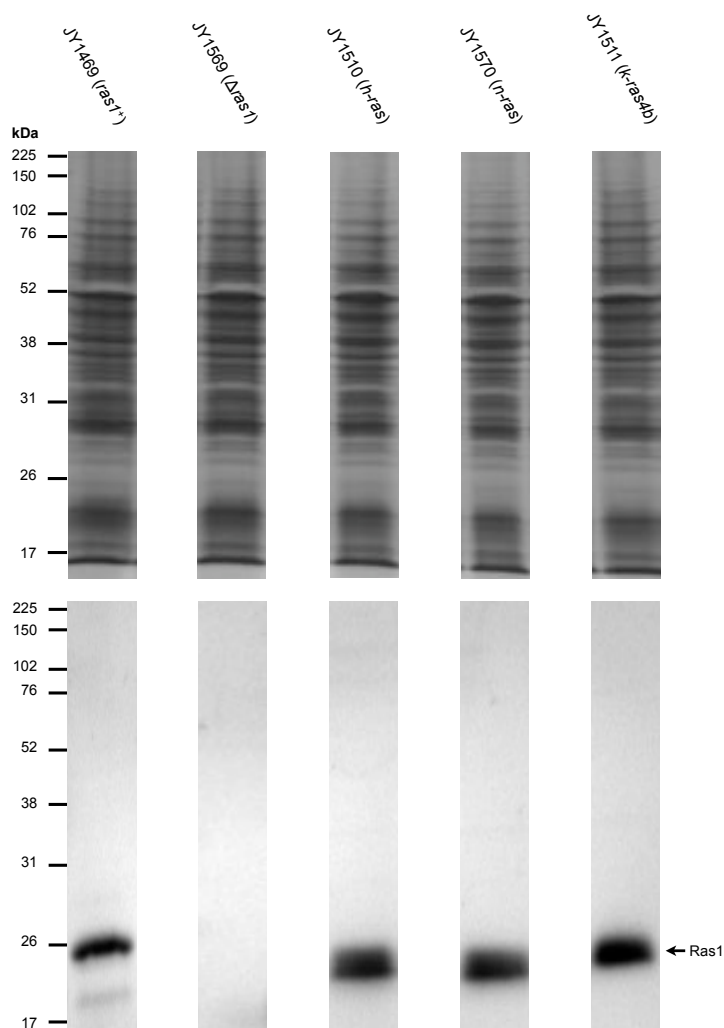


**Figure 7.4. Integration of human H-Ras, N-Ras and K-Ras4B at the *ras1* locus of the Tea1-mCherry strain**

Integration of human H-Ras, N-Ras and K-Ras4B in the *ras1::ura4<sup>+</sup>, tea1-mcherry* strain JY1569 (B) was confirmed via immunoblotting using an anti-ras RAS10 antibody. Coomassie stains of whole protein are included above the immunoblot as loading controls.

the *sxa2>lacZ* reporter (Figure 7.5). Expression was again confirmed by immunoblotting, giving a signal at a position consistent with the predicted size of the fusion ( $\sim 53$  kDa).

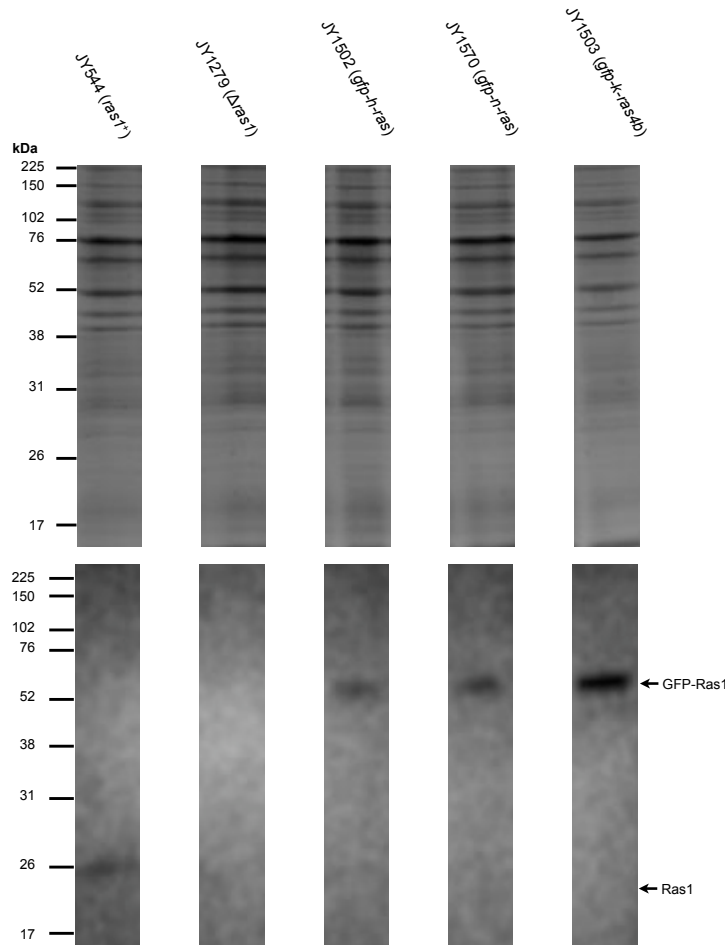


**Figure 7.5. Integration of GFP-H-Ras, GFP-N-Ras and GFP-K-Ras4B at the *ras1* locus**

Integration of GFP-H-Ras, GFP-N-Ras and GFP-K-Ras4B in the *ras1::ura4<sup>+</sup>, sxa2>lacZ* strain JY1247 was confirmed via immunoblotting using an anti-ras RAS10 antibody. Coomassie stains of whole protein are included above the immunoblot as loading controls.

#### 7.4. The function of human ras proteins in *Sz. pombe*

##### 7.4.1. H-Ras, N-Ras and K-Ras4B all signal through Scd1.

The function of human ras proteins in fission yeast was first assessed through analysis of polar cell morphology and Tea1-mCherry localisation. The localisation of Tea1-mCherry was assessed in cells expressing each of the three human ras isoforms from the *ras1* locus. Images were obtained using a Nikon E800 epifluorescence microscope fitted with an Andor EM-CCD camera (Figure 7.6C). All three human ras isoforms appeared to support polar Tea1-mCherry localisation in the majority of cells observed. These strains displayed defined tip

localisation of Tea1-mCherry with little Tea1-mCherry present at other areas of the cell periphery, and with an accompanying elongated polar morphology. These results suggest significant ras signalling through the cell morphology pathway.

To further determine the activity of human ras in regulating cell polarity, the morphologies of cells expressing each human ras isoforms were analysed using quantitative image analysis. Images of each strain were obtained using a Leica SP5 confocal microscope (Figure 7.6A) and expression of GFP from pREP3x, following growth in DMM lacking thiamine, was used to allow detection of the cell. Quimp software was then used to determine the circularity of 30 cells of each strain. All strains expressing human ras isoforms exhibited a significantly lower percentage circularity than cells lacking Ras1 ( $87.5 \pm 1.2$  %). JY1461 (*h-ras*) and JY1463 (*k-ras4b*) showed comparable morphologies, with JY1461 (*h-ras*) giving a percentage circularity of  $77.0 \pm 1.4$  % and JY1463 (*k-ras4b*) giving a percentage circularity of  $79.3 \pm 1.5$  %. JY1462 (*n-ras*) exhibited a slightly higher percentage circularity ( $81.4 \pm 1.1$  %), possibly indicating a lower level of signalling through Scd1 (Figure 7.6B). Due to the high degree of homology in the N-termini of each isoform it is possible that this reduced activity is due to the markedly lower level of N-Ras at the plasma membrane compared to the other two human ras isoforms (Figure 7.2).

#### **7.4.2. H-Ras, N-Ras and K-Ras4B all propagate signalling in response to pheromone.**

Human H-Ras, N-Ras and K-Ras4B displayed significant signalling through the cell morphology pathway. To determine whether they could also support pheromone-dependent signalling, strains expressing human H-Ras (JY1461), N-Ras (JY1462) and K-Ras4B (JY1463) from the *ras1* locus were analysed using assays for  $\beta$ -galactosidase activity and cell volume.  $\beta$ -galactosidase activity and average cell volume were determined following growth in a range of

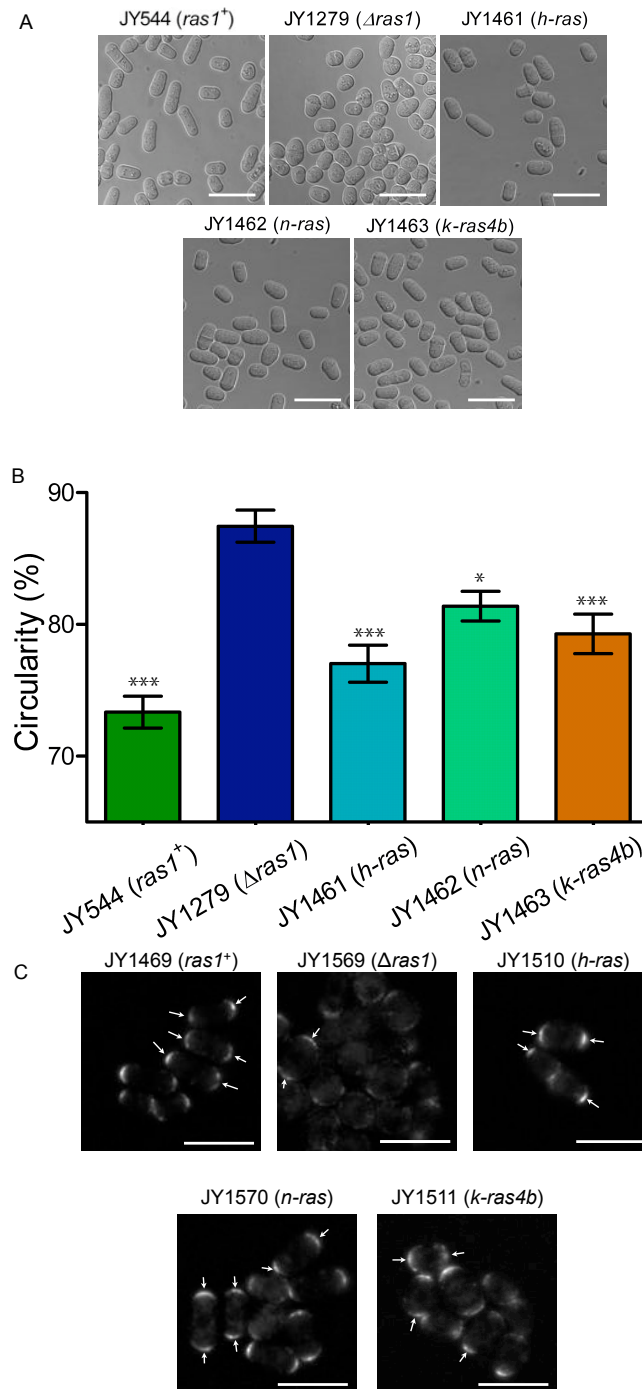


**Figure 7.6. Analysis of the morphology of cells expressing human H-Ras, N-Ras and K-Ras4B**

Images of *ras1*<sup>+</sup> (JY544),  $\Delta$ *ras1* (JY1279), *h-ras* (JY1461), *n-ras* (JY1462) and *k-ras4b* (JY1463) cells, expressing GFP from pREP3x, were obtained using a Leica SP5 scanning confocal microscope. Representative DIC images are displayed in panel A. Cell circularity was determined using Quimp software (B). Cells expressing all three isoforms displayed a lower percentage circularity than cells lacking Ras1. Data representative of 30 individual cells  $\pm$  SEM. The localisation of Tea1-mCherry was determined in *ras1*<sup>+</sup> (JY1469),  $\Delta$ *ras1* (JY1569), *h-ras* (JY1510), *n-ras* (JY1570) and *k-ras4b* (JY1511) cells using a Nikon E800 epifluorescence microscope fitted with an Andor EM-CCD camera (C). Cells expressing all three human ras isoforms displayed some polar Tea1-mCherry localisation. Arrows indicate the tip localisation of Tea1-mCherry. The scale bar represents 10  $\mu$ m. Three asterisks indicates a P-value of 0.001 and one asterisks a value of 0.05.

pheromone concentrations (1 nM to 100  $\mu$ M) in DMM for 16 h. All three human ras isoforms supported a pheromone-dependent increase in  $\beta$ -galactosidase activity (Figure 7.7A). JY1463 (*k-ras4b*) displayed the highest maximal response of the three strains ( $8.9 \pm 0.86$ ), followed by JY1461 (*h-ras*) ( $5.47 \pm 0.25$ ) and JY1462 (*n-ras*) ( $2.9 \pm 0.2$ ). The extent of signalling observed was lower than that seen in cells expressing wild-type Ras1 ( $29.0 \pm 1.2$ ). The level of maximal signalling through each human ras isoform matched closely the level of plasma membrane localisation each exhibited (Figure 7.2).

H-Ras and K-Ras4B supported a small increase in cell volume at higher pheromone concentrations (Figure 7.7B). *h-ras* cells (JY1461) increased from  $82.3 \pm 0.8$  fl to  $87.1 \pm 5.2$  fl in response to pheromone and *k-ras4b* (JY1463) cells increased from  $83.8 \pm 0.4$  fl to  $88.8 \pm 1.1$  fl. Cells expressing N-Ras displayed no pheromone-responsive increase in cell volume.

Cells displaying less elongated morphologies exhibit a higher cell volume due to increased cell width (Kelly and Nurse 2011). As a consequence, the analysis of shmoo formation using average cell volume is complicated by high basal figures. Due to the confounding effect of cell width, cell elongation in response to pheromone was also analysed using quantitative imaging. Cell length was measured after growth in the presence (10  $\mu$ M) and absence of pheromone in DMM lacking thiamine for 16 h. Images were obtained using a Leica SP5 scanning confocal microscope, with cells expressing GFP from pREP3x to allow segmentation of cells within the image. Quimp software was then used to determine the length of 30 cells for each strain under each assay condition. All strains expressing human ras isoforms displayed no significant elongation in response to pheromone. JY1463 (*k-ras4b*) displayed the strongest trend towards increased cell length ( $65.3 \pm 2.4$  pixels to  $69.0 \pm 2.6$  pixels). No visible change in morphology was observed in any of these strains following pheromone stimulation (Figure 7.8).

As a final measure of signalling in response to pheromone, cell cycle position was analysed in cells grown in the presence (10  $\mu$ M) and absence of

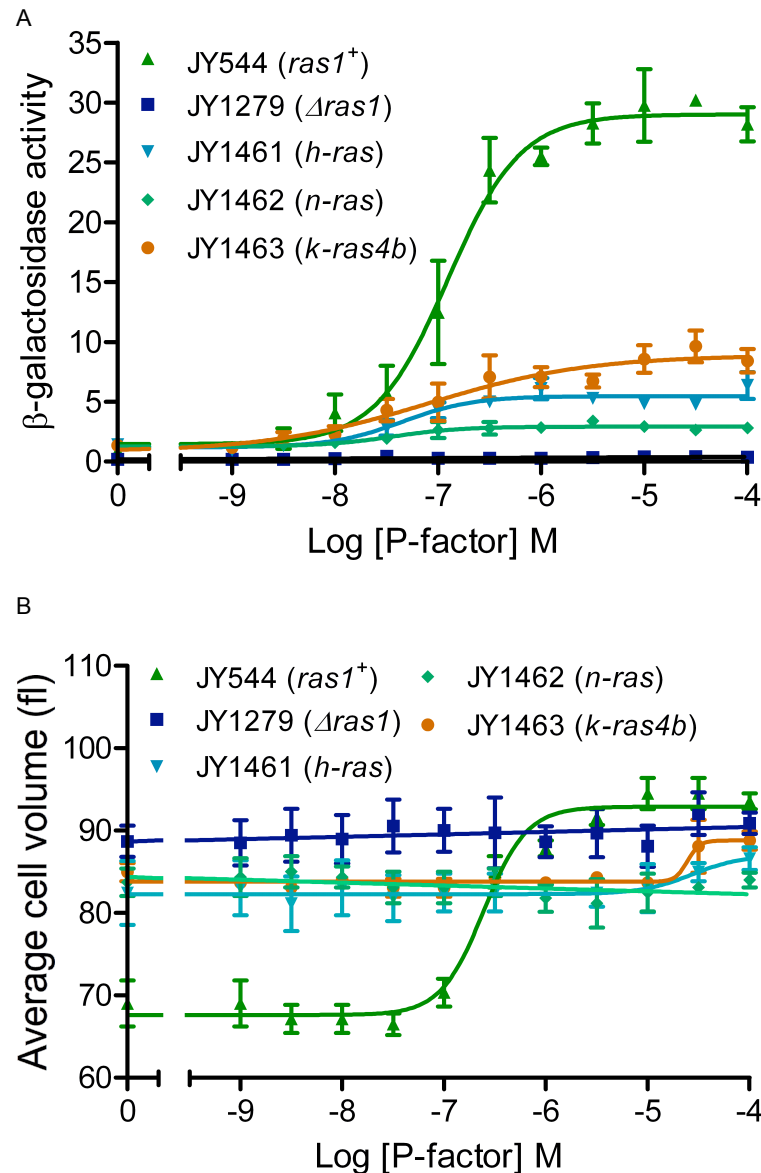


**Figure 7.7. Phormone-dependent changes in transcription and cell volume in cells expressing human ras isoforms**

Phormone-responsive changes in transcription and cell volume were observed in *ras1*<sup>+</sup> (JY544),  $\Delta$ *ras1* (JY1279), *h-ras* (JY1461), *n-ras* (JY1462) and *k-ras4b* (JY1463) cells. Cells were grown in 1 nM to 100  $\mu$ M phormone in DMM for 16 h. Assays were then performed for  $\beta$ -galactosidase activity (A) and average cell volume (B). All strains expressing human ras isoforms displayed some phormone-responsive  $\beta$ -galactosidase activity. H-Ras and K-Ras4B supported some increase in cell volume in response to phormone. Data shown is an average of three independent determinants ( $\pm$ SEM).

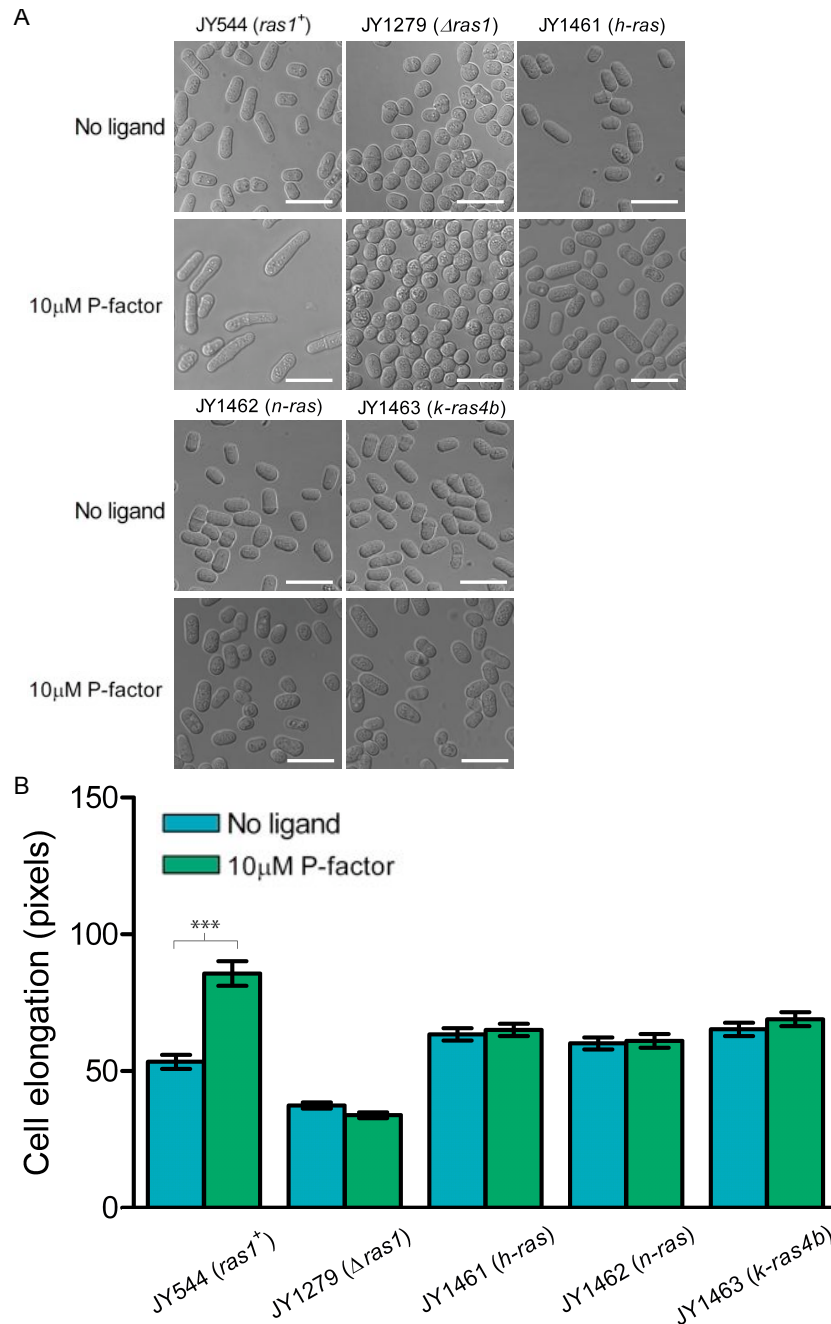


**Figure 7.8. Pheromone-dependent cell elongation in cells expressing human ras isoforms from the *ras1* locus**

Images of *ras1*<sup>+</sup> (JY544),  $\Delta$ *ras1* (JY1279), *h-ras* (JY1461), *n-ras* (JY1462) and *k-ras4b* (JY1463) cells, expressing GFP from pREP3x, were obtained using a Leica SP5 scanning confocal microscope. Images were taken following growth in the presence (10  $\mu$ M) and absence of pheromone in DMM for 16 h. Representative DIC images are displayed in panel A. Cell length was determined using Quimp software (B). Cells expressing H-Ras, N-Ras and K-Ras4B displayed no significant increase in cell length in response to pheromone. Data shown is representative of 30 individual cells  $\pm$  SEM. Statistical significance was determined using a one-way anova with a Tukey multiple comparison post test. Three asterisks indicates a P-value of 0.001. Images from the populations analysed demonstrate no change in morphology in response to pheromone. The scale bar represents 10  $\mu$ m.

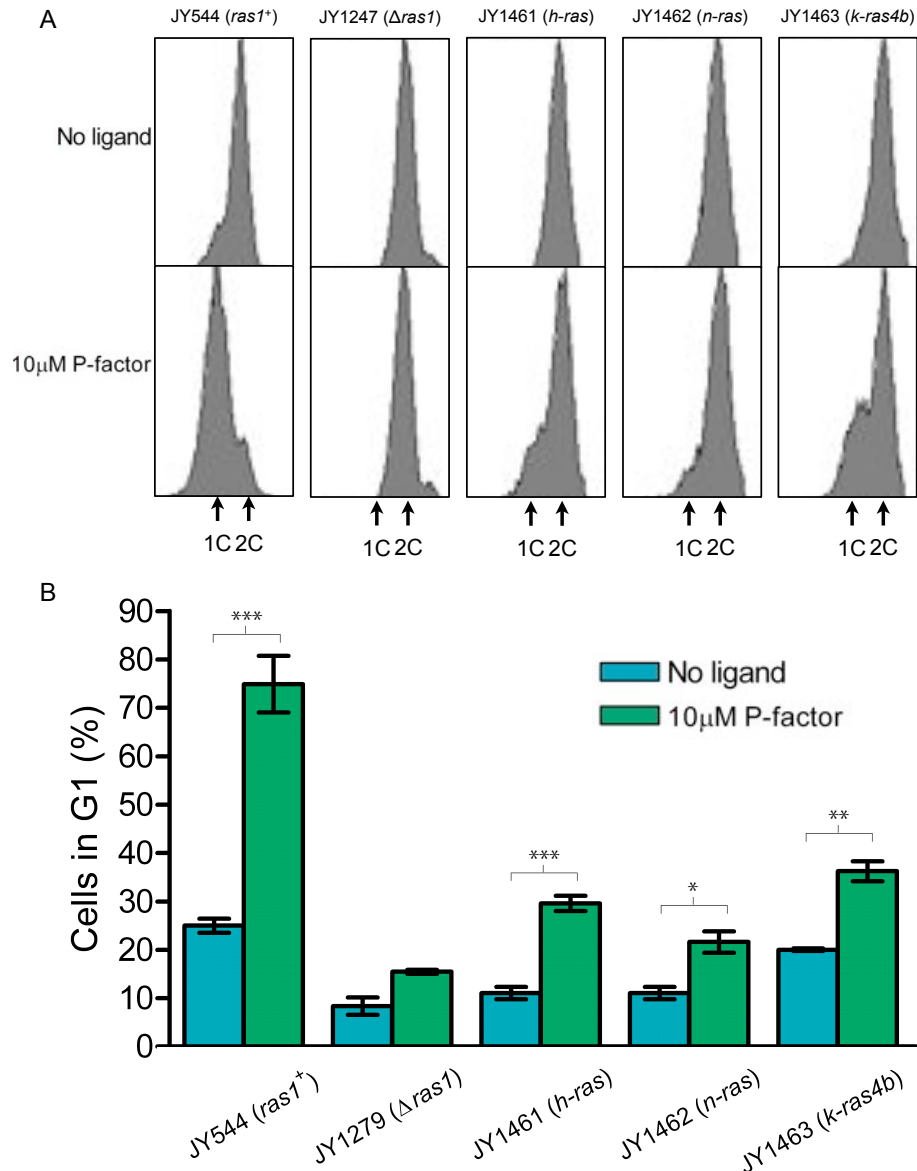


**Figure 7.9. Pheromone-responsive changes in cell cycle position in cells expressing human ras isoforms from the *ras1* locus**

Cell cycle arrest was analysed in *ras1*<sup>+</sup> (JY544),  $\Delta$ *ras1* (JY1279), *h-ras* (JY1461), *n-ras* (JY1462) and *k-ras4b* (JY1463) cells using propidium iodide staining and flow cytometry, after growth in the presence (10 µM) and absence of pheromone in DMM for 6 h. This analysis allowed the distinction between cells containing a single complement (1C) and double complement (2C) of DNA (A). Cells expressing human ras isoforms displayed some pheromone-dependent G<sub>1</sub> arrest (B). Data shown representative of three independent determinants  $\pm$  SEM. Analysis was performed for 30000 cells. Statistical significance was determined using a one-way anova with a Tukey multiple comparison post test. Three asterisks indicates a P-value of 0.001, two asterisks a value of 0.01 and one asterisks a value of 0.05.

pheromone in DMM for 6 h, using propidium iodide staining and flow cytometry. Analysis was performed for 30000 cells. H-Ras, N-Ras and K-Ras4B all supported a significant pheromone dependent G<sub>1</sub> arrest (Figure 7.9). JY1463 (*k-ras4b*) displayed the highest percentage of cells in G<sub>1</sub> following stimulation with pheromone, increasing from  $20.0 \pm 0.3$  % to  $36.2 \pm 2.1$  %. JY1461 (*h-ras*) displayed the most statistically significant arrest, but a lower levels of arrest following stimulation ( $11.0 \pm 1.3$  % to  $29.6 \pm 1.6$ ). JY1462 (*n-ras*) exhibited the lowest percentage of cells in G<sub>1</sub> following incubation with pheromone ( $10.35 \pm 1.9$  % to  $21.6 \pm 2.2$ ). The levels of maximal response in these strains again matches closely the level of each human ras isoform at the plasma membrane (Figure 7.2).

#### 7.4.3. Addition of GFP to the N-terminus reduces pheromone-responsive signalling through H-Ras, N-Ras and K-Ras4B.

To determine the effect of the GFP tag upon GFP-H-Ras, GFP-N-Ras and GFP-K-Ras4B,  $\beta$ -galactosidase activity and cell volume were analysed in response to pheromone, following growth in a range of pheromone concentrations (1 nM to 100  $\mu$ M) in DMM for 16 h. All three displayed a small pheromone-dependent increase in  $\beta$ -galactosidase activity (JY1461 (*h-ras*) =  $0.6 \pm 0.1$  to  $2.6 \pm 0.1$ , JY1462 (*n-ras*) =  $0.6 \pm 0.2$  to  $2.6 \pm 0.3$  and JY1463 (*k-ras4b*) =  $0.3 \pm 0.2$  to  $2.1 \pm 0.2$ ) (Figure 7.10). The level of signalling observed was markedly lower than that seen in cells expressing each human ras isoform without GFP fused to the N-terminus. None of these strains displayed a pheromone-responsive increase in cell volume. All also exhibited a high basal cell volume, similar to cells lacking Ras1 (JY1461 (*h-ras*) =  $85.0 \pm 1.0$  fl, JY1462 (*n-ras*) =  $85.0 \pm 2.2$  fl, JY1463 (*k-ras4b*) =  $87.7 \pm 1.5$  fl and JY1279 ( $\Delta ras1$ ) =  $89.4 \pm 0.4$  fl).

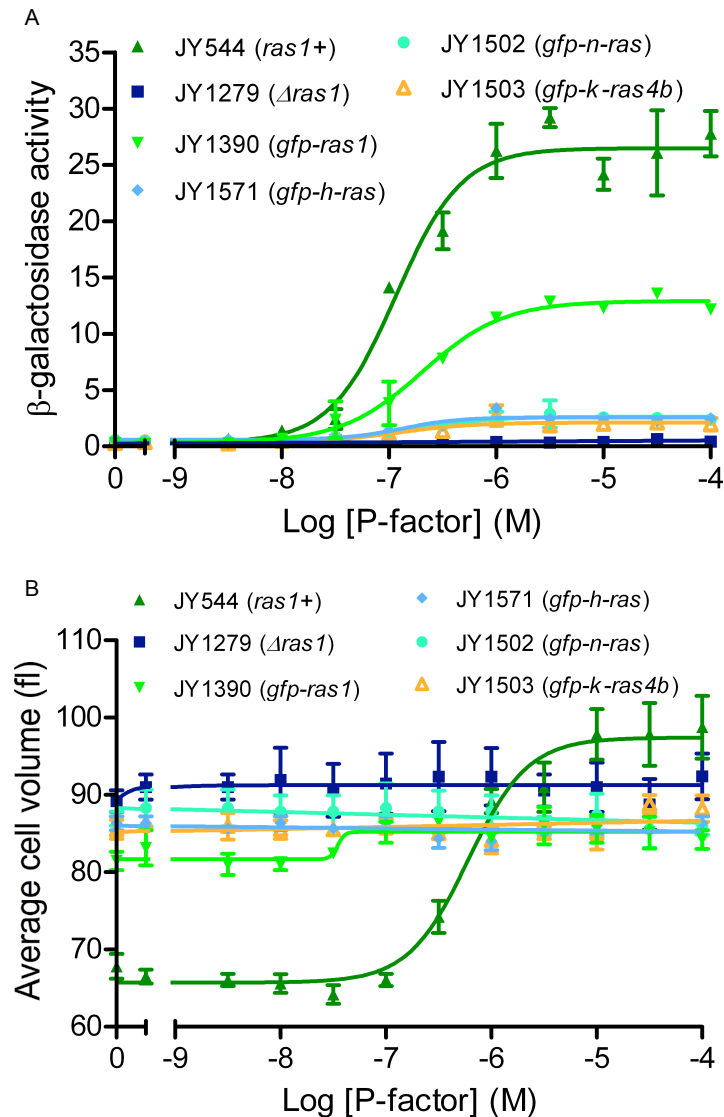


**Figure 7.10. Pheromone-dependent changes in transcription and cell volume in cells expressing GFP tagged human ras isoforms**

Pheromone-responsive changes in transcription and cell volume were observed in *ras1*<sup>+</sup> (JY544),  $\Delta$ *ras1* (JY1279), *gfp-ras1* (JY1390), *gfp-h-ras* (JY1571), *gfp-n-ras* (JY1502) and *gfp-k-ras4b* (JY1503) cells. Cells were grown in 1 nM to 100  $\mu$ M pheromone in DMM for 16 h. Assays were then performed for  $\beta$ -galactosidase activity (A) and average cell volume (B). GFP tagged human ras isoforms supported some pheromone-reponsive  $\beta$ -galactosidase activity, but no increase in cell volume upon pheromone stimulation. Data shown is an average of three independent determinants ( $\pm$ SEM).

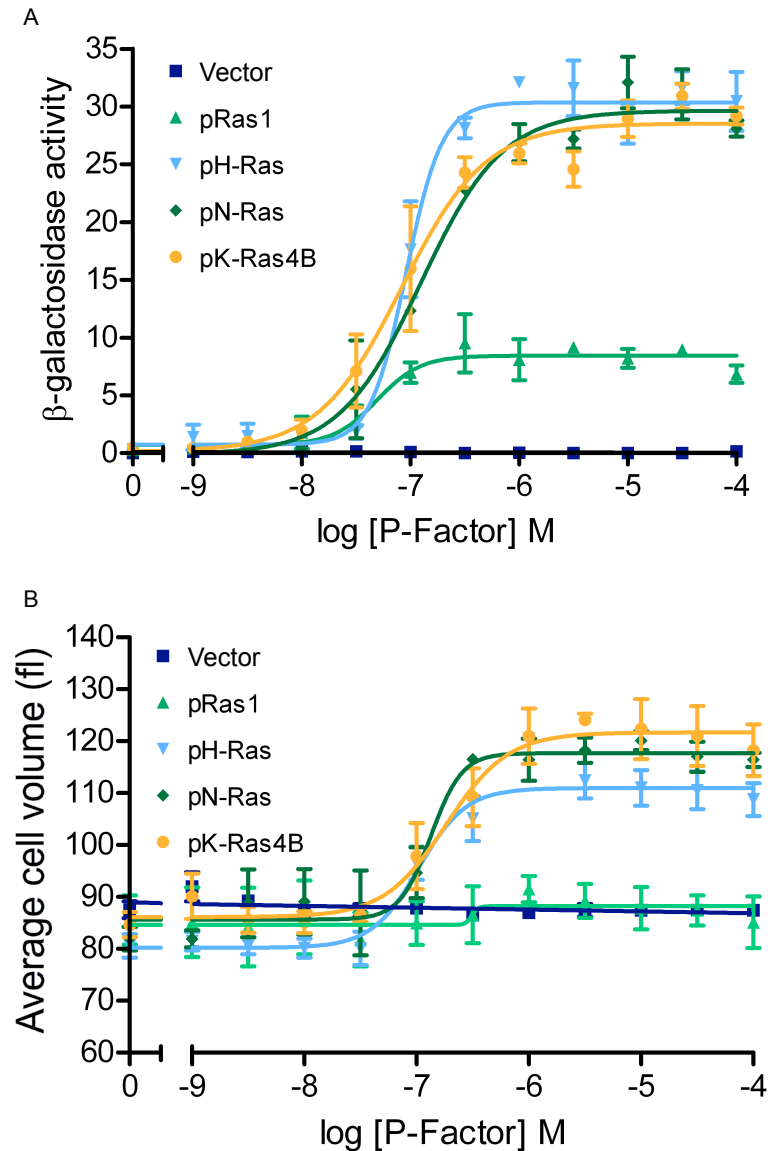


**Figure 7.11. Phormone-dependent changes in transcription and cell volume in cells expressing human ras isoforms from pREP3x**

Phormone-responsive changes in transcription and cell volume were observed in  $\Delta ras1$  (JY1279) cells expressing Ras1, H-Ras, N-Ras and K-Ras4B from pREP3x, in addition to a vector alone control. Cells were grown in 1 nM to 100  $\mu$ M phormone in DMM lacking thiamine for 16 h. Assays were then performed for  $\beta$ -galactosidase activity (A) and average cell volume (B). Cells expressing human ras isoforms from pREP3x exhibited strong phormone-responsive increases in  $\beta$ -galactosidase activity and cell volume. Data shown is an average of three independent determinants ( $\pm$ SEM).

#### 7.4.4. H-Ras, N-Ras and K-Ras4B display high levels of pheromone-responsive signalling upon expression from pREP3x.

All three human ras isoforms displayed a lower level of activity than Ras1. To determine whether signalling could be increased upon constitutive expression, the signalling of H-Ras, N-Ras and K-Ras4B was also investigated upon expression from pREP3x in the  $\Delta ras1$  strain JY1279. Signalling was analysed in response to pheromone using assays for  $\beta$ -galactosidase activity and cell volume, following growth in a range of pheromone concentrations (1 nM to 100  $\mu$ M) in DMM lacking thiamine for 16 h. All three human ras isoforms displayed strong pheromone-responsive signalling in  $\beta$ -galactosidase assays when expressed from pREP3x (Figure 7.11). Each gave a maximal signal greater than that observed in cells expressing wild-type Ras1 from pREP3x (H-Ras =  $30.4 \pm 0.8$ , N-Ras =  $29.7 \pm 0.9$ , K-Ras4B =  $28.5 \pm 1.0$  and Ras1 =  $8.5 \pm 0.5$ ). The maximal signal was close to that observed in JY544, suggesting that expression of H-Ras, N-Ras and K-Ras4B from pREP3x did not impair cell viability. Cells expressing each human ras isoform from pREP3x also displayed a pEC<sub>50</sub> (H-Ras =  $7.0 \pm 0.1$ , N-Ras =  $6.9 \pm 0.1$  and K-Ras4B =  $7.1 \pm 0.1$ ) comparable to cells expressing wild-type Ras1 ( $7.3 \pm 0.1$ ). In addition, all displayed a marked pheromone-dependent increase in cell volume. Cells expressing H-Ras from pREP3x displayed an increase from  $80.2 \pm 1.5$  fl to  $111.0 \pm 1.4$  fl, those expressing N-Ras from  $85.6 \pm 1.9$  fl to  $117.7 \pm 1.8$  fl and those expressing K-Ras4B from  $86.1 \pm 2.0$  fl to  $121.7 \pm 2.0$  fl.

#### 7.4.5. H-Ras, N-Ras and K-Ras4B are only able to support limited mating.

H-Ras, N-Ras and K-Ras4B all exhibited pheromone-dependent signalling. In order to determine whether this signalling was sufficient to support mating, the efficiency of mating in cells expressing H-Ras, N-Ras and K-Ras4B from the endogenous *ras1* promoter was determined using the quantitative mating

assay described in section 4.2.1. Expression of Sxa2 from pREP41x was used to restore Sxa2 activity. No mating (0 % in all cases) was observed using this assay in strains expressing any of the three human ras isoforms. Microscopic examination revealed some, limited ascus spore formation (Figure 7.12), indicating that H-Ras, N-Ras and K-Ras4B are able to support some mating activity. This observation is in concert with previous findings (Nadin-Davis *et al.* 1986) which suggested human H-Ras could support only limited mating.

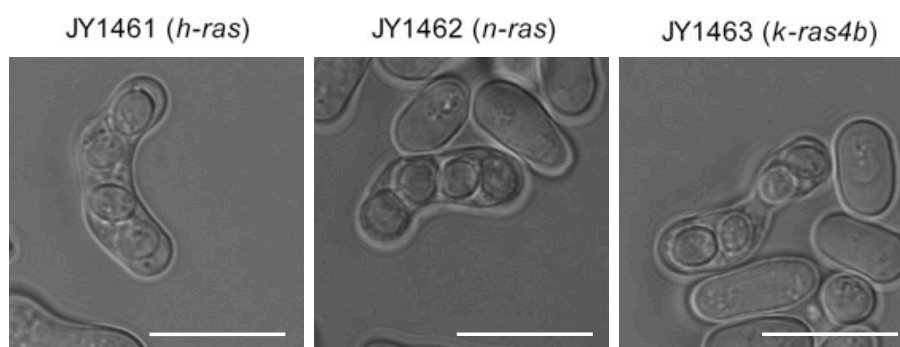


**Figure 7.12. Mating in cells expressing human H-Ras, N-Ras and K-Ras4B**

The mating of *h-ras* (JY1461), *n-ras* (JY1462) and *k-ras4b* (JY1463) cells expressing Sxa2 from pREP4x was assessed by microscopic examination. All displayed some, limited ascus spore formation. Images were obtained using a Leica SP5 scanning confocal microscope. The scale bar represents 10  $\mu\text{m}$ .

## 7.5. Summary

In the preceding chapter, the signalling activity of human H-Ras, N-Ras and K-Ras4B in *Sz. pombe* was detailed. Each human ras isoform displayed functional activity in both the pheromone-dependent signalling pathway and cell morphology pathway. In addition, each human ras isoform exhibited quite differing localisation profiles. Like Ras1, each displayed localisation to the endomembranes and plasma membrane. Marked differences however were observed in the level of each isoform at either membrane compartment. The localisation of K-Ras4B, which is determined by farnesylation and a polybasic stretch of residues at the C-terminus, was largely to the plasma membrane.

H-Ras, which contains a farnesyl and two palmitoyl residues, displayed a lower level of plasma membrane localisation and N-Ras, which contains a palmitoyl and farnesyl group, displayed the lowest level of plasma membrane localisation. Further to this observation, it appeared in both assays for  $\beta$ -galactosidase activity and G<sub>1</sub> arrest that the level of maximal signalling each displayed matched closely with the level of these isoforms at the plasma membrane. This observation is in good agreement with the results detailed in chapters five and six, which suggest that the level of Ras1 at the plasma membrane is critical in determining the level of signalling output.

Despite their functional activity when expressed from the *ras1* locus, the level of signalling observed through these isoforms was considerably lower than that observed through Ras1. Possibly as a consequence of this reduced signalling output, no significant mating was observed in strains containing these human ras isoforms. Some mating however was still supported by H-Ras, N-Ras and K-Ras4B, as spores could be seen upon incubation of each strain (transformed with pREP41x-Sxa2 to rescue Sxa2 activity) with cells of the opposite mating type.

Finally, it was also demonstrated that constitutive expression of H-Ras, N-Ras and K-Ras4B, through expression from the *nmt1* promoter of pREP3x, caused a significant increase in the level of pheromone-dependent signalling through these isoforms. Cells expressing Ras1 from pREP3x display a lower maximal signal than those expressing Ras1 from the *ras1* locus due to a reduced cell viability (section 4.6.6). It is possible that the high level of signalling observed upon expression of H-Ras, N-Ras and K-Ras4B from pREP3x is due to their lower intrinsic levels of signalling activity in *Sz. pombe* (section 7.4.2), resulting in a reduced effect upon cell viability.

## CHAPTER 8

### Discussion

#### 8.1. Overview

This thesis details a number of studies which expand our understanding of Ras1 signalling in *Sz. pombe*. These studies aimed to use a quantitative approach to the analysis of Ras1 localisation and function. To this end, a quantitative assay for mating was developed and quantitative imaging techniques were employed to investigate cell morphology and Ras1 localisation. These approaches were then combined with existing assays, such as reporter gene assays for pheromone-dependent transcription (Didmon *et al.* 2002), to provide a more complete view of Ras1 function. The use of these techniques to analyse the constitutive expression of Ras1 and the function of oncogenic mutants of Ras1 revealed the importance of the magnitude of Ras1 signalling in function output, cell viability and chromosome segregation.

This thesis also explores the role of Ras1 localisation in function. The use of mutants with altered C-terminal modification, in addition chimeric proteins with increased plasma membrane avidity, revealed the importance of Ras1 plasma membrane targeting in all measures of Ras1 function. Based upon this observation, a revised model is presented for the role of Ras1 localisation in dictating the activation of differing downstream pathways.

Finally, the function and localisation of three human ras isoforms, H-Ras, N-Ras and K-Ras4B, was also characterised in *Sz. pombe*. Analyses revealed that all three human ras proteins functioned in *Sz. pombe*. In addition, analysis of localisation revealed a similar relationship between localisation and signalling function to that observed for the Ras1 mutants detailed in these studies.

## 8.2. Quantifying Ras1 function and localisation in *Sz. pombe*

Most previous studies exploring Ras1 localisation and function in *Sz. pombe* have employed qualitative analysis techniques. In this study, quantitative measures of mating, morphology and Ras1 localisation were developed to complement existing assays, such as the  $\beta$ -galactosidase assay for pheromone-responsive transcription (Didmon *et al.* 2002). These assays were then employed to gain a more detailed understanding of Ras1 in *Sz. pombe*.

### 8.2.1. Developing a quantitative assay for mating.

The observation of spore formation, either using microscopy or iodine staining (Egel *et al.* 1994), provides an indication as to the extent of mating within a population. In this study, a major aim was to produce a reproducible quantitative assay for mating efficiency, allowing more effective comparison between differing strains. Spore heat-resistance was employed to allow the rapid killing of vegetative cells within a population at high temperatures, with no discernible effect upon spore viability. Spores were then allowed to recover on rich solid media, and spore numbers were assessed through the analysis of colony forming unit numbers (Figure 4.1). This method provided a relatively rapid and reproducible means of assessing mating efficiency in *Sz. pombe*.

### 8.2.2. The use of quantitative imaging techniques in *Sz. pombe*.

Observation of cell morphology and fluorescence localisation can prove highly subjective. As a consequence, the use of techniques to quantitatively analyse microscopy images can prove very informative. In this thesis, the Quantitative imaging of membrane protein (Quimp) plugin of Image J (Dormann *et al.* 2002; Bosgraaf *et al.* 2009) was employed to analyse cell morphology, cell length and the levels of plasma membrane localisation exhibited by a variety of GFP-tagged ras proteins.

Analysis of cell morphology was performed using a measure of percentage circularity. This analysis not only demonstrated significant differences between the morphologies of cells containing and lacking Ras1, but also provided an assay with a sufficient window to resolve intermediate morphologies (Figure 4.9). Additionally, the software provided a direct measure of cell length, allowing analysis of cell elongation in response to pheromone (Figure 4.13).

One of the primary functions of Quimp is to allow the analysis of cortical fluorescence. This function is ideally suited to the analysis of Ras1 localisation, as one of the key factors of interest is the level of plasma membrane localised ras compared to endomembrane localised ras. Quimp software was used in this study to allow accurate analysis of the plasma membrane targeting of all the GFP-tagged ras mutants and isoforms investigated.

### 8.3. Altering the activation and deactivation of Ras1

A number of mutations in ras have been described which alter either nucleotide binding or GTPase activity. The best characterised class of ras mutants are those based upon oncogenic mutations in human ras isoforms. Two such Ras1 mutants, Ras1<sup>G17V</sup> and Ras1<sup>Q66L</sup>, in addition to one inactive mutant, Ras1<sup>S22N</sup>, were analysed in this study.

Ras1<sup>S22N</sup> displayed little significant signalling activity. A small increase in  $\beta$ -galactosidase activity was observed in cells expressing Ras1<sup>S22N</sup> upon pheromone stimulation (Figure 4.31). The level of activity did not change upon constitutive expression (Figure 4.34), which would be expected in mutants which display impaired activity. This result suggests that Ras1<sup>S22N</sup> remains GDP bound, but retains some function, possibly by scaffolding or interacting with some pathway components. This mutant also exhibited a significantly lower level of plasma membrane localisation than wild-type Ras1 (Figure 5.4). This observation could indicate that either Ras1 activation, or the functional interactions of Ras1, contribute to plasma membrane targeting. The Ras1<sup>S22N</sup>

mutation is based upon a mutation in human ras proteins known to prevent GEF binding (Feig and Cooper, 1988; Jung *et al.* 1994). The interaction of Ras1 with GEFs, such as Ste6, or larger GEF/effector complexes, such as the Efc25/Scd1/Scd2 complex, could contribute to the effective trafficking of Ras1 (Figure 5.4).

Constitutive expression of Ras1<sup>G17V</sup> and Ras1<sup>Q66L</sup> caused increased maximal signalling compared to wild-type Ras1 (Figure 4.41). In addition, cells expressing Ras1<sup>G17V</sup> from the endogenous *ras1* locus displayed a hyper-elongated morphology (Figure 4.35). These data are all consistent with the results expected from mutants with increased signalling activity. Despite this, neither mutant could support mating, and cells expressing either mutant from the *ras1* locus demonstrated a reduction in signalling at higher pheromone concentrations. Both these observations indicate that preventing the GTPase activity of Ras1 has a detrimental effect on pheromone-responsive signalling.

#### 8.4. The effects of increasing Ras1 signalling

Few studies have made a detailed analysis of the effect of increased ras signalling in *Sz. pombe*. In this study a number of experiments are described illustrating the detrimental effect that increased Ras1 signalling has upon signalling output and cell viability.

##### 8.4.1. Morphological defects and impaired mating upon constitutive expression of Ras1.

Expression from the thiamine-repressible *nmt1* promoter of pREP3x allows the expression of exogenous genes at high levels. Analysis of morphology in cells expressing Ras1 from pREP3x indicated that they were more rounded than wild-type cells, and did not demonstrate wild-type Tea1 distribution. These

observations suggest that an increase in Ras1 prevents effective cell polarisation (Figure 4.19). Increased Ras1 expression levels could cause ectopic Ras1 signalling, preventing the correct selection of the growth site. Additionally, increased levels of Ras1 signalling could result in aberrant growth due to an increase in Ras1 activity at the tip beyond that in a wild-type cell.

This observation could be linked to the reduced mating efficiency observed in cells expressing Ras1 from pREP3x (Figure 4.18). One of the most noticeable features of cells containing pREP3x-Ras1 is that upon pheromone stimulation a number of cells form multiple shmoo tips (Figure 4.20). This once again is indicative of impaired cell polarisation when more Ras1 is present in the cell. These results highlight the importance of the level of Ras1 signalling in functional activity, possibly in limiting Ras1 signalling to the correct site of Ras1 function.

#### **8.4.2. Pheromone-dependent cell death in cells containing oncogenic Ras1 mutants.**

The effect of mutations in Ras1 which prevent GTP hydrolysis further highlights the importance of the extent of Ras1 signalling. Upon pheromone stimulation, cells expressing Ras1<sup>G17V</sup> and Ras1<sup>Q66L</sup> displayed a reduced level of signalling at higher pheromone concentrations (above 100 nM) (Figure 4.36). This reduced signalling corresponded to a dose-dependent increase in cell death (Figure 4.39). Ras1 signalling is intimately linked with processes which are essential for viability. The loss of downstream components of Ras1 pathways, such as Cdc42 (Miller and Johnson 1994) and Shk1 (Marcus *et al.* 1995) for example, is lethal to the cell. In addition, the cell morphology pathway interacts with cell division processes at a number of levels (Yen and Chang 2000; Padte *et al.* 2006) (Figure 8.1). As a consequence, increased levels of Ras1 signalling could impact upon essential cellular processes, possibly by sequestering components of pathways involved in cell division, such as Cdc42 and Shk1.

These effects upon cell viability could also contribute to the lack of mating observed in cells expressing Ras1<sup>G17V</sup> and Ras1<sup>Q66L</sup>. The inability of Ras1<sup>G17V</sup> and Ras1<sup>Q66L</sup> to support mating demonstrates parallels with other strains which exhibit increased signalling but reduced mating efficiency. Strains which display this phenotype include  $\Delta pmp1$  (Didmon *et al.* 2002),  $\Delta sxa1$  and  $\Delta sxa2$  (Imai and Yamamoto, 1992). A cell's recovery following stimulation is a key factor in functional signalling networks. The prevention of processes such as GTP hydrolysis on Ras1, dephosphorylation of MAP kinases (Pmp1) and the degradation of ligand (Sxa2) could prevent functional signalling by not allowing recovery from pheromone-stimulation. As a result, the cell may undergo protracted shmoo formation without conjugation.

The constitutive expression of Ras1, Ras1<sup>G17V</sup> and Ras1<sup>Q66L</sup> had more profound effects upon cell viability (Figure 4.42). Significant cell death was observed even in the absence of pheromone. This result suggests that the precise regulation of Ras1 expression levels is vital to Ras1 function. The overexpression of a fully functional wild-type Ras1 protein was more detrimental to cell viability than the expression of Ras1<sup>G17V</sup> and Ras1<sup>Q66L</sup> from the endogenous Ras1 locus. This reduced cell viability could contribute to both the loss of mating observed in cells expressing Ras1 from pREP3x (Figure 4.18) and the reduced level of pheromone-responsive transcription in these cells (Figure 4.17).

Expression of GFP-Ras1 from the endogenous Ras1 locus revealed very low expression levels (Figure 4.22). It is possible that this low level of expression is important in the regulation of correct Ras1 function. Ras1 signalling interacts directly with multiple pathways. It is feasible that the concentration of Ras1 is tightly regulated to prevent active Ras1 from drawing components of other pathways away from other roles in the cell. As a consequence increasing the levels of Ras1 may result in an effective reduction in key components of other pathways, including essential proteins such as Cdc42.

### 8.4.3. The effect of constitutive Ras1 expression on chromosome segregation.

Ras1 and Cdc42 influence chromosome segregation through the regulation of Yin6 and Moe1 (Yen and Chang 2000). As a result, one mechanism by which increased Ras1 activity may influence cell viability is through preventing correct chromosome segregation. A link between the loss of Ras1 and chromosome instability has already been established (Li *et al.* 2000), however the effects of increased Ras1 expression or increased Ras1 activity has not. Expression of Ras1 from pREP3x caused an increase in minichromosome loss in strains containing a non-essential minichromosome with an adenine auxotrophic marker. This effect was further compounded by the introduction of mutations which prevented GTP hydrolysis. The impaired cell viability in cells overexpressing Ras1 may also mask some of the chromosome loss resulting from Ras1 overexpression (Figure 4.43).

These data extend the observation that increased Ras1 is detrimental to cell viability, demonstrating a functional consequence of increased Ras1 in a process which is essential to the cell.

## 8.5. The role of C-terminal Ras1 modification

The importance of ras C-terminal modification in function is well established (Eisenberg and Henis 2008). Only one previous study has explored the role of the C-terminus of Ras1 in *Sz. pombe* (Onken *et al.* 2006). A key finding of this study was that the prevention of Ras1 palmitoylation constrained Ras1 to the endomembranes, and that this prevented mating but not the maintenance of polar cell morphology. In this thesis, a number of studies demonstrated a differing view of the role of palmitoylation in Ras1 localisation and function.

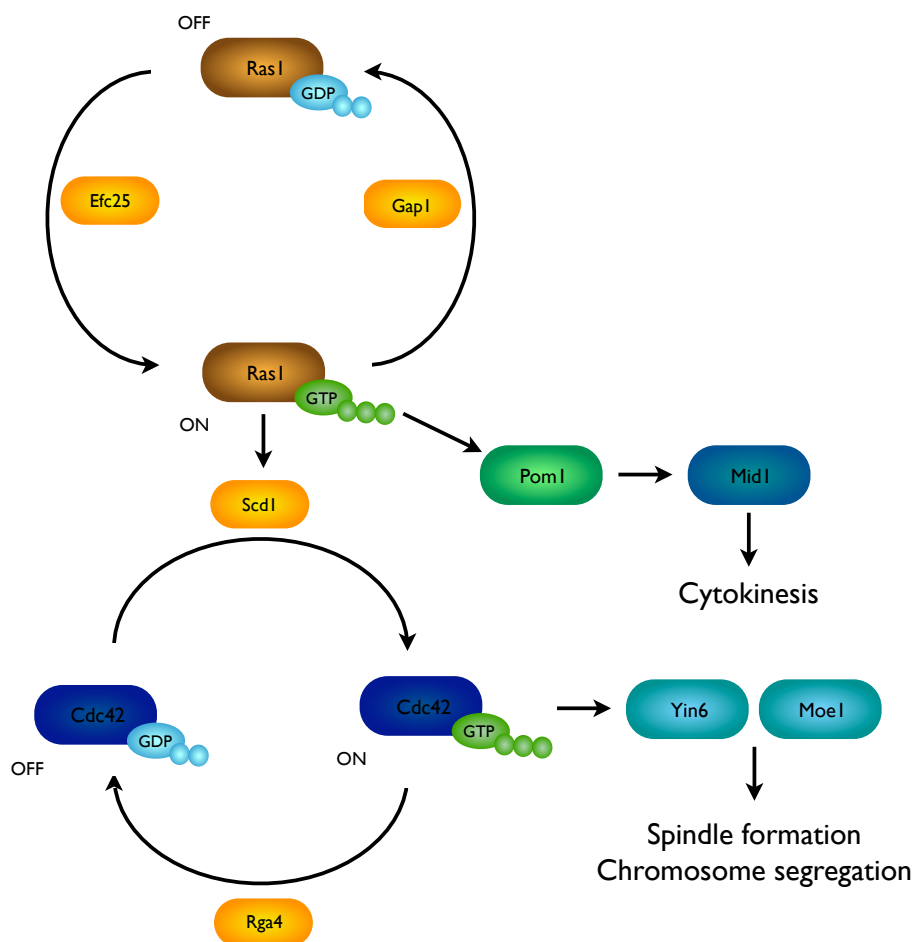


**Figure 8.1. The interaction between Ras1 signalling and cell division** Ras1 signalling and cell division are intimately linked. Ras1 directly regulates the DYRK (dual-specificity Yak-related kinase) family protein Pom1, which is involved in defining the midline of the cell through the protein Mid1. This process is required for cytokinesis and defining the position of the septum (Padte *et al.* 2006). Cdc42 also acts downstream of Ras1 signalling to regulate Yin6 and Moe1, which are required for spindle formation and chromosome segregation (Yen and Chang 2000).

### 8.5.1. The effects of altering C-terminal modification on Ras1 localisation.

The farnesylation of Ras1 is absolutely required for membrane association. Preventing the farnesylation of Ras1 by mutating the farnesylated cysteine to a serine (Ras1<sup>C216S</sup>) causes Ras1 to become cytosolic (Figure 5.7). This observation is in concert with previous studies exploring the role of farnesylation in Ras1 localisation (Onken *et al.* 2006).

Preventing the palmitoylation of Ras1, again through a cysteine to serine mutation (Ras1<sup>C215S</sup>), caused Ras1 to display indiscriminate membrane association (Figure 5.7). However, Ras1<sup>C215S</sup> had previously been described as showing specific localisation to the endomembranes (Onken *et al.* 2006). The current model for ras localisation suggests that farnesylation occurs in the cytoplasm, resulting in an increase in hydrophobicity. This does not however lead to a membrane constrained protein, but one displaying dynamic and transient interactions with cellular membranes. It would therefore be expected that farnesylated proteins, even if initially directed to the endomembranes, would display entropy-driven association to all available cellular membranes. More recent studies have suggested that other monolipidated substrates display a similar entropy-driven general membrane association (Rocks *et al.* 2010). Such observations could have implications on the functional analysis of Ras1<sup>C215S</sup>, as Quimp software analysis indicated that ~15 % of Ras1<sup>C215S</sup> was present at the plasma membrane.

### 8.5.2. The functional implications of preventing C-terminal Ras1 modification.

Based upon previous studies, it would be expected that both Ras1<sup>C215S</sup> and Ras1<sup>C216S</sup> would not support pheromone-dependent signalling. Initial analysis of both mutants indicated that expression from pREP3x supported high levels of pheromone-responsive transcription (Figure 5.17). This result indicates that increasing the concentration of even cytosolic Ras1 could allow signalling in response to pheromone. It has been suggested that the membrane tethering of signalling proteins acts as a means to concentrate pathway components (Kholodenko *et al.* 2000). Increasing the concentration of Ras1 throughout the cell could overcome the need for increased local concentration, allowing effective signalling through the pheromone response pathway.

Upon integration, Ras1<sup>C216S</sup> displayed little signalling activity through either the pheromone response pathway or the polar cell morphology pathway (Figure 5.10-5.14). This observation is in agreement with those presented in Onken *et al.* (2006), suggesting that at lower endogenous expression levels membrane association is required to allow propagation of signalling. However, the activity of Ras1<sup>C215S</sup> differed from that previously reported. Ras1<sup>C215S</sup> supported some pheromone-dependent transcription, which could be mediated by the fraction of Ras1<sup>C215S</sup> at the plasma membrane. Analysis of the morphology of cells expressing Ras1<sup>C215S</sup> revealed no significant signalling through Scd1-Cdc42 (Figure 5.10-5.14). This observation contradicts the results presented in Onken *et al.* (2006), where it is suggested that Ras1 mediates polar cell morphology from the endomembranes. Polar morphology was also not rescued upon the addition of exogenous cAMP (Figure 5.11), which has been shown to rescue the loss of adenylate cyclase and cause hyper-elongated morphologies at higher concentrations (Demirbas *et al.* 2011). These data suggest that plasma membrane localised Ras1 may play some role in the maintenance of cell polarity, in addition to mating.

### 8.5.3. Prolonging the activity of mislocalised Ras1.

Some of the most informative results gained from this study came from the double mutant Ras1<sup>Q66L, C215S</sup>. Increasing the duration of Ras1<sup>C215S</sup> activity using the GTPase deficient mutation Gln66Leu caused an increase in pheromone-responsive transcription (Figure 5.24-5.26). This observation indicates that reducing the concentration of Ras1 at the plasma membrane results in it becoming limiting through the pheromone-response pathway, as increasing the duration of its activity restores signalling. These data are consistent with the current model, in which Ras1 at the plasma membrane is responsible for pheromone-dependent signalling.

Ras1<sup>Q66L, C215S</sup> also supported a partial rescue of polar cell morphology (Figure 5.23). These data also allude to a role for plasma membrane localised Ras1 in regulating cell polarity, as they also suggest that Ras1<sup>C215S</sup> is a limiting factor in the cell morphology pathway.

## 8.6. Increasing the level of Ras1 at the plasma membrane

The data presented in this thesis detailing the activity of Ras1 mutants with altered C-terminal modification suggest that Ras1 at the plasma membrane is key to pheromone-dependent signalling and cell morphology. In order to further investigate the role of plasma membrane localisation in signalling, a number of chimeric proteins were characterised which display increased plasma membrane localisation.

### 8.6.1. The limitations of the Ras1-RitC fusion protein.

One previous Ras1 chimera has been described as demonstrating plasma membrane specific localisation. This chimera contained the N-terminus of Ras1 and the C-terminal localisation domain of the monomeric GTPase Rit (RitC). Ras1-RitC was chosen as it did not traffic through the endomembranes (Onken *et al.* 2006). Ras1-RitC exhibited largely plasma membrane localisation. Despite this, Ras1-RitC was also present in the cytosol and the nucleus, indicating that there was a pool of soluble Ras1-RitC (Figure 6.8).

It was previously suggested that Ras1-RitC could support mating but not polar cell morphology. Using quantitative assays for Ras1 function, it was determined that Ras1-RitC exhibited reduced pheromone-dependent signalling (Figure 6.5) and little mating (Figure 6.3). This would indicate that the function of Ras1 was impaired by altering the C-terminus, as a large amount of the chimera was present at the site of pheromone-dependent signalling. These data indicate that, although Ras1-RitC supports pheromone-responsive signalling,

this activity is impaired. In addition, Ras1-RitC partially rescued polar cell morphology (Figure 6.4). This observation again contradicts the assertion of Onken *et al.* (2006), that Ras1 localised to the plasma membrane is unable to regulate cell morphology. Further, as Ras1-RitC is not trafficked through the endomembranes, the polar cell morphology observed is unlikely to be regulated from the endomembranes. These data again support the notion of a revised model for Ras1 signalling, in which plasma membrane localised Ras1 is involved in the regulation of polar cell morphology.

### 8.6.2. The effect of 1-40Gpa1 on Ras1 localisation.

The first 40 amino acids of the G $\alpha$  subunit Gpa1 have previously been shown to be an efficient plasma membrane targeting domain (Dr Emma Godfrey, unpublished data), containing a consensus MG<sup>2</sup>XXXS<sup>6</sup> myristoylation sequence (Johnson *et al.* 1994) and a downstream cysteine, which could be a target for palmitoylation. The addition of 1-40Gpa1 to the N-terminus of Ras1 proteins with wild-type C-terminal localisation domains caused a slight increase in plasma membrane targeting (Figure 6.12). The labelling of endomembrane structures in these cells was also less pronounced.

An increase in plasma membrane localisation was observed for mutants which lack one or both C-terminal modifications upon the addition of 1-40Gpa1 to the N-terminus. With the exception of Ras1<sup>C216S</sup> (Figure 5.7), the addition of 1-40Gpa1 restored plasma membrane targeting to near wild-type levels in all mutants assayed (Figure 6.12).

### 8.6.3. The effect of 1-40Gpa1 on Ras1 function.

The addition of 1-40Gpa1 to GFP tagged Ras1 had little effect upon function, with 1-40Gpa1-GFP-Ras1 exhibiting similar levels of pheromone-dependent signalling, mating and polar cell morphology to GFP-Ras1 alone. Similarly, all GFP tagged Ras1 mutants with wild-type C-terminal localisation domains

displayed comparable signalling profiles when fused to the first 40 amino acids of Gpa1 (Figure 6.15-6.24).

The most striking observation came upon the analysis of 1-40Gpa1-GFP-Ras1 fusions which lacked one or both C-terminal modifications. The addition of 1-40Gpa1 to GFP-Ras1<sup>C215S</sup> and GFP-Ras1<sup>C216S</sup> increased pheromone-dependent signalling (Figure 6.18-6.23) and restored mating (Figure 6.24). This result highlights the importance of plasma membrane localisation in pheromone-dependent signalling, indicating that increasing the plasma membrane localisation of C-terminal modification mutants, through an entirely distinct localisation domain, increases signalling in response to pheromone.

Most significantly, it was also demonstrated that the addition of 1-40Gpa1 to GFP-Ras1<sup>C215S</sup> elicited a statistically significant partial rescue of polar cell morphology (Figure 6.16), with an accompanying increase in the polar localisation of Tea1 (Figure 6.17). 1-40Gpa1-GFP-Ras1<sup>C216S</sup> also displayed a lower percentage circularity than cells lacking Ras1 and some polar Tea1 localisation. These results demonstrate that moving Ras1 mutants from other cellular compartments to the plasma membrane increases signalling through Scd1-Cdc42. The results generated using 1-40Gpa1 as a plasma membrane targeting motif again highlight a need for Ras1 at the plasma membrane in the regulation of cell polarity.

#### 8.6.4. The limitations of the 1-40Gpa1-GFP-Ras1 fusion.

One of the main reasons cited for the use of the Ras1-RitC fusion was that it did not traffic through the endomembranes before reaching the plasma membrane. As a result, it was suggested that the activity seen in strains expressing Ras1-RitC could be solely attributed to Ras1 activity at the plasma membrane. By contrast 1-40Gpa1-GFP-Ras1 is processed on the endomembranes prior to transport to the plasma membrane. Despite this possible limitation, all 1-40Gpa1-GFP-Ras1 fusions displayed strong plasma membrane localisation. In

addition, the most informative data presented in this study concerns varying the concentration of Ras1 at the plasma membrane rather than attempting to limit Ras1 exclusively to one cellular compartment. Previous work has also suggested that the HVR of ras proteins is important in effector interaction, allowing the ras protein to adopt the correct orientation to interact with a specific binding partner (Abankwa *et al.* 2010). Using 1-40Gpa1 as a localisation domain, the aim was to maintain an intact Ras1 protein while altering the proportion of Ras1 present at the endomembranes or plasma membrane.

Another possible limitation of the 1-40Gpa1-GFP-Ras1 fusion is the reduced functional output observed upon the addition of a tag to the N-terminus of Ras1 (Figure 4.23-4.26). GFP-Ras1 does, however, retain all its functions at a reduced level. As GFP-Ras1 provides a relevant control with which to compare the activities of 1-40Gpa1-GFP-Ras1 fusions, it was felt that this limitation would not significantly affect the interpretation of these data.

### 8.7. A revised model of Ras1 signalling in *Sz. pombe*

The current model for Ras1 signalling in *Sz. pombe* suggests that polar cell morphology is controlled from the endomembranes and that mating is controlled from the plasma membrane (Onken *et al.* 2006). The results presented in this thesis all suggest a role for the plasma membrane localisation of Ras1 in all signalling processes, including cell polarity. These data do not obviate the possibility that Ras1 at the endomembranes has a functional role. Activation of Ras1 by Efc25 may, for example, occur on the endomembranes prior to the transport of active Ras1 to the plasma membrane. Similarly, Ras1 may become active at the periphery of the cell, but interact with effectors on the endomembranes.

Recent studies have suggested that the palmitoylation and depalmitoylation of ras proteins exists primarily to allow the directed transport of ras to the plasma membrane, while preventing the entropy-driven distribution of

ras to all membrane compartments upon processes such as endocytosis and membrane turnover (Rocks *et al.* 2010). These observations would suggest that one of the main roles for endomembrane localised Ras1 is as a trafficking intermediate to allow efficient plasma membrane targeting (Figure 8.2). In addition, a recent study has suggested that Gap1 localises to the growing tip during mitotic growth (Cathryn Weston, unpublished data). These data further highlight a role for Ras1 at the cell periphery in regulating cell polarity.

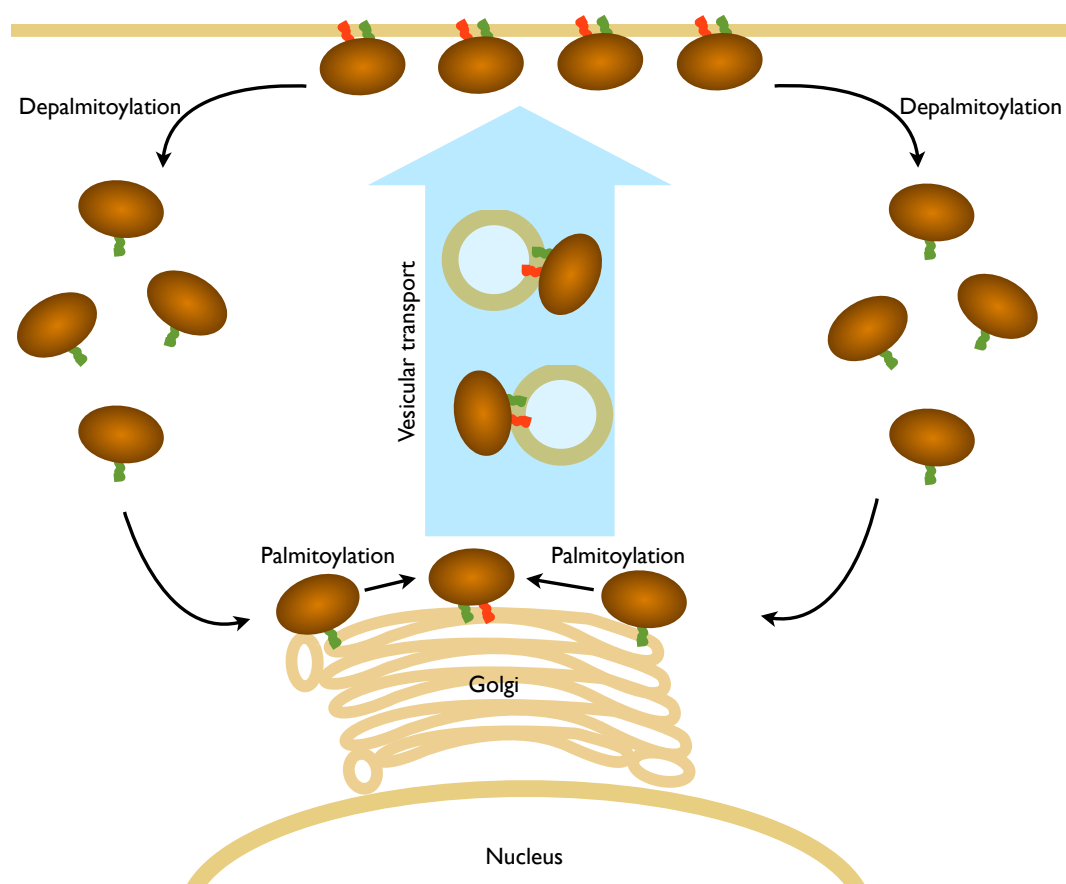


**Figure 8.2. The directed transport of palmitoylated ras**

The palmitoylation and depalmitoylation cycle is required for the directed transport of palmitoylated ras isoforms to the plasma membrane. Palmitoylation of ras on the Golgi increases membrane affinity allowing vesicular transport of ras to the plasma membrane. Without depalmitoylation endocytic processes would cause the eventual redistribution of ras to other cellular membrane compartments. Depalmitoylation allows ras to return to the Golgi where it is able to undergo palmitoylation and transport back to the plasma membrane. This process allows the preferential localisation of ras to the periphery of the cell.

### 8.8. Human ras function in *Sz. pombe*

The final section of this thesis details the functional expression of three human ras isoforms in *Sz. pombe*. Human H-Ras, N-Ras and K-Ras4B all displayed signalling activity in *Sz. pombe* both in response to pheromone and in regulating cell polarity (Figure 7.6-7.9). All three also supported some spore formation upon mating, but with very low efficiency (Figure 7.12). The level of pheromone-dependent signalling also matched closely the level of each isoform present at the periphery of the cell, further supporting the notion that the plasma membrane localisation of ras is key to pheromone-dependent signalling (Figure 7.7).

Human H-Ras, N-Ras and K-Ras4B all displayed quite differing localisation patterns in *Sz. pombe* (Figure 7.2). In addition, these localisation patterns did not just appear to be a function of their C-terminal modifications, as N-Ras and Ras1 displayed highly divergent localisation despite both containing a single palmitoyl and a single farnesyl modification. Previous studies have suggested the importance of regions upstream of these modifications. Ras1 in particular has a very large C-terminus, which could account for the differences in localisation observed between N-Ras and Ras1 (Hancock 2003). Confirmation that the human ras isoforms are correctly modified in *Sz. pombe* would be required to draw meaningful comparisons between their localisations and that of Ras1.

The functional expression of human ras in *Sz. pombe* raises the possibility of studying individual ras isoforms in isolation in a simple model system, in addition to the investigation of human regulatory proteins, such as human GAPs.

### 8.9. Perspectives and future directions

The results presented in this study indicate the importance of Ras1 plasma membrane localisation in all aspects of Ras1 signalling. However, further work is needed to determine the exact mechanism of Ras1 activity at the plasma membrane. It is known that Ras1 acts downstream of Gpa1 to recruit Byr2 to the cell periphery during mating (Bauman *et al.* 1998), however the mechanism by which Efc25 regulates Ras1 and brings about cell polarisation is not fully understood. This study has demonstrated that Ras1 is required at the plasma membrane during this process, however it is still possible that there is a role for endomembrane localised Ras1 in fission yeast. It is also still not fully understood how cells undergo the switch from vegetative cell growth to shmoo formation, and the exact role of Ras1 in this process.

The results presented in this thesis also support the emerging theory, suggesting that the primary role of the palmitoylation cycle is in the maintenance of proteins at a steady state at the plasma membrane (Rocks *et al.* 2010). Finally, a further study in mammalian systems has questioned the impact of endomembrane ras signalling (Augsten *et al.* 2006). This study illustrated that the plasma membrane is the predominant site of ras activation, and suggested that experimentally elevated expression levels was the primary confounding factor in determining the localisation of ras signalling. This finding demonstrates a number of parallels with those reported in this thesis.

### 8.10. Conclusions

The data presented in this thesis demonstrates that the localisation of Ras1 to the plasma membrane is key to all signalling outputs, raising the possibility of a revised model for the regulation of Ras1 in *Sz. pombe*. It was also indicated that the extent of Ras1 signalling and the regulation of Ras1 expression are key to signalling output. Increased Ras1 signalling negatively

affected cell viability and essential processes such as chromosome segregation. Finally, the functional expression of human ras isoforms validated the use of *Sz. pombe* as a model system for the heterologous expression of human ras signalling components.

## Bibliography

- Abankwa, D., Gorfe, A. A. and Hancock, J. F.** (2007). Ras nanoclusters: Molecular structure and assembly. *Semin. Cell Dev. Biol.* **18**, 599–607.
- Abankwa, D., Gorfe, A. A., Inder, K. and Hancock, J. F.** (2010). Ras membrane orientation and nanodomain localization generate isoform diversity. *Proc. Natl. Acad. Sci. U S A* **107**, 1130–1135.
- Akasaka, K., Tamada, M., Wang, F., Kariya, K., Shima, F., Kikuchi, A., Yamamoto, M., Shirouzu, M., Yokoyama, S. and Kataoka, T.** (1996). Differential structural requirements for interaction of Ras protein with its distinct downstream effectors. *J. Biol. Chem.* **271**, 5353–5360.
- Allshire, R. C., Nimmo, E. R., Ekwall, K., Javerzat, J. P. and Cranston, G.** (1995). Mutations derepressing silent centromeric domains in fission yeast disrupt chromosome segregation. *Genes Dev.* **9**, 218–233.
- Apolloni, A., Prior, I. A., Lindsay, M., Parton, R. G. and Hancock, J. F.** (2000). H-Ras but not K-Ras traffics to the plasma membrane through the exocytic pathway. *Mol. Cell. Biol.* **20**, 2475–2487.
- Appels, N. M. G. M., Beijnen, J. H. and Schellens, J. H. M.** (2005). Development of farnesyl transferase inhibitors: a review. *Oncologist* **10**, 565–578.
- Arkininstall, S., Edgerton, M., Payton, M. and Maundrell, K.** (1995). Co-expression of the neurokinin NK<sub>2</sub> receptor and G-protein components in the fission yeast *Schizosaccharomyces pombe*. *FEBS Lett.* **375**, 183–187.
- Arozarena, I., Matallanas, D., Berciano, M. T., Sanz-Moreno, V., Calvo, F., Munoz, M. T., Egea, G., Lafarga, M. and Crespo, P.** (2004). Activation of H-Ras in the endoplasmic reticulum by the rasGRF family guanine nucleotide exchange factors. *Mol. Cell. Biol.* **24**, 1516–1530.

- Augsten, M., Pusch, R., Biskup, C., Rennert, K., Wittig, U., Beyer, K., Blume, A., Wetzker, R., Friedrich, K. and Rubio, I.** (2006). Live-cell imaging of endogenous Ras-GTP illustrates predominant Ras activation at the plasma membrane. *EMBO Rep.* **7**, 46–51.
- Bähler, J. and Nurse, P.** (2001). Fission yeast pom1p kinase activity is cell cycle regulated and essential for cellular symmetry during growth and division. *Embo J.* **20**, 1064–1073.
- Baldwin, J. M.** (1993). The probable arrangement of the helices in G protein-coupled receptors. *EMBO J.* **12**, 1693–1703.
- Ballester, R., Marchuk, D., Boguski, M., Saulino, A., Letcher, R., Wigler, M. and Collins, F.** (1990). The NF1 locus encodes a protein functionally related to mammalian GAP and yeast IRA proteins. *Cell* **63**, 851–859.
- Ballesteros, J. A., Jensen, A. D., Liapakis, G., Rasmussen, S. G., Shi, L., Gether, U. and Javitch, J. A.** (2001). Activation of the beta 2-adrenergic receptor involves disruption of an ionic lock between the cytoplasmic ends of transmembrane segments 3 and 6. *J. Biol. Chem.* **276**, 29171–29177.
- Bauman, P., Cheng, Q. C. and Albright, C. F.** (1998). The Byr2 kinase translocates to the plasma membrane in a Ras1-dependent manner. *Biochem. Biophys. Res. Commun.* **244**, 468–474.
- Behrens, R. and Nurse, P.** (2002). Roles of fission yeast tea1p in the localization of polarity factors and in organizing the microtubular cytoskeleton. *J. Cell Biol.* **157**, 783–793.
- Bijlmakers, M.-J. and Marsh, M.** (2003). The on-off story of protein palmitoylation. *Trends Cell Biol.* **13**, 32–42.
- Bivona, T. G., Perez De Castro, I., Ahearn, I. M., Grana, T. M., Chiu, V. K., Lockyer, P. J., Cullen, P. J., Pellicer, A., Cox, A. D. and Philips, M. R.** (2003). Phospholipase  $\gamma$  activates Ras on the Golgi apparatus by means of RasGRP1. *Nature* **424**, 694–698.

- Bivona, T. G., Quatela, S. E., Bodemann, B. O., Ahearn, I. M., Soskis, M. J., Mor, A., Miura, J., Wiener, H. H., Wright, L., Saba, S. G., Yim, D., Fein, A., Perez de Castro, I., Li, C., Thompson, C. B., Cox, A. D. and Philips, M. R.** (2006). PKC regulates a farnesyl-electrostatic switch on K-Ras that promotes its association with Bcl-X<sub>L</sub> on mitochondria and induces apoptosis. *Mol. Cell* **21**, 481–493.
- Blumer, J. B., Cismowski, M. J., Sato, M. and Lanier, S. M.** (2005). AGS proteins: receptor-independent activators of G-protein signaling. *Trends Pharmacol. Sci.* **26**, 470–476.
- Boguski, M. S. and McCormick, F.** (1993). Proteins regulating Ras and its relatives. *Nature* **366**, 643–654.
- Bos, J. L.** (1989). ras oncogenes in human cancer: a review. *Cancer Res.* **49**, 4682–4689.
- Bos, J. L., Rehmann, H. and Wittinghofer, A.** (2007). GEFs and GAPs: critical elements in the control of small G proteins. *Cell* **129**, 865–877.
- Bosgraaf, L., van Haastert, P. J. M. and Bretschneider, T.** (2009). Analysis of cell movement by simultaneous quantification of local membrane displacement and fluorescent intensities using Quimp2. *Cell Motil. Cytoskeleton* **66**, 156–165.
- Broek, D., Toda, T., Michaeli, T., Levin, L., Birchmeier, C., Zoller, M., Powers, S. and Wigler, M.** (1987). The *S. cerevisiae* CDC25 gene product regulates the RAS/adenylate cyclase pathway. *Cell* **48**, 789–799.
- Bunney, T. D., Harris, R., Gandarillas, N. L., Josephs, M. B., Roe, S. M., Sorli, S. C., Paterson, H. F., Rodrigues-Lima, F., Esposito, D., Ponting, C. P., Gierschik, P., Pearl, L. H., Driscoll, P. C. and Katan, M.** (2006). Structural and mechanistic insights into ras association domains of phospholipase C $\epsilon$ . *Mol. Cell* **21**, 495–507.
- Campbell, S. L., Khosravi-Far, R., Rossman, K. L., Clark, G. J. and Der, C. J.** (1998). Increasing complexity of ras signaling. *Oncogene* **17**, 1395–1413.

- Chang, E. C., Barr, M., Wang, Y., Jung, V., Xu, H. P. and Wigler, M. H.** (1994). Cooperative interaction of *S. pombe* proteins required for mating and morphogenesis. *Cell* **79**, 131–141.
- Chang, E. C. and Philips, M. R.** (2006). Spatial segregation of Ras signaling: new evidence from fission yeast. *Cell Cycle* **5**, 1936–1939.
- Chen, Z. Q., Ulsh, L. S., DuBois, G. and Shih, T. Y.** (1985). Post-translational processing of p21 ras proteins involves palmitoylation of the C-terminal tetrapeptide containing cysteine-186. *J. Virol.* **56**, 607–612.
- Chiu, V. K., Bivona, T., Hach, A., Sajous, J. B., Silletti, J., Wiener, H., Johnson, Ronald L., n., Cox, A. D. and Philips, M. R.** (2002). Ras signalling on the endoplasmic reticulum and the Golgi. *Nat. Cell Biol.* **4**, 343–350.
- Choy, E., Chiu, V. K., Silletti, J., Feoktistov, M., Morimoto, T., Michaelson, D., Ivanov, I. E. and Philips, M. R.** (1999). Endomembrane trafficking of ras: the CAAX motif targets proteins to the ER and Golgi. *Cell* **98**, 69–80.
- Clapham, D. E. and Neer, E. J.** (1997). G protein  $\beta\gamma$  subunits. *Annu. Rev. Pharmacol. Toxicol.* **37**, 167–203.
- Clarke, S.** (1992). Protein isoprenylation and methylation at carboxyl-terminal cysteine residues. *Annu. Rev. Biochem.* **61**, 355–86.
- Coffin, J. M., Varmus, H. E., Bishop, J. M., Essex, M., Hardy, Jr, W. D., Martin, G. S., Rosenberg, N. E., Scolnick, E. M., Weinberg, R. A. and Vogt, P. K.** (1981). Proposal for naming host cell-derived inserts in retrovirus genomes. *J. Virol.* **40**, 953–7.
- Corpet, F.** (1988). Multiple sequence alignment with hierarchical clustering. *Nucleic Acids Res.* **16**, 10881–10890.
- Cowley, S., Paterson, H., Kemp, P. and Marshall, C. J.** (1994). Activation of MAP kinase kinase is necessary and sufficient for PC12 differentiation and for transformation of NIH 3T3 cells. *Cell* **77**, 841–852.
- Das, M., Wiley, D. J., Chen, X., Shah, K. and Verde, F.** (2009).

- The conserved NDR kinase Orb6 controls polarized cell growth by spatial regulation of the small GTPase Cdc42. *Curr. Biol.* **19**, 1314–1319.
- Daub, H., Wallasch, C., Lankenau, A., Herrlich, A. and Ullrich, A.** (1997). Signal characteristics of G protein-transactivated EGF receptor. *EMBO J.* **16**, 7032–7044.
- Davey, J.** (1991). Isolation and quantification of M-factor, a diffusible mating pheromone from the fission yeast, *Schizosaccharomyces pombe*. *Yeast* **7**, 357–366.
- Davey, J.** (1998). Fusion of a fission yeast. *Yeast* **14**, 1529–1566.
- Davey, J., Egel, R. and Nielsen, O.** (1995). Microbial Gene Techniques, Methods in Molecular Genetics, **6B**, Academic Press, San Diego, p.247 .
- Davey, J. and Nielsen, O.** (1994). Mutations in *cyr1* and *pat1* reveal pheromone-induced G1 arrest in the fission yeast *Schizosaccharomyces pombe*. *Curr. Genet.* **26**, 105–112.
- Dekker, F. J., Rocks, O., Vartak, N., Menninger, S., Hedberg, C., Balamurugan, R., Wetzels, S., Renner, S., Gerauer, M., Schölermann, B., Rusch, M., Kramer, J. W., Rauh, D., Coates, G. W., Brunsveld, L., Bastiaens, P. I. H. and Waldmann, H.** (2010). Small-molecule inhibition of APT1 affects Ras localization and signaling. *Nat. Chem. Biol.* **6**, 449–456.
- Demirbas, D., Ceyhan, O., Wyman, A. R., Ivey, F. D., Allain, C., Wang, L., Sharuk, M. N., Francis, S. H. and Hoffman, C. S.** (2011). Use of a *Schizosaccharomyces pombe* PKA-repressible reporter to study cGMP metabolising phosphodiesterases. *Cell. Signal.* **23**, 594–601.
- Der, C. J., Krontiris, T. G. and Cooper, G. M.** (1982). Transforming genes of human bladder and lung carcinoma cell lines are homologous to the ras genes of Harvey and Kirsten sarcoma viruses. *Proc. Natl. Acad. Sci. U S A* **79**, 3637–3640.
- Di Guglielmo, G. M., Baass, P. C., Ou, W. J., Posner, B. I. and Bergeron, J. J.** (1994). Compartmentalization of SHC, GRB2 and mSOS, and

- hyperphosphorylation of Raf-1 by EGF but not insulin in liver parenchyma. *EMBO J.* **13**, 4269–77.
- Didmon, M., Davis, K., Watson, P., Ladds, G., Broad, P. and Davey, J.** (2002). Identifying regulators of pheromone signalling in the fission yeast *Schizosaccharomyces pombe*. *Curr. Genet.* **41**, 241–253.
- Dohlman, H. G., Apaniesk, D., Chen, Y., Song, J. and Nusskern, D.** (1995). Inhibition of G-protein signaling by dominant gain-of-function mutations in Sst2p, a pheromone desensitization factor in *Saccharomyces cerevisiae*. *Mol. Cell. Biol.* **15**, 3635–3643.
- Donaldson, J. G.** (2008). Arfs and membrane lipids: sensing, generating and responding to membrane curvature. *Biochem. J.* **414**, 1–2.
- Dormann, D., Libotte, T., Weijer, C. J. and Bretschneider, T.** (2002). Simultaneous quantification of cell motility and protein-membrane-association using active contours. *Cell Motil. Cytoskeleton* **52**, 221–230.
- Downward, J.** (2003). Targeting RAS signalling pathways in cancer therapy. *Nat. Rev. Cancer* **3**, 11–22.
- Egel, R. and Egel-Mitani, M.** (1974). Premeiotic DNA synthesis in fission yeast. *Exp. Cell Res.* **88**, 127–134.
- Egel, R., Willer, M., Kjaerulff, S., Davey, J. and Nielsen, O.** (1994). Assessment of pheromone production and response in fission yeast by a halo test of induced sporulation. *Yeast* **10**, 1347–1354.
- Eisenberg, S. and Henis, Y. I.** (2008). Interactions of ras proteins with the plasma membrane and their roles in signaling. *Cell. Signal.* **20**, 31–39.
- Ellis, R. W., Defeo, D., Shih, T. Y., Gonda, M. A., Young, H. A., Tsuchida, N., Lowy, D. R. and Scolnick, E. M.** (1981). The p21 *src* genes of Harvey and Kirsten sarcoma viruses originate from divergent members of a family of normal vertebrate genes. *Nature* **292**, 506–511.
- Endo, M., Shirouzu, M. and Yokoyama, S.** (2003). The Cdc42 binding and scaffolding activities of the fission yeast adaptor protein Scd2. *J. Biol. Chem.* **278**, 843–852.

- Evanko, D. S., Thiyagarajan, M. M. and Wedegaertner, P. B.** (2000). Interaction with G $\beta\gamma$  is required for membrane targeting and palmitoylation of G $\alpha_s$  and G $\alpha_q$ . *J. Biol. Chem.* **275**, 1327–2336.
- Feierbach, B. and Chang, F.** (2001). Roles of the fission yeast formin for3p in cell polarity, actin cable formation and symmetric cell division. *Curr. Biol.* **11**, 1656–1665.
- Feig, L. A. and Cooper, G. M.** (1988). Inhibition of NIH 3T3 cell proliferation by a mutant ras protein with preferential affinity for GDP. *Mol. Cell. Biol.* **8**, 3235–3243.
- Ferguson, S. S.** (2001). Evolving concepts in G protein-coupled receptor endocytosis: the role in receptor desensitization and signaling. *Pharmacol. Rev.* **53**, 1–24.
- Fernández-Medarde, A. and Santos, E.** (2011). The RasGRF family of mammalian guanine nucleotide exchange factors. *Biochim Biophys Acta* **1815**, 170–188.
- Ficca, A. G., Testa, L. and Tocchini Valentini, G. P.** (1995). The human beta 2-adrenergic receptor expressed in *Schizosaccharomyces pombe* retains its pharmacological properties. *FEBS Lett.* **377**, 140–144.
- Fivaz, M. and Meyer, T.** (2005). Reversible intracellular translocation of KRas but not HRas in hippocampal neurons regulated by Ca<sup>2+</sup>/calmodulin. *J. Cell Biol.* **170**, 429–41.
- Fredriksson, R., Lagerström, M. C., Lundin, L.-G. and Schiöth, H. B.** (2003). The G-protein-coupled receptors in the human genome form five main families. Phylogenetic analysis, paralogon groups, and fingerprints. *Mol. Pharmacol.* **63**, 1256–72.
- Fukui, Y., Kaziro, Y. and Yamamoto, M.** (1986a). Mating pheromone-like diffusible factor released by *Schizosaccharomyces pombe*. *EMBO J.* **5**, 1991–1993.
- Fukui, Y., Kozasa, T., Kaziro, Y., Takeda, T. and Yamamoto, M.** (1986b). Role of a ras homolog in the life cycle of *Schizosaccharomyces*

- pombe*. *Cell* **44**, 329–336.
- Fukui, Y., Miyake, S., Satoh, M. and Yamamoto, M.** (1989). Characterization of the *Schizosaccharomyces pombe* *ral2* gene implicated in activation of the *ras1* gene product. *Mol. Cell. Biol.* **9**, 5617–5622.
- Garcia, P., Tajadura, V., Garcia, I. and Sanchez, Y.** (2006). Role of Rho GTPases and Rho-GEFs in the regulation of cell shape and integrity in fission yeast. *Yeast* **23**, 1031–1043.
- Gibbs, J. B., Sigal, I. S., Poe, M. and Scolnick, E. M.** (1984). Intrinsic GTPase activity distinguishes normal and oncogenic ras p21 molecules. *Proc. Natl. Acad. Sci. U S A* **81**, 5704–5708.
- Gilman, A. G.** (1987). G proteins: transducers of receptor-generated signals. *Annu. Rev. Biochem.* **56**, 615–649.
- Glynn, J. M., Lustig, R. J., Berlin, A. and Chang, F.** (2001). Role of bud6p and tea1p in the interaction between actin and microtubules for the establishment of cell polarity in fission yeast. *Curr. Biol.* **11**, 836–845.
- Goddard, A., Ladds, G., Forfar, R. and Davey, J.** (2006). Identification of Gnr1p, a negative regulator of G $\alpha$  signalling in *Schizosaccharomyces pombe*, and its complementation by human G $\beta$  subunits. *Fungal Genet. Biol.* **43**, 840–851.
- Godfrey, E. L.** (2009). Investigating the signalling characteristics of G $\alpha$  subunits in the fission yeast *Schizosaccharomyces pombe*.
- Grimm, C., Kohli, J., Murray, J. and Maundrell, K.** (1988). Genetic engineering of *Schizosaccharomyces pombe*: a system for gene disruption and replacement using the *ura4* gene as a selectable marker. *Mol. Gen. Genet.* **215**, 81–86.
- Gutierrez, L., Magee, A. I., Marshall, C. J. and Hancock, J. F.** (1989). Post-translational processing of p21ras is two-step and involves carboxyl-methylation and carboxy-terminal proteolysis. *EMBO J.* **8**, 1093–1098.
- Hancock, J. F.** (2003). Ras proteins: different signals from different locations. *Nat. Rev. Mol. Cell Biol.* **4**, 373–384.

- Hancock, J. F., Magee, A. I., Childs, J. E. and Marshall, C. J.** (1989). All ras proteins are polyisoprenylated but only some are palmitoylated. *Cell* **57**, 1167–1177.
- Harvey, J. J.** (1964). An unidentified virus which causes the rapid production of tumors in mice. *Nature* **204**, 1104–1105.
- Hepler, J. R. and Gilman, A. G.** (1992). G proteins. *Trends Biochem. Sci.* **17**, 383–387.
- Hill, C., Brownlie, Z., Davey, J., Milligan, G. and Ladds, G.** (2008). Isolation and characterization of a novel human RGS mutant displaying gain-of-function activity. *Cell. Signal.* **20**, 323–336.
- Hirota, K., Tanaka, K., Watanabe, Y. and Yamamoto, M.** (2001). Functional analysis of the C-terminal cytoplasmic region of the M-factor receptor in fission yeast. *Genes Cells* **6**, 201–214.
- Hoffman, C. S.** (2005a). Except in every detail: comparing and contrasting G-protein signaling in *Saccharomyces cerevisiae* and *Schizosaccharomyces pombe*. *Eukaryot. Cell* **4**, 495–503.
- Hoffman, C. S.** (2005b). Glucose sensing via the protein kinase A pathway in *Schizosaccharomyces pombe*. *Biochem. Soc. Trans.* **33**, 257–260.
- Hoffman, C. S. and Winston, F.** (1987). A ten-minute DNA preparation from yeast efficiently releases autonomous plasmids for transformation of *Escherichia coli*. *Gene* **57**, 267–272.
- Howe, C. L., Valletta, J. S., Rusnak, A. S. and Mobley, W. C.** (2001). NGF signaling from clathrin-coated vesicles: evidence that signaling endosomes serve as a platform for the Ras-MAPK pathway. *Neuron* **32**, 801–814.
- Hughes, D. A., Fukui, Y. and Yamamoto, M.** (1990). Homologous activators of ras in fission and budding yeast. *Nature* **344**, 355–357.
- Hughes, M. and Davey, J.** (1997). The role of Sxa1 in pheromone recovery in *Schizosaccharomyces pombe*. *Biochem. Soc. Trans.* **25**, 229–229.
- Hurley, J. B., Simon, M. I., Teplow, D. B., Robishaw, J. D. and Gilman, A. G.** (1984). Homologies between signal transducing G proteins

- and ras gene products. *Science* **226**, 860–862.
- Imai, Y., Miyake, S., Hughes, D. A. and Yamamoto, M.** (1991). Identification of a GTPase-activating protein homolog in *Schizosaccharomyces pombe*. *Mol. Cell. Biol.* **11**, 3088–3094.
- Imai, Y. and Yamamoto, M.** (1992). *Schizosaccharomyces pombe* *sxa1*<sup>+</sup> and *sxa2*<sup>+</sup> encode putative proteases involved in the mating response. *Mol. Cell. Biol.* **12**, 1827–1834.
- Imai, Y. and Yamamoto, M.** (1994). The fission yeast mating pheromone P-factor: its molecular structure, gene structure, and ability to induce gene expression and G<sub>1</sub> arrest in the mating partner. *Genes Dev.* **8**, 328–338.
- Isshiki, T., Mochizuki, N., Maeda, T. and Yamamoto, M.** (1992). Characterization of a fission yeast gene, *gpa2*, that encodes a G alpha subunit involved in the monitoring of nutrition. *Genes Dev.* **6**, 2455–2462.
- Ivey, F. D. and Hoffman, C. S.** (2005). Direct activation of fission yeast adenylate cyclase by the Gpa2 G $\alpha$  of the glucose signaling pathway. *Proc. Natl. Acad. Sci. U S A* **102**, 6108–6113.
- Iwashita, S. and Song, S.-Y.** (2008). RasGAPs: a crucial regulator of extracellular stimuli for homeostasis of cellular functions. *Mol. Biosyst.* **4**, 213–222.
- Jackson, J. H., Li, J. W., Buss, J. E., Der, C. J. and Cochrane, C. G.** (1994). Polylysine domain of K-Ras4b protein is crucial for malignant transformation. *Proc. Natl. Acad. Sci. U S A* **91**, 12730–12734.
- Jin, M., Fujita, M., Culley, B. M., Apolinario, E., Yamamoto, M., Maundrell, K. and Hoffman, C. S.** (1995). *sck1*, a high copy number suppressor of defects in the cAMP-dependent protein kinase pathway in fission yeast, encodes a protein homologous to the *Saccharomyces cerevisiae* SCH9 kinase. *Genetics* **140**, 457–467.
- Johnson, D. R., Bhatnagar, R. S., Knoll, L. J. and Gordon, J. I.** (1994). Genetic and biochemical studies of protein N-myristoylation. *Annu. Rev. Biochem.* **63**, 869–914.

- Jones, S., Vignais, M. L. and Broach, J. R.** (1991). The CDC25 protein of *Saccharomyces cerevisiae* promotes exchange of guanine nucleotides bound to ras. *Mol. Cell. Biol.* **11**, 2641–2646.
- Josefsson, L. G.** (1999). Evidence for kinship between diverse G-protein coupled receptors. *Gene* **239**, 333–340.
- Jung, V., Wei, W., Ballester, R., Camonis, J., Mi, S., Van Aelst, L., Wigler, M. and Broek, D.** (1994). Two types of RAS mutants that dominantly interfere with activators of RAS. *Mol. Cell. Biol.* **14**, 3707–3718.
- Kae, H., Lim, C. J., Spiegelman, G. B. and Weeks, G.** (2004). Chemoattractant-induced ras activation during *Dictyostelium* aggregation. *EMBO Rep.* **5**, 602–606.
- Kamata, T. and Feramisco, J. R.** (1984). Epidermal growth factor stimulates guanine nucleotide binding activity and phosphorylation of *ras* oncogene proteins. *Nature* **310**, 147–150.
- Kelley, G. G., Reks, S. E., Ondrako, J. M. and Smrcka, A. V.** (2001). Phospholipase C $\epsilon$ : a novel Ras effector. *EMBO J.* **20**, 743–754.
- Kelly, F. D. and Nurse, P.** (2011). Spatial control of Cdc42 activation determines cell width in fission yeast. *Mol. Biol. Cell* , 10.1091/mbc.E11-01-0057.
- Kholodenko, B. N., Hoek, J. B. and Westerhoff, H. V.** (2000). Why cytoplasmic signalling proteins should be recruited to cell membranes. *Trends Cell Biol.* **10**, 173–178.
- Kim, H., Yang, P., Catanuto, P., Verde, F., Lai, H., Du, H., Chang, F. and Marcus, S.** (2003). The kelch repeat protein, Tea1, is a potential substrate target of the p21-activated kinase, Shk1, in the fission yeast, *Schizosaccharomyces pombe*. *J. Biol. Chem.* **278**, 30074–30082.
- Kirsten, W. H. and Mayer, L. A.** (1967). Morphologic responses to a murine erythroblastosis virus. *J. Natl. Cancer Inst.* **39**, 311–335.
- Kitamura, K. and Shimoda, C.** (1991). The *Schizosaccharomyces pombe* *mam2* gene encodes a putative pheromone receptor which has a significant

- homology with the *Saccharomyces cerevisiae* Ste2 protein. *EMBO J.* **10**, 3743–3751.
- Kjaerulff, S., Lautrup-Larsen, I., Truelsen, S., Pedersen, M. and Nielsen, O.** (2005). Constitutive activation of the fission yeast pheromone-responsive pathway induces ectopic meiosis and reveals *ste11* as a mitogen-activated protein kinase target. *Mol. Cell. Biol.* **25**, 2045–2059.
- Klar, A. J. and Miglio, L. M.** (1986). Initiation of meiotic recombination by double-strand DNA breaks in *S. pombe*. *Cell* **46**, 725–731.
- Krengel, U., Schlichting, I., Scherer, A., Schumann, R., Frech, M., John, J., Kabsch, W., Pai, E. F. and Wittinghofer, A.** (1990). Three-dimensional structures of H-Ras p21 mutants: molecular basis for their inability to function as signal switch molecules. *Cell* **62**, 539–548.
- La Carbona, S., Le Goff, C. and Le Goff, X.** (2006). Fission yeast cytoskeletons and cell polarity factors: connecting at the cortex. *Biol. Cell* **98**, 619–631.
- Ladds, G. and Davey, J.** (2000). Sxa2 is a serine carboxypeptidase that degrades extracellular P-factor in the fission yeast *Schizosaccharomyces pombe*. *Mol. Microbiol.* **36**, 377–390.
- Ladds, G., Davis, K., Hillhouse, E. W. and Davey, J.** (2003). Modified yeast cells to investigate the coupling of G protein-coupled receptors to specific G proteins. *Mol. Microbiol.* **47**, 781–792.
- Ladds, G., Goddard, A. and Davey, J.** (2005). Functional analysis of heterologous GPCR signalling pathways in yeast. *Trends Biotechnol.* **23**, 367–373.
- Ladds, G., Goddard, A., Hill, C., Thornton, S. and Davey, J.** (2007). Differential effects of RGS proteins on G  $\alpha_q$  and G  $\alpha_{11}$  activity. *Cell. Signal.* **19**, 103–113.
- Ladds, G., Rasmussen, E. M., Young, T., Nielsen, O. and Davey, J.** (1996). The *sxa2*-dependent inactivation of the P-factor mating pheromone in the fission yeast *Schizosaccharomyces pombe*. *Mol. Microbiol.* **20**, 35–42.

- Lambright, D. G., Noel, J. P., Hamm, H. E. and Sigler, P. B.** (1994). Structural determinants for activation of the  $\alpha$ -subunit of a heterotrimeric G protein. *Nature* **369**, 621–628.
- Lee, E., Taussig, R. and Gilman, A. G.** (1992). The G226A mutant of  $G_{as}$  highlights the requirement for dissociation of G protein subunits. *J. Biol. Chem.* **267**, 1212–8.
- Leipe, D. D., Wolf, Y. I., Koonin, E. V. and Aravind, L.** (2002). Classification and evolution of P-loop GTPases and related ATPases. *J. Mol. Biol.* **317**, 41–72.
- Levkowitz, G., Waterman, H., Zamir, E., Kam, Z., Oved, S., Langdon, W. Y., Beguinot, L., Geiger, B. and Yarden, Y.** (1998). c-Cbl/Sli-1 regulates endocytic sorting and ubiquitination of the epidermal growth factor receptor. *Genes Dev.* **12**, 3663–3674.
- Li, Y. C., Chen, C. R. and Chang, E. C.** (2000). Fission yeast Ras1 effector Scd1 interacts with the spindle and affects its proper formation. *Genetics* **156**, 995–1004.
- Lui, K. and Huang, Y.** (2009). RanGTPase: A key regulator of nucleocytoplasmic trafficking. *Mol. Cell. Pharmacol.* **1**, 148–156.
- Luttrell, L. M., Daaka, Y. and Lefkowitz, R. J.** (1999). Regulation of tyrosine kinase cascades by G-protein-coupled receptors. *Curr. Opin. Cell Biol.* **11**, 177–183.
- Maeda, T., Mochizuki, N. and Yamamoto, M.** (1990). Adenylyl cyclase is dispensable for vegetative cell growth in the fission yeast *Schizosaccharomyces pombe*. *Proc. Natl. Acad. Sci. U S A* **87**, 7814–7818.
- Malumbres, M. and Barbacid, M.** (2003). Ras oncogenes: the first 30 years. *Nat. Rev. Cancer* **3**, 459–465.
- Marcus, S., Polverino, A., Chang, E., Robbins, D., Cobb, M. H. and Wigler, M. H.** (1995). Shk1, a homolog of the *Saccharomyces cerevisiae* Ste20 and mammalian p65PAK protein kinases, is a component of a Ras/Cdc42 signaling module in the fission yeast *Schizosaccharomyces pombe*.

- Proc. Natl. Acad. Sci. U S A* **92**, 6180–6184.
- Marks, J., Hagan, I. M. and Hyams, J. S.** (1986). Growth polarity and cytokinesis in fission yeast: the role of the cytoskeleton. *J. Cell Sci. Suppl.* **5**, 229–241.
- Marrari, Y., Crouthamel, M., Irannejad, R. and Wedegaertner, P. B.** (2007). Assembly and trafficking of heterotrimeric G proteins. *Biochemistry* **46**, 7665–7677.
- Mata, J. and Nurse, P.** (1997). Tea1 and the microtubular cytoskeleton are important for generating global spatial order within the fission yeast cell. *Cell* **89**, 939–949.
- Matallanas, D., Sanz-Moreno, V., Arozarena, I., Calvo, F., Agudo-Ibanez, L., Santos, E., Berciano, M. T. and Crespo, P.** (2006). Distinct utilization of effectors and biological outcomes resulting from site-specific ras activation: Ras functions in lipid rafts and Golgi complex are dispensable for proliferation and transformation. *Mol. Cell. Biol.* **26**, 100–116.
- Maundrell, K.** (1993). Thiamine-repressible expression vectors pREP and pRIP for fission yeast. *Gene* **123**, 127–130.
- McCormick, F.** (1989). Ras GTPase activating protein: signal transmitter and signal terminator. *Cell* **56**, 5–8.
- McCormick, F.** (1993). Signal transduction. How receptors turn Ras on. *Nature* **363**, 15–16.
- Miller, P. J. and Johnson, D. I.** (1994). Cdc42p GTPase is involved in controlling polarized cell growth in *Schizosaccharomyces pombe*. *Mol. Cell. Biol.* **14**, 1075–1083.
- Mineo, C., Gill, G. N. and Anderson, R. G.** (1999). Regulated migration of epidermal growth factor receptor from caveolae. *J. Biol. Chem.* **274**, 30636–30643.
- Mitin, N., Rossman, K. L. and Der, C. J.** (2005). Signaling interplay in Ras superfamily function. *Curr. Biol.* **15**, 563–574.

- Miyata, M., Matsuoka, M. and Inada, T.** (1997). Induction of sexual co-flocculation of heterothallic fission yeast (*Schizosaccharomyces pombe*) cells by mating pheromones. *J. Gen. Appl. Microbiol.* **43**, 169–174.
- Mondesert, O., McGowan, C. H. and Russell, P.** (1996). Cig2, a B-type cyclin, promotes the onset of S in *Schizosaccharomyces pombe*. *Mol. Cell. Biol.* **16**, 1527–1533.
- Mor, A. and Philips, M. R.** (2006). Compartmentalized Ras/MAPK signaling. *Annu. Rev. Immunol.* **24**, 771–800.
- Moreno, S. and Nurse, P.** (1994). Regulation of progression through the G<sub>1</sub> phase of the cell cycle by the *rum1*<sup>+</sup> gene. *Nature* **367**, 236–242.
- Nadin-Davis, S. A., Nasim, A. and Beach, D.** (1986). Involvement of ras in sexual differentiation but not in growth control in fission yeast. *EMBO J.* **5**, 2963–2971.
- Neves, S. R., Ram, P. T. and Iyengar, R.** (2002). G protein pathways. *Science* **296**, 1636–1639.
- Niccoli, T. and Nurse, P.** (2002). Different mechanisms of cell polarisation in vegetative and shmooing growth in fission yeast. *J. Cell Sci.* **115**, 1651–1662.
- Nielsen, O. and Davey, J.** (1995). Pheromone communication in the fission yeast *Schizosaccharomyces pombe*. *Semin. Cell Biol.* **6**, 95–104.
- Nielsen, O., Davey, J. and Egel, R.** (1992). The *ras1* function of *Schizosaccharomyces pombe* mediates pheromone-induced transcription. *Embo J.* **11**, 1391–5.
- Niwa, O., Matsumoto, T., Chikashige, Y. and Yanagida, M.** (1989). Characterization of *Schizosaccharomyces pombe* minichromosome deletion derivatives and a functional allocation of their centromere. *EMBO J.* **8**, 3045–3052.
- Obara, T., Nakafuku, M., Yamamoto, M. and Kaziro, Y.** (1991). Isolation and characterization of a gene encoding a G-protein  $\alpha$  subunit from *Schizosaccharomyces pombe*: involvement in mating and sporulation

- pathways. *Proc. Natl. Acad. Sci. U S A* **88**, 5877–5881.
- Okazaki, K., Okazaki, N., Kume, K., Jinno, S., Tanaka, K. and Okayama, H.** (1990). High-frequency transformation method and library transducing vectors for cloning mammalian cDNAs by trans-complementation of *Schizosaccharomyces pombe*. *Nucleic Acids Res.* **18**, 6485–6489.
- Onken, B., Wiener, H., Philips, M. R. and Chang, E. C.** (2006). Compartmentalized signaling of ras in fission yeast. *Proc. Natl. Acad. Sci. U S A* **103**, 9045–9050.
- Padte, N. N., Martin, S. G., Howard, M. and Chang, F.** (2006). The cell-end factor pom1p inhibits mid1p in specification of the cell division plane in fission yeast. *Curr. Biol.* **16**, 2480–2487.
- Papadaki, P., Pizon, V., Onken, B. and Chang, E. C.** (2002). Two ras pathways in fission yeast are differentially regulated by two ras guanine nucleotide exchange factors. *Mol. Cell. Biol.* **22**, 4598–4606.
- Parada, L. F., Tabin, C. J., Shih, C. and Weinberg, R. A.** (1982). Human EJ bladder carcinoma oncogene is homologue of Harvey sarcoma virus ras gene. *Nature* **297**, 474–478.
- Petersen, J., Heitz, M. J. and Hagan, I. M.** (1998). Conjugation in *S. pombe*: identification of a microtubule-organising centre, a requirement for microtubules and a role for Mad2. *Curr. Biol.* **8**, 963–966.
- Pierce, K. L., Premont, R. T. and Lefkowitz, R. J.** (2002). Seven-transmembrane receptors. *Nat. Rev. Mol. Cell Biol.* **3**, 639–650.
- Prior, I. A., Harding, A., Yan, J., Sluimer, J., Parton, R. G. and Hancock, J. F.** (2001). GTP-dependent segregation of H-Ras from lipid rafts is required for biological activity. *Nat. Cell Biol.* **3**, 368–375.
- Reichelt, B. Y. and Fleet, G. H.** (1981). Isolation, properties, function, and regulation of endo-(1 leads to 3)- $\beta$ -glucanases in *Schizosaccharomyces pombe*. *J. Bacteriol.* **147**, 1085–1094.
- Resat, H., Straatsma, T. P., Dixon, D. A. and Miller, J. H.** (2001).

- The arginine finger of RasGAP helps Gln-61 align the nucleophilic water in GAP-stimulated hydrolysis of GTP. *Proc. Natl. Acad. Sci. U S A* **98**, 6033–6038.
- Resh, M. D.** (1996). Regulation of cellular signalling by fatty acid acylation and prenylation of signal transduction proteins. *Cell. Signal.* **8**, 403–412.
- Resh, M. D.** (1999). Fatty acylation of proteins: new insights into membrane targeting of myristoylated and palmitoylated proteins. *Biochim. Biophys. Acta* **1451**, 1–16.
- Resh, M. D.** (2006). Use of analogs and inhibitors to study the functional significance of protein palmitoylation. *Methods* **40**, 191–197.
- Rocks, O., Gerauer, M., Vartak, N., Koch, S., Huang, Z.-P., Pechlivanis, M., Kuhlmann, J., Brunsveld, L., Chandra, A., Ellinger, B., Waldmann, H. and Bastiaens, P. I. H.** (2010). The palmitoylation machinery is a spatially organizing system for peripheral membrane proteins. *Cell* **141**, 458–471.
- Rocks, O., Peyker, A., Kahms, M., Verveer, P. J., Koerner, C., Lumbierres, M., Kuhlmann, J., Waldmann, H., Wittinghofer, A. and Bastiaens, P. I. H.** (2005). An acylation cycle regulates localization and activity of palmitoylated ras isoforms. *Science* **307**, 1746–1752. ISSN 1095-9203 (Electronic).
- Rodriguez-Viciano, P., Warne, P. H., Dhand, R., Vanhaesebroeck, B., Gout, I., Fry, M. J., Waterfield, M. D. and Downward, J.** (1994). Phosphatidylinositol-3-OH kinase as a direct target of Ras. *Nature* **370**, 527–532.
- Roose, J. and Weiss, A.** (2000). T cells: getting a GRP on ras. *Nat. Immunol.* **1**, 275–6.
- Ross, E. M. and Wilkie, T. M.** (2000). GTPase-activating proteins for heterotrimeric G proteins: regulators of G protein signaling (RGS) and RGS-like proteins. *Annu. Rev. Biochem.* **69**, 795–827.
- Rotblat, B., Prior, I. A., Muncke, C., Parton, R. G., Kloog, Y.,**

- Henis, Y. I. and Hancock, J. F.** (2004). Three separable domains regulate GTP-dependent association of H-Ras with the plasma membrane. *Mol. Cell. Biol.* **24**, 6799–6810.
- Roy, S., Plowman, S., Rotblat, B., Prior, I. A., Muncke, C., Grainger, S., Parton, R. G., Henis, Y. I., Kloog, Y. and Hancock, J. F.** (2005). Individual palmitoyl residues serve distinct roles in H-Ras trafficking, microlocalization, and signaling. *Mol. Cell. Biol.* **25**, 6722–6733.
- Sambrook, J., Fritsch, E. and Maniatis, T.** (1989). *Molecular Cloning: A Laboratory Manual*, 2nd edn. Cold Spring Harbor, NY: Cold Spring Harbor Laboratory Press .
- Sander, P., Grünewald, S., Reiländer, H. and Michel, H.** (1994). Expression of the human D<sub>2S</sub> dopamine receptor in the yeasts *Saccharomyces cerevisiae* and *Schizosaccharomyces pombe*: a comparative study. *FEBS Lett.* **344**, 41–46.
- Santos, E., Tronick, S. R., Aaronson, S. A., Pulciani, S. and Barbacid, M.** (1982). T24 human bladder carcinoma oncogene is an activated form of the normal human homologue of BALB- and Harvey-MSV transforming genes. *Nature* **298**, 343–347.
- Saraste, M., Sibbald, P. R. and Wittinghofer, A.** (1990). The P-loop: a common motif in ATP- and GTP-binding proteins. *Trends Biochem. Sci.* **15**, 430–434.
- Sato, M., Blumer, J. B., Simon, V. and Lanier, S. M.** (2006). Accessory proteins for G proteins: partners in signaling. *Annu. Rev. Pharmacol. Toxicol.* **46**, 151–187.
- Sawin, K. E. and Nurse, P.** (1998). Regulation of cell polarity by microtubules in fission yeast. *J. Cell Biol.* **142**, 457–471.
- Sazer, S. and Sherwood, S. W.** (1990). Mitochondrial growth and DNA synthesis occur in the absence of nuclear DNA replication in fission yeast. *J. Cell Sci.* **97**, 509–516.
- Scolnick, E. M., Papageorge, A. G. and Shih, T. Y.** (1979). Guanine

- nucleotide-binding activity as an assay for src protein of rat-derived murine sarcoma viruses. *Proc. Natl. Acad. Sci. U S A* **76**, 5355–5359.
- Scolnick, E. M., Rands, E., Williams, D. and Parks, W. P.** (1973). Studies on the nucleic acid sequences of Kirsten sarcoma virus: a model for formation of a mammalian RNA-containing sarcoma virus. *J. Virol.* **12**, 458–463.
- Sharifmoghadam, M. R., Bustos-Sanmamed, P. and Valdivieso, M.-H.** (2006). The fission yeast Map4 protein is a novel adhesin required for mating. *FEBS Lett.* **580**, 4457–4462.
- Silvius, J. R.** (2002). Mechanisms of Ras protein targeting in mammalian cells. *J. Membr. Biol.* **190**, 83–92.
- Simon, M. A., Bowtell, D. D., Dodson, G. S., Laverty, T. R. and Rubin, G. M.** (1991). Ras1 and a putative guanine nucleotide exchange factor perform crucial steps in signaling by the sevenless protein tyrosine kinase. *Cell* **67**, 701–716.
- Simons, K. and Toomre, D.** (2000). Lipid rafts and signal transduction. *Nat. Rev. Mol. Cell Biol.* **1**, 31–39.
- Smith, B., Hill, C., Godfrey, E. L., Rand, D., van den Berg, H., Thornton, S., Hodgkin, M., Davey, J. and Ladds, G.** (2009). Dual positive and negative regulation of GPCR signaling by GTP hydrolysis. *Cell. Signal.* **21**, 1151–1160.
- Smotrýs, J. E. and Linder, M. E.** (2004). Palmitoylation of intracellular signaling proteins: regulation and function. *Annu. Rev. Biochem.* **73**, 559–587.
- Snaith, H. A. and Sawin, K. E.** (2003). Fission yeast mod5p regulates polarized growth through anchoring of tea1p at cell tips. *Nature* **423**, 647–651.
- Sprang, S. R.** (1997). G protein mechanisms: insights from structural analysis. *Annu. Rev. Biochem.* **66**, 639–678.
- Stern, B. and Nurse, P.** (1997). Fission yeast pheromone blocks S-phase

- by inhibiting the G<sub>1</sub> cyclin B-p34cdc2 kinase. *EMBO J.* **16**, 534–544.
- Stern, B. and Nurse, P.** (1998). Cyclin B proteolysis and the cyclin-dependent kinase inhibitor rum1p are required for pheromone-induced G<sub>1</sub> arrest in fission yeast. *Mol. Biol. Cell* **9**, 1309–1321.
- Sugimoto, A., Iino, Y., Maeda, T., Watanabe, Y. and Yamamoto, M.** (1991). *Schizosaccharomyces pombe ste11<sup>+</sup>* encodes a transcription factor with an HMG motif that is a critical regulator of sexual development. *Genes Dev.* **5**, 1990–1999.
- Sullivan, M. and Folk, W. R.** (1988). An improved procedure for measuring DNA replication with transient assays in eukaryotic cells. *Gene Anal. Tech.* **5**, 54–56.
- Sweet, R. W., Yokoyama, S., Kamata, T., Feramisco, J. R., Rosenberg, M. and Gross, M.** (1984). The product of ras is a GTPase and the T24 oncogenic mutant is deficient in this activity. *Nature* **311**, 273–5.
- Tanaka, K., Davey, J., Imai, Y. and Yamamoto, M.** (1993). *Schizosaccharomyces pombe map3<sup>+</sup>* encodes the putative M-factor receptor. *Mol. Cell. Biol.* **13**, 80–88.
- Tanaka, K. and Hirata, A.** (1982). Ascospore development in the fission yeasts *Schizosaccharomyces pombe* and *S. japonicus*. *J. Cell Sci.* **56**, 263–279.
- Teis, D., Wunderlich, W. and Huber, L. A.** (2002). Localization of the MP1-MAPK scaffold complex to endosomes is mediated by p14 and required for signal transduction. *Dev. Cell* **3**, 803–814.
- Tian, T., Harding, A., Inder, K., Plowman, S., Parton, R. G. and Hancock, J. F.** (2007). Plasma membrane nanoswitches generate high-fidelity Ras signal transduction. *Nat. Cell. Biol.* **9**, 905–914.
- Tinline-Purvis, H., Savory, A. P., Cullen, J. K., Davé, A., Moss, J., Bridge, W. L., Marguerat, S., Bähler, J., Ragoussis, J., Mott, R., Walker, C. A. and Humphrey, T. C.** (2009). Failed gene conversion leads to extensive end processing and chromosomal rearrangements in fission

- yeast. *EMBO J.* **28**, 3400–3412.
- Toda, T., Shimanuki, M. and Yanagida, M.** (1991). Fission yeast genes that confer resistance to staurosporine encode an AP-1-like transcription factor and a protein kinase related to the mammalian ERK1/MAP2 and budding yeast FUS3 and KSS1 kinases. *Genes Dev.* **5**, 60–73.
- Tong, L. A., de Vos, A. M., Milburn, M. V. and Kim, S. H.** (1991). Crystal structures at 2.2 Å resolution of the catalytic domains of normal ras protein and an oncogenic mutant complexed with GDP. *J. Mol. Biol.* **217**, 503–516.
- Torii, S., Kusakabe, M., Yamamoto, T., Maekawa, M. and Nishida, E.** (2004). Sef is a spatial regulator for Ras/MAP kinase signaling. *Dev. Cell* **7**, 33–44.
- Trahey, M. and McCormick, F.** (1987). A cytoplasmic protein stimulates normal N-Ras p21 GTPase, but does not affect oncogenic mutants. *Science* **238**, 542–545.
- Tratner, I., Fourticq-Esqueoute, A., Tillit, J. and Baldacci, G.** (1997). Cloning and characterization of the *S. pombe* gene *efc25<sup>+</sup>*, a new putative guanine nucleotide exchange factor. *Gene* **193**, 203–210.
- Ullrich, A. and Schlessinger, J.** (1990). Signal transduction by receptors with tyrosine kinase activity. *Cell* **61**, 203–212.
- Vanhaesebroeck, B., Guillermet-Guibert, J., Graupera, M. and Bilanges, B.** (2010). The emerging mechanisms of isoform-specific PI3K signalling. *Nat. Rev. Mol. Cell Biol.* **11**, 329–341.
- Venter, J. C., Adams, M. D., Myers, E. W. and *et al.*** (2001). The sequence of the human genome. *Science* **291**, 1304–1351.
- Verde, F., Mata, J. and Nurse, P.** (1995). Fission yeast cell morphogenesis: identification of new genes and analysis of their role during the cell cycle. *J. Cell. Biol.* **131**, 1529–1538.
- Vetter, I. R. and Wittinghofer, A.** (2001). The guanine nucleotide-binding switch in three dimensions. *Science* **294**, 1299–1304.

- Vieira, A. V., Lamaze, C. and Schmid, S. L.** (1996). Control of EGF receptor signaling by clathrin-mediated endocytosis. *Science* **274**, 2086–2089.
- Vogel, U. S., Dixon, R. A., Schaber, M. D., Diehl, R. E., Marshall, M. S., Scolnick, E. M., Sigal, I. S. and Gibbs, J. B.** (1988). Cloning of bovine GAP and its interaction with oncogenic ras p21. *Nature* **335**, 90–93.
- Wang, Y., Xu, H. P., Riggs, M., Rodgers, L. and Wigler, M.** (1991). *byr2*, a *Schizosaccharomyces pombe* gene encoding a protein kinase capable of partial suppression of the *ras1* mutant phenotype. *Mol. Cell. Biol.* **11**, 3554–3563.
- Watson, P., Davis, K., Didmon, M., Broad, P. and Davey, J.** (1999). An RGS protein regulates the pheromone response in the fission yeast *Schizosaccharomyces pombe*. *Mol. Microbiol.* **33**, 623–634.
- Wei, W., Mosteller, R. D., Sanyal, P., Gonzales, E., McKinney, D., Dasgupta, C., Li, P., Liu, B. X. and Broek, D.** (1992). Identification of a mammalian gene structurally and functionally related to the CDC25 gene of *Saccharomyces cerevisiae*. *Proc Natl Acad Sci U S A* **89**, 7100–7104.
- Welton, R. M. and Hoffman, C. S.** (2000). Glucose monitoring in fission yeast via the Gpa2 G $\alpha$ , the Git5 G $\beta$  and the Git3 putative glucose receptor. *Genetics* **156**, 513–521.
- Wennerberg, K., Rossman, K. and Der, C.** (2005). The Ras superfamily at a glance. *J. Cell Sci.* **118**, 843–846.
- Wettschureck, N. and Offermanns, S.** (2005). Mammalian G proteins and their cell type specific functions. *Physiol. Rev.* **85**, 1159–1204.
- Willingham, M. C., Pastan, I., Shih, T. Y. and Scolnick, E. M.** (1980). Localization of the src gene product of the Harvey strain of MSV to plasma membrane of transformed cells by electron microscopic immunocytochemistry. *Cell* **19**, 1005–1014.
- Willumsen, B. M., Norris, K., Papageorge, A. G., Hubbert, N. L.**

- and Lowy, D. R.** (1984). Harvey murine sarcoma virus p21 ras protein: biological and biochemical significance of the cysteine nearest the carboxy terminus. *EMBO J.* **3**, 2581–2585.
- Yamamoto, M.** (1996). Regulation of meiosis in fission yeast. *Cell Struct. Funct.* **21**, 431–436.
- Yen, H. C. and Chang, E. C.** (2000). Yin6, a fission yeast Int6 homolog, complexes with Moe1 and plays a role in chromosome segregation. *Proc. Nat.l Acad. Sci. U S A* **97**, 14370–14375.
- Zhang, T. and Fang, H. H. P.** (2004). Quantification of *Saccharomyces cerevisiae* viability using BacLight. *Biotechnol. Lett.* **26**, 989–992.